Catalytic and Electrocatalytic Pathways in Fuel Cells

A Dissertation

Submitted to the Faculty of the

WORCESTER POLYTECHNIC INSTITUTE

Department of Chemical Engineering

In partial fulfillment of the requirements for the

Degree of Doctor of Philosophy in Chemical Engineering

By

_____

Saurabh A. Vilekar
April 11, 2010

Approved:

_____

Prof. Ravindra Datta, Advisor
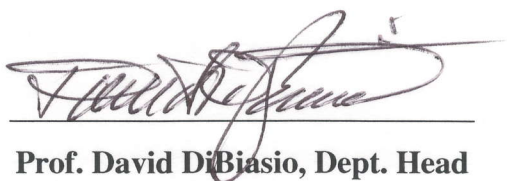WPI Department of Chemical Engineering

_____

Prof. Ilie Fishtik, Co-Advisor
WPI Department of Chemical Engineering

_____

Prof. N. Aaron Deskins
WPI Chemical Engineering Department

_____

Prof. Erkan Tüzel
WPI Department of Physics

_____

Prof. David DiBiasio, Dept. Head
WPI Chemical Engineering Department

Abstract

Materialization of the hydrogen economy can provide a long-term solution to our ever-increasing and pressing energy needs. However, significant challenges must be overcome before this shift in energy paradigm can occur. If hydrogen is indeed to become the energy-vector of future, a fundamental understanding of the kinetics and mechanisms of the catalytic reaction steps involved in the process of converting a fuel into hydrogen rich stream suitable for a fuel cell, as well as the electro-catalytic reactions within a fuel cell, is not only conceptually appealing, but could provide a sound basis for the design and development of efficient fuel processor/fuel cell systems. With the quantum chemical calculations on kinetics of elementary catalytic reaction steps becoming rather commonplace, and with increasing information now available in terms of electronic structures, vibration spectra, and kinetic data (activation energy and pre-exponential factors), the stage is set for development of a comprehensive approach.

Toward this end, we have developed a framework that can utilize this basic information to develop a comprehensive understanding of catalytic and electrocatalytic reaction networks. The approach is based on the development of Reaction Route (RR) Graphs, which not only represent the reaction pathways pictorially, but are quantitative networks consistent with the Kirchhoff's laws of flow networks, allowing a detailed quantitative analysis by exploiting the analogy with electrical circuits. The result is an unambiguous portrayal of the reaction scheme that lays bare the dominant pathways. Further, the rate-limiting steps are identified rationally with ease, based on comparison of step resistances, as are the dominant pathways via flux analysis. In fact, explicit steady-state overall reaction (OR) rate expression can also be derived in an Ohm's law form, i.e. OR rate = OR motive force/OR resistance of an equivalent electric circuit, which derives directly from the RR graph of its mechanism.

This approach is utilized for a detailed analysis of the catalytic and electro-catalytic reaction systems involved in reformer/fuel cell systems. The catalytic reaction systems considered include methanol decomposition, water gas shift, ammonia decomposition, and methane steam reforming, which have been studied mechanistically and kinetically. A detailed analysis of the electro-catalytic reactions in connection to the anode and

cathode of fuel cells, i.e. hydrogen electrode reaction and the oxygen reduction reaction, has also been accomplished. These reaction systems have not so far been investigated at this level of detail. The basic underlying principles of the RR graphs and the topological analysis for these reaction systems are discussed.

Acknowledgements

First and foremost, I would like to thank my advisor Prof. Ravindra Datta, without whom this dissertation would not have been possible. It has truly been an honor to be his advisee and I couldn't have asked for a better advisor, a friend and a philosopher. His passion, dedication and enthusiasm for research sure are contagious and have motivated me throughout my stay at WPI. I appreciate all his contributions, his kind and timely advice and critical comments in making this an enriching and productive experience and transforming me into an individual thinker. I am at a loss of words to describe his role which has been pivotal in shaping my professional and personal growth. I have thoroughly enjoyed working with him and learnt a great deal from him, all of which is impossible to pen down on a mere scrap of paper. All I can say is that I strive hard, not only to be a better researcher, but also to be a better person like him. Thank you for believing in me even in times when I had my own doubts.

I am also grateful to my co-advisor Prof. Ilie Fishtik for patiently explaining the basics of reaction route theory in my early days as a graduate student. I would like to thank Prof. Deskins and Prof. Tüzel for serving on my thesis committee and for their time and interest. Special thanks to all of my teachers at various levels of my education, from whom I have gained more than just academic knowledge.

I would like to thank Worcester Polytechnic Institute and the Department of Chemical Engineering for accepting me as a graduate student and supporting me as a Teaching Assistant all these years. It has most certainly sharpened by teaching skills and instilled in me the desire to venture a career in academics at some stage. Thanks to all the faculty members of our department for their guidance and advice.

I would like to take this opportunity to thank Laura Hanlan and other staff at our library for all their help and assistance with acquisition of journal articles. It is hard to fathom, how else would I have been able to perform a thorough literature review.

Special thanks to the current and past administrative staff of our department: Felicia Vidito, Tiffany Royal, Sandra Natale, Elaine Brady, Joseph Kaupu for helping me on numerous occasions. Thanks to Paula Moravek for all her timely help with purchase

In the loving memory of my grandparents........

"Without kinetic guidance, to go through a combinatorial campaign is to play dice with high technology."

-M. Boudart

Table of Contents

Chapter III: A Graph-Theoretic/DFT Analysis of Methanol Decomposition Reaction Network on Pt(111)

Chapter IV: A Reaction Route Network Analysis of Water Gas Shift Catalysis on Pt(111)

Chapter V: A Reaction Route Network Analysis of Ammonia Decomposition on Fe

Catalytic and Electrocatalytic Pathways in Fuel Cells

Chapter VI: Reaction Circuitry of Methane Steam Reforming on Ni(111): Mechanism and Kinetics

Chapter VII: H$_2$ – O$_2$ Polymer Electrolyte Membrane (PEM) Fuel Cells

Chapter VIII: Topology, Mechanism and Kinetics of Electro-catalytic Reaction Systems in Fuel Cells

List of Figures

Catalytic and Electrocatalytic Pathways in Fuel Cells

List of Tables

Catalytic and Electrocatalytic Pathways in Fuel Cells

Nomenclature

Symbols

a_i	Activity of terminal species i
A_ρ	Affinity of elementary reaction ρ
$\mathscr{A}_\rho$	Dimensionless reaction affinity of elementary reaction ρ
$\mathscr{A}_{OR}$	Dimensionless affinity of the overall reaction
$\mathscr{A}_{IR}$	Dimensionless affinity of intermediate reaction
$BE_{I_k \cdot S}$	Binding energy of intermediate species, I_k
c_i	Concentration of species i
C_t	Site density
D_i	Diffusion coefficient of gaseous species i within Nafion
$\vec{E}_\rho$	Activation energy of the forward reaction
$\overleftarrow{E}_\rho$	Activation energy of the reverse reaction
E_{OR}	Electro-motive force
E_{HOR,Φ_0}	Effective activation energy for HOR
E_{ORR,Φ_0}	Effective activation energy for ORR
F	Faraday's constant, 96,487 C eq^{-1}
ΔG_ρ	Gibbs free energy change of the elementary reaction ρ
ΔG_ρ	Gibbs free energy change of the elementary reaction ρ
$\Delta G_\rho^{\ddagger,o}$	Gibbs-free energy of activation
ΔG_{ad}^o	Standard adsorption free energy for $1/2H_2 + S \rightarrow H \cdot S$ at zero overpotential
H	Hamiltonian (total energy operator)
$H_{I_k(g)}^o$	Standard enthalpy of formation in the gas phase
$H_{I_k \cdot S}^o$	Standard enthalpy of formation in the adsorbed phase
$\Delta H_\rho^{\ddagger,o}$	Enthalpy of activation

Catalytic and Electrocatalytic Pathways in Fuel Cells

h	Planck's constant
I_k	Intermediate species k
$I_\rho^\bullet$	Maximum branch current
i	Fuel cell current density
i_{int}	Total internal current consisting of short-circuiting and crossover currents
$i_{S,M}$	Electrical-short circuit current
$i_{X,C}$	Crossover current at the cathode
$i_{X,A}$	Crossover current at the anode
i_0	Exchange current density
i^*	Current density (per metal catalyst surface)
i_0^*	Exchange current density (per metal catalyst surface)
$i_{0,ref}^*$	Exchange current density at reference conditions (per metal catalyst surface)
$i_{A,L}$	Anode limiting current density
$i_{C,L}$	Cathode limiting current density
k_i	Permeability of gaseous species i within Nafion
κ_i	Partition coefficient of gaseous species i within Nafion
k_{H_2}	Permeability of hydrogen within Nafion
k_{O_2}	Permeability of oxygen within Nafion
K_ρ	Equilibrium constant of the elementary reaction ρ
K_{OR}	Equilibrium constant of the overall reaction
$\vec{k}_\rho$	Forward rate constant of the elementary reaction ρ
$\overleftarrow{k}_\rho$	Backward rate constant of the elementary reaction ρ
k_B	Boltzman's constant
L_M	Membrane thickness

L_{EL}	Thickness of the electrolyte, ($L_{EL} = L_M$)
m	Number of independent ORs
M	distinct direct ORs
m_{mol}	mass of a molecule
$m_{\rho j}$	Incidence coefficient
n	Number of terminal species
N_{Av}	Avogadro's number
$N_{i,z}$	Flux of species i in the membrane along the z direction
OCV	Open-circuit voltage (V)
p	Number of elementary reactions
p_i	Partial pressure of species i
q	Number of linearly independent intermediate species
Q_k	intermediate QSS condition
r	Rank of formula matrix
R	Gas Constant
R_{ρ}	Resistance of elementary reaction ρ
$R_{\rho}^{\bullet}$	Resistance of elementary reaction s_{ρ}, when s_{ρ} is the RDS
R_{OR}	Total resistance of the overall reaction network
R_I	Interfacial resistance
r_{ρ}	Net rate of the elementary reaction ρ
r_{OR}	Net rate of the overall reaction
$\vec{r}_{\rho}$	Forward rate of elementary reaction ρ
$\overleftarrow{r}_{\rho}$	Reverse rate of elementary reaction ρ
$r_{\rho}^{\bullet}$	Maximum rate of the elementary reaction ρ
$\vec{r}_{\rho}^{\bullet}$	Maximum forward rate of the elementary reaction ρ
S	Unoccupied surface site
S_t	Active catalyst surface area
ΔS_{ρ}	Entropy change the elementary reaction ρ

$\Delta S_\rho^{\ddagger,o}$	Entropy of activation
$S_{I_k(g)}^o$	Standard entropy of formation of the species I_k in gas phase
$S_{trans,I_{k(g)}}$	Translational entropy of the species I_k in the gas phase
s_ρ	Elementary reaction ρ
T	Temperature
T_{ref}	Reference temperature (K)
T_i	Terminal species i
V_0	Thermodynamic open circuit potential $= (\Phi_{0,C} - \Phi_{0,A})$ (V)
V	Fuel cell voltage (V)
W	Mass of the catalyst bed
x_i	Mole fraction of species i
z_ρ	Reversibility of reaction s_ρ
z_{OR}	Reversibility of overall reaction
z_{IR}	Reversibility of an intermediate reaction
$\Delta(ZPE_{I_k})$	zero point energy correction to binding energy of the intermediate species, I_k

Greek Symbols

$\vec{\alpha}_{\rho k}$	Stoichiometric coefficient of intermediate species I_k in reaction step s_ρ as a reactant
$\overleftarrow{\alpha}_{\rho k}$	Stoichiometric coefficient of intermediate species I_k in reaction step s_ρ as a product
$\boldsymbol{\alpha}$	intermediate sub-matrix
$\vec{\beta}_{\rho i}$	Stoichiometric coefficient of the terminal species i in reaction step s_ρ as a reactant
$\overleftarrow{\beta}_{\rho i}$	Stoichiometric coefficient of the terminal species i in reaction step s_ρ as a product
β_ρ	Symmetry factor

ρ	Elementary reaction
σ_ρ	Stoichiometric number for the elementary reaction ρ
Λ_ρ	Pre-exponential factor
θ_k	Surface coverage of intermediate species k
$\theta_{k,\rho}^\bullet$	Surface coverage of intermediate species k when s_ρ is the RDS
μ	Number of linearly independent reaction routes
ω_ρ	Step weight for reaction s_ρ
$\vec{\omega}_\rho$	Forward step weight for reaction s_ρ
$\overleftarrow{\omega}_\rho$	Reverse step weight for reaction s_ρ
v_i	Stoichiometric coefficient of terminal species i in an overall reaction
$v_{\rho i}$	Stoichiometric coefficient of species i in reaction ρ
$v_{\rho e^-}$	Stoichiometric coefficient of electrons in reaction ρ
γ	reduced stoichiometric sub-matrix
γ_k	Stoichiometric coefficient of intermediate species I_k in an intermediate reaction
γ_{ki}	Stoichiometric coefficient of terminal species i in an intermediate reaction
ε	Fuel cell efficiency
Φ	Electrode potential
$\Phi_{\rho,0}$	Half-cell thermodynamic (reversible) potential (V) of electrode reaction ρ
$\Phi_{\rho,0}^\circ$	Standard half-cell thermodynamic potential (V) of electrode reaction ρ, i.e., for unit activities
Φ_0°	Standard electrode potentials
Φ_C	Cathode potential
$\Phi_{A,0}$	Thermodynamic potential of HOR
η_ρ	Overpotential of electrode reaction $\rho = \Phi - \Phi_{\rho,0}$ (V)

$\eta_{X,A}$	Anodic overpotential (V)
$\eta_{X,C}$	Cathodic overpotential (V)
ψ	Dimensionless electrode overpotential, $0.5F\eta/RT$
$\alpha_\rho^\bullet$	Effective transfer coefficient of the electrode reaction ρ
γ_M	Roughness factor (cm^2 metal cm^{-2} geometric electrode area)
σ_{M,e^-}	Electronic conductivity of the membrane
σ_{EL}	Protonic conductivity of the membrane
$\upsilon_{I_{k(g)}}$	Molar volume of gas-phase I_k

Abbreviations

AFC	Alkaline fuel cell
BE	Binding energy
CI	Configuration Interaction
CHP	Combined heat and power generation
DFT	Density Functional Theory
ER	Empty route
FCA	Frozen Core Approximation
FR	Full route
GGA	Generalized Gradient Approximation
GT	Gas turbine
HER	Hydrogen evolution reaction
HFSCF	Hartree Fock Self-Consistent Field
HOR	Hydrogen oxidation reaction
HT	Heyrovsky-Tafel
HTS	High temperature shift
IN	Intermediate node
IR	Intermediate reaction
IRR	Intermediate reaction route
KFL	Kirchhoff's Flux law
KPL	Kirchhoff's Potential law

LDA	Local Density Approximation
LFER	Linear free energy relation
LHHW	Langmuir-Hinshelwood-Hougen-Watson
LTS	Low temperature shift
MARI	Most abundant reactive intermediate
MCFC	Molten carbonate fuel cell
MEA	Membrane electrode assembly
MSR	Methane steam reforming
OCV	Open circuit voltage
OR	Overall reaction
ORR	Oxygen reduction reaction
PAFC	Phosphoric acid fuel cell
PES	Potential energy surface
PEH	Pseudo-equilibrium hypothesis
PEM	Polymer electrolyte membrane
PBR	Packed-bed reactor
PrOx	Preferential oxidation
ECPrOx	Electrochemical Preferential oxidation
QSS	Quasi-steady state
QE	Quasi-equilibrium
RH	Relative humidity
RR	Reaction Route
RDS	Rate determining step
RLS	Rate limiting step
SOFC	Solid oxide fuel cell
SR	Steam reforming
TE	Total electronic energy
TISE	Time-Independent Schrödinger Equation
TN	Terminal node
TST	Transition state theory
UBI-QEP	Unity Bond Index – Quadratic Exponential Potential

VH	Volmer-Heyrovsky
VT	Volmer-Tafel
XC	Exchange-correlation

Catalytic and Electrocatalytic Pathways in Fuel Cells

Chapter I

Motivation and Objectives

1.1 Background and Rationale

Fuel cells have been touted as the next-generation power sources for decades. They offer the potential of revolutionizing energy production through highly efficient and pollution-free power generators for use in applications such as consumer electronics, home, and transportation. Enormous technological progress has been made since the invention of the first fuel cell ever by William Grove in 1839; however, even the most advanced of the technologies is far from being commercialized. A summary of the different type of fuel cells as a result of the active research for more than a century is presented in Table 1-1 [1] and shown schematically in Figure 1-1.

The low temperature fuel cells, namely the $H_2 - O_2$ PEM fuel cells demand pure hydrogen as the feed. Hydrogen, in spite of being the most abundant element in nature, does not exist by itself, and is intended to be produced either on site or centrally via catalytic reforming of hydrocarbon fuels. However, despite the considerable advantages of a hydrogen economy compared to the current fossil fuel economy, like the possibility of finding a long-term energy source with H_2 being produced from both fossil fuels, renewable resources and atomic energy, there are still significant challenges that must be overcome before this shift in energy paradigm can occur.

Hydrogen comprises of three times the energy content of petrol on weight basis; however, on volume basis the situation is reversed. If hydrogen is indeed to replace gasoline, in the much hyped hydrogen economy, and is to be more environmentally benign as compared to gasoline, momentous effort needs to be devoted to the advancement of technologies for reliable, efficient, safe, and cost-effective production, distribution and use of the fuel, which currently is a major technological impediment for the commercialization of PEM fuel cells.

Table 1-1: Comparison of different types of fuel cells [1].

Fuel Cell Type	Common Electrolyte	Operating T	System Output	Electrical Efficiency	Combined Heat and Power (CHP) Efficiency	Applications	Advantages
Polymer Electrolyte Membrane (PEM)/ or DMFCs	Solid organic polymer poly-perfluorosulfonic acid	50 - 100°C 122 - 212°F 80 - 150°C (for DMFCs)	< 1kW – 250kW	53-58% (transportation) 25-35% (stationary)	70-90% (low-grade waste heat)	• Backup power • Portable power • Small distributed generation • Transportation • Specialty vehicles	• Solid electrolyte reduces corrosion & electrolyte management problems • Low temperature • Quick start-up
Alkaline (AFC)	Aqueous solution of potassium hydroxide soaked in a matrix	90 - 100°C 194 - 212°F	10kW – 100kW	60%	> 80% (low-grade waste heat)	• Military • Space	• Cathode reaction faster in alkaline electrolyte, leads to higher performance • Can use a variety of catalysts
Phosphoric Acid (PAFC)	Liquid phosphoric acid soaked in a matrix	150 - 200°C 302 - 392°F	50kW – 1MW (250kW module typical)	>40%	> 85%	• Distributed generation	• Higher overall efficiency with CHP • Increased tolerance to impurities in hydrogen
Molten Carbonate (MCFC)	Liquid solution of lithium, sodium, and/or potassium carbonates, soaked in a matrix	600 - 700°C 1112 - 1292°F	< 1kW – 1MW (250kW module typical)	45-47%	> 80%	• Electric utility • Large distributed generation	• High efficiency • Fuel flexibility • Can use a variety of catalysts • Suitable for CHP
Solid Oxide (SOFC)	Yttria stabilized zirconia	600 - 1000°C 1202 - 1832°F		35-43%	< 90%	• Auxiliary power • Electric utility • Large distributed generation	• High efficiency • Fuel flexibility • Can use a variety of catalysts • Solid electrolyte reduces electrolyte management problems • Suitable for CHP • Hybrid /GT cycle
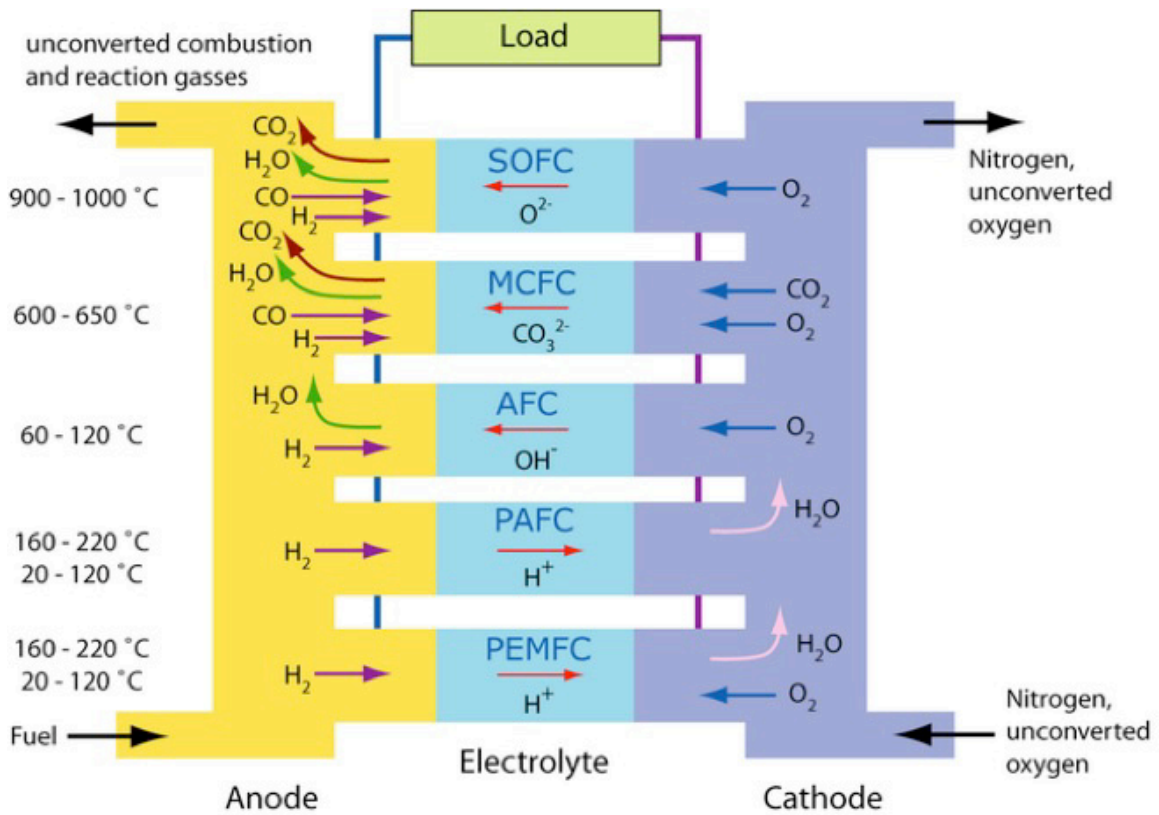
Figure 1-1: Schematics of different type of fuel cells.

Even though liquefaction leads to a form of hydrogen that is potentially attractive for use in larger fuel-cell systems, the energy density is low (2.70 Wh/cm^3). Furthermore, if the energy spent in the liquefaction process is considered, the energy density is lowered even further, by as much as 40% [2]. Of course, central production and distribution of hydrogen could be a potential solution, however, that calls for a huge capital investment, making the use of pipelines unlikely to transition to the hydrogen economy. Currently, no efficient, practical method of storing hydrogen for fuel cell applications exists, which is not too heavy, bulky or costly. The alternate option is to use some sort of hydrogen carrier. A two way carrier is a material that is transported to a distribution site in a "hydrogenated" form, dehydrogenated to yield hydrogen, and the dehydrogenated material returned to a processing site where it would be re-hydrogenated for reuse, e.g. complex hydrides like $LiBH_4$ which has high gravimetric hydrogen wt% (18.5%) and can theoretically release about 13.9 wt% hydrogen. A great deal of research effort has been invested in the area of onboard storage of hydrogen and it is clear from Figure 1-2 that storing as little as 4 kg of H_2 (the required amount of H_2 for an automobile to give an acceptable driving range of 300 miles) onboard presents a daunting prospect [3].

On the other hand, conventional fuels e.g., natural gas, gasoline or alcohols, might be construed as one-way hydrogen carriers, i.e., they could be reformed at the point of use, e.g., on board an automobile. Such distributed generation (i.e., at the point of consumption) proffers the advantage of cost reduction, reduces interdependencies and inefficiencies with the associated transmission and distribution. This, however, requires a compact fuel processor, often with a number of issues. Any hydrocarbon used for onboard hydrogen generation will essentially produce a reformate stream containing CO and CO_2. The susceptibility of low temperature PEM fuel cells to CO poisoning makes the integrated onboard fuel processors rather complex, comparable to a small-scale version of an industrial reforming unit. The amount of CO produced during the reforming process is greatly influenced by the hydrocarbon being processed and the temperature of reforming. Lower the H/C ratio, and higher the temperature, greater is the propensity toward formation of CO. For example steam reforming of n-dodecane might produce CO in the order of ~8 − 10%, while for methanol steam reforming CO might be in the range of ~1%.

Figure 1-2: Volume of 4 kg of hydrogen compacted in different ways, with size relative to the size of a car [3].

Thus, the degree of fuel processing, post the reformer would change substantially so as to produce reformate of PEM fuel cell quality, and many technical issues exists in this proposed reformer/fuel cell scheme that remain unresolved at this time.

An alternate and potentially extremely attractive technology is the direct methanol fuel cell (DMFC), operating at around 80 to 150 ºC, which would obviate the multi-step reforming process and its associated complexities, albeit at the expense of substantial overpotential or electrical energy. This presents a genuine predicament as to what is really an optimum configuration? Is it utilization of the hydrogen rich reformate stream in a $H_2 - O_2$ PEM fuel or direct internal reforming of methanol in a direct methanol fuel cell? Indeed, the optimum solution depends upon the application, e.g., in portable power unit, a DMFC may be better, while in a stationary unit, a reformer followed by a PEM fuel cell may be better. There is a strong possibility, nonetheless, that *the molecular mechanism of the overall process remains largely the same* regardless of the process scheme.

Another such an example is the case of solid oxide fuel cell (SOFC). SOFC's operate at much higher temperatures, which provide them the opportunity to utilize readily available liquid fuels like gasoline for direct internal reforming. However, it should be noted that the high temperature of operation that provides leverage in terms of fuel flexibility has the associated material stability and sealing issues, adding system complexities. Further, the Ni anode of the SOFC is susceptible to H_2S poisoning, and thus calls for upstream desulfurization. Moreover, with direct internal reforming of liquid fuels, proclivity for the formation of coke precursors (i.e, higher hydrocarbons > C2s) and eventual performance degradation has been well documented. Moreover, SOFC's also function better with H_2-rich reformate from reforming of liquid hydrocarbons, which allows performance longevity. Some level of fuel processing is, thus, inevitable. Of course, natural gas can be utilized directly as fuel for internal reforming in a SOFC (See Figure 6-1). On the other hand, hydrogen can be produced from steam reforming of natural gas, which can be utilized in a PEM fuel cell, which again presents the same quandary: Which configuration is optimum?
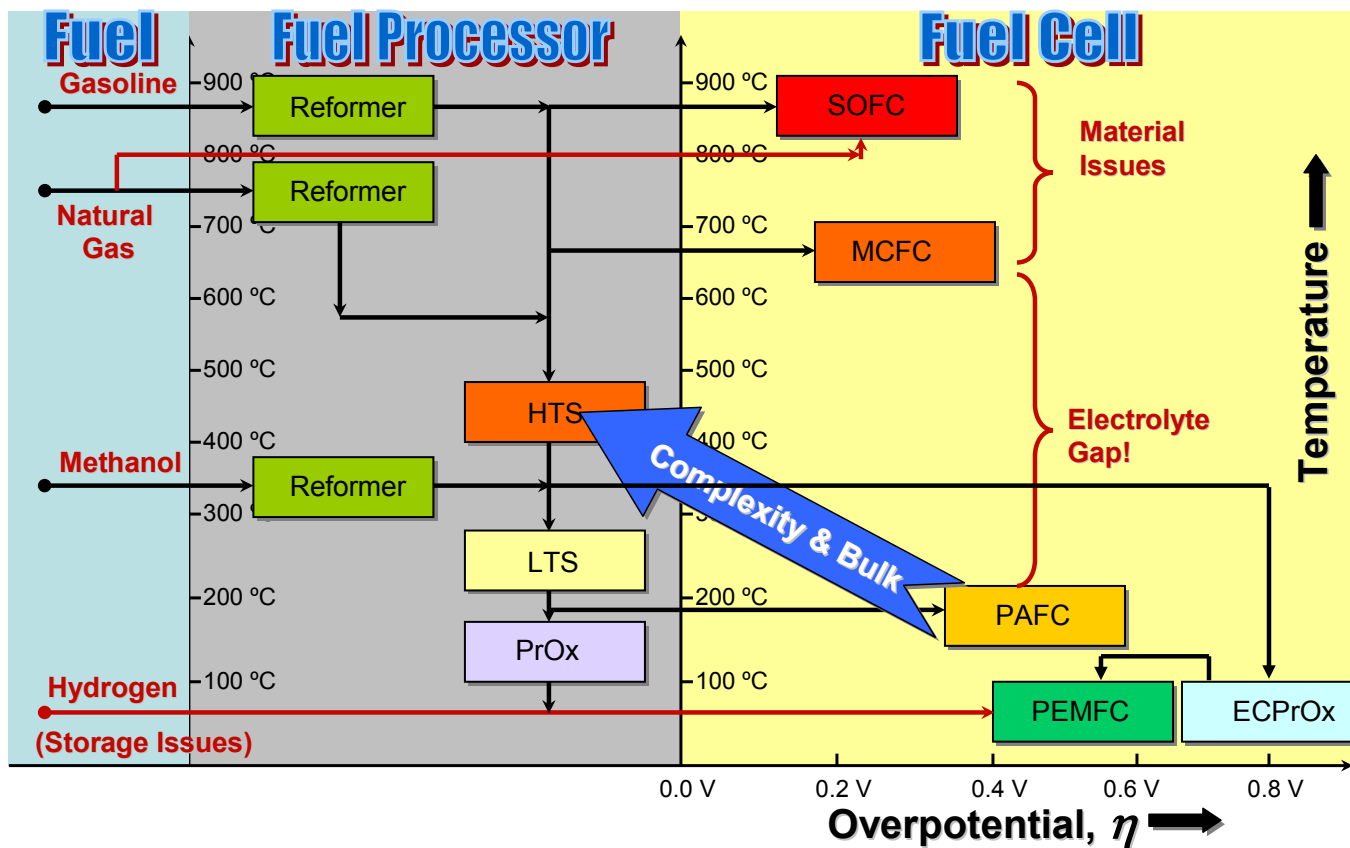
Figure 1-3: Various reformer / fuel cell systems options.

Thus, for any fuel cell, H_2-rich reformate might be the best suited fuel, where hydrogen is simply an energy vector, in turn derived from another fossil fuel or renewable fuel. This journey of a fuel (e.g. methane or methanol) to electricity involves a number of catalytic steps in fuel reformation into hydrogen as well as electro-catalytic steps in the conversion of hydrogen to electricity in a fuel cell. This journey should, in fact, be viewed as a continuum, in order to optimize the process of a temperature versus potential scale. These various fuel cell/reforming options are summarized in Figure 1-3. Thus, the reformer complexity is dictated by the choice of the fuel cell and the fuel, the latter determining its temperature. For example, gasoline reforming requires a higher temperature than methane, which reforms at a higher temperature than methanol. A high temperature reformer is followed by high and low temperature shift, i.e., HTS or LTS, reactor, and preferential oxidation, or PrOx, reactor, to reduce the CO to tolerable levels. However, for the phosphoric acid fuel cell (PAFC) operating at around 200 ºC, the PrOx stage is unnecessary, while PEM fuel cell requires it. In the higher temperature fuel cells, namely molten carbonate fuel cell (MCFC) and SOFC, the HTS and LTS are unnecessary, since they can use CO and CH_4 directly, and also do not need precious metal catalysts.

As is evident, on the one extreme, the fuel may be utilized directly in a high temperature fuel cell without reformation, to the other extreme involving several catalytic steps (reforming, water-gas shift, and preferential oxidation reactions) to produce hydrogen feeding a low temperature fuel cell. The optimum perhaps lies in the middle somewhere, with a simpler reforming process combined with an intermediate temperature fuel cell, which currently does not exist due to lack of electrolytes that function at those temperatures. It is with this view that we embark on a fundamental understanding of the catalytic reaction steps involved in the process of converting the fossil fuels into hydrogen rich streams capable of being utilized in fuel cells and the electro-catalytic reactions in a fuel cell that eventually produces power. A detailed mechanistic and kinetic understanding of these molecular events should eventually enable us to develop efficient fuel processor/fuel cell systems.

The earliest approach to developing catalytic kinetics based on a molecular mechanism was that of Langmuir-Hinshelwood-Hougen-Watson, or LHHW [4, 5], which is still the standard approach today. However, such an approach is limited in the sense

that it is applicable to only *single* RLS systems and is also fraught with the risk of identifying the wrong RLS, since more than one such rate expression might concur with the experimental findings. On the other hand, quasi-steady state (QSS) and the microkinetic approach require detailed kinetics of the mechanistic steps, which have so far been based largely on fitting of experimental data along with the use of semiempirical relations, e.g., the Polanyi relation [6].

Prediction of surface kinetics from fundamental principles was first attempted by Shustorovich [7] employing a semi-empirical method, namely Unity Bond Index – Quadratic Exponential Potential method (UBI-QEP), that provides activation energy barriers within ±4–12 kJ/mol and has been rigorously employed to probe into surface chemistry [8-11]. With the advent of user-friendly quantum mechanics software, theoretical study of molecular catalytic reaction mechanisms has become rather commonplace as a very insightful tool [8-13]. For instance, until relatively recently, surface intermediates could only be guessed or identified via elaborate surface science experiments, whereas now, quantum chemistry calculations provides a detailed picture [14]. For instance, the optimized molecular structures of the reaction intermediates for methanol decomposition on Pt(111) are reported in detail in refs [15-19]. In fact, it is not even possible to experimentally detect all of these intermediates even with a broad array of sophisticated techniques including TPD, EELS, IRS, UPS, AES, and molecular beam [16]. First principle calculations can provide not only structural information but also thermochemical and energetic parameters for the surface reactions. In short, the density functional method (DFT) is an inimitable tool for determining the reaction intermediates and building a detailed molecular mechanism for catalytic reactions. The interest in fuel cells has also spurred some work in first-principles modeling of electrocatalysis [20-26], but the field is still in its infancy. The accuracy of predictions can be expected to only improve in the future.

However, this is only the starting point for developing a complete understanding of a catalytic system, including the most favorable reaction pathway and the key reaction steps. What is needed is an easy to use addendum to the quantum mechanical software that can utilize its first principles predictions to construct a comprehensive picture of the catalytic system, including elucidation of all parallel pathways and the dominant reaction

routes and steps. While software tools such as CHEMKIN are available for this purpose, they are based on rather brute-force numerical methodologies. A more insightful graphic approach is called for that might be readily utilized by the catalytic scientist, without the necessity of being fully conversant with its theoretical underpinnings. One of the objectives here, thus, is to develop such a consistent graph-theoretic approach and utilize it for a host of catalytic and electro-catalytic systems in connection to fuel cells.

Graph-theoretical approaches to visualize reaction networks are, of course, not new [14, 27, 28]. Such mathematical depiction of network topology while useful is, however, not enough. Quantitative reaction networks involving flux of material must also conform to certain laws dealing with interdependence of flows in the interconnected networks, namely, mass balance at junctures, and consistency with thermodynamics. These, in fact, take the form of Kirchhoff's laws of current (charge balance) and potential (thermodynamic driving force) in electrical circuits [29], for instance. Thus, rules for graph-theoretic depiction of reaction networks need to be clearly enunciated and followed so that the resulting graphs are consistent with these basic requirements. Otherwise, the result is a little more than a pretty picture.

Unfortunately, practically all the existing reaction graph and theoretical approaches are inconsistent with these requirements, as is readily discerned, for instance, if one studies Figure 1-4 of Broadbelt and Pfaendtner [14], which is inconsistent except for the case of linear mechanisms. Most catalytic mechanisms are non-linear although enzyme reactions are often linear. This is due to the unfortunate, but universal, practice of identifying nodes, or vertices with *individual* species, while branches, or edges, represent the reaction steps in conventional graph-theoretic representation. This practice no doubt derives from the mechanisms depicted in chemistry texts, where species, often including structural details, are drawn at hubs interconnected by arrows depicting reactions.

Our graph-theoretic approach [30-32] is developed further here that avoids this pitfall, overcoming the limitations of current methodologies and providing a self-consistent topological and mechanistic and kinetic analysis tool, based on the reaction route theory.
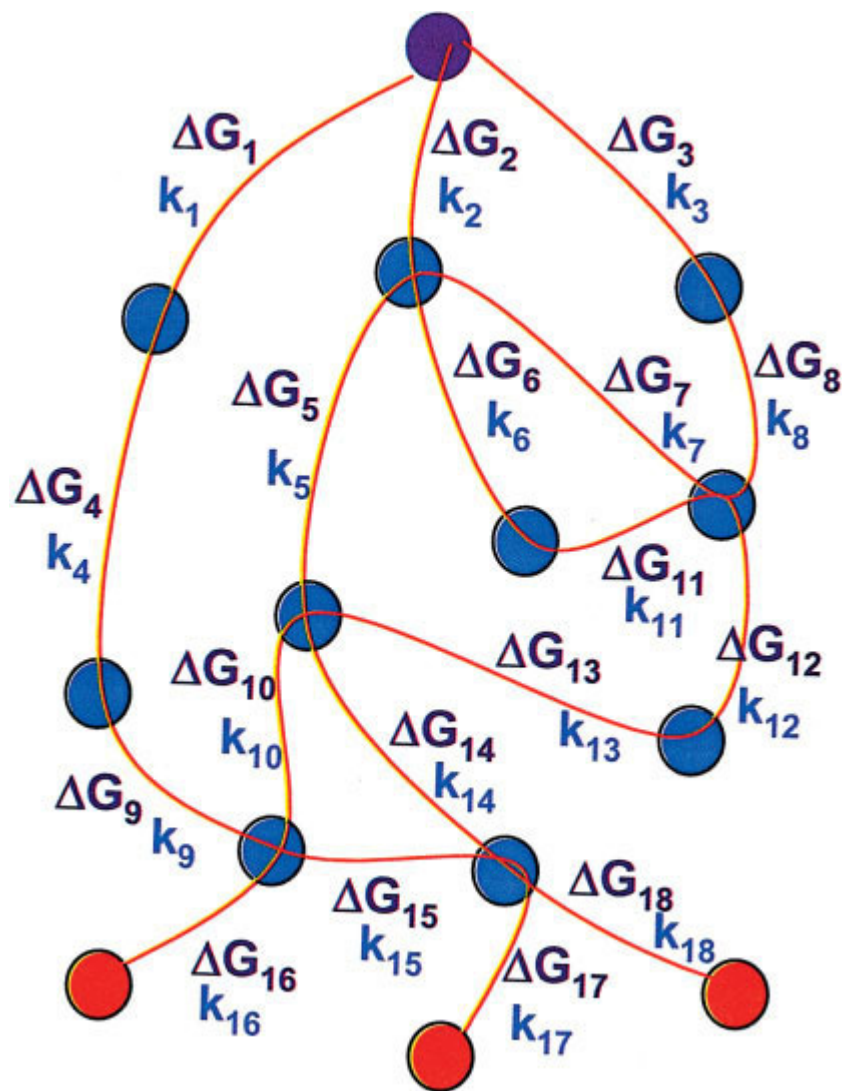
Figure 1-4: Conventional graph-theoretic representation with nodes representing individual species [14].

The basic difference from the conventional approach is that the nodes, or hubs, do not necessarily represent an individual species, but rather simply represent the connectivity among elementary reaction steps in the network at a juncture. As a result, the RR Graphs become quantitative that follow network laws. For instance, they can be directly converted into an equivalent electrical circuit, thus, allowing the well-developed and familiar methods of electric circuit theory, including Kirchhoff's laws, to be utilized in a direct and transparent fashion for network analysis. Thus, our new graph-theoretic approach, in conjunction with DFT calculations, forms a powerful combination for visualizing the myriad pathways, developing detailed network kinetics, and performing flux analysis and network pruning. The proposed algorithm provides a framework by which the improved experimental and theoretical knowledge could be used to better probe and discern reaction mechanisms and kinetics. An adequate understanding of the reaction mechanism thus developed not only allows one to develop robust rate expressions required for reactor design but also allows rational improvement of catalysts and processes to make them more selective and, consequently, more energy and resource efficient.

Our approach toward robust mechanistic and kinetic analysis is schematically shown in Figure 1-5. Further, such analysis could be of immense practical utility in the *a priori* catalyst screening and design by performing such analysis for different catalysts to predict reaction kinetics and selectivity, thus reducing the experimental screening work and expense. Our overall approach (Figure 1-5) involves the following steps: 1) determination of surface intermediates on a given catalyst; 2) generation of a set of plausible surface elementary reaction steps involved in the overall reaction (OR); 3) graph-theoretic generation of a reaction network that depicts the overall mechanism as well as the multitude of reaction routes (RRs); 4) prediction of pre-exponential factors and activation energies, from which energy diagrams are drawn; 5) conversion of the reaction network into an equivalent electrical network that, not only pictorially represents the "circuitry" of reaction pathways, but also allows rigorous flux and kinetic analysis by making use of the vast array of tools available for the analysis of electrical circuits, namely Kirchhoff's flux and potential law.
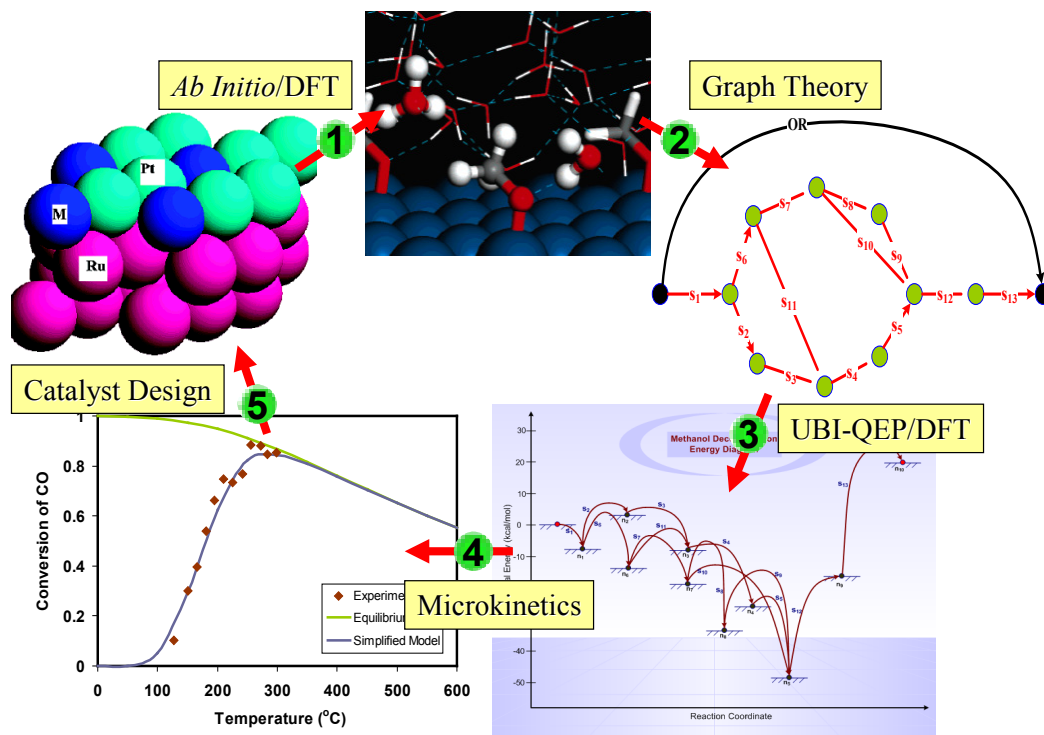
Figure 1-5: Network approach to catalyst design.

Furthermore, the reaction circuitry allows a reduction of the network by a direct and transparent comparison of the reaction step resistances along with a logical identification of slow or rate-limiting steps. The approach provides for development of explicit rate expressions for the considered reaction system. Moreover, the approach also allows for incorporation of time-honored principles of quasi-equilibrium (QE) hypothesis, most-abundant reactive intermediate (MARI), LHHW formulation without any *ad hoc* assumption of rate-limiting steps (RLS) and so on.

In chapter II the theory of Reaction Route (RR) Graphs and its analogy with electrical circuits is explicated without undue mathematical details using relatively simple examples of gas-phase hydrogen-bromine non-catalytic reaction and zeolite catalyzed N_2O decomposition reaction. The approach is then be utilized in subsequent chapters with rigor to analyze thermo- and electro-catalytic reaction systems involving *parallel* pathways in fuel cells.

Chapter III deals with methanol decomposition on Pt, which is important first step not only in methanol steam reforming but also in a direct methanol fuel cell. Here we show that the electrical analogy of the RR Graph approach could be combined with *ab initio* prediction of step kinetics to do a detailed flux analysis that lays bare the important pathways and steps in a reaction network allowing insightful pruning of the mechanism. It is, thus, found that methanol decomposition proceeds exclusively via the initial C-H dehydrogenation step rather than through O-H bond activation.

Chapter IV evaluates the case of water-gas-shit (WGS), an integral part of the fuel processing train for low temperature fuel cells. A rigorous analysis of the comprehensive 17-step mechanism with DFT-predicted kinetics for the WGS reaction on Pt(111) is accomplished, where we show how to assemble all the 71 reaction pathways into a RR graph. Based on the reaction circuitry approach, the mechanism is reduced to a network involving only a single dominant RR mediated via carboxyl species. Rate limiting steps are next identified logically to derive a simple and accurate rate expression, without any *ad hoc* assumptions.

As an alternative to a metal-hydride carrier for hydrogen storage, chemical storage of hydrogen has been suggested, e.g., as NH_3, a very effective and inexpensive hydrogen

carrier available in large quantities. Chapter V probes the mechanism and kinetics of a 7-step commonly accepted mechanism for NH_3 decomposition on Fe. The mechanism is whittled down to a single RLS. A rate expression subsequently derived is in complete agreement with our experimental data.

As discussed in this chapter, natural gas can be utilized directly for internal reforming in a SOFC on a Ni-based anode or hydrogen can be produced via steam reforming which is eventually used in a low temperature PEM fuel cell. Fundamental understanding of this important reaction mechanism is pivotal for the development of compact and efficient fuel processors/fuel cell systems. A 22-step reaction mechanism based on exhaustive literature review is analyzed using the RR graph approach in chapter VI. We unequivocally show that a dual-pathway mechanism exists depending on the temperature of operation. Rate expressions are next derived based on logical identification of the RLSs. The model predictions are in concurrence with the experimental data by Xu and Froment [33], considered as the standard reference on methane steam reforming (MSR).

In chapter VII, we consider the typical membrane-electrode-assembly (MEA) consisting of a five layer assembly in terms of RR Graph approach to develop a lumped fuel cell model. We also discuss the cause and the extent of the effect of the fuel and/or oxidant crossover on the fuel cell open-circuit voltage (OCV) and provide a logical explanation based on *a priori* parameters, that the hydrogen cross-over to the cathode explains all of the observed loss of ~20% under open circuit conditions.

Chapter VIII considers the electro-catalytic reactions in connection to low temperature fuel cells, namely the hydrogen electrode reaction at the anode and the oxygen reduction reaction at the cathode. An improved understanding of these archetypical electrochemical reactions is essential for deeper fundamental understanding of fuel cells, which would assist better catalyst design and detailed fuel cell modeling. Based on *a priori* activation energies, explicit rate expressions are reported for the first time ever, agreeing reasonably well with the experimental findings. Finally, we show for the hydrogen oxidation reaction in acidic system that the exchange current density is two orders of magnitude higher than what has been assumed for more than four decades. The

approach developed here can be extended to a host of other electrochemical systems like methanol electro-oxidation occurring at the anode of DMFCs.

In summary, the premise of this study is that a better understanding of the catalytic and electrocatalytic processes that occur within a reformer/fuel cell system can lead to improved catalysts, devices, operating conditions, and overall system. Toward this end, this work represents the initial steps taken to understand this important energy generation system of the future.

1.2 References

[1] http://www.eere.energy.gov.

[2] R. Harris, D. Book, P. Anderson, P. Edwards, Fuel Cell Review. June/July (2004) 17.

[3] L. Schlapbach, A. Züttel, Nature. 414 (2001) 353-358.

[4] O.A. Hougen, K.M. Watson, J. Ind. Eng. Chem. 35 (1943) 529-541.

[5] M. Boudart, G. Djega-Mariadassou, Kinetics of Heterogeneous Catalytic Reactions, Princeton University Press, Princeton, N. J., 1984.

[6] J.A. Dumesic, D.F. Rudd, L.M. Aparicio, J.E. Rekoske, A.A. Trevino, The Microkinetics of Heterogeneous Catalysis, ACS, Washington, DC, 1993.

[7] E. Shustorovich, H. Sellers, Surf. Sci. Reports. 31 (1998) 1-119.

[8] A. GroB, Surf. Sci. 500 (2002) 347-367.

[9] M. Neurock, J Catal. 216 (2003) 73-88.

[10] F. Ruette, M. Sanchez, A. Sierraalta, C. Mendoza, R. Anez, L. Rodriguez, O. Lisboa, J. Daza, P. Manrique, Z. Perdomo, M. Rosa-Brussin, J. Mol. Catal. A: Chemical. 228 (2005) 211-225.

[11] S. Desai, M. Neurock, Electrochimica Acta. 48 (2003) 3759-3773.

[12] G.-C. Wang, L. Jian, Y. Morikawa, J. Nakamura, Z.-S. Cai, Y.-M. Pan, X.-Z. Zhao, Surface Science. 570 (2004) 205-217.

[13] Y.-A. Zhu, D. Chen, X.-G. Zhou, W.-K. Yuan, Catal. Today. 148 (2009) 260–267.

[14] L.J. Broadbelt, J. Pfaendtner, AIChE Journal. 51 (2005) 2112-2121.

[15] J. Greeley, M. Mavrikakis, J. Am. Chem. Soc. 124 (2002) 7193-7201.

[16] J. Greeley, M. Mavrikakis, J. Am. Chem. Soc. 126 (2004) 3910-3919.

[17] D. Cao, G.-Q. Lu, A. Wieckowski, S.A. Wasileski, M. Neurock, J. Phys. Chem. B. 109 (2005) 11622-11633.

[18] J. Kua, W.A. Goddard, III., J. Am. Chem. Soc. 121 (1999) 10928-10941.

[19] Y. Ishikawa, M. Liao, C. Cabrera, Surf. Sci. 463 (2000) 66-80.

[20] Y. Ishikawa, J.J. Mateo, D.A. Tryk, C.R. Cabrera, J. Electroanal. Chem. 607 (2007) 37-46.

[21] A.B. Anderson, T.V. Albu, J. Am. Chem. Soc. 121 (1999) 11855-11863.

[22] Y. Cai , A.B. Anderson, J. Phys. Chem. B. 108 (2004) 9829 -9833.

[23] E. Skulason, G.S. Karlberg, J. Rossmeisl, T. Bligaard, Greeley J., H. Jonsson, J.K. Nørskov, Phys. Chem. Chem. Phys. 9 (2007) 3241–3250.

[24] J.X. Wang, T.E. Springer, P. Liu, M. Shao, R.R. Adzic, J. Phys. Chem. C. 111 (2007) 12425-12433.

[25] P. Liu, J.K. Nørskov, Fuel Cells. 1 (2001) 192-201.

[26] C.D. Taylor, M. Neurock, Curr. Opinion Solid State & Mat. Sci. 9 (2005) 49-65.

[27] A.T. Balaban, in: D. Bonchev, O. Mekenyan (Eds.), Graph Theoretical Approaches to Chemical Reactivity, Kluwer Academic Publishers, Dordrecht, Netherlands, 1994, pp. 137-180.

[28] O.N. Temkin, A.V. Zeigarnik, D.G. Bonchev, Chemical Reaction Networks: A Graph-Theoretical Approach, CRC Press, New York, 1996.

[29] N. Balabanian, T. Bickart, Electrical Network Theory, John Wiley, New York, 1969.

[30] I. Fishtik, C.A. Callaghan, R. Datta, J. Phys. Chem. B. 108 (2004) 5671-5682.

[31] I. Fishtik, C.A. Callaghan, R. Datta, J. Phys. Chem. B. 108 (2004) 5683-5697.

[32] I. Fishtik, C.A. Callaghan, R. Datta, J. Phys. Chem. B. 109 (2005) 2710-2722.

[33] J. Xu, G.F. Froment, AIChE Journal. 35 (1989) 88-96.

Chapter II

Topological and Kinetic Analysis Based on Reaction Route (RR) Graphs

The conventional kinetic analysis of an overall reaction (OR) is limited to a *single* sequential pathway of molecular steps at a time, based either on the general quasi-steady state (QSS) approach of Bodenstein, or on the much simpler but limited Langmuir-Hinshelwood-Hougen-Watson (LHHW) approach based on assuming a *single* rate-determining step (RDS), the remaining being quasi-equilibrated (QE). In this chapter the theory of Reaction Route (RR) Graphs and its analogy with electrical circuits is explicated, which will be utilized with rigor to subsequently analyze thermo- and electro-catalytic reaction systems involving *parallel* pathways in fuel cells. Based on RR Graphs/circuitry, QSS rate expression for a reaction system can be simply cast into an Ohm's law form, i.e., OR rate = OR motive force/OR resistance of an equivalent electric circuit. Moreover, logical pruning and identification of rate-*limiting* steps is afforded based on flux analysis and step resistance comparison quantitatively. The approach is independent of how the step kinetics are derived. In order to describe the basic framework for the approach, we utilize the relatively simple examples of: 1) the gas-phase hydrogen-bromine non-catalytic reaction (non-linear kinetics), and 2) zeolite catalyzed N_2O decomposition reaction (linear kinetics). In subsequent chapters, the approach is applied to practical and more complex reactions networks relevant to fuel cells.

2.1 Introduction

Many of the industrially significant reactions involve parallel reaction pathways. For instance water-gas-shift (WGS) reaction of central importance in fuel reforming has many possible reaction pathways like redox pathway, associative pathway and so on, which could potentially occur in parallel on a given catalyst surface depending on reaction conditions. A quandary for the reaction engineer has been how to explicitly account for these alternate pathways in describing the overall reaction (OR) rate, r_{OR}, in terms of the kinetics of the elementary reaction steps, i.e., in determining the so-called OR "rate law" in terms of the known step weights, ω_ρ [1-4], which represent the step mass-action kinetics with the exclusion of the unknown intermediates compositions. The most general approach for this is the quasi-steady-state (QSS) approximation of Bodenstein [1-4], based simply on the assumption of time-invariance of reaction intermediates. However, an explicit QSS rate expression for overall rate r_{OR} is often unwieldy, or not possible at all when step kinetics are nonlinear in intermediates concentrations [5], only numerical results then being possible for a given set of reaction conditions.

The Langmuir-Hinshelwood-Hougen-Watson (LHHW) methodology [6], on the other hand, does generally allow the development of simple explicit expressions for r_{OR}, but it is based on the often arbitrary assumption of a *single* rate-*determining* step (RDS), the remaining being at quasi-equilibrium (QE). Further, the *a priori* identification of such a RDS in the mechanism, if it exists at all, is not simple. Dumesic [7] has presented an approach based on De Donder relations for identification of the RDS involving the concept of step reversibility. Thus, the RDS is defined as the step, s_ρ, whose step reversibility, z_ρ $(\equiv \vec{r}_\rho / \vec{r}_\rho = \exp(-\mathscr{A}_\rho))$, the ratio of the step rate in the backward, to that in the forward direction), is approximately equal to that of the OR, $z_{OR} \equiv \vec{r}_{OR} / \vec{r}_{OR} = \exp(-\mathscr{A}_{OR})$. Here, the dimensionless De Donder affinity, $\mathscr{A}_\rho = -\Delta G_\rho / RT$ for the step, and $\mathscr{A}_{OR} = -\Delta G_{OR} / RT$ for the overall reaction.

Campbell [8] has, however, pointed out that such a criterion for identifying the RDS is limited, since reversibility of a step represents only its thermodynamic driving force,

not containing any information, for instance, on its activation barrier, or kinetics. On the other hand, identification of RDS simply based on activation barriers is fraught with risk as well. In fact, the net step rate involves both kinetics and thermodynamics, i.e., $r_\rho = \vec{r}_\rho - \overleftarrow{r}_\rho = \vec{r}_\rho(1 - z_\rho) = \vec{r}_\rho(E_\rho)$, where $E_\rho = 1 - \exp(-\mathcal{A}_\rho)$ represents the thermodynamic driving force [1-4], while $1/\vec{r}_\rho$ represents a kinetic resistance. Campbell's degree of control approach, on the other hand, based on sensitivity analysis to identify the step rate constant(s) that most influence r_{OR}, provides a more robust approach for the identification of the RDS. However, it is based on a numerical analysis. The reaction step resistance, R_ρ, discussed below, in fact, is the most convenient criterion for identifying the slow or rate-limiting steps in a sequence. We assume, in fact, that there can, in general, be more than a single rate-*limiting* step (RLS), the latter being distinct from the rate-*determining* step (RDS).

Furthermore, given that there are now first-principles and semi-theoretical methods [9-12] available that can predict the kinetics of the elementary reaction steps with increasing accuracy, it is now increasingly important that more comprehensive methods for the analysis of reaction networks be developed, which is the objective here, based on an intuitively appealing electrical analogy of reaction networks.

The electrical analogy is, in fact, commonly invoked in a *qualitative* discussion of reaction mechanism and kinetics [13, 14], wherein reaction steps are represented by individual resistances, with the current (rate) being driven by an overall motive force (Figure 2-1). Thus, we see from Figure 2-1, that when justified, the *smaller* of the two resistances in series is dropped in pruning a mechanism, while the *larger* of the two resistances in parallel is neglected. The electrical analogy was, in fact, first proposed by Nernst [15], who suggested that the rate of a chemical reaction might be represented in analogy to Ohm's law, being equal to a "chemical force" divided by a "chemical resistance." Besides its intuitive appeal, the analogy is useful in visualizing the network, and especially when rationalizing the assumption of a RLS, as one with the highest "resistance" in a sequence. However, it is rarely utilized in a *quantitative* analysis.

$$I = \frac{E}{R_{tot}} = \frac{E}{R_{AD} + R_S + R_D}$$

For $R_S \gg R_{AD}, R_D$

$$I \approx \frac{E}{R_S}$$

$$I = \frac{E}{R_{tot}} = \frac{E}{R_1 + \left(\dfrac{R_2 R_3}{R_2 + R_3} \right)}$$

For $R_1 \ll R_2, R_3$ and for $R_2 \ll R_3$

$$I \approx \frac{E}{\dfrac{R_2 R_3}{R_2 + R_3}} \qquad I \approx \frac{E}{R_2}$$

i.e., parallel branch with *smaller* resistance determines current
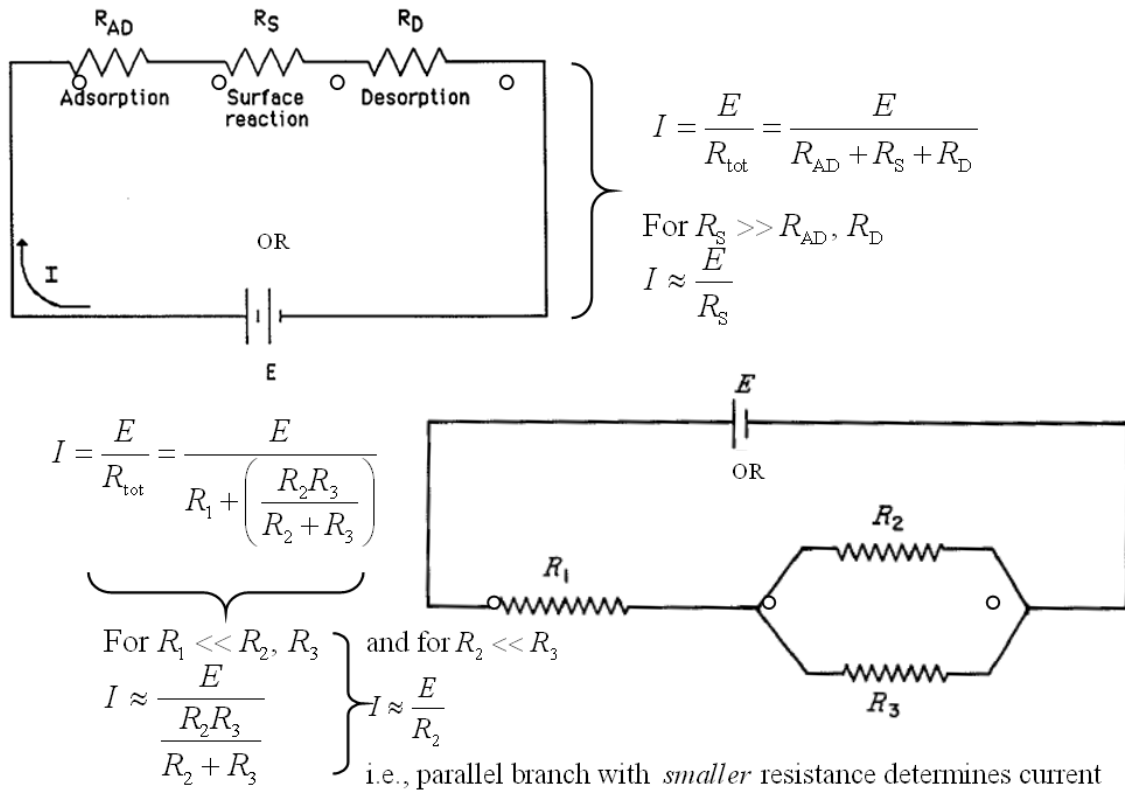
Figure 2-1: Qualitative representation of electrical analogy in kinetics.

This is so, because the relationships of the step resistance and the motive force to the conventional reaction kinetic and thermodynamic quantities have remained unclear, and it is not known how one might draw an appropriate equivalent electric circuit for a complex mechanism.

We have, actually, more recently developed a Reaction Route (RR) Graph approach [16-19] that puts this analogy on a rigorous footing by: 1) providing the equivalent electrical circuit for a given mechanism adapted directly from its RR Graph, and 2), defining the step resistance in terms of step kinetics via the relation $R_\rho \equiv \ln(\vec{r}_\rho / \bar{r}_\rho)/(\vec{r}_\rho - \bar{r}_\rho)$, and the dimensionless De Donder affinity, $\mathscr{A}_\rho$, as the driving force, resulting in Ohm's law form for step kinetics, $r_\rho = \mathscr{A}_\rho / R_\rho$. The corresponding overall rate then takes the form $r_{OR} = \mathscr{A}_{OR} / R_{OR}$, where R_{OR} may be obtained in terms of R_ρ from the RR Graph in a manner completely equivalent to that in electrical circuits (Fishtik et al. 2005b). However, only numerical analysis is possible in this manner, since the step rates, $\vec{r}_\rho$ and $\bar{r}_\rho$, and, hence, the step resistances are not known *a priori*, involving the unknown intermediates concentrations.

In a recent paper [20], however, we followed an alternate algebraic methodology for the QSS analysis of a reaction *sequence,* in which the final result was of a form that could be cast into an alternate Ohm's law form, i.e., $r_{OR} = E_{OR} / R_{OR}^\bullet$, where the OR driving force is in the conventional form, $E_{OR} = 1 - z_{OR} = \{1 - \exp(-\mathscr{A}_{OR})\}$, and the OR resistance could be expressed as a sum of the step resistances in series, $R_{OR}^\bullet = \sum_\rho R_\rho^\bullet$, while the step resistances $R_\rho^\bullet$ could be determined *a priori* via the LHHW methodology, thus providing a new analytical approach based on the electrical analogy. In this Chapter, we show that this new form can be extended readily to *parallel* reaction networks as well, where $R_{OR}^\bullet$ relates to step resistances $R_\rho^\bullet$ in the usual manner of electrical circuits. This approach not only provides an explicit QSS rate expression for a given mechanism in terms of step kinetics, but also affords perceptive insights into the dominant pathways and rate-limiting steps, thus allowing rigorous network pruning.

We first describe how one might use the given molecular mechanism of an OR to construct its RR Graph, which depicts reaction steps as branches interconnected at nodes such that *all* possible reaction pathways for the OR are represented simply as walks on the RR graph. Next, the RR Graph is converted into an equivalent circuit by simply replacing the branches by resistors representing the steps, followed by Ohm's law representation of overall rate, with the overall resistance being obtained from the resulting circuit. We show, for the case of linear step kinetics, that the result is exactly the same as that obtained via linear algebra from the conventional QSS analysis. Further, we show that, while approximate, the results are very accurate for non-linear kinetics as well. All the necessary details along with definitions from our previous work are also summarized so that the treatment below is self-contained.

For ease of comprehension, further, the application of our approach to parallel pathway reaction networks is illustrated here for the relatively simple cases of: 1) gas-phase hydrogen-bromine reaction (non-linear kinetics), and 2) zeolite catalyzed N_2O decomposition reaction (linear kinetics) mechanism, both involving only a handful of steps. Of course, more complex mechanisms are similarly amenable to kinetic analysis, which will be the focus in the subsequent chapters.

2.2 Theory

2.2.1 Reaction Routes: Basic Definitions

We first consider a simple generic 4-step mechanism with parallel pathways given in Eq. (2.1), in order to explain the essentials of RR Graphs approach, while avoiding the mathematical details [16-19].

$$
\begin{array}{lllcc}
\underline{s_\rho} & & & \underline{\sigma_{1\rho}} & \underline{\sigma_{2\rho}} \\
s_1: & A \rightleftharpoons I_1 & & +1 & +1 \\
s_2: & I_1 \rightleftharpoons I_2 + C & & +1 & 0 \\
s_3: & I_2 \rightleftharpoons B & & +1 & 0 \\
s_4: & I_1 \rightleftharpoons B + C & & 0 & +1 \\
\hline
OR: & A \rightleftharpoons B + C & & &
\end{array} \tag{2.1}
$$
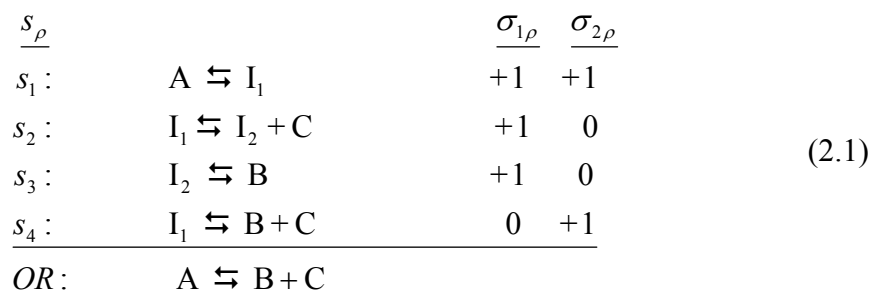
This mechanism admits two parallel pathways, or reaction routes (RRs), as indicated above by the stoichiometric numbers in the two columns. Thus, steps s_1, s_2, and s_3, when added, result in a cancellation of the intermediates I_1 and I_2, resulting in the OR. Similarly, $s_1 + s_4$ provides the OR, which is a second RR. More formally, thus, we define:

> *Reaction Route (RR)*: or a reaction pathway, or a reaction sequence, is a linear combination of elementary steps, $\sum_{\rho=1}^{p} \sigma_{g\rho} s_{\rho}$ that eliminates a specified number of intermediate and terminal species to produce a reaction, where $\sigma_{g\rho}$ is the stoichiometric number (usually, 0, ±1 or ±2) of step s_{ρ} in the gth RR. If *all* the intermediate species are eliminated the reaction route is called a *Full Route (FR)*.

Thus, for the above example, the two RRs may be written as

$$\left.\begin{array}{ll} FR_1: & OR = (+1)s_1 + (+1)s_2 + (+1)s_3 \\ FR_2: & OR = (+1)s_1 + (+1)s_4 \end{array}\right\} \qquad (2.2)$$

On the other hand, an

> *Empty Route (ER)*: or a cycle is a linear combination of the elementary steps such that *all* of the species, both intermediate and terminal, are cancelled, thus producing the so-called "zero" OR (i.e., the stoichiometric coefficients of all the species are zero).

In fact, since subtracting one FR from the other, e.g., $FR_1 - FR_2$, would eliminate all the species, it can provide an empty route (ER), e.g.,

$$ER_1: \quad 0 = (+1)s_2 + (+1)s_3 + (-1)s_4 \qquad (2.3)$$

A negative stoichiometric number, as above, simply indicates that the step in the given RR is followed in the reverse direction to that indicated in Eq. (2.1). Since all elementary steps are reversible, in principle, although the reversibility of a step z_{ρ} can vary widely, this does not present any problem.

Of course, an infinite number of such RRs may be obtained via a linear combination of two or more RRs. However, we are only interested in the so called *direct RR*,

following Milner's [21] concept of directness or minimality. Such a direct FR and ER contains no more than $q + 1$ and $q + 2$ steps, respectively, from a given reaction mechanism, where q is the number of linearly independent intermediate species, I_k. This limitation results in a finite and unique set of RRs.

In order to construct the Reaction Route (RR) Graph, and hence the electrical circuit, for a given mechanism, in fact, a knowledge of not even the entire set of direct RRs is needed. Actually, only a set of *independent* RRs is needed for this purpose, i.e. any set of $\mu = p - q$ RRs, which can include both FRs and ERs, that among them include all of the steps of the given mechanism. This is, in fact, related to the fundamental RR matrix of the RR Graph [16-18]. All the other direct RRs of the unique set can be topologically traced on the thus generated RR Graph as walks, as explained later on. A more formal approach for enumerating the entire set of (direct) FRs and ERs based on the stoichiometric coefficient matrix of the mechanism is described by Fishtik et al. [16-18].

We will also be concerned with reaction routes that produce a given *intermediate* I_k from terminal species. Thus, an

> *Intermediate Reaction Route (IRR)*: is the RR, or pathway, in which all the intermediate species except the one of interest I_k (often along with a reference intermediate, say the vacant surface site, S, in case of catalytic reaction system) are eliminated.

The set of stoichiometrically distinct intermediate reactions, IRs, produced by these IRRs may be written as

$$\text{IR}_h: \quad \gamma_k I_k + (-\gamma_k)S + \sum_{i=1}^{n}(\gamma_{ki})T_i = 0 \tag{2.4}$$

where γ_k is positive, since the intermediate I_k is considered as a product in the IR.

For the example considered above, i.e., Eq. (2.1), in fact, no surface site is involved. Thus,

$$\text{IRR}_1: \quad \text{IR}_1 = (+1)s_1 \tag{2.5}$$

is an example of an IRR for the formation of the intermediate species, I_1.

2.2.2 Reaction Route (RR) Graph

The typical goals of kinetic analysis are:

1) to determine the elementary step rates r_ρ, by first determining the unknown intermediate concentrations in terms of the step rate constants and the terminal species activities (concentrations), and

2) to relate the OR rate, r_{OR} to the step rates r_ρ.

Both of these goals are facilitated by the availability of the Reaction Route (RR) Graph of the mechanism, which shows graphically how the various step rates are interconnected in a reaction network depicting the overall reaction system and its pathways, and how these interconnections constrain the rates of the individual steps, and that of the OR. Of course, one could accomplish this goal without the help of the RR Graph, just as one could solve an electric circuit problem mathematically without drawing a circuit diagram, but the process, as in the case of electric circuits, is assisted by the graphic visualization afforded by the RR Graph. In fact, since RR Graphs follow flow network laws, namely, Kirchhoff's laws, they can be directly converted into an equivalent electric circuit by simply replacing the branches representing the elementary reactions by resistors and the OR by a battery with an EMF related to the affinity, or Gibbs free energy, of the OR.

Thus,

Reaction Route (RR) Graph: for an OR is a graphical representation of its mechanism that is comprised of elementary reactions, and is drawn in a manner so that:

1) the directed (with arrows) branches representing the individual steps s_ρ are interconnected at intermediate nodes (INs) such that all reaction routes (RRs) can be traced on it simply as walks between terminal nodes (TNs), with the overall reaction (OR) drawn as a branch between the TNs; and

2) the interconnectivity of the branches at the INs is consistent with the QSS condition for the intermediates, while the connectivity of branches at the

TNs, including the OR, is consistent with the QSS condition of the terminal species. These are, in fact, the equivalent of Kirchhoff's Flux (or Current) Law (KFL or KCL) in electrical circuits.

Thus, INs interconnect only elementary steps while the TNs interconnect elementary steps to the OR. Both set of nodes are, further, consistent with KFL and the minimality of incidence or directness, in the sense that eliminating a reaction step will violate the QSS condition.

> *Kirchhoff's Flux (or Current) Law:* states that the step rate r_ρ (likened to branch current I_ρ) of all branches incident at a node j sum up to zero (from mass conservation, along with the fact that $V_{node} = 0$). In other words, $\Delta r_j \equiv \sum_{\rho=1}^{p} m_{\rho j} r_\rho = 0$, where the incidence coefficient $m_{\rho j} = +1$, if a branch leaves the node j, and $m_{\rho j} = -1$, if a branch is coming into the node j. In fact $m_{\rho j}$ are elements of the incidence matrix of the RR Graph [16].

Of course, KFL is analogous to the QSS assumption for the intermediate and the terminal species.

> *Quasi-Steady-State (QSS) Assumption:* implies the time invariance of the species concentration, i.e., the net rate of production of a species is zero, $\Delta r_i = \sum_{\rho=1}^{p} v_{\rho i} r_\rho = 0$.

It is, thus, clear from the above that KFL and QSS approximation are equivalent.

Let us apply QSS approximation to the intermediate species in the homogeneous decomposition reaction mechanism (Eq. 1), i.e.,

$$
\left.
\begin{array}{ll}
Q_{I_1}: & r_{I_1} = (-1)r_1 + (+1)r_2 + (+1)r_4 = 0 \\
Q_{I_2}: & r_{I_2} = (-1)r_2 + (+1)r_3 = 0
\end{array}
\right\} \tag{2.6}
$$

Since these two relations are the equivalent of KFL, the connectivity of the reaction steps at intermediate nodes implied by these QSS approximation relations is shown in Figure 2-2a.

Catalytic and Electrocatalytic Pathways in Fuel Cells
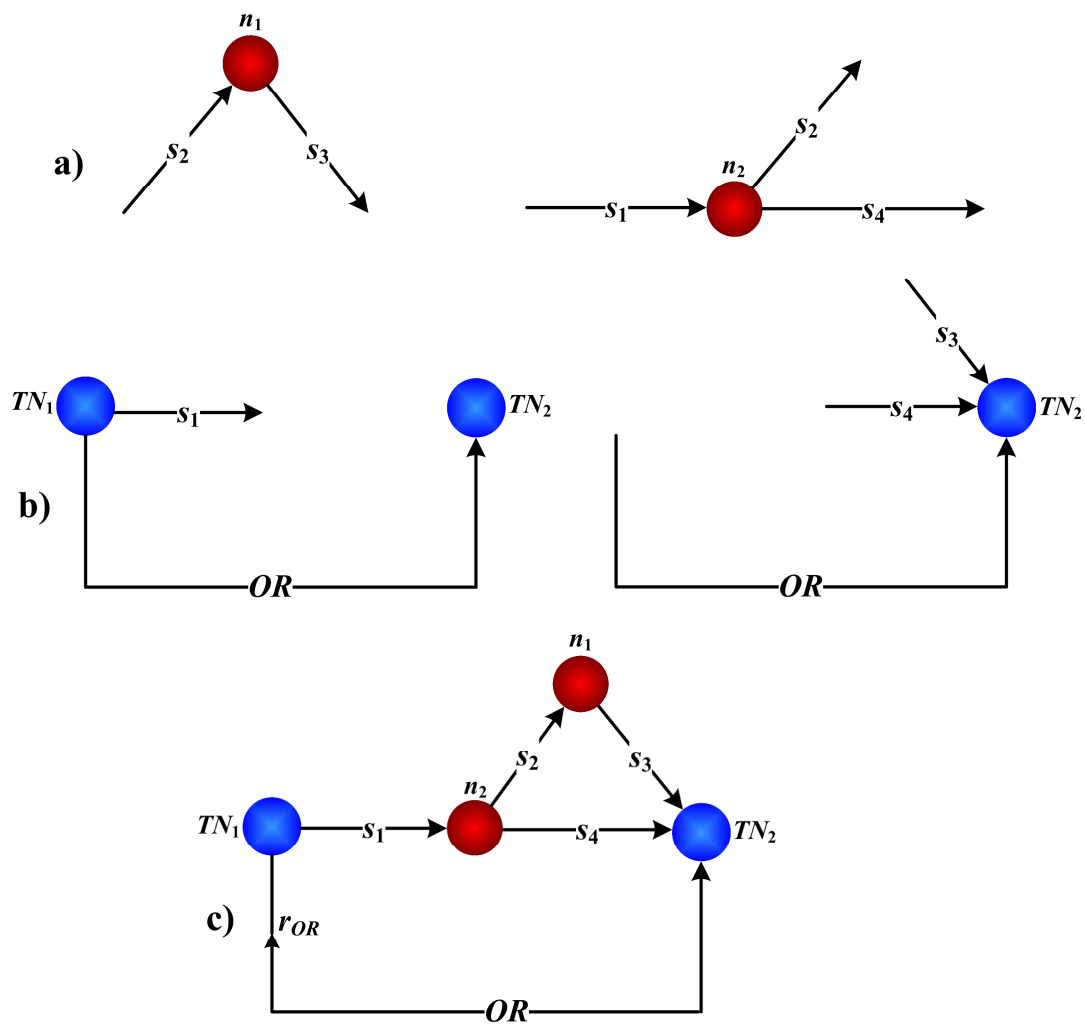
Figure 2-2: a) KFL condition for intermediates, b) KFL condition for terminal species, c) RR Graph

The second of these relations indicates that s_2 and s_3 are interconnected at one intermediate node (in red), with s_2 coming in and s_3 leaving, while the first relation indicates an intermediate node with s_1 coming in and s_2 as well as s_4 leaving. These two subgraphs are depicted in Figure 2-2a.

Let us next consider the QSS approximation for the 3 terminal species, which participate both in the elementary reactions as well as in the OR

$$\left.\begin{aligned}
Q_A: &\quad r_A = (-1)r_1 + (-1)r_{OR} = 0\\
Q_B: &\quad r_B = (+1)r_3 + (+1)r_4 + (+1)r_{OR} = 0\\
Q_C: &\quad r_C = (+1)r_2 + (+1)r_4 + (+1)r_{OR} = 0
\end{aligned}\right\} \tag{2.7}$$

Because from Eq. (2.6), $r_2 = r_3$, the QSS approximation for both B and C are the same, i.e., only one of these two equations is independent. The remaining two independent conditions can be represented by the KFL subgraphs shown in Figure 2-2b, where blue nodes represent the terminal nodes. The only way that all these sub-graphs (Figure 2-2a and b) can be coalesced into a single RR graph is by overlaying the common branches, resulting in Figure 2-2c, which is, hence the RR Graph for the mechanism in Eq. (1).

It can be seen that this RR Graph is appropriate. Firstly, all of the RRs (FR$_1$, FR$_2$ and ER$_1$) enumerated above can be traced on this as walks.

In general, a

> *Walk*: from a starting node to an ending node is an alternating sequence of nodes and branches such that a given node may not be crossed more than once. If a walk begins and ends at the same node, it is called a cycle, while if a walk begins at one terminal node and ends at the other terminal node, it is a full route.

Secondly, the nodes evidently satisfy the QSS approximation for both the intermediate (INs) and terminal species (TNs). Thus, Figure 2-2c is an appropriate RR Graph for the mechanism as it satisfies both of the basic criteria outlined above.

Moreover, RR Graphs are also thermodynamically consistent, given that they concur with Kirchhoff's Potential Law (KPL).

Kirchhoff's Potential Law (KPL): implies that the branch affinity, i.e., negative Gibbs free energy change for a reaction step, $A_\rho = -\Delta G_\rho$ (likened to branch voltage V_ρ) of all branches in a closed walk (starting and ending at the same node), or a cycle, sum up to zero, i.e., $\sum_{\rho=1}^{p} \sigma_{g\rho} A_\rho = 0$, where the stoichiometric number $\sigma_{g\rho} = +1$, if a branch is directed in the direction of the walk around a cycle, and $\sigma_{g\rho} = -1$, if a branch is directed in the opposite direction.

For example, if we apply KPL to the cycle (ER$_1$) in the considered mechanism, Eq. (2.1), there results, $A_2 + A_3 - A_4 = 0$, or $\dfrac{\vec{k}_2}{\overleftarrow{k}_2} \dfrac{\vec{k}_3}{\overleftarrow{k}_3} \dfrac{\vec{k}_4}{\overleftarrow{k}_4} = 1$. Thus, the predicted (or measured) kinetics must be consistent with this KPL condition. In other words, not all rate constants need to be predicted (measured), some can be obtained from KPL relations.

2.2.3 Electrical Analogy

Since the RR Graphs follow the flow network laws (namely, KFL and KPL), they can be directly converted into an equivalent electric circuit by simply replacing the branches representing the elementary reactions by resistors, R_ρ, and the OR by a battery with an EMF, $\mathscr{A}_{OR}$. Thus, for the above 4-step decomposition example with the RR Graph in Figure 2-2c, the equivalent electrical circuit is shown in Figure 2-3.

In order to complete the analogy, we define [16-18]

Reaction or Step Affinity A_ρ: is negative of reaction Gibbs free energy, $A_\rho = -\Delta G_\rho$. It is, in turn, related to the ratio of the rate in the forward direction $\vec{r}_\rho$ to that in the reverse direction, $\overleftarrow{r}_\rho$, via $\mathscr{A}_\rho = \ln(\vec{r}_\rho / \overleftarrow{r}_\rho)$, where the dimensionless affinity, $\mathscr{A}_\rho \equiv A_\rho / RT$.
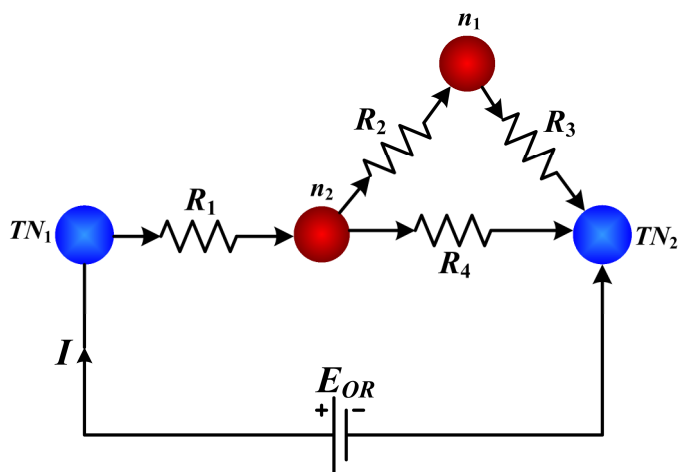
Figure 2-3: Electrical analog of the RR Graph shown in Figure 2-2c.

Reaction or Step Resistance R_ρ: is the mean value of the inverse of the net step rate, $r_\rho = \vec{r}_\rho - \bar{r}_\rho$, between its limiting values, namely, $\vec{r}_\rho$ and $\bar{r}_\rho$, i.e.,

$$R_\rho \equiv \frac{1}{\vec{r}_\rho - \bar{r}_\rho} \int_{\bar{r}_\rho}^{\vec{r}_\rho} \frac{1}{r_\rho} dr_\rho = \frac{\ln(\vec{r}_\rho / \bar{r}_\rho)}{\vec{r}_\rho - \bar{r}_\rho}.$$

Unfortunately, unlike in electric circuits, we don't know the reaction resistance *a priori*, since it involves the unknown intermediates concentrations.

Ohm's Law Form of Step Kinetics: From the definitions of branch affinity and branch resistance for a step s_ρ as provided above, it is easy to see that step rate follows Ohm's law: $r_\rho = \dfrac{\mathscr{A}_\rho}{R_\rho}$

It is to be noted that this does not represent a linearization of reaction kinetics, but is simply a definition of a reaction resistance, which unlike the resistance in electrical circuits, is not a constant, but rather changes with reaction conditions, especially temperature, as $\vec{r}_\rho$ and $\bar{r}_\rho$ change with composition and temperature.

Since the RR Graphs are drawn so that they are consistent with KFL and KPL and Ohm's law kinetics representation, there is a quantitative correspondence between RR Graphs and their electrical circuit analogs. As a result, the overall resistance of the network might be calculated in terms of step resistances, with the result that the overall rate may be written as

$$r_{OR} = \frac{\mathscr{A}_{OR}}{R_{OR}} \tag{2.8}$$

where standard electrical circuit techniques are used to evaluate R_{OR} in terms of R_ρ, e.g., via $\Delta - to - Y$ conversions, and other tools of electrical circuit analysis.

For instance, for the above equivalent circuit (Figure 2-3) involving series and parallel resistors

$$r_{OR} = \frac{\mathcal{A}_{OR}}{R_{OR}} = \frac{\mathcal{A}_{OR}}{R_1 + \cfrac{1}{\cfrac{1}{R_4} + \cfrac{1}{R_2 + R_3}}} \tag{2.9}$$

While this rate expression is precise, it is not predictive, as the step rates $\vec{r}_\rho$ and $\bar{r}_\rho$, and hence the step resistances R_ρ, are not known *a priori*. A predictive approach is developed below.

2.2.4 New Form of the Electrical Analogy

Next, we discuss the alternate formulation of the electrical analogy that leads to an explicit expression for the OR rate. First, however, we define (Dumesic, [7]

> *Reversibility:* of an elementary step $z_\rho \equiv \bar{r}_\rho / \vec{r}_\rho$, i.e., it is the ratio of the rate in the reverse to the forward direction for a step, and is related to step affinity via De Donder relation, [22, 23] i.e., $z_\rho = \exp(-\mathcal{A}_\rho)$.

Further, for the OR, it is

$$z_{OR} = \bar{r}_{OR} / \vec{r}_{OR} = \exp(-\mathcal{A}_{OR}) = \frac{1}{K_{OR}} \prod_{i=1}^{n} a_i^{\nu_i} \tag{2.10}$$

Furthermore, since it is a thermodynamic property, from KPL we have

$$z_{OR} = \frac{\bar{r}_{OR}}{\vec{r}_{OR}} = \prod_{\rho=1}^{q+1} \left(\frac{\bar{r}_\rho}{\vec{r}_\rho} \right)^{\sigma_\rho} = \prod_{\rho=1}^{q+1} (z_\rho)^{\sigma_\rho} \tag{2.11}$$

In fact, since the intermediate species get cancelled in a FR

$$z_{OR} = \prod_{\rho=1}^{q+1} \left(\frac{\bar{\omega}_\rho}{\vec{\omega}_\rho} \right)^{\sigma_\rho} \tag{2.12}$$

i.e., the OR reversibility, z_{OR}, is a *known* quantity for a given set of reaction conditions. Here ω_ρ is the reaction step weight, which includes the observable (known) quantities, i.e., the rate constants and activities of the terminal species (e.g. $\vec{\omega}_\rho = \vec{k}_\rho a_i^\beta$).

Further, we formally define

_____

Catalytic and Electrocatalytic Pathways in Fuel Cells

Quasi-Equilibrium (QE): A step is quasi-equilibrated if its reversibility, $z_\rho \to 1$, or alternately, if its affinity $\mathcal{A}_\rho \to 0$. At true equilibrium, of course, $z_\rho = 1$, and $\mathcal{A}_\rho = 0$.

Rate-Limiting Step (RLS): in a sequence is one, whose resistance R_ρ contributes significantly to R_{OR}. There may, of course, be more than one RLS in a sequence.

Interestingly, however, it may be noted that for a constant flux through a sequence of steps, this implies that reversibility z_ρ contributes significantly to z_{OR}, in agreement with (Dumesic, [7]. This may be seen by noting that $R_\rho / R_{OR} = \mathcal{A}_\rho / \mathcal{A}_{OR}$ in a sequence with $r_\rho = r_{OR}$ for unit stoichiometric numbers ($\sigma_\rho = +1$).

At any rate, for the equivalent circuit shown in Figure 2-3, rearranging the OR rate, Eq. (2.9), we have

$$\frac{1}{r_{OR}} = \frac{R_{OR}}{\mathcal{A}_{OR}} = \frac{R_1}{\mathcal{A}_{OR}} + \frac{1}{\dfrac{\mathcal{A}_{OR}}{R_4} + \dfrac{1}{\dfrac{R_2}{\mathcal{A}_{OR}} + \dfrac{R_3}{\mathcal{A}_{OR}}}} \tag{2.13}$$

so that, we may write

$$\frac{1}{r_{OR}} \approx \frac{1}{r_1^\bullet} + \frac{1}{r_4^\bullet + \dfrac{1}{\dfrac{1}{r_2^\bullet} + \dfrac{1}{r_3^\bullet}}} \tag{2.14}$$

where the rate-*determining* step (RDS) is given by

$$r_\rho^\bullet \cong \frac{\mathcal{A}_{OR}}{R_\rho} \tag{2.15}$$

where the bullet in the subscript denotes the step as the rate-*determining* step (RDS). Thus,

Rate-Determining Step (RDS): $r_\rho^\bullet$ ($I_\rho^\bullet$) is the rate (current) of the branch (resistor) s_ρ (R_ρ) if *all* other resistors in the circuit were short-circuited, i.e., if the entire

motive force $\mathcal{A}_{OR}$ (E_{OR}) occurred across a chosen step (resistor) s_ρ (R_ρ), which, of course, would be the *maximum step rate* (current) in the step (resistor) for the given motive force.

By the same token, since the driving force ($\mathcal{A}_\rho$) drop across the remaining steps is virtually zero, they may be considered to be at quasi-equilibrium (QE). In other words, the RDS and quasi-equilibrium (QE) hypothesis (also called pseudo-equilibrium hypothesis, PEH) go hand-in-hand, as inherent in the LHHW approach. It is to be noted, however, that while in an electric circuit the resistance is constant and, thus, independent of the driving force, this is not entirely correct in a reaction network. Eq. (2.14) is predicated on the assumption that R_ρ remains constant as $\mathcal{A}_\rho$ changes to $\mathcal{A}_{OR}$, which is not true in general in kinetics, unlike in electrical circuits, hence the approximate sign.

In fact, $r_\rho^\bullet$ may be obtained via the LHHW methodology, with s_ρ as the RDS, all the other steps being at QE. Since s_ρ is the RDS and all other steps are at QE, i.e., $z_\rho = z_{OR}$, for $\sigma_\rho = +1$, then

$$r_\rho^\bullet \equiv \vec{r}_\rho^\bullet (1 - z_{OR}) \tag{2.16}$$

From Eqs. (2.14) and (2.16), thus, we have

$$r_{OR} = \cfrac{E_{OR}}{R_1^\bullet + \cfrac{1}{\cfrac{1}{R_4^\bullet} + \cfrac{1}{R_2^\bullet + R_3^\bullet}}} = \frac{E_{OR}}{R_{OR}^\bullet} \tag{2.17}$$

where

$$E_{OR} \equiv 1 - z_{OR} = \{1 - \exp(-\mathcal{A}_{OR})\} \tag{2.18}$$

and

$$R_\rho^\bullet \equiv \frac{1}{r_\rho^\bullet} \tag{2.19}$$

Here, E_{OR} is the thermodynamic motive force term as defined by Christiansen [1] rather than the OR affinity, $\mathcal{A}_{OR}$, and $R_\rho^\bullet$ is the resistance of the step s_ρ when it is

considered as the RDS, i.e., when the entire driving force for the OR occurs across the step, the other steps being quasi-equilibrated. As a result, this allows $R_\rho^\bullet$ to be determined explicitly *a priori*, following the LHHW algorithm. Hence, Eq. (2.17) provides an explicit predictive rate expression for the QSS rate of the OR.

We next show how to obtain the $R_\rho^\bullet$ employing the LHHW approach along with the notion of IRRs. We will, thereafter, show that this rate expression in the form of alternate Ohm's law provides exact results for the case of linear kinetics mechanisms (similar to the considered reaction mechanism, Eq. (2.1)). We further contend that it provides an approximate, albeit, accurate results in other cases [20]. Furthermore, Eq. (2.17), is in a form that is readily amenable to comprehension as well as pruning via comparison of resistances.

2.2.5 LHHW Methodology for Reaction Resistance, $R_\rho^\bullet$

The resistances $R_\rho^\bullet$ can be obtained *a priori*, by treating each of the steps as RDS, in turn, and using the QE approximation for the remaining [20]. The basic idea is that for a given RDS, the q linearly independent unknown intermediate site fractions are determined by identifying the appropriate intermediate reactions, or IRs, or pathways for the formation of intermediates. As mentioned above, an IR (Eq.(2.4)) results from an appropriate linear combination of steps s_j that eliminates all of the intermediate species except that of interest, I_k, formed from terminal species along with some reference intermediate, e.g., the vacant site S in case of catalytic reactions [24, 25], i.e.,

$$\sum_{IR_k} \sigma_{kj} s_j = IR_k \tag{2.20}$$

In analogy with KPL, the affinity of this IR_k

$$\sum_{IR_k} \sigma_{kj} \mathscr{A}_\rho = \mathscr{A}_{IR_k} \tag{2.21}$$

Using the definition of step reversibility

$$z_\rho = \vec{r}_\rho / \vec{r}_\rho = \exp(-\mathscr{A}_\rho) \tag{2.22}$$

we have

$$z_{IR_k} = \prod_{IR_k} (z_j)^{\sigma_{kj}} = \prod_{IR_k} \left(\frac{\vec{r}_j}{\overleftarrow{r}_j} \right)^{\sigma_{kj}} \tag{2.23}$$

Using in this the step kinetics in terms of step weights, and noting that, all intermediates but I_k and the reference intermediate, i.e., vacant sites S (in case of a catalytic reaction) are eliminated by the stoichiometric numbers chosen to produce the IR (Eq. (2.20))

$$z_{IR_k} = \left(\frac{\theta_k}{\theta_0} \right)^{\gamma_k} \prod_{IR_k} \left(\frac{\vec{\omega}_j}{\overleftarrow{\omega}_j} \right)^{\sigma_{kj}} \tag{2.24}$$

Further, if we select all the steps s_j in Eq. (2.20), such that it does not include the step s_ρ under consideration as the RDS, or in other words all the selected steps are among the QE steps, $z_{IR_k} = 1$, we have

$$\frac{\theta_{k,\rho}^\bullet}{\theta_{0,\rho}^\bullet} = \left\{ \prod_{IR_k} \left(\frac{\vec{\omega}_j}{\overleftarrow{\omega}_j} \right)^{\sigma_{kj}} \right\}^{1/\gamma_k} \tag{2.25}$$

Note that we use the notation $\theta_{k,\rho}^\bullet$ to represent site fraction of I_k when s_ρ is the RDS. Finally, the site fractions thus calculated are used in the site balance, $1 = \sum_{k=0}^{q} \theta_{k,\rho}^\bullet$, written in the form

$$\frac{1}{\theta_{0,\rho}^\bullet} = \sum_{k=0}^{q} \frac{\theta_{k,\rho}^\bullet}{\theta_{0,\rho}^\bullet} \tag{2.26}$$

Thus, the reference site fraction $\theta_{0,\rho}^\bullet$ can be determined and, from it, all the remaining site fractions $\theta_{k,\rho}^\bullet$. As a result, the forward rate of the RDS, and hence the step resistance, $R_\rho^\bullet$ as per Eq. (2.19), can be evaluated *a priori*.

We next show that the rate expression derived via Eq. (2.17), i.e. $r_{OR} = E_{OR}/R_{OR}^{\bullet}$ is the same as that obtained via QSS approximation for the simple 4-step homogeneous (non-catalytic) reaction mechanism (Eq. (2.1)).

2.2.6 Comparison of QSS Analysis of the 4-Step Homogeneous Reaction and the Electrical Analogy Approach

The rates of the elementary steps of the 4-step homogeneous decomposition reaction mechanism depicted in Eq. (2.1), in terms of species activities, a_i

$$
\begin{aligned}
r_1 &= \vec{r}_1 - \overleftarrow{r}_1 = \underbrace{\vec{k}_1 a_A}_{\vec{\omega}_1} - \underbrace{\overleftarrow{k}_1 a_{I_1}}_{\overleftarrow{\omega}_1} = \vec{\omega}_1 - \overleftarrow{\omega}_1 a_{I_1} \\
r_2 &= \vec{r}_2 - \overleftarrow{r}_2 = \underbrace{\vec{k}_2 a_{I_1}}_{\vec{\omega}_2} - \underbrace{\overleftarrow{k}_2 a_C a_{I_2}}_{\overleftarrow{\omega}_2} = \vec{\omega}_2 a_{I_1} - \overleftarrow{\omega}_2 a_{I_2} \\
r_3 &= \vec{r}_3 - \overleftarrow{r}_3 = \underbrace{\vec{k}_3 a_{I_2}}_{\vec{\omega}_3} - \underbrace{\overleftarrow{k}_3 a_B}_{\overleftarrow{\omega}_3} = \vec{\omega}_3 a_{I_2} - \overleftarrow{\omega}_3 \\
r_4 &= \vec{r}_4 - \overleftarrow{r}_4 = \underbrace{\vec{k}_4 a_{I_1}}_{\vec{\omega}_4} - \underbrace{\overleftarrow{k}_4 a_B a_C}_{\overleftarrow{\omega}_4} = \vec{\omega}_4 a_{I_1} - \overleftarrow{\omega}_4
\end{aligned}
\tag{2.27}
$$

where the corresponding step weights ω_ρ (i.e., products of rate constants and activities of the terminal species) are also defined.

The QSS approximation for the intermediates in this mechanism is provided in Eq. (2.6). Using the step rate kinetics in this and rearranging

$$
\begin{aligned}
(\overleftarrow{\omega}_1 + \vec{\omega}_2 + \vec{\omega}_4)a_{I_1} &- & (\overleftarrow{\omega}_2)a_{I_2} &= (\vec{\omega}_1 + \overleftarrow{\omega}_4) \\
-(\vec{\omega}_2)a_{I_1} &+ & (\overleftarrow{\omega}_2 + \vec{\omega}_3)a_{I_2} &= \overleftarrow{\omega}_3
\end{aligned}
\tag{2.28}
$$

This may be written in a matrix form, i.e., $\mathbf{W}_m \cdot \mathbf{x} = \mathbf{b}$, where the various matrices are

$$
\mathbf{W}_m = \begin{bmatrix} (\overleftarrow{\omega}_1 + \vec{\omega}_2 + \vec{\omega}_4) & -\overleftarrow{\omega}_2 \\ -\vec{\omega}_2 & (\overleftarrow{\omega}_2 + \vec{\omega}_3) \end{bmatrix}; \mathbf{x} = \begin{pmatrix} a_{I_1} \\ a_{I_2} \end{pmatrix}; \text{ and } \mathbf{b} = \begin{pmatrix} \vec{\omega}_1 + \overleftarrow{\omega}_4 \\ \overleftarrow{\omega}_3 \end{pmatrix}
\tag{2.29}
$$

The solution via Cramer's rule (or by substitution) is

$$\left.\begin{aligned} a_{I_1} &= \frac{\bar{\omega}_2\bar{\omega}_4 + \bar{\omega}_2\bar{\omega}_3 + \bar{\omega}_1\bar{\omega}_2 + \bar{\omega}_3\bar{\omega}_4 + \bar{\omega}_1\bar{\omega}_3}{\bar{\omega}_1\bar{\omega}_2 + \bar{\omega}_1\bar{\omega}_3 + \bar{\omega}_2\bar{\omega}_3 + \bar{\omega}_2\bar{\omega}_4 + \bar{\omega}_3\bar{\omega}_4} \\ a_{I_2} &= \frac{\bar{\omega}_1\bar{\omega}_3 + \bar{\omega}_2\bar{\omega}_4 + \bar{\omega}_2\bar{\omega}_3 + \bar{\omega}_1\bar{\omega}_2 + \bar{\omega}_3\bar{\omega}_4}{\bar{\omega}_1\bar{\omega}_2 + \bar{\omega}_1\bar{\omega}_3 + \bar{\omega}_2\bar{\omega}_3 + \bar{\omega}_2\bar{\omega}_4 + \bar{\omega}_3\bar{\omega}_4} \end{aligned}\right\} \tag{2.30}$$

With the unknown intermediate concentrations known in terms of ω_ρ, all step rates can now be found. Further, OR rate can be found from the relation between OR and step rates, which can be discerned from the RR Graph as well. Thus, from Figure 2-3

$$\begin{aligned} r_{OR} &= r_1 \\ r_{OR} &= r_3 + r_4 \end{aligned} \tag{2.31}$$

Either of these relations could be used. For instance, from the first of these, i.e., $r_{OR} = r_1 = \vec{\omega}_1 - \bar{\omega}_1 a_{I_1}$ and rearranging

$$r_{OR} = \frac{\left\{ \vec{\omega}_1\vec{\omega}_2\vec{\omega}_3 \left(1 - \frac{\bar{\omega}_1\bar{\omega}_2\bar{\omega}_3}{\vec{\omega}_1\vec{\omega}_2\vec{\omega}_3}\right) + (\vec{\omega}_2 + \vec{\omega}_3)\vec{\omega}_1\vec{\omega}_4 \left(1 - \frac{\bar{\omega}_1\bar{\omega}_4}{\vec{\omega}_1\vec{\omega}_4}\right) \right\}}{\bar{\omega}_1\bar{\omega}_2 + \bar{\omega}_1\bar{\omega}_3 + \bar{\omega}_2\bar{\omega}_3 + \bar{\omega}_2\bar{\omega}_4 + \bar{\omega}_3\bar{\omega}_4} \tag{2.32}$$

Using Eq. (2.34) below for the driving force (via KPL) for the two parallel pathways, we can factor out E_{OR} to provide an alternate form for the OR rate

$$r_{OR} = \frac{\vec{\omega}_1\vec{\omega}_2\vec{\omega}_3 + (\vec{\omega}_2 + \vec{\omega}_3)\vec{\omega}_1\vec{\omega}_4}{\bar{\omega}_1\bar{\omega}_2 + \bar{\omega}_1\bar{\omega}_3 + \bar{\omega}_2\bar{\omega}_3 + \bar{\omega}_2\bar{\omega}_4 + \bar{\omega}_3\bar{\omega}_4} \left(1 - \frac{1}{K_{OR}}\frac{a_B a_C}{a_A}\right) \tag{2.33}$$

where from KPL (Figure 2-3)

$$E_{OR} = \left(1 - \frac{\bar{\omega}_1\bar{\omega}_2\bar{\omega}_3}{\vec{\omega}_1\vec{\omega}_2\vec{\omega}_3}\right) = \left(1 - \frac{\bar{\omega}_1\bar{\omega}_4}{\vec{\omega}_1\vec{\omega}_4}\right) = \left(1 - \frac{1}{K_{OR}}\frac{a_B a_C}{a_A}\right) \tag{2.34}$$

We next describe the methodology for deriving the rate expression using the RR Graph approach utilizing Eq. (2.17). Thus, using Eqs. (2.17) and (2.34)

$$r_{OR} = \frac{E_{OR}}{R_1^\bullet + \dfrac{1}{\dfrac{1}{R_4^\bullet} + \dfrac{1}{R_2^\bullet + R_3^\bullet}}} = \frac{1}{R_1^\bullet + \dfrac{1}{\dfrac{1}{R_4^\bullet} + \dfrac{1}{R_2^\bullet + R_3^\bullet}}} \left(1 - \frac{1}{K_{OR}}\frac{a_B a_C}{a_A}\right) \tag{2.35}$$

In order to derive $R_\rho^\bullet$, let us first consider step s_1 as the RDS, the remaining steps being at QE. Thus,

$$R_1^\bullet = \frac{1}{\vec{r}_1^\bullet} = \frac{1}{\vec{\omega}_1} \tag{2.36}$$

For step s_2, similarly

$$R_2^\bullet = \frac{1}{\vec{r}_2^\bullet} = \frac{1}{\vec{\omega}_2 a_{1,2}^\bullet} \tag{2.37}$$

where $a_{1,2}^\bullet$ denotes the activity of I_1 when step s_2 is considered as the RDS and all other steps are at QE. The activity $a_{1,2}^\bullet$, as explained above, is obtained by identifying IRR for the formation of I_1, from reaction steps other than the RDS, s_2. An appropriate IRR for I_1 that does not include s_2 is

$$\text{IRR}_1: \quad \text{IR}_1 = (+1)s_1 \tag{2.38}$$

Thus, with no catalyst site involved in this homogeneous mechanism, using Eq. (2.25), we have

$$a_{1,2}^\bullet = \frac{\vec{\omega}_1}{\overleftarrow{\omega}_1} \tag{2.39}$$

Using Eq. (2.39) in Eq. (2.37) we have

$$R_2^\bullet = \frac{1}{\vec{\omega}_2 \left(\dfrac{\vec{\omega}_1}{\overleftarrow{\omega}_1}\right)} = \frac{1}{\vec{\omega}_2} \frac{\overleftarrow{\omega}_1}{\vec{\omega}_1} \tag{2.40}$$

Similarly, we have for the two remaining steps

$$R_3^\bullet = \frac{1}{\vec{r}_3^\bullet} = \frac{1}{\vec{\omega}_3 a_{2,3}^\bullet} = \frac{1}{\vec{\omega}_3 \left(\dfrac{\vec{\omega}_1 \vec{\omega}_2}{\overleftarrow{\omega}_1 \overleftarrow{\omega}_2}\right)} = \frac{1}{\vec{\omega}_3} \frac{\overleftarrow{\omega}_1 \overleftarrow{\omega}_2}{\vec{\omega}_1 \vec{\omega}_2} \tag{2.41}$$

$$R_4^\bullet = \frac{1}{\vec{r}_4^\bullet} = \frac{1}{\vec{\omega}_4 a_{1,4}^\bullet} = \frac{1}{\vec{\omega}_4 \left(\dfrac{\vec{\omega}_1}{\overleftarrow{\omega}_1}\right)} = \frac{1}{\vec{\omega}_4} \frac{\overleftarrow{\omega}_1}{\vec{\omega}_1} \tag{2.42}$$

Using Eq. (2.36) and (2.40) – (2.42) in Eq. (2.35), thus,

$$r_{OR} = \cfrac{1}{\cfrac{1}{\vec{\omega}_1} + \cfrac{1}{\cfrac{1}{\cfrac{1}{\vec{\omega}_4}\cfrac{\bar{\omega}_1}{\vec{\omega}_1}} + \cfrac{1}{\cfrac{1}{\vec{\omega}_2}\cfrac{\bar{\omega}_1}{\vec{\omega}_1} + \cfrac{1}{\vec{\omega}_3}\cfrac{\bar{\omega}_1\bar{\omega}_2}{\vec{\omega}_1\vec{\omega}_2}}}} \left(1 - \cfrac{1}{K_{OR}}\cfrac{a_B a_C}{a_A}\right) \tag{2.43}$$

which is just a rearranged form of Eq. (2.33). However, as seen here the RR Graph approach is easy to follow. Furthermore, logical pruning of the rate expression is possible via comparison of the $R_\rho^\bullet$ as illustrated below.

The practical utility of the approach is next highlighted with a non-linear kinetics example first, namely, the 4-step gas phase hydrogen-bromine reaction, followed by a linear kinetics mechanism example, i.e., zeolite catalyzed N_2O decomposition.

2.3 Illustration: Nonlinear Kinetics Mechanism, H₂-Br₂ Example

We first define

Nonlinear Kinetics Mechanism: as one that includes some mechanistic steps involving more than one intermediate species on either or both sides, so that the kinetics of these steps are nonlinear in a_{I_k}, e.g., $\vec{r}_\rho = \vec{\omega}_\rho a_{I_k}^2$, and $\vec{r}_\rho = \vec{\omega}_\rho a_{I_j} a_{I_l}$. For example, for the bromine decomposition step: $Br_2 \leftrightarrows 2Br\cdot$, the rate in the reverse direction $\bar{r}_\rho = \bar{\omega}_1 a_{Br\cdot}^2$.

It is, of course, unlikely that more than two intermediates are involved in an elementary reaction, so that higher than quadratic terms in a_{I_k} are unlikely.

Let us next illustrate the feasibility of the application of the above approach to a non-linear kinetics mechanism with $\sigma_\rho = \pm 1$. Thus, we consider the classical 4-step H₂-Br₂ reaction mechanism

$$
\begin{array}{llcc}
 & & \sigma_{\rho 1} & \sigma_{\rho 2} \\
\text{Initiation}: \{s_1: & Br_2 \leftrightarrows 2Br\cdot & +1 & 0 \\
\text{Propagation}: \begin{cases} s_2: & Br\cdot + H_2 \leftrightarrows HBr + H\cdot & +1 & +1 \\ s_3: & H\cdot + Br_2 \leftrightarrows HBr + Br\cdot & 0 & +1 \end{cases} & & \\
\text{Termination}: \{s_4: & Br\cdot + H\cdot \leftrightarrows HBr & +1 & 0 \\
\hline
OR: & Br_2 + H_2 \leftrightarrows 2HBr & &
\end{array}
\tag{2.44}
$$
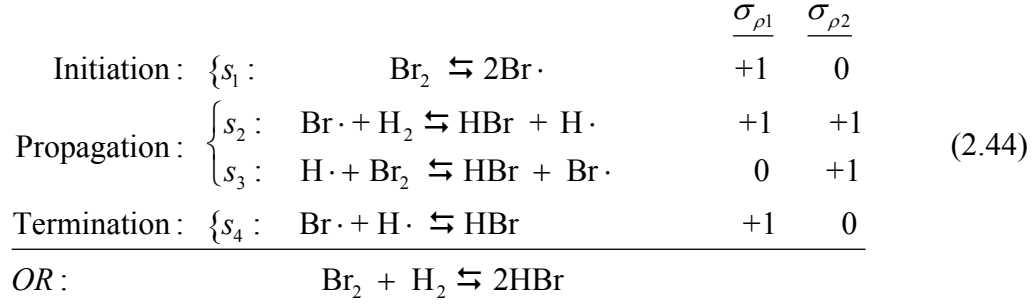
Clearly, the mechanism is nonlinear in intermediate concentrations. The kinetic data for the reaction mechanism is provided in the Ref. [26].

For the non-linear case, the expression

$$
r_{OR} \approx \frac{E_{OR}}{R_{OR}^{\bullet}}
\tag{2.45}
$$

provides only approximate, but accurate results, as shown below. In general, of course, for the non-linear case, an explicit solution via the QSS approach is not possible. Rather, only numerical solution is generally obtained. Therefore, even though approximate, an explicit solution is very useful, for instance, in reactor design and analysis.

2.3.1 Rate Expression Based on Electrical Analogy

For the given reaction mechanism, Eq. (2.44), thus, the step kinetics are

$$
\left. \begin{aligned}
r_1 &= \vec{r}_1 - \overleftarrow{r}_1 = \underbrace{\vec{k}_1 c_{Br_2}}_{\vec{\omega}_1} - \underbrace{\overleftarrow{k}_1 c_{Br\cdot}^2}_{\overleftarrow{\omega}_1} = \vec{\omega}_1 - \overleftarrow{\omega}_1 c_{Br\cdot}^2 \\
r_2 &= \vec{r}_2 - \overleftarrow{r}_2 = \underbrace{\vec{k}_2 c_{H_2}}_{\vec{\omega}_2} c_{Br\cdot} - \underbrace{\overleftarrow{k}_2 c_{HBr}}_{\overleftarrow{\omega}_2} c_{H\cdot} = \vec{\omega}_2 c_{Br\cdot} - \overleftarrow{\omega}_2 c_{H\cdot} \\
r_3 &= \vec{r}_3 - \overleftarrow{r}_3 = \underbrace{\vec{k}_3 c_{Br_2}}_{\vec{\omega}_3} c_{H\cdot} - \underbrace{\overleftarrow{k}_3 c_{HBr}}_{\overleftarrow{\omega}_3} c_{Br\cdot} = \vec{\omega}_3 c_{H\cdot} - \overleftarrow{\omega}_3 c_{Br\cdot} \\
r_4 &= \vec{r}_4 - \overleftarrow{r}_4 = \underbrace{\vec{k}_4}_{\vec{\omega}_4} c_{Br\cdot} c_{H\cdot} - \underbrace{\overleftarrow{k}_4 c_{HBr}}_{\overleftarrow{\omega}_4} = \vec{\omega}_4 c_{H\cdot} c_{Br\cdot} - \overleftarrow{\omega}_4
\end{aligned} \right\}
\tag{2.46}
$$

Further, as can be seen from Eq. (2.44), this reaction mechanism has two full routes and one empty route, similar to the generic example, i.e., Eq. (2.1),

$$
\left.
\begin{array}{lll}
\text{FR}_1: & OR = (+1)s_1 + (+1)s_2 + (+1)s_4 \\
\text{FR}_2: & OR = (+1)s_2 + (+1)s_3 \\
\text{ER}_1: & 0 = (+1)s_1 + (-1)s_3 + (+1)s_4
\end{array}
\right\}
\tag{2.47}
$$

The equivalent circuit for the mechanism is shown in Figure 2-4, which is obtained following a similar procedure as explained for the academic example, and is identical to it, although with different step labels.

Thus, we have from Figure 2-4, as before

$$
R_{OR}^{\bullet} = R_2^{\bullet} + \cfrac{1}{\cfrac{1}{R_3^{\bullet}} + \cfrac{1}{R_1^{\bullet} + R_4^{\bullet}}}
\tag{2.48}
$$

Let us calculate the resistances from the step kinetics. For step s_1 as RDS, and all others at QE, we have

$$
R_1^{\bullet} = \frac{1}{\vec{r}_1^{\bullet}} = \frac{1}{\vec{\omega}_1}
\tag{2.49}
$$

For step s_2 as RDS, and all others at QE, we have

$$
R_2^{\bullet} = \frac{1}{\vec{r}_2^{\bullet}} = \frac{1}{\vec{\omega}_2 c_{\text{Br}\cdot,2}^{\bullet}}
\tag{2.50}
$$

where $c_{\text{Br}\cdot,2}^{\bullet}$ is the concentration of $\text{Br}\cdot$ when step s_2 is the RDS. An appropriate IR for formation of $\text{Br}\cdot$ is

$$
\text{IRR}_1: \quad \text{IR}_1 = (+1)s_1: \quad \text{Br}_2 \leftrightarrows 2\text{Br}\cdot
\tag{2.51}
$$
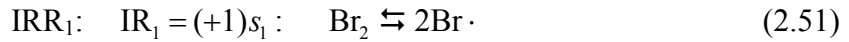
which gives

$$
c_{\text{Br}\cdot,2}^{\bullet} = \sqrt{\frac{\vec{\omega}_1}{\overleftarrow{\omega}_1}}
\tag{2.52}
$$

Thus, using Eq. (2.52) in Eq. (2.50), we have

$$
R_2^{\bullet} = \frac{1}{\vec{r}_2^{\bullet}} = \frac{1}{\vec{\omega}_2 c_{\text{Br}\cdot,2}^{\bullet}} = \frac{1}{\vec{\omega}_2} \sqrt{\frac{\overleftarrow{\omega}_1}{\vec{\omega}_1}}
\tag{2.53}
$$
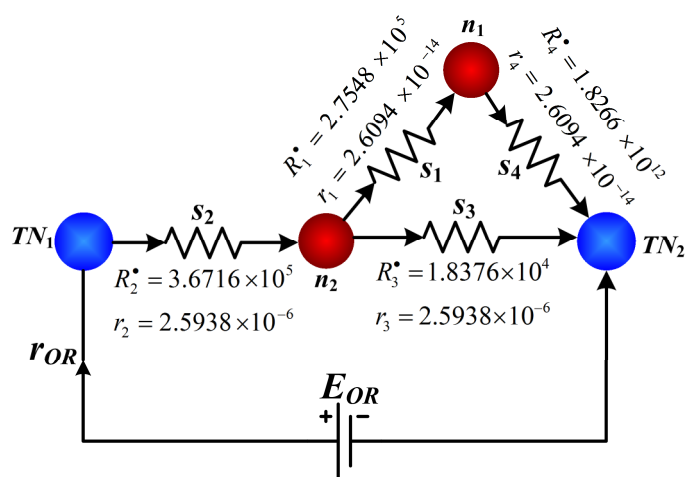
Figure 2-4: Equivalent electrical circuit for the 4-step HBr example along with representative values of $R_1^\bullet$, $R_2^\bullet$, $R_3^\bullet$, $R_4^\bullet$ and the corresponding flux at conditions reported in the text.

Similarly, we can obtain $R_3^\bullet$ and $R_4^\bullet$

$$R_3^\bullet = \frac{1}{\vec{r}_3^\bullet} = \frac{1}{\vec{\omega}_3 c_{H\cdot,3}^\bullet} = \frac{1}{\vec{\omega}_3} \frac{\bar{\omega}_2}{\vec{\omega}_2 c_{Br\cdot,3}^\bullet} = \frac{1}{\vec{\omega}_3} \frac{\bar{\omega}_2}{\vec{\omega}_2} \sqrt{\frac{\bar{\omega}_1}{\vec{\omega}_1}} \tag{2.54}$$

$$R_4^\bullet = \frac{1}{\vec{r}_4^\bullet} = \frac{1}{\vec{\omega}_4 c_{H\cdot,4}^\bullet c_{Br\cdot,4}^\bullet} = \frac{1}{\vec{\omega}_4} \frac{\bar{\omega}_2}{\vec{\omega}_2} \sqrt{\frac{\bar{\omega}_1}{\vec{\omega}_1}} \sqrt{\frac{\bar{\omega}_1}{\vec{\omega}_1}} = \frac{1}{\vec{\omega}_4} \frac{\bar{\omega}_2}{\vec{\omega}_2} \frac{\bar{\omega}_1}{\vec{\omega}_1} \tag{2.55}$$

As a result

$$r_{OR} = \frac{E_{OR}}{R_2^\bullet + \cfrac{1}{\cfrac{1}{R_3^\bullet} + \cfrac{1}{R_1^\bullet + R_4^\bullet}}} = \frac{E_{OR}}{\cfrac{1}{\vec{\omega}_2}\sqrt{\cfrac{\bar{\omega}_1}{\vec{\omega}_1}} + \cfrac{1}{\cfrac{1}{\cfrac{1}{\vec{\omega}_3}\cfrac{\bar{\omega}_2}{\vec{\omega}_2}\sqrt{\cfrac{\bar{\omega}_1}{\vec{\omega}_1}}} + \cfrac{1}{\cfrac{1}{\vec{\omega}_1} + \cfrac{1}{\vec{\omega}_4}\cfrac{\bar{\omega}_2}{\vec{\omega}_2}\cfrac{\bar{\omega}_1}{\vec{\omega}_1}}}} \tag{2.56}$$

where

$$E_{OR} = 1 - z_{OR} = 1 - \frac{\bar{\omega}_2 \bar{\omega}_3}{\vec{\omega}_2 \vec{\omega}_3} = 1 - \frac{\bar{\omega}_1 \bar{\omega}_2 \bar{\omega}_4}{\vec{\omega}_1 \vec{\omega}_2 \vec{\omega}_4} \tag{2.57}$$

2.3.2 QSS Kinetics

Let us compare the accuracy of the above expression to numerical QSS analysis. An explicit expression for this case via QSS procedure, of course, is not possible. For numerical comparison, we utilize the kinetic data (Table 2-1) provided by Cooley and Anderson [26]. However, before we apply the QSS approximation, let us check the thermodynamic consistence of the reported kinetic data afforded by the RR Graph approach.

Applying KPL to the empty route, ER$_1$, we have $\mathcal{A}_1 + \mathcal{A}_4 - \mathcal{A}_3 = 0$. Using de Donder's relationship we have, $\left(\dfrac{\vec{k}_1}{\bar{k}_1}\right)\left(\dfrac{\vec{k}_4}{\bar{k}_4}\right)\left(\dfrac{\bar{k}_3}{\vec{k}_3}\right) = 1$. However, the reported data [26] yields this product as 0.68, rather than 1.

Table 2-1: The kinetic data for H_2-Br_2 reaction. Activation energies in kcal/mol; pre-exponential factors are in units of mol/cm^3 and sec [26]

s_ρ	Reaction Step	$\vec{E}_\rho$	$\overleftarrow{E}_\rho$	$\vec{\Lambda}_\rho$	$\overleftarrow{\Lambda}_\rho$	$\vec{m}_\rho$	$\overleftarrow{m}_\rho$
s_1	$Br_2 \leftrightharpoons 2Br\cdot$	45.25 $^\#$	0	1.05 10^{13} $^\#$	5.7 10^{15}	1	0
s_2	$Br\cdot + H_2 \leftrightharpoons HBr + H\cdot$	17.7	1.1	8.05 10^{10}	3.08 10^{10}	1	1
s_3	$H\cdot + Br_2 \leftrightharpoons HBr + Br\cdot$	1.1	41.7	2.59 10^{11}	9.31 10^{10}	1	1
s_4	$Br\cdot + H\cdot \leftrightharpoons HBr$	0	85.85	9 10^{15}	5.95 10^{12}	0	1

$^\#$ $\vec{E}_1$ changed from 45.23 and $\vec{\Lambda}_1$ changed from 7.18 10^{12}, to ensure thermodynamic consistency via KPL.

$$k_\rho = \Lambda_\rho T^m \exp\left(-\frac{E_\rho}{RT}\right)$$

Furthermore, for the empty route ER_1, $\Delta H_1 + \Delta H_4 - \Delta H_3 = 0$. The reported data [26] yields this summation as $-20\,\text{cal/mol}$, rather than 0, pointing to the slight thermodynamic inconsistency of the data available in literature. Thus, the original value of $\vec{E}_1$ was replaced from 45230 cal/mol to 45250 cal/mol and $\vec{\Lambda}_1$ from 7.18×10^{12} to 1.05×10^{13} $\text{cm}^3\text{mol}^{-1}\text{s}^{-1}$, to ensure thermodynamic consistency via KPL. Such inconsistencies in the rate data become glaring via the RR Graph approach.

The conventional QSS result is obtained by algebraic solution of the QSS equations for the two intermediates, into which the mass action kinetics is substituted. Alternately, we could use the simpler KFL equations, i.e., Eq. (2.58), which are evident from Figure 2-4 at the two intermediate nodes (red)

$$\left.\begin{array}{c} r_4 - r_1 = 0 \\ r_1 + r_3 - r_2 = 0 \end{array}\right\} \tag{2.58}$$

Using step kinetics in this

$$(\vec{\omega}_4 c_{\text{H.}} c_{\text{Br.}} - \bar{\omega}_4) - (\vec{\omega}_1 - \bar{\omega}_1 c_{\text{Br.}}^2) = 0 \tag{2.59}$$

$$(\vec{\omega}_1 - \bar{\omega}_1 c_{\text{Br.}}^2) + (\vec{\omega}_3 c_{\text{H.}} - \bar{\omega}_3 c_{\text{Br.}}) - (\vec{\omega}_2 c_{\text{Br.}} - \bar{\omega}_2 c_{\text{H.}}) = 0 \tag{2.60}$$

which are two simultaneous non-linear algebraic equations which may be solved for the two unknown intermediate concentrations $c_{\text{H.}}$ and $c_{\text{Br.}}$, and then substituted back into Eq. (2.46), or KFL equations at the terminal nodes, in order to determine the OR rate. This is not trivial, however, since substituting for $c_{\text{H.}}$ from Eq. (2.60) into Eq. (2.59) results in a third order equation in $c_{\text{Br.}}$ with three possible roots. This clearly demonstrates the strength and intuitive power of the described electrical analogy approach. Therefore, we will use the QSS analysis below simply to numerically verify the result obtained above, using the kinetic parameters from Cooley and Anderson [26] and experimental data provided by Levy [27].

2.3.3 QSS vs. Electrical Analogy Rates

Calculations based on the above QSS analysis were made for a temperature, $T = 473$ K, and for $c_{\text{H}_2} = 0.428\,\text{mol/cm}^3$, $c_{\text{Br}_2} = 0.594$ mol/cm^3 and $c_{\text{HBr}} = 0.25$ mol/cm^3. Thus, the

overall rate, $r_{OR} = r_2 = r_4 + r_3 = 2.5938 \times 10^{-6}$ s^{-1} was obtained from solving the QSS equations, (2.59) and (2.60), and substituting the resulting concentrations of the intermediate species $c_{H.}$ and $c_{Br.}$ in Eq. (2.46) to calculate the corresponding step rates. These QSS step rates are shown on the RR Graph in Figure 2-4. It can, clearly, be seen from Figure 2-4 that KFL for the QSS step rates is followed at all the nodes. Further, the right-hand-side of Eq. (2.56), along with Eq. (2.57), was used to also directly calculate a rate of $r_{OR} = 2.5938 \times 10^{-6}$ s^{-1} from the derived rate expression for the given set of conditions. Clearly, Eq. (2.56) provides an accurate explicit rate expression! Further, unlike the QSS numerical approach, the rate expression, Eq. (2.56), is in a form that is amenable to pruning as explained below.

For this, $R_\rho^\bullet$ were calculated from the explicit Eqs. (2.49) and (2.53) – (2.55) for the specified conditions, as they provide an indication of the rate limiting steps, if any. These calculated values of $R_1^\bullet$, $R_2^\bullet$, $R_3^\bullet$, $R_4^\bullet$ are also shown in Figure 2-4. A comparison of activation energies or rate constants alone is not enough to identify the RLS, since the concentrations of intermediates are also needed to determine the step rates. However, a comparison of $R_\rho^\bullet$ is more rigorous in identifying the RLSs, as discussed before. Of course, these $R_\rho^\bullet$ may also be used in the first equality in Eq. (2.56) along with Eq. (2.57), to calculate the overall rate from the electrical analogy, which not surprisingly, also provides $r_{OR} = 2.5938 \times 10^{-6}$ s^{-1}.

For the mixture composition assumed above, a comparison of $R_1^\bullet + R_4^\bullet$, $R_3^\bullet$, $R_4^\bullet$ as a function of temperature is provided in Figure 2-5. It can be seen that $R_1^\bullet + R_4^\bullet \approx R_4^\bullet$, and, hence, $R_1^\bullet$ can be easily eliminated from Eq. (2.56). It can be further concluded from Figure 2-5, that $R_3^\bullet \ll R_4^\bullet$, i.e., $1/R_3^\bullet \gg 1/R_4^\bullet$.

Thus, $R_4^\bullet$ can also be eliminated from Eq. (2.56), resulting in a reduced expression for the overall resistance,

$$R_{OR}^\bullet \approx R_2^\bullet + \frac{1}{\dfrac{1}{R_3^\bullet}} = R_2^\bullet + R_3^\bullet \qquad (2.61)$$
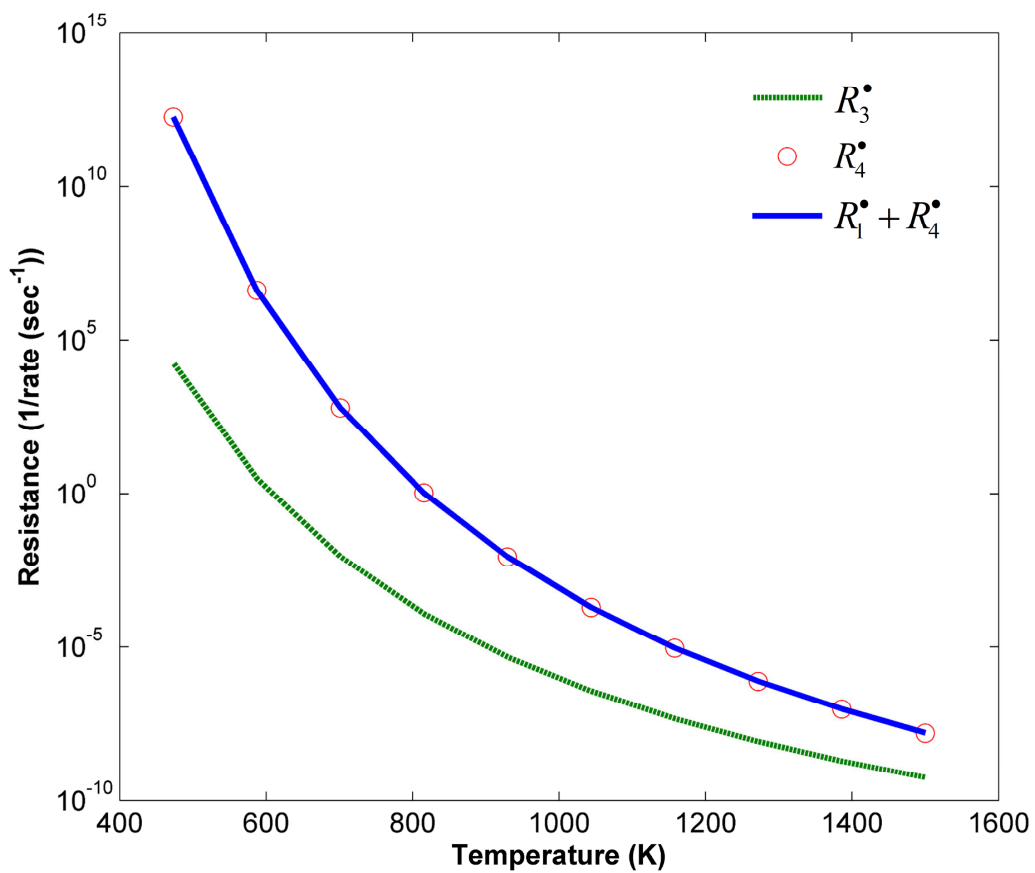
Figure 2-5: A comparison of $R_1^\bullet + R_4^\bullet$, $R_3^\bullet$, $R_4^\bullet$ as a function of temperature for the conditions reported in the text.

One could have arrived at this conclusion also from a comparison of the branch fluxes in Figure 3. Furthermore, the reaction is essentially irreversible at these conditions, i.e.,

$$z_{OR} \to 0 \text{, hence } E_{OR} \to 1 \tag{2.62}$$

When Eq. (2.61) and (2.62) are used in Eq. (2.56), a substantially simplified expression results, i.e.,

$$r_{OR} = \frac{E_{OR}}{\dfrac{1}{\vec{\omega}_2}\sqrt{\dfrac{\bar{\omega}_1}{\vec{\omega}_1}} + \dfrac{1}{\vec{\omega}_3}\dfrac{\bar{\omega}_2}{\vec{\omega}_2}\sqrt{\dfrac{\bar{\omega}_1}{\vec{\omega}_1}}} = \frac{\vec{\omega}_2\sqrt{\vec{\omega}_1/\bar{\omega}_1}}{1+\dfrac{\bar{\omega}_2}{\vec{\omega}_3}} \tag{2.63}$$

Finally, using the reaction weights in Eq. (2.63), we obtain

$$r_{OR} = \frac{\left(\vec{k}_2\sqrt{\vec{k}_1/\bar{k}_1}\right)c_{H_2}c_{Br_2}^{1/2}}{1+\dfrac{\bar{k}_2}{\vec{k}_3}\dfrac{c_{HBr}}{c_{Br_2}}} \tag{2.64}$$

as determined from the early experiments by Bodenstein and Lind [28] in the temperature range of 200 – 300 ºC. Later experiments by Levy (1958) show that this simplified rate law is also valid at higher temperatures. Thus, only reaction steps s_2 and s_3 are *kinetically* significant for the reaction conditions mentioned above. Of course, *mechanistically*, the other steps of initiation and termination are also significant.

Next, we illustrate the utility of our approach by using it for a practical system with linear kinetics mechanism.

2.4 Illustration: Linear Kinetics Mechanism, N₂O Decomposition on Fe-ZSM-5

First, we define

Linear Kinetics Mechanism: as one that includes mechanistic steps that involve only one intermediate species on either or both sides, so that the kinetics of these steps are linear in a_{I_k}, e.g., $\vec{r}_\rho = \vec{\omega}_\rho a_{I_k}$.

Here, a 7-step mechanism is adopted from Heyden et al., [10] who performed quantum chemical calculations for N₂O decomposition on dehydrated mononuclear iron

sites in Fe-ZSM-5, using the TURBOMOLE V5.6 suite of programs following the DFT-B3LYP approach, as an example for a linear kinetics mechanism. The step kinetics, found to be consistent with KPL requirements, are summarized in Table 2-2 [29].

The system has two full routes and one empty route

$$\left. \begin{array}{l} FR_1 : s_1 + s_2 + s_4 + s_5 + s_6 + s_7 = OR \\ FR_2 : s_1 + s_3 + s_5 + s_6 + s_7 = OR \\ ER_1 : s_2 - s_3 + s_4 = 0 \end{array} \right\} \tag{2.65}$$

The corresponding RR Graph/electric circuit for this system obtained from this independent RR set, by following a procedure similar to that described above for the generic example, is shown in Figure 2-6. From this, thus, the overall rate can be written as

$$r_{OR} = \frac{E_{OR}}{R_{OR}^\bullet} = \frac{E_{OR}}{R_1^\bullet + R_5^\bullet + R_6^\bullet + R_7^\bullet + \cfrac{1}{\cfrac{1}{R_2^\bullet + R_4^\bullet} + \cfrac{1}{R_3^\bullet}}} \tag{2.66}$$

To obtain the step resistances in this, let us first consider step s_1 as the RDS, the remaining steps being at QE. Thus,

$$R_1^\bullet = \frac{1}{\vec{r}_1^\bullet} = \frac{1}{\vec{\omega}_1 \theta_{0,1}^\bullet} \tag{2.67}$$

where, as explained above, the first subscript 0 in θ denotes I_0, and the second subscript 1 denotes s_1 as the RDS. With s_1 as the RDS, thus, and all subsequent steps at QE, the appropriate IRs for the formation of five linearly independent surface intermediates, I_1, I_2, I_3, I_4, I_5, from the reference intermediate I_0, comprising of steps other than s_1, are

$$\begin{array}{lll} IR_{I_1} : & (-1)s_3 + (-1)s_5 + (-1)s_6 + (-1)s_7 : & O_2 + 2N_2 - N_2O + I_0 \leftrightarrows I_1 \\ IR_{I_2} : & (-1)s_4 + (-1)s_5 + (-1)s_6 + (-1)s_7 : & O_2 + N_2 - N_2O + I_0 \leftrightarrows I_2 \\ IR_{I_3} : & (-1)s_5 + (-1)s_6 + (-1)s_7 : & O_2 + N_2 - N_2O + I_0 \leftrightarrows I_3 \\ IR_{I_4} : & (-1)s_6 + (-1)s_7 : & O_2 + N_2 + I_0 \leftrightarrows I_4 \\ IR_{I_5} : & (-1)s_7 : & O_2 + I_0 \leftrightarrows I_5 \end{array} \tag{2.68}$$

Table 2-2: Elementary reaction steps and their rates in the N_2O decomposition on Fe-ZSM-5 [10]

s_ρ	Reaction Step	$r_\rho = \vec{r}_\rho - \overset{\leftarrow}{r}_\rho$	$\vec{\omega}_\rho$	$\overset{\leftarrow}{\omega}_\rho$	$\vec{\Lambda}_\rho$	$\overset{\leftarrow}{\Lambda}_\rho$	$\vec{E}_\rho$	$\overset{\leftarrow}{E}_\rho$
s_1:	$N_2O + I_0 \leftrightarrows I_1$	$r_1 = \vec{\omega}_1\theta_0 - \overset{\leftarrow}{\omega}_1\theta_1$	$\vec{k}_1 p_{N_2O}$	$\overset{\leftarrow}{k}_1$	$1.06\ 10^7$	$1.67\ 10^{13}$	0.0	6.4
s_2:	$I_1 \leftrightarrows I_2 + N_2$	$r_2 = \vec{\omega}_2\theta_1 - \overset{\leftarrow}{\omega}_2\theta_2$	$\vec{k}_2$	$\overset{\leftarrow}{k}_2 p_{N_2}$	$2.09\ 10^{14}$	$4.43\ 10^8$	30.7	41.9
s_3:	$I_1 \leftrightarrows I_3 + N_2$	$r_3 = \vec{\omega}_3\theta_1 - \overset{\leftarrow}{\omega}_3\theta_3$	$\vec{k}_3$	$\overset{\leftarrow}{k}_3 p_{N_2}$	$6.98\ 10^{13}$	$5.82\ 10^7$	30.4	50.0
s_4:	$I_2 \leftrightarrows I_3$	$r_4 = \vec{\omega}_4\theta_2 - \overset{\leftarrow}{\omega}_4\theta_3$	$\vec{k}_4$	$\overset{\leftarrow}{k}_4$	$2.15\ 10^{13}$	$8.46\ 10^{12}$	14.1	22.5
s_5:	$N_2O + I_3 \leftrightarrows I_4$	$r_5 = \vec{\omega}_5\theta_3 - \overset{\leftarrow}{\omega}_5\theta_4$	$\vec{k}_5 p_{N_2O}$	$\overset{\leftarrow}{k}_5$	$4.39\ 10^{8\ \#}$	$1.67\ 10^{13}$	0.0	2.7
s_6:	$I_4 \leftrightarrows I_5 + N_2$	$r_6 = \vec{\omega}_6\theta_4 - \overset{\leftarrow}{\omega}_6\theta_5$	$\vec{k}_6$	$\overset{\leftarrow}{k}_6 p_{N_2}$	$3.12\ 10^{12\ \#}$	$3.19\ 10^8$	$20.2\ ^*$	31.5
s_7:	$I_5 \leftrightarrows I_0 + O_2$	$r_7 = \vec{\omega}_7\theta_5 - \overset{\leftarrow}{\omega}_7\theta_0$	$\vec{k}_7$	$\overset{\leftarrow}{k}_7 p_{O_2}$	$1.67\ 10^{13}$	$1.51\ 10^5$	8.0	8.1

$I_0=Z^-[FeO]^+$; $I_1=Z^-[FeO]^+(ON_2)$; $I_2=Z^-[OFeO]^+$; $I_3=Z^-[FeO_2]^+$; $I_4=Z^-[FeO_2]^+(ON_2)$; $I_5=Z^-[O_2FeO]^+$

Activation energies in $k_\rho = \Lambda_\rho \exp(-E_\rho / RT)$ are in kcal/mol; the units of the pre–exponential factors are $bar^{-1}\ s^{-1}$ for adsorption/desorption reactions and s^{-1} for surface reactions.

modified $\vec{\Lambda}_\rho$, * modified $\vec{E}_\rho$ [29]
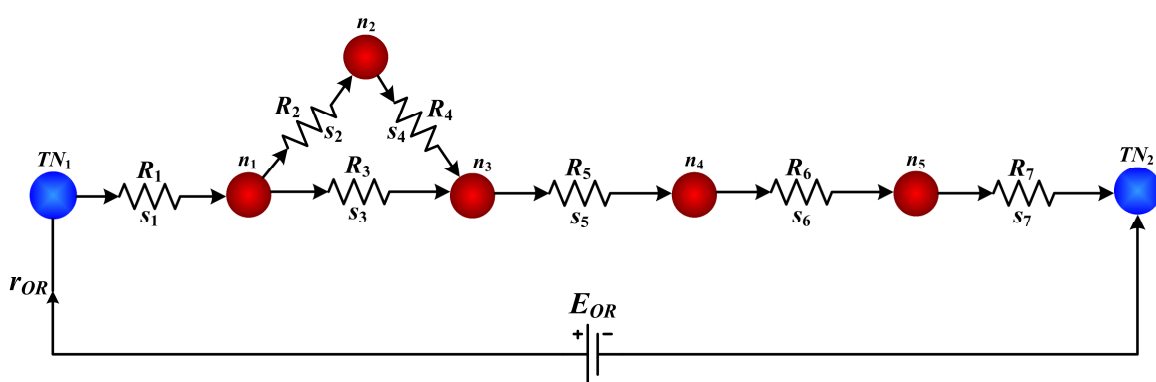
Figure 2-6: Equivalent electrical circuit for the 7-step N_2O decomposition reaction mechanism on Fe-ZSM-5

Then, using Eq. (2.25), for the QE steps, the site fraction ratios are

$$
\left.
\begin{aligned}
\frac{\theta_{1,1}^{\bullet}}{\theta_{0,1}^{\bullet}} &= \left(\frac{\vec{\omega}_3}{\vec{\omega}_3}\right)^{-1}\left(\frac{\vec{\omega}_5}{\vec{\omega}_5}\right)^{-1}\left(\frac{\vec{\omega}_6}{\vec{\omega}_6}\right)^{-1}\left(\frac{\vec{\omega}_7}{\vec{\omega}_7}\right)^{-1} \\[2mm]
\frac{\theta_{2,1}^{\bullet}}{\theta_{0,1}^{\bullet}} &= \left(\frac{\vec{\omega}_4}{\vec{\omega}_4}\right)^{-1}\left(\frac{\vec{\omega}_5}{\vec{\omega}_5}\right)^{-1}\left(\frac{\vec{\omega}_6}{\vec{\omega}_6}\right)^{-1}\left(\frac{\vec{\omega}_7}{\vec{\omega}_7}\right)^{-1} \\[2mm]
\frac{\theta_{3,1}^{\bullet}}{\theta_{0,1}^{\bullet}} &= \left(\frac{\vec{\omega}_5}{\vec{\omega}_5}\right)^{-1}\left(\frac{\vec{\omega}_6}{\vec{\omega}_6}\right)^{-1}\left(\frac{\vec{\omega}_7}{\vec{\omega}_7}\right)^{-1} \\[2mm]
\frac{\theta_{4,1}^{\bullet}}{\theta_{0,1}^{\bullet}} &= \left(\frac{\vec{\omega}_6}{\vec{\omega}_6}\right)^{-1}\left(\frac{\vec{\omega}_7}{\vec{\omega}_7}\right)^{-1} \\[2mm]
\frac{\theta_{5,1}^{\bullet}}{\theta_{0,1}^{\bullet}} &= \left(\frac{\vec{\omega}_7}{\vec{\omega}_7}\right)^{-1}
\end{aligned}
\right\}
\tag{2.69}
$$

Finally using these in site balance, Eq. (2.26),

$$
\frac{1}{\theta_{0,1}^{\bullet}} = 1 + \left(\frac{\theta_{1,1}^{\bullet}}{\theta_{0,1}^{\bullet}}\right) + \left(\frac{\theta_{2,1}^{\bullet}}{\theta_{0,1}^{\bullet}}\right) + \left(\frac{\theta_{3,1}^{\bullet}}{\theta_{0,1}^{\bullet}}\right) + \left(\frac{\theta_{4,1}^{\bullet}}{\theta_{0,1}^{\bullet}}\right) + \left(\frac{\theta_{5,1}^{\bullet}}{\theta_{0,1}^{\bullet}}\right)
\tag{2.70}
$$

Thus, we have from Eq. (2.67)

$$
R_1^{\bullet} = \frac{1}{\vec{\omega}_1}\left(1 + \frac{\vec{\omega}_3\vec{\omega}_5\vec{\omega}_6\vec{\omega}_7}{\vec{\omega}_3\vec{\omega}_5\vec{\omega}_6\vec{\omega}_7} + \frac{\vec{\omega}_4\vec{\omega}_5\vec{\omega}_6\vec{\omega}_7}{\vec{\omega}_4\vec{\omega}_5\vec{\omega}_6\vec{\omega}_7} + \frac{\vec{\omega}_5\vec{\omega}_6\vec{\omega}_7}{\vec{\omega}_5\vec{\omega}_6\vec{\omega}_7} + \frac{\vec{\omega}_6\vec{\omega}_7}{\vec{\omega}_6\vec{\omega}_7} + \frac{\vec{\omega}_7}{\vec{\omega}_7}\right)
\tag{2.71}
$$

We next consider step s_2 as the RDS, and the remaining steps at QE, to derive an explicit expression for $R_2^{\bullet}$, where

$$
R_2^{\bullet} = \frac{1}{\vec{r}_2^{\bullet}} = \frac{1}{\vec{\omega}_2\theta_{1,2}^{\bullet}} = \frac{1}{\vec{\omega}_2\left(\dfrac{\theta_{1,2}^{\bullet}}{\theta_{0,2}^{\bullet}}\right)\theta_{0,2}^{\bullet}}
\tag{2.72}
$$

Following a similar procedure as above, there result

$$
R_2^{\bullet} = \frac{1}{\vec{\omega}_2\left(\dfrac{\vec{\omega}_1}{\vec{\omega}_1}\right)}\left(1 + \frac{\vec{\omega}_1}{\vec{\omega}_1} + \frac{\vec{\omega}_4\vec{\omega}_5\vec{\omega}_6\vec{\omega}_7}{\vec{\omega}_4\vec{\omega}_5\vec{\omega}_6\vec{\omega}_7} + \frac{\vec{\omega}_5\vec{\omega}_6\vec{\omega}_7}{\vec{\omega}_5\vec{\omega}_6\vec{\omega}_7} + \frac{\vec{\omega}_6\vec{\omega}_7}{\vec{\omega}_6\vec{\omega}_7} + \frac{\vec{\omega}_7}{\vec{\omega}_7}\right)
\tag{2.73}
$$

$$R_3^{\bullet} = \cfrac{1}{\vec{\omega}_3 \left(\cfrac{\vec{\omega}_1}{\overleftarrow{\omega}_1} \right)} \left(1 + \frac{\vec{\omega}_1}{\overleftarrow{\omega}_1} + \frac{\vec{\omega}_4 \vec{\omega}_5 \vec{\omega}_6 \vec{\omega}_7}{\overleftarrow{\omega}_4 \overleftarrow{\omega}_5 \overleftarrow{\omega}_6 \overleftarrow{\omega}_7} + \frac{\vec{\omega}_5 \vec{\omega}_6 \vec{\omega}_7}{\overleftarrow{\omega}_5 \overleftarrow{\omega}_6 \overleftarrow{\omega}_7} + \frac{\vec{\omega}_6 \vec{\omega}_7}{\overleftarrow{\omega}_6 \overleftarrow{\omega}_7} + \frac{\vec{\omega}_7}{\overleftarrow{\omega}_7} \right) \tag{2.74}$$

$$R_4^{\bullet} = \cfrac{1}{\vec{\omega}_4 \left(\cfrac{\vec{\omega}_1 \vec{\omega}_2}{\overleftarrow{\omega}_1 \overleftarrow{\omega}_2} \right)} \left(1 + \frac{\vec{\omega}_1}{\overleftarrow{\omega}_1} + \frac{\vec{\omega}_1 \vec{\omega}_2}{\overleftarrow{\omega}_1 \overleftarrow{\omega}_2} + \frac{\vec{\omega}_5 \vec{\omega}_6 \vec{\omega}_7}{\overleftarrow{\omega}_5 \overleftarrow{\omega}_6 \overleftarrow{\omega}_7} + \frac{\vec{\omega}_6 \vec{\omega}_7}{\overleftarrow{\omega}_6 \overleftarrow{\omega}_7} + \frac{\vec{\omega}_7}{\overleftarrow{\omega}_7} \right) \tag{2.75}$$

$$R_5^{\bullet} = \cfrac{1}{\vec{\omega}_5 \left(\cfrac{\vec{\omega}_1 \vec{\omega}_3}{\overleftarrow{\omega}_1 \overleftarrow{\omega}_3} \right)} \left(1 + \frac{\vec{\omega}_1}{\overleftarrow{\omega}_1} + \frac{\vec{\omega}_1 \vec{\omega}_2}{\overleftarrow{\omega}_1 \overleftarrow{\omega}_2} + \frac{\vec{\omega}_1 \vec{\omega}_3}{\overleftarrow{\omega}_1 \overleftarrow{\omega}_3} + \frac{\vec{\omega}_6 \vec{\omega}_7}{\overleftarrow{\omega}_6 \overleftarrow{\omega}_7} + \frac{\vec{\omega}_7}{\overleftarrow{\omega}_7} \right) \tag{2.76}$$

$$R_6^{\bullet} = \cfrac{1}{\vec{\omega}_6 \left(\cfrac{\vec{\omega}_1 \vec{\omega}_3 \vec{\omega}_5}{\overleftarrow{\omega}_1 \overleftarrow{\omega}_3 \overleftarrow{\omega}_5} \right)} \left(1 + \frac{\vec{\omega}_1}{\overleftarrow{\omega}_1} + \frac{\vec{\omega}_1 \vec{\omega}_2}{\overleftarrow{\omega}_1 \overleftarrow{\omega}_2} + \frac{\vec{\omega}_1 \vec{\omega}_3}{\overleftarrow{\omega}_1 \overleftarrow{\omega}_3} + \frac{\vec{\omega}_1 \vec{\omega}_3 \vec{\omega}_5}{\overleftarrow{\omega}_1 \overleftarrow{\omega}_3 \overleftarrow{\omega}_5} + \frac{\vec{\omega}_7}{\overleftarrow{\omega}_7} \right) \tag{2.77}$$

and
$$R_7^{\bullet} = \cfrac{1}{\vec{\omega}_7 \left(\cfrac{\vec{\omega}_1 \vec{\omega}_3 \vec{\omega}_5 \vec{\omega}_6}{\overleftarrow{\omega}_1 \overleftarrow{\omega}_3 \overleftarrow{\omega}_5 \overleftarrow{\omega}_6} \right)} \left(1 + \frac{\vec{\omega}_1}{\overleftarrow{\omega}_1} + \frac{\vec{\omega}_1 \vec{\omega}_2}{\overleftarrow{\omega}_1 \overleftarrow{\omega}_2} + \frac{\vec{\omega}_1 \vec{\omega}_3}{\overleftarrow{\omega}_1 \overleftarrow{\omega}_3} + \frac{\vec{\omega}_1 \vec{\omega}_3 \vec{\omega}_5}{\overleftarrow{\omega}_1 \overleftarrow{\omega}_3 \overleftarrow{\omega}_5} + \frac{\vec{\omega}_1 \vec{\omega}_3 \vec{\omega}_5 \vec{\omega}_6}{\overleftarrow{\omega}_1 \overleftarrow{\omega}_3 \overleftarrow{\omega}_5 \overleftarrow{\omega}_6} \right) \tag{2.78}$$

Finally, these equations, i.e., Eq. (2.71) and Eqs. (2.73) – (2.78), are used in Eq. (2.66) to provide the OR rate explicitly in terms of ω_ρ. The resulting expression is in fact, identical to that derived via the conventional QSS approach for this linear kinetics mechanism using linear algebra, as illustrated above for the generic example. However, the conventional QSS approach provides a rate expression that is in a considerably more complex looking and hard to discern form.

For typical experimental conditions [11], namely, with a feed of 15,000 ppm N$_2$O in He passed over Fe-ZSM-5 at T = 800 K, $p_{N_2O} = 0.0015\,\text{bar}$; $p_{N_2} = 0.0135\,\text{bar}$; $p_{O_2} = p_{N_2} / 2\,\text{bar}$ and using Eq. (2.71) and Eq. (2.73) – (2.78) we have

$$\left. \begin{aligned}
R_1^\bullet &= 6.2893 \times 10^{-5} \text{ s} \\
R_2^\bullet &= 2.1871 \times 10^{1} \text{ s} \\
R_3^\bullet &= 5.4224 \times 10^{1} \text{ s} \\
R_4^\bullet &= 3.3101 \times 10^{-10} \text{ s} \\
R_5^\bullet &= 1.5216 \times 10^{-6} \text{ s} \\
R_6^\bullet &= 4.9184 \times 10^{-1} \text{ s} \\
R_7^\bullet &= 9.2286 \times 10^{-12} \text{ s}
\end{aligned} \right\} \tag{2.79}$$

Using Eq. (2.79) in Eq. (2.66), thus, the overall rate of the reaction is

$$r_{OR} = 6.2202 \times 10^{-2} \text{ s}^{-1} \tag{2.80}$$

which is identical to that obtained from solving the QSS equations numerically for the 7-step mechanism.

2.4.1 Reduced Rate Expression

The rate expression, Eq. (2.66), is in a revealing form and allows judicious network pruning. Let us first compare the resistance of the steps in series, namely, steps s_1, s_5, s_6, and s_7. As is the case with electrical circuits, the step with maximum step resistance in series may be taken as the slowest step or the RLS for the sequence. It can be clearly seen from Eq. (2.79), that $R_6^\bullet$ is four orders of magnitude higher than $R_1^\bullet + R_5^\bullet + R_7^\bullet$. Thus,

$$R_6^\bullet \gg R_1^\bullet + R_5^\bullet + R_7^\bullet \tag{2.81}$$

Next, note that there are two parallel pathways starting at intermediate node n_1 and ending at n_3. For parallel pathways, the path with the least resistance would be the dominant pathway. The total resistance of the first pathway, namely $s_2 + s_4$ is $R_2^\bullet + R_4^\bullet$ while that for the other pathway, step s_3 is simply $R_3^\bullet$. It is evident from Eq. (2.79), that both the pathways have comparable resistances and it is imperative to retain both. Hence, the simplified overall resistance is

$$R_{OR}^\bullet \approx R_6^\bullet + \cfrac{1}{\cfrac{1}{R_2^\bullet + R_4^\bullet} + \cfrac{1}{R_3^\bullet}} \tag{2.82}$$

Further, in the series combination, $s_2 + s_4$, $R_4^\bullet$ is several orders of magnitude lower than $R_2^\bullet$ and, hence, can be eliminated without materially affecting the overall flux (rate). Thus, we may further simplify the overall resistance

$$R_{OR}^\bullet \approx R_6^\bullet + \cfrac{1}{\cfrac{1}{R_2^\bullet} + \cfrac{1}{R_3^\bullet}} \tag{2.83}$$

In other words, we simply have three steps s_2, s_3, and s_6 that are the RLSs with resistances of similar order, so that the reduced rate expression is

$$r_{OR} = \cfrac{1}{R_6^\bullet + \cfrac{1}{\cfrac{1}{R_2^\bullet} + \cfrac{1}{R_3^\bullet}}} \left(1 - \frac{\bar{\omega}_1 \bar{\omega}_3 \bar{\omega}_5 \bar{\omega}_6 \bar{\omega}_7}{\vec{\omega}_1 \vec{\omega}_3 \vec{\omega}_5 \vec{\omega}_6 \vec{\omega}_7} \right) \tag{2.84}$$

where $R_2^\bullet$, $R_3^\bullet$ and $R_6^\bullet$, given by Eqs. (2.73), (2.74) and (2.77) are of a comparable order and need to be retained.

$R_2^\bullet$, $R_3^\bullet$ and $R_6^\bullet$ can, in fact, be further simplified based on the concept of most abundant reactive intermediate (MARI) [30], i.e., by comparing the values of $\theta_{k,\rho}^\bullet / \theta_{0,\rho}^\bullet$ in $R_\rho^\bullet$. For both, steps s_2 and s_3, $\theta_{k,\rho}^\bullet / \theta_{0,\rho}^\bullet \approx 0$ for all intermediate species under the conditions mentioned above, which implies $1/\theta_{0,\rho}^\bullet \approx 1$ and, hence, the simplified expressions for $R_2^\bullet$ and $R_3^\bullet$ are

$$\left.\begin{aligned} R_2^\bullet &= \frac{\bar{\omega}_1}{\vec{\omega}_2 \vec{\omega}_1} \\[2mm] R_3^\bullet &= \frac{\bar{\omega}_1}{\vec{\omega}_3 \vec{\omega}_1} \end{aligned}\right\} \tag{2.85}$$

Similarly, by comparing the values of $\theta_{k,\rho}^\bullet / \theta_{0,\rho}^\bullet$ in $R_6^\bullet$ we have,

$$R_6^\bullet = \cfrac{1}{\bar{\omega}_6 \left(\cfrac{\vec{\omega}_1 \vec{\omega}_3 \vec{\omega}_5}{\bar{\omega}_1 \bar{\omega}_3 \bar{\omega}_5} \right)} \left(1 + \frac{\vec{\omega}_1 \vec{\omega}_3}{\bar{\omega}_1 \bar{\omega}_3} \right) \tag{2.86}$$

Using Eqs. (2.85) and (2.86) in Eq. (2.84), the simplified rate expression, thus, is

$$r_{OR} = \cfrac{1}{\cfrac{1}{\bar{\omega}_6\left(\cfrac{\vec{\omega}_1\vec{\omega}_3\vec{\omega}_5}{\bar{\omega}_1\bar{\omega}_3\bar{\omega}_5}\right)}\left(1+\cfrac{\vec{\omega}_1\vec{\omega}_3}{\bar{\omega}_1\bar{\omega}_3}\right)+\cfrac{1}{\cfrac{1}{\cfrac{\bar{\omega}_1}{\vec{\omega}_2\vec{\omega}_1}}+\cfrac{1}{\cfrac{\bar{\omega}_1}{\vec{\omega}_3\vec{\omega}_1}}}}\left(1-\cfrac{\bar{\omega}_1\bar{\omega}_3\bar{\omega}_5\bar{\omega}_6\bar{\omega}_7}{\vec{\omega}_1\vec{\omega}_3\vec{\omega}_5\vec{\omega}_6\vec{\omega}_7}\right) \qquad (2.87)$$

Using the expressions for ω_ρ (Table 2-2), thus, the simplified rate expression for the aforementioned experimental conditions, in the conventional form, is

$$r_{OR} = \cfrac{1}{\cfrac{\bar{k}_1\bar{k}_3\bar{k}_5\,p_{N_2}}{\vec{k}_1\vec{k}_3\vec{k}_5\vec{k}_6\,p_{N_2O}^2}\left(1+\cfrac{\vec{k}_1\vec{k}_3\,p_{N_2O}}{\bar{k}_1\bar{k}_3\,p_{N_2}}\right)+\cfrac{\bar{k}_1}{\vec{k}_1(\vec{k}_2+\vec{k}_3)\,p_{N_2O}}}\left(1-\cfrac{1}{K_{OR}}\cfrac{p_{N_2}^2\,p_{O_2}}{p_{N_2O}^2}\right) \qquad (2.88)$$

Finally, since we have an essentially irreversible reaction, i.e.,

$$E_{OR} \equiv (1-z_{OR}) = \left(1-\cfrac{1}{K_{OR}}\cfrac{p_{N_2}^2\,p_{O_2}}{p_{N_2O}^2}\right) \approx 1 \qquad (2.89)$$

as $z_{OR} \to 0$, the above expression can be further simplified to

$$r_{OR} = \cfrac{K_1(\vec{k}_2+\vec{k}_3)\,p_{N_2O}}{1+\cfrac{(\vec{k}_2+\vec{k}_3)\,p_{N_2}}{K_3K_5\vec{k}_6\,p_{N_2O}}\left(1+\cfrac{K_1K_3\,p_{N_2O}}{p_{N_2}}\right)} \qquad (2.90)$$

where K_ρ is the equilibrium constant for step s_ρ.

In conclusion, as a result of the systematic analysis of this example, rate-limiting steps have been identified in an intuitive manner, following the evaluation of $R_\rho^\bullet$. Thus, steps s_2, s_3, and s_6 i.e., the decomposition of adsorbed N_2O on $Z^-[FeO]^+$ and $Z^-[FeO_2]^+$ are concluded to be the RLSs. We finally wind up with a highly simplified, but accurate, rate expression for N_2O decomposition on Fe-ZSM-5. Thus, the simplified rate expression, i.e., Eq. (2.90) provides $r_{OR} = 6.2206 \times 10^{-2}$ s^{-1} for the reaction conditions mentioned above, which is close to that obtained from Eq. (2.66), or the QSS analysis, i.e., $r_{OR} = 6.2202 \times 10^{-2}$ s^{-1}.

2.5 Conclusions

A simple and intuitively appealing approach is described here for the treatment of quasi-steady state (QSS) kinetics of overall reaction (OR) mechanisms involving parallel pathways. It is based on first determining the Reaction Route (RR) Graph for a given molecular mechanism, in which reaction steps are represented by branches meeting at the nodes such that all pathways can be traced as walks between terminal nodes. The RR Graphs are consistent with Kirchhoff's laws of flow networks, e.g., electric circuits, and can, thus, can be directly adapted into an equivalent electrical circuit, in which the branches are replaced by resistors representing individual mechanistic steps. The OR rate can, hence, be expressed in Ohm's law form, i.e., OR rate = OR motive force/OR resistance, where the overall resistance in terms of individual step resistances is obtained following the common tools of electrical circuit analysis.

The individual step resistance, in turn, is replaced by the virtual maximum step rate, i.e., the rate of the step, if the entire OR affinity were available to the reaction step, with all other steps being quasi-equilibrated (QE), i.e., their affinities being zero. This can be ascertained following the LHHW approach involving a combination of the RDS/QE assumptions. In this manner, the QSS rate law for a complex mechanisms can be determined, which may be difficult or impossible to obtain by simply solving the QSS equations algebraically. The results are exact for a reaction network with steps linear in intermediates, while they are approximate, *albeit* accurate, for nonlinear step kinetics.

The algorithm is illustrated here for a case of the gas-phase H_2-Br_2 system (non-linear kinetics mechanism) involving 4 steps and a 7-step linear zeolite catalyzed N_2O decomposition mechanism, both with 2 parallel pathways. These simple systems were chosen so as to render the process comprehensible, although the approach is widely applicable. It is also shown how the thermodynamic consistence of the kinetic data can be verified easily using the RR Graph. Further, reaction flux and resistance can be used for insightful pruning and mechanistic reduction. The methodology described here when utilized with intuitive predictions of step kinetics either via first principles or semi-empirical methods, provides a comprehensive and consistent framework for mechanistic and kinetic analysis. Subsequent chapters will illustrate with examples relevant to fuel

cells that the RR network approach is a valuable new weapon in the arsenal of the catalytic scientist.

2.6 References

[1]   J.A. Christiansen, Adv. Catal. 5 (1953) 311-353.

[2]   C. Wagner, Adv. Catal. 21 (1970) 323-381.

[3]   J. Horiuti, Ann. N.Y. Acad. Sci. 213 (1973) 5-30.

[4]   M.I. Temkin, Adv. Catal. 28 (1979) 173.

[5]   M.Z. Lazman, G.S. Yablonskii, Patterns and Dynamics in Reactive Media, The IMA Volumes in Mathematics and its Applications, Springer, Berlin - Heidelberg - New York, 1991, pp. 117-150.

[6]   O.A. Hougen, K.M. Watson, J. Ind. Eng. Chem. 35 (1943) 529-541.

[7]   J.A. Dumesic, J. Catal. 185 (1999) 496-505.

[8]   Cambell, J. Catal. 204 (2001) 520-524.

[9]   A. Heyden, A.T. Bell, F.J. Keil, J. Catal. 233 (2005) 26-35.

[10] A. Heyden, B. Peters, A.T. Bell, F.J. Keil, J. Phys. Chem. B. 109 (2005) 1857-1873.

[11] A. Heyden, Department of Chemical Reaction Engineering, Ph.D. Thesis, Hamburg University of Technology, Germany, 2005.

[12] E. Shustorovich, H. Sellers, Surf. Sci. Rep. 31 (1998) 1-119.

[13] H.S. Fogler, The Elements of Chemical Reaction Engineering, 4th ed., Prentice Hall, Upper Saddle River, NJ 2006.

[14] J.O.M. Bockris, Fuel Cells: Their Electrochemistry, McGraw-Hill, New York, 1969.

[15] W. Nernst, Theoretical chemistry from the standpoint of Avogadro's rule and thermodynamics (German, Theoretische Chemie vom Standpunkte der Avogadroschen Regel und der Thermodynamik), F. Enke, Stuttgart, Germany, 1926.

[16] I. Fishtik, C.A. Callaghan, R. Datta, J. Phys. Chem. B. 108 (2004) 5671-5682.

[17] I. Fishtik, C.A. Callaghan, R. Datta, J. Phys. Chem. B. 108 (2004) 5683-5697.

[18] I. Fishtik, C.A. Callaghan, R. Datta, J. Phys. Chem. B. 109 (2005) 2710-2722.

[19] I. Fishtik, C.A. Callaghan, R. Datta, Ind. Eng. Chem. Res. 45 (2006) 6468-6476.

[20] S.A. Vilekar, I. Fishtik, R. Datta, Chem. Eng. Sci. 64 (2009) 1968-1979.

[21] P.C. Milner, J. Electrochem. Soc. 111 (1964) 228-232.

[22] T. De Donder, P. Rysselberghe, Thermodynamic Theory of Affinity, Stanford University Press, Stanford, 1936.

[23] P. van Rysselberghe, J. Chem. Phys. 29 (1958) 640-642.

[24] I. Fishtik, R. Datta, Studies in Surf. Sci. Catal. 133 (2001) 123-130.

[25] I. Fishtik, R. Datta, Ind. Eng. Chem. Res. 40 (2001) 2416-2427.

[26] S.D. Cooley, R.C. Anderson, Ind. Eng. Chem. 44 (1952) 1402-1406.

[27] A. Levy, J. Phys. Chem. 62 (1958) 570-574.

[28] M. Bodenstein, S.C. Lind, Z. Phys. Chem. 57 (1907) 168-192.

[29] S.A. Vilekar, I. Fishtik, R. Datta, in: I. Halasz (Ed.), Silica and Silicates in Modern Catalysis, Transworld Research Network, Kerala, India, 2010, pp. 49-79.

[30] M. Boudart, G. Djega-Mariadassou, Kinetics of Heterogeneous Catalytic Reactions, Princeton University Press, Princeton, N. J., 1984.

Chapter III

A Graph-Theoretic/DFT Analysis of Methanol Decomposition Reaction Network on Pt(111)

The Reaction Route (RR) Graph approach described in chapter II as a powerful new tool for topological, mechanistic and kinetic analysis of catalytic reaction networks, is utilized here for in depth analysis of methanol decomposition on Pt(111). In this approach a graph-theoretic network of molecular reaction steps is first constructed for the overall reaction (OR), on which each mechanistic step is represented by a directed branch interconnected at nodes, such that all conceivable reaction pathways can then be traced on it simply as walks or paths. The thermodynamic consistence of the DFT predicted kinetics in the literature is verified, simply from the fact that the network is consistent with the basic laws of flow graphs and its direct analogy with electrical circuits, namely, Kirchhoff's laws of current (rate) and potential (affinity). Next, rigorous flux analysis of the network is accomplished. As a result, the dominant pathways as well as the rate-limiting steps (RLS) become transparent. This furthermore facilitates network pruning to retain only the essential steps and pathways. The RR Graph approach when combined with *ab initio* kinetics, thus, provides a rigorous new framework for analyzing the mechanism and kinetics of catalytic reactions. It is, thus, found that methanol decomposition proceeds exclusively via the initial C–H dehydrogenation step rather than through O–H bond activation.

3.1 Introduction

Catalytic decomposition of methanol is an important reaction in that it occurs in several processes, e.g., methanol steam reforming [1-3], Fischer-Tropsch synthesis [4], methanol partial oxidation [5-7], methanol electro-oxidation in direct methanol fuel cells (DMFCs) [8, 9]. The reverse reaction is involved in methanol synthesis. It is therefore useful to develop a fundamental understanding of the reaction mechanism and kinetics on different catalysts. Decomposition of methanol on Pt is one of the main reactions occurring at the anode of DMFCs. A deeper understanding of the reaction mechanism can aid better catalyst design which provides additional motivation for the study to gain qualitative insights which can be applied to more complex electrochemical environment like the one occurring at the anode of direct methanol fuel cell.

The catalysts active in methanol decomposition are metals from group 10 of periodic table. The decomposition of methanol have been investigated on a variety of metal surfaces, for example, Ni(100) [10], Ni(111) [11], Cu(100) [12, 13], Cu(110) [14-16], Cu(111) [17-20], Ag(110) [21], Ag(111) [22], Pd(110) [23], Pd(111) [24], Pt(100) [25], Pt(110) [26], Pt(111) [27], Mo(110) [28] and so on. For most these surfaces, methoxy species has been reported as the dominant surface intermediate at temperatures below 350 K, formed by the O-H cleavage of the adsorbed methanol. Several researchers have studied methanol decomposition reaction using experimental techniques like IR, DEMS, ECTDMS, EELS, TDS, AES, LEED, HREELS, UPS, SEXAFS, NEXAFS, SXPS, XPD and other molecular beam techniques in order to probe its reaction intermediates [17, 29-40]. The catalytic cycle may be initiated via the activation of: *i*) the C–H; *ii*) O–H; or *iii*) the C–O bond of the adsorbed methanol, forming the corresponding intermediates hydroxymethyl ($CH_2OH \cdot S$), methoxy ($CH_3O \cdot S$), and $CH_3 \cdot S / OH \cdot S$, respectively, where S is a surface site.

C-O activation is much less likely [41] than the C-H or O-H activation pathways on Pt(110). Greeley and Mavrikakis [42] have shown that C-O bond scission has an extremely high activation energy barrier (2.19 eV) on Pt(111), and hence less likely similar to that for Pt(110). In their review, Mavrikakis and Barteau [43] opine that O-H bond cleavage of alcohols upon their adsorption on most transition metals appears to be a

common phenomenon, occurring at low temperatures and leading to the formation of stable alkoxide intermediate. Franaszczuk et al. [44] examined the decomposition of methanol over Pt(110) under ultrahigh-vacuum conditions. Using isotope substitution, they showed that the decomposition reaction proceeds via O-H bond scission to yield a methoxide intermediate, which then decomposes to CO. The methoxide intermediate is also thought to form on oxygen-precovered Pt(111) and Pt(100) surfaces [25]. On Pt(111) covered with oxygen, EELS data shows that molecularly adsorbed methanol transforms to methoxide at 170 K [29]. However, no direct spectroscopic observations for methoxide species were detected on clean Pt(111). Peck et al. [31], however detected methoxide species on clean Pt(111) by using methyl nitrite precursor. As suggested by Desai et al. [45], the mechanism of methanol decomposition over clean Pt(111) is different from that over oxygen-precovered Pt(111). Oxygen acts a promoter for the activation of O-H bond according to Kizhakevarium and Stuve [25]. In the absence of coadsorbed oxygen, however, a stable surface methoxide intermediate has only been identified on Pt(110) [41, 44].

Bagotsky et al. [46], in late 70's, formulated the dehydrogenation scheme in which H-atoms are successively removed, starting with those of the methyl group, i.e. the first dehydrogenation step was assumed to proceed via C-H bond activation. DFT analysis of the nature and thermodynamics of the reaction intermediates in methanol decomposition was initially reported by Kua and Goddard [47] and by Ishikawa et al. [48], using a finite cluster model to represent the catalyst. In fact, these studies have extended the dehydrogenation scheme in which H-atoms are successively removed, starting with those of the methyl group, originally formulated by Bagotzky et al. [46] in 1977 into a dual path mechanism, i.e. either C-H or O-H bond activation. Kua and Goddard [47] have shown CO to be a thermodynamic sink on Pt, much in accordance to the experimental findings that CO poisons the catalyst surface. Both the studies show methoxy intermediates to be thermodynamically unstable, and hence, the dehydrogenation mechanism to proceed via C-H bond activation in preference to O-H bond activation. Ishikawa et al. [48] predict the C-H bond activation to be about 33.8 kJ/mol lower than O-H bond activation on Pt(111). Thus, both, Kua and Goddard [47] and Ishikawa et al. [48] predict methanol decomposition to proceed via sequential removal of hydrogen

atoms off the carbon end as shown in Figure 3-1. Kua and Goddard [47] favor hydroxymethylidyne (COH) species over formyl (CHO), while Ishikawa et al. [48] recognize that the formation of both species is feasible and likely and the preferred species depends on the experimental conditions.

More recently, Cao et al. [49] have investigated the reaction intermediates and the mechanism for methanol decomposition on well-defined low Miller index platinum single crystal planes, Pt(111), Pt(110), and Pt(100), in an aqueous environment (in connection with direct methanol fuel cell), using a combination of chronoamperometry, fast scan cyclic voltammetry as well as an *ab initio*/DFT investigation using a three-layer periodic slab model. Their results also support a dual path dehydrogenation mechanism, proceeding via both C–H and O–H bond activation as represented in Figure 3-1.

The pathway proceeding via C-H cleavage of adsorbed methanol is, in fact, the same as that proposed by Bagotsky et al. [46]. For CH_3OH decomposition in the gas-phase (UHV) over Pt(111), on the other hand, Greeley and Mavrikakis [42, 50] and Kandoi et al. [51] have also theoretically investigated the intermediates resulting from homolytic C–H or O–H cleavage.

Thus, the intermediates resulting from successive dehydrogenation of the methyl group are in hydroxymethyl ($CH_2OH·S$), hydroxymethylene (CHOH·S), and hydroxymethylidyne (COH·S) or formyl (CHO·S), which finally results in adsorbed CO, CO·S (Figure 3-1). Some of these intermediates are also assumed to undergo parallel reactions involving O–H bond scission (Figure 3-1). While, the pathway starting with O–H bond cleavage of adsorbed methanol leads first to the methoxy ($CH_3O·S$). Subsequent sequential abstraction of H forms formaldehyde ($CH_2O·S_2$), formyl (CHO·S) and CO·S species (Figure 3-1).

The optimized molecular structures of these intermediates are reported in refs. [42, 47-50]. One such example is shown in Figure 3-2, where Cao et al. [49] has provided optimized molecular structures of the reaction intermediates over aqueous-solvated Pt(111), an environment similar to that at the anode of DMFCs. Thus, the overall reaction scheme is largely similar, be it thermal of electrochemical reaction system.
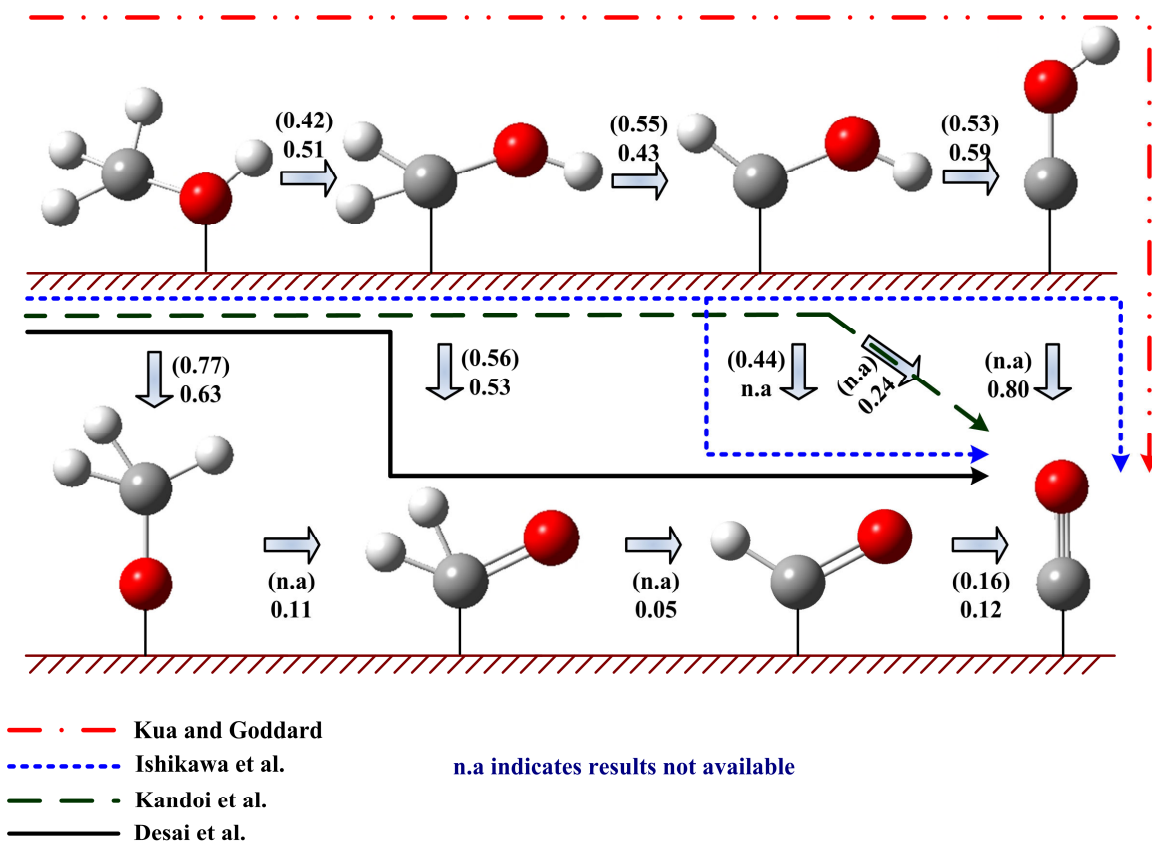
Figure 3-1: Reaction mechanism and activation energies (eV). The values in the parenthesis correspond to the calculations by Ishikawa et al. [48] and the lower numbers to the prediction by Wisconsin group [51, 52]
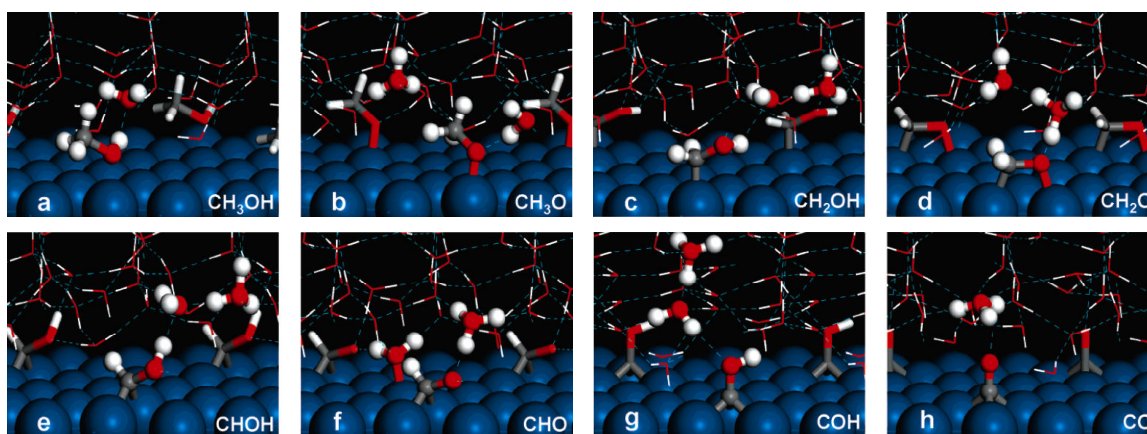
Figure 3-2: DFT predictions of optimized structures of surface intermediates in methanol decomposition over aqueous-solvated Pt(111) [49].

Such theoretical insights are of tremendous utility in building a robust molecular reaction network. Thus, the DFT method is an inimitable starting point for predicting the intermediates and building a molecular mechanism. However, a systematic analysis of the reaction pathways has not been accomplished. The most favorable decomposition mechanism is difficult to be deduced from DFT studies alone, since the relative rates depend upon the reaction conditions [52].

One of the earlier attempts to predict the reaction energetics of methanol decomposition on Pt was by Ishikawa et al. [48], where a hybrid approach of combination of DFT and unity-bond index quadratic exponential potential (UBI-QEP) was utilized. Ishikawa et al. [48] calculated the adsorption energies of various intermediates involved in methanol oxidation on Pt and mixed metals Pt-M (M=Ru, Sn) using quantum chemical calculations using the Amsterdam density functional (ADF) package. All intermediates, except atomic hydrogen was found to prefer the on-top site. Moreover, the DFT results indicated that the coordination via carbon is more favorable than via oxygen for all intermediates except, adsorbed CH_3OH, CH_3O and CH_2O. The predictions by Greeley et al. [42, 50] using the total energy calculation code, DACAPO are consistent with these results, except that for CH_2O, as they predict the binding configuration to be via both oxygen and carbon. Ishikawa et al. [48] predicted the formations of adsorbed CH_3O and CH_2O species to be less favorable than adsorbed CH_2OH and $CHOH$, implying the dehydrogenation of adsorbed methanol on Pt to be energetically favorable with hydrogen atom first stripped off the carbon end, i.e., the C-H bond scission. Predictions by Greeley et al. [42, 50] are much in agreement with the findings of Ishikawa et al. [48].

In addition to thermodynamics, the Wisconsin group [42, 50-52] has, also utilized the DFT method based on the extended-surface periodic-slab model, to determine the activation energy barriers for a 13-step mechanism comprising of both, the O–H and C–H bond scission pathways of methanol decomposition on Pt(111). They initially provided activation energy barriers (not corrected for zero-point energy, ZPE) for elementary reaction steps in methanol decomposition on Pt(111) [42], which were refined in the subsequent publication to provide ZPE corrected energetics [52]. These were then utilized in a microkinetic analysis of the reaction network, the results of which were

found to be in agreement with experimental results. It should be noted that the early predictions by Ishikawa et al. [48] are largely in agreement with those of the Wisconsin group [42, 50-52], with an average deviation of ±2 kcal/mol, as seen from Figure 3-1.

In this chapter, the 13-step Wisconsin mechanism for methanol decomposition is adopted, since it is the most comprehensive mechanism available providing many necessary details for our analysis to judge the efficacy of the competitive parallel pathways. More specifically, the Wisconsin mechanism for methanol decomposition on Pt(111) comprising 13 elementary steps is assembled into a graph-theoretic reaction route (RR) network [53-55]. The RR network is next converted into an equivalent reaction electrical circuit which is further analyzed, simplified and pruned using the tools of electric circuit analysis. The result is the emergence of an unambiguous picture of methanol decomposition on Pt(111), with a clear portrayal of all possible pathways, and irrefutable identification of the dominant pathways and rate limiting steps. This example, thus, clearly illustrates the utility of our approach in conjunction with DFT for unraveling catalytic reaction mechanism and kinetics.

3.2 Reaction Mechanism and Kinetics

The $p = 13$ elementary reaction steps comprising the mechanism of methanol decomposition on Pt(111) developed by, Greeley and Mavrikakis [42] and Gokhale et al. [52], is adopted here, and is summarized in Table 3-1. The mechanism consists of two initial dehydrogenation pathways, one proceeding via O–H bond scission (step s_2) and the other proceeding via C–H bond scission (step s_6). Steps s_1, s_{12} and s_{13} are the adsorption-desorption steps for methanol, carbon monoxide and hydrogen respectively, while the rest are all surface reaction steps. All reactions are considered to be reversible. The extent of reversibility of a step, of course, varies and is indicated by its affinity, A_ρ.

Gokhale et al. [52] have also provided the thermodynamic properties of the surface intermediate species, I_k·S, based on the DFT prediction of the total electronic energy (TE) of the system and the vibrational spectra of the species.

Thus, the standard enthalpy of formation of a surface species was calculated by them via

Table 3-1: The microkinetic model for methanol decomposition on Pt(111). The letter 'S' denotes a surface site. Activation energies and enthalpy changes in kJ/mol; the units of the pre–exponential factors are $atm^{-1} s^{-1}$ for adsorption/desorption reactions and s^{-1} for surface reactions.

	$\vec{E}_\rho$	$\vec{\Lambda}_\rho$	Elementary Reactions	$\overline{E}_\rho$	$\overline{\Lambda}_\rho$	ΔH°_ρ
s_1:	0	1.00×10^6	$CH_3OH + S \leftrightarrows CH_3OH \cdot S$	31.845	8.64×10^{13}	−31.845
s_2:	60.795	1.04×10^{15}	$CH_3OH \cdot S + S \leftrightarrows CH_3O \cdot S + H \cdot S$	18.335	1.12×10^{15}	42.46
s_3:	10.615	4.61×10^{14}	$CH_3O \cdot S + 2S \leftrightarrows CH_2O \cdot S_2 + H \cdot S$	56.935	1.16×10^{15}	−46.32
s_4:	4.825	1.00×10^{13}	$CH_2O \cdot S_2 \leftrightarrows CHO \cdot S + H \cdot S$	80.095	2.36×10^{12}	−75.27
s_5:	11.58	1.16×10^{14}	$CHO \cdot S + S \leftrightarrows CO \cdot S + H \cdot S$	106.15	1.32×10^{15}	−94.57
s_6:	49.215	4.06×10^{15}	$CH_3OH \cdot S + S \leftrightarrows CH_2OH \cdot S + H \cdot S$	76.235	1.12×10^{15}	−27.02
s_7:	41.495	2.99×10^{14}	$CH_2OH \cdot S + S \leftrightarrows CHOH \cdot S + H \cdot S$	59.83	1.37×10^{15}	−18.335
s_8:	56.935	6.10×10^{13}	$CHOH \cdot S + S \leftrightarrows COH \cdot S + H \cdot S$	116.765	2.72×10^{13}	−59.83
s_9:	77.2	7.87×10^{12}	$COH \cdot S + S \leftrightarrows CO \cdot S + H \cdot S$	145.715	1.02×10^{14}	−68.515
s_{10}:	23.16	1.76×10^{13}	$CHOH \cdot S + 2S \leftrightarrows CO \cdot S + 2H \cdot S$	151.505	1.01×10^{14}	−128.345
s_{11}:	51.145	1.95×10^{13}	$CH_2OH \cdot S + 2S \leftrightarrows CH_2O \cdot S_2 + H \cdot S$	27.985	1.92×10^{14}	23.16
s_{12}:	133.888	1.00×10^{13}	$CO \cdot S \leftrightarrows CO + S$	0	1.41×10^5	133.888
s_{13}:	88.2824	1.00×10^{13}	$H \cdot S + H \cdot S \leftrightarrows H_2 + 2S$	13	6.33×10^6	75.3

$$H^{\circ}_{I_k \cdot S} = H^{\circ}_{I_k(g)} + BE_{I_k \cdot S} + \Delta(ZPE_{I_k}) \tag{3.1}$$

where $H^{\circ}_{I_k(g)}$ is the standard enthalpy of formation in the gas phase, $BE_{I_k \cdot S}$ is the binding energy, and $\Delta(ZPE_{I_k})$ is the zero point energy correction to binding energy of the intermediate species I_k, all of which are provided by Gokhale et al. [52]. The thermodynamic properties of the surface reaction steps were then calculated by them based on the species thermodynamic properties. Thus, for the surface reaction s_ρ, defined as

$$\sum_{k=1}^{l} \alpha_{\rho k} I_k \cdot S + \sum_{i=1}^{n} \beta_{\rho i} T_i = 0, \tag{3.2}$$

The enthalpy change and the entropy change are

$$\Delta H^{\circ}_{\rho} = \sum_{k=1}^{l} \alpha_{\rho k}(H^{\circ}_{I_k \cdot S}) + \sum_{i=1}^{n} \beta_{\rho i}(H^{\circ}_{T_i(g)}); \text{ and } \Delta S^{\circ}_{\rho} = \sum_{k=1}^{l} \alpha_{\rho k}(S^{\circ}_{I_k \cdot S}) + \sum_{i=1}^{n} \beta_{\rho i}(S^{\circ}_{T_i(g)}) \tag{3.3}$$

where, $\alpha_{\rho k}$ is the stoichiometric coefficient of surface intermediate $I_k \cdot S$ ($k = 1, 2, \ldots, l$) and $\beta_{\rho i}$ of the terminal species T_i ($i = 1, 2, \ldots, n$), in the reaction step s_ρ.

The standard entropy of formation of a surface species, $I_k \cdot S$ is based on the assumption that adsorption causes a total loss of translational entropy [56], i.e.,

$$S^{\circ}_{I_k \cdot S} = S^{\circ}_{I_k(g)} - S_{trans, I_{k(g)}} \tag{3.4}$$

where, $S^{\circ}_{I_k(g)}$ is the standard entropy of formation and $S_{trans, I_{k(g)}}$ is the translational entropy of the species I_k in the gas phase

$$S_{trans, I_{k(g)}} = R \left[\frac{5}{2} + \ln\left(\frac{(2\pi m_{mol} k_B T)^{3/2} \upsilon_{I_{k(g)}}}{h^3} \right) \right] \tag{3.5}$$

where $\upsilon_{I_{k(g)}}$ is the molar volume of gas-phase I_k. The entropy values for species in the gas phase, $S^{\circ}_{I_k(g)}$ were taken from standard handbooks [57-59]. The entropies of formation of CHOH and COH in the gas phase were, however, determined by us using Gaussian 03 [60] at the B3LYP/LANL2DZ level of theory with harmonic oscillator approximation, at

_____ 101

reference temperature of 298 K and 1 bar, due to lack of reported values in the literature. The vibrational frequencies, thus, predicted were similar to those reported by Gokhale et al. [52].

The forward and reverse rate constants in are written in the Arrhenius form

$$\vec{k}_\rho = \vec{\Lambda}_\rho \exp\left(-\frac{\vec{E}_\rho}{RT}\right); \ \overleftarrow{k}_\rho = \overleftarrow{\Lambda}_\rho \exp\left(-\frac{\overleftarrow{E}_\rho}{RT}\right) \text{ and } \vec{E}_\rho - \overleftarrow{E}_\rho = \Delta H_\rho^\circ \qquad (3.6)$$

where Λ_ρ are the pre-exponential factors. The activation energies for steps s_2 through s_{11} were taken from ref. [52] and are based on DFT calculations, while those for the adsorption and desorption steps (s_1, s_{12}, s_{13}), not provided in ref. [52] were calculated by us using the UBI-QEP method [61], which is based solely on the heats of chemisorption and bond dissociation energies of the species involved, already available.

The pre-exponential factors in the exothermic direction were taken from ref. [52], while the ones in the opposite direction were calculated by us from the standard reaction entropies as estimated above and the following relation shown below [56], to ensure thermodynamic consistency with the known thermodynamics of the overall reaction.

$$\overleftarrow{\Lambda}_\rho = \vec{\Lambda}_\rho \cdot \exp(-\Delta S_\rho^o / R) \qquad (3.7)$$

The pre-exponential factors listed in Table 3-1 were not subsequently varied from these initial estimates. It must be noted, that there are some differences between the Wisconsin model and ours, especially, the methodology for calculation of the pre-exponential factors in the reverse direction. Moreover, for the sake of simplicity, we haven't utilized binding energy of CO as a function of surface coverage.

3.3 Reaction Route (RR) Graph

3.3.1 Enumeration of RRs and Nodes

The first step in our RR Graph approach is the enumeration of atleast some of the reaction routes, or pathways [62]. Then, the RR Graph is drawn on which all the RRs can be traced as walks or paths. According to the stoichiometric RR formalism, the species comprising the mechanism are divided into terminal, i.e., reactants (CH$_3$OH) and

products (CO and H_2), and, surface intermediates (S, $CH_3OH \cdot S$, $CH_2OH \cdot S$, $CHOH \cdot S$, $COH \cdot S$, $CH_3O \cdot S$, $CH_2O \cdot S_2$, $CHO \cdot S$, $CO \cdot S$ and $H \cdot S$) where S stands for a free active site on the catalyst surface. Due to the site conservation, however, only $q = 9$ out of $l = 10$ intermediates are linearly independent.

However, one does not need to enumerate all possible direct pathways for the analysis, and only the knowledge of so called *independent set* is essential. According to Horiuti-Temkin theorem, only $\mu = p - q = 13 - 9 = 4$ RRs are linearly independent from the *complete* set of enumerated FRs and ERs for this system. Any appropriate set may be chosen. Moreover, the number of linearly independent ERs is given by $p - (q + 1) = 13 - 9 - 1 = 3$ for the reaction mechanism considered. Thus, a set of 4 linearly independent RRs may be readily determined by finding 3 independent ERs and one FR for the mechanism. These, in fact, can be determined simply from an inspection of the mechanism, thus avoiding the step of systematic stoichiometric enumeration as described in our earlier publications [53-55]. In fact, as shown here, all these FRs and ERs can be determined topologically as walks, once the RR Graph is constructed.

A direct FR for this system, as defined earlier, involves no more than $q + 1 = 9 + 1 = 10$ elementary steps. Many may include fewer steps. A simple inspection of the reaction mechanism (Table 3-1) shows that $s_1 + s_2 + s_3 + s_4 + s_5 + s_{12} + 2s_{13} = OR$, is an appropriate full route, labeled here as FR_1. A direct ER for this system, involves no more than $q + 2 = 9 + 2 = 11$ elementary steps, most involving far fewer. Thus, from Table 3-1, we can identify the following three ERs or cycles via inspection labeled here as, ER_1: $s_2 + s_3 - s_6 - s_{11} = 0$; ER_2: $s_4 + s_5 - s_7 - s_{10} + s_{11} = 0$ and ER_3: $s_8 + s_9 - s_{10} = 0$. It can be seen that this set of 4 RRs (1 FR and 3 ERs) comprises all reaction steps and is, thus, an adequate independent set.

Next, the direct INs may be stoichiometrically enumerated based on the QSS of the linearly independent intermediate species (Table 3-2) [53-55]. By definition, a direct QSS condition at a node involves no more than $p - (q - 1) = 13 - 9 + 1 = 5$ rates and can be obtained by linearly combining Qs listed in Table 3-2. In other words, the degree of INs is ≤ 5. Clearly Q_6 does not satisfy this criterion.

Table 3-2: QSS conditions for surface intermediates and terminal species involved in methanol decomposition

Intermediate Species:

$CH_3OH \cdot S$: (Q_1) $r_1 - r_2 - r_6 = 0$

$CH_3O \cdot S$: (Q_2) $r_2 - r_3 = 0$

$CH_2O \cdot S_2$: (Q_3) $r_3 - r_4 + r_{11} = 0$

$CHO \cdot S$: (Q_4) $r_4 - r_5 = 0$

$CO \cdot S$: (Q_5) $r_5 + r_9 + r_{10} - r_{12} = 0$

$H \cdot S$: (Q_6) $r_2 + r_3 + r_4 + r_5 + r_6 + r_7 + r_8 + r_9 + 2r_{10} + r_{11} - 2r_{13} = 0$

$CH_2OH \cdot S$: (Q_7) $r_6 - r_7 - r_{11} = 0$

$CHOH \cdot S$: (Q_8) $r_7 - r_8 - r_{10} = 0$

$COH \cdot S$: (Q_9) $r_8 - r_9 = 0$

Terminal Species:

CH_3OH: $r_1 = r_{OR}$

CO: $r_{12} = r_{OR}$

H_2: $r_{13} = 2r_{OR}$

Table 3-3: List of Intermediate and Terminal Nodes for the 13-step methanol decomposition reaction mechanism.

Intermediate Nodes	
$IN_1 = s_1 - s_2 - s_6$	$IN_{17} = 2s_4 + 2s_8 + 2s_{10} - s_{13}$
$IN_2 = s_2 - s_3$	$IN_{18} = 2s_4 + 2s_7 - s_{13}$
$IN_3 = s_3 - s_4 + s_{11}$	$IN_{19} = 2s_4 + 2s_6 - 2s_{11} - s_{13}$
$IN_4 = s_4 - s_5$	$IN_{20} = 2s_3 + 2s_9 + 2s_{10} + 2s_{11} - s_{13}$
$IN_5 = 2s_5 + 2s_9 + 2s_{10} - s_{13}$	$IN_{21} = 2s_3 + 2s_8 + 2s_{10} + 2s_{11} - s_{13}$
$IN_6 = s_6 - s_7 - s_{11}$	$IN_{22} = 2s_3 + 2s_7 + 2s_{11} - s_{13}$
$IN_7 = s_7 - s_8 - s_{10}$	$IN_{23} = 2s_3 + 2s_6 - s_{13}$
$IN_8 = s_8 - s_9$	$IN_{24} = s_3 - s_5 + s_{11}$
$IN_9 = 2s_{12} - s_{13}$	$IN_{25} = 2s_2 + 2s_9 + 2s_{10} + 2s_{11} - s_{13}$
$IN_{10} = s_7 - s_9 - s_{10}$	$IN_{26} = 2s_2 + 2s_8 + 2s_{10} + 2s_{11} - s_{13}$
$IN_{11} = s_6 - s_9 - s_{10} - s_{11}$	$IN_{27} = 2s_2 + 2s_7 + 2s_{11} - s_{13}$
$IN_{12} = s_6 - s_8 - s_{10} - s_{11}$	$IN_{28} = 2s_2 + 2s_6 - s_{13}$
$IN_{13} = 2s_5 + 2s_8 + 2s_{10} - s_{13}$	$IN_{29} = s_2 - s_5 + s_{11}$
$IN_{14} = 2s_5 + 2s_7 - s_{13}$	$IN_{30} = s_2 - s_4 + s_{11}$
$IN_{15} = 2s_5 + 2s_6 - 2s_{11} - s_{13}$	$IN_{31} = 2s_1 - s_{13}$
$IN_{16} = 2s_4 + 2s_9 + 2s_{10} - s_{13}$	$IN_{32} = s_1 - s_{12}$
Terminal Nodes	
$TN_1 = OR - s_1$	$TN_2 = 2OR - s_{13}$
$TN_3 = OR - s_{12}$	

An appropriate set of INs may be obtained by linearly combining Q_k listed in Table 3-2. This is useful, since it is not known *a priori* which nodes will be needed for construction of the RR Graph.

A complete set of INs by linear combination of those in Table 3-2 is listed in Table 3-3. The TNs, similarly are enumerated based on the QSS of the terminal species [53-55]. The complete list of hence enumerated INs and TNs is presented above in Table 3-3. The alternate stoichiometric algorithm is described by us [53-55].

3.3.2 RR Graph Construction

Now that, the list of the linearly independent RRs (1 FR and 3 ERs) and nodes (INs and TNs) for the system is determined as described above or via stoichiometric algorithms, the next step in our procedure is to construct the graph-theoretic RR Graph, on which each reaction step s_ρ is drawn as a directed branch, showing assumed direction, while the nodes represent reaction connectivity, such that all the remaining FRs and ERs can be visualized on the graph as walks or paths. One starts with the construction of the RR Graph based on the 4 linearly independent RRs, i.e., ER_1, ER_2, ER_3 and FR_1. The ERs are first assembled into what is called a cycle graph (Figure 3-3A). For instance, ER_1 and ER_2 have step s_{11} in common, and, may thus be combined (Figure 3-3A). ER_2 and ER_3 have step s_{10} in common and may thus be fused resulting in the cycle graph. Next, the adsorption/desorption steps, i.e., s_1, s_{12} and s_{13} which are not involved in any of the ER, are added to the cycle graph such that FR_1 may be traced as a walk on the network.

While seemingly straightforward, the last step is actually rather tricky due to the fact that non-unit stoichiometric numbers are present in the FR [55]. This is, in fact, characteristic of most catalytic reactions. Thus s_{13} must occur twice on the RR Graph. Further, the addition of these steps to the cycle graph must be done such that all nodes are among the INs. It is, further, seen from Table 3-3 that the INs for s_{13} all involve doubled other steps, e.g., n_5: $2s_5 + 2s_9 + 2s_{10} - s_{13} = 0$. Moreover, since the step s_{13} is involved twice in FR_1, the two steps s_{13} should appear in the network in series. This is so because the mass balance conditions of the terminal species, CH_3OH, CO and H_2, require the rates

of the desorption/adsorption steps to satisfy the condition $2r_1 = 2r_{12} = r_{13} = 2r_{OR}$ (Table 3-2). Because of these constraints, all of the steps (including the OR) must be doubled, i.e., two identical steps in parallel between two given nodes. This is readily accomplished by fusing together two cycle graphs shown in Figure 3-3A and adding the remaining steps as depicted in Figure 3-3. It can be checked that all the nodes are among the enumerated INs and TNs. Thus, the final RR Graph for methanol decomposition is shown in Figure 3-3B.

It may be noted that all reaction steps are present twice in the RR Graph. This is, in fact, a general property of balanced RR Graphs, i.e., the mass balance conditions require every step in a RR network, including the ORs, to be present in the network an equal number of times, in this case 2, because of the particular stoichiometry. The final RR network thus assembled is shown in Figure 3-3B. Upon inspection of this graph, it is seen that all nodes are balanced in that they satisfy the quasi-state conditions of surface intermediates. The topological enumeration of all reaction pathways or RRs can now be easily accomplished by tracing walks on the RR Graph topology. A total of 6 direct FRs can be easily traced as walks between the terminal nodes, and 6 direct ERs can be traced as cycles. Of course, only $p - q = 13 - 9 = 4$ FRs are linearly independent, i.e., the others can be resulted by their linear combination. The complete list of thus generated FRs and ERs is listed in Table 3-4. It must be noted that exactly the same set of direct RRs (FRs and ERs) can be generated based on our stoichiometric algorithm [53-55]. Thus, topological enumeration of FRs and ERs is an effective alternate to stoichiometric enumeration [62].

Amongst the enumerated FRs, three FRs are initiated via O–H cleavage (Paths 1, 4 and 5), whilst the rest start via C–H cleavage of adsorbed methanol (Paths 2, 3 and 6). From among these, Paths 1, 3 and 6 have been identified by Greeley and Mavrikakis [42] and Gokhale et al. [52]. On the other hand, Paths 1, 2 and 6 have been identified by Neurock and coworkers [49, 63]. Further, Paths 2 and 6 were proposed by Bagotzky et al. [64]. Kua and Goddard [47] and Ishikawa et al. [48] have recognized Path 2.

However, Paths 4 and 5 for methanol decomposition have apparently not so far been identified in the literature. Clearly, rigorous stoichiometric enumeration of FRs as done here is essential.
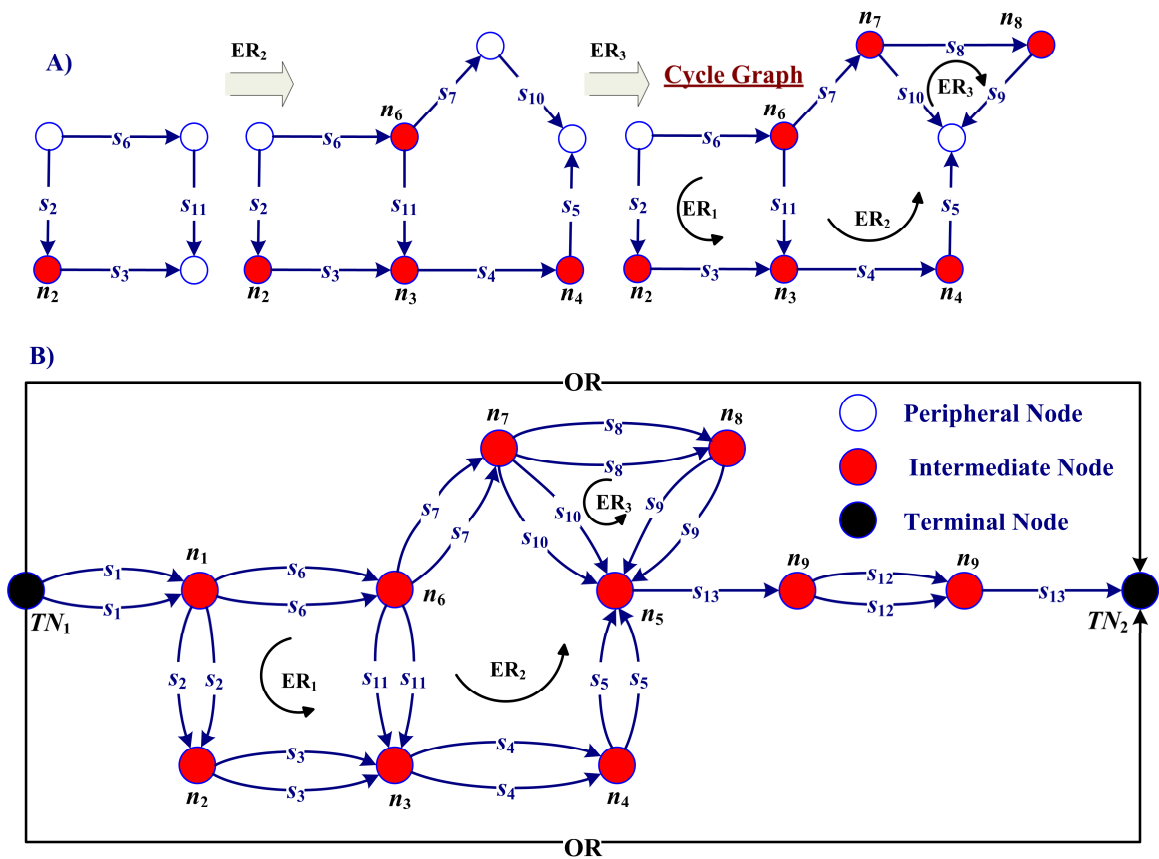
Figure 3-3: Systematic construction of RR Graph for the considered methanol decomposition reaction mechanism.

Table 3-4: Stoichiometrically distinct direct FRs and ERs for methanol decomposition reaction.

Reaction Route	Expression
	Full RRs
FR_1 (Path 1):	$s_1 + s_2 + s_3 + s_4 + s_5 + s_{12} + 2s_{13} = OR$ $CH_3OH \rightarrow CH_3O \rightarrow CH_2O \rightarrow CHO \rightarrow CO$
FR_2 (Path 2):	$s_1 + s_6 + s_7 + s_8 + s_9 + s_{12} + 2s_{13} = OR$ $CH_3OH \rightarrow CH_2OH \rightarrow CHOH \rightarrow COH \rightarrow CO$
FR_3 (Path 3):	$s_1 + s_6 + s_7 + s_{10} + s_{12} + 2s_{13} = OR$ $CH_3OH \rightarrow CH_2OH \rightarrow CHOH \rightarrow CO$
FR_4 (Path 4):	$s_1 + s_2 + s_3 - s_{11} + s_7 + s_8 + s_9 + s_{12} + 2s_{13} = OR$ $CH_3OH \rightarrow CH_3O \rightarrow CH_2O \rightarrow CH_2OH \rightarrow CHOH \rightarrow COH \rightarrow CO$
FR_5 (Path 5):	$s_1 + s_2 + s_3 - s_{11} + s_7 + s_{10} + s_{12} + 2s_{13} = OR$ $CH_3OH \rightarrow CH_3O \rightarrow CH_2O \rightarrow CH_2OH \rightarrow CHOH \rightarrow CO$
FR_6 (Path 6):	$s_1 + s_6 + s_{11} + s_4 + s_5 + s_{12} + 2s_{13} = OR$ $CH_3OH \rightarrow CH_2OH \rightarrow CH_2O \rightarrow CHO \rightarrow CO$
	Empty RRs
ER_1:	$s_2 + s_3 - s_6 - s_{11} = 0$
ER_2:	$s_4 + s_5 - s_7 - s_{10} + s_{11} = 0$
ER_3:	$s_8 + s_9 - s_{10} = 0$
ER_4:	$s_2 + s_3 + s_4 + s_5 - s_6 - s_7 - s_8 - s_9 = 0$
ER_5:	$s_4 + s_5 - s_7 - s_8 - s_9 + s_{11} = 0$
ER_6:	$s_2 + s_3 + s_4 + s_5 - s_6 - s_7 - s_{10} = 0$

Of course, not all FRs may contribute significantly towards the total flux of the OR. The dominant FRs can be identified readily using the RR circuit approach as described next.

The RR Graph can also be used to directly generate appropriate energy diagrams, as shown in Figure 3-4. As mentioned above, each node is characterized by a potential energy or enthalpy on the diagram.

Thus, each plateau corresponds to the respective node on the RR graph. In addition to reaction enthalpy or the difference between its nodes, the energy diagram also depicts both the forward and reverse activation energies for each elementary step (Table 3-1). The FRs and ERs are evident on the energy diagram as well.

3.4 Reaction Network, Thermodynamics, and Kinetics

Each cycle or ER in the RR Graph is subject to KPL. As an example of KPL, consider ER_1, i.e., $s_2 + s_3 - s_6 - s_{11} = 0$. The corresponding linear combination of affinities is, of course, equal to zero

$$A_2 + A_3 - A_6 - A_{11} = 0, \text{ i.e., } \left(\frac{\vec{r}_2}{\overleftarrow{r}_2}\right)\left(\frac{\vec{r}_3}{\overleftarrow{r}_3}\right)\left(\frac{\overleftarrow{r}_6}{\vec{r}_6}\right)\left(\frac{\overleftarrow{r}_{11}}{\vec{r}_{11}}\right) = 1 \tag{3.8}$$

Since in a cycle, the species activities cancel out, we have a thermodynamic consistency check on the predicted rate constants of steps in a cycle, i.e.,

$$\frac{\vec{k}_2}{\overleftarrow{k}_2}\frac{\vec{k}_3}{\overleftarrow{k}_3}\frac{\overleftarrow{k}_6}{\vec{k}_6}\frac{\overleftarrow{k}_{11}}{\vec{k}_{11}} = 1 = K_2 K_3 K_6^{-1} K_{11}^{-1} \tag{3.9}$$

The calculated rate constants must be consistent with these constraints. There are two other such constraints for the remaining two independent ERs. Alternatively, not all rate constants need to be predicted, some may be found from KPL relations.

Furthermore, the affinities, A_ρ of the elementary reactions ($A_\rho = -\Delta G_\rho$), in a FR are interrelated with the affinity of the OR, A_{OR}, via similar KPL relation. For instance, for $FR_1: s_1 + s_2 + s_3 + s_4 + s_5 + s_{12} + 2s_{13}$, we have

$$A_1 + A_2 + A_3 + A_4 + A_5 + A_{12} + 2A_{13} = A_{OR}, \text{ i.e., } K_1 K_2 K_3 K_4 K_5 K_{12} K_{13}^2 = K_{OR} \tag{3.10}$$
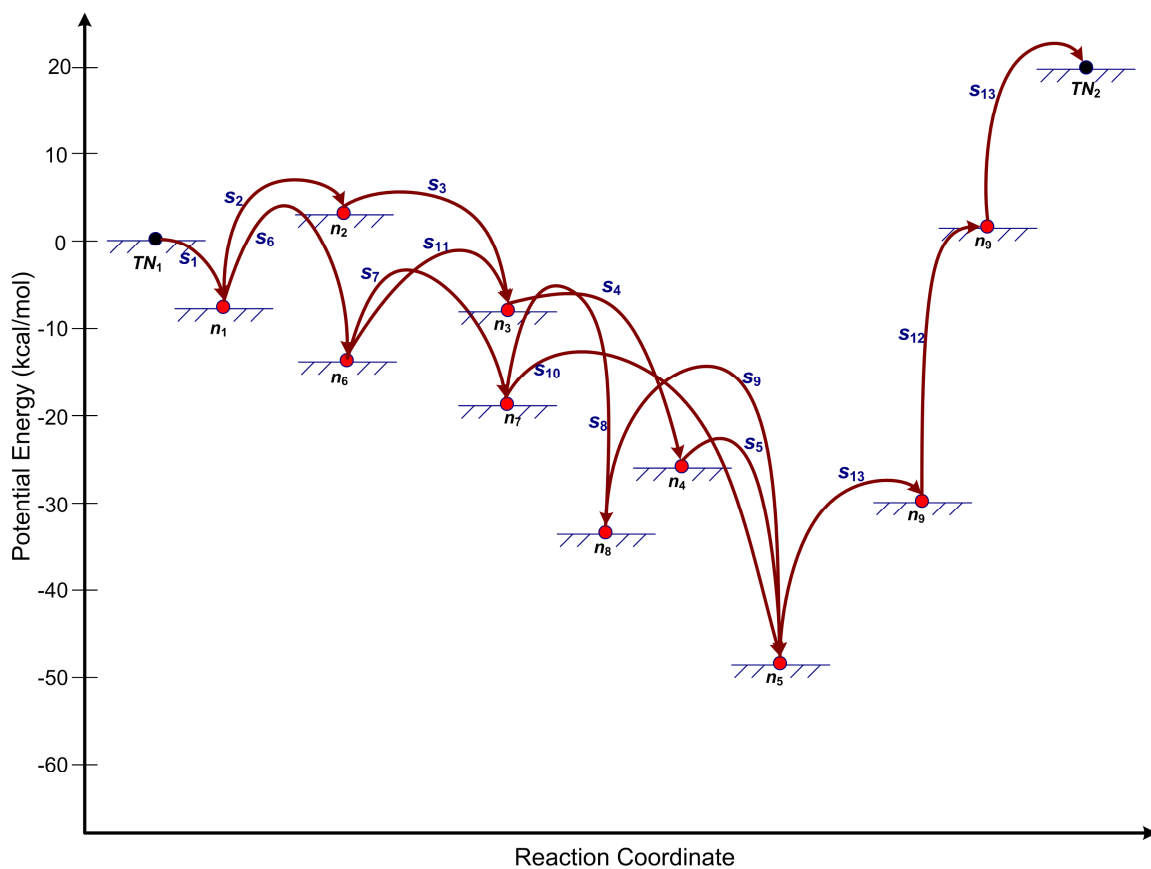
Figure 3-4: Energy diagram corresponding to the RR Graph for methanol decomposition reaction on Pt(111).

where, K_ρ and K_{OR} is the equilibrium constant of the elementary reaction step s_ρ and OR respectively. The data in Table 3-1 are consistent with this.

Each node on the RR graph follows Kirchhoff's Flux Law (KFL). Thus, KPL ensures thermodynamic consistency while KFL is used to rigorously determine the network kinetics. For the case of methanol decomposition, the following equations result as per the application of KFL at the 9 linearly independent nodes, i.e., (Figure 3-3)

$$
\begin{aligned}
&n_1 : r_1 - r_2 - r_6 = 0; \\
&n_2 : r_2 - r_3 = 0; \\
&n_3 : r_3 - r_4 + r_{11} = 0; \\
&n_4 : r_4 - r_5 = 0; \\
&n_5 : 2r_5 + 2r_9 + 2r_{10} - r_{13} = 0; \\
&n_6 : r_6 - r_7 - r_{11} = 0; \\
&n_7 : r_7 - r_8 - r_{10} = 0; \\
&n_8 : r_8 - r_9 = 0; \\
&n_9 : r_{13} - 2r_{12} = 0
\end{aligned}
\tag{3.11}
$$

which provide the network constraints on the rates of elementary steps. Using mass action kinetics, these KFL equations reduce to the following set

$$\left(\vec{k}_1 p_{CH_3OH}\theta_0 - \bar{k}_1\theta_{CH_3OH\cdot S}\right) - \left(\vec{k}_2\theta_{CH_3OH\cdot S}\theta_0 - \bar{k}_2\theta_{CH_3O\cdot S}\theta_{H\cdot S}\right) - \left(\vec{k}_6\theta_{CH_3OH\cdot S}\theta_0 - \bar{k}_6\theta_{CH_2OH\cdot S}\theta_{H\cdot S}\right) = 0$$

$$\left(\vec{k}_2\theta_{CH_3OH\cdot S}\theta_0 - \bar{k}_2\theta_{CH_3O\cdot S}\theta_{H\cdot S}\right) - \left(\vec{k}_3\theta_{CH_3O\cdot S}\theta_0^2 - \bar{k}_3\theta_{CH_2O\cdot S_2}\theta_{H\cdot S}\right) = 0$$

$$\left(\vec{k}_3\theta_{CH_3O\cdot S}\theta_0^2 - \bar{k}_3\theta_{CH_2O\cdot S_2}\theta_{H\cdot S}\right) - \left(\vec{k}_4\theta_{CH_2O\cdot S_2} - \bar{k}_4\theta_{CHO\cdot S}\theta_{H\cdot S}\right) + \left(\vec{k}_{11}\theta_{CH_2OH\cdot S}\theta_0^2 - \bar{k}_{11}\theta_{CH_2O\cdot S_2}\theta_{H\cdot S}\right) = 0$$

$$\left(\vec{k}_4\theta_{CH_2O\cdot S_2} - \bar{k}_4\theta_{CHO\cdot S}\theta_{H\cdot S}\right) - \left(\vec{k}_5\theta_{CHO\cdot S}\theta_0 - \bar{k}_5\theta_{CO\cdot S}\theta_{H\cdot S}\right) = 0$$

$$2\left(\vec{k}_5\theta_{CHO\cdot S}\theta_0 - \bar{k}_5\theta_{CO\cdot S}\theta_{H\cdot S}\right) + 2\left(\vec{k}_9\theta_{COH\cdot S}\theta_0 - \bar{k}_9\theta_{CO\cdot S}\theta_{H\cdot S}\right) + 2\left(\vec{k}_{10}\theta_{CHOH\cdot S}\theta_0^2 - \bar{k}_{10}\theta_{CO\cdot S}\theta_{H\cdot S}^2\right)$$
$$- \left(\vec{k}_{13}\theta_{H\cdot S}^2 - \bar{k}_{13}p_{H_2}\theta_0^2\right) = 0$$

$$\left(\vec{k}_6\theta_{CH_3OH\cdot S}\theta_0 - \bar{k}_6\theta_{CH_2OH\cdot S}\theta_{H\cdot S}\right) - \left(\vec{k}_7\theta_{CH_2OH\cdot S}\theta_0 - \bar{k}_7\theta_{CHOH\cdot S}\theta_{H\cdot S}\right) - \left(\vec{k}_{11}\theta_{CH_2OH\cdot S}\theta_0^2 - \bar{k}_{11}\theta_{CH_2O\cdot S_2}\theta_{H\cdot S}\right) = 0$$

$$\left(\vec{k}_7\theta_{CH_2OH\cdot S}\theta_0 - \bar{k}_7\theta_{CHOH\cdot S}\theta_{H\cdot S}\right) - \left(\vec{k}_8\theta_{CHOH\cdot S}\theta_0 - \bar{k}_8\theta_{COH\cdot S}\theta_{H\cdot S}\right) - \left(\vec{k}_{10}\theta_{CHOH\cdot S}\theta_0^2 - \bar{k}_{10}\theta_{CO\cdot S}\theta_{H\cdot S}^2\right) = 0$$

$$\left(\vec{k}_8\theta_{CHOH\cdot S}\theta_0 - \bar{k}_8\theta_{COH\cdot S}\theta_{H\cdot S}\right) - \left(\vec{k}_9\theta_{COH\cdot S}\theta_0 - \bar{k}_9\theta_{CO\cdot S}\theta_{H\cdot S}\right) = 0$$

$$\left(\vec{k}_{13}\theta_{H\cdot S}^2 - \bar{k}_{13}p_{H_2}\theta_0^2\right) - 2\left(\vec{k}_{12}\theta_{CO\cdot S} - \bar{k}_{12}p_{CO}\theta_0\right) = 0$$

$$(3.12)$$

The above set of 9 non-linear algebraic KFL equations, along with the site balance equation,

$$\theta_{CH_3OH\cdot S} + \theta_{CH_2OH\cdot S} + \theta_{CH_3O\cdot S} + \theta_{CH_2O\cdot S_2} + \theta_{CHOH\cdot S} + \theta_{CHO\cdot S} + \theta_{COH\cdot S} + \theta_{CO\cdot S} + \theta_{H\cdot S} + \theta_0 = 1 \quad (3.13)$$

may be numerically solved simultaneously, for given input conditions (temperature and partial pressures of reactants) and conversion, to obtain the unknown site fractions of intermediate species, θ_k. Thereupon, one may readily calculate the rate, affinity and resistance of each elementary reaction step. Finally, the rate of the overall reaction may be obtained from the TNs, e.g., $r_{OR} = r_1 = r_{12} = r_{13}/2$ (Figure 3-3). Moreover, if combined with mass-balance conditions for a given reactor, one can predict the reactor performance. This procedure is distinct from conventional microkinetics analysis [52],

wherein differential equations for a given reactor are solved numerically to obtain conversion, from which rate of a reaction is inferred indirectly.

Finally, once the step resistances are calculated, the elimination of parallel routes with higher "resistance" and identification of steps with highest resistance in a sequence as rate limiting steps (RLS) can be accomplished rigorously and transparently, as described next.

3.5 Network Analysis and Pruning

As a first approximation, as is commonly done, the most favorable reaction routes may be identified based on the energetic considerations by simply comparing the energy diagrams of the various pathways (Figure 3-4). For instance, one may expect pathways involving step s_2 to be less favorable than those involving s_6. In other words, the initial dehydrogenation step is indicated to proceed via the C–H cleavage of adsorbed methanol to yield hydroxymethyl (CH$_2$OH·S) in preference to the O–H cleavage producing methoxide (CH$_3$O·S) on Pt(111), owing to the higher activation energy barrier for step s_2. However, such qualitative arguments can lead to erroneous conclusions because the rate of a step depends not only upon the energy barrier but also on concentration of the reactants. Further, flux along a pathway may not be determined by a single RLS.

A more accurate and robust simplification and reduction may be accomplished based on a comparison of the flux (current) along different pathways in the reaction circuit or via a comparison of pathway resistance (Figure 3-5). As mentioned above, being consistent, RR Graphs can be directly converted into an equivalent electric circuit, or wiring diagram allowing use of the gamut of techniques available for electric circuit analysis. For the methanol decomposition example, the equivalent electrical circuit can be obtained simply by replacing the branches in Figure 3-3B by the step resistances. Figure 3-5, thus, provides the electrical analog or the reaction circuit of the methanol decomposition. The branch currents in Figure 3-5, simulated using Multisim software, a schematic simulation and programmable logic tool produced by Electronics Workbench [65], as an alternate to the above mentioned KFL approach, represent the turnover frequencies (TOFs, s^{-1}) for the corresponding elementary steps on Pt(111) simulated in a packed bed reactor (PBR) with W/F = 100 s at 553 K, 1 atm and 1% methanol in feed.

First of all note that KFL is followed at all nodes. Figure 3-5 is a very revealing diagram, from which many important conclusions regarding the network may be drawn via an inspection of branch currents, current splitting at nodes, and a comparison of resistances. The total current is 4.4 A ($2r_{OR} = 4.4$ s^{-1}) under these conditions, split equally between two parallel s_1. At n_1, it is seen that the current (flux) flows almost entirely through the upper branch (s_6), even though R_6 is only an order of magnitude lower than R_2. This is because of a very large R_3 in series with R_2. Thus, the O-H cleavage pathway contributes virtually nothing to the overall methanol decomposition pathway under these conditions. The upper branch (C-H cleavage pathway) splits again at node n_6. Again, due to the large difference in R_7 and R_{11}, the flux through the upper branch dominates. A further split occurs at n_7. Here, while almost 90% of the flux is through lower branch (R_{10}), the upper branch ($R_8 + R_9$) contribution (about 10%) cannot be neglected. It can be readily seen that steps s_8 and s_9 are an order of magnitude lower than step s_{10}, a conclusion similar to that of Gokhale et al. [52] and Kandoi et al. [51] based on their microkinetic analysis. It can further be seen from Figure 3-5 that Path 3, i.e. $s_1 + s_6 + s_7 + s_{10} + s_{12} + 2s_{13}$, (CH$_3$OH $\rightarrow$ CH$_2$OH $\rightarrow$ CHOH $\rightarrow$ CO) is the dominant reaction pathway for these typical reaction conditions, since majority of the current (flux) flows through this pathway. However, the parallel pathway, FR$_2$ comprising of steps s_8 and s_9, also contributes non-negligibly.

To further, confirm these findings, detailed comparison of the resistances is called for under a variety of conditions along parallel paths so that irrefutable conclusions can be made about the mechanism and kinetics of methanol decomposition. This is most readily accomplished by a comparison of resistances of the two parallel pathways between two given nodes, which have the same affinity drop by virtue of KPL, i.e., by considering each ER as two parallel paths and comparing the total resistance of each path for the sub-mechanism between two nodes. If the resistance along one path is much larger than the other, it would be safe to assume that the path contributes little to the flux and may be neglected.
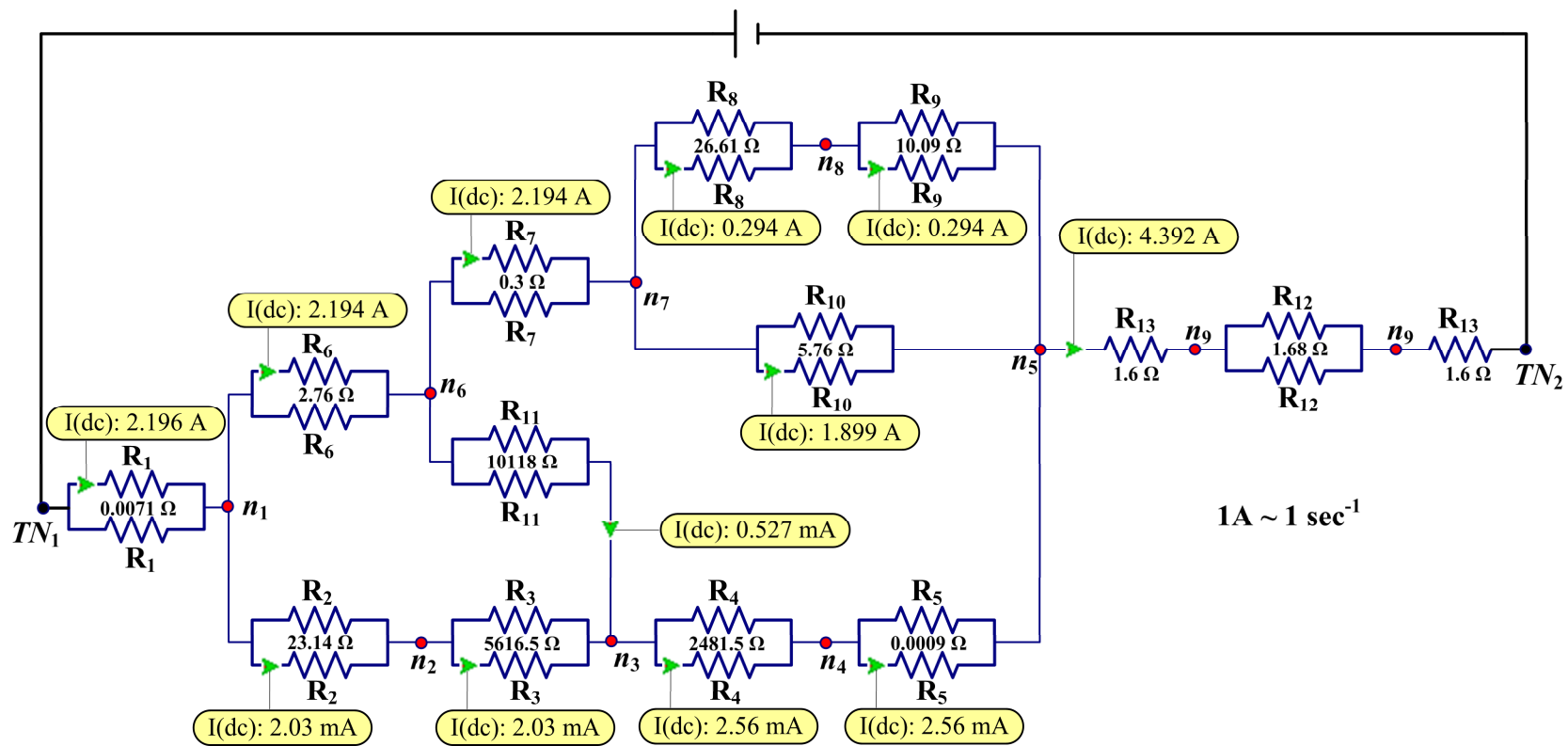
Figure 3-5: Reaction Circuitry/Electrical analog of the RR network for methanol decomposition reaction. The branch currents represent the TOFs (s^{-1}) for the corresponding elementary steps on Pt(111) at 553 K, 1 atm and 1% methanol in feed, PBR *W/F=*100 s

As an example, consider ER_3, i.e., let us compare the resistances along parallel pathways between nodes n_7 and n_5, namely, the two parallel paths that produce CO·S species. In the first path, i.e. s_{10}, CHOH·S directly decomposes into CO·S, where as in the second path, i.e., $s_8 + s_9$, COH·S is first formed, which then decomposes into CO·S. The first path consists of a single resistance, R_{10} while the second path consists of two resistances in series, R_8 and R_9, the overall resistance being $R_8 + R_9$. To compare these two parallel paths for this sub-mechanism under a broad range of conditions, these resistances as a function of temperature are shown in Figure 3-6. $R_8 + R_9$ is found to have a higher resistance than R_{10} in the entire temperature range, except around 400 K – 425 K, for the considered reaction conditions. Although, as can be seen from Figure 3-5, flux through s_8 and s_9 is only about 10% of the total flux, it is clear that deletion of s_8 and s_9 is not justifiable. To further investigate this, the effect of composition of terminal species on path resistance is investigated.

Figure 3-7, thus, compares the resistance of these two parallel paths to produce CO·S species in ER_3 at a temperature of 503 K as a function of methanol conversion. It can be seen that for conversion < 10%, direct decomposition of CHOH·S to CO·S is the dominant reaction pathway, while at higher conversion, CHOH·S first decomposes to COH·S and then to CO·S. A similar analysis at T = 553 K, shows FR_3 to be a dominant reaction pathway for conversions < 75% while at higher conversions, FR_2 is the dominant reaction pathway. Thus, both FR_2 and FR_3 are significant depending upon the reaction conditions, and the parallel pathways via s_{10} and, s_8 and s_9, are hence retained in the pruned mechanism.

Similar comparisons for ER_2, i.e., $s_4 + s_5 - s_7 - s_{10} + s_{11} = 0$, and ER_1, i.e., $s_2 + s_3 - s_6 - s_{11} = 0$, are shown in Figure 3-8 and Figure 3-9, respectively. Thus, pathways involving steps s_2, s_3, s_4, s_5 and s_{11} are unlikely, although from Figure 3-9 it seems that, the pathway proceeding via steps s_2 and s_3, i.e. initial O–H cleavage of adsorbed methanol begins to contribute more at temperatures above 525 K. However, the subsequent steps for the pathway via initial O–H cleavage of adsorbed methanol, say ($s_4 + s_5$) have much higher resistance than steps involved in the pathway via initial C–H cleavage of adsorbed methanol, say ($s_7 + s_{10}$). Thus, s_2, s_3, s_4, s_5 and s_{11} may be dropped from the mechanism.
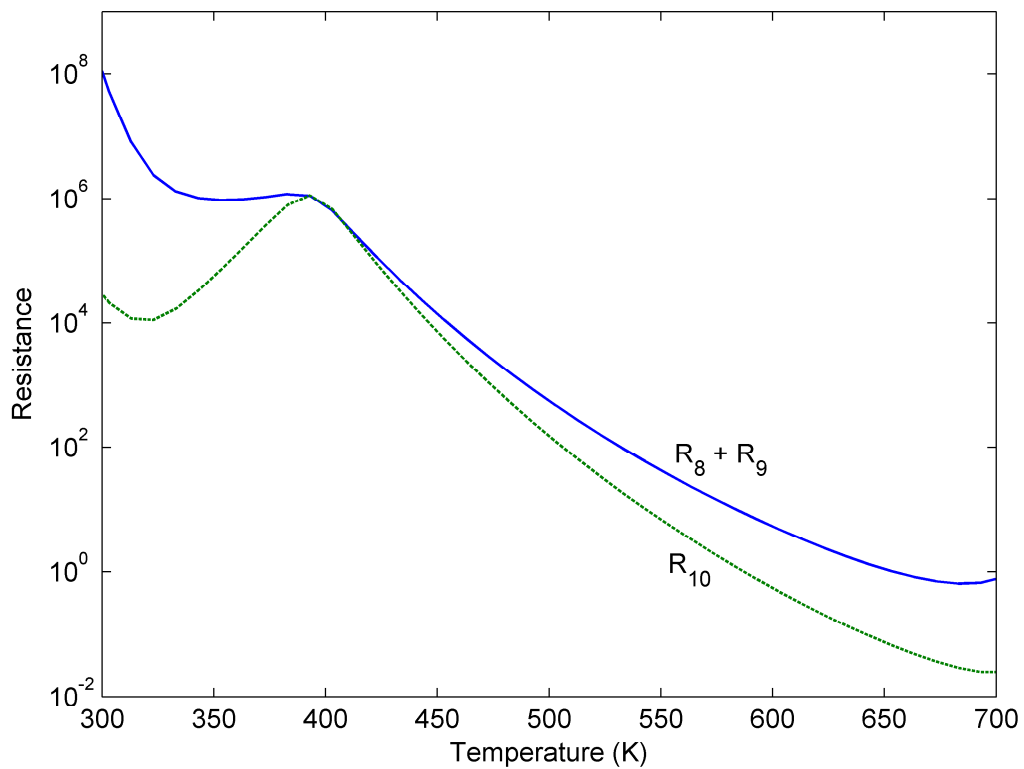
Figure 3-6: R_{10} vs $R_8 + R_9$, as a function of temperature for methanol decomposition reaction on Pt(111). [1% methanol in feed, 1 atm, PBR with $W/F = 100$ s]
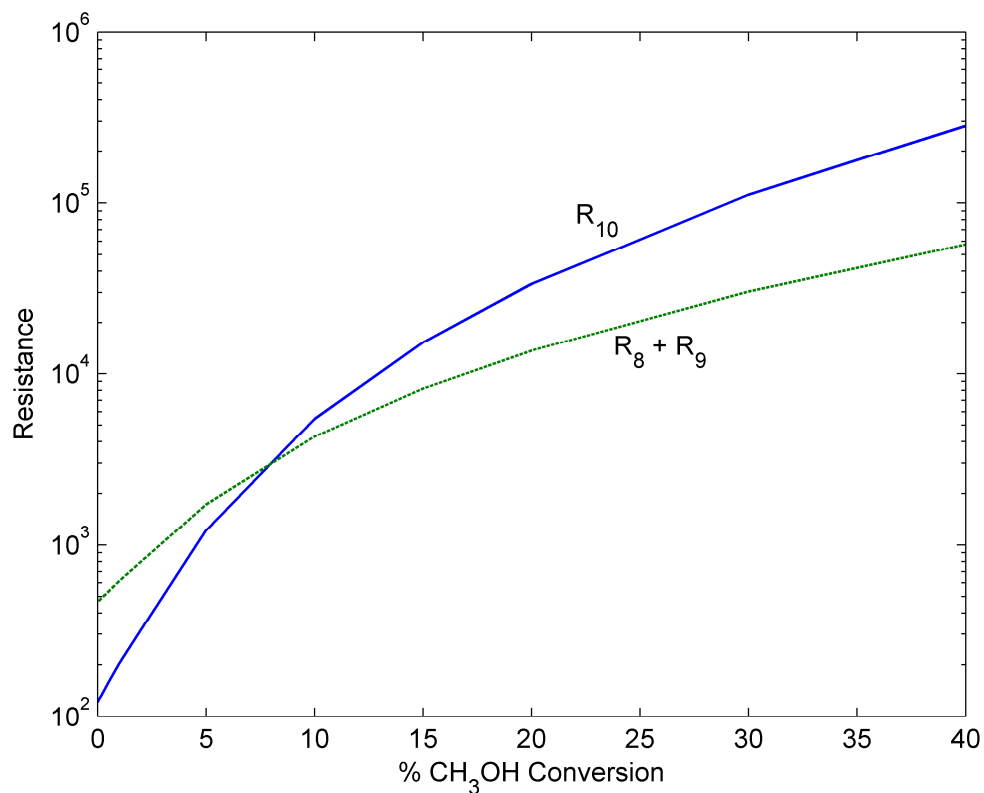
Figure 3-7: R_{10} vs $R_8 + R_9$, as a function of conversion at $T = 503$ K for methanol

decomposition reaction on Pt(111). [1% methanol in feed, 1 atm]
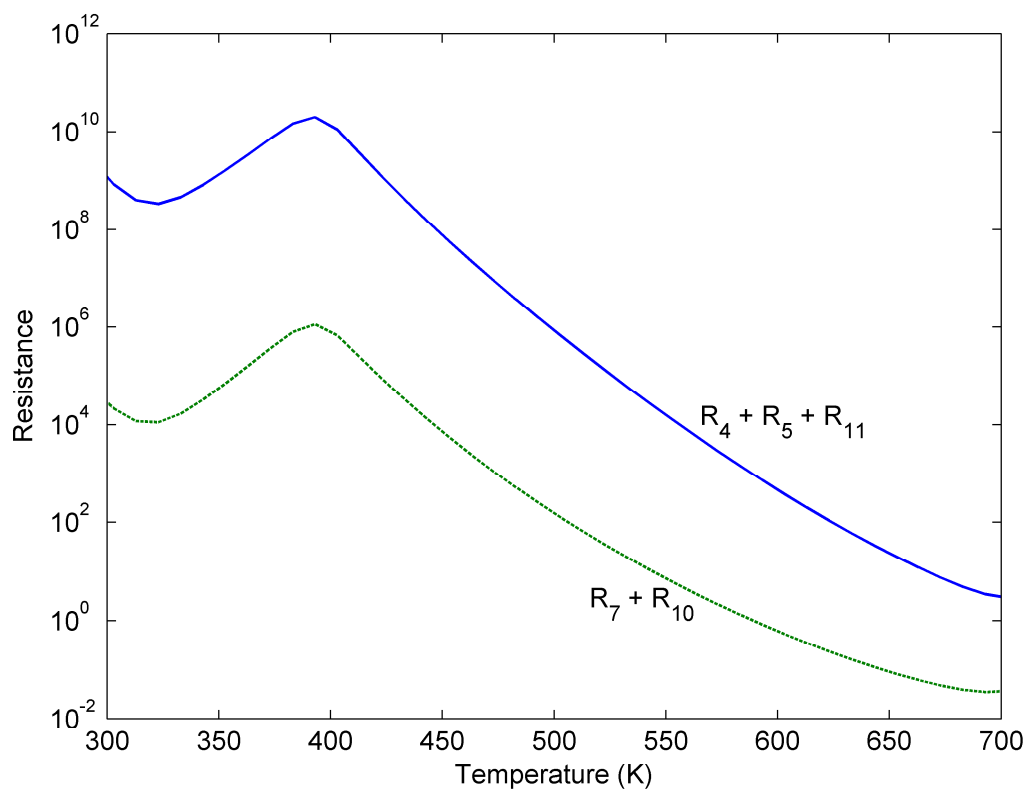
Figure 3-8: $R_4 + R_5 + R_{11}$ vs $R_7 + R_{10}$ as a function of temperature for methanol decomposition reaction on Pt(111). [1% methanol in feed, 1 atm, PBR with *W/F* = 100 s]
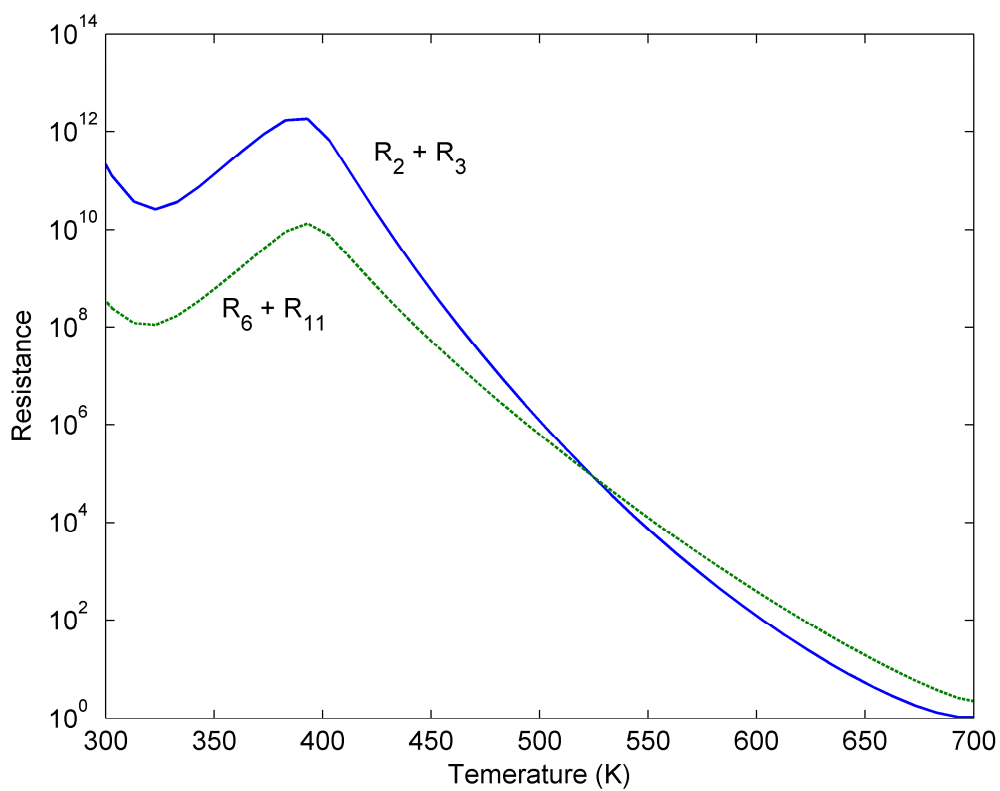
Figure 3-9: $R_2 + R_3$ vs $R_6 + R_{11}$, as a function of temperature for methanol decomposition reaction on Pt(111). [1% methanol in feed, 1 atm, PBR with $W/F = 100$ s]

A third way of network pruning is to evaluate the overall resistance of the network. Then, the FRs or steps whose resistance has no effect on the overall resistance of the network could be disregarded. The overall network resistance of the reaction circuit shown in Figure 3-5 was evaluated from individual elementary reaction step resistances, using conventional electrical circuit theory [66]. Mesh analysis was utilized to evaluate the resistance of the sub-network between nodes n_1 and n_5, the rest of the steps being in series as shown in Figure 3-10. Because of the complexity of the network, an explicit expression for the overall network resistance is cumbersome and is not provided here. The individual pathway resistance comprises of sequential branches between nodes n_i and n_j, the total resistance being given by Eq. (3.14) [53],

$$R_{k,n_i \to n_j} = \sum_{n_i \to n_j} \sigma_{k\rho}^2 R_\rho \qquad (3.14)$$

A comparison among the individual path resistances and the overall resistance of the entire network is shown in Figure 3-11. It is seen that the resistance along Path 3, i.e. FR_3 compares well with the overall resistance of the network, while the resistance of all other paths, with the exception of Path 2, is significantly higher, suggesting FR_3 and FR_2 as dominant parallel reaction pathways for methanol decomposition reaction on Pt(111) under the conditions considered in this study. Even if all of the FRs, excepting FR_3 and FR_2, are eliminated, the overall resistance of the network still remains largely unaffected, as is the rate of the overall reaction.

It must be noted that reaction steps s_2, s_3, s_4, s_5 and s_{11} are not involved in FR_3 and FR_2 (Table 3-4) and, consequently this analysis also justifies their elimination from the reaction mechanism, resulting into a 8 step simplified reaction network for methanol decomposition on Pt(111), as shown in Figure 3-12.
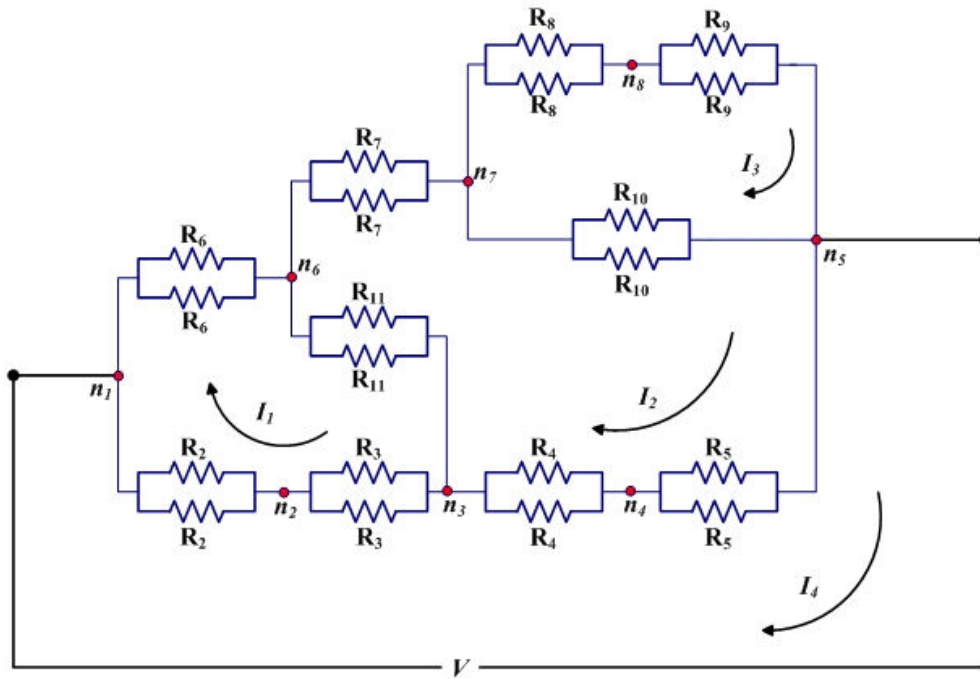
$$\begin{bmatrix} \left(\dfrac{R_6 + R_{11} + R_3 + R_2}{2}\right) & \dfrac{-R_{11}}{2} & 0 & \left(\dfrac{-R_3 - R_2}{2}\right) \\[2em] \dfrac{-R_{11}}{2} & \left(\dfrac{R_5 + R_4 + R_{11} + R_7 + R_{10}}{2}\right) & \dfrac{-R_{10}}{2} & \left(\dfrac{-R_5 - R_4}{2}\right) \\[2em] 0 & \dfrac{-R_{10}}{2} & \left(\dfrac{R_8 + R_9 + R_{10}}{2}\right) & 0 \\[2em] \left(\dfrac{-R_2 - R_3}{2}\right) & \left(\dfrac{-R_4 - R_5}{2}\right) & 0 & \left(\dfrac{R_2 + R_3 + R_4 + R_5}{2}\right) \end{bmatrix} \begin{bmatrix} I_1 \\ I_2 \\ I_3 \\ I_4 \end{bmatrix} = \begin{bmatrix} 0 \\ 0 \\ 0 \\ V \end{bmatrix}$$

$$R_{mesh} = \frac{V}{I_4}$$

$$R_{Network} = R_{mesh} + \frac{R_1}{2} + \frac{R_{12}}{2} + 2 \cdot R_{13}$$

Figure 3-10: Overall network resistance calculation using Mesh Analysis.
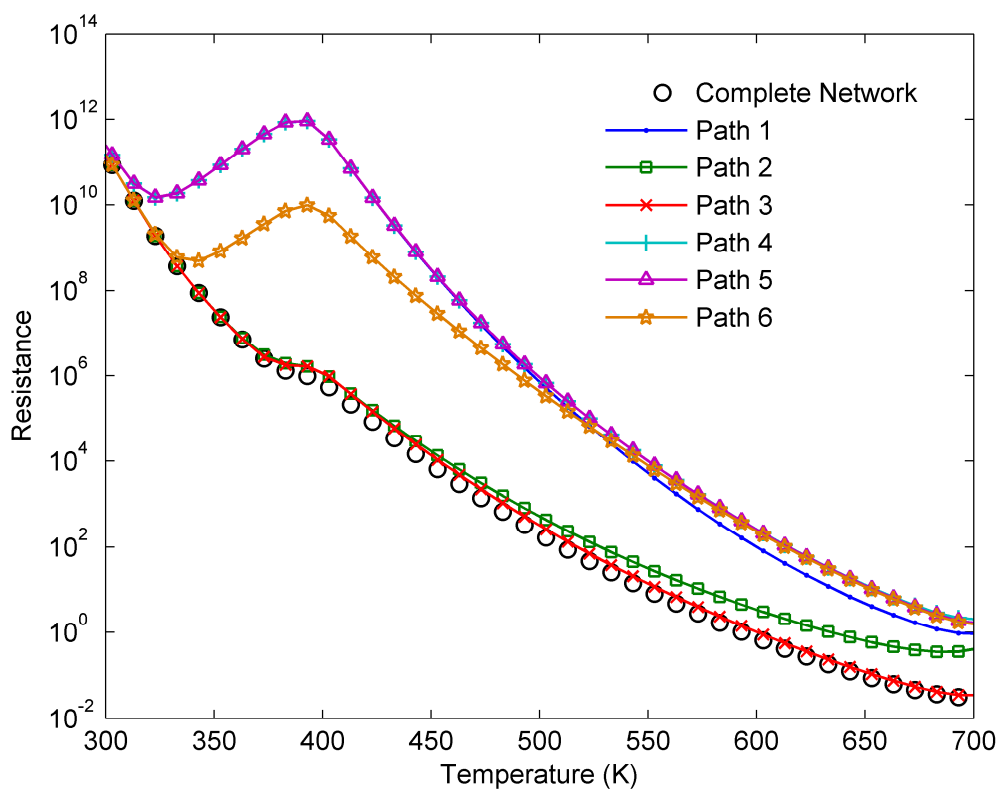
Figure 3-11: Comparison of the path resistance with the overall network resistance.

[1% methanol in feed, 1 atm, PBR with *W/F* = 100 s]

Finally, to further validate the elimination of steps s_2, s_3, s_4, s_5, and s_{11}, we checked the effect of neglecting these steps on the overall kinetics by comparing the simulated overall rate of the 13-step mechanism (Table 3-1) to the mechanism less s_2, s_3, s_4, s_5, and s_{11}. As seen in Figure 3-13, the elimination of steps s_2, s_3, s_4, s_5 and s_{11} (simplified 8 step mechanism) does not materially affect the overall kinetics.

Moreover, as can be seen from Figure 3-13, FR_2 does contribute to the net rate non-negligibly, and must be retained in the reduced network. It is noteworthy that all of the eliminated steps are based on the initial O–H bond scission pathway. It is, thus, clear that this is not a significant pathway in methanol decomposition on Pt(111).

This pruned network shows that the initial dehydrogenation step for methanol is via step s_6, i.e., via initial C–H cleavage of adsorbed methanol. The O–H cleavage pathway plays little or no role in the overall methanol decomposition on Pt(111), which agrees with the experimental and theoretical findings of several researchers. To the authors' knowledge, no direct spectroscopic evidence for methoxide species on clean Pt(111) has been reported in the literature except for Peck et al. [67], who detected methoxide species on clean Pt(111) by using a methyl nitrite precursor. Quantum chemical calculations performed over platinum clusters also suggest that methanol prefers to dehydrogenate by the activation of its C–H rather than O–H bond [47, 48]. Franaszczuk et al. [68] have experimentally concluded the first step to be the C–H scission of methanol on platinum clusters in electrochemical environment. Recently, Desai et al. [63], based on nonlocal gradient corrected periodic DFT calculations, have also reported the methanol decomposition pathway involving an initial activation of C–H bond to be thermodynamically more favorable than O–H bond activation on Pt(111). The model predictions by Greeley and Mavrikakis [42] based on DFT analysis suggest that the adsorbed hydroxymethyl, product of the C–H bond activation is ~0.8 eV more stable than the adsorbed methoxy, product of the O–H bond activation on Pt(111).
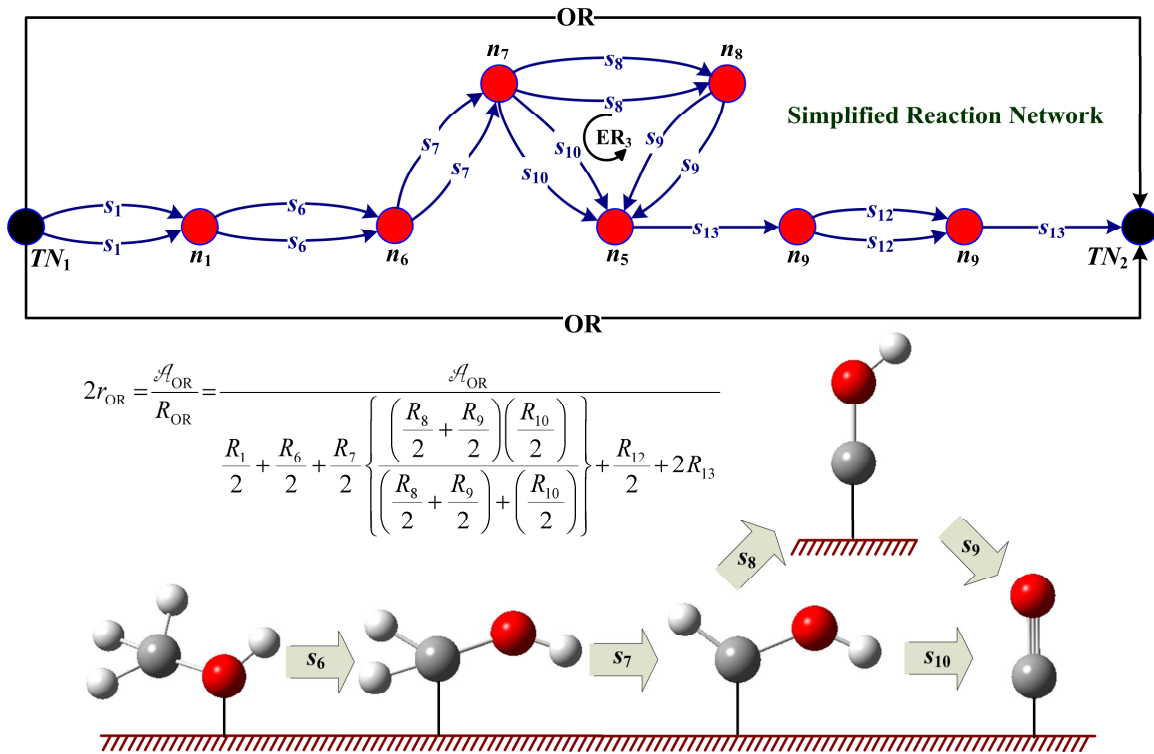
Figure 3-12: Simplified reaction network and schematic of the dominant reaction pathways for methanol decomposition reaction on Pt(111).
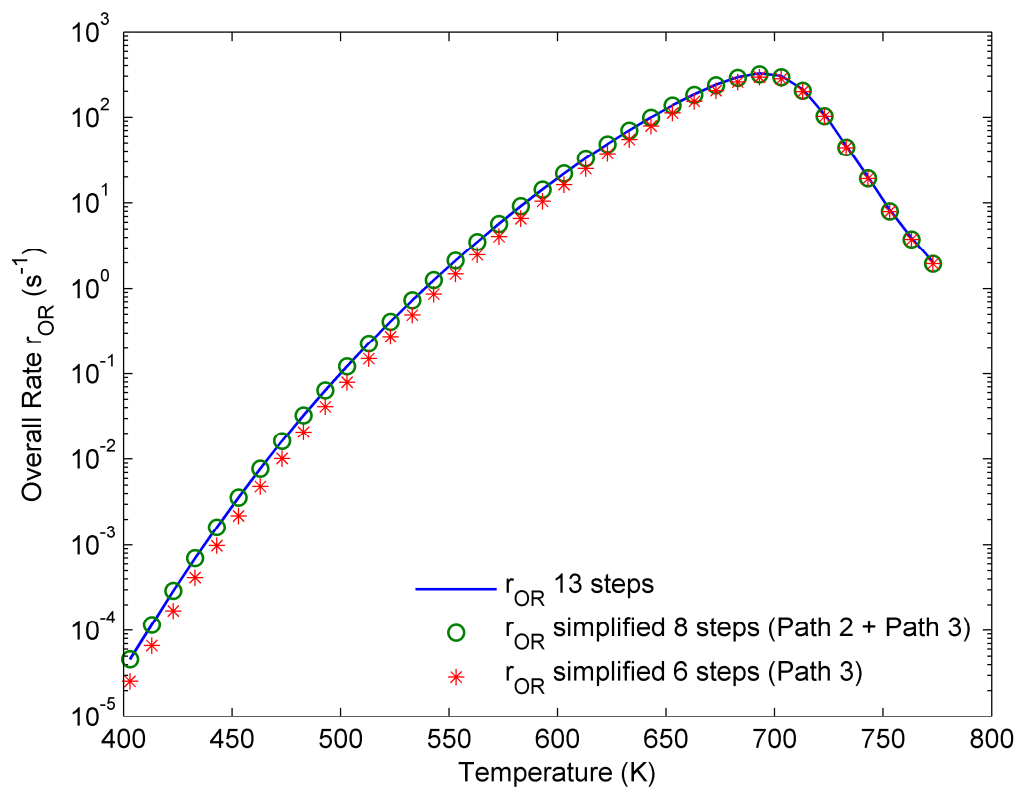
Figure 3-13: Comparison of overall mechanism kinetics with and without s_2, s_3, s_4, s_5 and s_{11}. [1% methanol in feed, 1 atm, PBR with $W/F = 100$ s]
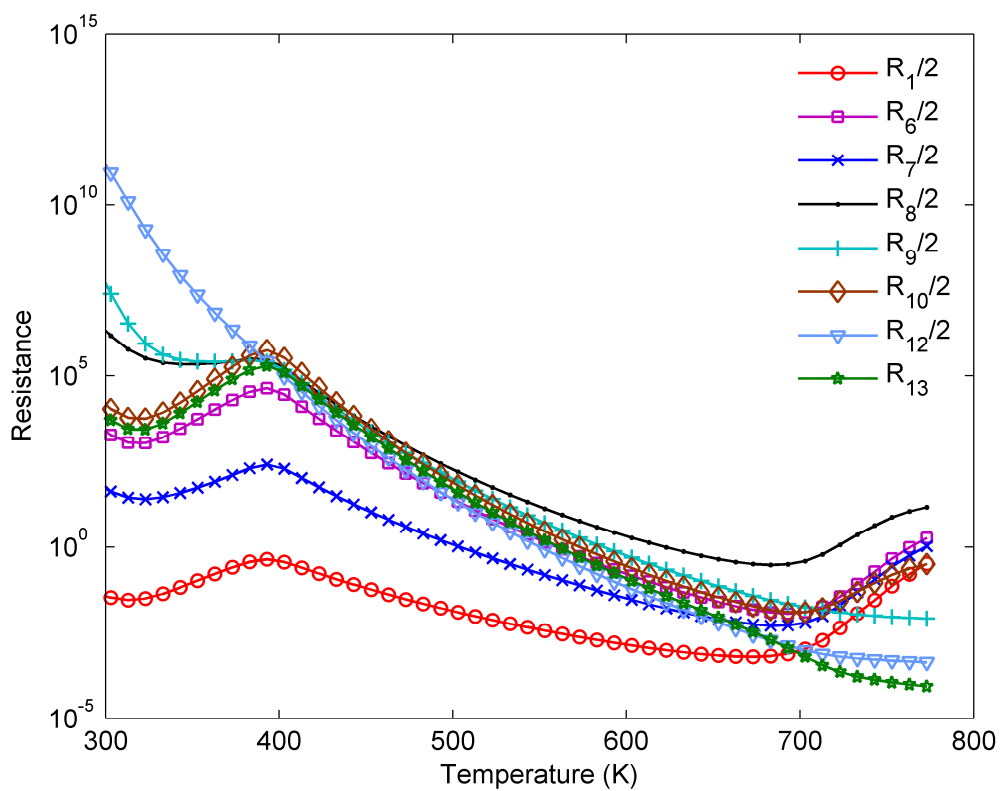
Figure 3-14: Determination of RLS by comparing the series resistances in the reduced RR network. [1% methanol in feed, 1 atm, PBR with *W/F* = 100 s]

It must be noted that reaction steps s_2, s_3, s_4, s_5 and s_{11} are not involved in FR_3 and FR_2 (Table 3-4) and, consequently this analysis also justifies their elimination from the reaction mechanism, resulting into a 8 step simplified reaction network for methanol decomposition on Pt(111), as shown in Figure 3-12.

Furthermore, Gokhale et al. [52] also show that the net rate of step s_6 is higher than that of step s_2, with a similar conclusion. The experimental findings by Kandoi et al. [51] coupled with microkinetic modeling using DFT, suggest FR_3 to be a dominant reaction pathway for methanol decomposition on Pt(111) which is in accord with our findings based on our graph-theoretic approach, although we find that in addition FR_2 must be retained.

Finally, RLS(s) may be identified by comparing the series step resistances, wherein the step with the highest resistance would govern the reaction kinetics and is the RLS. Figure 3-5 indicates that s_8, s_9 and s_{10} are the RLSs under the reaction conditions of Figure 3-5. To further investigate this, Figure 3-14 evaluates the resistance of the reaction steps at other temperatures. It is seen that, in the temperature range of $300 - 400$ K, step s_{12} is the RLS. In the temperature range, $400 - 500$ K, steps s_8, s_9 and s_{10}, are the slowest. While at temperature above 500 K, step s_8 is the RLS. Thus, it is clear that it is not possible to further reduce this mechanism down to a single RLS under all conditions.

3.6 Conclusions

The RR graph analysis has been applied for detailed study of catalytic decomposition of methanol on Pt(111). The analysis shows two dominant reaction pathways, FR_3 and FR_2 depending upon the reaction conditions, both with an initial C–H bond activation of methanol over Pt(111). Thus, the reaction proceeds exclusively via an initial dehydrogenation of the C–H bond rather than through the O–H bond of methanol.

Methanol decomposition is an important reaction taking place at the anode of DMFC. The analysis can be easily extended to methanol electro-oxidation by assuming that the mechanism largely remains same. In fact, Janik et al. [69] have shown that a similar dual-path mechanism exists for methanol decomposition in an electrochemical environment using *ab initio* quantum chemical methods. The authors [69] provide an approach to

theoretically calculate potential dependent activation energies. However, one could well assume, the activation energies and pre-exponential factors to be similar for both catalytic and electrocatalytic systems. The only difference being for electrochemical counterparts of the catalytic reactions, the reaction rate would be affected by the electrode potential described by the Butler-Volmer equation. The said approach coupled with RR graph analysis can possibly provide a detailed portrayal of the electrochemical reaction system at the DMFC anode.

3.7 References

[1]   G. Jacobs, B.H. Davis, Applied Catalysis A: General. 285 (2005) 49.

[2]   B.A. Peppley, J.C. Amphlett, L.M. Kearns, R.F. Mann, Applied Catalysis A: General. 179 (1999) 49.

[3]   R.O. Idem, N.N. Bakhshi, Chemical Engineering Science. 51 (1996) 3708.

[4]   J. Nerlov, S. Sckerl, J. Wambach, I. Chorkendorff, Applied Catalysis A: General. 191 (2000) 109.

[5]   S. Sakong, C. Sendner, A. Gro, Journal of Molecular Structure: THEOCHEM. 771 (2006) 122.

[6]   C. Sendner, S. Sakong, A. Gro, Surface Science. 600 (2006) 3265.

[7]   I. Eswaramoorthi, V. Sundaramurthy, A.K. Dalai, Applied Catalysis A: General. 313 (2006) 34.

[8]   S. Sriramulu, T.D. Jarvi, E.M. Stuve, Journal of Electroanalytical Chemistry. 467 (1999) 142.

[9]   D.S. Corrigan, M.J. Weaver, Journal of Electroanalytical Chemistry. 241 (1988) 162.

[10] J.S. Huberty, R.J. Madix, Surface Science. 360 (1996) 144.

[11] R. Zenobi, J. Xu, J. T. Yates Jr., B. N. J. Persson, A.I. Volotkin, Chem. Phys. Lett. 208 (1993) 414.

[12] J. P. Camplin, E.M. McCash, Surf. Sci. 360 (1996) 229.

[13] M. A. Karolewski, R.G. Cavell, Surf. Sci. 344 (1995) 74.

[14] S. L. Silva, A. A. Patel, T. M. Pham, F.M. Leibsle, Surf. Sci. 441 (1999) 351.

[15] A. F. Carley, P. R. Davies, G. G. Mariotti, S. Read, Surf. Sci. 364 (1996) L525.

[16] S. L. Silva, R. M. Lemor, F.M. Leibsle, Surf. Sci. 421 (1999) 135.

[17] P. Hofmann, K.-M. Schindler, S. Bao, V. Fritzche, D. E. Ricken, A. M. Bradshaw, D.P. Woodruff, Surf. Sci. 304 (1994) 74.

[18] M. Witko, K. Hermann, D. Ricken, W. Stenzel, H. Conrad, A.M. Bradshaw, Chem. Phys. 177 (1993) 363.

[19] J. Greeley, M. Mavrikakis, Journal of Catalysis. 208 (2002) 291-300.

[20] J. R. B. Gomes , J.A.N.F. Gomes, Surf. Sci. 471 (2001) 59-70.

[21] Q. Dai, A.J. Gellman, Surf. Sci. 102 (1991) 271.

[22] W. S. Sim, P. Gardner, D.A. King, J. Phys. Chem. 99 (1995) 16002.

[23] N. Hartmann, F. Esch, R. Imbihl, Surf. Sci. 297 (1993) 175.

[24] J.-J. Chen, Z.-C. Jiang, Y. Zhou, B. R. Chakraborty, N. Wirnograd, Surf. Sci. 328 (1995) 248.

[25] N. Kizhakevarium, E.M. Stuve, Surf. Sci. 286 (1993) 246.

[26] J. Wang, M. A. de Angelis, D. Zaikos, M. Setiadi, R.I. Masel, Surf. Sci. 318 (1994) 307.

[27] M. Endo, T. Matsumoto, J. Kubota, K. Domen, C. Hirose, Surf. Sci. 441 (1999) L931.

[28] M. K. Weldon, P. Uvdal, C. M. Friend, J.G. Serafin, J. Chem. Phys. 103 (1995) 5075.

[29] B.A. Sexton, Surf. Sci. 102 (1981) 271.

[30] L. Diekhohner, D. A. Butler, A. Baurichter, A.C. Luntz, Surf. Sci. 409 (1998) 384-391.

[31] J. W. Peck, D. I. Mahon, D. E. Beck, B. Bansenaur, B.E. Koel, Surf. Sci. 410 (1998).

[32] A. V. de Carvalho, M. C. Asensio, D.P. Woodruff, Surface Science. 273 (1992) 381-384.

[33] K. Amemiya, Y. Kitajima, Y. Yonamoto, S. Terada, H. Tsukabayashi, T. Yokoyama, T. Ohta, Physical Review B. 59 (1999) 2307-2312.

[34] D. R. Mullins, M. D. Robbins, J. Zhou, Surface Science. 600 (2006) 1547-1558.

[35] X.H. Xia, T. Iwasita, F. Ge, W. Vielstich, Electrochim. Acta. 41 (1996) 711.

[36] Y.X. Chen, A. Miki, S. Ye, H. Sakai, M. Osawa, J. Am. Chem. Soc. 125 (2003) 3680.

[37] M. I. S. Lopes, B. Beden, F. Hahn, J. M. Leger, C. Lamy, J. Electroanal. Chem. 313 (1991) 323.

[38] St.G. Christoskova, M. Stoyanova, N. Danova, O. Argirov, Applied Catalysis A: General. 173 (1998) 101-105.

[39] S. Wilhelm, T. Iwasita, W. Vielstich, J. Electroanal. Chem. 238 (1987) 383.

[40] T. Iwasita, W. Vielstich, E. Santos, J. Electroanal. Chem. 229 (1987) 367.

[41] W. T. Lee, F. Thomas, R.I. Masel, Surf. Sci. 418 (1998) 479.

[42] J. Greeley, M. Mavrikakis, J. Am. Chem. Soc. 126 (2004) 3910-3919.

[43] M. Mavrikakis, M.A. Barteau, J. Mol. Cat. A. 131 (1998) 135-147.

[44] K. Franaszczuk, E. Herrero, P. Zelenay, A. Wieckowski, J. Wang, R.I. Masel, J. Phys. Chem. 96 (1992) 8509-8516.

[45] S. K. Desai, M. Neurock, K. Kourtakis, J. Phys. Chem. B. 106 (2002) 2559-2568.

[46] V.S. Bagotzki, Y.B. Vassiliev, O.A. Khazova, J. Electroanal. Chem. 81 (1977) 229-238.

[47] J. Kua, W.A. Goddard, III., J. Am. Chem. Soc. 121 (1999) 10928-10941.

[48] Y. Ishikawa, M. Liao, C. Cabrera, Surf. Sci. 463 (2000) 66-80.

[49] D. Cao, G.-Q. Lu, A. Wieckowski, S.A. Wasileski, M. Neurock, J. Phys. Chem. B. 109 (2005) 11622-11633.

[50] J. Greeley, M. Mavrikakis, J. Am. Chem. Soc. 124 (2002) 7193-7201.

[51] S. Kandoi, J. Greeley, M.A. Sanchez-Castillo, S.T. Evans, A.A. Gokhale, J.A. Dumesic, M. Mavrikakis, Topics in Catal. 37 (2006) 17-28.

[52] A.A. Gokhale, S. Kandoi, J.P. Greeley, M. Mavrikakis, J.A. Dumesic, Chem. Eng. Sci. 59 (2004) 4679-4691.

[53] I. Fishtik, C.A. Callaghan, R. Datta, J. Phys. Chem. B. 108 (2004) 5671-5682.

[54] I. Fishtik, C.A. Callaghan, R. Datta, J. Phys. Chem. B. 108 (2004) 5683-5697.

[55] I. Fishtik, C.A. Callaghan, R. Datta, J. Phys. Chem. B. 109 (2005) 2710-2722.

[56] C.R.F. Lund, Ind. Eng. Chem. Res. 35 (1996) 2531-2538.

[57] L.V. Gurvich, I.V. Veyts, C.B. Alcock, Thermodynamic Properties of Individual Substances, 4th ed., Hemisphere Pub. Co., New York, 1989.

[58] J.D. Cox, D.D. Wagman, V.A. Medvedev, CODATA Key Values for Thermodynamics, Hemisphere, New York, 1989.

[59] P.J. Linstrom, W.G. Mallard, Gaithersburg MD, 20899, National Institute of Standards and Technology, June 2005, (http://webbook.nist.gov).

[60] Gaussian 03, Revision C.02, M. J. Frisch, G. W. Trucks, H. B. Schlegel, G. E. Scuseria, M. A. Robb, J. R. Cheeseman, J. J. A. Montgomery, T. Vreven, K. N. Kudin, J. C. Burant, J. M. Millam, S. S. Iyengar, J. Tomasi, V. Barone, B. Mennucci, M. Cossi, G. Scalmani, N. Rega, G. A. Petersson, H. Nakatsuji, M. Hada, M. Ehara, K. Toyota, R. Fukuda, J. Hasegawa, M. Ishida, T. Nakajima, Y. Honda, O. Kitao, H. Nakai, M. Klene, X. Li, J. E. Knox, H. P. Hratchian, J. B. Cross, V. Bakken, C. Adamo, J. Jaramillo, R. Gomperts, R. E. Stratmann, O. Yazyev, A. J. Austin, R. Cammi, C. Pomelli, J. W. Ochterski, P. Y. Ayala, K. Morokuma, G. A. Voth, P. Salvador, J. J. Dannenberg, V. G. Zakrzewski, S. Dapprich, A. D. Daniels, M. C. Strain, O. Farkas, D. K. Malick, A. D. Rabuck, K. Raghavachari, J. B. Foresman, J. V. Ortiz, Q. Cui, A. G. Baboul, S. Clifford, J. Cioslowski, B. B. Stefanov, G. Liu, A. Liashenko, P. Piskorz, I. Komaromi, R. L. Martin, D. J. Fox, T. Keith, M. A. Al-Laham, C. Y. Peng, A. Nanayakkara, M. Challacombe, P. M. W. Gill, B. Johnson, W. Chen, M. W. Wong, C. Gonzalez, J.A. Pople, Wallingford CT, 2004.

[61] E. Shustorovich, H. Sellers, Surf. Sci. Reports. 31 (1998) 1-119.

[62] J. Happel, P.H. Sellers, Adv. Catal. 32 (1983) 273-323.

[63] S.K. Desai, M. Neurock, K. Kourtakis, J. Phys. Chem. B. 106 (2002) 2559-2568.

[64] V.S. Bagotzky, Y.B. Vassiliev, O.A. Khazova, J. Electroanal. Chem. 81 (1977) 229-238.

[65] Multisim v. 9, Electronics Workbench, Prentice Hall Publishing.

[66] L.O. Chua, C.A. Desoer, E.S. Kuh, Linear and Nonlinear Circuits, Mc-Graw Hill, New York, 1987.

[67] J.W. Peck, D.I. Mahon, D.E. Beck, B. Bansenaur, B.E. Koel, Surf. Sci. 410 (1998).

[68] K. Franaszczuk, E. Herrero, P. Zelenay, A. Wieckowski, J. Wang, R.I. Masel, J. Phys. Chem. 96 (1992) 8509-8516.

[69] M.J. Janik, C.D. Taylor, M. Neurock, Top. Catal. 46 (2007) 306–319.

Chapter IV

A Reaction Route Network Analysis of Water Gas Shift Catalysis on Pt(111)

After more than a century of intensive research, the mechanism of the water gas shift (WGS) reaction continues to be a focus of *ab initio* and microkinetic modeling. Moreover, new catalysts are sought for the WGS reaction in connection with distributed hydrogen generation. This quest would be aided by improved fundamental understanding of WGS catalysis. We utilize here, the systematic theoretical approach of Reaction Route (RR) Graph, for developing a comprehensive understanding of the WGS reaction based on a detailed molecular mechanism with *a priori* kinetics. Furthermore, the problem of thermodynamic consistency of the reaction kinetics may also naturally be treated in terms of RR graphs in a simple intuitive manner.

We consider literature reported WGS mechanism along with predicted kinetics of the elementary steps in this chapter. These are next used for a graph-theoretic generation of a reaction network that depicts the overall mechanism as well as the multitude of reaction routes (RRs). The flux analysis afforded by the RR graph allows the dominant reaction pathways and the rate-limiting steps to be identified in a transparent and perceptive manner. A highly simplified rate expression is next derived based on the alternate electrical circuitry.

4.1 Introduction

Recent advances in *ab initio* chemistry have made it possible to develop a more complete theoretical understanding of the elementary molecular steps in heterogeneous catalysis, along with reasonably accurate prediction of reaction energetics. One such example is provided in Figure 4-1, where the authors investigate the role of step sites in water-gas-shift (WGS) reaction by using a stepped surface Cu(321) and periodic DFT within a supercell approach [1]. The next logical step is to utilize these calculations to develop a comprehensive picture of the reaction mechanism and to elucidate the myriad parallel pathways and dominant reaction routes and steps. This step is crucial in translating our improved understanding into improved catalysts. The Reaction Route graph approach described in detail in chapter II is such a network tool that can translate the information obtained from quantum chemical software into useful information, based on which many important details can be extracted in a logical manner.

The performance of the low temperature proton-exchange membrane (PEM) fuel cells is limited by CO poisoning of the Pt-based anode catalyst. Thus, there is a need for developing an efficient and compact reforming process for distributed generation of hydrogen that is devoid of CO. The WGS reaction is an essential part of this. Although a well established industrial process, alternate catalysts are sought for distributed hydrogen generation because of different operating conditions, design constraints, and safety concerns [2]. It is, thus, useful to develop a deeper fundamental understanding of the molecular steps involved in the WGS reaction, so that a more systematic and theory-guided approach may be used to select new catalysts.

Because of the industrial significance of the WGS reaction, numerous investigations have been made into its reaction mechanism and kinetics over common industrial catalysts (i.e., copper, and iron) [3-9]. These investigations suggest that the WGS reaction mainly occurs via four mechanisms: 1) the so-called formate mechanism [3-7], 2) the redox mechanism [4, 5, 8-13], 3) the associative mechanism [14-16], and, 4) the carbonate mechanism [12, 13, 17-19]. These parallel mechanisms are pictorially depicted in Figure 4-2.
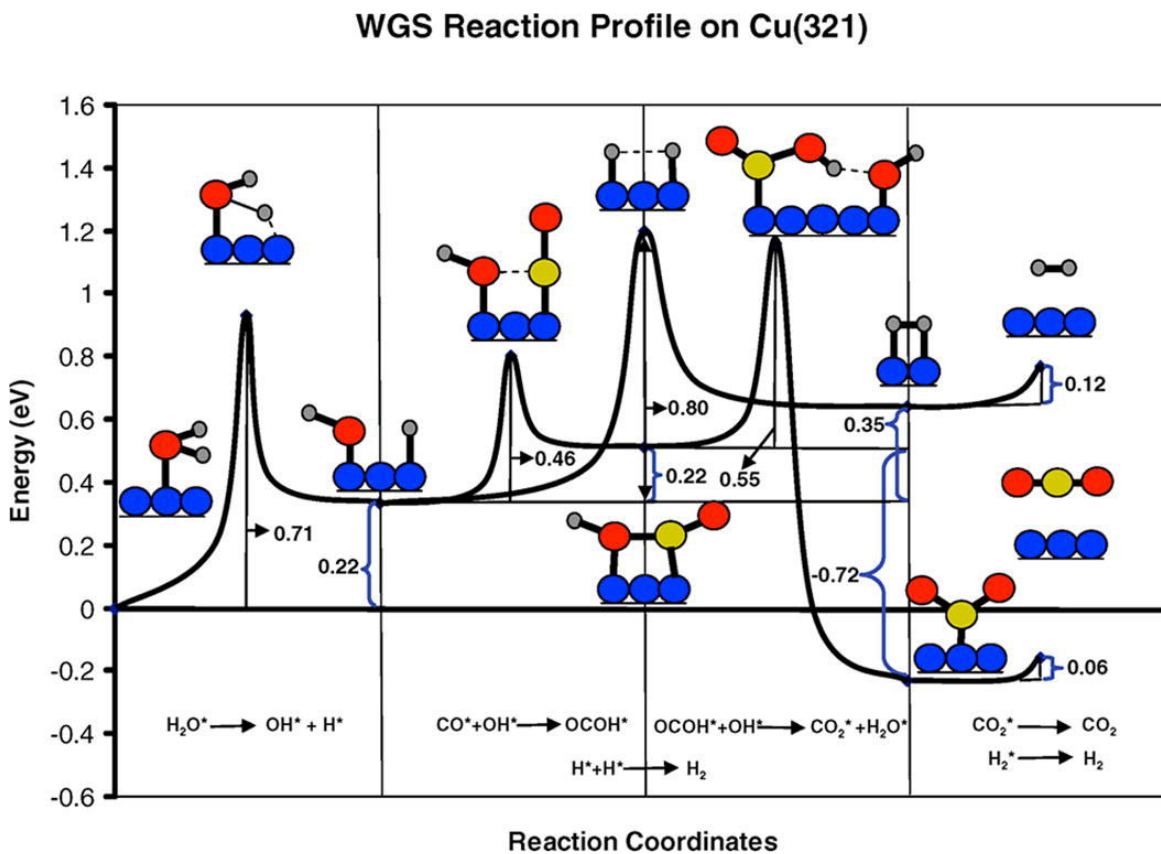
Figure 4-1: Reaction profile for WGS mechanism on Cu(321) with DFT predicted energetics [1].
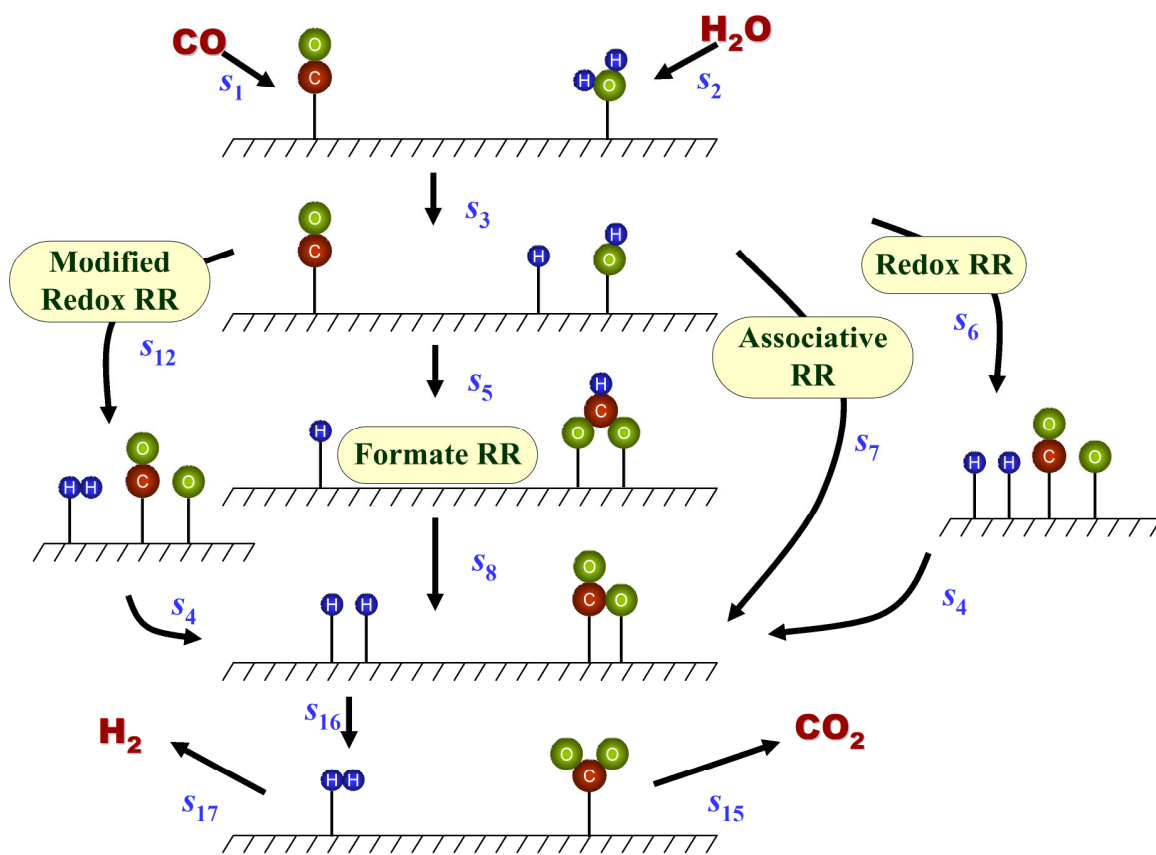
Figure 4-2: Schematic of possible mechanisms of the WGS reaction

Campbell and Daube [4] explored the water-gas-shift reaction in terms of a formate mechanism. Investigating the WGS reaction on a single crystal copper catalyst, their surface analysis by AES indicated low levels of carbon. The dissociation of H_2O into a surface hydroxyl was identified as the rate-limiting step, the surface hydroxyl then combining with surface CO to form surface formate. It was noted that the presence of adsorbed oxygen could significantly enhance the WGS reaction via: $H_2O \cdot S + O \cdot S \leftrightarrows OH \cdot S + OH \cdot S$, where S is a surface site.

Nakamura, et al. [8] suggested the occurrence of the OH disproportionation reaction, $2OH \cdot S \leftrightarrows O \cdot S + H_2O \cdot S$, the surface oxygen then reacting with CO(g) to produce CO_2(g). This conclusion was based on studies where the group was unable to produce measurable amounts of surface formate, but the OH disproportionation reaction to adsorbed water and adsorbed atomic oxygen occurred rapidly, thus resulting in the redox mechanism. Based on the work of Nakamura, et al. [8] and Campbell and Daube [4], Ovesen, et al. [5, 9] considered an 8-step mechanism, but excluded the formate species. The authors concluded that H_2O dissociation and the oxidation of CO were both plausible rate-limiting steps. The carbonate species [18, 19] was also neglected by these authors, because attempted synthesis of carbonate via exposure of an oxygen-covered Cu surface did not produce any carbonate [5]. Millar, et al. [17] considered a carbonate mechanism based on experimental IR spectroscopy results which showed a band corresponding to "symmetrical" carbonate ions on the catalyst surface. Lund et al. [18, 19] have also investigated the WGS reaction via the carbonate mechanism.

Tserpe and Waugh [12] and Waugh [13] examined the redox microkinetic mechanism vis-à-vis experimental data for the reverse WGS reaction. They utilized theoretical activation energies and pre-exponential factors. Waugh [13], thus, suggested that the forward WGS reaction proceeds by water adsorbing on the copper catalyst and then decomposing to give gas phase H_2 and adsorbed atomic oxygen. CO also adsorbs on to the surface and proceeds to remove the adsorbed atomic oxygen via a Langmuir-Hinshelwood mechanism yielding adsorbed CO_2 and ultimately CO_2(g). In both the forward and reverse WGS reaction mechanisms, the pre-exponential factors of the desorption reactions were assumed to have the value of 10^{13} s^{-1}. The microkinetic model

showed a good agreement with the experimental data. However, the activation energy for the adsorption of hydrogen (as atoms) on Cu was assumed to be zero. Subsequent work by Waugh has shown that the chemisorption of hydrogen on Cu is, infact, activated [13]. As a consequence, the modeling results were found to overpredict the hydrogen surface coverage.

The 9-step redox mechanism of Nakamura et al. [8] was also considered by Schumacher et al. [10], who predicted trends in low-temperature WGS activity via microkinetics on transition metals based on DFT energetics. The experimental trend found by Grenoble et al. [20] at 300°C on an aluminum oxide support is Cu > Re > Co > Ru > Ni > Pt > Os > Au > Fe > Pd > Rh > Ir. Based on chemisorption energy calculations on step sites by Nørskov and co-workers [21], Schumacher et al. [10] suggested the WGS activity trend as Cu > Co > Ru > Fe > Ni > Rh > Au > Ir > Pd > Pt. On the other hand, utilizing the chemisorption energies on terraces, the WGS activity trend was predicted as Cu > Ni > Pt > Rh > Ru > Au > Ir > Pd. Thus, in the former case the rates for Fe and Rh are overestimated, and the rate over Pt is underestimated, while in the latter, the rate over Rh is overestimated and that over Ru is underestimated. Although the order of activity of the metals is predicted well, the model fails to quantitatively agree with experimental data. Zeigarnik et al. [22] have also predicted the WGS activity in the order Cu > Ni > Fe > Pt, Pd > Ag > Au, where the rate for Pt seems to be underestimated, when compared with the experimentally observed trend. The experimental findings by Wheeler et al. [23] indicate the effectiveness of the metal catalysts follows the order Ni > Ru > Rh > Pt > Pd.

A complexity on many of these catalysts is that methanation is unavoidable under WGS conditions. The order in which metals promote methanation [23] was shown to be Ru > Rh > Ni > Pt > Pd. Thus, both experimental and theoretical trends must account for this. Further, many supports such as CeO_2 [23-27] have a substantial effect on WGS activity. Pt was shown to have pronounced effect of ceria addition by Wheeler et al. [23] and ceria supported catalyst showed the following trend, Ni ~ Ru > Pt > Rh > Pd. It is worth nothing that Pt/ceria was found to more effective than Rh/ceria, whereas Rh was more effective than Pt metal.

Mhadeshwar and Vlachos [28] considered the kinetics of the WGS reaction on a Pt catalyst as a part of a multiple overall reaction. A 23-step mechanism was proposed to describe simultaneous CO oxidation, H_2 oxidation, WGS reaction, as well as the preferential oxidation (PrOx) of CO. This was based on their previous work [29], in which the CO-H_2 coupling was considered and implied that the reactions may proceed through a carboxyl (COOH·S) intermediate. Earlier studies of the WGS reaction by our group [16] suggested a 13-step mechanism for the WGS reaction. The analysis was performed for a Cu(111) catalyst and indicated that three different mechanisms dominated the kinetics of the WGS reaction. This mechanism was further expanded with the addition of two more steps [14]. The analysis revealed an alternative to the conventional redox reaction mechanism, namely, the modified redox mechanism, which was shown to dominate the kinetics at higher temperatures in place of the conventional redox mechanism. Recently, we [30] considered a comprehensive set of 19 plausible elementary reaction steps proposed in the literature on Cu(111) along with detailed kinetics based on pre-exponential factors and energetic parameters calculated via the UBI-QEP method. A subsequent systematic pruning of the network identified three dominant routes, along with rate-limiting and quasi-equilibrated elementary reaction steps, eventually yielding a 11-step simplified mechanism from which a predictive rate expression was derived. This was found to be in good agreement not only with the complete microkinetic mechanism, but also with our own experimental data. The analysis on Cu(111) surface revealed that associative route and formate route are dominant at temperatures < 550 K, while the modified redox mechanism dominants at higher temperatures. The rate limiting step for the associative mechanism was identified as the formation of adsorbed CO_2, while that for formate route was the formation of adsorbed HCOO species from adsorbed CO and OH species. The rate-limiting step for the modified redox pathway was formation of adsorbed CO_2 from adsorbed CO and O species. Fajín et al. [1] recently studied the WGS mechanism on stepped Cu surface and showed that the presence of step sites decreases the activation energy of the rate-limiting steps, compared to a perfect Cu(111) surface.

Very recently, Gokhale et al. [31] and Grabow et al. [32] suggested an associative mechanism through a carboxyl intermediate based on periodic, self-consistent density

functional theory (DFT-GGA) calculations on Cu(111) and Pt(111), respectively. The associative mechanism via formate intermediate was shown to very minimally contribute to the overall reaction rate. Direct decomposition of carboxyl species was predicted as the rate-limiting step. Liu et al. [33] on the other hand, based on their DFT calculations using DMOL code, suggested that the redox and the associative route via carboxyl intermediate could co-exist and the dominant reaction pathway depends on the system under consideration, typically the nature of the catalytic surface. However, the authors predicted water dissociation as the rate-limiting step, which remains the same for all the systems investigated. The experimental study by Meunier et al. [34-36] based on DRIFTS and isotopic labeling suggested the IR-observable formate species to be only a minor reaction intermediates on Pt and Au based catalysts, supporting the claim the formate route could only be a minor contributor to the overall reaction rate. Further, the authors also suggested that these formate species should not be labeled as "spectator" species since they do lead to some reaction product, although at relatively lower rate as compared to the dominant route.

In this chapter, we consider the 17-step mechanism and the DFT-GGA energetics provided by Grabow et al. [32] on Pt(111) for a detailed network analysis by utilizing the RR graph approach and its electrical analogy.

4.2 Reaction Mechanism and Kinetics

The $p = 17$ step mechanism, comprising of the redox and carboxyl-mediated associative pathways, considered here is summarized in Table 4-1. Grabow et al. [32] performed periodic, self-consistent density functional theory (DFT-GGA) using DACAPO total energy calculation code, based on which a microkinetic model was formulated. The authors assumed a pre-exponential factor of 10^{13} sec^{-1} for spontaneous reactions (s_{12}, s_{13}, s_{14}, s_{15} and s_{17}) where no transition state could be identified. Finally, the authors [32] also employed an additional fitting parameter to describe the fraction of rotational and vibrational entropy of the gas-phase molecules that is retained by the adsorbed species. Lastly, the activation energies utilized in the microkinetic model were obtained from activation energy barrier and energy change derived from DFT via a fitting parameter that reflects the chemical property of the transition state [32].

Table 4-1: The microkinetic model for WGS on Pt(111). The letter 'S' denotes a surface site. Activation energies and enthalpy changes in kJ/mol; the units of the pre–exponential factors are atm^{-1} s^{-1} for adsorption/desorption reactions and s^{-1} for surface reactions. The pre-exponential factor in bold taken from Ref. [32].

	$\vec{E}_\rho$	$\vec{\Lambda}_\rho$	Elementary Reactions	$\bar{E}_\rho$	$\bar{\Lambda}_\rho$	ΔH^o_ρ
s_1:	0	1.00×10^6	$H_2O + S \leftrightarrows H_2O{\cdot}S$	18.335	3.6453×10^{13}	−18.335
s_2:	0	1.00×10^6	$CO + S \leftrightarrows CO{\cdot}S$	104.22	7.0722×10^{13}	−104.22
s_3:	4.825	1.00×10^{13}	$2H{\cdot}S \leftrightarrows H_2 + 2S$	0	6.3276×10^6	4.825
s_4:	10.615	1.00×10^{13}	$CO_2{\cdot}S \leftrightarrows CO_2 + S$	0	4.9955×10^5	10.615
s_5:	46.32	$\mathbf{1.04 \times 10^{13}}$	$H_2O{\cdot}S + S \leftrightarrows OH{\cdot}S + H{\cdot}S$	26.055	8.5904×10^{12}	20.265
s_6:	266.34	$\mathbf{1.60 \times 10^{13}}$	$OH{\cdot}S + S \leftrightarrows O{\cdot}S + H{\cdot}S$	0	1.0828×10^{14}	266.34
s_7:	246.075	$\mathbf{9.24 \times 10^{12}}$	$OH{\cdot}S + OH{\cdot}S \leftrightarrows H_2O{\cdot}S + O{\cdot}S$	0	7.5704×10^{13}	246.075
s_8:	94.57	$\mathbf{1.12 \times 10^{13}}$	$CO{\cdot}S + O{\cdot}S \leftrightarrows CO_2{\cdot}S + S$	312.66	2.6840×10^{13}	−218.09
s_9:	44.39	$\mathbf{9.89 \times 10^{12}}$	$CO{\cdot}S + OH{\cdot}S \leftrightarrows COOH{\cdot}S + S$	34.74	3.2259×10^{12}	9.65
s_{10}:	66.585	$\mathbf{1.99 \times 10^{12}}$	$COOH{\cdot}S + S \leftrightarrows CO_2{\cdot}S + H{\cdot}S$	27.985	9.8943×10^{13}	38.6
s_{11}:	0	$\mathbf{3.74 \times 10^{12}}$	$COOH{\cdot}S + O{\cdot}S \leftrightarrows CO_2{\cdot}S + OH{\cdot}S$	227.74	2.7477×10^{13}	−227.74
s_{12}:	27.985	$\mathbf{1.00 \times 10^{13}}$	$COOH{\cdot}S + OH{\cdot}S \leftrightarrows CO_2{\cdot}S + H_2O{\cdot}S$	9.65	6.0194×10^{14}	18.335
s_{13}:	147.645	$\mathbf{1.00 \times 10^{13}}$	$COOH{\cdot}S + CO{\cdot}S \leftrightarrows CO_2{\cdot}S + HCO{\cdot}S$	77.2	4.2003×10^{13}	70.445
s_{14}:	157.295	$\mathbf{1.00 \times 10^{13}}$	$HCOO{\cdot}S + S \leftrightarrows CO_2{\cdot}S + H{\cdot}S$	105.185	5.5962×10^{14}	52.11
s_{15}:	257.655	8.2692×10^{13}	$CO_2{\cdot}S + OH{\cdot}S \leftrightarrows HCOO{\cdot}S + O{\cdot}S$	43.425	$\mathbf{1.00 \times 10^{13}}$	214.23
s_{16}:	144.75$^{\#}$	1.1179×10^{13}	$CO_2{\cdot}S + H_2O{\cdot}S \leftrightarrows HCOO{\cdot}S + OH{\cdot}S$	176.595	$\mathbf{1.65 \times 10^{11}}$	−31.845
s_{17}:	41.495	$\mathbf{1.00 \times 10^{13}}$	$HCO{\cdot}S + S \leftrightarrows CO{\cdot}S + H{\cdot}S$	73.34	1.1837×10^{14}	−31.845

Modified from 143.785, owing to KPL as explained in the text

The pre-exponential factors (shown as bold in Table 4-1) are taken from Ref. [32], while those in the opposite direction are calculated by us using Lund's approach [37] from the standard reaction entropies estimated following a procedure explained in chapter III.

Thus, the entropy values for species in the gas phase, $S^{o}_{I_k(g)}$ were taken from standard handbooks [38]. The entropies of formation of COOH and HCOO in the gas phase were, however, determined by us using Gaussian 03 [39] at the B3LYP/LANL2DZ level of theory with harmonic oscillator approximation, at reference temperature of 298 K and 1 bar, due to lack of reported values in the literature.

Finally, following Dumesic et al. [40], the forward pre-exponential factors for steps s_1 through s_4 were assumed by us as shown in Table 4-1. The pre-exponential factors and activation energies listed in Table 4-1 were not subsequently varied from these initial estimates.

4.3 Reaction Route Graph

4.3.1 Enumeration of RRs and Nodes

RR Graph for a mechanism as explained earlier depicts *all* possible reaction routes or reaction paths as walks between the terminal nodes (TNs). Thus, the first step in our RR Graph approach is the enumeration of the reaction routes (RRs), or reaction pathways [41]. In chapters II and III, we followed the graphical enumeration approach for the reaction routes. In this chapter, let us follow our stoichiometric algorithm (Appendix A) [42-44] that provides all "direct" RRs, i.e., those that are the shortest for a given mechanism, the "nondirect" RRs resulting from their linear combination. It should, however, be noted that stoichiometric reaction route enumeration is certainly not necessary, since the knowledge of the *independent set* is more than sufficient to define the topological characteristics of a RR graph including the FRs, and ERs, which in turn strongly affects the flux and affinity (Gibbs free energy) of steps.

For the WGS mechanism, our starting point for the stoichiometric analysis is a list of species (reactants, intermediates, and products), which for this system includes the so-called terminal species H_2O and CO as reactants, and CO_2 and H_2 as products (i.e., $n = 4$),

and $H_2O \cdot S$, $CO \cdot S$, $H \cdot S$, $CO_2 \cdot S$, $OH \cdot S$, $O \cdot S$, $COOH \cdot S$, $HCOO \cdot S$, and $HCO \cdot S$ ($q = 9$) as the independent surface intermediates, in addition to vacant surface site, S. The intermediates stoichiometric matrix [42-44], thus,

$$
\alpha =
\begin{array}{c}
\begin{array}{ccccccccc}
H_2O\cdot S & CO\cdot S & H\cdot S & CO_2\cdot S & OH\cdot S & O\cdot S & COOH\cdot S & HCOO\cdot S & HCO\cdot S
\end{array} \\
\left[
\begin{array}{ccccccccc}
+1 & 0 & 0 & 0 & 0 & 0 & 0 & 0 & 0 \\
0 & +1 & 0 & 0 & 0 & 0 & 0 & 0 & 0 \\
0 & 0 & -2 & 0 & 0 & 0 & 0 & 0 & 0 \\
0 & 0 & 0 & -1 & 0 & 0 & 0 & 0 & 0 \\
-1 & 0 & +1 & 0 & +1 & 0 & 0 & 0 & 0 \\
0 & 0 & +1 & 0 & -1 & +1 & 0 & 0 & 0 \\
+1 & 0 & 0 & 0 & -2 & +1 & 0 & 0 & 0 \\
0 & -1 & 0 & +1 & 0 & -1 & 0 & 0 & 0 \\
0 & -1 & 0 & 0 & -1 & 0 & +1 & 0 & 0 \\
0 & 0 & +1 & +1 & 0 & 0 & -1 & 0 & 0 \\
0 & 0 & 0 & +1 & +1 & -1 & -1 & 0 & 0 \\
+1 & 0 & 0 & +1 & -1 & 0 & -1 & 0 & 0 \\
0 & -1 & 0 & +1 & 0 & 0 & -1 & 0 & +1 \\
0 & 0 & +1 & +1 & 0 & 0 & 0 & -1 & 0 \\
0 & 0 & 0 & -1 & -1 & +1 & 0 & +1 & 0 \\
-1 & 0 & 0 & -1 & +1 & 0 & 0 & +1 & 0 \\
0 & 1 & +1 & 0 & 0 & 0 & 0 & 0 & -1
\end{array}
\right]
\begin{array}{l}
s_1 \\ s_2 \\ s_3 \\ s_4 \\ s_5 \\ s_6 \\ s_7 \\ s_8 \\ s_9 \\ s_{10} \\ s_{11} \\ s_{12} \\ s_{13} \\ s_{14} \\ s_{15} \\ s_{16} \\ s_{17}
\end{array}
\end{array}
\tag{4.1}
$$

where, the columns correspond to the 9 linearly independent intermediate species and the rows to the elementary steps of the mechanism listed in Table 4-1. The FRs are enumerated based on this intermediates stoichiometric matrix α [42-44]. A direct FR for this system, as mentioned earlier, involves no more than $q + 1 = \text{rank } \alpha + 1 = 9 + 1 = 10$ elementary steps, and is obtained from a submatrix of α. For example, the linearly independent set of 10 elementary reactions s_1, s_2, s_3, s_4, s_5, s_6, s_8, s_9, s_{13}, and s_{14} provides the following FR;

FR: $(s_1, s_2, s_3, s_4, s_5, s_6, s_8, s_9, s_{13}, s_{14})$

$H_2O \cdot S$	$CO \cdot S$	$H \cdot S$	$CO_2 \cdot S$	$OH \cdot S$	$O \cdot S$	$COOH \cdot S$	$HCOO \cdot S$	$HCO \cdot S$	
+1	0	0	0	0	0	0	0	0	s_1
0	+1	0	0	0	0	0	0	0	s_2
0	0	-2	0	0	0	0	0	0	s_3
0	0	0	-1	0	0	0	0	0	s_4
-1	0	+1	0	+1	0	0	0	0	s_5
0	0	+1	0	-1	+1	0	0	0	s_6
0	-1	0	+1	0	-1	0	0	0	s_8
0	-1	0	0	-1	0	+1	0	0	s_9
0	-1	0	+1	0	0	-1	0	+1	s_{13}
0	0	+1	+1	0	0	0	-1	0	s_{14}

$$= s_1 + s_2 + s_3 + s_4 + s_5 + s_6 + s_8$$

which, is FR_1 in the Table 4-2.

In the usual format, this FR, or reaction pathway, may be presented as $OR = \sum_\rho \sigma_\rho s_\rho$, i.e.,

$$\sigma_\rho$$

		σ_ρ
s_1:	$H_2O + S \leftrightarrows H_2O \cdot S$	+1
s_2:	$CO + S \leftrightarrows CO \cdot S$	+1
s_3:	$2H \cdot S \leftrightarrows H_2 + 2S$	+1
s_4:	$CO_2 \cdot S \leftrightarrows CO_2 + S$	+1
s_5:	$H_2O \cdot S + S \leftrightarrows OH \cdot S + H \cdot S$	+1
s_6:	$OH \cdot S + S \leftrightarrows O \cdot S + H \cdot S$	+1
s_8:	$CO \cdot S + O \cdot S \leftrightarrows CO_2 \cdot S + S$	+1

Net: $H_2O + CO \leftrightarrows CO_2 + H_2$

On the other hand, the RR or reaction path involving the elementary reactions s_1, s_2, s_3, s_4, s_5, s_6, s_7, s_9, s_{13}, and s_{14} is an ER, i.e.,

$ER(s_1, s_2, s_3, s_4, s_5, s_6, s_7, s_9, s_{13}, s_{14})$

H₂O·S	CO·S	H·S	CO₂·S	OH·S	O·S	COOH·S	HCOO·S	HCO·S	
+1	0	0	0	0	0	0	0	0	s_1
0	+1	0	0	0	0	0	0	0	s_2
0	0	−2	0	0	0	0	0	0	s_3
0	0	0	−1	0	0	0	0	0	s_4
−1	0	+1	0	+1	0	0	0	0	s_5
0	0	+1	0	−1	+1	0	0	0	s_6
+1	0	0	0	−2	+1	0	0	0	s_7
0	−1	0	0	−1	0	+1	0	0	s_9
0	−1	0	+1	0	0	−1	0	+1	s_{13}
0	0	+1	+1	0	0	0	−1	0	s_{14}

$$= s_5 - s_6 + s_7$$

or

	σ_ρ
s_5: $\quad H_2O·S + S \leftrightarrows OH·S + H·S$	+1
s_6: $\quad OH·S + S \leftrightarrows O·S + H·S$	−1
s_7: $\quad OH·S + OH·S \leftrightarrows H_2O·S + O·S$	+1

Net: $0 = 0$

The total number of direct RRs does not exceed the number of ways 10 elementary reactions may be selected from the 17 elementary steps of the mechanism, i.e., $17!/10!/7! = 19448$. In reality, the number is considerably smaller by virtue of the fact that not all of the possible sets of 10 elementary reactions involved in a RR are unique. The complete list of thus generated FRs and ERs is provided in Table 4-2 and Table 4-3, respectively. Thus, a total of 71 FRs and 49 ERs were found to be distinct. Of course, not all FRs may contribute significantly toward the total flux of the OR. Moreover, according to Horiuti-Temkin theorem, only $\mu = p - q = 17 - 9 = 8$ RRs are linearly independent, which may include both, FRs and ERs. Additionally, only $p - (q + 1) = 17 - 9 - 1 = 7$ of the ERs are linearly independent.

Table 4-2: The complete list of stoichiometrically enumerated direct FRs for the 17-step WGS reaction mechanism

FR_1: $s_1 + s_2 + s_3 + s_4 + s_5 + s_6 + s_8$

FR_2: $s_1 + s_2 + s_3 + s_4 + s_5 + s_9 + s_{10}$

FR_3: $s_1 + s_2 + s_3 + s_4 + s_5 + s_6 + s_9 + s_{11}$

FR_4: $s_1 + s_2 + s_3 + s_4 + 2s_5 + s_9 + s_{12}$

FR_5: $s_1 + s_2 + s_3 + s_4 + s_5 + s_9 + s_{13} + s_{17}$

FR_6: $s_1 + s_2 + s_3 + s_4 + 2s_5 + s_7 + s_8$

FR_7: $s_1 + s_2 + s_3 + s_4 + 2s_5 + s_7 + s_9 + s_{11}$

FR_8: $s_1 + s_2 + s_3 + s_4 + s_5 + s_8 + s_{14} + s_{15}$

FR_9: $s_1 + s_2 + s_3 + s_4 + 2s_5 + s_8 + s_{15} - s_{16}$

FR_{10}: $s_1 + s_2 + s_3 + s_4 + s_5 + s_8 + s_{10} - s_{11}$

FR_{11}: $s_1 + s_2 + s_3 + s_4 + 2s_5 + s_8 - s_{11} + s_{12}$

FR_{12}: $s_1 + s_2 + s_3 + s_4 + s_5 + s_8 - s_{11} + s_{13} + s_{17}$

FR_{13}: $s_1 + s_2 + s_3 + s_4 + s_5 + s_9 + s_{11} + s_{14} + s_{15}$

FR_{14}: $s_1 + s_2 + s_3 + s_4 + 2s_5 + s_9 + s_{11} + s_{15} - s_{16}$

FR_{15}: $s_1 + s_2 + s_3 + s_4 + 2s_6 - s_7 + s_8$

FR_{16}: $s_1 + s_2 + s_3 + s_4 + s_6 - s_7 + s_9 + s_{10}$

FR_{17}: $s_1 + s_2 + s_3 + s_4 + 2s_6 - s_7 + s_9 + s_{11}$

FR_{18}: $s_1 + s_2 + s_3 + s_4 + 2s_6 - 2s_7 + s_9 + s_{12}$

FR_{19}: $s_1 + s_2 + s_3 + s_4 + s_6 - s_7 + s_9 + s_{13} + s_{17}$

FR_{20}: $s_1 + s_2 + s_3 + s_4 + 2s_6 + 2s_8 - s_9 - s_{12}$

FR_{21}: $s_1 + s_2 + s_3 + s_4 + s_6 + s_8 + s_{14} + s_{16}$

FR_{22}: $s_1 + s_2 + s_3 + s_4 + 2s_6 + s_8 - s_{15} + s_{16}$

FR_{23}: $s_1 + s_2 + s_3 + s_4 + s_6 + s_8 + s_{10} - s_{12}$

FR_{24}: $s_1 + s_2 + s_3 + s_4 + 2s_6 + s_8 + s_{11} - s_{12}$

FR_{25}: $s_1 + s_2 + s_3 + s_4 + s_6 + s_8 - s_{12} + s_{13} + s_{17}$

FR_{26}: $s_1 + s_2 + s_3 + s_4 + s_9 + 2s_{10} - s_{12}$

FR_{27}: $s_1 + s_2 + s_3 + s_4 + s_9 + s_{10} + s_{14} + s_{16}$

FR_{28}: $s_1 + s_2 + s_3 + s_4 + s_6 + s_9 + s_{10} - s_{15} + s_{16}$

FR_{29}: $s_1 + s_2 + s_3 + s_4 + 2s_6 + s_9 + 2s_{11} - s_{12}$

FR_{30}: $s_1 + s_2 + s_3 + s_4 + s_6 + s_9 + s_{11} + s_{14} + s_{16}$

FR_{31}: $s_1 + s_2 + s_3 + s_4 + 2s_6 + s_9 + s_{11} - s_{15} + s_{16}$

FR_{32}: $s_1 + s_2 + s_3 + s_4 + s_9 + s_{12} + 2s_{14} + 2s_{16}$

FR_{33}: $s_1 + s_2 + s_3 + s_4 + s_9 - s_{12} + 2s_{13} + 2s_{17}$

FR_{34}: $s_1 + s_2 + s_3 + s_4 + 2s_6 + s_9 + s_{12} - 2s_{15} + 2s_{16}$

FR_{35}: $s_1 + s_2 + s_3 + s_4 + s_9 + s_{13} + s_{14} + s_{16} + s_{17}$

FR_{36}: $s_1 + s_2 + s_3 + s_4 + s_6 + s_9 + s_{13} - s_{15} + s_{16} + s_{17}$

FR_{37}: $s_1 + s_2 + s_3 + s_4 - s_7 - s_8 + 2s_9 + 2s_{10}$

FR_{38}: $s_1 + s_2 + s_3 + s_4 - s_7 + s_8 + 2s_{14} + 2s_{15}$

FR_{39}: $s_1 + s_2 + s_3 + s_4 + s_7 + s_8 + 2s_{14} + 2s_{16}$

FR_{40}: $s_1 + s_2 + s_3 + s_4 - s_7 - s_8 + 2s_9 + 2s_{13} + 2s_{17}$

FR_{41}: $s_1 + s_2 + s_3 + s_4 - s_7 + s_8 + 2s_{10} - 2s_{11}$

FR_{42}: $s_1 + s_2 + s_3 + s_4 + s_7 + s_8 + 2s_{10} - 2s_{12}$

FR_{43}: $s_1 + s_2 + s_3 + s_4 - s_7 + s_8 - 2s_{11} + 2s_{13} + 2s_{17}$

FR_{44}: $s_1 + s_2 + s_3 + s_4 + s_7 + s_8 - 2s_{12} + 2s_{13} + 2s_{17}$

FR_{45}: $s_1 + s_2 + s_3 + s_4 - s_7 + s_9 + 2s_{10} - s_{11}$

FR_{46}: $s_1 + s_2 + s_3 + s_4 - s_7 + s_9 + s_{10} + s_{14} + s_{15}$

FR_{47}: $s_1 + s_2 + s_3 + s_4 - s_7 + s_9 + s_{11} + 2s_{14} + 2s_{15}$

FR_{48}: $s_1 + s_2 + s_3 + s_4 + s_7 + s_9 + s_{11} + 2s_{14} + 2s_{16}$

FR_{49}: $s_1 + s_2 + s_3 + s_4 - s_7 + s_9 - s_{11} + 2s_{13} + 2s_{17}$

FR_{50}: $s_1 + s_2 + s_3 + s_4 - 2s_7 + s_9 + s_{12} + 2s_{14} + 2s_{15}$

FR_{51}: $s_1 + s_2 + s_3 + s_4 - s_7 + s_9 + s_{13} + s_{14} + s_{15} + s_{17}$

FR_{52}: $s_1 + s_2 + s_3 + s_4 - s_8 + 2s_9 + 2s_{10} - s_{15} + s_{16}$

FR_{53}: $s_1 + s_2 + s_3 + s_4 + 2s_8 - s_9 - s_{12} + 2s_{14} + 2s_{15}$

FR_{54}: $s_1 + s_2 + s_3 + s_4 + s_8 + 2s_{14} + s_{15} + s_{16}$

FR_{55}: $s_1 + s_2 + s_3 + s_4 - s_8 + 2s_9 + 2s_{13} - s_{15} + s_{16} + 2s_{17}$

FR_{56}: $s_1 + s_2 + s_3 + s_4 + s_8 + 2s_{10} - s_{11} - s_{12}$

FR_{57}: $s_1 + s_2 + s_3 + s_4 + s_8 + s_{10} - s_{11} + s_{14} + s_{16}$

FR_{58}: $s_1 + s_2 + s_3 + s_4 + s_8 + 2s_{10} - 2s_{11} - s_{15} + s_{16}$

FR_{59}: $s_1 + s_2 + s_3 + s_4 + s_8 + s_{10} - s_{12} + s_{14} + s_{15}$

FR_{60}: $s_1 + s_2 + s_3 + s_4 + s_8 + 2s_{10} - 2s_{12} + s_{15} - s_{16}$

FR_{61}: $s_1 + s_2 + s_3 + s_4 + s_8 + s_{11} - s_{12} + 2s_{14} + 2s_{15}$

FR_{62}: $s_1 + s_2 + s_3 + s_4 + s_8 - s_{11} + s_{12} + 2s_{14} + 2s_{16}$

FR_{63}: $s_1 + s_2 + s_3 + s_4 + s_8 - s_{11} - s_{12} + 2s_{13} + 2s_{17}$

FR_{64}: $s_1 + s_2 + s_3 + s_4 + s_8 - s_{11} + s_{13} + s_{14} + s_{16} + s_{17}$

FR_{65}: $s_1 + s_2 + s_3 + s_4 + s_8 - 2s_{11} + 2s_{13} - s_{15} + s_{16} + 2s_{17}$

FR_{66}: $s_1 + s_2 + s_3 + s_4 + s_8 - s_{12} + s_{13} + s_{14} + s_{15} + s_{17}$

FR_{67}: $s_1 + s_2 + s_3 + s_4 + s_8 - 2s_{12} + 2s_{13} + s_{15} - s_{16} + 2s_{17}$

FR_{68}: $s_1 + s_2 + s_3 + s_4 + s_9 + 2s_{10} - s_{11} - s_{15} + s_{16}$

FR_{69}: $s_1 + s_2 + s_3 + s_4 + s_9 + 2s_{11} - s_{12} + 2s_{14} + 2s_{15}$

FR_{70}: $s_1 + s_2 + s_3 + s_4 + s_9 + s_{11} + 2s_{14} + s_{15} + s_{16}$

FR_{71}: $s_1 + s_2 + s_3 + s_4 + s_9 - s_{11} + 2s_{13} - s_{15} + s_{16} + 2s_{17}$

Table 4-3: The complete list of stoichiometrically enumerated direct ERs for the 17-step WGS reaction mechanism

ER_1: $s_5 - s_6 + s_7$

ER_2: $s_6 + s_8 - s_9 - s_{10}$

ER_3: $s_8 - s_9 - s_{11}$

ER_4: $s_5 - s_6 - s_8 + s_9 + s_{12}$

ER_5: $s_6 - s_{14} - s_{15}$

ER_6: $s_5 - s_{14} - s_{16}$

ER_7: $s_6 + s_8 - s_9 - s_{13} - s_{17}$

ER_8: $s_5 - s_6 + s_{15} - s_{16}$

ER_9: $s_6 - s_{10} + s_{11}$

ER_{10}: $s_5 - s_{10} + s_{12}$

ER_{11}: $s_{10} - s_{13} - s_{17}$

ER_{12}: $s_5 - s_6 - s_{11} + s_{12}$

ER_{13}: $s_6 + s_{11} - s_{13} - s_{17}$

ER_{14}: $s_5 + s_{12} - s_{13} - s_{17}$

ER_{15}: $s_5 + s_7 + s_8 - s_9 - s_{10}$

ER_{16}: $s_7 + s_8 - s_9 - s_{12}$

ER_{17}: $s_5 + s_7 - s_{14} - s_{15}$

ER_{18}: $s_5 + s_7 + s_8 - s_9 - s_{13} - s_{17}$

ER_{19}: $s_7 - s_{15} + s_{16}$

ER_{20}: $s_5 + s_7 - s_{10} + s_{11}$

ER_{21}: $s_7 + s_{11} - s_{12}$

ER_{22}: $s_5 + s_7 + s_{11} - s_{13} - s_{17}$

ER_{23}: $s_8 - s_9 - s_{10} + s_{14} + s_{15}$

ER_{24}: $s_5 + s_8 - s_9 - s_{10} + s_{15} - s_{16}$

ER_{25}: $s_5 - s_8 + s_9 + s_{12} - s_{14} - s_{15}$

ER_{26}: $s_8 - s_9 - s_{12} + s_{15} - s_{16}$

ER_{27}: $s_8 - s_9 - s_{13} + s_{14} + s_{15} - s_{17}$

ER_{28}: $s_5 + s_8 - s_9 - s_{13} + s_{15} - s_{16} - s_{17}$

ER_{29}: $s_{10} - s_{11} - s_{14} - s_{15}$

ER_{30}: $s_5 - s_{10} + s_{11} + s_{15} - s_{16}$

ER_{31}: $s_5 - s_{11} + s_{12} - s_{14} - s_{15}$

ER_{32}: $s_{11} - s_{12} + s_{15} - s_{16}$

ER_{33}: $s_{11} - s_{13} + s_{14} + s_{15} - s_{17}$

ER_{34}: $s_5 + s_{11} - s_{13} + s_{15} - s_{16} - s_{17}$

ER_{35}: $s_6 - s_7 - s_{14} - s_{16}$

ER_{36}: $s_6 - s_7 - s_{10} + s_{12}$

ER_{37}: $s_6 - s_7 + s_{12} - s_{13} - s_{17}$

ER_{38}: $s_6 + s_8 - s_9 - s_{12} - s_{14} - s_{16}$

ER_{39}: $s_{10} - s_{12} - s_{14} - s_{16}$

ER_{40}: $s_6 - s_{10} + s_{12} - s_{15} + s_{16}$

ER_{41}: $s_6 + s_{11} - s_{12} - s_{14} - s_{16}$

ER_{42}: $s_{12} - s_{13} + s_{14} + s_{16} - s_{17}$

ER_{43}: $s_6 + s_{12} - s_{13} - s_{15} + s_{16} - s_{17}$

ER_{44}: $s_7 + s_8 - s_9 - s_{10} + s_{14} + s_{16}$

ER_{45}: $s_7 + s_8 - s_9 - s_{13} + s_{14} + s_{16} - s_{17}$

ER_{46}: $s_7 - s_{10} + s_{11} + s_{14} + s_{16}$

ER_{47}: $s_7 + s_{10} - s_{12} - s_{14} - s_{15}$

ER_{48}: $s_7 + s_{11} - s_{13} + s_{14} + s_{16} - s_{17}$

ER_{49}: $s_7 - s_{12} + s_{13} - s_{14} - s_{15} + s_{17}$

Next, the connectivity of reaction steps at direct INs in the RR Graph is stoichiometrically enumerated based on the QSS (Q_k) of the linearly independent intermediate species (Table 4-4) [42-44]. By definition, a direct IN has a degree of no more than $p - (q - 1) = 17 - 9 + 1 = 11$ rates and can be obtained by linearly combining Qs listed in Table 4-4, i.e., INs represent linear combination of QSS conditions for the q intermediates. Only q of the INs are independent from the complete list presented in Table 4-5. The TNs, similarly are enumerated based on the QSS of the terminal species [42-44].

4.3.2 RR Graph Construction

We begin by drawing the cycle graph by assembling the ERs together. For this, let us consider a set of 7 linearly independent ERs comprising of minimum number of steps, say ER_6, ER_5, ER_{19}, ER_9, ER_{21}, ER_{11}, and ER_3. We first draw ER_6 as shown in Figure 4-3a. ER_6 and ER_5 have step s_{14} in common and can then be combined together as show in Figure 4-3a. Next, ER_{19} has steps s_{16} and s_{15} in common with ER_6 and ER_5, respectively and can be fused together. ER_9 has step s_6 common with ER_5 and can be added appropriately. ER_{21} has steps s_7 and s_{11} common with ER_{19} and ER_9 and can be aptly added. Next, ER_{11} has step s_{10} common with ER_9 and can be subsequently merged. Finally, ER_3 has step s_8 common with ER_9 can be added together to yield the cycle graph. It should be noted that any other set of 7 linearly independent ERs would also lead to a similar cycle graph and that choice of the linearly independent ERs is arbitrary. However, it is easier to work with the ERs with minimum number of steps, typically three, as done here. Moreover, all the other ERs can also be traced on the cycle graph.

Upon examination of the compilation of the direct FRs given in Table 4-2, it is next noted that there are non-unit stoichiometric numbers in several of the FRs; specifically, it is seen that some FRs have stoichiometric numbers of ±2, suggesting that the RR graph will have each step s_ρ as well as the OR twice, which must furthermore be symmetrical. This is achieved by duplicating the cycle graph as shown in Figure 4-3b and fusing the two together to form a symmetric cycle graph. The characteristics associated with each of the unfused nodes are not lost; instead, they are represented collectively by the fused node.

Table 4-4: Steady-state mass balance conditions for surface intermediates and terminal species involved in WGS reaction

Intermediate Species:

$H_2O \cdot S$: (Q_1) $\quad r_1 - r_5 + r_7 + r_{12} - r_{16} = 0$

$CO \cdot S$: (Q_2) $\quad r_2 - r_8 - r_9 - r_{13} + r_{17} = 0$

$H \cdot S$: (Q_3) $\quad -2r_3 + r_5 + r_6 + r_{10} + r_{14} + r_{17} = 0$

$CO_2 \cdot S$: (Q_4) $\quad r_8 - r_4 + r_{10} + r_{11} + r_{12} + r_{13} + r_{14} - r_{15} - r_{16} = 0$

$OH \cdot S$: (Q_5) $\quad r_5 - r_6 - 2r_7 - r_9 + r_{11} - r_{12} - r_{15} + r_{16} = 0$

$O \cdot S$: (Q_6) $\quad r_6 + r_7 - r_8 - r_{11} + r_{15} = 0$

$COOH \cdot S$: (Q_7) $\quad r_9 - r_{10} - r_{11} - r_{12} - r_{13} = 0$

$HCOO \cdot S$: (Q_8) $\quad -r_{14} + r_{15} + r_{16} = 0$

$HCO \cdot S$: (Q_9) $\quad r_{13} - r_{17} = 0$

Terminal Species:

CO: $\quad -r_2 = r_{OR}$
H_2O: $\quad -r_1 = r_{OR}$
CO_2: $\quad r_4 = r_{OR}$
H_2: $\quad r_3 = r_{OR}$

Table 4-5: The complete list of stoichiometrically enumerated direct INs for the 17-step WGS reaction mechanism

IN_1: $s_{14} - s_{15} - s_{16}$
IN_2: $s_{13} - s_{17}$
IN_3: $s_9 - s_{10} - s_{11} - s_{12} - s_{17}$
IN_4: $s_9 - s_{10} - s_{11} - s_{12} - s_{13}$
IN_5: $s_6 + s_7 - s_8 - s_{11} + s_{15}$
IN_6: $s_6 + s_7 - s_8 - s_{11} + s_{14} - s_{16}$
IN_7: $s_6 + s_7 - s_8 - s_9 + s_{10} + s_{12} + s_{15} + s_{17}$
IN_8: $s_6 + s_7 - s_8 - s_9 + s_{10} + s_{12} + s_{14} - s_{16} + s_{17}$
IN_9: $s_6 + s_7 - s_8 - s_9 + s_{10} + s_{12} + s_{13} + s_{15}$
IN_{10}: $s_6 + s_7 - s_8 - s_9 + s_{10} + s_{12} + s_{13} + s_{14} - s_{16}$
IN_{11}: $s_5 - s_7 - s_8 - s_{10} - s_{11} - 2s_{12} + s_{16} - s_{17}$
IN_{12}: $s_5 - s_7 - s_8 - s_{10} - s_{11} - 2s_{12} + s_{14} - s_{15} - s_{17}$
IN_{13}: $s_5 - s_7 - s_8 - s_{10} - s_{11} - 2s_{12} - s_{13} + s_{16}$
IN_{14}: $s_5 - s_7 - s_8 - s_{10} - s_{11} - 2s_{12} - s_{13} + s_{14} - s_{15}$
IN_{15}: $s_5 - s_7 - s_8 - s_9 - s_{12} + s_{16}$
IN_{16}: $s_5 - s_7 - s_8 - s_9 - s_{12} + s_{14} - s_{15}$
IN_{17}: $s_5 - s_7 - s_8 - 2s_9 + s_{10} + s_{11} + s_{16} + s_{17}$
IN_{18}: $s_5 - s_7 - s_8 - 2s_9 + s_{10} + s_{11} + s_{14} - s_{15} + s_{17}$
IN_{19}: $s_5 - s_7 - s_8 - 2s_9 + s_{10} + s_{11} + s_{13} + s_{16}$
IN_{20}: $s_5 - s_7 - s_8 - 2s_9 + s_{10} + s_{11} + s_{13} + s_{14} - s_{15}$
IN_{21}: $s_5 + s_6 - 2s_8 - s_{10} - 2s_{11} - 2s_{12} + s_{15} + s_{16} - s_{17}$
IN_{22}: $s_5 + s_6 - 2s_8 - s_{10} - 2s_{11} - 2s_{12} + s_{14} - s_{17}$
IN_{23}: $s_5 + s_6 - 2s_8 - s_{10} - 2s_{11} - 2s_{12} - s_{13} + s_{15} + s_{16}$
IN_{24}: $s_5 + s_6 - 2s_8 - s_{10} - 2s_{11} - 2s_{12} - s_{13} + s_{14}$
IN_{25}: $s_5 + s_6 - 2s_8 - s_9 - s_{11} - s_{12} + s_{15} + s_{16}$
IN_{26}: $s_5 + s_6 - 2s_8 - s_9 - s_{11} - s_{12} + s_{14}$
IN_{27}: $s_5 + s_6 - 2s_8 - 2s_9 + s_{10} + s_{15} + s_{16} + s_{17}$
IN_{28}: $s_5 + s_6 - 2s_8 - 2s_9 + s_{10} + s_{14} + s_{17}$
IN_{29}: $s_5 + s_6 - 2s_8 - 2s_9 + s_{10} + s_{13} + s_{15} + s_{16}$
IN_{30}: $s_5 + s_6 - 2s_8 - 2s_9 + s_{10} + s_{13} + s_{14}$
IN_{31}: $s_5 - s_6 - 2s_7 - s_{10} - 2s_{12} - s_{15} + s_{16} - s_{17}$
IN_{32}: $s_5 - s_6 - 2s_7 - s_{10} - 2s_{12} - s_{14} + 2s_{16} - s_{17}$
IN_{33}: $s_5 - s_6 - 2s_7 - s_{10} - 2s_{12} + s_{14} - 2s_{15} - s_{17}$
IN_{34}: $s_5 - s_6 - 2s_7 - s_{10} - 2s_{12} - s_{13} - s_{15} + s_{16}$
IN_{35}: $s_5 - 6 - 2s_7 - s_{10} - 2s_{12} - s_{13} - s_{14} + 2s_{16}$
IN_{36}: $s_5 - s_6 - 2s_7 - s_{10} - 2s_{12} - s_{13} + s_{14} - 2s_{15}$
IN_{37}: $s_5 - s_6 - 2s_7 - s_9 + s_{11} - s_{12} - s_{15} + s_{16}$
IN_{38}: $s_5 - s_6 - 2s_7 - s_9 + s_{11} - s_{12} - s_{14} + 2s_{16}$
IN_{39}: $s_5 - s_6 - 2s_7 - s_9 + s_{11} - s_{12} + s_{14} - 2s_{15}$
IN_{40}: $s_5 - s_6 - 2s_7 - 2s_9 + s_{10} + 2s_{11} - s_{15} + s_{16} + s_{17}$
IN_{41}: $s_5 - s_6 - 2s_7 - 2s_9 + s_{10} + 2s_{11} - s_{14} + 2s_{16} + s_{17}$
IN_{42}: $s_5 - s_6 - 2s_7 - 2s_9 + s_{10} + 2s_{11} + s_{14} - 2s_{15} + s_{17}$
IN_{43}: $s_5 - s_6 - 2s_7 - 2s_9 + s_{10} + 2s_{11} + s_{13} - s_{15} + s_{16}$
IN_{44}: $s_5 - s_6 - 2s_7 - 2s_9 + s_{10} + 2s_{11} + s_{13} - s_{14} + 2s_{16}$
IN_{45}: $s_5 - s_6 - 2s_7 - 2s_9 + s_{10} + 2s_{11} + s_{13} + s_{14} - 2s_{15}$
IN_{46}: $s_4 - s_8 - s_{10} - s_{11} - s_{12} - s_{17}$
IN_{47}: $s_4 - s_8 - s_{10} - s_{11} - s_{12} - s_{13}$
IN_{48}: $s_4 - s_8 - s_9$
IN_{49}: $s_4 - s_6 - s_7 - s_{10} - s_{12} - s_{15} - s_{17}$
IN_{50}: $s_4 - s_6 - s_7 - s_{10} - s_{12} - s_{14} + s_{16} - s_{17}$
IN_{51}: $s_4 - s_6 - s_7 - s_{10} - s_{12} - s_{13} - s_{15}$
IN_{52}: $s_4 - s_6 - s_7 - s_{10} - s_{12} - s_{13} - s_{14} + s_{16}$
IN_{53}: $s_4 - s_6 - s_7 - s_9 + s_{11} - s_{15}$
IN_{54}: $s_4 - s_6 - s_7 - s_9 + s_{11} - s_{14} + s_{16}$
IN_{55}: $s_4 - s_5 + s_7 + s_{12} - s_{16}$
IN_{56}: $s_4 - s_5 + s_7 + s_{12} - s_{14} + s_{15}$
IN_{57}: $s_4 - s_5 + s_7 + s_9 - s_{10} - s_{11} - s_{16} - s_{17}$
IN_{58}: $s_4 - s_5 + s_7 + s_9 - s_{10} - s_{11} - s_{14} + s_{15} - s_{17}$
IN_{59}: $s_4 - s_5 + s_7 + s_9 - s_{10} - s_{11} - s_{13} - s_{16}$
IN_{60}: $s_4 - s_5 + s_7 + s_9 - s_{10} - s_{11} - s_{13} - s_{14} + s_{15}$
IN_{61}: $2s_4 - s_5 + s_7 - s_8 - s_{10} - s_{11} - s_{16} - s_{17}$
IN_{62}: $2s_4 - s_5 + s_7 - s_8 - s_{10} - s_{11} - s_{14} + s_{15} - s_{17}$
IN_{63}: $2s_4 - s_5 + s_7 - s_8 - s_{10} - s_{11} - s_{13} - s_{16}$
IN_{64}: $2s_4 - s_5 + s_7 - s_8 - s_{10} - s_{11} - s_{13} - s_{14} + s_{15}$

IN_{65}: $2s_4 - s_5 - s_6 - s_{10} - s_{15} - s_{16} - s_{17}$
IN_{66}: $2s_4 - s_5 - s_6 - s_{10} - s_{14} - s_{17}$
IN_{67}: $2s_4 - s_5 - s_6 - s_{10} - s_{13} - s_{15} - s_{16}$
IN_{68}: $2s_4 - s_5 - s_6 - s_{10} - s_{13} - s_{14}$
IN_{69}: $2s_4 - s_5 - s_6 - s_9 + s_{11} + s_{12} - s_{15} - s_{16}$
IN_{70}: $2s_4 : - s_5 - s_6 - s_9 + s_{11} + s_{12} - s_{14}$
IN_{71}: $s_4 - s_5 - s_6 + s_8 + s_{11} + s_{12} - s_{15} - s_{16}$
IN_{72}: $s_4 - s_5 - s_6 + s_8 + s_{11} + s_{12} - s_{14}$
IN_{73}: $s_3 - s_8 - s_{10} - s_{11} - s_{12} - s_{17}$
IN_{74}: $s_3 - s_8 - s_{10} - s_{11} - s_{12} - s_{13}$
IN_{75}: $s_3 - s_8 - s_9$
IN_{76}: $s_3 - s_6 - s_7 - s_{10} - s_{12} - s_{15} - s_{17}$
IN_{77}: $s_3 - s_6 - s_7 - s_{10} - s_{12} - s_{14} + s_{16} - s_{17}$
IN_{78}: $s_3 - s_6 - s_7 - s_{10} - s_{12} - s_{13} - s_{15}$
IN_{79}: $s_3 - s_6 - s_7 - s_{10} - s_{12} - s_{13} - s_{14} + s_{16}$
IN_{80}: $s_3 - s_6 - s_7 - s_9 + s_{11} - s_{15}$
IN_{81}: $s_3 - s_6 - s_7 - s_9 + s_{11} - s_{14} + s_{16}$
IN_{82}: $s_3 - s_5 + s_7 + s_{12} - s_{16}$
IN_{83}: $s_3 - s_5 + s_7 + s_{12} - s_{14} + s_{15}$
IN_{84}: $s_3 - s_5 + s_7 + s_9 - s_{10} - s_{11} - s_{16} - s_{17}$
IN_{85}: $s_3 - s_5 + s_7 + s_9 - s_{10} - s_{11} - s_{14} + s_{15} - s_{17}$
IN_{86}: $s_3 - s_5 + s_7 + s_9 - s_{10} - s_{11} - s_{13} - s_{16}$
IN_{87}: $s_3 - s_5 + s_7 + s_9 - s_{10} - s_{11} - s_{13} - s_{14} + s_{15}$
IN_{88}: $2s_3 - s_5 + s_7 - s_8 - s_{10} - s_{11} - s_{16} - s_{17}$
IN_{89}: $2s_3 - s_5 + s_7 - s_8 - s_{10} - s_{11} - s_{14} + s_{15} - s_{17}$
IN_{90}: $2s_3 - s_5 + s_7 - s_8 - s_{10} - s_{11} - s_{13} - s_{16}$
IN_{91}: $2s_3 - s_5 + s_7 - s_8 - s_{10} - s_{11} - s_{13} - s_{14} + s_{15}$
IN_{92}: $2s_3 - s_5 - s_6 - s_{10} - s_{15} - s_{16} - s_{17}$
IN_{93}: $2s_3 - s_5 - s_6 - s_{10} - s_{14} - s_{17}$
IN_{94}: $2s_3 - s_5 - s_6 - s_{10} - s_{13} - s_{15} - s_{16}$
IN_{95}: $2s_3 - s_5 - s_6 - s_{10} - s_{13} - s_{14}$
IN_{96}: $2s_3 - s_5 - s_6 - s_9 + s_{11} + s_{12} - s_{15} - s_{16}$
IN_{97}: $2s_3 - s_5 - s_6 - s_9 + s_{11} + s_{12} - s_{14}$
IN_{98}: $s_3 - s_5 - s_6 + s_8 + s_{11} + s_{12} - s_{15} - s_{16}$
IN_{99}: $s_3 - s_5 - s_6 + s_8 + s_{11} + s_{12} - s_{14}$
IN_{100}: $s_3 - s_4$
IN_{101}: $s_2 - s_8 - s_{10} - s_{11} - s_{12} - s_{17}$
IN_{102}: $s_2 - s_8 - s_{10} - s_{11} - s_{12} - s_{13}$
IN_{103}: $s_2 - s_8 - s_9$
IN_{104}: $s_2 - s_6 - s_7 - s_{10} - s_{12} - s_{15} - s_{17}$
IN_{105}: $s_2 - s_6 - s_7 - s_{10} - s_{12} - s_{14} + s_{16} - s_{17}$
IN_{106}: $s_2 - s_6 - s_7 - s_{10} - s_{12} - s_{13} - s_{15}$
IN_{107}: $s_2 - s_6 - s_7 - s_{10} - s_{12} - s_{13} - s_{14} + s_{16}$
IN_{108}: $s_2 - s_6 - s_7 - s_9 + s_{11} - s_{15}$
IN_{109}: $s_2 - s_6 - s_7 - s_9 + s_{11} - s_{14} + s_{16}$
IN_{110}: $s_2 - s_5 + s_7 + s_{12} - s_{16}$
IN_{111}: $s_2 - s_5 + s_7 + s_{12} - s_{14} + s_{15}$
IN_{112}: $s_2 - s_5 + s_7 + s_9 - s_{10} - s_{11} - s_{16} - s_{17}$
IN_{113}: $s_2 - s_5 + s_7 + s_9 - s_{10} - s_{11} - s_{14} + s_{15} - s_{17}$
IN_{114}: $s_2 - s_5 + s_7 + s_9 - s_{10} - s_{11} - s_{13} - s_{16}$
IN_{115}: $s_2 - s_5 + s_7 + s_9 - s_{10} - s_{11} - s_{13} - s_{14} + s_{15}$
IN_{116}: $2s_2 - s_5 + s_7 - s_8 - s_{10} - s_{11} - s_{16} - s_{17}$
IN_{117}: $2s_2 - s_5 + s_7 - s_8 - s_{10} - s_{11} - s_{14} + s_{15} - s_{17}$
IN_{118}: $2s_2 - s_5 + s_7 - s_8 - s_{10} - s_{11} - s_{13} - s_{16}$
IN_{119}: $2s_2 - s_5 + s_7 - s_8 - s_{10} - s_{11} - s_{13} - s_{14} + s_{15}$
IN_{120}: $2s_2 - s_5 - s_6 - s_{10} - s_{15} - s_{16} - s_{17}$
IN_{121}: $2s_2 - s_5 - s_6 - s_{10} - s_{14} - s_{17}$
IN_{122}: $2s_2 - s_5 - s_6 - s_{10} - s_{13} - s_{15} - s_{16}$
IN_{123}: $2s_2 - s_5 - s_6 - s_{10} - s_{13} - s_{14}$
IN_{124}: $2s_2 - s_5 - s_6 - s_9 + s_{11} + s_{12} - s_{15} - s_{16}$
IN_{125}: $2s_2 - s_5 - s_6 - s_9 + s_{11} + s_{12} - s_{14}$
IN_{126}: $s_2 - s_5 - s_6 + s_8 + s_{11} + s_{12} - s_{15} - s_{16}$
IN_{127}: $s_2 - s_5 - s_6 + s_8 + s_{11} + s_{12} - s_{14}$
IN_{128}: $s_2 - s_4$

IN_{129}: $s_2 - s_3$
IN_{130}: $s_1 - s_8 - s_{10} - s_{11} - s_{12} - s_{17}$
IN_{131}: $s_1 - s_8 - s_{10} - s_{11} - s_{12} - s_{13}$
IN_{132}: $s_1 - s_8 - s_9$
IN_{133}: $s_1 - s_6 - s_7 - s_{10} - s_{12} - s_{15} - s_{17}$
IN_{134}: $s_1 - s_6 - s_7 - s_{10} - s_{12} - s_{14} + s_{16} - s_{17}$
IN_{135}: $s_1 - s_6 - s_7 - s_{10} - s_{12} - s_{13} - s_{15}$
IN_{136}: $s_1 - s_6 - s_7 - s_{10} - s_{12} - s_{13} - s_{14} + s_{16}$
IN_{137}: $s_1 - s_6 - s_7 - s_9 + s_{11} - s_{15}$
IN_{138}: $s_1 - s_6 - s_7 - s_9 + s_{11} - s_{14} + s_{16}$
IN_{139}: $s_1 - s_5 + s_7 + s_{12} - s_{16}$
IN_{140}: $s_1 - s_5 + s_7 + s_{12} - s_{14} + s_{15}$
IN_{141}: $s_1 - s_5 + s_7 + s_9 - s_{10} - s_{11} - s_{16} - s_{17}$
IN_{142}: $s_1 - s_5 + s_7 + s_9 - s_{10} - s_{11} - s_{14} + s_{15} - s_{17}$
IN_{143}: $s_1 - s_5 + s_7 + s_9 - s_{10} - s_{11} - s_{13} - s_{16}$
IN_{144}: $s_1 - s_5 + s_7 + s_9 - s_{10} - s_{11} - s_{13} - s_{14} + s_{15}$
IN_{145}: $2s_1 - s_5 + s_7 - s_8 - s_{10} - s_{11} - s_{16} - s_{17}$
IN_{146}: $2s_1 - s_5 + s_7 - s_8 - s_{10} - s_{11} - s_{14} + s_{15} - s_{17}$
IN_{147}: $2s_1 - s_5 + s_7 - s_8 - s_{10} - s_{11} - s_{13} - s_{16}$
IN_{148}: $2s_1 - s_5 + s_7 - s_8 - s_{10} - s_{11} - s_{13} - s_{14} + s_{15}$
IN_{149}: $2s_1 - s_5 - s_6 - s_{10} - s_{15} - s_{16} - s_{17}$
IN_{150}: $2s_1 - s_5 - s_6 - s_{10} - s_{14} - s_{17}$
IN_{151}: $2s_1 - s_5 - s_6 - s_{10} - s_{13} - s_{15} - s_{16}$
IN_{152}: $2s_1 - s_5 - s_6 - s_{10} - s_{13} - s_{14}$
IN_{153}: $2s_1 - s_5 - s_6 - s_9 + s_{11} + s_{12} - s_{15} - s_{16}$
IN_{154}: $2s_1 - s_5 - s_6 - s_9 + s_{11} + s_{12} - s_{14}$
IN_{155}: $s_1 - s_5 - s_6 + s_8 + s_{11} + s_{12} - s_{15} - s_{16}$
IN_{156}: $s_1 - s_5 - s_6 + s_8 + s_{11} + s_{12} - s_{14}$
IN_{157}: $s_1 - s_4$
IN_{158}: $s_1 - s_3$
IN_{159}: $s_1 - s_2$

The only steps missing in the so-assembled fused cycle graph are the adsorption/desorption steps, namely steps s_1, s_2, s_3 and s_4. These are next added to as depicted in Figure 4-3c. Steps s_1, s_2, s_3 and s_4 are added twice across the nodes in order to satisfy the KFL at the respective node. For example, node n_2 (Figure 4-3c) corresponds to IN_{121}: $2s_2 - s_5 - s_6 - s_{10} - s_{14} - s_{17}$ (Table 4-5), which implies step s_2 needs to be added twice at the node. Similarly, it can be checked that all the other nodes are among the enumerated INs and TNs, i.e., they concur with the mass balance conditions for the intermediate/terminal species. The final step in the construction of the RR graph is the addition of two ORs ($2r_{OR} = 2r_1 = 2r_4$), completing the connectivity of TNs. Thus, the final RR Graph for the 17-step WGS on Pt(111) is shown in Figure 4-3c. It may be verified that the entire list of FRs and ERs can be traced on the resulting RR graph as walks or paths.

4.4 Network Consistence with Kirchhoff's Laws

As shown in chapter II, RR graphs concur with KFL and KPL. Thus, each ER in the RR graph is subject to thermodynamic constraints imposed by KPL. Let us take the example of ER_6: $s_5 - s_{14} - s_{16}$. The corresponding linear combination of thermodynamic properties must be equal to zero

$$A_5 - A_{14} - A_{16} = 0, \text{ i.e., } \left(\frac{\vec{r}_5}{\bar{r}_5}\right)\left(\frac{\bar{r}_{14}}{\vec{r}_{14}}\right)\left(\frac{\bar{r}_{16}}{\vec{r}_{16}}\right) = 1 \tag{4.2}$$

Since all the species (both terminal and intermediate) cancel in an ER, thus producing a zero overall reaction, all the potentials should sum up to zero in the light of KPL, i.e.,

$$\Delta H_5 - \Delta H_{14} - \Delta H_{16} = 0, \left(\frac{\vec{\Lambda}_5}{\bar{\Lambda}_5}\right)\left(\frac{\bar{\Lambda}_{14}}{\vec{\Lambda}_{14}}\right)\left(\frac{\bar{\Lambda}_{16}}{\vec{\Lambda}_{16}}\right) = 1 \tag{4.3}$$

The pre-exponential factors reported in Table 4-1 calculated based on Lund's approach [37], indeed yields $\left(\frac{\vec{\Lambda}_5}{\bar{\Lambda}_5}\right)\left(\frac{\bar{\Lambda}_{14}}{\vec{\Lambda}_{14}}\right)\left(\frac{\bar{\Lambda}_{16}}{\vec{\Lambda}_{16}}\right) = 1$, however the energetics reported in [32] yields $\Delta H_5 - \Delta H_{14} - \Delta H_{16} = 20.265 - 52.11 - (-32.81) = 0.965 \text{ kJ/mol}$, which is well within the error range of DFT predictions.
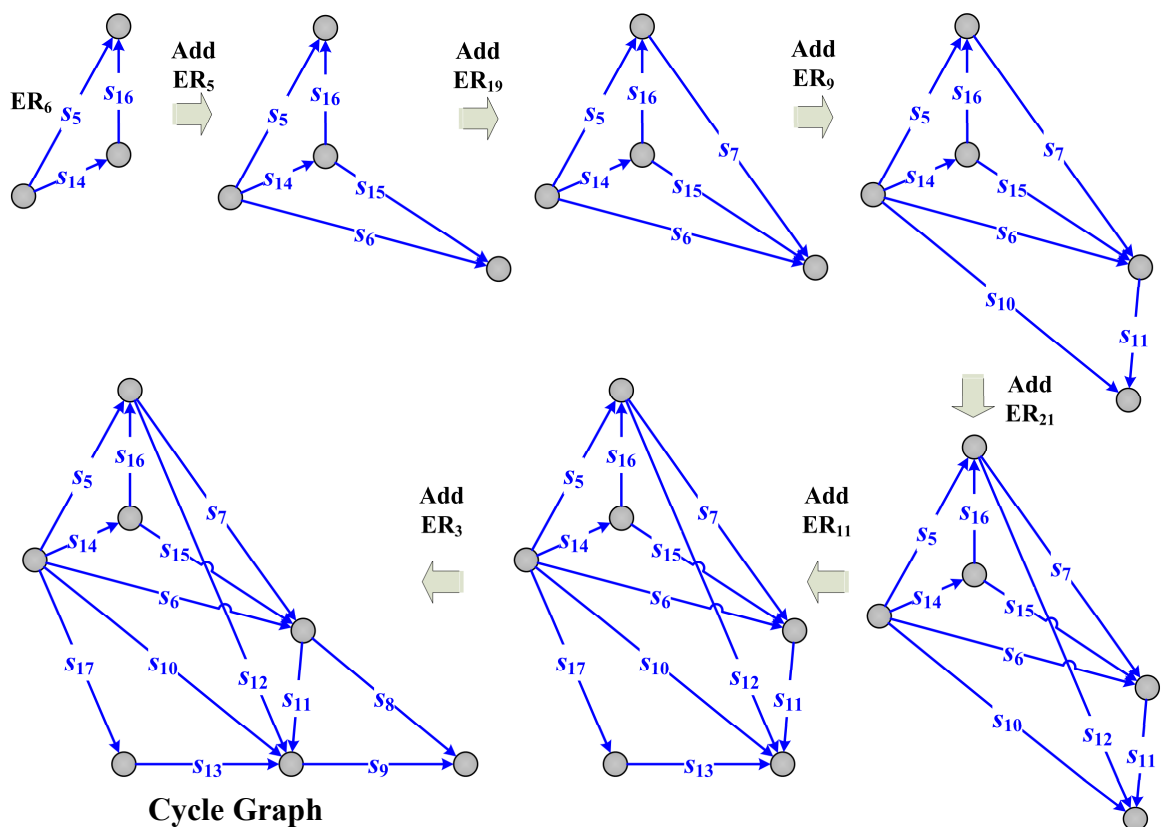
Figure 4-3a: Systematic construction of the 19-step WGS reaction mechanism RR Graph.
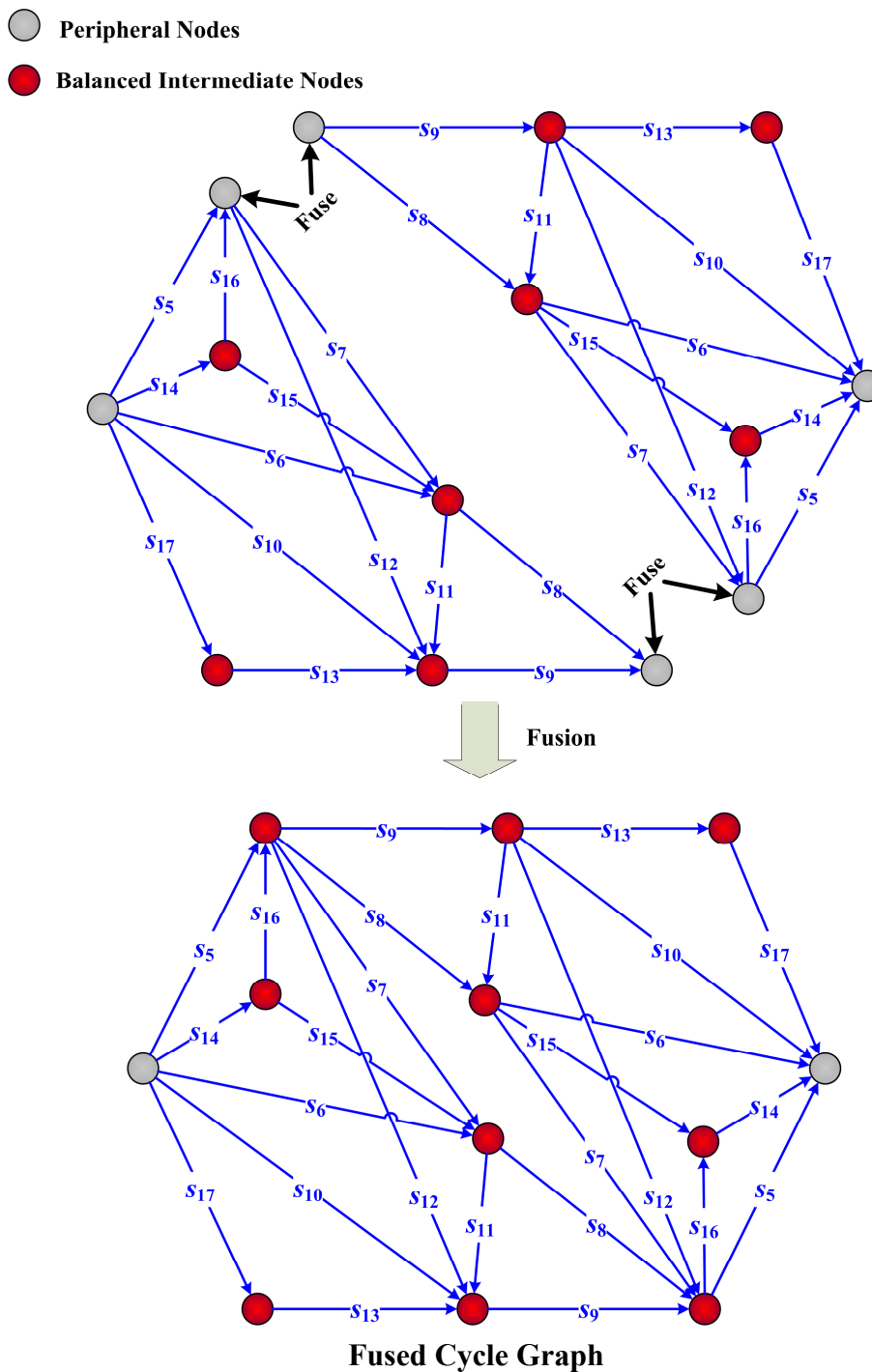
Figure 4-3b: Systematic construction of the 19-step WGS reaction mechanism RR Graph.
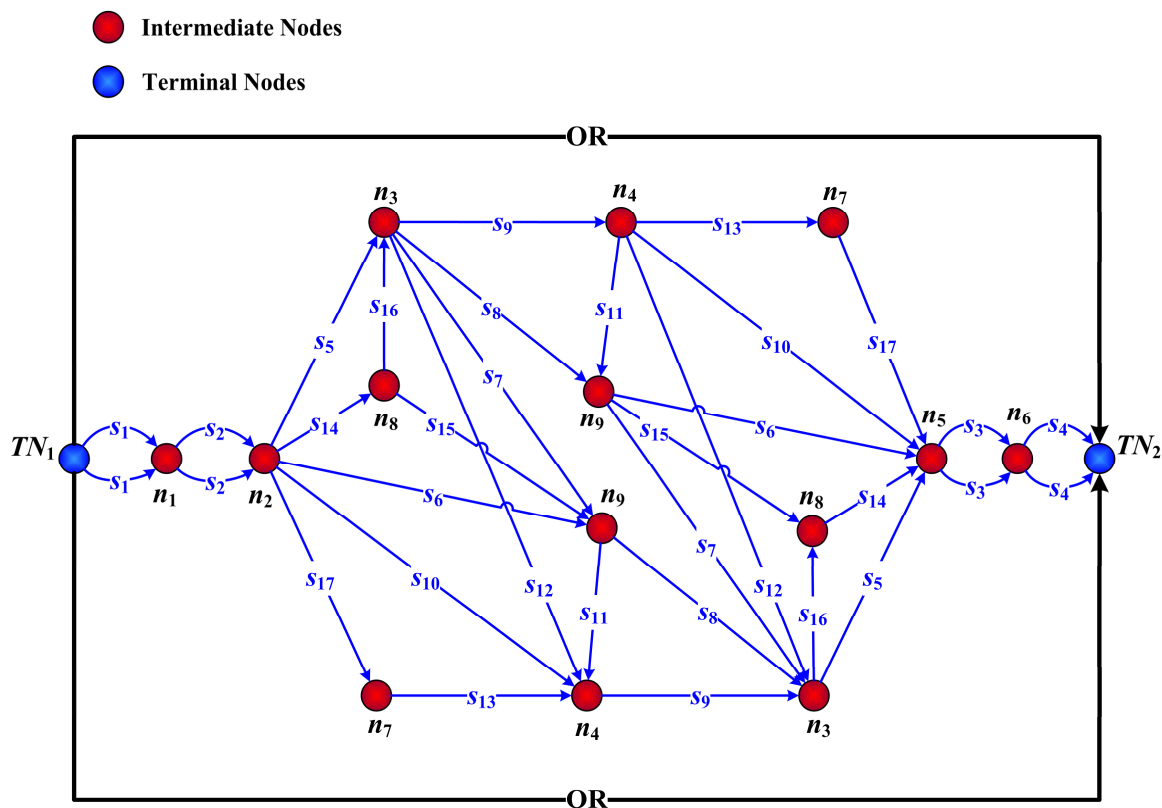
Figure 4-3c: Systematic construction of the 19-step WGS reaction mechanism RR Graph.

However, to be entirely consistent with thermodynamics $\vec{E}_{16}$ from Ref. [32] was modified to 144.75 from 143.785 kJ/mol, as given in Table 4-1. With the hence modified $\vec{E}_{16}$, all the KPL relations are satisfied for all the rest of the ERs.

Furthermore, the affinities, A_ρ of the elementary reactions ($A_\rho = -\Delta G_\rho$), in a FR are interrelated with the affinity of the OR, A_{OR}, via similar KPL relation. For instance, for FR_1: $s_1 + s_2 + s_3 + s_4 + s_5 + s_6 + s_8$, we have

$$A_1 + A_2 + A_3 + A_4 + A_5 + A_6 + A_8 = A_{OR}, \text{ i.e., } K_1K_2K_3K_4K_5K_6K_8 = K_{OR} \tag{4.4}$$

where, K_ρ and K_{OR} is the equilibrium constant of the elementary reaction step s_ρ and OR respectively. The data in Table 4-1 are consistent with this. Thus, KPL ensures thermodynamic consistency while KFL followed at each node is used to rigorously determine the network kinetics.

4.5 Network Analysis and Pruning

For the 17-step water gas shift reaction, the equivalent electrical circuit can be obtained simply by replacing the branches in the final RR Graph in Figure 4-3c by the step resistances. Figure 4-4, thus, provides the electrical analog or the reaction circuit of the WGS reaction. An accurate and robust simplification and reduction may be accomplished based on a comparison of the flux (current) along different pathways in the reaction circuit. The fractional surface coverage of the $q = 9$ linear independent intermediate species, namely, $H_2O \cdot S$, $CO \cdot S$, $H \cdot S$, $CO_2 \cdot S$, $OH \cdot S$, $O \cdot S$, $COOH \cdot S$, $HCOO \cdot S$, and $HCO \cdot S$, along with the free sites are obtained by solving KFL equations (and using mass action kinetics for the elementary steps) at 9 linearly independent INs along with site conservation equation. This set of QSS equations for the linearly independent intermediate species can be obtained directly from the step connectivity shown on the RR graph Figure 4-4,

$$n_1 : 2r_1 - 2r_2 = 0;$$
$$n_2 : 2r_2 - r_5 - r_6 - r_{10} - r_{14} - r_{17} = 0;$$
$$n_3 : r_5 - r_7 - r_8 - r_9 - r_{12} + r_{16} = 0;$$
$$n_4 : r_9 - r_{10} - r_{11} - r_{12} - r_{13} = 0;$$
$$n_5 : 2r_3 - r_5 - r_6 - r_{10} - r_{14} - r_{17} = 0; \qquad (4.5)$$
$$n_6 : 2r_3 - 2r_4 = 0;$$
$$n_7 : r_{13} - r_{17} = 0;$$
$$n_8 : r_{14} - r_{15} - r_{16} = 0;$$
$$n_9 : r_6 + r_7 - r_8 - r_{11} + r_{15} = 0$$

i.e.,

$$n_1 : 2(\vec{k}_1 p_{H_2O}\theta_0 - \bar{k}_1\theta_{H_2O\cdot S}) - 2(\vec{k}_2 p_{CO}\theta_0 - \bar{k}_2\theta_{CO\cdot S}) = 0;$$

$$n_2 : 2(\vec{k}_2 p_{CO}\theta_0 - \bar{k}_2\theta_{CO\cdot S}) - (\vec{k}_5\theta_{H_2O\cdot S}\theta_0 - \bar{k}_5\theta_{OH\cdot S}\theta_{H\cdot S}) - (\vec{k}_6\theta_{OH\cdot S}\theta_0 - \bar{k}_6\theta_{O\cdot S}\theta_{H\cdot S}) - (\vec{k}_{10}\theta_{COOH\cdot S}\theta_0 - \bar{k}_{10}\theta_{CO_2\cdot S}\theta_{H\cdot S})$$
$$- (\vec{k}_{14}\theta_{HCOO\cdot S}\theta_0 - \bar{k}_{14}\theta_{CO_2\cdot S}\theta_{H\cdot S}) - (\vec{k}_{17}\theta_{HCO\cdot S}\theta_0 - \bar{k}_{17}\theta_{CO\cdot S}\theta_{H\cdot S}) = 0;$$

$$n_3 : (\vec{k}_5\theta_{H_2O\cdot S}\theta_0 - \bar{k}_5\theta_{OH\cdot S}\theta_{H\cdot S}) - (\vec{k}_7\theta_{OH\cdot S}\theta_{OH\cdot S} - \bar{k}_7\theta_{H_2O\cdot S}\theta_{O\cdot S}) - (\vec{k}_8\theta_{CO\cdot S}\theta_{O\cdot S} - \bar{k}_8\theta_{CO_2\cdot S}\theta_0) - (\vec{k}_9\theta_{CO\cdot S}\theta_{OH\cdot S} - \bar{k}_9\theta_{COOH\cdot S}\theta_0)$$
$$- (\vec{k}_{12}\theta_{COOH\cdot S}\theta_{OH\cdot S} - \bar{k}_{12}\theta_{CO_2\cdot S}\theta_{H_2O\cdot S}) + (\vec{k}_{16}\theta_{CO_2\cdot S}\theta_{H_2O\cdot S} - \bar{k}_{16}\theta_{HCOO\cdot S}\theta_{OH\cdot S}) = 0;$$

$$n_4 : (\vec{k}_9\theta_{CO\cdot S}\theta_{OH\cdot S} - \bar{k}_9\theta_{COOH\cdot S}\theta_0) - (\vec{k}_{10}\theta_{COOH\cdot S}\theta_0 - \bar{k}_{10}\theta_{CO_2\cdot S}\theta_{H\cdot S}) - (\vec{k}_{11}\theta_{COOH\cdot S}\theta_{O\cdot S} - \bar{k}_{11}\theta_{CO_2\cdot S}\theta_{OH\cdot S})$$
$$- (\vec{k}_{12}\theta_{COOH\cdot S}\theta_{OH\cdot S} - \bar{k}_{12}\theta_{CO_2\cdot S}\theta_{H_2O\cdot S}) - (\vec{k}_{13}\theta_{COOH\cdot S}\theta_{CO\cdot S} - \bar{k}_{13}\theta_{CO_2\cdot S}\theta_{HCO\cdot S}) = 0;$$

$$n_5 : 2(\vec{k}_3\theta_{H\cdot S}^2 - \bar{k}_3 p_{H_2}\theta_0^2) - (\vec{k}_5\theta_{H_2O\cdot S}\theta_0 - \bar{k}_5\theta_{OH\cdot S}\theta_{H\cdot S}) - (\vec{k}_6\theta_{OH\cdot S}\theta_0 - \bar{k}_6\theta_{O\cdot S}\theta_{H\cdot S}) - (\vec{k}_{10}\theta_{COOH\cdot S}\theta_0 - \bar{k}_{10}\theta_{CO_2\cdot S}\theta_{H\cdot S})$$
$$- (\vec{k}_{14}\theta_{HCOO\cdot S}\theta_0 - \bar{k}_{14}\theta_{CO_2\cdot S}\theta_{H\cdot S}) - (\vec{k}_{17}\theta_{HCO\cdot S}\theta_0 - \bar{k}_{17}\theta_{CO\cdot S}\theta_{H\cdot S}) = 0;$$

$$n_6 : 2(\vec{k}_3\theta_{H\cdot S}^2 - \bar{k}_3 p_{H_2}\theta_0^2) - 2(\vec{k}_4\theta_{CO_2\cdot S} - \bar{k}_4 p_{CO_2}\theta_0) = 0;$$

$$n_7 : (\vec{k}_{13}\theta_{COOH\cdot S}\theta_{CO\cdot S} - \bar{k}_{13}\theta_{CO_2\cdot S}\theta_{HCO\cdot S}) - (\vec{k}_{17}\theta_{HCO\cdot S}\theta_0 - \bar{k}_{17}\theta_{CO\cdot S}\theta_{H\cdot S}) = 0;$$

$$n_8 : (\vec{k}_{14}\theta_{HCOO\cdot S}\theta_0 - \bar{k}_{14}\theta_{CO_2\cdot S}\theta_{H\cdot S}) - (\vec{k}_{15}\theta_{CO_2\cdot S}\theta_{OH\cdot S} - \bar{k}_{15}\theta_{HCOO\cdot S}\theta_{O\cdot S}) - (\vec{k}_{16}\theta_{CO_2\cdot S}\theta_{H_2O\cdot S} - \bar{k}_{16}\theta_{HCOO\cdot S}\theta_{OH\cdot S}) = 0;$$

$$n_9 : (\vec{k}_6\theta_{OH\cdot S}\theta_0 - \bar{k}_6\theta_{O\cdot S}\theta_{H\cdot S}) + (\vec{k}_7\theta_{OH\cdot S}\theta_{OH\cdot S} - \bar{k}_7\theta_{H_2O\cdot S}\theta_{O\cdot S}) - (\vec{k}_8\theta_{CO\cdot S}\theta_{O\cdot S} - \bar{k}_8\theta_{CO_2\cdot S}\theta_0)$$
$$- (\vec{k}_{11}\theta_{COOH\cdot S}\theta_{O\cdot S} - \bar{k}_{11}\theta_{CO_2\cdot S}\theta_{OH\cdot S}) + (\vec{k}_{15}\theta_{CO_2\cdot S}\theta_{OH\cdot S} - \bar{k}_{15}\theta_{HCOO\cdot S}\theta_{O\cdot S}) = 0$$
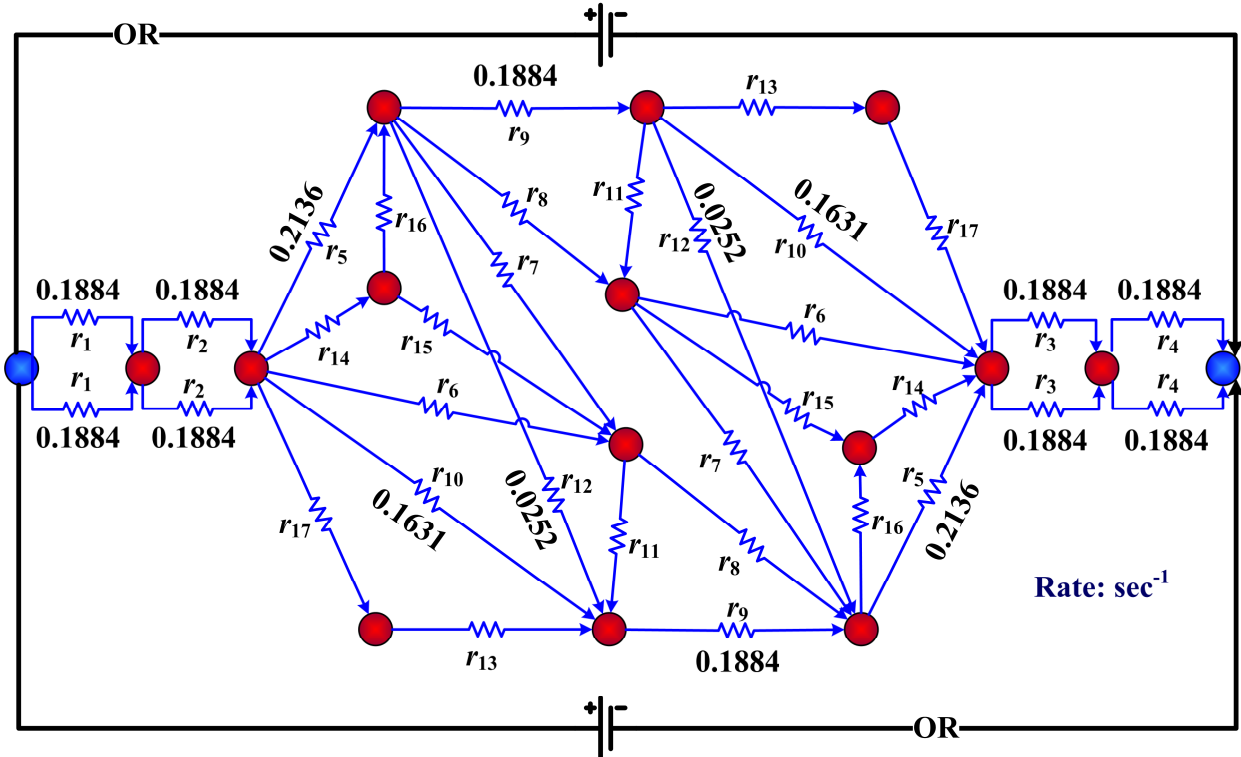
$$(4.6)$$

Figure 4-4: The electrical/reaction circuit analog of the reaction network for the WGS reaction along with the rates, resistances and reversibilities of elementary reaction steps for conditions quoted in text.

The above set of 9 non-linear algebraic KFL equations, along with the site balance equation,

$$\theta_{H_2O \cdot S} + \theta_{CO \cdot S} + \theta_{H \cdot S} + \theta_{CO_2 \cdot S} + \theta_{OH \cdot S} + \theta_{O \cdot S} + \theta_{COOH \cdot S} + \theta_{HCOO \cdot S} + \theta_{HCO \cdot S} + \theta_0 = 1 \qquad (4.7)$$

may be numerically solved simultaneously, for given input conditions (temperature and partial pressures of reactants) and conversion, to obtain the unknown site fractions of intermediate species, θ_k. Thereupon, one may readily calculate the rate, affinity, and resistance of each elementary reaction step. Finally, the rate of the OR can be obtained from TNs, e.g. $r_{OR} = r_1 = r_4$ (Figure 4-4). Moreover, if combined with the mass-balance equation for a given reactor, one can predict the reactor performance, or conversion, X.

For Pt catalyst in a well-mixed reactor, $T = 548$ $^{\circ}$C; feed composition of H_2O(10%), CO(10%) and N_2(balance), the calculated rate (flux) along with reversibility and resistance for the elementary reaction steps is mentioned in Figure 4-4. Note, that only flux through dominant steps is mentioned on Figure 4-4. For all other steps, the flux is negligible (close to zero). Thus, for the said conditions, the adsorption/desorption steps s_1, s_2, s_3, s_4, dissociation of water, i.e. step s_5, formation of carboxyl species, i.e., step s_9, and subsequent direct decomposition of adsorbed carboxyl, i.e. step s_{10} and the decomposition of adsorbed carboxyl via adsorbed hydroxyl species, i.e. step s_{12} are the only kinetically significant elementary reaction steps.

Further, flux (current) comparison in the various branches (reaction steps) for the above reaction conditions reveal that there are only two dominant pathways, namely FR_2: $s_1 + s_2 + s_3 + s_4 + s_5 + s_9 + s_{10}$ and FR_4: $s_1 + s_2 + s_3 + s_4 + 2s_5 + s_9 + s_{12}$ comprising of the steps mentioned above. Furthermore, it is evident from Figure 4-4, that direct decomposition of adsorbed carboxyl, i.e. s_{10}: COOH·S + S $\leftrightarrows$ CO_2·S + H·S contributes significantly to the overall flux rather than decomposition of adsorbed carboxyl via adsorbed hydroxyl species, i.e. s_{12}: COOH·S + OH·S $\leftrightarrows$ CO_2·S + H_2O·S. Thus, FR_2 provides for ~87% of the overall flux, while the remaining 13% is contributed by FR_4. It should be noted that a higher steam-to-carbon ratio could lead to an increase in the concentration of adsorbed hydroxyl species and could potentially increase the flux contribution via step s_{12}.
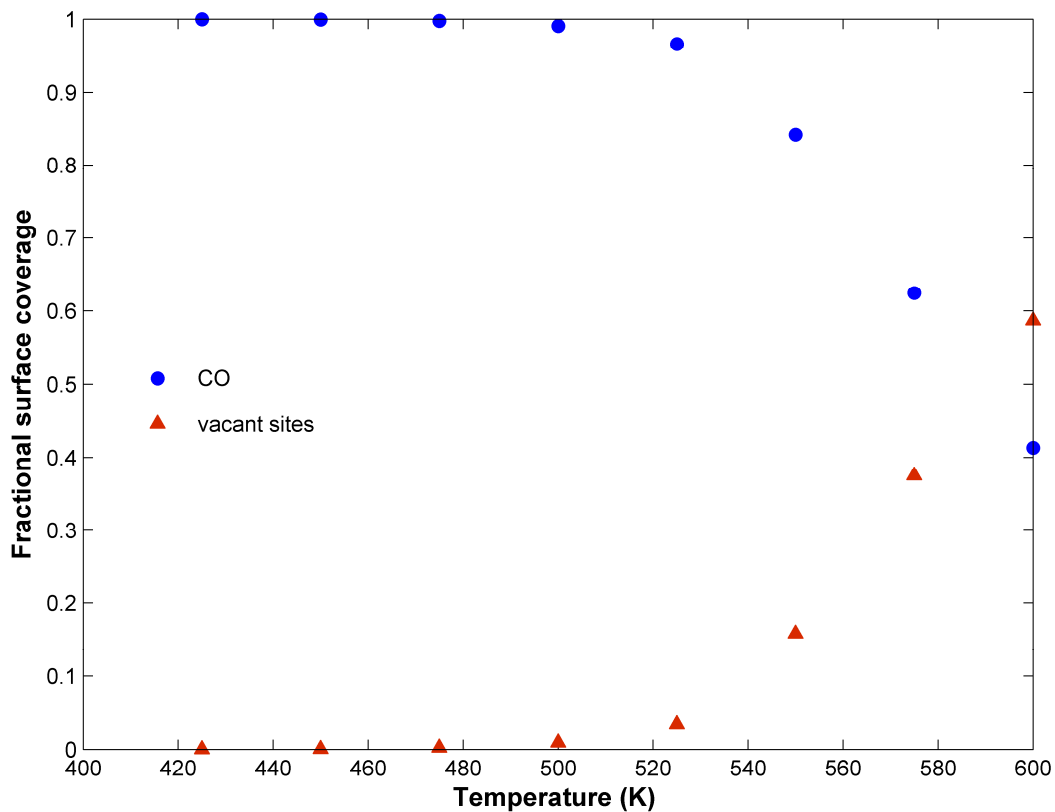
Figure 4-5: Surface coverage of the dominant reaction species as a function of temperature for WGS for the reaction conditions mentioned in Figure 4-4.

On the other hand, higher affinity of CO toward Pt (Figure 4-5), i.e. higher surface coverage of CO·S could render step s_{12} to be limited by the small OH·S surface coverage. Finally, the step reversibilites and resistances (Figure 4-4) reveal that amongst the key elementary steps, only steps s_5, s_{10} and s_{12} are slow or non-QE steps, while rest of the steps are all quasi-equilibrated for the said reaction conditions. However, these conclusions may or may not be valid at other conditions.

Validation of this reduction and simplification of the RR network over a broad range of temperatures can be accomplished by comparing the resistances along parallel paths between two nodes, which have the same affinity drop by virtue of KPL, i.e., by considering each ER as two parallel paths and comparing the total resistance of each path. If the resistance along one path is much larger than the other, it would be safe to assume that the path contributes little to the flux and may be neglected. Finally, the effect of eliminating a step or pathway is validated by calculating the overall kinetics without the elementary reaction step in question.

Let us consider ER$_6$: $s_5 - s_{14} - s_{16}$, which implies there are two parallel pathways for formation of adsorbed hydrogen and hydroxyl species. One pathway is the direct dissociation of adsorbed water via step s_5, i.e. $H_2O·S + S \leftrightarrows OH·S + H·S$. The other pathway proceeds through the formate species, via steps s_{14} and s_{16} as shown below

$$\underline{\sigma_\rho}$$

s_{14}:	$HCOO·S + S \leftrightarrows CO_2·S + H·S$	+1
s_{16}:	$CO_2·S + H_2O·S \leftrightarrows HCOO·S + OH·S$	+1

Net: $H_2O·S + S \leftrightarrows OH·S + H·S$
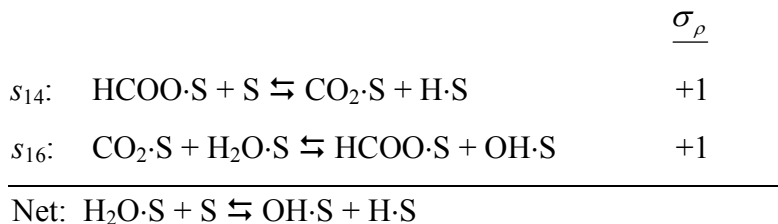
The resistance of the first pathway is simply R_5, while that for the second pathway comprising of two steps in series is $R_{14} + R_{16}$. Figure 4-6 compares the resistance of these two pathways as a function of temperature for the reaction conditions mentioned above. It is evident from Figure 4-6, that $R_{14} + R_{16}$ is several orders of magnitude higher than R_5 over a broad temperature range. Since a reaction will always proceed largely via the minimum resistance pathway, it is reasonable to conclude that it may be possible to eliminate steps s_{14} and s_{16} from the mechanism.
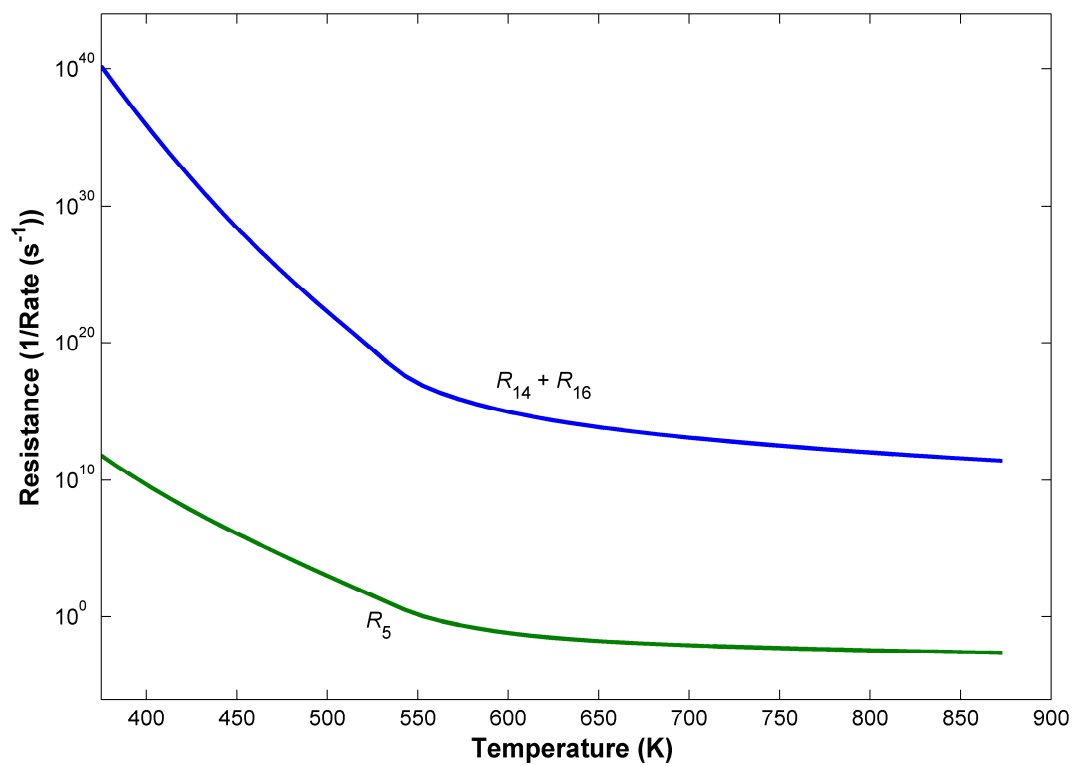
Figure 4-6: Parallel pathway resistance ($R_{14} + R_{16}$ vs. R_5) comparison as a function of temperature for the conditions quoted in the text.

To validate this elimination, we check the effect of s_{14} and s_{16} on the overall kinetics by comparing the simulated overall kinetics of the complete mechanism to the mechanism less s_{14} and s_{16} and find that these steps do not contribute significantly to the overall reaction flux.

We next consider the parallel pathways represented by ER_5: $s_6 - s_{14} - s_{15}$ for the formation of O·S and H·S. Figure 4-7 reveals that $R_{14} + R_{15}$ is several orders of magnitude higher than R_6 and hence can be logically deemed kinetically insignificant. Continuing the pruning of the RR graph thus, ER_{11}: $s_{10} - s_{13} - s_{17}$ provides two pathways, first being the direct decomposition of adsorbed carboxyl species into CO_2·S and H·S (step s_{10}), while the other being a two-step decomposition via steps s_{13} and s_{17}. The resistance of the first pathway is simply R_{10} while that for the other with two series resistors is $R_{13} + R_{17}$. Numerical simulations of these two resistances as a function of temperature are presented in Figure 4-8. It is seen that $R_{13} + R_{17}$ is several orders of magnitude higher than R_{10} at all temperatures. Hence, there is ample justification to neglect steps s_{13} and s_{17}.

Continuing the pruning of the RR graph in this vein, the next step is to consider the two parallel branches via ER_{21}: $s_7 + s_{11} - s_{12}$. One pathway, i.e. step s_{12} represents the decomposition of COOH·S via OH·S, while the other is a two step pathway, comprising of steps s_7 and s_{11}. From numerical simulations it may be concluded (Figure 4-9) that single step s_{12} offers the minimum resistance pathway and, consequently, the steps s_7 and s_{11} may be disregarded. Finally, we compare the resistances of the two parallel branches for formation of CO_2·S and H·S as represented by ER_2: $s_6 + s_8 - s_9 - s_{10}$. Both pathways comprise of two steps (resistors) in series where the resistance is given as $R_6 + R_8$ and $R_9 + R_{10}$, for the respective pathway. Based on numerical results (Figure 4-10), we conclude that the resistance $R_6 + R_8$ is much higher than $R_9 + R_{10}$ and, hence, the formation of CO_2·S and H·S via carboxyl species (i.e. steps s_9 and s_{10}) is much faster than that via steps s_6 and s_8. In other words, the steps s_6 and s_8 can be eliminated from the mechanism without materially affecting the overall reaction flux.
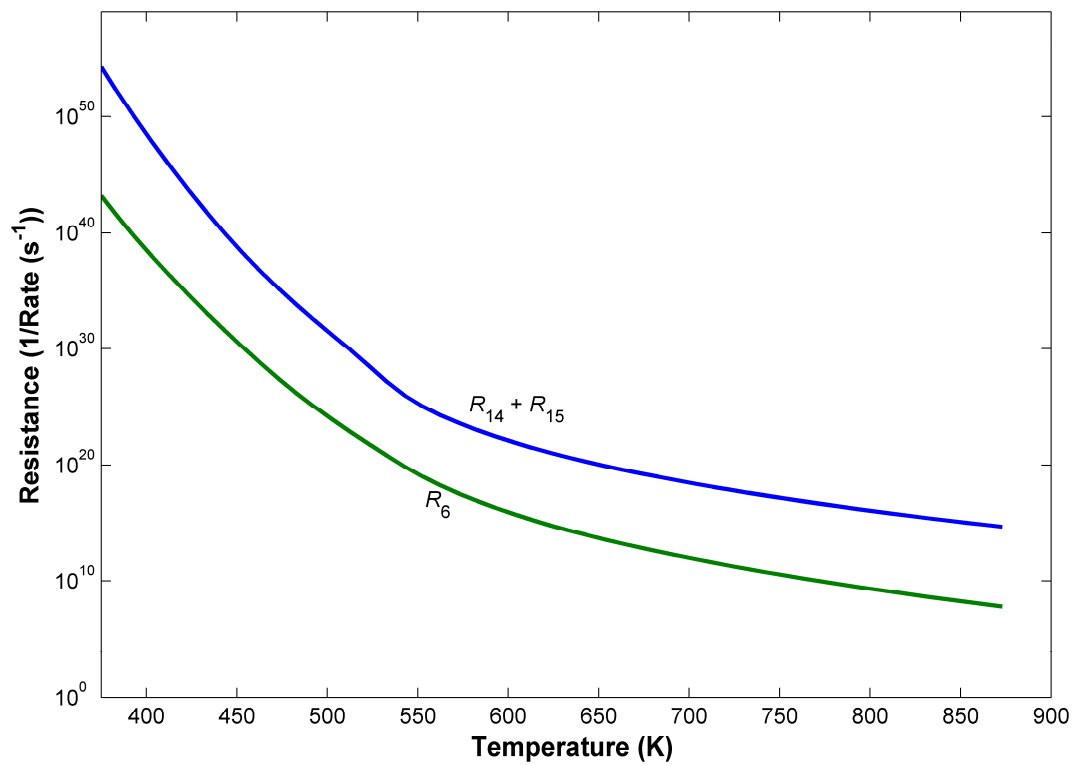
Figure 4-7: Parallel pathway resistance ($R_{14} + R_{15}$ vs. R_6) comparison as a function of temperature for the conditions quoted in the text.
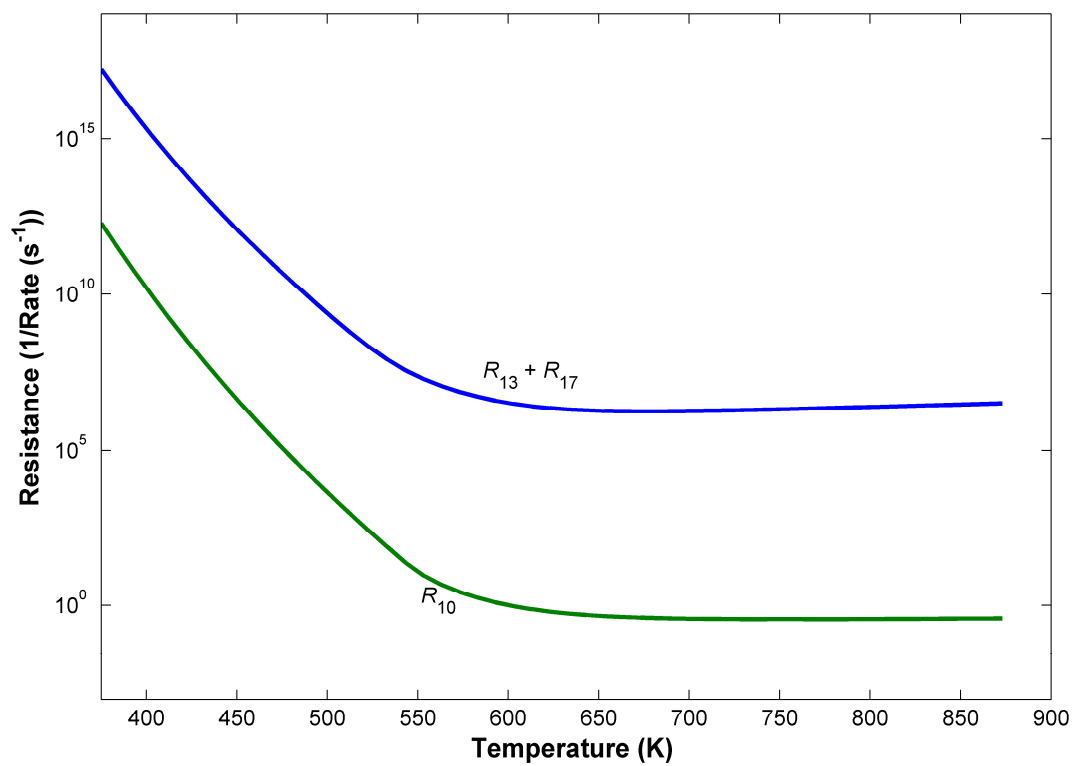
Figure 4-8: Parallel pathway resistance ($R_{13} + R_{17}$ vs. R_{10}) comparison as a function of temperature for the conditions quoted in the text.
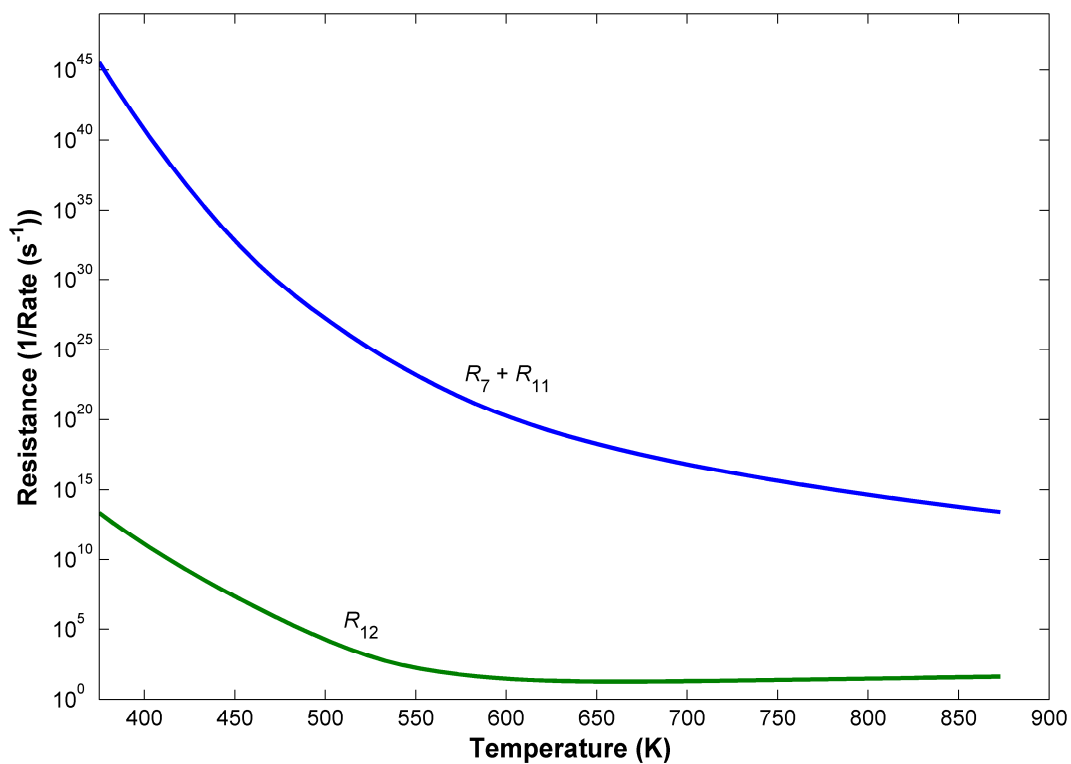
Figure 4-9: Parallel pathway resistance ($R_7 + R_{11}$ vs. R_{12}) comparison as a function of temperature for the conditions quoted in the text.
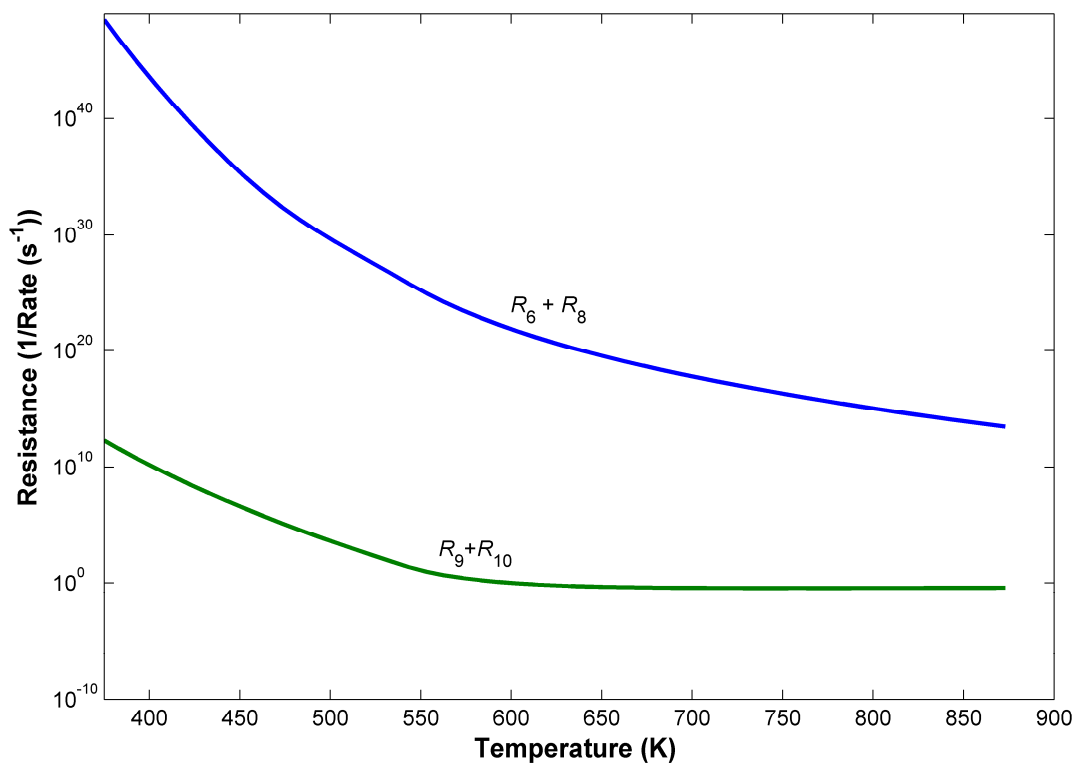
Figure 4-10: Parallel pathway resistance ($R_6 + R_8$ vs. $R_9 + R_{10}$) comparison as a function of temperature for the conditions quoted in the text.

The elimination of steps, s_6, s_7, s_8, s_{11}, s_{13}, $s_{14,}$ s_{15}, s_{16} and s_{17} from the mechanism based on the above logic is validated by comparing simulated results of the complete mechanism with results from the mechanism excluding s_6, s_7, s_8, s_{11}, s_{13}, $s_{14,}$ s_{15}, s_{16} and s_{17}, i.e., the simplified 8 step model. Eliminating the above steps leave us with a reduced network comprising of only 8 elementary reactions and 2 FRs, namely, FR_2 and FR_4 from the list in Table 4-2. The overall resistances of each of these FRs is equal to

$$R_{FR_2}:\quad R_1 + R_2 + R_3 + R_4 + R_5 + R_9 + R_{10}$$

$$R_{FR_4}:\quad R_1 + R_2 + R_3 + R_4 + 4R_5 + R_9 + R_{12}$$

As can be seen from Figure 4-11, FR_4 has a higher resistance as compared to FR_2, more so at temperatures > 500 K, i.e. in the temperature region of interest with Pt catalyst. Thus, the overall WGS mechanism is dominated by FR_2, conventionally written as follows:

$$\underline{\sigma_\rho}$$

		σ_ρ
s_1:	$H_2O + S \leftrightarrows H_2O{\cdot}S$	+1
s_2:	$CO + S \leftrightarrows CO{\cdot}S$	+1
s_3:	$2H{\cdot}S \leftrightarrows H_2 + 2S$	+1
s_4:	$CO_2{\cdot}S \leftrightarrows CO_2 + S$	+1
s_5:	$H_2O{\cdot}S + S \leftrightarrows OH{\cdot}S + H{\cdot}S$	+1
s_9:	$CO{\cdot}S + OH{\cdot}S \leftrightarrows COOH{\cdot}S + S$	+1
s_{10}:	$COOH{\cdot}S + S \leftrightarrows CO_2{\cdot}S + H{\cdot}S$	+1

Net: $H_2O + CO \leftrightarrows CO_2 + H_2$
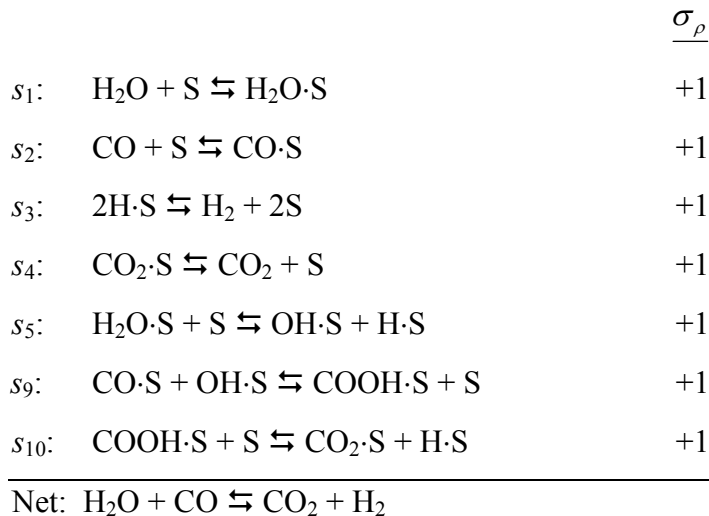
However, as mentioned above, a higher steam-to-carbon ratio could potentially increase the concentration of OH·S species, thereby increasing the rate consumption of carboxyl species via step s_{12}. However, in light of the high surface coverage of CO on Pt, it is unlikely that the surface coverage of OH·S species will be increased dramatically except at very high temperatures (Figure 4-5). The thus reduced RR graph for the WGS mechanism on Pt(111) is shown in Figure 4-12, which is simply a catalytic sequence.
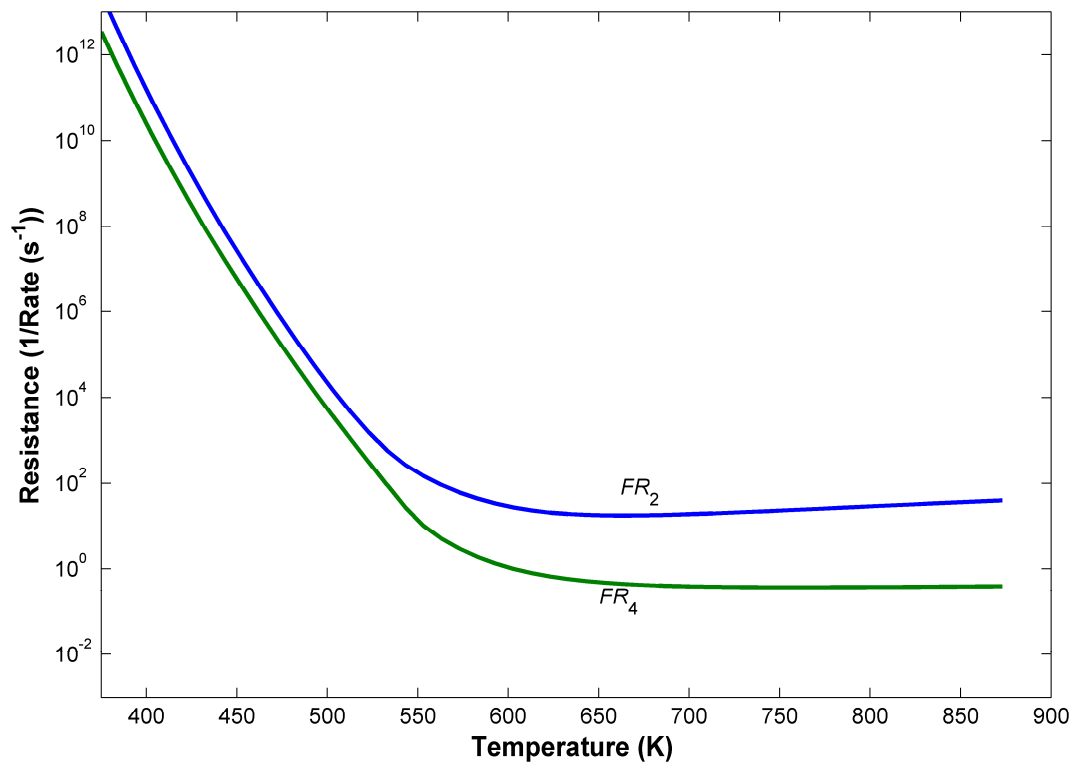
Figure 4-11: Resistances of FR_2 and FR_4 vs. temperature for the conditions quoted in the text.
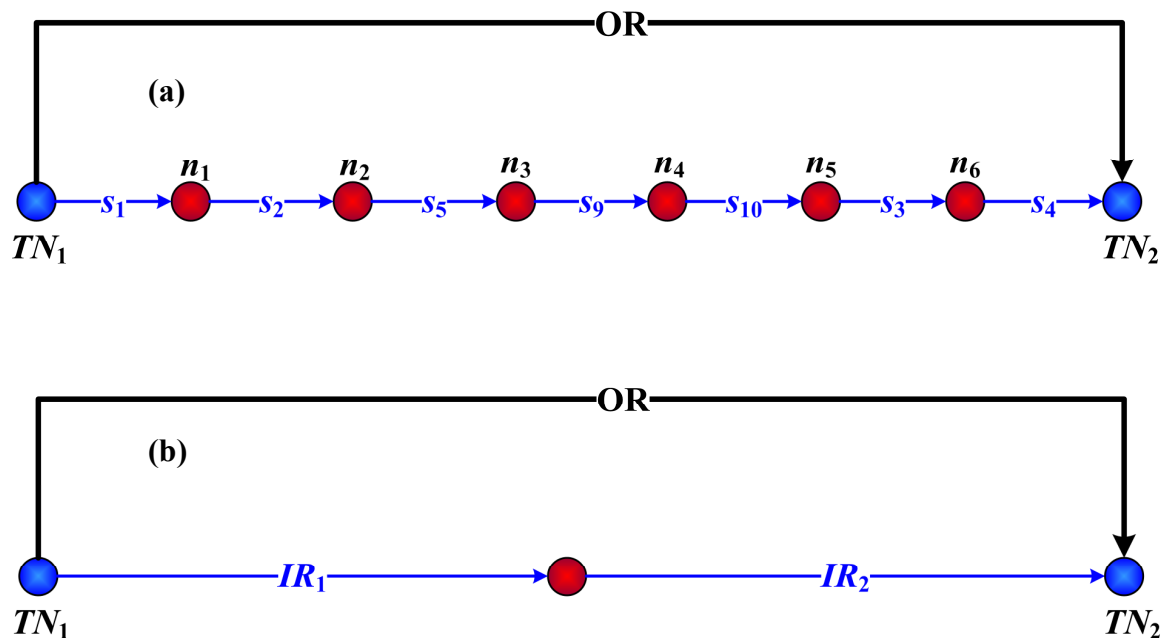
Figure 4-12: Pruned RR graph for the WGS mechanism on Pt(111).

4.6 Overall Reaction Rate via Electrical Analogy

Now that the mechanism has been dramatically pruned, we are in a position to consider a rate expression for the overall reaction. First, we write a formal rate equation for the kinetics of the reduced reaction network, Figure 4-12a, by employing the electrical circuit analogy and the linear rate law analogous to Ohm's law.

Thus, the overall rate (overall current) is the ratio of the affinity of the OR and the overall resistance of the reaction network, i.e., $r_{OR} = \dfrac{\mathscr{A}_{OR}}{R_{OR}}$, where the overall resistance of the reduced reaction network (Figure 4-12a) is R_{FR_2} : $R_1 + R_2 + R_3 + R_4 + R_5 + R_9 + R_{10}$

Thus,

$$r_{OR} = \frac{\mathscr{A}_{OR}}{R_1 + R_2 + R_3 + R_4 + R_5 + R_9 + R_{10}} \tag{4.8}$$

where, the resistance of a step is defined in chapter II. It can be seen from Figure 4-13, that R_5 and R_{10} are the dominant reaction steps for the above sequence. Thus,

$$r_{OR} \approx \frac{\mathscr{A}_{OR}}{R_5 + R_{10}} \tag{4.9}$$

All the other steps, s_1, s_2, s_3, s_4, and s_9 are at QE (Figure 4-14). Following Temkin, now the reduced WGS mechanism can be simply written as a 2-step lumped pathway, as follows, which is represented in Figure 4-12b.

$$\underline{\sigma_\rho}$$

$IR_1 : (+1)s_1 + (+1/2)s_3 + (+1)s_5$: $H_2O + S \leftrightarrows OH{\cdot}S + 1/2H_2$ $+1$

$IR_2 : (+1)s_2 + (+1/2)s_3 + (+1)s_4 + (+1)s_9 + (+1)s_{10}$: $CO + OH{\cdot}S \leftrightarrows CO_2 + 1/2H_2 + S$ $+1$

Net: $CO + H_2O \leftrightarrows CO_2 + H_2$
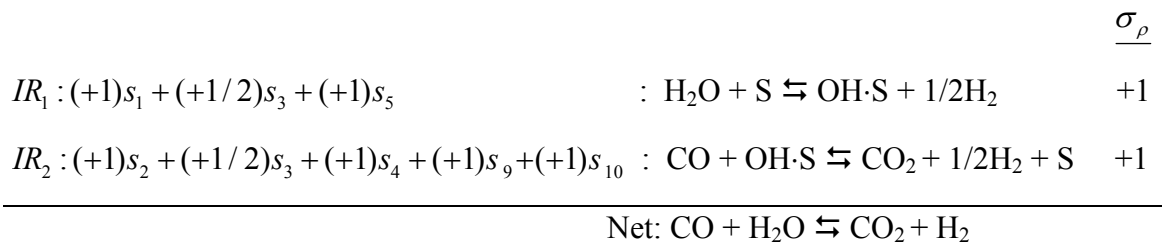
While the above formal rate expression (Eq. (4.9)) is adequate for numerical computation of the rate from numerically calculated resistances, it is more desirable to obtain, if possible, an explicit rate expression in terms of the terminal species composition.
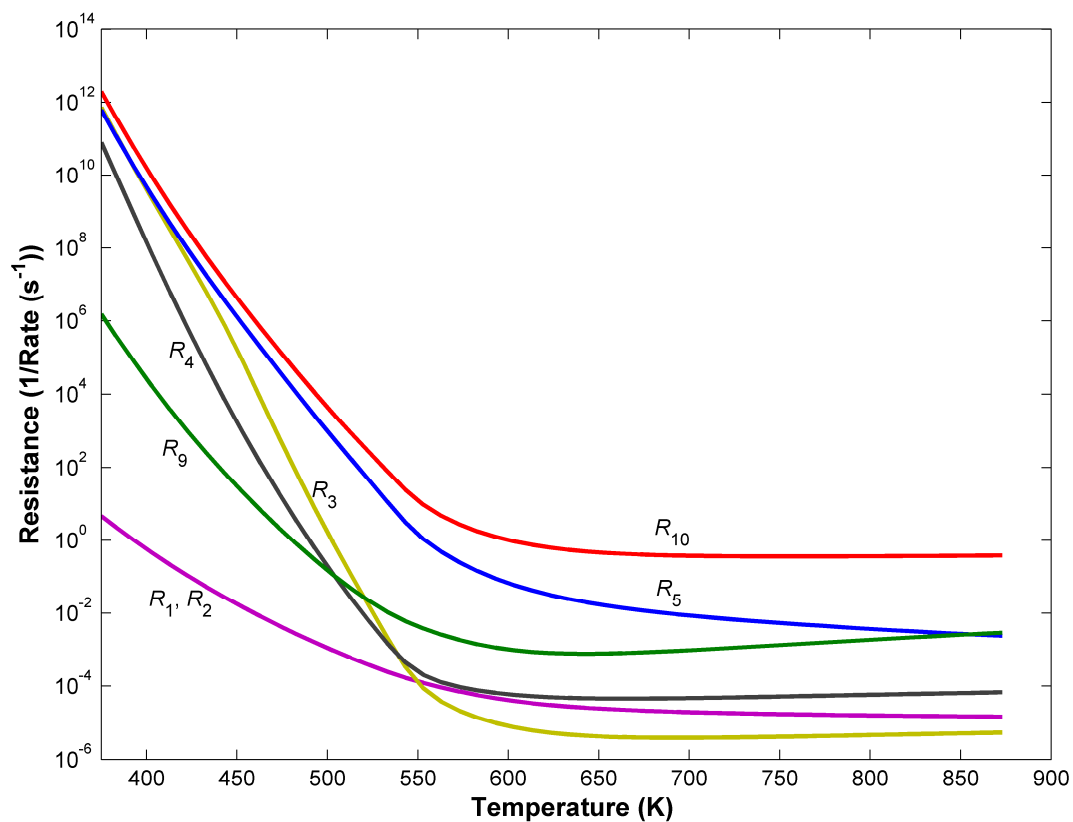
Figure 4-13: Comparison of series resistance as a function of temperature in the dominant reaction pathway for WGS for conditions mentioned in the text.
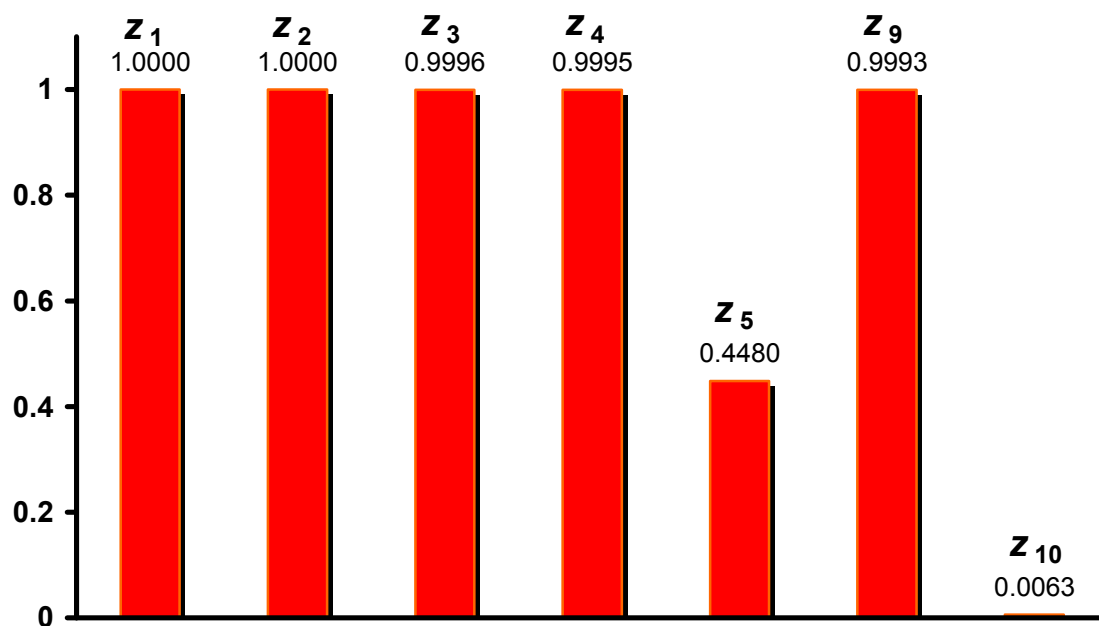
Figure 4-14: Step reversibilites for the elementary reaction steps in the dominant reaction
sequence for WGS for conditions mentioned in Figure 4-4.

This is accomplished by following the alternate electrical analogy proposed in chapter 2. Based on the approach presented in chapter II, the overall reaction rate can be approximated as

$$r_{OR} \approx \frac{E_{OR}}{R_{OR}^{\bullet}} = \frac{E_{OR}}{R_{IR_1}^{\bullet} + R_{IR_2}^{\bullet}} \tag{4.10}$$

IR_1 above is comprised of steps s_1, s_3 and s_5. Based on step reversibilities, z_ρ (Figure 4-14) we see that steps s_1 and s_3 are both QE. Thus, the flux through IR_1 is governed by step s_5, i.e. dissociation of water. Similarly, the flux through IR_2 is governed by step s_{10}, i.e. direct decomposition of carboxyl, others being QE steps.

Thus,

$$\left. \begin{aligned} R_{IR_1}^{\bullet} &\approx R_5^{\bullet} \\ R_{IR_2}^{\bullet} &\approx R_{10}^{\bullet} \end{aligned} \right\} \tag{4.11}$$

Substituting Eq. (4.11) in Eq. (4.10), we have

$$r_{OR} \approx \frac{E_{OR}}{R_5^{\bullet} + R_{10}^{\bullet}} \tag{4.12}$$

$R_5^{\bullet}$ and $R_{10}^{\bullet}$ can be ascertained *a priori* following the LHHW approach detailed in chapter II. To obtain the step resistances above, let us first consider step s_5 as the RDS, the remaining steps being at QE. Thus,

$$R_5^{\bullet} = \frac{1}{\vec{r}_5^{\bullet}} = \frac{1}{\vec{\omega}_5 \theta_{H_2O\cdot S,5}^{\bullet} \theta_{0,5}^{\bullet}} = \frac{1}{\vec{\omega}_5 \left(\dfrac{\theta_{H_2O\cdot S,5}^{\bullet}}{\theta_{0,5}^{\bullet}} \right) (\theta_{0,5}^{\bullet})^2} \tag{4.13}$$

where $\theta_{k,\rho}^{\bullet}$ and $\theta_{0,\rho}^{\bullet}$ represents site fraction of intermediate k and vacant surface sites S, respectively, when s_ρ is the RDS. With s_5 as the RDS, thus, and all other steps at QE, the appropriate IRs for the formation of six linearly independent surface intermediates, $H_2O\cdot S$, $CO\cdot S$, $H\cdot S$, $CO_2\cdot S$, $COOH\cdot S$, $OH\cdot S$ (in the reduced 7-step mechanism) from the vacant surface sites S, comprising of steps other than s_5, are

$IR_{H_2O \cdot S} : (+1)s_1$ $: H_2O + S \leftrightarrows H_2O \cdot S$

$IR_{CO \cdot S} : (+1)s_2$ $: CO + S \leftrightarrows CO \cdot S$

$IR_{H \cdot S} : (-1/2)s_3$ $: 1/2H_2 + S \leftrightarrows H \cdot S$

$IR_{CO_2 \cdot S} : (-1)s_4$ $: CO_2 + S \leftrightarrows CO_2 \cdot S$

$IR_{COOH \cdot S} : (-1/2)s_3 + (-1)s_4 + (-1)s_{10}$ $: 1/2H_2 + CO_2 + S \leftrightarrows COOH \cdot S$

$IR_{OH \cdot S} : (-1)s_2 + (-1/2)s_3 + (-1)s_4 + (-1)s_9 + (-1)s_{10}$ $: 1/2H_2 + CO_2 + S \leftrightarrows CO + OH \cdot S$

$$(4.14)$$
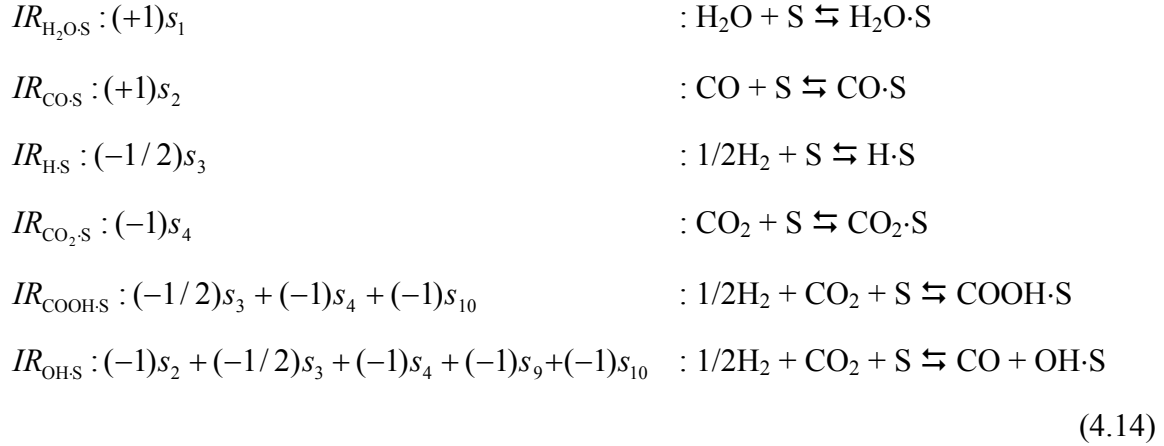
Then, using Eq. 2.25, for the QE steps, the site fraction ratios are

$$
\left.
\begin{aligned}
\frac{\theta^{\bullet}_{H_2O \cdot S,5}}{\theta^{\bullet}_{0,5}} &= \left(\frac{\vec{\omega}_1}{\bar{\omega}_1} \right)^{+1} \\[2mm]
\frac{\theta^{\bullet}_{CO \cdot S,5}}{\theta^{\bullet}_{0,5}} &= \left(\frac{\vec{\omega}_2}{\bar{\omega}_2} \right)^{+1} \\[2mm]
\frac{\theta^{\bullet}_{H \cdot S,5}}{\theta^{\bullet}_{0,5}} &= \left(\frac{\vec{\omega}_3}{\bar{\omega}_3} \right)^{-1/2} \\[2mm]
\frac{\theta^{\bullet}_{CO_2 \cdot S,5}}{\theta^{\bullet}_{0,5}} &= \left(\frac{\vec{\omega}_4}{\bar{\omega}_4} \right)^{-1} \\[2mm]
\frac{\theta^{\bullet}_{COOH \cdot S,5}}{\theta^{\bullet}_{0,5}} &= \left(\frac{\vec{\omega}_3}{\bar{\omega}_3} \right)^{-1/2} \left(\frac{\vec{\omega}_4}{\bar{\omega}_4} \right)^{-1} \left(\frac{\vec{\omega}_{10}}{\bar{\omega}_{10}} \right)^{-1} \\[2mm]
\frac{\theta^{\bullet}_{OH \cdot S,5}}{\theta^{\bullet}_{0,5}} &= \left(\frac{\vec{\omega}_2}{\bar{\omega}_2} \right)^{-1} \left(\frac{\vec{\omega}_3}{\bar{\omega}_3} \right)^{-1/2} \left(\frac{\vec{\omega}_4}{\bar{\omega}_4} \right)^{-1} \left(\frac{\vec{\omega}_9}{\bar{\omega}_9} \right)^{-1} \left(\frac{\vec{\omega}_{10}}{\bar{\omega}_{10}} \right)^{-1}
\end{aligned}
\right\}
\qquad (4.15)
$$

Finally using these in site balance, Eq. 2.26,

$$
\frac{1}{\theta^{\bullet}_{0,5}} = 1 + \frac{\theta^{\bullet}_{H_2O \cdot S,5}}{\theta^{\bullet}_{0,5}} + \frac{\theta^{\bullet}_{CO \cdot S,5}}{\theta^{\bullet}_{0,5}} + \frac{\theta^{\bullet}_{H \cdot S,5}}{\theta^{\bullet}_{0,5}} + \frac{\theta^{\bullet}_{CO_2 \cdot S,5}}{\theta^{\bullet}_{0,5}} + \frac{\theta^{\bullet}_{COOH \cdot S,5}}{\theta^{\bullet}_{0,5}} + \frac{\theta^{\bullet}_{OH \cdot S,5}}{\theta^{\bullet}_{0,5}}
\qquad (4.16)
$$

Thus, we have from Eq. (4.13)

$$
R^{\bullet}_5 = \frac{1}{\bar{\omega}_5 \left(\dfrac{\vec{\omega}_1}{\bar{\omega}_1} \right)} \left(1 + \frac{\vec{\omega}_1}{\bar{\omega}_1} + \frac{\vec{\omega}_2}{\bar{\omega}_2} + \sqrt{\frac{\bar{\omega}_3}{\vec{\omega}_3}} + \frac{\vec{\omega}_4}{\bar{\omega}_4} + \sqrt{\frac{\bar{\omega}_3}{\vec{\omega}_3}} \frac{\vec{\omega}_4}{\bar{\omega}_4} \frac{\vec{\omega}_{10}}{\bar{\omega}_{10}} + \frac{\vec{\omega}_2}{\bar{\omega}_2} \sqrt{\frac{\bar{\omega}_3}{\vec{\omega}_3}} \frac{\vec{\omega}_4}{\bar{\omega}_4} \frac{\vec{\omega}_9}{\bar{\omega}_9} \frac{\vec{\omega}_{10}}{\bar{\omega}_{10}} \right)^2
\qquad (4.17)
$$

Let us next consider step s_{10} as the RDS while the others at QE in order to obtain an explicit expression for $R_{10}^\bullet$.

$$R_{10}^\bullet = \frac{1}{\vec{r}_{10}^\bullet} = \frac{1}{\vec{\omega}_{10}\theta_{COOH\cdot S,10}^\bullet\theta_{0,10}^\bullet} = \frac{1}{\vec{\omega}_{10}\left(\dfrac{\theta_{COOH\cdot S,10}^\bullet}{\theta_{0,10}^\bullet}\right)(\theta_{0,10}^\bullet)^2} \qquad (4.18)$$

With s_{10} as the RDS, and all other steps at QE, the appropriate IRs for the formation of six linearly independent surface intermediates, $H_2O\cdot S$, $CO\cdot S$, $H\cdot S$, $CO_2\cdot S$, $COOH\cdot S$, $OH\cdot S$ from the vacant surface sites S, comprising of steps other than s_{10}, are

$$IR_{H_2O\cdot S} : (+1)s_1 \qquad\qquad\qquad : H_2O + S \leftrightarrows H_2O\cdot S$$

$$IR_{CO\cdot S} : (+1)s_2 \qquad\qquad\qquad : CO + S \leftrightarrows CO\cdot S$$

$$IR_{H\cdot S} : (-1/2)s_3 \qquad\qquad\qquad : 1/2H_2 + S \leftrightarrows H\cdot S$$

$$IR_{CO_2\cdot S} : (-1)s_4 \qquad\qquad\qquad : CO_2 + S \leftrightarrows CO_2\cdot S$$

$$IR_{COOH\cdot S} : (+1)s_1 + (+1)s_2 + (+1/2)s_3 + (+1)s_5 + (+1)s_9 : H_2O + CO + S \leftrightarrows COOH\cdot S + 1/2H_2$$

$$IR_{OH\cdot S} : (+1)s_1 + (+1/2)s_3 + (+1)s_5 \qquad : H_2O + S \leftrightarrows OH\cdot S + 1/2H_2$$

$$(4.19)$$
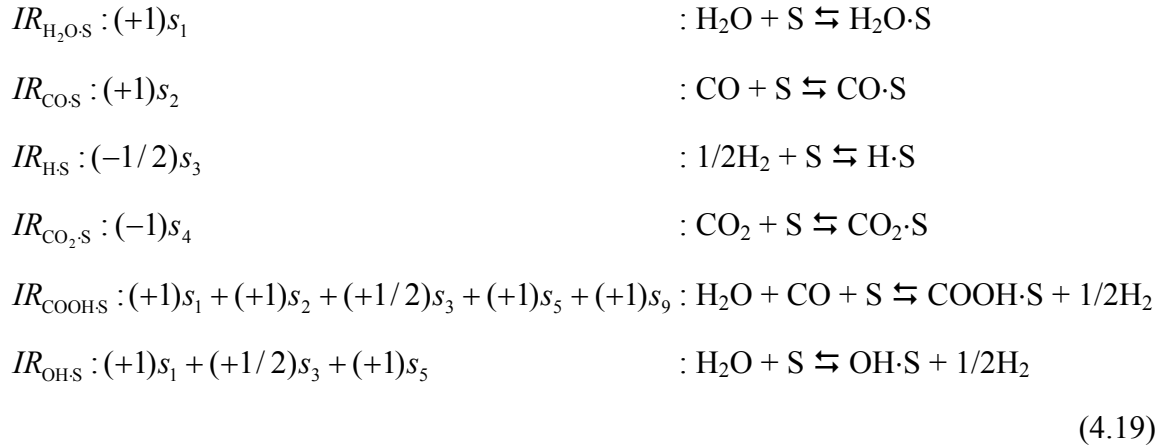
Then, using Eq. 2.25, for the QE steps, the site fraction ratios are

$$
\left.
\begin{aligned}
\frac{\theta^{\bullet}_{H_2O\cdot S,10}}{\theta^{\bullet}_{0,10}} &= \left(\frac{\vec{\omega}_1}{\overleftarrow{\omega}_1}\right)^{+1} \\[6pt]
\frac{\theta^{\bullet}_{CO\cdot S,10}}{\theta^{\bullet}_{0,10}} &= \left(\frac{\vec{\omega}_2}{\overleftarrow{\omega}_2}\right)^{+1} \\[6pt]
\frac{\theta^{\bullet}_{H\cdot S,10}}{\theta^{\bullet}_{0,10}} &= \left(\frac{\vec{\omega}_3}{\overleftarrow{\omega}_3}\right)^{-1/2} \\[6pt]
\frac{\theta^{\bullet}_{CO_2\cdot S,10}}{\theta^{\bullet}_{0,10}} &= \left(\frac{\vec{\omega}_4}{\overleftarrow{\omega}_4}\right)^{-1} \\[6pt]
\frac{\theta^{\bullet}_{COOH\cdot S,10}}{\theta^{\bullet}_{0,10}} &= \left(\frac{\vec{\omega}_1}{\overleftarrow{\omega}_1}\right)^{+1}\left(\frac{\vec{\omega}_2}{\overleftarrow{\omega}_2}\right)^{+1}\left(\frac{\vec{\omega}_3}{\overleftarrow{\omega}_3}\right)^{+1/2}\left(\frac{\vec{\omega}_5}{\overleftarrow{\omega}_5}\right)^{+1}\left(\frac{\vec{\omega}_9}{\overleftarrow{\omega}_9}\right)^{+1} \\[6pt]
\frac{\theta^{\bullet}_{OH\cdot S,10}}{\theta^{\bullet}_{0,10}} &= \left(\frac{\vec{\omega}_1}{\overleftarrow{\omega}_1}\right)^{+1}\left(\frac{\vec{\omega}_3}{\overleftarrow{\omega}_3}\right)^{+1/2}\left(\frac{\vec{\omega}_5}{\overleftarrow{\omega}_5}\right)^{+1}
\end{aligned}
\right\}
\tag{4.20}
$$

Finally using these in site balance, Eq. 2.26,

$$
\frac{1}{\theta^{\bullet}_{0,10}} = 1 + \frac{\theta^{\bullet}_{H_2O\cdot S,10}}{\theta^{\bullet}_{0,10}} + \frac{\theta^{\bullet}_{CO\cdot S,10}}{\theta^{\bullet}_{0,10}} + \frac{\theta^{\bullet}_{H\cdot S,10}}{\theta^{\bullet}_{0,10}} + \frac{\theta^{\bullet}_{CO_2\cdot S,10}}{\theta^{\bullet}_{0,10}} + \frac{\theta^{\bullet}_{COOH\cdot S,10}}{\theta^{\bullet}_{0,10}} + \frac{\theta^{\bullet}_{OH\cdot S,10}}{\theta^{\bullet}_{0,10}}
\tag{4.21}
$$

Thus, we have from Eq. (4.18)

$$
R^{\bullet}_{10} = \frac{1}{\overleftarrow{\omega}_{10}\,\frac{\vec{\omega}_1}{\overleftarrow{\omega}_1}\frac{\vec{\omega}_2}{\overleftarrow{\omega}_2}\sqrt{\frac{\vec{\omega}_3}{\overleftarrow{\omega}_3}}\frac{\vec{\omega}_5}{\overleftarrow{\omega}_5}\frac{\vec{\omega}_9}{\overleftarrow{\omega}_9}} \left(1 + \frac{\vec{\omega}_1}{\overleftarrow{\omega}_1} + \frac{\vec{\omega}_2}{\overleftarrow{\omega}_2} + \sqrt{\frac{\overleftarrow{\omega}_3}{\vec{\omega}_3}} + \frac{\vec{\omega}_4}{\overleftarrow{\omega}_4} + \frac{\vec{\omega}_1}{\overleftarrow{\omega}_1}\frac{\vec{\omega}_2}{\overleftarrow{\omega}_2}\sqrt{\frac{\vec{\omega}_3}{\overleftarrow{\omega}_3}}\frac{\vec{\omega}_5}{\overleftarrow{\omega}_5}\frac{\vec{\omega}_9}{\overleftarrow{\omega}_9} + \frac{\vec{\omega}_1}{\overleftarrow{\omega}_1}\sqrt{\frac{\vec{\omega}_3}{\overleftarrow{\omega}_3}}\frac{\vec{\omega}_5}{\overleftarrow{\omega}_5}\right)^2
$$

$$\tag{4.22}$$

Finally,

$$
E_{OR} = 1 - z_{OR} = 1 - \frac{\overleftarrow{\omega}_1\overleftarrow{\omega}_2\overleftarrow{\omega}_3\overleftarrow{\omega}_4\overleftarrow{\omega}_5\overleftarrow{\omega}_9\overleftarrow{\omega}_{10}}{\vec{\omega}_1\vec{\omega}_2\vec{\omega}_3\vec{\omega}_4\vec{\omega}_5\vec{\omega}_9\vec{\omega}_{10}} = 1 - \frac{1}{K_{OR}}\frac{P_{CO_2}P_{H_2}}{P_{H_2O}P_{CO}}
\tag{4.23}
$$

where, K_{OR} is the equilibrium constant for WGS reaction.

Thus, Eq. (4.12), (4.17), (4.22) and (4.23) provide an explicit rate expression for the WGS mechanism on Pt.

$R_5^\bullet$ and $R_{10}^\bullet$ can, in fact, be further simplified based on the concept of most abundant reactive intermediate (MARI) [45], i.e., by comparing the values of $\theta_{k,\rho}^\bullet / \theta_{0,\rho}^\bullet$ in $R_\rho^\bullet$. We find that $\theta_{CO\cdot S,5}^\bullet / \theta_{0,5}^\bullet$ and $\theta_{CO\cdot S,10}^\bullet / \theta_{0,10}^\bullet$ is significantly higher than others for s_5 and s_{10}, respectively (Figure 4-5). Thus,

$$R_5^\bullet \approx \frac{1}{\bar{\omega}_5 \left(\dfrac{\vec{\omega}_1}{\overleftarrow{\omega}_1}\right)}\left(1+\frac{\vec{\omega}_2}{\overleftarrow{\omega}_2}\right) = \frac{\overleftarrow{\omega}_1}{\bar{\omega}_5 \vec{\omega}_1}\left(1+\frac{\vec{\omega}_2}{\overleftarrow{\omega}_2}\right)^2 \tag{4.24}$$

and

$$R_{10}^\bullet \approx \frac{1}{\bar{\omega}_{10}\,\dfrac{\vec{\omega}_1}{\overleftarrow{\omega}_1}\dfrac{\vec{\omega}_2}{\overleftarrow{\omega}_2}\sqrt{\dfrac{\vec{\omega}_3}{\overleftarrow{\omega}_3}\dfrac{\vec{\omega}_5}{\overleftarrow{\omega}_5}\dfrac{\vec{\omega}_9}{\overleftarrow{\omega}_9}}}\left(1+\frac{\vec{\omega}_2}{\overleftarrow{\omega}_2}\right)^2 = \frac{\overleftarrow{\omega}_1 \overleftarrow{\omega}_2 \sqrt{\overleftarrow{\omega}_3 \overleftarrow{\omega}_5 \overleftarrow{\omega}_9}}{\bar{\omega}_{10}\vec{\omega}_1\vec{\omega}_2\sqrt{\vec{\omega}_3\vec{\omega}_5\vec{\omega}_9}}\left(1+\frac{\vec{\omega}_2}{\overleftarrow{\omega}_2}\right)^2 \tag{4.25}$$

Using the thus reduced expressions for $R_5^\bullet$ and $R_{10}^\bullet$ along with Eq. (4.23) in Eq. (4.12), we have

$$r_{OR} \approx \frac{1}{\left(\dfrac{1}{\bar{\omega}_5}+\dfrac{\vec{\omega}_2\sqrt{\vec{\omega}_3\vec{\omega}_5\vec{\omega}_9}}{\bar{\omega}_{10}\overleftarrow{\omega}_2\sqrt{\overleftarrow{\omega}_3\overleftarrow{\omega}_5\overleftarrow{\omega}_9}}\right)\dfrac{\vec{\omega}_1}{\overleftarrow{\omega}_1}\left(1+\dfrac{\vec{\omega}_2}{\overleftarrow{\omega}_2}\right)^2}\left(1-\frac{1}{K_{OR}}\frac{P_{CO_2}P_{H_2}}{P_{H_2O}P_{CO}}\right) \tag{4.26}$$

Finally, substituting the rate constants and concentration of terminal species for reaction step weights ω_ρ, we have the overall reaction rate in the conventional form

$$r_{OR} \approx \frac{\vec{k}_5\vec{k}_{10}K_1K_2K_3^{1/2}K_5K_9 P_{H_2O}P_{CO}}{(\vec{k}_5 P_{H_2}^{1/2}+\vec{k}_{10}K_2K_3^{1/2}K_5K_9 P_{CO})(1+K_2P_{CO})^2}\left(1-\frac{1}{K_{OR}}\frac{P_{CO_2}P_{H_2}}{P_{H_2O}P_{CO}}\right) \tag{4.27}$$

where, K_ρ is the equilibrium constant for step s_ρ.

Eq. (4.19) reveals that $K_1K_2K_3^{1/2}K_5K_9$ represents the equilibrium constant for the intermediate reaction for the formation of COOH·S species when step s_{10} is considered as the RDS, i.e.

$$K_1K_2K_3^{1/2}K_5K_9 = K_{IR_{COOHS,10}} \tag{4.28}$$

Using Eq. (4.28) in Eq. (4.27), we thus, have

$$r_{OR} \approx \frac{\vec{k}_5 \vec{k}_{10} K_1 K_{IR_{COOHS,10}} P_{H_2O} P_{CO}}{(\vec{k}_5 K_1 P_{H_2}^{1/2} + \vec{k}_{10} K_{IR_{COOHS,10}} P_{CO})(1 + K_2 P_{CO})^2} \left(1 - \frac{1}{K_{OR}} \frac{P_{CO_2} P_{H_2}}{P_{H_2O} P_{CO}}\right) \tag{4.29}$$

If appropriate rate constants in Eq. (4.29) are combined, we obtain the following simple rate expression for WGS on Pt,

$$r_{OR} \approx \frac{k_A P_{H_2O} P_{CO}}{(k_B P_{H_2}^{1/2} + k_C P_{CO})(1 + k_D P_{CO})^2} \left(1 - \frac{1}{K_{OR}} \frac{P_{CO_2} P_{H_2}}{P_{H_2O} P_{CO}}\right)$$

$$\text{where, } k_A = 1.0276 \times 10^6 \exp\left(\frac{-4342.5}{RT}\right)$$

$$k_B = 2.8530 \times 10^5 \exp\left(\frac{-27985}{RT}\right) \tag{4.30}$$

$$k_C = 3.6017 \exp\left(\frac{23642.5}{RT}\right)$$

$$k_D = 1.414 \times 10^{-8} \exp\left(\frac{104220}{RT}\right)$$

where R is the gas constant in J/(mol K) and T is the temperature in K. The above explicit rate expression is in good agreement with the QSS rate obtained numerically for the 17-step WGS mechanism on Pt(111) from the microkinetic model as shown in Figure 4-15. For example, the overall reaction rate for conditions mentioned in Figure 4-4 via Eq. (4.30) is 0.1878 s^{-1} which compares well with 0.1884 s^{-1} obtained from numerical computation, which points to the robustness of the reaction network analysis and reduction approach presented here.

Finally, from Eq. (4.30), it is easy to see that the reaction order with respect to H$_2$O is 1, while H$_2$ and CO, both, have inhibitive effect on the overall rate. This is supported by Ribeiro and co-workers [24], who reported (slightly) negative kinetic order with respect to CO of –0.03 over Pt/CeO$_2$. On the other hand, Meunier et al. [46] reported apparent reaction order with respect to CO to be –0.27. This is not entirely surprising for Pt catalyst, owing to the extremely high affinity of CO toward Pt and perhaps competitive adsorption of CO and H$_2$O.
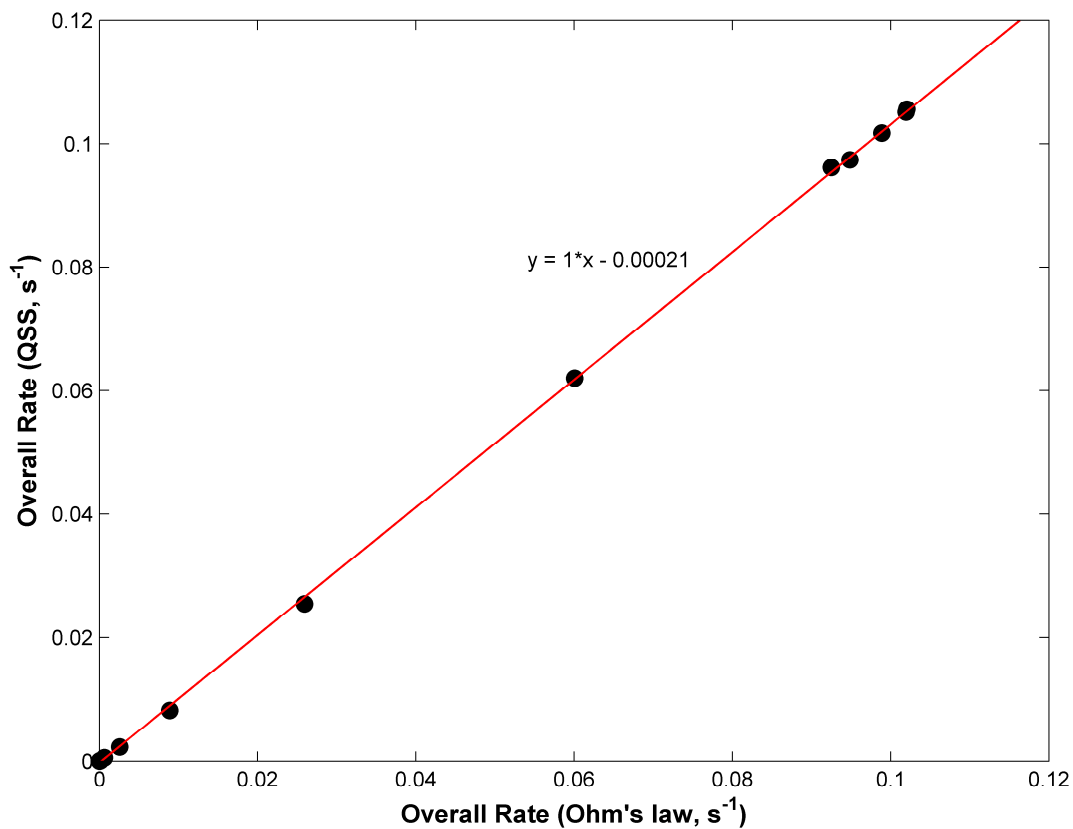
Figure 4-15: Comparison of overall QSS rate obtained from Ohm's law form, i.e. Eq. (4.29) and that calculated numerically via microkinetic modeling for the 17-step WGS reaction on Pt(111).

4.7 Conclusions

A comprehensive 17-step mechanism with predicted kinetics for the water-gas-shift (WGS) reaction on Pt(111) has been rigorously analyzed, simplified and pruned into a 7-step, single reaction route model, using the RR Graph approach, a comprehensive framework for analyzing complex mechanisms and network kinetics. A RR Graph has been constructed for the given WGS mechanism that incorporates all the 17 steps, on which all of the 71 direct FRs and 49 ERs may be traced as walks!

The RR network was subsequently simplified and reduced to a network involving only a single dominant RR, namely FR_4, i.e. associative mechanism mediated via carboxyl species. Microkinetic analysis by Grabow et al. [32] also conclude the said pathway as dominant. Further, the authors concluded the direct decomposition of carboxyl species, i.e. step s_{10} as the RLS for the sequence, based on sensitivity analysis. However, our graph theoretic based resistance comparison suggests that both, dissociation of water, i.e. step s_5 and direct decomposition of carboxyl species, i.e. step s_{10} are non-QE steps (or slow steps) and hence RLSs for the said pathway. For example, if step s_5 is not considered as a slow step and dropped from the rate expression, i.e., $r_{OR} \approx E_{OR} / R_{10}^{\bullet}$, we obtain the overall rate as 0.3657 s^{-1}, significantly higher than the actual overall rate of 0.1884 s^{-1} for the reaction conditions mentioned in Figure 4-4. Thus, following the RR network approach, the RLSs have been identified without making any *ad hoc* assumptions. Based on these two slow steps, a QSS rate expression has been derived based on the electrical analogy where the overall reaction rate is cast into an Ohm's law form, i.e. rate = overall driving force/overall resistance. The derived rate expression was next pruned based on standard MARI approach, with adsorbed CO as the dominant species on Pt, yielding a highly simplified rate expression agreeing reasonably well with the 17-step microkinetic model. Further, it is clear from the rate expression and MARI that the strong adsorption of CO on Pt is self-poisoning and limits the rate of the OR.

4.8 References

[1] J.L.C. Fajín, M.N.D.S. Cordeiro, F. Illas, J.R.B. Gomes, J. Catal. 268 (2009) 131-141.

[2] R. Farrauto, L. Shore, W. Ruettinger, J. Lampert, T. Giroux, Y. Liu, O. Ilinich, Annu. Rev. Mater. Res. 33 (2003) 1-27.

[3] T.S. Askgaard, J.K. Nørskov, C.V. Ovesen, P. Stoltze, J. Catal. 156 (1995) 229-242.

[4] C.T. Campbell, K.A. Daube, J. Catal. 104 (1987) 109-119.

[5] C.V. Ovesen, B.S. Clausen, B.S. Hammershoi, G. Steffensen, T. Askgaard, I. Chorkendorff, J.T. Norskov, P.B. Rasmussen, P. Stoltze, P. Taylor, J. Catal. 158 (1996) 170-180.

[6] T. Shido, Y. Iwasawa, J. Catal. 140 (1993) 575-584.

[7] T. Van Herwijnen, W.A. De Jong, J. Catal. 63 (1980) 83-93.

[8] J. Nakamura, J.M. Campbell, C.T. Campbell, J. Chem. Soc. Faraday Trans. 86 (1990) 2725-2734.

[9] C.V. Ovesen, P. Stoltze, J.K. Norskov, C.T. Campbell, J. Catal. 134 (1992) 445-468.

[10] N. Schumacher, A. Boisen, S. Dahl, A.A. Gokhale, S. Kandoi, L.C. Grabow, J.A. Dumesic, M. Mavrikakis, I. Chorkendorff, J. Catal. 229 (2005) 265-275.

[11] M.I. Temkin, in: D.D. Eley, H. Pines, P.B. Weisz (Eds.), Advances in Catalysis, Academic Press, New York, 1979, pp. 173-291.

[12] E. Tserpe, K.C. Waugh, in: K.C.W. G. F. Froment (Ed.), Dynamics of Surfaces and Reaction Kinetics in Heterogeneous Catalysis, Elsevier, Amsterdam, 1997, pp. 401-416.

[13] K.C. Waugh, Catal. Today. 53 (1999) 161-176.

[14] C.A. Callaghan, I. Fishtik, R. Datta, M. Carpenter, M. Chmielewski, A. Lugo, Surf. Sci. 541 (2003) 21-30.

[15] C. Rhodes, G.J. Hutchings, A.M. Ward, Catal. Today. 23 (1995) 43-58.

[16] I. Fishtik, R. Datta, Surf. Sci. 512 (2002) 229.

[17] G.J. Millar, C.H. Rochester, C. Howe, K.C. Waugh, Molecular Physics. 76 (1991) 833-849.

[18] C.R.F. Lund, SUNY-Buffalo, 2001, pp. 1-19.

[19] D. Ma, C.R.F. Lund, Ind. Eng. Chem. Res. 42 (2003) 711-717.

[20] D.C. Grenoble, M.M. Estadt, D.F. Ollis, J. Catal. 67 (1981) 90-102.

[21] T. Bligaard, J.K. Nørskov, S. Dahl, J. Matthiesen, C.H. Christensen, J. Sehested, J. Catal. 224 (2004) 206-217.

[22] A.V. Zeigarnik, C.A. Callaghan, R. Datta, I. Fishtik, E. Shustorovich, Kinetics and Catalysis. 46 (2005) 509-515.

[23] C. Wheeler, A. Jhalani, E.J. Klein, S. Tummala, L.D. Schmidt, J. Catal. 223 (2004) 191-199.

[24] A.A. Phatak, N. Koryabkina, S. Rai, J.L. Ratts, W. Ruettinger, R.J. Farrauto, G.E. Blau, W.N. Delgass, F.H. Ribeiro, Catalysis Today. 123 (2007) 224-234.

[25] Q. Fu, W. Deng, H. Saltsburg, M. Flytzani-Stephanopoulos, Applied Catalysis B: Environmental. 56 (2005) 57-68.

[26] W. Deng, J.D. Jesus, H. Saltsburg, M. Flytzani-Stephanopoulos, Applied Catalysis A: General. 291 (2005) 126-135.

[27] Q. Fu, S. Kudriavtseva, H. Saltsburg, M. Flytzani-Stephanopoulos, Chemical Engineering Journal. 93 (2003) 41-53.

[28] A.B. Mhadeshwar, D.G. Vlachos, Catalysis Today (2005).

[29] A.B. Mhadeshwar, D.G. Vlachos, J. Phys. Chem. B. 108 (2004) 15246-15258.

[30] C.A. Callaghan, S.A. Vilekar, I. Fishtik, R. Datta, Appl. Catal. A: General. 345 (2008) 213-232.

[31] A. A. Gokhale, J. A. Dumesic, M. Mavrikakis, J. Am. Chem. Soc. 130 (2008) 1402-1414.

[32] L. C. Grabow, A. A. Gokhale, S. T. Evans, J. A. Dumesic, M. Mavrikakis, J. Phys. Chem. C (2008) A-J.

[33] P. Liu, J.A. Rodriguez, J. Chem. Phys. 126 (2007) 164705.

[34] D. Tibiletti, F.C. Meunier, A. Goguet, D. Reid, R. Burch, M. Boaro, M. Vicario, A. Trovarelli, J. Catal. 244 (2006) 183.

[35] F.C. Meunier, D. Reid, A. Goguet, S. Shekhtman, C. Hardacre, R. Burch, W. Deng, M. Flytzani-Stephanopoulos, J. Catal. 247 (2007) 277.

[36] F.C. Meunier, A. Goguet, C. Hardacre, R. Burch, D. Thompsett, J. Catal. 252 (2007) 18.

[37] C.R.F. Lund, Ind. Eng. Chem. Res. 35 (1996) 2531-2538.

[38] NIST Chemistry WebBook (http://webbook.nist.gov/chemistry).

[39] Gaussian 03, Revision C.02, M. J. Frisch, G. W. Trucks, H. B. Schlegel, G. E. Scuseria, M. A. Robb, J. R. Cheeseman, J. J. A. Montgomery, T. Vreven, K. N. Kudin, J. C. Burant, J. M. Millam, S. S. Iyengar, J. Tomasi, V. Barone, B. Mennucci, M. Cossi, G. Scalmani, N. Rega, G. A. Petersson, H. Nakatsuji, M. Hada, M. Ehara, K. Toyota, R. Fukuda, J. Hasegawa, M. Ishida, T. Nakajima, Y. Honda, O. Kitao, H. Nakai, M. Klene, X. Li, J. E. Knox, H. P. Hratchian, J. B. Cross, V. Bakken, C. Adamo, J. Jaramillo, R. Gomperts, R. E. Stratmann, O. Yazyev, A. J. Austin, R. Cammi, C. Pomelli, J. W. Ochterski, P. Y. Ayala, K. Morokuma, G. A. Voth, P. Salvador, J. J. Dannenberg, V. G. Zakrzewski, S. Dapprich, A. D. Daniels, M. C. Strain, O. Farkas, D. K. Malick, A. D. Rabuck, K. Raghavachari, J. B. Foresman, J. V. Ortiz, Q. Cui, A. G. Baboul, S. Clifford, J. Cioslowski, B. B. Stefanov, G. Liu, A. Liashenko, P. Piskorz, I. Komaromi, R. L. Martin, D. J. Fox, T. Keith, M. A. Al-Laham, C. Y. Peng, A. Nanayakkara, M. Challacombe, P. M. W. Gill, B. Johnson, W. Chen, M. W. Wong, C. Gonzalez, J.A. Pople, Wallingford CT, 2004.

[40] J.A. Dumesic, D.F. Rudd, L.M. Aparicio, J.E. Rekoske, A.A. Trevino, The Microkinetics of Heterogeneous Catalysis, ACS, 1993.

[41] J. Happel, H. Sellers, Adv. Catal. 32 (1983) 272-323.

[42] I. Fishtik, C.A. Callaghan, R. Datta, J. Phys. Chem. B. 108 (2004) 5671-5682.

[43] I. Fishtik, C.A. Callaghan, R. Datta, J. Phys. Chem. B. 108 (2004) 5683-5697.

[44] I. Fishtik, C.A. Callaghan, R. Datta, J. Phys. Chem. B. 109 (2005) 2710-2722.

[45] M. Boudart, G. Djega-Mariadassou, Kinetics of Heterogeneous Catalytic Reactions, Princeton University Press, Princeton, 1984.

[46] F.C. Meunier, G. Yablonsky, D. Reid, S.O. Shekhtman, C. Hardacre, R. Burch, M. Lazman, Catal. Today. 138 (2008) 216–221.

Chapter V

A Reaction Route Network Analysis of Ammonia Decomposition on Fe

A key impediment to the universal application of PEM fuel cells is the lack of hydrogen storage and distribution infrastructure. Ammonia, which is easy to store and transport, and possesses attractive energy density can act as a potential hydrogen carrier due to its relative ease of decomposition. Moreover, being carbon free, it does not produce any CO, which could act as a poison to the low-temperature fuel cells. The N_2 produced is an inert in a fuel cell. Detailed microkinetic modeling of NH_3 decomposition has been a subject of interest for decades. However, in spite being a well-researched reaction system, there is disagreement in the literature as to which step is indeed the rate-determining step (RDS) for the reaction mechanism.

In this chapter, we utilize our Reaction Route Graph analysis for detailed mechanistic and kinetic analysis of the well-accepted 7-step NH_3 decomposition reaction mechanism. The RLS(s) are identified in a logical manner following a comparison of the step resistances. Next, based on the Ohm's law representation of kinetics we develop quasi-steady state rate expression. The thus developed simplified rate expression is found to be in complete agreement with our experimental data on Fe.

5.1 Introduction

Hydrogen storage is an area of active research, where chemical storage of hydrogen has also been suggested, e.g., as NH_3, which is actually a very effective and inexpensive hydrogen carrier available in large quantities. Sørensen et al. [1] have shown that adequate amount of hydrogen for a 1 W fuel cell (sufficient for common cell phones) can be produced in a reactor volume of only 20 μl with Ru-based catalyst.

In fact, the proposition has been around for a while; e.g. Figure 5-1 shows an ammonia cracker built for US Army 500W-fuel cells almost three decades ago [2, 3]. Moreover, a PEM fuel cell with 80% fuel utilization can provide enough hydrogen (combusted with air) to provide the heat of reaction. Ammonia is one of the few materials that can be produced cheaply, transported efficiently, and transformed directly to yield hydrogen and a non-polluting byproduct. It has a proven storage/delivery infrastructure and safety record. Ammonia is a potential hydrogen carrier with many desirable properties [4]. It is produced in very large quantities on the industrial scale (109 MT/y worldwide in 2004), as the main source for nitrogen in synthetic fertilizers. With a boiling point of ~ 33.3 ºC (240 K) and a vapor pressure of roughly 10 atm at room temperature (1061 kPa at 300 K), it is a readily liquefied vapor under ambient conditions, with a liquid density of 0.682 kg/L at ~33.3 ºC, and 0.639 kg/L at 0 ºC, which is high for a small molecule and is because of its polar nature. It contains 17.6% by weight of hydrogen, i.e., around 0.11 kg/L of hydrogen. This compares with 0.07 kg/L for liquid hydrogen, and 0.123 kg/L for octane. With a heat of combustion of 18.6 kJ/g (LHV) and 22.5 kJ/g (HHV), its energy density is very attractive. Even though corrosive and toxic with a strong odor, procedure and facilities for its safe handling, transportation and storage are available throughout the world. Furthermore, it can be fed into a reformer as a vapor without a pump, and is relatively easily decomposed at around 500 - 600 ºC over an Fe or Ru catalyst to provide clean hydrogen with ppm levels of unconverted NH_3. Being carbon free, it does not produce any CO, which could poison the low temperature fuel cells, thus, eliminating the need for further processing, e.g. shift converter or selective oxidation. The N_2 produced along with H_2 is an inert diluent for fuel cell.
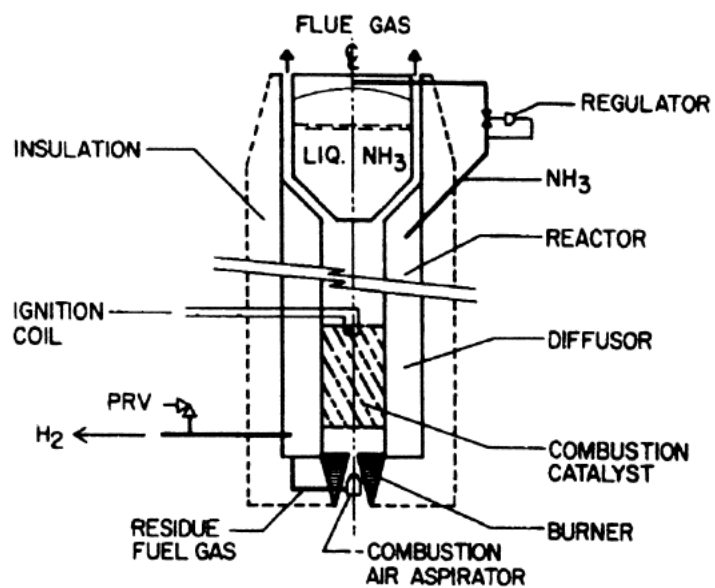
Figure 5-1: Diagram of an Ammonia Cracker built for US Army 500W-fuel cells [2, 3].
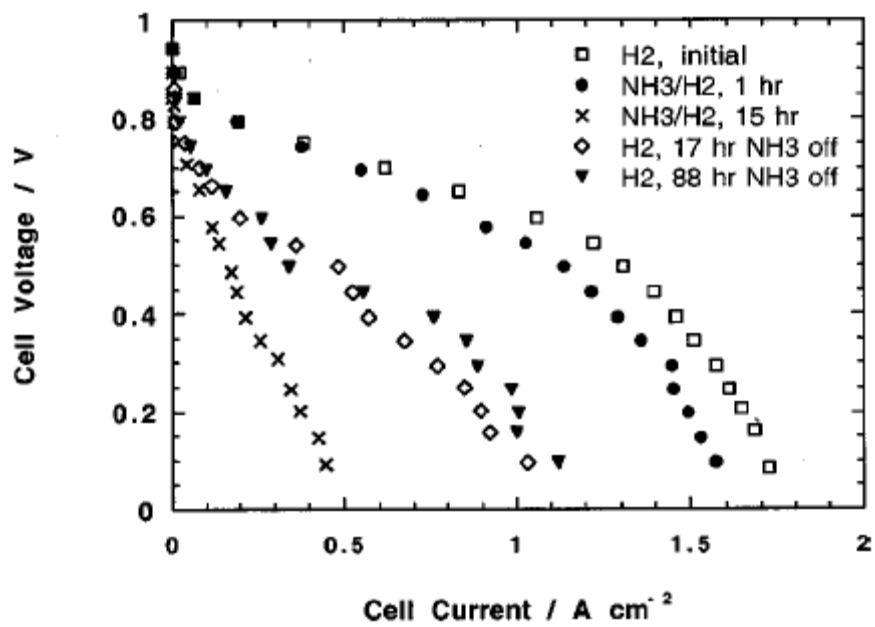
Figure 5-2: Effect of NH$_3$ (30 ppm) exposure at anode on H$_2$-air fuel cell performance at 80 $^{\circ}$C [5].

However, trace amount of ammonia as low as 13 ppm in the anode feed is known to poison PEM fuel cells [6]. Short term exposure (< 1 hr) shows reversible poisoning effect, however, long term exposure causes severe and irreversible loss in performance as can be seen from Figure 5-2 [5]. It was conjectured that replacement of H^+ by NH_4^+ ions and the ensuing loss of protonic conductivity was the primary reason for performance drop. Thus, a challenge is to reduce ammonia in the reformate to below ppb levels to ensure long life, since the losses are cumulative as a consequence of ammonia build up in the electrolyte [5, 6]. Uribe et al. [5] utilized Dowex H-ion exchange resin to clean up H_2 fuel streams contaminated with traces of ammonia. Of course, a membrane reactor could also be implemented for a combined catalytic reforming and separation of hydrogen [7]. The advantage arises as a result of shift in the reaction thermodynamic equilibrium, thus increasing the yield at lower operating temperatures while combining processes of generating and separating the hydrogen into a single unit operation, the downside being the associated higher cost. The use of an ion-exchange resin [5] or an adsorbent filter e.g., Calgon-URC [8], to remove traces of ammonia down to ppb levels is an attractive, practical, simple and cost-effective approach. Of course, no adsorber is needed if an alkaline fuel cell (AFC) is employed and the heat required for ammonia decomposition can be supplied directly by the fuel cell. In fact, comparison of hydrogen production economics via ammonia decomposition as opposed to that via methanol steam reforming for AFC suggested that ammonia is indeed a better choice [9, 10]. Consequently, CO_x-free hydrogen from a single-step source like ammonia decomposition can be an attractive alternative to hydrocarbon fuels for small-scale fuel cell applications, and a green pathway, since every gallon of gasoline/diesel replaced saves ~20 pounds of CO_2 from entering the atmosphere. It must, further, be noted that, for SOFC, ammonia can be directly reformed internally [11, 12].

Decomposition of ammonia has been investigated on a host of single crystal surfaces. The experimental studies showed that on most of these single-crystal metal surfaces the recombinative desorption of N_2 is the RDS for NH_3 catalytic decomposition [13]. However, the N-H bond cleavage has also been found to be the RDS in some studies [14-17].

Earlier studies show that at low temperatures and high hydrogen partial pressures, the reaction is inhibited by hydrogen, and is described by the Temkin–Pyzhev mechanism [18], while at high temperatures and low hydrogen partial pressure, the reaction is only dependent on ammonia partial pressure, referred to as the Tamaru model [18, 19]. Löffler and Schmidt [20, 21] observed that at low temperatures (<500 ∘C for Pt and Ru) and low ammonia partial pressure (typically <1 Torr) the reaction is zero-order with respect to ammonia, and at high temperatures the reaction becomes first-order with respect to ammonia.

Oyama [22] and by Djèga–Mariadassou et al. [19], suggested that a simple rate expression may be derived by applying Langmuir–Hinshelwood analysis to a sequence that involves equilibrium adsorption of ammonia, followed by decomposition of adsorbed ammonia to products. However, it does not address the inhibitive effect of H_2 observed on Ru, particularly at low temperatures and when H_2 is co-fed along with NH_3 [18, 19, 21, 23]. To explain, these effects a power-law model of the form

$$r = k \, p_{NH_3}^{a} \, p_{H_2}^{b} \tag{5.1}$$

has been suggested. When hydrogen inhibition is significant, (high hydrogen partial pressures and low temperatures), b in the above equation is negative, and it becomes equivalent to the Temkin–Pyzhev expression

$$r = k \left(\frac{p_{NH_3}^{2}}{p_{H_2}^{3}} \right)^{\beta} \tag{5.2}$$

Chellappa et al. [24] studied the kinetics of pure ammonia over Ni–Pt/Al_2O_3, the results varying greatly with the previous work with dilute NH_3. The authors analyzed their experimental data and fitted the same to a power–law model as given by Eq. (5.1). The analysis of the experimental data between 520 and 660 ^{o}C revealed a first-order dependence on ammonia. This simple first-order model was shown to satisfactorily predict conversions >80% over a wide range of W/F values and operating temperatures. Mechanistically, this would imply that N–H bond cleavage is not the RDS under these conditions with no hydrogen inhibition and no apparent change in the reaction order with respect to ammonia. However, when data between 520 and 560 ^{o}C was analyzed

separately, with the Temkin–Pyzhev model Eq. (5.2), the reaction orders of ammonia and hydrogen were 0.67 and −1, respectively, indicating hydrogen inhibition effect. Thus, different conclusions were reached depending on how the analysis was developed. The authors later hinted at the possibility of ammonia decomposition being governed by more than one RLS.

Bradford et al. [25] showed that the rate has first-order dependence on NH_3 with both N–H bond cleavage and recombinative desorption of nitrogen as the RLSs, along with nitrogen atoms as the MARI. N_2-TPD and TOF data by Yin et al. [26] supports the proposition that the recombinative desorption of nitrogen atoms is the RDS in NH_3 decomposition. Shustorovich and Bell [27], based on BOC Morse potential method suggested a *single* RDS as the recombinative desorption of N_2 on Ru, Pt, Fe and Re. The experimental study by Tsai et al. [14] on the other hand showed that the RDS for NH_3 decomposition on Ru at low partial pressures is the temperature dependent, the recombinative desorption of N_2 being the RDS at $T < 650\,^{\circ}C$, while at higher temperature the N–H bond cleavage of adsorbed NH_3 being the RDS. DFT calculations by Stolbov et al. [15] and Huang et al. [28] also suggest that the first dissociation step ($NH_3 \cdot S + S \leftrightarrows NH_2 \cdot S + H \cdot S$) is the RDS for NH_3 decomposition on Pd(211) and Ir(100), respectively, based on the calculated energy barriers.

Vlachos and co-workers [16, 17] utilized a hybrid approach, where the N-N adsorbate–adsorbate interactions were taken from the DFT simulations, while UBI-QEP method was utilized to calculate the step activation energies for a 6-step mechanism, which were utilized in a microkinetic modeling of NH_3 decomposition on Ru(0001). The authors [16] showed that in the absence of the N–N interactions, N·S was the MARI, while in the presence of the N–N interactions, H·S was the dominant species. The RDS based on sensitivity analysis was found to be N–H bond cleavage of adsorbed NH_2 species ($NH_2 \cdot S + S \leftrightarrows NH \cdot S + H \cdot S$) and that desorption of nitrogen only plays a secondary role in the presence of the N–N interactions. Subsequent work showed that at low temperatures $NH_3 \cdot S$ dominates as a result of its slow decomposition, while H·S is the dominant species at high temperatures with N·S only being the second dominant species [17].

Thus, even for such a simple reaction as ammonia decomposition, which has been a subject of intensive investigation for decades, there exists no consensus as to which step(s) are the slow step(s), or even whether there is a *single* RDS, and which surface species are significant. We address these questions based on our Reaction Route Graph approach in this chapter. The rate-limiting step(s) are identified in a logical manner based on comparison of step resistances, allowing us to deduce a simplified rate expression. The resulting rate expression can be further pruned based on the concept of MARI, and agrees reasonably well with our experimental data on Fe.

5.2 Experimental

A schematic of the experimental set up by Skoplyak et al. [29] is shown in Figure 5-3 [29]. As shown in Figure 5-3, Argon (99.998% [zero-grade] purity, SpecAir), Hydrogen (99.95% purity, BOC), Anhydrous Ammonia (99.99% purity, AGA), and Nitrogen (99.999% [Ultra High Purity] purity, SpecAir) gases were fed to the system. MKS Type 119A Mass-Flow® controllers, controlled by model 247C 4-channel readout were used. The reactor was a 0.4 cm I.D., 0.6 cm O.D. quartz U-tube that contained approximately 1 cm of catalyst bed. 0.2 g of unsupported crushed pre-reduced iron catalyst (AS-4F), supplied by Süd-Chemie was used in the experiments. The received pellets were crushed using a ceramic mortar and pestle and then sieved to obtain a range of particles between 40 and 60 mesh. The composition was 78.0 wt% Fe, 11.0 wt% Fe_2O_3 / FeO, 3.8 wt% Al_2O_3, and 3.2 wt% CaO, 0.7 wt% K_2O. The bulk density of the catalyst was 130 ±10 lbs/ft^3. The specific surface area of the catalyst and the site density were 12 m^2/g and 4.43×10^{15} sites/cm^2, respectively.

The fresh catalyst was reduced prior to experimentation. The reduction consisted of exposing the catalyst bed to a mixture of 37.5 sccm H_2, 12.5 sccm N_2, and 50 sccm Ar. The bed temperature was ramped up from room temperature to 500 °C in one hour, and then held at 500 °C for three hours followed by a stream of 20 sccm NH_3 and 80 sccm Ar at a bed temperature of 350 °C in order to ensure that the system would quickly equilibrate during experimental runs. During the experiments, ammonia at a constant partial pressure of 0.2 atm was fed with argon, the total pressure being 1 atm.
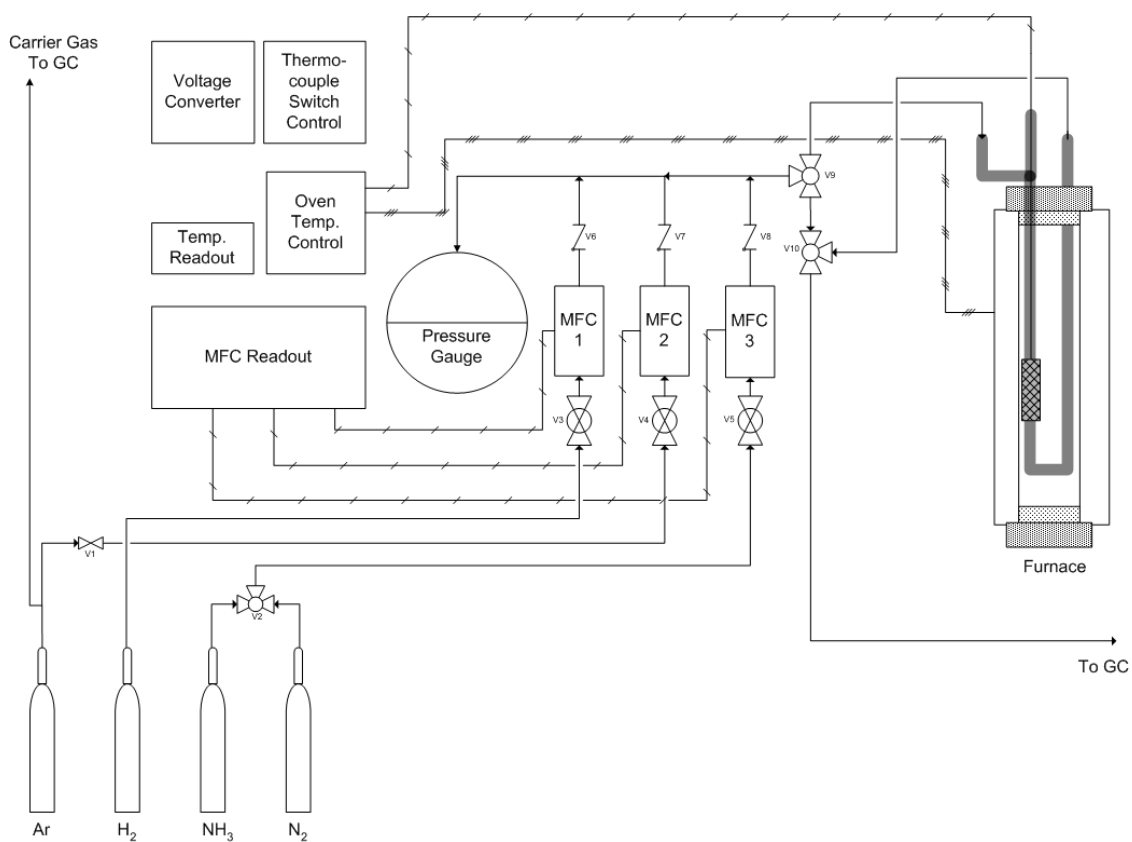
Figure 5-3: Experimental setup for NH$_3$ decomposition on Fe [29].
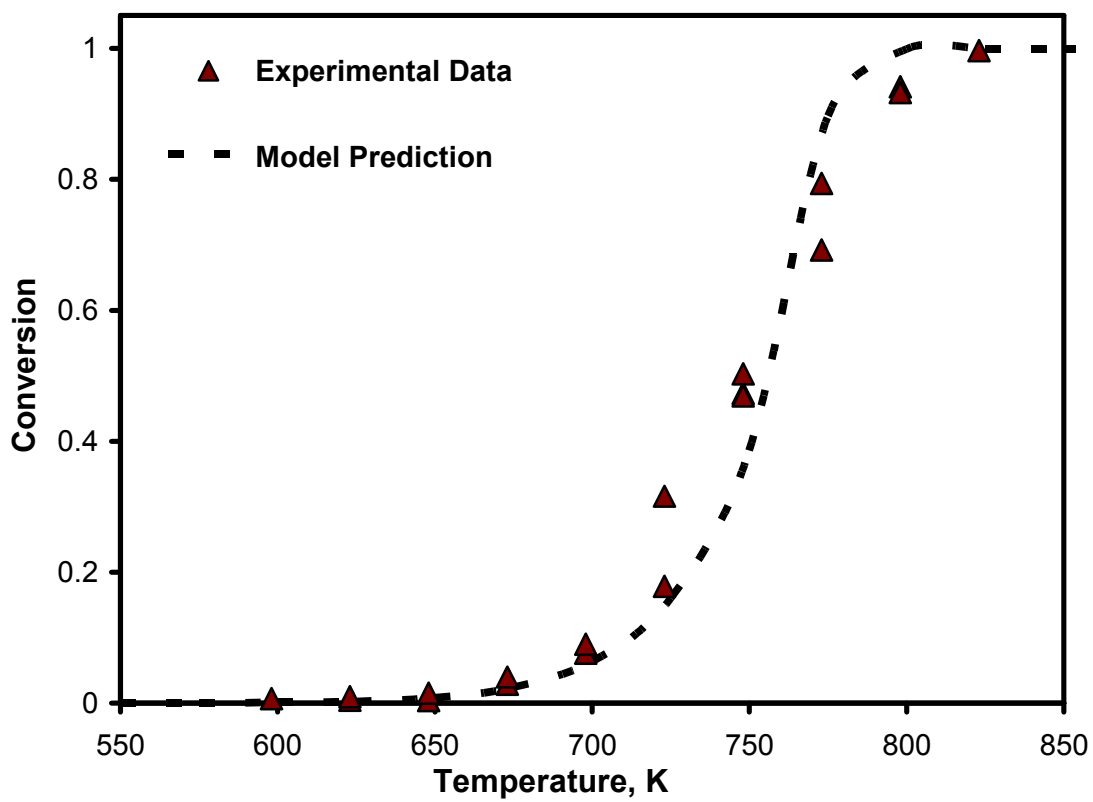
Figure 5-4: Conversion of NH_3 as a function of temperature on Fe in a packed-bed reactor. (0.2 g of catalyst; Feed: NH_3 20 cm^3/min, N_2 80 cm^3/min, 1 atm)

The reactor effluent was analyzed by a SRI model 8610C thermoconductivity detector (TCD) gas chromatograph with a HayeSep T packed column. Additional details can be found in Ref. [29]. The experimental data of conversion versus temperature is provided in Figure 5-4.

5.3 Reaction Mechanism and Kinetics

We consider here the commonly proposed and well-accepted 7-step mechanism for NH_3 decomposition as shown in Eq. (5.3)

$$
\begin{array}{lll}
& & \underline{\sigma_\rho} \\
s_1: & NH_3 + S \leftrightarrows NH_3 \cdot S & +2 \\
s_2: & NH_3 \cdot S + S \leftrightarrows NH_2 \cdot S + H \cdot S & +2 \\
s_3: & NH_2 \cdot S + S \leftrightarrows NH \cdot S + H \cdot S & +2 \\
s_4: & NH \cdot S + S \leftrightarrows N \cdot S + H \cdot S & +2 \\
s_5: & 2N \cdot S \leftrightarrows N_2 \cdot S + S & +1 \\
s_6: & N_2 \cdot S \leftrightarrows N_2 + S & +1 \\
s_7: & 2H \cdot S \leftrightarrows H_2 + 2S & +3 \\
\hline
OR: & N_2 + 3H_2 \leftrightarrows 2NH_3 &
\end{array}
\tag{5.3}
$$
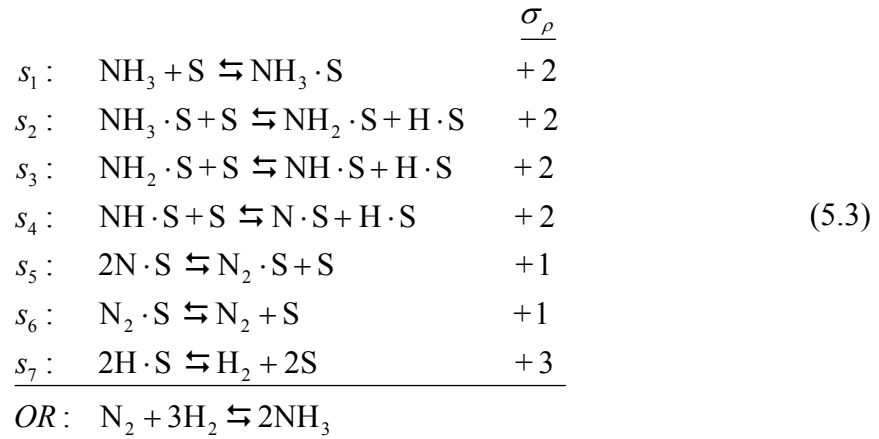
where S represents a vacant surface site. This describes a reaction system with $p = 7$ elementary steps, involving $n = 3$ terminal species, i.e., reactants N_2 and H_2, and the product NH_3, and $q = 6$ independent intermediate species, namely, $N \cdot S$, $N_2 \cdot S$, $H \cdot S$, $NH \cdot S$, $NH_2 \cdot S$, and $NH_3 \cdot S$, in addition to the vacant surface site S. As per the Horiuti-Temkin theorem [30, 31], thus, the number of independent RRs, or pathways, $\mu = p - q = 7 - 6 = 1$. This is, of course, given by

$$
FR_1: \quad OR = (+2)s_1 + (+2)s_2 + (+2)s_3 + (+2)s_4 + (+1)s_5 + (+1)s_6 + (+3)s_7 \tag{5.4}
$$

There are no empty routes (ERs). Thus, we have a reaction system with a single RR for a single overall reaction (OR), i.e., $\sum_{i=1}^{n} \nu_i T_i = 0$, where ν_i is the stoichiometric coefficient of the terminal (observable) species T_i ($i = 1, 2, \ldots, n$), i.e., reactants and products of the OR. Moreover, it also represents a non-linear kinetics mechanism, one of the most complex, but well-investigated, cases of sequential reactions.

Following mass action kinetics, the net rate of an elementary step, $r_\rho = \vec{r}_\rho - \bar{r}_\rho$, is written in the form

$$\vec{r}_\rho = \vec{k}_\rho \underbrace{\prod_{i=1}^{n} a_i^{-\vec{\beta}_{\rho i}}}_{\vec{\omega}_\rho} \prod_{k=0}^{q} \theta_k^{-\vec{\alpha}_{\rho k}} = \vec{\omega}_\rho \prod_{k=0}^{q} \left(\frac{\theta_k}{\theta_0}\right)^{-\vec{\alpha}_{\rho k}} (\theta_0)^{-\vec{\alpha}_{\rho k}} \quad ;$$

$$\bar{r}_\rho = \bar{k}_\rho \underbrace{\prod_{i=1}^{n} a_i^{\bar{\beta}_{\rho i}}}_{\bar{\omega}_\rho} \prod_{k=0}^{q} \theta_k^{\bar{\alpha}_{\rho k}} = \bar{\omega}_\rho \prod_{k=0}^{q} \left(\frac{\theta_k}{\theta_0}\right)^{\bar{\alpha}_{\rho k}} (\theta_0)^{\bar{\alpha}_{\rho k}}$$

(5.5)

Here θ_k is the (unknown) activity of intermediate species $I_k \cdot S$, a_i is the (known, or specified) activity of terminal species T_i and ω_ρ is the reaction step weight.

For ammonia decomposition we, thus, have:

$$r_1 = \vec{\omega}_1 \theta_0 - \bar{\omega}_1 \left(\frac{\theta_{NH_3 \cdot S}}{\theta_0}\right) \theta_0 \qquad ; \quad \vec{\omega}_1 = \vec{k}_1 p_{NH_3} ; \quad \bar{\omega}_1 = \bar{k}_1$$

$$r_2 = \vec{\omega}_2 \left(\frac{\theta_{NH_3 \cdot S}}{\theta_0}\right) \theta_0^2 - \bar{\omega}_2 \left(\frac{\theta_{NH_2 \cdot S}}{\theta_0}\right)\left(\frac{\theta_{H \cdot S}}{\theta_0}\right) \theta_0^2 \quad ; \quad \vec{\omega}_2 = \vec{k}_2 \qquad ; \quad \bar{\omega}_2 = \bar{k}_2$$

$$r_3 = \vec{\omega}_3 \left(\frac{\theta_{NH_2 \cdot S}}{\theta_0}\right) \theta_0^2 - \bar{\omega}_3 \left(\frac{\theta_{NH \cdot S}}{\theta_0}\right)\left(\frac{\theta_{H \cdot S}}{\theta_0}\right) \theta_0^2 \quad ; \quad \vec{\omega}_3 = \vec{k}_3 \qquad ; \quad \bar{\omega}_3 = \bar{k}_3$$

$$r_4 = \vec{\omega}_4 \left(\frac{\theta_{NH \cdot S}}{\theta_0}\right) \theta_0^2 - \bar{\omega}_4 \left(\frac{\theta_{N \cdot S}}{\theta_0}\right)\left(\frac{\theta_{H \cdot S}}{\theta_0}\right) \theta_0^2 \quad ; \quad \vec{\omega}_4 = \vec{k}_4 \qquad ; \quad \bar{\omega}_4 = \bar{k}_4$$

$$r_5 = \vec{\omega}_5 \left(\frac{\theta_{N \cdot S}}{\theta_0}\right)^2 \theta_0^2 - \bar{\omega}_5 \left(\frac{\theta_{N_2 \cdot S}}{\theta_0}\right) \theta_0^2 \qquad ; \quad \vec{\omega}_5 = \vec{k}_5 \qquad ; \quad \bar{\omega}_5 = \bar{k}_5$$

$$r_6 = \vec{\omega}_6 \left(\frac{\theta_{N_2 \cdot S}}{\theta_0}\right) \theta_0 - \bar{\omega}_6 \theta_0 \qquad ; \quad \vec{\omega}_6 = \vec{k}_6 \qquad ; \quad \bar{\omega}_6 = \bar{k}_6 p_{N_2}$$

$$r_7 = \vec{\omega}_7 \left(\frac{\theta_{H \cdot S}}{\theta_0}\right)^2 \theta_0^2 - \bar{\omega}_7 \theta_0^2 \qquad ; \quad \vec{\omega}_7 = \vec{k}_7 \qquad ; \quad \bar{\omega}_7 = \bar{k}_7 p_{H_2} \quad (5.6)$$

The step kinetics provided by Stolze and Nørskov [32-34], utilized in this study are summarized in Table 5-1.

Table 5-1: The microkinetic model for NH_3 decomposition on Fe. The letter 'S' denotes a surface site. Activation energies and enthalpy changes in kJ/mol; the units of the pre–exponential factors are $atm^{-1}\ s^{-1}$ for adsorption/desorption reactions and s^{-1} for surface reactions [32-34].

	$\vec{E}_\rho$	$\vec{\Lambda}_\rho$	Elementary Reactions	$\overleftarrow{E}_\rho$	$\overleftarrow{\Lambda}_\rho$
s_1:	0.0	2.00×10^8	$NH_3 + S \leftrightarrows NH_3{\cdot}S$	39.0	4.00×10^{12}
s_2:	0.0	2.00×10^{13}	$NH_3{\cdot}S + S \leftrightarrows NH_2{\cdot}S + H{\cdot}S$	39.0	4.00×10^{13}
s_3:	0.0	1.00×10^{12}	$NH_2{\cdot}S + S \leftrightarrows NH{\cdot}S + H{\cdot}S$	36.0	1.00×10^{13}
s_4:	23.0	1.00×10^7	$NH{\cdot}S + S \leftrightarrows N{\cdot}S + H{\cdot}S$	81.0	2.00×10^9
s_5:	155.0	1.00×10^9	$2N{\cdot}S \leftrightarrows N_2{\cdot}S + S$	29.0	4.00×10^9
s_6:	43.0	2.00×10^{14}	$N_2{\cdot}S \leftrightarrows N_2 + S$	0.0	2.00×10^6
s_7:	94.0	3.00×10^{13}	$2H{\cdot}S \leftrightarrows H_2 + 2S$	0.0	7.00×10^6

5.4 QSS Rate

As discussed in chapter II, an explicit QSS rate expression for the overall rate r_{OR} is generally not possible [35] for a system as non-linear as the one under consideration, typically only numerical results being possible for a given set of reaction conditions. However, we provide one here based on the algorithm described in chapter II.

The q intermediate activities θ_k in terms of $\bar{\omega}_\rho$ and $\bar{\omega}_\rho$, may be determined numerically by simultaneously solving the q algebraic QSS equations that relate r_ρ to r_{OR},

$$r_\rho = \sigma_\rho r_{OR} \quad (\rho = 1, 2, ..., q + 1) \tag{5.7}$$

along with the site conservation equation and the constitutive equations (Eq. (5.5))

The QSS relations represented by Eq. (5.7) are a special case of the so-called Kirchhoff's Flux Law (KFL), representing mass balance at the nodes in reaction route graphs [31], for the case of a reaction sequence. For the case of the ammonia decomposition example, it may be written in the form

$$6r_{OR} = 3r_1 = 3r_2 = 3r_3 = 3r_4 = 6r_5 = 6r_6 = 2r_7 \tag{5.8}$$

In order to derive an explicit QSS rate expression we, next utilize our RR graph approach to logically identify the RLS in the sequence based on resistance comparison of steps in the sequence. The step that significantly contributes to the overall reaction resistance can be labeled as the RLS. It should, however, be noted that there could be more than one RLS in a given sequence.

5.5 RR Graph and Network Analysis

For the considered non-linear reaction mechanism consisting of a single RR, the construction of the RR graph is rather straight-forward as shown in Figure 5-5. The connectivity of the reaction steps at the nodes in this RR Graph is governed by the KFL (QSS), (Eq. (5.7)), expressed as integers as given above, i.e., Eq. (5.8), along with the FR, i.e. Eq. (5.4).
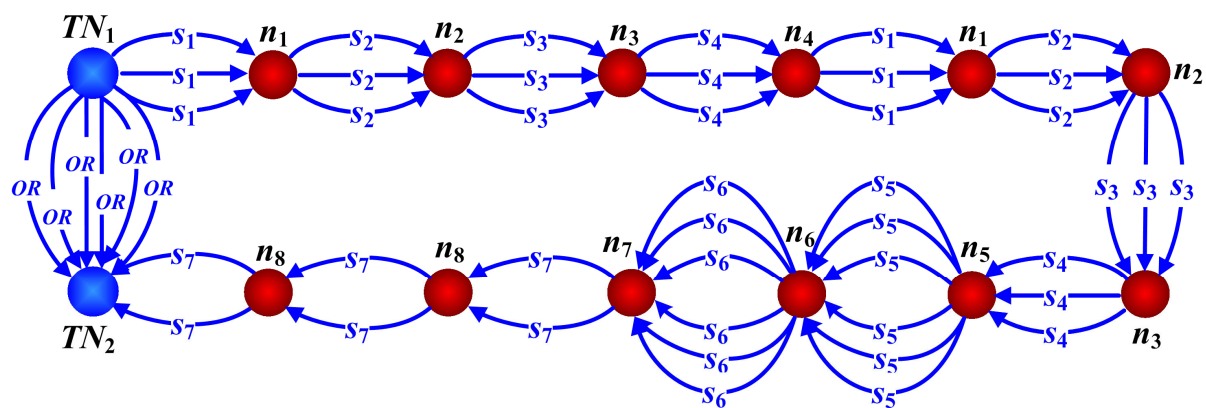
Figure 5-5: Reaction Route (RR) Graph for the 7-step NH$_3$ decomposition reaction mechanism.

The overall reaction rate can next be written in the Ohm's law form

$$r_{OR} \equiv \frac{\mathcal{A}_{OR}}{R_{OR}} \tag{5.9}$$

where the resistance of the overall network, may be obtained in terms of the branch resistances directly for the case of a single sequence under consideration as follows.

Using the Ohm's law for the OR as well as for the individual step in the KPL relation, $\mathcal{A}_{OR} = \sum_{\rho=1}^{q+1} \sigma_\rho \mathcal{A}_\rho$, we have,

$$R_{OR}(r_{OR}) = \sum_{\rho=1}^{q+1} \sigma_\rho \{(R_\rho)r_\rho\} \tag{5.10}$$

Further, using the KFL, Eq. (5.7) in the above, i.e., $r_\rho = \sigma_\rho r_{OR}$, provides the necessary relation between R_{OR} and R_ρ, i.e.,

$$R_{OR} = \sum_{\rho=1}^{q+1} \sigma_\rho^2 (R_\rho) \tag{5.11}$$

In other words, this results from a combination of KPL, KFL, and Ohm's law. The use of Eq. (5.9) along with Eq. (5.11) for r_{OR} requires a knowledge of the step resistances R_ρ. Unfortunately, the step resistances, in turn, involve step kinetics including concentrations of intermediate species, which are, of course, not known *a priori*. We will therefore follow the alternate Ohm's law form of kinetics, which is approximate but predictive, as developed in chapter II. Thus,

$$r_{OR} \cong \frac{E_{OR}}{R_{OR}^\bullet} \tag{5.12}$$

where, the overall resistance for this form is $R_{OR}^\bullet = 1/\vec{r}_{OR}$. The motive force, E_{OR} can be obtained from the overall reaction reversibility, which is a known quantity.

$$E_{OR} = 1 - z_{OR} = \prod_{\rho=1}^{q+1} (z_\rho)^{\sigma_\rho} = \prod_{\rho=1}^{q+1} \left(\frac{\overleftarrow{r}_\rho}{\overrightarrow{r}_\rho} \right)^{\sigma_\rho} = \prod_{\rho=1}^{q+1} \left(\frac{\overleftarrow{\omega}_\rho}{\overrightarrow{\omega}_\rho} \right)^{\sigma_\rho} \tag{5.13}$$

For the ammonia decomposition, the overall driving force, thus

$$E_{OR} = 1 - \left(\frac{\bar{\omega}_1}{\vec{\omega}_1}\right)^2 \left(\frac{\bar{\omega}_2}{\vec{\omega}_2}\right)^2 \left(\frac{\bar{\omega}_3}{\vec{\omega}_3}\right)^2 \left(\frac{\bar{\omega}_4}{\vec{\omega}_4}\right)^2 \left(\frac{\bar{\omega}_5}{\vec{\omega}_5}\right) \left(\frac{\bar{\omega}_6}{\vec{\omega}_6}\right) \left(\frac{\bar{\omega}_7}{\vec{\omega}_7}\right)^3 = 1 - \frac{1}{K_{OR}} \frac{p_{N_2} p_{H_2}^3}{p_{NH_3}^2} \qquad (5.14)$$

In analogy with Eq. (5.11), we have

$$R_{OR}^{\bullet} = \sum_{\rho=1}^{q+1} \sigma_\rho^2 (R_\rho^{\bullet}) \qquad (5.15)$$

Combining Eq. (5.14), (5.15) in Eq. (5.12), thus, the overall rate

$$r_{OR} = \frac{1}{4R_1^{\bullet} + 4R_2^{\bullet} + 4R_3^{\bullet} + 4R_4^{\bullet} + R_5^{\bullet} + R_6^{\bullet} + 9R_7^{\bullet}} \left(1 - \frac{1}{K_{OR}} \frac{p_{N_2} p_{H_2}^3}{p_{NH_3}^2}\right) \qquad (5.16)$$

where the step resistance for E_{OR} as the driving force (rather than affinity)

$$R_\rho^{\bullet} \equiv \frac{1}{\vec{r}_\rho^{\bullet}} \qquad (5.17)$$

The resistances $R_\rho^{\bullet}$ are next obtained *a priori*, by treating each of the steps as rate-determining step (RDS), in turn, and using the QE approximation for the remaining [36], i.e. following the LHHW approach, along with the notion of intermediate reactions.

Let us, thus, calculate the resistance for step s_1 as the RDS from Eq. (5.17)

$$R_1^{\bullet} = \frac{1}{\vec{r}_1^{\bullet}} = \frac{1}{\bar{\omega}_1 \theta_{0,1}^{\bullet}} \qquad (5.18)$$

with all other steps being at QE. Note that the subscript 1 in θ indicates step s_1 as the RDS, while others at QE. Then the IRs for the six intermediates may be written based on the QE steps

$$IR_{N \cdot S}: \quad (-)s_5 + (-1)s_6: \qquad\qquad N_2 + 2S \leftrightarrows 2N \cdot S$$
$$IR_{N_2 \cdot S}: \quad (-1)s_6: \qquad\qquad N_2 + S \leftrightarrows N_2 \cdot S$$
$$IR_{H \cdot S}: \quad (-1)s_7: \qquad\qquad H_2 + 2S \leftrightarrows 2H \cdot S$$
$$IR_{NH \cdot S}: \quad (-1)s_4 + (-1/2)s_5 + (-1/2)s_6 + (-1/2)s_7: \qquad 1/2N_2 + 1/2H_2 + S \leftrightarrows NH \cdot S$$
$$IR_{NH_2 \cdot S}: \quad (-1)s_3 + (-1)s_4 + (-1/2)s_5 + (-1/2)s_6 + (-1)s_7: \qquad 1/2N_2 + H_2 + S \leftrightarrows NH_2 \cdot S$$
$$IR_{NH_3 \cdot S}: \quad (-1)s_2 + (-1)s_3 + (-1)s_4 + (-1/2)s_5 + (-1/2)s_6 + (-3/2)s_7: \quad 1/2N_2 + 3/2H_2 + S \leftrightarrows NH_3 \cdot S$$

$$(5.19)$$
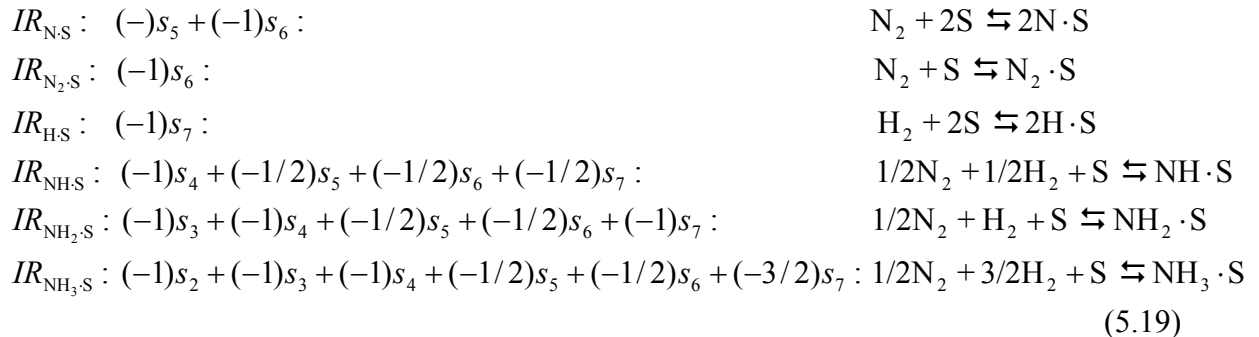
Using these in Eq. 2.25 for obtaining the intermediate site fraction ratio $\theta_{k,\rho}^{\bullet}/\theta_{0,\rho}^{\bullet}$ in terms of $\vec{\omega}_\rho$ and $\bar{\omega}_\rho$ of the QE steps, and then substituting into the site balance, i.e., in

$$\frac{1}{\theta_{0,1}^{\bullet}} = 1 + \left(\frac{\theta_{N\cdot S,1}^{\bullet}}{\theta_{0,1}^{\bullet}}\right) + \left(\frac{\theta_{N_2\cdot S,1}^{\bullet}}{\theta_{0,1}^{\bullet}}\right) + \left(\frac{\theta_{H\cdot S,1}^{\bullet}}{\theta_{0,1}^{\bullet}}\right) + \left(\frac{\theta_{NH\cdot S,1}^{\bullet}}{\theta_{0,1}^{\bullet}}\right) + \left(\frac{\theta_{NH_2\cdot S,1}^{\bullet}}{\theta_{0,1}^{\bullet}}\right) + \left(\frac{\theta_{NH_3\cdot S,1}^{\bullet}}{\theta_{0,1}^{\bullet}}\right) \quad (5.20)$$

to find $1/\theta_{0,1}^{\bullet}$, which when used in Eq. (5.18) provides

$$R_1^{\bullet} = \frac{1}{\vec{\omega}_1}\left[1 + \sqrt{\frac{\bar{\omega}_5\bar{\omega}_6}{\vec{\omega}_5\vec{\omega}_6}} + \frac{\bar{\omega}_6}{\vec{\omega}_6} + \sqrt{\frac{\bar{\omega}_7}{\vec{\omega}_7}} + \frac{\bar{\omega}_4}{\vec{\omega}_4}\sqrt{\frac{\bar{\omega}_5\bar{\omega}_6\bar{\omega}_7}{\vec{\omega}_5\vec{\omega}_6\vec{\omega}_7}} + \frac{\bar{\omega}_3\bar{\omega}_4}{\vec{\omega}_3\vec{\omega}_4}\sqrt{\frac{\bar{\omega}_5\bar{\omega}_6}{\vec{\omega}_5\vec{\omega}_6}}\frac{\bar{\omega}_7}{\vec{\omega}_7} + \frac{\bar{\omega}_2\bar{\omega}_3\bar{\omega}_4}{\vec{\omega}_2\vec{\omega}_3\vec{\omega}_4}\sqrt{\frac{\bar{\omega}_5\bar{\omega}_6}{\vec{\omega}_5\vec{\omega}_6}}\left(\frac{\bar{\omega}_7}{\vec{\omega}_7}\right)^{3/2}\right] \quad (5.21)$$

In a similar manner, using Eq. (5.17) for the resistance for step s_2

$$R_2^{\bullet} = \frac{1}{\vec{r}_2^{\bullet}} = \frac{1}{\vec{\omega}_2}\frac{1}{\theta_{NH_3\cdot S,2}^{\bullet}\theta_{0,2}^{\bullet}} = \frac{1}{\vec{\omega}_2}\frac{1}{\left(\dfrac{\theta_{NH_3\cdot S,2}^{\bullet}}{\theta_{0,2}^{\bullet}}\right)(\theta_{0,2}^{\bullet})^2} \quad (5.22)$$

The appropriate IRs for the six intermediates, with step s_2 as RLS may be written based on the QE steps

$$
\begin{array}{lll}
IR_{N\cdot S}: & (-)s_5 + (-1)s_6: & N_2 + 2S \leftrightarrows 2N\cdot S \\
IR_{N_2\cdot S}: & (-1)s_6: & N_2 + S \leftrightarrows N_2\cdot S \\
IR_{H\cdot S}: & (-1)s_7: & H_2 + 2S \leftrightarrows 2H\cdot S \\
IR_{NH\cdot S}: & (-1)s_4 + (-1/2)s_5 + (-1/2)s_6 + (-1/2)s_7: & 1/2N_2 + 1/2H_2 + S \leftrightarrows NH\cdot S \\
IR_{NH_2\cdot S}: & (-1)s_3 + (-1)s_4 + (-1/2)s_5 + (-1/2)s_6 + (-1)s_7: & 1/2N_2 + H_2 + S \leftrightarrows NH_2\cdot S \\
IR_{NH_3\cdot S}: & (+1)s_1: & NH_3 + S \leftrightarrows NH_3\cdot S
\end{array}
$$

$$\quad (5.23)$$

Following a similar procedure for obtaining the intermediate site fractions we have after some algebra

$$R_2^{\bullet} = \frac{1}{\vec{\omega}_2\left(\dfrac{\bar{\omega}_1}{\vec{\omega}_1}\right)}\left[1 + \sqrt{\frac{\bar{\omega}_5\bar{\omega}_6}{\vec{\omega}_5\vec{\omega}_6}} + \frac{\bar{\omega}_6}{\vec{\omega}_6} + \sqrt{\frac{\bar{\omega}_7}{\vec{\omega}_7}} + \frac{\bar{\omega}_4}{\vec{\omega}_4}\sqrt{\frac{\bar{\omega}_5\bar{\omega}_6\bar{\omega}_7}{\vec{\omega}_5\vec{\omega}_6\vec{\omega}_7}} + \frac{\bar{\omega}_3\bar{\omega}_4}{\vec{\omega}_3\vec{\omega}_4}\sqrt{\frac{\bar{\omega}_5\bar{\omega}_6}{\vec{\omega}_5\vec{\omega}_6}}\frac{\bar{\omega}_7}{\vec{\omega}_7} + \frac{\bar{\omega}_1}{\vec{\omega}_1}\right]^2 \quad (5.24)$$

Similarly, the resistance for step s_3

$$R_3^\bullet = \frac{1}{\vec{\omega}_3} \frac{1}{\left(\dfrac{\theta_{NH_2 \cdot S,3}^\bullet}{\theta_{0,3}^\bullet} \right) \left(\theta_{0,3}^\bullet \right)^2} \tag{5.25}$$

resulting in

$$R_3^\bullet = \frac{1}{\vec{\omega}_3 \left(\dfrac{\vec{\omega}_1 \vec{\omega}_2}{\vec{\omega}_1 \vec{\omega}_2} \sqrt{\dfrac{\vec{\omega}_7}{\vec{\omega}_7}} \right)} \left[1 + \sqrt{\dfrac{\vec{\omega}_5 \vec{\omega}_6}{\vec{\omega}_5 \vec{\omega}_6}} + \dfrac{\vec{\omega}_6}{\vec{\omega}_6} + \sqrt{\dfrac{\vec{\omega}_7}{\vec{\omega}_7}} + \dfrac{\vec{\omega}_4}{\vec{\omega}_4} \sqrt{\dfrac{\vec{\omega}_5 \vec{\omega}_6 \vec{\omega}_7}{\vec{\omega}_5 \vec{\omega}_6 \vec{\omega}_7}} + \dfrac{\vec{\omega}_1 \vec{\omega}_2}{\vec{\omega}_1 \vec{\omega}_2} \sqrt{\dfrac{\vec{\omega}_7}{\vec{\omega}_7}} + \dfrac{\vec{\omega}_1}{\vec{\omega}_1} \right]^2 \tag{5.26}$$

For step s_4

$$R_4^\bullet = \frac{1}{\vec{\omega}_4} \frac{1}{\left(\dfrac{\theta_{NH \cdot S,4}^\bullet}{\theta_{0,4}^\bullet} \right) \left(\theta_{0,4}^\bullet \right)^2} \tag{5.27}$$

resulting in

$$R_4^\bullet = \frac{1}{\vec{\omega}_4 \left(\dfrac{\vec{\omega}_1 \vec{\omega}_2 \vec{\omega}_3 \vec{\omega}_7}{\vec{\omega}_1 \vec{\omega}_2 \vec{\omega}_3 \vec{\omega}_7} \right)} \left[1 + \sqrt{\dfrac{\vec{\omega}_5 \vec{\omega}_6}{\vec{\omega}_5 \vec{\omega}_6}} + \dfrac{\vec{\omega}_6}{\vec{\omega}_6} + \sqrt{\dfrac{\vec{\omega}_7}{\vec{\omega}_7}} + \dfrac{\vec{\omega}_1 \vec{\omega}_2 \vec{\omega}_3 \vec{\omega}_7}{\vec{\omega}_1 \vec{\omega}_2 \vec{\omega}_3 \vec{\omega}_7} + \dfrac{\vec{\omega}_1 \vec{\omega}_2}{\vec{\omega}_1 \vec{\omega}_2} \sqrt{\dfrac{\vec{\omega}_7}{\vec{\omega}_7}} + \dfrac{\vec{\omega}_1}{\vec{\omega}_1} \right]^2 \tag{5.28}$$

For step s_5

$$R_5^\bullet = \frac{1}{\vec{\omega}_5} \frac{1}{\left(\dfrac{\theta_{N \cdot S,5}^\bullet}{\theta_{0,5}^\bullet} \right)^2 \left(\theta_{0,5}^\bullet \right)^2} \tag{5.29}$$

resulting in

$$R_5^\bullet = \frac{1}{\vec{\omega}_5 \left(\dfrac{\vec{\omega}_1 \vec{\omega}_2 \vec{\omega}_3 \vec{\omega}_4}{\vec{\omega}_1 \vec{\omega}_2 \vec{\omega}_3 \vec{\omega}_4} \right)^2 \left(\dfrac{\vec{\omega}_7}{\vec{\omega}_7} \right)^3} \left[1 + \dfrac{\vec{\omega}_1 \vec{\omega}_2 \vec{\omega}_3 \vec{\omega}_4}{\vec{\omega}_1 \vec{\omega}_2 \vec{\omega}_3 \vec{\omega}_4} \left(\dfrac{\vec{\omega}_7}{\vec{\omega}_7} \right)^{3/2} + \dfrac{\vec{\omega}_6}{\vec{\omega}_6} + \sqrt{\dfrac{\vec{\omega}_7}{\vec{\omega}_7}} + \dfrac{\vec{\omega}_1 \vec{\omega}_2 \vec{\omega}_3 \vec{\omega}_7}{\vec{\omega}_1 \vec{\omega}_2 \vec{\omega}_3 \vec{\omega}_7} + \dfrac{\vec{\omega}_1 \vec{\omega}_2}{\vec{\omega}_1 \vec{\omega}_2} \sqrt{\dfrac{\vec{\omega}_7}{\vec{\omega}_7}} + \dfrac{\vec{\omega}_1}{\vec{\omega}_1} \right]^2$$

$$\tag{5.30}$$

For step s_6

$$R_6^\bullet = \frac{1}{\vec{\omega}_6} \frac{1}{\left(\dfrac{\theta_{N_2 \cdot S,6}^\bullet}{\theta_{0,6}^\bullet}\right)\left(\theta_{0,6}^\bullet\right)} \tag{5.31}$$

resulting in

$$R_6^\bullet = \frac{1}{\vec{\omega}_6\left(\dfrac{\vec{\omega}_1\vec{\omega}_2\vec{\omega}_3\vec{\omega}_4}{\overleftarrow{\omega}_1\overleftarrow{\omega}_2\overleftarrow{\omega}_3\overleftarrow{\omega}_4}\right)^2 \dfrac{\vec{\omega}_5}{\overleftarrow{\omega}_5}\left(\dfrac{\vec{\omega}_7}{\overleftarrow{\omega}_7}\right)^3} \times$$

$$\left[1 + \frac{\vec{\omega}_1\vec{\omega}_2\vec{\omega}_3\vec{\omega}_4}{\overleftarrow{\omega}_1\overleftarrow{\omega}_2\overleftarrow{\omega}_3\overleftarrow{\omega}_4}\left(\frac{\vec{\omega}_7}{\overleftarrow{\omega}_7}\right)^{3/2} + \left(\frac{\vec{\omega}_1\vec{\omega}_2\vec{\omega}_3\vec{\omega}_4}{\overleftarrow{\omega}_1\overleftarrow{\omega}_2\overleftarrow{\omega}_3\overleftarrow{\omega}_4}\right)^2 \frac{\vec{\omega}_5}{\overleftarrow{\omega}_5}\left(\frac{\vec{\omega}_7}{\overleftarrow{\omega}_7}\right)^3 + \sqrt{\frac{\overleftarrow{\omega}_7}{\vec{\omega}_7}} + \frac{\vec{\omega}_1\vec{\omega}_2\vec{\omega}_3\vec{\omega}_7}{\overleftarrow{\omega}_1\overleftarrow{\omega}_2\overleftarrow{\omega}_3\overleftarrow{\omega}_7} + \frac{\vec{\omega}_1\vec{\omega}_2}{\overleftarrow{\omega}_1\overleftarrow{\omega}_2}\sqrt{\frac{\overleftarrow{\omega}_7}{\vec{\omega}_7}} + \frac{\vec{\omega}_1}{\overleftarrow{\omega}_1}\right] \tag{5.32}$$

and, finally, for step s_7

$$R_7^\bullet = \frac{1}{\vec{\omega}_7} \frac{1}{\left(\dfrac{\theta_{H\cdot S,7}^\bullet}{\theta_{0,7}^\bullet}\right)^2 \left(\theta_{0,7}^\bullet\right)^2} \tag{5.33}$$

resulting in

$$R_7^\bullet = \frac{1}{\vec{\omega}_7\left(\dfrac{\vec{\omega}_1\vec{\omega}_2\vec{\omega}_3\vec{\omega}_4}{\overleftarrow{\omega}_1\overleftarrow{\omega}_2\overleftarrow{\omega}_3\overleftarrow{\omega}_4}\sqrt{\dfrac{\overleftarrow{\omega}_5\overleftarrow{\omega}_6}{\vec{\omega}_5\vec{\omega}_6}}\right)^2} \times$$

$$\left[1 + \sqrt{\frac{\overleftarrow{\omega}_5\overleftarrow{\omega}_6}{\vec{\omega}_5\vec{\omega}_6}} + \frac{\overleftarrow{\omega}_6}{\vec{\omega}_6} + \left(\frac{\vec{\omega}_1\vec{\omega}_2\vec{\omega}_3\vec{\omega}_4}{\overleftarrow{\omega}_1\overleftarrow{\omega}_2\overleftarrow{\omega}_3\overleftarrow{\omega}_4}\sqrt{\frac{\overleftarrow{\omega}_5\overleftarrow{\omega}_6}{\vec{\omega}_5\vec{\omega}_6}}\right)^{1/3} + \left(\frac{\vec{\omega}_1\vec{\omega}_2\vec{\omega}_3\vec{\omega}_4}{\overleftarrow{\omega}_1\overleftarrow{\omega}_2\overleftarrow{\omega}_3\overleftarrow{\omega}_4}\sqrt{\frac{\overleftarrow{\omega}_5\overleftarrow{\omega}_6}{\vec{\omega}_5\vec{\omega}_6}}\right)^{1/3}\frac{\vec{\omega}_4}{\overleftarrow{\omega}_4}\sqrt{\frac{\overleftarrow{\omega}_5\overleftarrow{\omega}_6}{\vec{\omega}_5\vec{\omega}_6}} + \right.$$

$$\left. \left(\frac{\vec{\omega}_1\vec{\omega}_2\vec{\omega}_3\vec{\omega}_4}{\overleftarrow{\omega}_1\overleftarrow{\omega}_2\overleftarrow{\omega}_3\overleftarrow{\omega}_4}\sqrt{\frac{\overleftarrow{\omega}_5\overleftarrow{\omega}_6}{\vec{\omega}_5\vec{\omega}_6}}\right)^{2/3}\frac{\vec{\omega}_3\vec{\omega}_4}{\overleftarrow{\omega}_3\overleftarrow{\omega}_4}\sqrt{\frac{\overleftarrow{\omega}_5\overleftarrow{\omega}_6}{\vec{\omega}_5\vec{\omega}_6}} + \frac{\vec{\omega}_1}{\overleftarrow{\omega}_1}\right]^2 \tag{5.34}$$

Thus, all step resistances are now available in explicit, albeit rather complex, form for use in the OR rate expression, Eq. (5.16). Even though complex-looking, it is, thus, possible to obtain a steady state rate expression for this highly non-linear kinetics example following our approach without making any assumptions pertaining to the RLS in a tractable manner, which otherwise would be virtually impossible. Further our approach allows for logical pruning of the rate-expression as explained further.

Let us first confirm that the rate expression, Eq. (5.16) thus obtained, is in good agreement with the conventional QSS approximation approach, where a set of non-linear equations are solved simultaneously in order to evaluate the surface coverage of the intermediate species, based on which the overall rate is obtained. It must be noted that this set of non-linear QSS equations can be directly obtained from the RR Graph, Figure 5-5, and is represented by the KFL at the independent intermediate nodes (represented by color red), i.e.,

$$n_1 : r_1 - r_2 = 0; \quad n_2 : r_2 - r_3 = 0; \quad n_3 : r_3 - r_4 = 0;$$
$$n_5 : r_4 - 2r_5 = 0; \quad n_6 : r_5 - r_6 = 0; \quad n_7 : 3r_6 - r_7 = 0 \tag{5.35}$$

Using mass action kinetics, these KFL equations reduce to the following set

$$(\vec{\omega}_1\theta_0 - \bar{\omega}_1\theta_{NH_3\cdot S}) - (\vec{\omega}_2\theta_{NH_3\cdot S}\theta_0 - \bar{\omega}_2\theta_{NH_2\cdot S}\theta_{H\cdot S}) = 0;$$
$$(\vec{\omega}_2\theta_{NH_3\cdot S}\theta_0 - \bar{\omega}_2\theta_{NH_2\cdot S}\theta_{H\cdot S}) - (\vec{\omega}_3\theta_{NH_2\cdot S}\theta_0 - \bar{\omega}_3\theta_{NH\cdot S}\theta_{H\cdot S}) = 0;$$
$$(\vec{\omega}_3\theta_{NH_2\cdot S}\theta_0 - \bar{\omega}_3\theta_{NH\cdot S}\theta_{H\cdot S}) - (\vec{\omega}_4\theta_{NH\cdot S}\theta_0 - \bar{\omega}_4\theta_{N\cdot S}\theta_{H\cdot S}) = 0;$$
$$(\vec{\omega}_4\theta_{NH\cdot S}\theta_0 - \bar{\omega}_4\theta_{N\cdot S}\theta_{H\cdot S}) - 2(\vec{\omega}_5\theta_{N\cdot S}^2 - \bar{\omega}_5\theta_{N_2\cdot S}\theta_0) = 0; \tag{5.36}$$
$$(\vec{\omega}_5\theta_{N\cdot S}^2 - \bar{\omega}_5\theta_{N_2\cdot S}\theta_0) - (\vec{\omega}_6\theta_{N_2\cdot S} - \bar{\omega}_6\theta_0) = 0;$$
$$3(\vec{\omega}_6\theta_{N_2\cdot S} - \bar{\omega}_6\theta_0) - (\vec{\omega}_7\theta_{H\cdot S}^2 - \bar{\omega}_7\theta_0^2) = 0$$

Eq. (5.36) along with the site balance equation,

$$\theta_{NH_3\cdot S} + \theta_{NH_2\cdot S} + \theta_{NH\cdot S} + \theta_{N\cdot S} + \theta_{N_2\cdot S} + \theta_{H\cdot S} + \theta_0 = 1 \tag{5.37}$$

can be solved numerically, for given concentration of terminal species (experimental data provided in Figure 5-4) to obtain the unknown site fractions of intermediate species, θ_k. The QSS rate of the overall reaction may be obtained from the TNs, e.g., $6r_{OR} = 3r_1 = 2r_7$ (Figure 5-5).

The kinetic parameters provided in Table 5-1, are used in the above two approaches to compute the steady state overall rate of the reaction for the reaction conditions mentioned in Figure 5-4. Figure 5-6 compares the rate obtained from the QSS approach (solving Eqs. (5.36) - (5.37)) and that obtained from the alternate electrical circuit treatment based on the concept of maximum step rate, i.e. Eq. (5.16) along with Eqs. (5.21), (5.24), (5.26), (5.28), (5.30), (5.32) and (5.34).
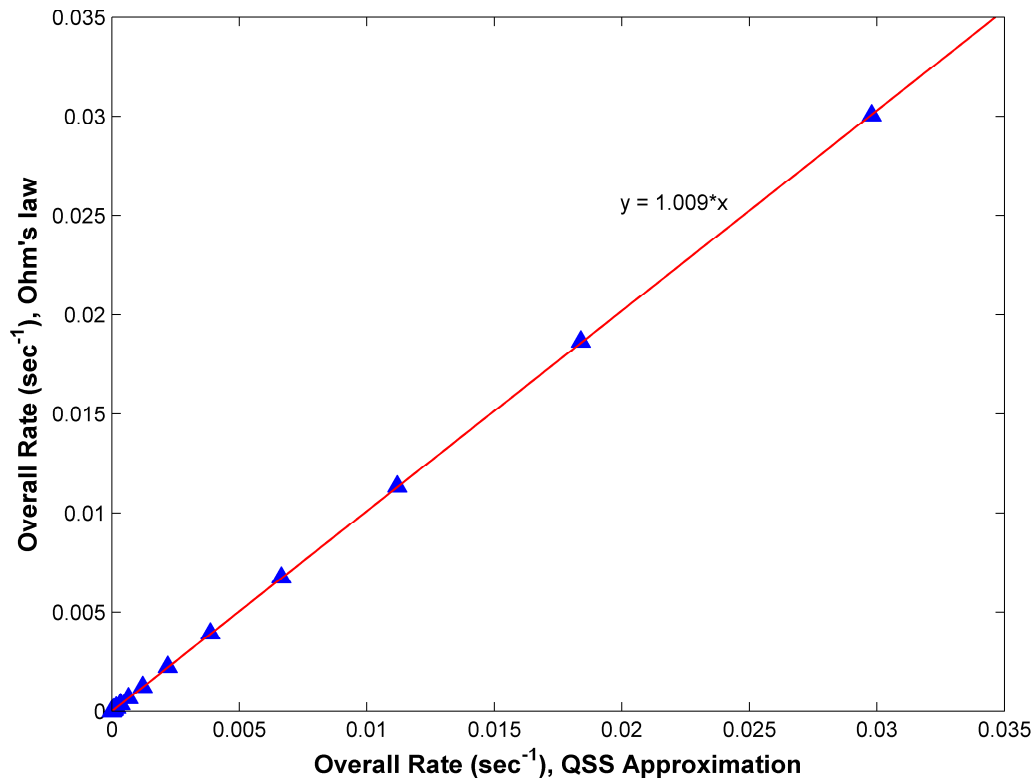
Figure 5-6: Parity plot for the experimental data shown in Figure 5-4.

As is evident from Figure 5-6, the two approaches are in close agreement with each other, which demonstrates the efficacy of the alternate electrical circuit approach elucidated above.

5.6 Sequence Pruning

The data may also be used for pruning and further reduction of the mechanism. By comparing the relative series resistances, one can quantitatively identify the rate-limiting step(s). Thus, the approach is not limited to the case of a single RLS. Figure 5-7 plots the seven step resistances, $R_\rho^\bullet$, for the given partial pressures of the terminal species as a function of temperature (Figure 5-4). It is clear from this plot (Figure 5-7) that step s_5 is the RDS, since for this reaction sequence; the step has the dominant resistance in comparison with the resistances of the remaining steps.

Thus, we have,

$$R_{OR}^\bullet = 4R_1^\bullet + 4R_2^\bullet + 4R_3^\bullet + 4R_4^\bullet + R_5^\bullet + R_6^\bullet + 9R_7^\bullet \approx R_5^\bullet \tag{5.38}$$

As a result, the overall rate expression for ammonia decomposition over Fe can be reduced suitably.

$$r_{OR} \approx \frac{E_{OR}}{R_5^\bullet} \tag{5.39}$$

Finally the approach also allows for the incorporation of the most abundant reactive intermediate (MARI) approximation. By comparing $\theta_{k,\rho}^\bullet / \theta_{0,\rho}^\bullet$, the expression for $\theta_{0,\rho}^\bullet$ can be appropriately reduced and so is $R_\rho^\bullet$. Figure 5-8 compares the $\theta_{k,5}^\bullet / \theta_{0,5}^\bullet$ as a function of temperature. We, thus, find the adsorbed nitrogen is the MARI, for the reaction conditions considered in this study, i.e.

$$\frac{1}{\theta_{0,5}^\bullet} = 1 + \left(\frac{\theta_{N\cdot S,5}^\bullet}{\theta_{0,5}^\bullet}\right) + \left(\frac{\theta_{N_2\cdot S,5}^\bullet}{\theta_{0,5}^\bullet}\right) + \left(\frac{\theta_{H\cdot S,5}^\bullet}{\theta_{0,5}^\bullet}\right) + \left(\frac{\theta_{NH\cdot S,5}^\bullet}{\theta_{0,5}^\bullet}\right) + \left(\frac{\theta_{NH_2\cdot S,5}^\bullet}{\theta_{0,5}^\bullet}\right) + \left(\frac{\theta_{NH_3\cdot S,5}^\bullet}{\theta_{0,5}^\bullet}\right) \approx 1 + \left(\frac{\theta_{N\cdot S,5}^\bullet}{\theta_{0,5}^\bullet}\right) \tag{5.40}$$
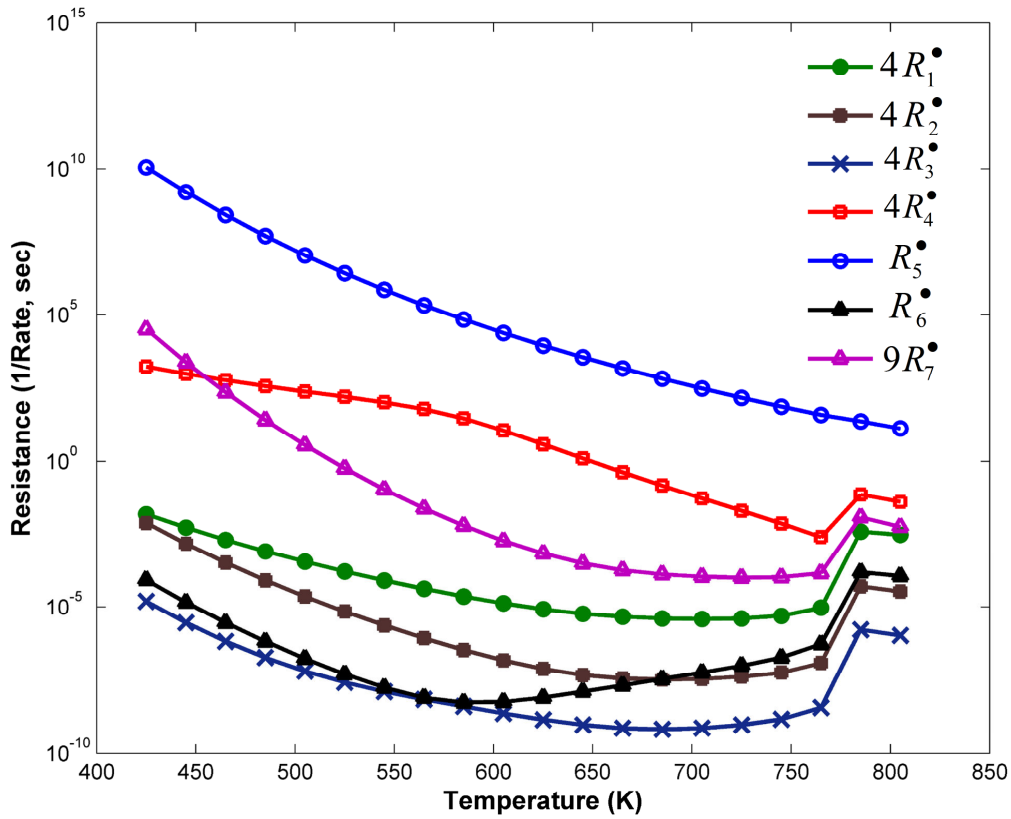
Figure 5-7: $R_\rho^\bullet$ as a function of temperature for the experimental data provided in Figure

5-4.
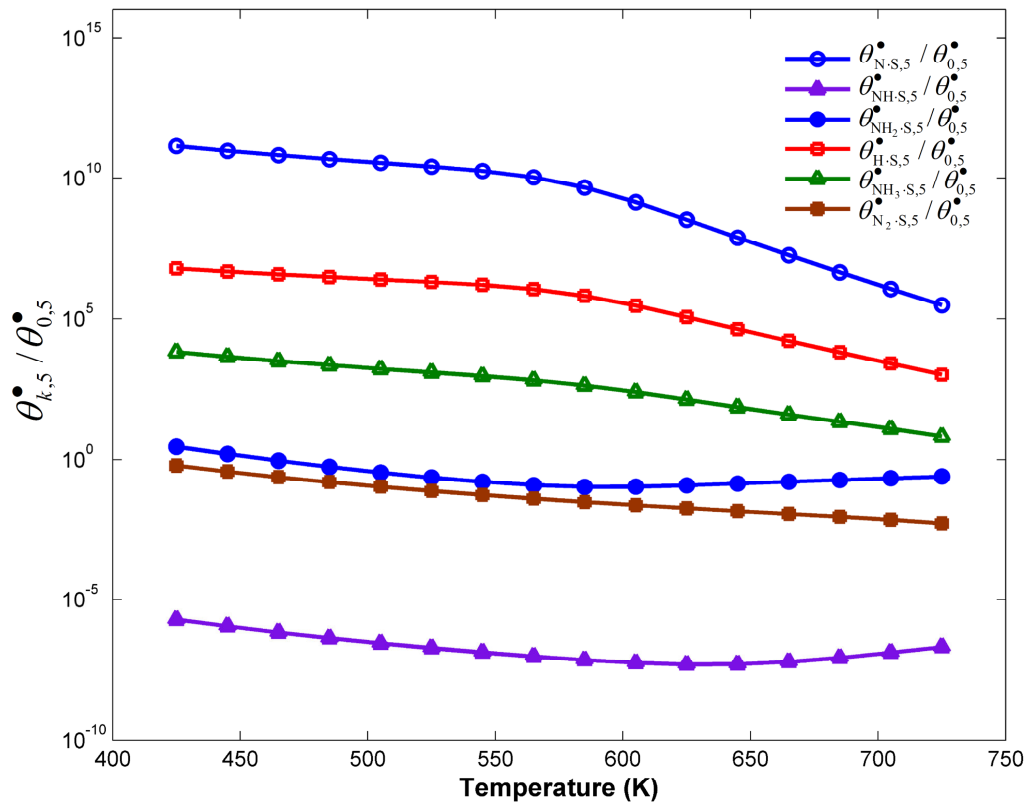
Figure 5-8: $\theta_{k,5}^{\bullet}\big/\theta_{0,5}^{\bullet}$ as a function of temperature for the experimental data provided in Figure 5-4.

Utilizing, Eq. (5.40), $R_5^\bullet$ can be reduced as follows

$$R_5^\bullet \approx \cfrac{1}{\bar{\omega}_5 \left(\cfrac{\vec{\omega}_1 \vec{\omega}_2 \vec{\omega}_3 \vec{\omega}_4}{\bar{\omega}_1 \bar{\omega}_2 \bar{\omega}_3 \bar{\omega}_4}\right)^2 \left(\cfrac{\vec{\omega}_7}{\bar{\omega}_7}\right)^3} \left[1 + \cfrac{\vec{\omega}_1 \vec{\omega}_2 \vec{\omega}_3 \vec{\omega}_4}{\bar{\omega}_1 \bar{\omega}_2 \bar{\omega}_3 \bar{\omega}_4}\left(\cfrac{\vec{\omega}_7}{\bar{\omega}_7}\right)^{3/2}\right]^2 \qquad (5.41)$$

Using Eq. (5.41) in Eq. (5.39), the overall rate expression for ammonia decomposition on Fe can be written in the conventional form as

$$r_{OR} \approx \cfrac{\vec{k}_5 (K_1 K_2 K_3 K_4 K_7^{1.5})^2 (p_{NH_3}^2 / p_{H_2}^3)}{\left[1 + K_1 K_2 K_3 K_4 K_7^{1.5}(p_{NH_3}/p_{H_2}^{1.5})\right]^2}\left(1 - \cfrac{1}{K_{OR}}\cfrac{p_{N_2} p_{H_2}^3}{p_{NH_3}^2}\right) \qquad (5.42)$$

where, K_ρ is the equilibrium constant for step s_ρ.

The NH$_3$ decomposition on Fe can now be simply written as two-step mechanism as shown below, with IR_1 at QE and step s_5 determining the rate of the overall reaction

$$\underline{\sigma_\rho}$$

$$IR_1 : (+1)s_1 + (+1)s_2 + (+1)s_3 + (+1)s_4 + (+3/2)s_7 : \qquad : \text{NH}_3 + \text{S} \leftrightarrows \text{N·S} + 3/2\text{H}_2 \qquad +2$$

$$IR_2 : (+1)s_5 + (+1)s_6 \qquad\qquad : 2\text{N·S} \leftrightarrows \text{N}_2 + \text{S} \qquad +1$$

$$\text{OR: } 2\text{NH}_3 \leftrightarrows \text{N}_2 + 3\text{H}_2 \qquad (5.43)$$
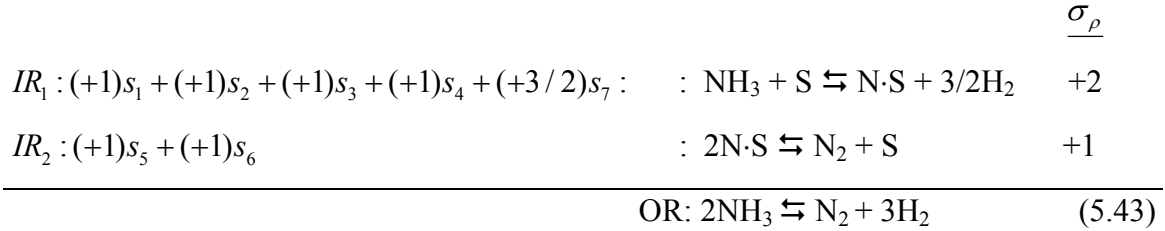
With step s_5 as the RLS and others at QE, $K_1 K_2 K_3 K_4 K_7^{1.5}$ represents the equilibrium constant for the formation of adsorbed nitrogen, i.e. N·S, as is evident from Eq. (5.43) Thus,

$$K_1 K_2 K_3 K_4 K_7^{1.5} = K_{IR_1} \qquad (5.44)$$

Using Eq. (5.44) in Eq. (5.42), we thus, have

$$r_{OR} \approx \cfrac{\vec{k}_5 (K_{IR_1})^2 (p_{NH_3}^2 / p_{H_2}^3)}{\left[1 + K_{IR_1}(p_{NH_3}/p_{H_2}^{1.5})\right]^2}\left(1 - \cfrac{1}{K_{OR}}\cfrac{p_{N_2} p_{H_2}^3}{p_{NH_3}^2}\right) \qquad (5.45)$$

Combining the appropriate rate constants in Eq. (5.45), we obtain the following simple rate expression for NH$_3$ decomposition on Fe,

$$r_{OR} \approx \frac{k_A(p_{NH_3}^2 / p_{H_2}^3)}{\left[1 + k_B(p_{NH_3} / p_{H_2}^{1.5})\right]^2} \left(1 - \frac{1}{K_{OR}} \frac{p_{N_2} p_{H_2}^3}{p_{NH_3}^2}\right)$$

$$\text{where, } k_A = 1.230 \times 10^{13} \exp\left(\frac{-93000}{RT}\right) \tag{5.46}$$

$$k_B = 1.1090 \times 10^2 \exp\left(\frac{31000}{RT}\right)$$

R is the gas constant in J/(mol K) and T is the temperature in K. Eq. (5.46) is in close agreement with the complete rate expression (Eq. (5.16)) as well as with the numerical QSS analysis. Further, the form of the above equation is similar to the Temkin–Pyzhev expression (Eq. (5.2)).

Eq. (5.45) can be used to predict the performance of the packed-bed reactor using the known kinetics (Table 5-1) for ammonia decomposition on Fe for a given input conditions, using the mass balance equation for the packed bed reactor [37],

$$\frac{dx_i}{d\left(\frac{W}{F_{0i}}\right)} = x_{0i} \frac{S_t C_t}{N_A} \left(\sum_{\rho=1}^{p} \beta_{\rho i} r_\rho - x_i \sum_{i=1}^{n} \sum_{\rho=1}^{p} \beta_{\rho i} r_\rho\right) \tag{5.47}$$

where C_t is the site density (sites/cm^2), S_t is the active catalyst surface area (cm^2/g), W is the mass, or weight of the catalyst, and x_i is the mole fraction of species i.

As seen from Figure 5-4, the kinetics predictions, without any fitted parameters, are in reasonable agreement with our experimental data for ammonia decomposition on Fe, indicative of the robustness of our theoretical approach. Furthermore, Eq. (5.45) also reveals hydrogen inhibition on the steady state rate of NH$_3$ decomposition, in agreement to the many reported studies in literature.

Finally, Skoplyak et al. [29] attempted sizing of an ammonia reformer for PEM fuel cell powered automobile application. An inlet ammonia flow rate of 5.40 kg/hr was calculated for an automobile cruising at 55 miles/hr with fuel efficiency of 55 miles/gallon, and fuel cell efficiency of ~40%. Furthermore, the calculations also incorporate roughly 10.5% hydrogen produced to be consumed in order to sustain the endothermic decomposition reaction at 600 °C. With a fuel tank capacity of 18.5 gallons

of liquid ammonia, the PEM fuel cell vehicle will be able to travel 434 miles, ~27% less than it would with a gasoline fueled automobile with internal combustion engine. Of course, for the PEM fuel cell automobile, impact on lower vehicle emissions would be immense. Finally, only 150 g of Fe catalyst would be required in the reformer in order to achieve equilibrium conversion. However, it should be noted that trace amounts of ammonia in the order of $100 - 1000$ ppm would be produced, because of thermodynamic limitations, which needs to be reduced to ppb levels, if the PEM fuel cell is not be poisoned. This would warrant the incorporation of an efficient adsorber downstream of the reformer.

5.7 Conclusions

Ammonia can serve as an excellent chemical carrier for hydrogen and allow compact systems for a single-step hydrogen production. In order to develop efficient ammonia reformer for fuel cell applications or for direct ammonia fuel cells, it is imperative to investigate in detail the decomposition reaction mechanism and kinetics. To this end, we have studied the 7-step NH_3 decomposition reaction mechanism, which is a case of non-linear kinetic reaction sequence, utilizing our RR graph approach. The steady state rate expression can be cast into a simple Ohm's law form, $r_{OR} = E_{OR} / R_{OR}^{\bullet}$, which allows further network pruning based on step resistance comparison to logically identify the rate-limiting step(s). The analysis based on comparison of step resistances, reveals unequivocally that the reaction mechanism can be reduced to a *single* rate-limiting step, namely the recombinative desorption of nitrogen, step s_5 (2N·S $\leftrightarrows$ N$_2$·S + S), for the reaction conditions considered in this study. Moreover, the analysis also allows for incorporation of the MARI assumption. Comparison of species surface coverage reveal the adsorbed nitrogen, N·S is indeed the MARI, agreeing with most of the literature reported studies. These simplifications allows for further reduction of the steady-state rate expression. The final simple rate expression is in good agreement with our experimental data on Fe. Thus, the convenient and insightful new framework based on electrical analogy described here, makes it possible to obtain steady state rate expressions without making arbitrary assumptions.

Finally, CO_x-free, SO_x-free and NO_x-free hydrogen from a single-step source like ammonia decomposition can be an attractive alternative to hydrocarbon fuels for small-scale fuel cell applications.

5.8 References

[1] R. Z. Sørensen, L. J. E. Nielsen, S. Jensen, O. Hansen, T. Johannessen, U. Quaade, C. H. Christensen, Cataly. Comm. 6 (2005) 229-232.

[2] P. Ross, Proceedings 16th Intersoc. Energy Conv. Eng. Conference, 1981.

[3] K. Kordesch, J. Gsellmann, M. Cifrain, S. Voss, V. Hacker, R.R. Aronson, C. Fabjan, T. Hejze, J. Daniel-Ivad, J. Power Sources. 80 (1999) 190-197.

[4] V. Hacker, K. Kordesch, in: W. Vielstich, A. Lamm, H.A. Gasteiger (Eds.), Handbook of Fuel Cells - Fundamentals Technology and Applications Vol. 3: Fuel Cell Technology and Applications: Part 1, John Wiley, Chichester, England, 2003, p. 121.

[5] F.A. Uribe, S. Gottesfeld, T.A. Zawodzinski, Jr., J. Electrochem. Soc. 149 (2002) A293-A296.

[6] F. Uribe, T.J. Zawodzinski, 200th Meeting Electrochem. Soc. Abstract 339, San Francisco, CA, 2001.

[7] F.R. García-García, Y.H. Ma, I. Rodríguez-Ramos, A. Guerrero-Ruiz, Catalysis Communications. 9 (2008) 482-486.

[8] A.S. Chellappa, C.M. Fischer, W.J. Thomson, Appl. Catal. A General. 227 (2002) 231-240.

[9] R. Metkemeijer, P. Achard, Int. J. Hydrogen Energy. 19 (1994) 535.

[10] R. Metkemeijer, P. Achard, J. Power Sources. 49 (1994) 271.

[11] A. Wojcik, H. Middleton, I. Damopoulos, J. Van Herle, J. Power Sources. 118 (2003) 342-348.

[12] B. Chachuat, A. Mitsos, P.I. Barton, Chem. Eng. Sci. 60 (2005) 4535–4556.

[13] A. K. Santra, B. K. Min, C. W. Yi, K. Luo, T. V. Choudhary, D. W. Goodman, J. Phys. Chem. B. 106 (2002) 340.

[14] W. Tsai, W.H. Weinberg, J. Phys. Chem. 91 (1987) 5307.

[15] S. Stolbov, T. S. Rahman, J. Chem. Phys. 123 (2005) 204716.

[16] A. B. Mhadeshwar, J. R. Kitchin, M. A. Barteau, D. G. Vlachos, Catal. Lett. 96 (2004) 13.

[17] S. R. Deshmukh, A. B. Mhadeshwar, D. G. Vlachos, Ind. Eng. Chem. Res. 43 (2004) 2986-2999.

[18] K. Tamaru, Acc. Chem. Res. 21 (1988) 88.

[19] G. Djèga-Mariadassou, C.-H. Shin, G. Bugli, J. Mol. Catal. A: Chem. 141 (1999) 263.

[20] D.G. Löffler, L.D. Schmidt, J. Catal. 44 (1976) 244.

[21] D.G. Löffler, L.D. Schmidt, J. Catal. 41 (1976) 440.

[22] S.T. Oyama, J. Catal. 133 (1992) 358.

[23] G. Ertl, M. Huber, J. Catal. 61 (1980) 537.

[24] A.S. Chellappa, C.M. Fischer, W.J. Thomson, Appl. Catal. A General. 227 (2002) 231–240.

[25] M.C.J. Bradford, P.E. Fanning, M.A. Vannice, J. Catal. 172 (1997) 479.

[26] S.F. Yin, Q.H. Zhang, B.Q. Xu, W.X. Zhu, C.F. Ng, C.T. Au, J. Catal. 224 (2004) 384.

[27] E. Shustorovich, A.T. Bell, Surf. Sci. Lett. 259 (1991) 791.

[28] W. Huang, W. Lai, D. Xie, Surf. Sci. 602 (2008) 1288–1294.

[29] O. Skoplyak, B.M. Grace, S.T. Castellani, Major Qualifying Project Report, Worcester Polytechnic Institute, Worcester, MA, 2003.

[30] M.I. Temkin, Adv. Catal. 28 (1979) 173.

[31] I. Fishtik, C.A. Callaghan, R. Datta, J. Phys. Chem. B. 108 (2004) 5671-5682.

[32] P. Stolze, J.K. Nørskov, Phys. Rev. Lett. 55 (1985) 2502.

[33] P. Stolze, J.K. Nørskov, Surf. Sci. Lett. 197 (1988) L230.

[34] P. Stolze, J.K. Nørskov, J. Catal. 110 (1988) 1.

[35] M.Z. Lazman, G.S. Yablonskii, Patterns and Dynamics in Reactive Media, The IMA Volumes in Mathematics and its Applications, Springer, Berlin - Heidelberg - New York, 1991, pp. 117-150.

[36] S.A. Vilekar, I. Fishtik, R. Datta, Chem. Eng. Sci. 64 (2009) 1968-1979.

[37] C.A. Callaghan, Department of Chemical Engineering, Worcester Polytechnic Institute, Worcester, MA, 2006.

Chapter VI

Reaction Circuitry of Methane Steam Reforming on Ni(111): Mechanism and Kinetics

In the preceding chapters we have utilized the RR Graph approach for *single* overall reaction systems. In this chapter, we extend this approach to provide a robust model, with predictive kinetics for methane steam reforming (MSR) on Ni(111), a case of multiple overall reactions. A detailed mechanism comprising of 22 elementary steps is considered based on literature reported mechanisms. The Unity Bond Index – Quadratic Exponential Potential (UBI-QEP) method and the transition-state theory are employed to calculate the elementary reaction step kinetics.

Following our RR graph approach, the 22-step mechanism is whittled down to a dual path mechanism for MSR, depending upon the reaction temperature. Further, only two independent overall reactions out of a total of five are necessary to adequately describe the system. Rate-limiting steps and quasi-equilibrated steps are next identified based on the concept of step resistance and reversibility, respectively, following which explicit rate expressions are developed. Finally, a comparison between the reduced model predictions for an isothermal PFR and the experimental results of Xu and Froment [1] is presented, showing good agreement.

6.1 Introduction

Natural gas is the preferred feedstock for hydrogen production via steam reforming (SR), as well as for direct internal reforming [2-5] in solid oxide fuel cells (Figure 6-1). Natural gas consists mostly of methane [6], and has the highest H/C ratio and, thus, the lowest CO_2 footprint of any hydrocarbon fuel. Methane steam reforming (MSR), typically on Ni, is currently the most common industrial process for the production of hydrogen [7], producing roughly half of the hydrogen worldwide. For this reason, the kinetics of the process has been intensively investigated [1, 8-11]. Most of the proposed kinetics and the underlying mechanisms have been developed using the conventional Langmuir-Hinshelwood-Hougen-Wantson (LHHW) approach. Here, for brevity, we mention only a selection of these models.

Early work on MSR was based on the assumption that the methane adsorption was rate-determining, which was in agreement with the assumption of first-order dependence on the methane. For example, Bodrov et al. [12] assumed methane adsorption to be rate-limiting and proposed the following expression based on experiments conducted over a nickel foil

$$r = \frac{kp_{CH_4}}{1 + a(p_{H_2O} / p_{H_2}) + bp_{CO}} \tag{6.1}$$

However, this could not explain the observed hydrogen inhibitive effect. Khomenko et al. on the other hand [13] proposed the following rate expression without considering a RDS and relying instead on the QSS analysis in terms of Temkin indentity

$$r = \frac{kp_{CH_4} p_{H_2O}}{f(p_{H_2O}, p_{H_2})(1 + K_{H_2O} P_{H_2O} / P_{H_2})} \left(1 - \frac{1}{K} \frac{p_{H_2}^3 p_{CO}}{p_{CH_4} p_{H_2O}}\right) \tag{6.2}$$

where $f(p_{H_2O}, p_{H_2})$ is a polynomial in p_{H_2O} and p_{H_2}. However, when this expression was tested at high pressure over a nickel foil, the rate constant was found to be a function of pressure.

Temkin and coworkers [8] proposed two different, 6-elementary reactions, 2-reaction routes (RRs), two OR mechanisms shown below, that result in the same overall rate expressions.

		RR_I	RR_{II}	
s_1:	$CH_4 + S \leftrightarrows \mathbf{CH_2 \cdot S} + H_2$	+1	0	
s_2:	$\mathbf{CH_2 \cdot S} + H_2O \leftrightarrows \mathbf{CH_2O \cdot S} + H_2$	+1	0	
s_3:	$\mathbf{CH_2O \cdot S} + S \leftrightarrows \mathbf{CO \cdot S} + H_2$	+1	0	
s_4:	$\mathbf{CO \cdot S} \leftrightarrows CO + S$	+1	0	(6.3)
s_5:	$H_2O + S \leftrightarrows \mathbf{O \cdot S} + H_2$	0	+1	
s_6:	$CO + \mathbf{O \cdot S} \leftrightarrows CO_2 + S$	0	+1	
RR_I:	$CH_4 + H_2O \leftrightarrows CO + 3H_2$	$r_I = r_1$		
RR_{II}:	$H_2O + CO \leftrightarrows CO_2 + H_2$	$r_{II} = r_5$		

		RR_I	RR_{II}	
s_1:	$CH_4 + S \leftrightarrows \mathbf{CH_2 \cdot S} + H_2$	+1	0	
s_2:	$\mathbf{CH_2 \cdot S} \leftrightarrows \mathbf{C \cdot S} + H_2$	+1	0	
s_3:	$\mathbf{C \cdot S} + H_2O \leftrightarrows \mathbf{CO \cdot S} + H_2$	+1	0	
s_4:	$\mathbf{CO \cdot S} \leftrightarrows CO + S$	+1	0	(6.4)
s_5:	$H_2O + S \leftrightarrows \mathbf{O \cdot S} + H_2$	0	+1	
s_6:	$CO + \mathbf{O \cdot S} \leftrightarrows CO_2 + S$	0	+1	
RR_I:	$CH_4 + H_2O \leftrightarrows CO + 3H_2$	$r_I = r_1$		
RR_{II}:	$H_2O + CO \leftrightarrows CO_2 + H_2$	$r_{II} = r_5$		
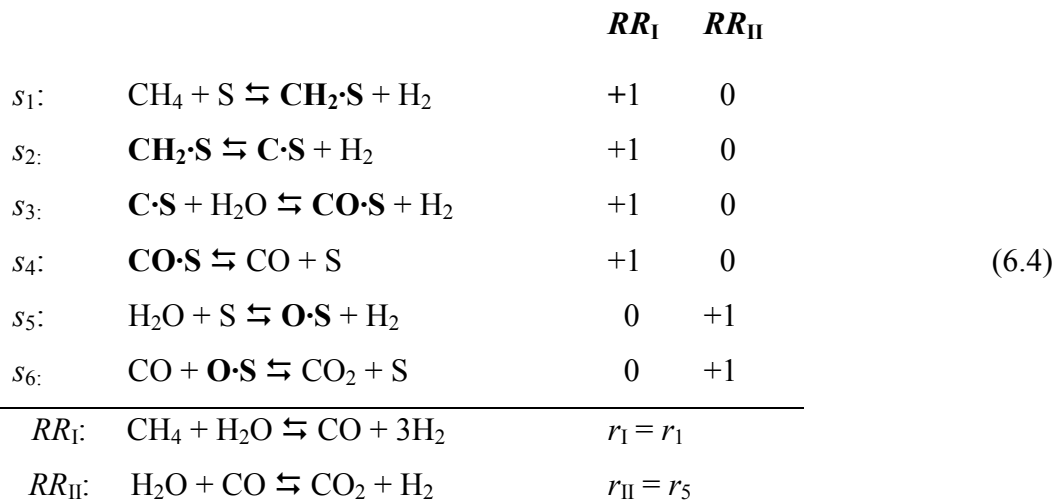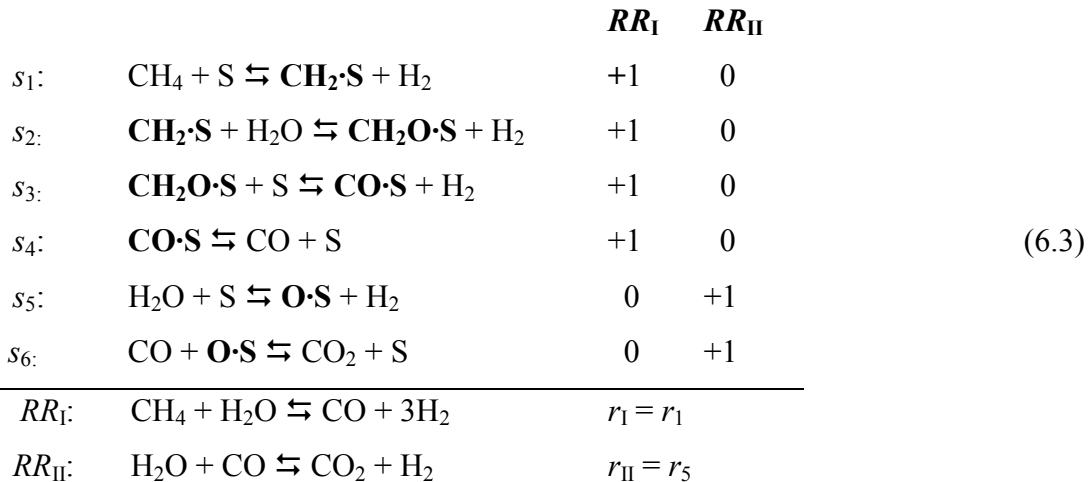
According to the first mechanism, the CO is produced via carbon oxygenates while in the second mechanism, the CO is produced via elemental carbon. In both mechanisms, the CO_2 is produced via the WGS reaction. It may be noted that in both of these mechanisms, the SR and the WGS reactions proceed independently, i.e. they have no common steps. The rate equations were derived employing the QSS assumption for the species written in bold letters. It can, however, be easily seen that most of the proposed reactions are not elementary reaction steps.
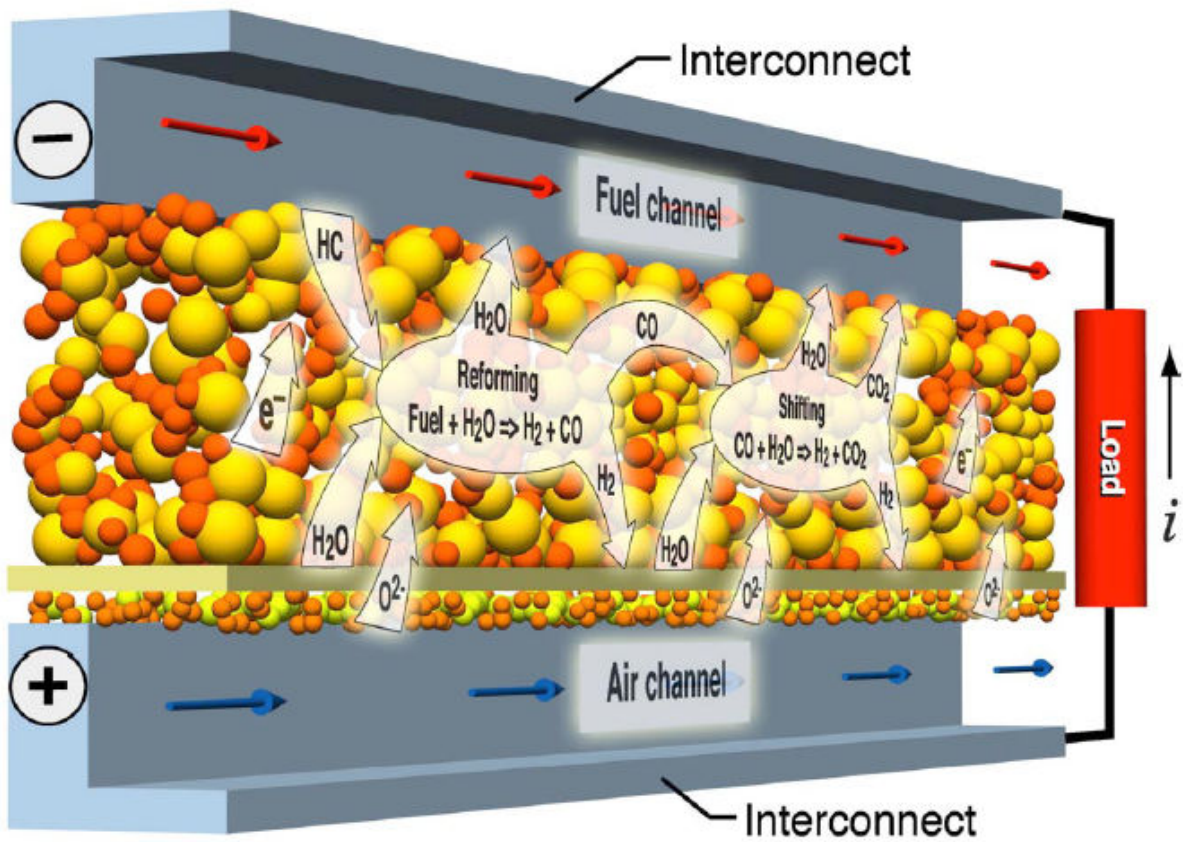
Figure 6-1: Direct internal reforming (DIR) on Ni/YSZ anode in a SOFC [14].

A 13-elementary reactions, 3-RRs mechanism shown below, has been proposed by Xu and Froment [1], which was an advancement over the mechanism proposed by Temkin.

		RR_I	RR_{II}	RR_{III}	
s_1:	$CH_4 + S \leftrightarrows CH_4 \cdot S$	+1	+1	0	QE
s_2:	$H_2O + S \leftrightarrows O \cdot S + H_2$	+1	+2	+1	QE
s_3:	$CO \cdot S \leftrightarrows CO + S$	+1	0	-1	QE
s_4:	$CO_2 \cdot S \leftrightarrows CO_2 + S$	0	+1	+1	QE
s_5:	$H \cdot S + H \cdot S \leftrightarrows H_2 \cdot S + S$	+3	+4	+1	QE
s_6:	$H_2 \cdot S \leftrightarrows H_2 + S$	+3	+4	+1	QE
s_7:	$CH_4 \cdot S + S \leftrightarrows CH_3 \cdot S + H \cdot S$	+1	+1	0	QE
s_8:	$CH_3 \cdot S + S \leftrightarrows CH_2 \cdot S + H \cdot S$	+1	+1	0	QE
s_9:	$CH_2 \cdot S + O \cdot S \leftrightarrows CH_2O \cdot S + S$	+1	+1	0	QE
s_{10}:	$CH_2O \cdot S + S \leftrightarrows CHO \cdot S + H \cdot S$	+1	+1	0	QE
s_{11}:	**$CHO \cdot S + S \leftrightarrows CO \cdot S + H \cdot S$**	**+1**	**0**	**0**	**RDS**
s_{12}:	**$CHO \cdot S + O \cdot S \leftrightarrows CO_2 \cdot S + H \cdot S$**	**0**	**+1**	**0**	**RDS**
s_{13}:	**$CO \cdot S + O \cdot S \leftrightarrows CO_2 \cdot S + S$**	**0**	**0**	**+1**	**RDS**

(6.5)

RR_I:	$CH_4 + H_2O \leftrightarrows CO + 3H_2$	$r_I = r_{11}$
RR_{II}:	$CH_4 + 2H_2O \leftrightarrows CO_2 + 4H_2$	$r_{II} = r_{12}$
RR_{III}:	$H_2O + CO \leftrightarrows CO_2 + H_2$	$r_{III} = r_{13}$

The following rate expressions were developed for the three overall reactions in the Xu and Froment model, derived using the LHHW formalism, with $CHO \cdot S + S = CO \cdot S + H \cdot S$, $CHO \cdot S + O \cdot S = CO_2 \cdot S + H \cdot S$ and $CO \cdot S + O \cdot S = CO_2 \cdot S + S$ assumed as rate-limiting steps (written as bold in Eq. (6.5)), S being a surface site.

$$r_1 = \frac{k_1 p_{CH_4} p_{H_2O} \theta_0^2}{p_{H_2}^{2.5}} \left(1 - \frac{1}{K_1} \frac{p_{H_2}^3 p_{CO}}{p_{CH_4} p_{H_2O}} \right)$$

(6.6)

for RR_I: $CH_4 + H_2O \leftrightarrows CO + 3H_2$

$$r_2 = \frac{k_2 p_{CH_4} p_{H_2O}^2 \theta_0^2}{p_{H_2}^{3.5}} \left(1 - \frac{1}{K_2} \frac{p_{H_2}^4 p_{CO_2}}{p_{CH_4} p_{H_2O}^2} \right)$$

(6.7)

for RR_{II}: $CH_4 + 2H_2O \leftrightarrows CO_2 + 4H_2$, and

$$r_3 = \frac{k_3 p_{CO} p_{H_2O} \theta_0^2}{p_{H_2}} \left(1 - \frac{1}{K_3} \frac{p_{H_2} p_{CO_2}}{p_{CO} p_{H_2O}} \right)$$

(6.8)

for RR_{III}: $H_2O + CO \leftrightarrows CO_2 + H_2$

Furthermore, it was also assumed that the surface is mostly covered with adsorbed oxygen atoms in addition to CO, H_2 and CH_4. Thus, in the Xu and Froment model,

$$\theta_0 = \frac{1}{1 + K_{CO} P_{CO} + K_{H_2} P_{H_2} + K_{CH_4} P_{CH_4} + K_{H_2O} P_{H_2O} / P_{H_2}}$$

(6.9)

The resulting rate equations were fitted to the experimental data and were shown to accurately reproduce and predict the kinetics over a large range of parameter values. The model predicts the order of methane consumption rate with respect to methane to be significantly lower than unity.

Since the work of Dumesic and coworkers [15] and the recent dramatic advancements in semi-empirical [16] and *ab-initio* [17] quantum chemical methods of calculation of the energetics of the elementary reactions, microkinetic modeling is becoming an increasingly powerful tool in the development of fundamental and accurate kinetics of heterogeneous catalytic reactions [18, 19]. Moreover, the mechanism of steam reforming (SR) is complex and there is always the potential for carbon formation on the catalyst in the SR process by a variety of mechanisms, i.e., whisker formation following C formation, dissolution, nucleation and growth, etc. Recently, the propensity to coking shown by Ni catalysts was explained by the strong adsorption of carbon atoms at the step sites on a Ni(211) surface, followed by the growth of graphitic carbon over the adjacent terrace sites [20]. Bengaard et al. [21] based on their DFT calculations also suggested the nucleation of graphite on Ni at step sites. It is, thus, known that the Ni catalysts normally suffer from carbon formation (Figure 6-2), and a rational kinetic model needs to incorporate the same for a realistic portrayal of the reaction mechanism. This aspect has certainly not been considered in the Xu and Froment [1] model.

(a)   **(b)**
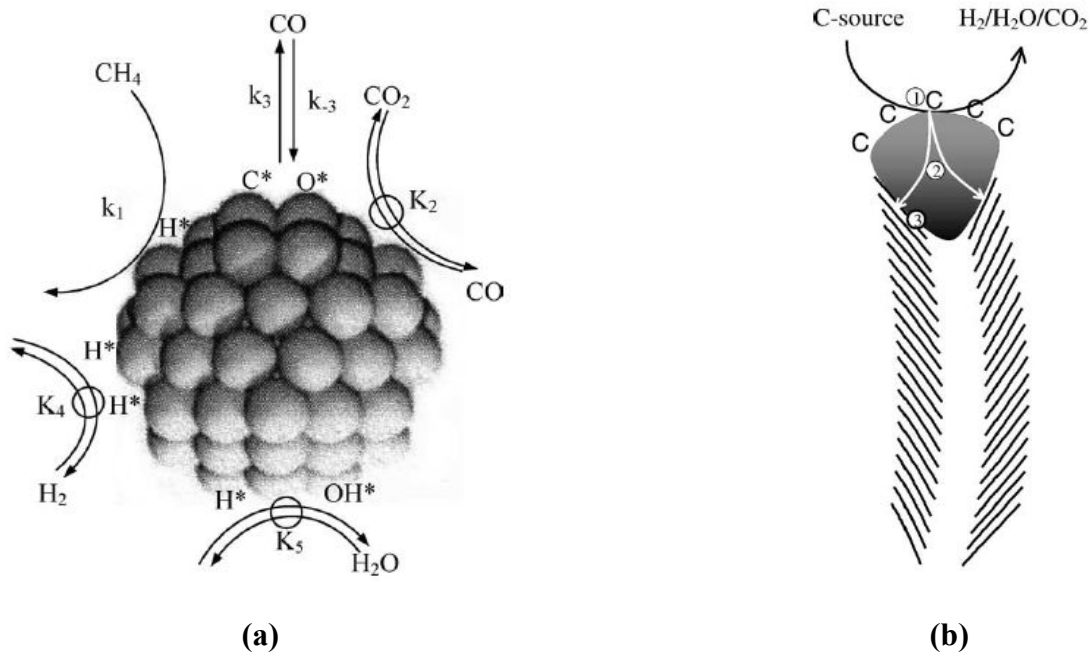
Figure 6-2: (a) Sequence of elementary steps for CH_4 reforming involving C formation [9]. (b) Schematic representation of catalytic growth of carbon nanofibres (CNF) [22], Step 1: decomposition of carbon-containing gases on the metal surface. Step 2: carbon atoms dissolve in and diffuse through the bulk of the metal. Step 3: precipitation of carbon in the form of a CNF consisting of graphite

Thus, more recently a 11-elementary steps, 2 RRs, microkinetic model for the MSR on Ni was proposed by Aparicio [10] as shown in Eq. (6.10), which incorporates the C formation mechanism.

		RR_I	RR_{II}
s_1:	$CH_4 + 2S \leftrightarrows CH_3 \cdot S + H \cdot S$	+1	0
s_2:	$CH_3 \cdot S + S \leftrightarrows CH_2 \cdot S + H \cdot S$	+1	0
s_3:	$CH_2 \cdot S + S \leftrightarrows CH \cdot S + H \cdot S$	+1	0
s_4:	$CH \cdot S + S \leftrightarrows C \cdot S + H \cdot S$	+1	0
s_5:	$H_2O + S \leftrightarrows H_2O \cdot S$	+1	+1
s_6:	$H_2O \cdot S + S \leftrightarrows OH \cdot S + H \cdot S$	+1	+1
s_7:	$C \cdot S + OH \cdot S \leftrightarrows CHO \cdot S_2$	+1	0
s_8:	$CO_2 + 2H \cdot S + 2S \leftrightarrows CHO \cdot S_2 + OH \cdot S + S$	0	-1
s_9:	$CHO \cdot S_2 + S \leftrightarrows CO \cdot S_2 + H \cdot S$	+1	-1
s_{10}:	$CO \cdot S_2 \leftrightarrows CO + 2S$	+1	-1
s_{11}:	$2H \cdot S \leftrightarrows H_2 + S$	+3	+1

$$(6.10)$$

RR_I:	$CH_4 + H_2O \leftrightarrows CO + 3H_2$
RR_{II}:	$H_2O + CO \leftrightarrows CO_2 + H_2$
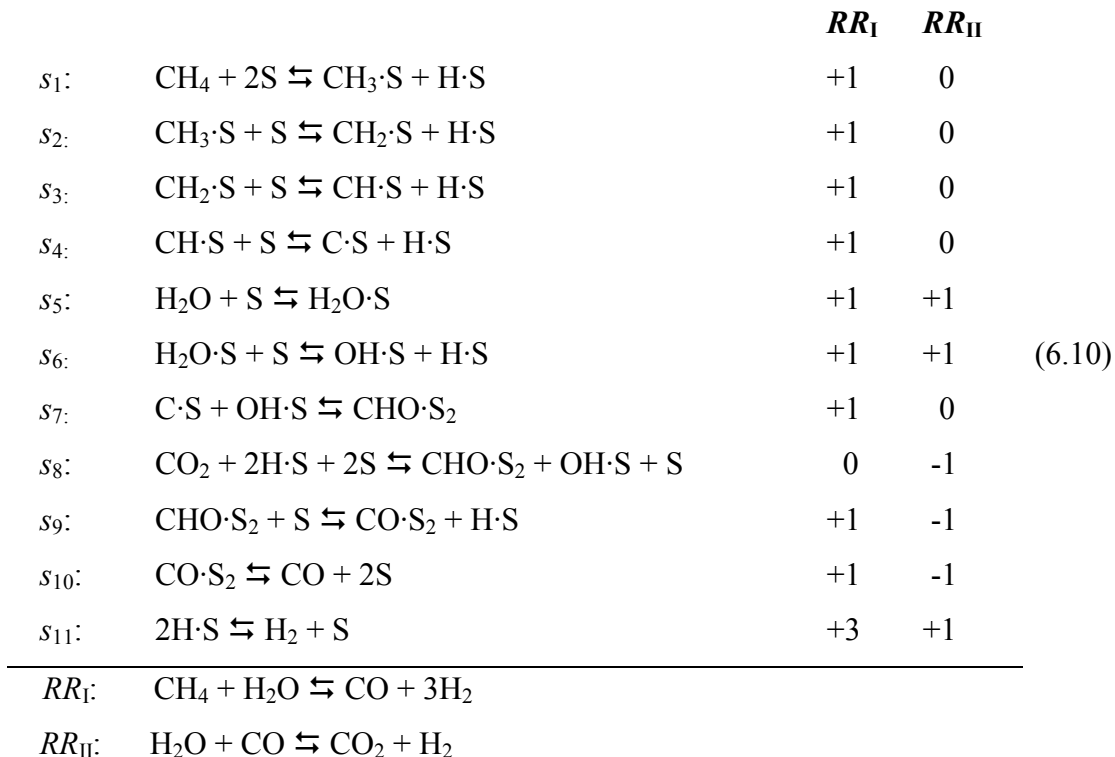
Most of the pre-exponential factors and activation energies of the elementary reactions in this model were theoretically estimated using the experimental molecular level information and statistical thermodynamics. Nonetheless, the rate constants of some of the elementary reactions were determined by fitting the model to the experimental kinetic data. More recently, the Aparicio model has also been adapted for dry (CO_2) reforming of methane [23]. For example, Avetisov et al. [24], have utilized the Xu and Froment as well as the Aparicio models to analyze their experimental data. The kinetic parameters were obtained using mathematical regression by minimizing the sum of squares of relative deviations of experimental and calculated values of CH_4 conversion and CO_2 yields.

Using power law model of the form

$$r = kp_{CH_4}^a p_{CO_2}^b \qquad (6.11)$$

Bhat and Sachtler [25] reported the dry reforming of methane to be first order in CH_4 and zero order in CO_2, indicating that C–H bond activation is the kinetically relevant step in CH_4 reforming reactions. The H_2 and CO_2 desorption reaction were found to be kinetically fast. Rostrup-Nielsen and Hansen [26] suggested that steam reforming and dry reforming of methane on Ni catalyst proceed with the same rate, and the CH_4 dissociation and C oxidation were predicted to determine the overall reaction rate.

Wei and Iglesia [27, 28] proposed a simple reaction mechanism for both steam and dry reforming of methane on Pt and Rh. The activation of C–H bonds was considered to be irreversible and first abstraction of hydrogen from CH_4 ($CH_4 + 2S \rightarrow CH_3 \cdot S + H \cdot S$) was shown to the RDS, regardless of the co-reactants. This indicates that the reactivity of the metal towards C–H bond activation governs the overall reaction kinetics. On the other hand, study by Xu and Froment [1] implies that reactions of carbon intermediates with oxygen are rate-limiting.

Chen et al. [29, 30] used Aparicio's microkinetic model [10] as basis for their model that included carbon formation and deactivation. Bond Conservation Energy (BOC) method was utilized to calculate the step activation energies. The model described both dry and steam reforming of methane on $Ni/MgO\text{-}Al_2O_3$ and $Ni/CaO\text{-}Al_2O_3$ in a temperature range of $773 - 923$ K. The sensitivity analysis by the authors revealed that the reaction mechanism could not be reduced to a case of *single* RDS, clearly demonstrating the limitation of conventional LHHW-type kinetic modeling based on a *single* RDS. The microkinetic modeling [30] concluded that although the surface coverage of C·S is relatively low, it plays a very important role in syngas formation. Moreover, the surface coverage of C·S was found to be larger than that of $CH_3 \cdot S$, $CH_2 \cdot S$ and $CH \cdot S$.

Jarosch et al. [31] utilized the Box-Hill function to statistically analyze six different literature reported models, concluding that the adsorption of methane plays a significant role in order to determine the observed rate of methane consumption in MSR. Bradford and Vannice [32] reported the reaction kinetics of dry reforming of CH_4 over various nickel catalysts and proposed a reaction model based on CH_4 activation to form CH_x and CH_xO decomposition as slow kinetic steps.

Figure 6-3: Reaction mechanism for methane reforming on Ni [33].

Hu and Ruckenstein [34, 35] employed a transient response analysis to study the reaction mechanism over Ni/SiO_2 and Ni/MgO, and found that the surface reaction between C·S and O·S constitutes the RDS.

Over the last decade, there has been a surge in first principles prediction of steam and dry reforming of methane. Blaylock et al. [36] combined thermodynamic data with electronic activation energies and developed microkinetic model to simulate steam reforming of methane under realistic conditions. The rate-limiting steps were found to be the CH_4 dissociative adsorption and the CH·S oxidation by O·S as well as OH·S.

Wang et al. [37, 38] based on their DFT calculations suggested CH_4 dissociation to be the RDS. However, the contribution of OH·S was neglected by the authors. Jones et al. [39], implemented DFT analysis using DACAPO code for a 9-step MSR reaction mechanism and predicted the catalytic activity trend as Ru > Rh > Ni > Ir > Pt ~ Pd, under the assumption that the support effects were negligible. Even though this agrees with the experimental trend, the analysis was based on a LHHW-type of rate expressions, derived by assuming $CH_4 + 2S \leftrightharpoons CH_3·S + S$ and $C·S + O·S \leftrightharpoons CO·S$ as RLSs. As elucidated earlier, such an analysis based on assumed RLS with experimental validation is fraught with the risk since more than one such rate expression can agree with the experimental observations. Moreover, for complex catalytic systems such as methane steam reforming, the RLS can very change with reaction conditions. In fact, Zhu et al. [33], very recently, investigated the dry methane reforming on Ni using Vienna ab initio simulation package (VASP) using a 34 elementary reaction step mechanism as shown in Figure 6-3 and suggested that RLS step does vary with reaction conditions based on comparison of the activation energies.

Thus, the kinetics of steam and dry reforming of methane have been investigated in great detail because of the industrial importance of the reaction system. Nonetheless, there is still considerable disagreement among the various reported studies in terms of mechanism and the kinetics providing detailed information of elementary reaction steps. It is the objective of this chapter to shed light on the reaction mechanism and logically identify the RLS(s), based on which a reaction rate expression can be derived which

would be useful for reactor design as well as rational design for a better anode catalyst for SOFCs.

In the preceding chapters we have utilized the RR Graph approach for *single* overall reaction systems. Here, we extend this approach to provide a robust model, with predictive kinetics for the MSR on Ni(111), a case of multiple overall reactions. A detailed mechanism comprising of 22 elementary steps is considered based on literature reported mechanisms. The Unity Bond Index – Quadratic Exponential Potential (UBI-QEP) method [16] is, utilized to calculate the enthalpy changes as well as activation energies of the elementary reactions of the forward and reverse directions. Further, the pre-exponential factors are estimated using the conventional transition-state theory [15]. Fine-tuning of some of the pre-exponential factors of the adsorption/desorption reactions, however, was necessary in order to be consistent with the known thermodynamics of the overall reactions.

6.2 Reaction Mechanism and Kinetics

A comprehensive summary of the literature reported mechanisms is provided in Table 6-1. We only consider CH_4, H_2O, H_2, CO and CO_2 as the terminal species. Thus, reaction steps with any other terminal species, e.g. formation of methanol as a side product, considered by Zhu et al. [33], has not been included in our analysis.

Of course, the idealistic approach would be to include all possible elementary reaction steps, provided their kinetics are available or can be predicted and assemble the same into a RR graph for mechanistic and kinetic analysis. However, the approach is, in fact, most revealing when used along with some *a priori* pruning based on chemical intuition. It is easy to see that many of the literature proposed steps are either not elementary reactions, i.e., they cannot be treated theoretically, or don't have kinetic and energetic parameters available. Clearly, including all of these steps would result in a RR Graph that is exceedingly complex, and would serve to obfuscate rather than illuminate. We, thus, judiciously picked a 22 steps mechanism which is considered to be comprehensive, but without causing undue complexity.

The mechanism adopted in this study comprises of the 13-step mechanism proposed by Xu and Froment [1]. However, it should be noted that the step $H_2O + S \leftrightarrows O \cdot S + H_2$ proposed by Xu and Froment [1] is certainly not an elementary reaction and is replaced by the following steps in order to be able to predict the step kinetics *a priori*.

$$
\begin{array}{lll}
 & & \underline{\sigma_\rho} \\
s_2: & H_2O + S \leftrightarrows H_2O \cdot S & +1 \\
s_5: & H \cdot S + H \cdot S \leftrightarrows H_2 \cdot S + S & +1 \\
s_6: & H_2 \cdot S \leftrightarrows H_2 + S & +1 \qquad (6.12)\\
s_7: & H_2O \cdot S + S \leftrightarrows OH \cdot S + H \cdot S & +1 \\
s_8: & OH \cdot S + S \leftrightarrows O \cdot S + H \cdot S & +1 \\
\hline
IR_1: & H_2O + S \leftrightarrows O \cdot S + H_2 &
\end{array}
$$
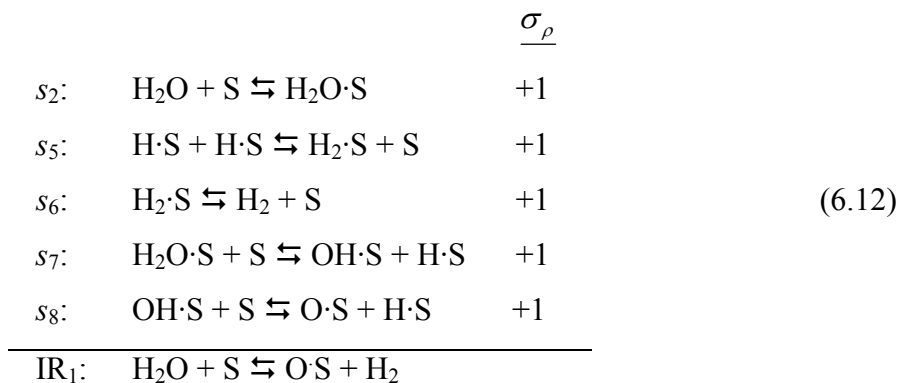
Steps s_{11} ($CH_2 \cdot S + S \leftrightarrows CH \cdot S + H \cdot S$) and s_{12} ($CH \cdot S + S \leftrightarrows C \cdot S + H \cdot S$) were next added which describe the sequential formation of carbon species, $C \cdot S$, suggested by many in the literature as shown in Table 6-1. Steps s_9 through s_{12} represent successive abstraction of hydrogen from adsorbed CH_4, i.e., $CH_4 \cdot S$ to form $CH_x \cdot S$. The, thus formed $CH_x \cdot S$ can further react with the adsorbed oxygen to form $CH_xO \cdot S$. Thus, steps s_{19} through s_{22} and step s_{13} have also been considered in our reaction mechanism so as to account for oxygenated carbon species.

Here, we utilize the semi-empirical Unity Bond Index–Quadratic Exponential Potential (UBI–QEP) method (formerly known as the Bond Order Conservation–Morse Potential, BOC–MP) to calculate the activation energies of the elementary reaction steps. The accuracy of UBI–QEP method to calculate energetics for a wide variety of complex reactions within 1-3 kcal/mol is well documented [16, 40-43]. The method solely depends on bond dissociation energies and heats of chemisorption. The heats of chemisorption, can in turn, be calculated from UBI–QEP formulation, first principles calculations or derived from reliable experimental measurements. Complete details of the UBI–QEP method can be found in Reference [16]. The bond dissociation energies and heat of chemisorption have been reported for a number of species in the literature [43-45].

Table 6-1: Literature reported mechanisms for methane reforming.

		WPI (This work)	Xu and Froment [1]	Aparicio [10]	Hou and Hughes [46]	Hecht et al. [3]	Wei and Iglesia [28]	Erdohelyi et al. [47]	Efstathiou et al. [48]	Deutschmann and Schmidt [49]	Bizzi et al. [50]	Galea et al. [20]	Jarosch et al. [31]	Avetisov et al. [51]	Chen et al. [30]	Yang et al. [52]	Wang et al. [53]	Aghalayam et al.	Alstrup [55]	Pistonesi et al. [56]	Jones et al. [39]	Zhu et al. [33]
s_1	$CH_4 + S \leftrightarrows CH_4{\cdot}S$	X	X		X	X			X	X	X	X	X	X		X						X
s_2	$H_2O + S \leftrightarrows H_2O{\cdot}S$	X		X	X	X	X		X	X	X	X		X	X	X	X					X
s_3	$CO{\cdot}S \leftrightarrows CO + S$	X	X		X	X	X		X	X	X	X		X		X	X	X			X	X
s_4	$CO_2{\cdot}S \leftrightarrows CO_2 + S$	X	X		X	X			X		X					X	X	X				X
s_5	$H{\cdot}S + H{\cdot}S \leftrightarrows H_2{\cdot}S + S$	X	X				X					X				X						X
s_6	$H_2{\cdot}S \leftrightarrows H_2 + S$	X	X				X					X				X						X
s_7	$H_2O{\cdot}S + S \leftrightarrows OH{\cdot}S + H{\cdot}S$	X		X	X	X			X	X	X	X		X	X	X	X					X
s_8	$OH{\cdot}S + S \leftrightarrows O{\cdot}S + H{\cdot}S$	X				X	X		X	X	X	X		X		X	X	X	X		X	X
s_9	$CH_4{\cdot}S + S \leftrightarrows CH_3{\cdot}S + H{\cdot}S$	X	X			X				X	X	X	X	X		X						X
s_{10}	$CH_3{\cdot}S + S \leftrightarrows CH_2{\cdot}S + H{\cdot}S$	X	X	X		X	X	X		X	X	X	X	X	X	X	X	X			X	X
s_{11}	$CH_2{\cdot}S + S \leftrightarrows CH{\cdot}S + H{\cdot}S$	X		X		X	X	X		X	X	X	X	X		X	X	X			X	X
s_{12}	$CH{\cdot}S + S \leftrightarrows C{\cdot}S + H{\cdot}S$	X		X		X	X	X	X	X	X	X	X	X		X	X	X			X	X
s_{13}	$C{\cdot}S + O{\cdot}S \leftrightarrows CO{\cdot}S + S$	X				X	X		X	X	X			X		X	X	X			X	X
s_{14}	$CH_2{\cdot}S + O{\cdot}S \leftrightarrows CH_2O{\cdot}S + S$	X	X													X						X
s_{15}	$CH_2O{\cdot}S + S \leftrightarrows CHO{\cdot}S + H{\cdot}S$	X	X													X						X
s_{16}	$CHO{\cdot}S + S \leftrightarrows CO{\cdot}S + H{\cdot}S$	X	X		X	X										X				X		X
s_{17}	$CO{\cdot}S + O{\cdot}S \leftrightarrows CO_2{\cdot}S + S$	X	X		X	X			X		X			X		X		X				X
s_{18}	$CHO{\cdot}S + O{\cdot}S \leftrightarrows CO_2{\cdot}S + H{\cdot}S$	X	X		X											X				X		
s_{19}	$CH_3{\cdot}S + O{\cdot}S \leftrightarrows CH_3O{\cdot}S + S$	X																				X
s_{20}	$CH_3O{\cdot}S + S \leftrightarrows CH_2O{\cdot}S + H{\cdot}S$	X																				X
s_{21}	$CHO{\cdot}S + S \leftrightarrows CH{\cdot}S + O{\cdot}S$	X				X																X
s_{22}	$CH{\cdot}S + O{\cdot}S \leftrightarrows CO{\cdot}S + H{\cdot}S$	X						X									X					

		WPI (This work)	Xu and Froment [1]	Aparicio [10]	Hou and Hughes [46]	Hecht et al. [3]	Wei and Iglesia [28]	Erdohelyi et al. [47]	Efstathiou et al. [48]	Deutschmann and Schmidt [49]	Bizzi et al. [50]	Galea et al. [20]	Jarosch et al. [31]	Avetisov et al. [51]	Chen et al. [30]	Yang et al. [52]	Wang et al. [53]	Aghalayam et al.	Alstrup [55]	Pistonesi et al. [56]		Zhu et al. [33]
IR$_1$	$H_2O + S \leftrightarrows H_2 + O{\cdot}S$	X	X		X																	
	$CO{\cdot}S_2 \leftrightarrows CO + 2S$			X										X	X							
	$CO_2 + 2S \leftrightarrows CO_2{\cdot}S_2$			X																		
	$CH{\cdot}S + 2S \leftrightarrows C{\cdot}S_2 + H{\cdot}S$														X							
	$CH_4{\cdot}S + O{\cdot}S \leftrightarrows CH_3{\cdot}S + OH{\cdot}S$					X		X	X		X				X							
	$CH_3{\cdot}S + O{\cdot}S \leftrightarrows CH_2{\cdot}S + OH{\cdot}S$					X			X		X				X			X				
	$CH_2{\cdot}S + O{\cdot}S \leftrightarrows CH{\cdot}S + OH{\cdot}S$					X			X		X				X			X				
	$CH{\cdot}S + O{\cdot}S \leftrightarrows C{\cdot}S + OH{\cdot}S$					X					X				X			X				
	$C{\cdot}S_2 + O{\cdot}S \leftrightarrows CO{\cdot}S_2 + S$																					
	$CHO{\cdot}S_2 + S \leftrightarrows CO{\cdot}S_2 + H{\cdot}S$			X											X							
	$CHO{\cdot}S + O{\cdot}S \leftrightarrows CO{\cdot}S + OH{\cdot}S$																					
	$CO{\cdot}S_2 + O{\cdot}S \leftrightarrows CO_2{\cdot}S_2 + S$																					
	$CO_2 + 2S \leftrightarrows CO{\cdot}S + O{\cdot}S$						X		X													
	$OH{\cdot}S + CO{\cdot}S \leftrightarrows HCOO{\cdot}S + S$																					
	$OH{\cdot}S + CO{\cdot}S \leftrightarrows CO_2{\cdot}S + H{\cdot}S$						X											X				
	$HCOO{\cdot}S + S \leftrightarrows CO_2{\cdot}S + H{\cdot}S$																					
	$CO_2{\cdot}S_2 + H{\cdot}S \leftrightarrows HCOO{\cdot}S_2 + S$			X																		
	$HCOO{\cdot}S + O{\cdot}S \leftrightarrows CO_2{\cdot}S + OH{\cdot}S$																					
	$C{\cdot}S + OH{\cdot}S \leftrightarrows CO{\cdot}S + H{\cdot}S$								X									X				
	$C{\cdot}S + CO_2{\cdot}S \leftrightarrows 2CO + 2S$																X					
	$C{\cdot}S + CO_2{\cdot}S \leftrightarrows 2CO{\cdot}S$																	X				
	$CH_4 + 2S \leftrightarrows CH_3{\cdot}S + H{\cdot}S$			X			X	X							X	X		X	X			X
	$C{\cdot}S + OH{\cdot}S \leftrightarrows CHO{\cdot}S_2$			X											X							
	$CO_2 + 2H{\cdot}S + 2S \leftrightarrows CHO{\cdot}S_2 + OH{\cdot}S + S$			X											X							

Reaction	WPI (This work)	Xu and Froment [1]	Aparicio [10]	Hou and Hughes [46]	Hecht et al. [3]	Wei and Iglesia [28]	Erdohelyi et al. [47]	Efstathiou et al. [48]	Deutschmann and Schmidt [49]	Bizzi et al. [50]	Galea et al. [20]	Jarosch et al. [31]	Avetisov et al. [51]	Chen et al. [30]	Yang et al. [52]	Wang et al. [53]	Aghalayam et al.	Alstrup [55]	Pistonesi et al. [56]		Zhu et al. [33]
$HCOO \cdot S_2 + H \cdot S + 2S \rightleftharpoons CHO \cdot S_2 + OH \cdot S + 2S$			X																		
$CHO \cdot S_2 + 3S \rightleftharpoons CO \cdot S_2 + H \cdot S + 2S$			X																		
$H \cdot S + H \cdot S \rightleftharpoons H_2 + 2S$			X	X	X			X	X	X			X	X	X		X	X			X
$CH_2 \cdot S + H_2O \cdot S \rightleftharpoons CH_3 \cdot S + OH \cdot S$																	X				
$CH \cdot S + H_2O \cdot S \rightleftharpoons CH_2 \cdot S + OH \cdot S$																	X				
$C \cdot S + H_2O \cdot S \rightleftharpoons CH \cdot S + OH \cdot S$																	X				
$CH_4 + 3S \rightleftharpoons CH_2 \cdot S + 2H \cdot S$				X																	
$CH_2 \cdot S + OS \rightleftharpoons CHO \cdot S + H \cdot S$				X																	
$H_2O \cdot S + O \cdot S \rightleftharpoons OH \cdot S + OH \cdot S$					X			X	X				X				X				
$H_2O + O \cdot S + S \rightleftharpoons OH \cdot S + OH \cdot S$							X	X													
$H_2O + 2S \rightleftharpoons OH \cdot S + H \cdot S$															X			X			X
$CH_4 \cdot S + 2S \rightleftharpoons CH_2 \cdot S + 2H \cdot S$								X													
$CH_4 \cdot S + 3S \rightleftharpoons CH \cdot S + 3H \cdot S$								X													
$CH_4 \cdot S + 4S \rightleftharpoons C \cdot S + 4H \cdot S$								X	X												
$CH_3 \cdot S + 3S \rightleftharpoons C \cdot S + 3H \cdot S$								X													
$CH_2 \cdot S + 2S \rightleftharpoons C \cdot S + 2H \cdot S$								X													
$CO_2 \cdot S + H \cdot S \rightleftharpoons COOH \cdot S$																					X
$COOH \cdot S \rightleftharpoons CO \cdot S + OH \cdot S$																					X
$CH_3 \cdot S + OH \cdot S \rightleftharpoons CH_3OH \cdot S$																					X
$CH_3OH \cdot S \rightleftharpoons CH_2OH \cdot S + H \cdot S$																					X
$CH_2 \cdot S + OH \cdot S \rightleftharpoons CH_2OH \cdot S$																					X
$CH_2OH \cdot S \rightleftharpoons CHOH \cdot S + H \cdot S$																					X
$CH \cdot S + OH \cdot S \rightleftharpoons CHOH \cdot S$																					X
$CHOH \cdot S \rightleftharpoons COH \cdot S + H \cdot S$																					X

	WPI (This work)	Xu and Froment [1]	Aparicio [10]	Hou and Hughes [46]	Hecht et al. [3]	Wei and Iglesia [28]	Erdohelyi et al. [47]	Efstathiou et al. [48]	Deutschmann and Schmidt [49]	Bizzi et al. [50]	Galea et al. [20]	Jarosch et al. [31]	Avetisov et al. [51]	Chen et al. [30]	Yang et al. [52]	Wang et al. [53]	Aghalayam et al.	Alstrup [55]	Pistonesi et al. [56]		Zhu et al. [33]
C·S + OH·S ⇆ COH·S																					X
COH·S ⇆ CO·S + H·S																					X
CH_3OH·S ⇆ CH_3O·S + H·S																					X
CH_2OH·S ⇆ CH_2O·S + H·S																					X
CHOH·S ⇆ CHO·S + H·S																					X
CH_3OH·S ⇆ CH_3OH + S																					X
CH_3 + S ⇆ CH_3·S																	X				
CH_2 + S ⇆ CH_2·S																	X				
CH + S ⇆ CH·S																	X				
C + S ⇆ C·S																	X				

Further, it should be noted that according to Patrito et al. [57], when the surface coverage of oxygen is high, the equations governing the prediction of the heat of adsorption of OH species indicate a lower value as compared to zero-coverage. This is the consequence of a true electronic effect of the surface coverage rather than adsorbate-adsorbate interactions. At low oxygen coverages, hydrogen bonding allows for attractive interactions between adsorbed hydroxyls leading to a higher heat of adsorption for OH. The difference is typically 20-30 kcal/mol. The activation energies of the elementary reaction steps including the OH·S species were calculated in this study including the "OH effect" that allows for lateral interaction and takes into account the formation of hydrogen bonds between OH groups.

Following Dumesic et al. [15], furthermore, we simply assume an immobile transition state without rotation for all of surface species, which results in a pre-exponential factor of 10^1 $Pa^{-1}s^{-1}$ for adsorption/desorption reactions, and 10^{13} s^{-1} for surface reactions. However, this simplification can provide results that are inconsistent with the overall reaction thermodynamics. Thus, some of the pre-exponential factors, namely, those of steps s_1, s_3, s_{11}, and s_{15} were adjusted somewhat to ensure consistency with the thermodynamics of the overall WGS and MSR reactions. The pre-exponential factors, thus, obtained are shown as bold in Table 6-2, while the ones in the opposite direction were obtained from Lund's approach [58] described in chapter III. The Lund's approach, however, requires the knowledge of the entropy change for the elementary reaction which can be obtained from the species entropy. The standard entropy of formation of a surface species, I_k·S is based on the assumption that adsorption causes a total loss of translational entropy, while the entropy values for species in the gas phase, $S^o_{I_k(g)}$ were taken from standard sources [59].

The complete kinetic model for the 22-step reaction mechanism considered in this study is provided in Table 6-2.

Table 6-2: The microkinetic model for methane steam reforming on Ni(111). The letter 'S' denotes a surface site. Activation energies in kcal/mol ($\theta \to 0$ limit); the units of the pre–exponential factors are $atm^{-1}\,s^{-1}$ for adsorption/desorption reactions and s^{-1} for surface reactions.

	$\vec{E}_\rho$	$\vec{\Lambda}_\rho$	Elementary Reactions	$\bar{E}_\rho$	$\bar{\Lambda}_\rho$
s_1:	0.0	5.5892×10^6	$CH_4 + S \leftrightarrows CH_4 \cdot S$	6.0	3.0518×10^{13}
s_2:	0.0	1.0×10^6	$H_2O + S \leftrightarrows H_2O \cdot S$	16.5	3.6415×10^{13}
s_3:	27.0	8.0718×10^{13}	$CO \cdot S \leftrightarrows CO + S$	0.0	1.0×10^6
s_4:	6.5	1.3917×10^{14}	$CO_2 \cdot S \leftrightarrows CO_2 + S$	0.0	1.0×10^6
s_5:	23.35	1.0×10^{13}	$H \cdot S + H \cdot S \leftrightarrows H_2 \cdot S + S$	8.15	8.5516×10^{12}
s_6:	6.8	1.3487×10^{12}	$H_2 \cdot S \leftrightarrows H_2 + S$	0.0	1.0×10^6
s_7:	14.41	1.0×10^{13}	$H_2O \cdot S + S \leftrightarrows OH \cdot S + H \cdot S$	20.41	8.2516×10^{12}
s_8:	21.1	1.0×10^{13}	$OH \cdot S + S \leftrightarrows O \cdot S + H \cdot S$	19.6	6.7606×10^{13}
s_9:	13.76	1.0×10^{13}	$CH_4 \cdot S + S \leftrightarrows CH_3 \cdot S + H \cdot S$	13.34	1.6984×10^{12}
s_{10}:	23.87	1.0×10^{13}	$CH_3 \cdot S + S \leftrightarrows CH_2 \cdot S + H \cdot S$	11.87	4.5019×10^{12}
s_{11}:	23.21	4.0×10^{12}	$CH_2 \cdot S + S \leftrightarrows CH \cdot S + H \cdot S$	17.61	6.4334×10^{12}
s_{12}:	4.52	1.0×10^{13}	$CH \cdot S + S \leftrightarrows C \cdot S + H \cdot S$	41.52	8.6385×10^{13}
s_{13}:	35.38	1.0×10^{13}	$C \cdot S + O \cdot S \leftrightarrows CO \cdot S + S$	33.38	2.5919×10^{12}
s_{14}:	24.19	1.0×10^{13}	$CH_2 \cdot S + O \cdot S \leftrightarrows CH_2O \cdot S + S$	23.89	1.3112×10^{13}
s_{15}:	10.62	1.8×10^{12}	$CH_2O \cdot S + S \leftrightarrows CHO \cdot S + H \cdot S$	17.22	4.1806×10^{11}
s_{16}:	0.0	1.0×10^{13}	$CHO \cdot S + S \leftrightarrows CO \cdot S + H \cdot S$	23.1	1.1825×10^{14}
s_{17}:	15.18	1.0×10^{13}	$CO \cdot S + O \cdot S \leftrightarrows CO_2 \cdot S + S$	6.68	2.3989×10^{13}
s_{18}:	10.1	1.0×10^{13}	$CHO \cdot S + O \cdot S \leftrightarrows CO_2 \cdot S + H \cdot S$	24.7	2.8367×10^{14}
s_{19}:	20.88	1.0×10^{13}	$CH_3 \cdot S + O \cdot S \leftrightarrows CH_3O \cdot S + S$	12.78	2.3989×10^{12}
s_{20}:	9.49	1.0×10^{13}	$CH_3O \cdot S + S \leftrightarrows CH_2O \cdot S + H \cdot S$	5.29	2.4607×10^{13}
s_{21}:	34.82	1.0×10^{13}	$CHO \cdot S + S \leftrightarrows CH \cdot S + O \cdot S$	22.92	5.2813×10^{13}
s_{22}:	11.37	1.0×10^{13}	$CH \cdot S + O \cdot S \leftrightarrows CO \cdot S + H \cdot S$	46.37	2.2390×10^{13}

6.3 Multiple Overall Reaction System: Which and how many ORs are important?

The question next arises as to how can one obtain a comprehensive set of ORs for a multiple overall reaction mechanism? In fact, innumerable ORs can be written for a specified set of reactants and products. How does, then, one determine which ORs are germane? Which of these ORs are really occurring, and which are superfluous? Does one need a rate expression for each of the chosen ORs? How many of these are unique? Further, how many are independent? The MSR is generally represented by the following reversible set of ORs [1, 60]

$$
\begin{aligned}
OR_1: & \quad CH_4 + H_2O \leftrightarrows CO + 3H_2 \\
OR_2: & \quad CO + H_2O \leftrightarrows CO_2 + H_2 \\
OR_3: & \quad CH_4 + 2H_2O \leftrightarrows CO_2 + 4H_2 \\
OR_4: & \quad CH_4 + CO_2 \leftrightarrows 2CO + 2H_2
\end{aligned} \tag{6.13}
$$
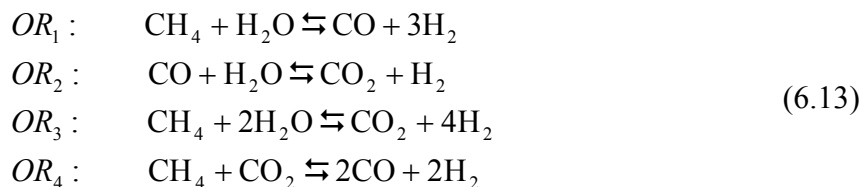
where the significance of OR_4 in this system, namely the CO_2 dry-reforming of methane [61], has been the subject of much recent discussion as a potential route for the abatement of green house gases, namely CO_2 and CH_4. In fact, in this case, only two ORs are adequate to describe the system, not for instance three, i.e., OR_1, OR_2, and OR_3, as assumed by Xu and Froment [1], in their seminal study of this very important industrial reaction system.

The number and identity of ORs whose rate expressions are needed to describe the kinetics in a multiple OR system, thus, remains a source of confusion. It is shown here that such questions are, in fact, superfluous. What actually matters is the list of the terminal (reactants and products) species, along with the list of elementary reaction steps occurring on the catalyst surface representing the molecular mechanism. The ORs are simply our invention to try to rationalize the overall stoichiometry of the process, which can rarely be captured by a single OR. It is the mechanistic steps that represent the real molecular events, not the ORs.

Moreover, ORs also need to be "direct," in the sense that they have a limitation on the number of species that can participate in them. For systems based on the elements C, H,

and O, this is actually 4 as shown below. Since ORs do not involve intermediate species, they may, in fact, be derived directly from the set of given terminal species, and their constituent elements, as the so-called response reactions, or RERs [62]. In this approach, the n terminal species are considered as made up of r "elements," or chemical building blocks, which are the radicals, or molecular fragments, that remain unchanged among the given terminal species. These are selected such that the rank of the formula matrix is equal to the number of elements r, and are frequently, but not always, the *actual* chemical elements [62]. For instance, the formula matrix for the MSR case is:

$$
\varepsilon = \begin{array}{c} \\ CH_4 \\ H_2O \\ CO \\ CO_2 \\ H_2 \end{array} \begin{array}{ccc} C & H & O \\ \left[\begin{array}{ccc} 1 & 4 & 0 \\ 0 & 2 & 1 \\ 1 & 0 & 1 \\ 1 & 0 & 2 \\ 0 & 2 & 0 \end{array}\right] \end{array} \tag{6.14}
$$

which has a rank, $r =$ rank$\varepsilon = 3$. Thus, for this case, C, H, and O are appropriate "elements."

It is, furthermore, known from chemical stoichiometry [63], that the number of linearly independent ORs, m, is related to the number of terminal species n and the rank of the formula matrix r via $m = n - r$. For the MSR case considered here, for instance, with $n = 5$ (CH_4, H_2O, CO, CO_2 and H_2), and $r = 3$, the number of independent ORs, $m = 5 - 3 = 2$.

As a result, the number of terminal species involved in a direct OR $= n - (m - 1) = n - (n - r) + 1 = r + 1$. For instance, for the MSR case, the maximum number of terminal species in a direct OR $= 3 + 1 = 4$. Thus, a complete enumeration of direct ORs may be accomplished by considering all possible combinations of 4 terminal species from among the total of 5. This results is $M = 5$ distinct direct ORs:

$$OR(CH_4, H_2O, CO, H_2) = OR_1: \quad CH_4 + H_2O \leftrightarrows CO + 3H_2$$

$$OR(H_2O, CO, CO_2, H_2) = OR_2: \quad CO + H_2O \leftrightarrows CO_2 + H_2$$

$$OR(CH_4, CO, CO_2, H_2) = OR_3: \quad CH_4 + 2H_2O \leftrightarrows CO_2 + 4H_2 \qquad (6.15)$$

$$OR(CH_4, H_2O, CO_2, H_2) = OR_4: \quad CH_4 + CO_2 \leftrightarrows 2CO + 2H_2$$

$$OR(CH_4, H_2O, CO, CO_2) = OR_5: \quad CH_4 + 3CO_2 \leftrightarrows 4CO + 2H_2O$$
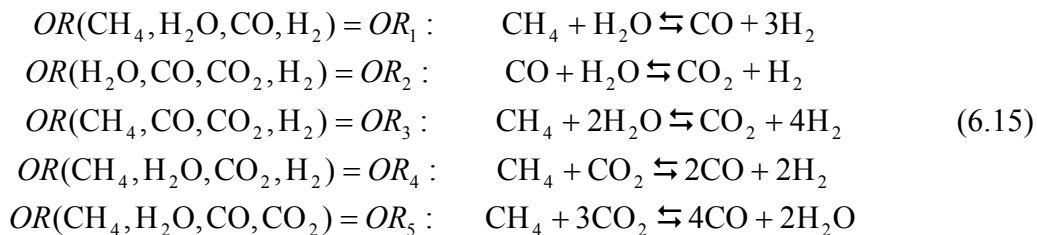
Thus, while unique, all the ORs (Eq. (6.15)) are not all linearly independent, as some of these ORs may be generated by linearly combining an independent set of ORs. Further, since the number of linearly independent ORs for this system is simply 2, we may pick any appropriate set. Thus, we pick OR_1 and OR_2 as the independent ORs for further analysis here. The remaining ORs may, thus, be derived from these via linear combination. For instance, $OR_4 = OR_1 - OR_2$, $OR_3 = OR_1 + OR_2$ and $OR_5 = OR_1 - 3OR_2$. This choice of independent ORs is not unique. Any other set would also suffice.

Finally, it may be mentioned that additional constraints may be imposed to reduce the set of direct ORs further. For instance, we could reject direct ORs involving stoichiometric coefficients larger than say 3, in which case OR_5 would be rejected. However, this is not necessary, as a set of independent ORs, i.e. any two ORs in this case, is all that is needed for further analysis.

6.4 Reaction Route Graph

Before we can generate the RR graph for MSR on Ni, we need to identify the independent reaction routes (RRs) for the two independent overall reactions, OR_1 and OR_2. In doing so, we take into account that steps s_2, s_5, s_6, s_7 and s_8 should be present in all stoichiometrically distinct RRs for both the ORs. The combination of these steps, in fact, represents the intermediate reaction IR_1: $H_2O + S \leftrightarrows O^{\cdot}S + H_2$ considered by Xu and Froment [1]. Thus, the combined IR_1, is utilized only for drawing the RR graph, while for kinetic analysis, individual steps s_2, s_5, s_6, s_7 and s_8 with *a priori* kinetics are employed.

It should be noted that this step is not essential, and the number of stoichiometrically distinct RRs, in the absence of this assumption would be different since we are altering the *q* value. However, all we are concerned is with the independent set of RRs, and not with the most exhaustive list of RRs for a given OR.

Table 6-3: 20-step lumped mechanism for MSR on Ni.

s_1:	$CH_4 + S \leftrightarrows CH_4 \cdot S$
IR_1:	$H_2O + S \leftrightarrows O \cdot S + H_2$
s_3:	$CO \cdot S \leftrightarrows CO + S$
s_4:	$CO_2 \cdot S \leftrightarrows CO_2 + S$
s_5:	$H \cdot S + H \cdot S \leftrightarrows H_2 \cdot S + S$
s_6:	$H_2 \cdot S \leftrightarrows H_2 + S$
s_9:	$CH_4 \cdot S + S \leftrightarrows CH_3 \cdot S + H \cdot S$
s_{10}:	$CH_3 \cdot S + S \leftrightarrows CH_2 \cdot S + H \cdot S$
s_{11}:	$CH_2 \cdot S + S \leftrightarrows CH \cdot S + H \cdot S$
s_{12}:	$CH \cdot S + S \leftrightarrows C \cdot S + H \cdot S$
s_{13}:	$C \cdot S + O \cdot S \leftrightarrows CO \cdot S + S$
s_{14}:	$CH_2 \cdot S + O \cdot S \leftrightarrows CH_2O \cdot S + S$
s_{15}:	$CH_2O \cdot S + S \leftrightarrows CHO \cdot S + H \cdot S$
s_{16}:	$CHO \cdot S + S \leftrightarrows CO \cdot S + H \cdot S$
s_{17}:	$CO \cdot S + O \cdot S \leftrightarrows CO_2 \cdot S + S$
s_{18}:	$CHO \cdot S + O \cdot S \leftrightarrows CO_2 \cdot S + H \cdot S$
s_{19}:	$CH_3 \cdot S + O \cdot S \leftrightarrows CH_3O \cdot S + S$
s_{20}:	$CH_3O \cdot S + S \leftrightarrows CH_2O \cdot S + H \cdot S$
s_{21}:	$CHO \cdot S + S \leftrightarrows CH \cdot S + O \cdot S$
s_{22}:	$CH \cdot S + O \cdot S \leftrightarrows CO \cdot S + H \cdot S$

Thus, the lumped mechanism considered for generating the RR graph is provided in Table 6-3. The number of independent RRs for the reaction system is given by $\mu = p - q$.

We have 20 elementary reactions, and 13 independent intermediate species (after combining s_2, s_5, s_6, s_7 and s_8 into IR_1), thus, $\mu = 20 - 13 = 7$. Thus, we may pick 5 independent ERs and one FR for each of the two independent ORs. For instance, we may pick the independent RRs set as

$$FR_1 : OR_1 = (+1)s_1 + (+1)IR_1 + (+1)s_3 + (+2)s_5 + (+2)s_6 + (+1)s_9 + (+1)s_{10} + (+1)s_{11} + (+1)s_{12} + (+1)s_{13}$$
$$FR_2 : OR_2 = (+1)IR_1 + (-1)s_3 + (+1)s_4 + (+1)s_{17}$$
$$ER_1 : 0 = (+1)s_{10} + (+1)s_{14} + (-1)s_{19} + (-1)s_{20}$$
$$ER_2 : 0 = (+1)s_{11} + (-1)s_{14} + (-1)s_{15} + (-1)s_{21}$$
$$ER_3 : 0 = (+1)s_{12} + (+1)s_{13} + (-1)s_{22}$$
$$ER_4 : 0 = (+1)s_{16} + (-1)s_{21} + (-1)s_{22}$$
$$ER_5 : 0 = (+1)s_{16} + (+1)s_{17} + (-1)s_{18}$$

$$(6.16)$$

It can be seen that this set of 7 RRs (2 FRs and 5 ERs) comprises of all the 22 reaction steps and is, thus, an adequate independent set. This set is, of course, not unique, as other sets of μ independent RRs may be chosen that fit these criteria. However, this set is enough to draw the RR Graph, from which the complete set of unique RRs can be determined *topologically*, as walks, once the RR Graph is constructed, which is however, not a prerequisite for further analysis.

We start by assembling the empty routes one at a time in to a cycle graph by fusing the ERs by their common steps. For e.g., ER_1 can be fused with ER_2 as they have step s_{14} in common. ER_4 can be next added by fusing it with ER_2 via the common step s_{21}. ER_3 is next fused to ER_4 along the common step s_{22}. Finally, the last of the independent empty routes, ER_5 is added to ER_4 via the common step s_{16} to generate the cycle graph shown in Figure 6-4a.

The nodes in the cycle graph are next checked, so as to identify the already balanced nodes, i.e. the nodes which agree with the mass balance conditions (or KFL) for the intermediate/terminal species provided in Table 6-4.
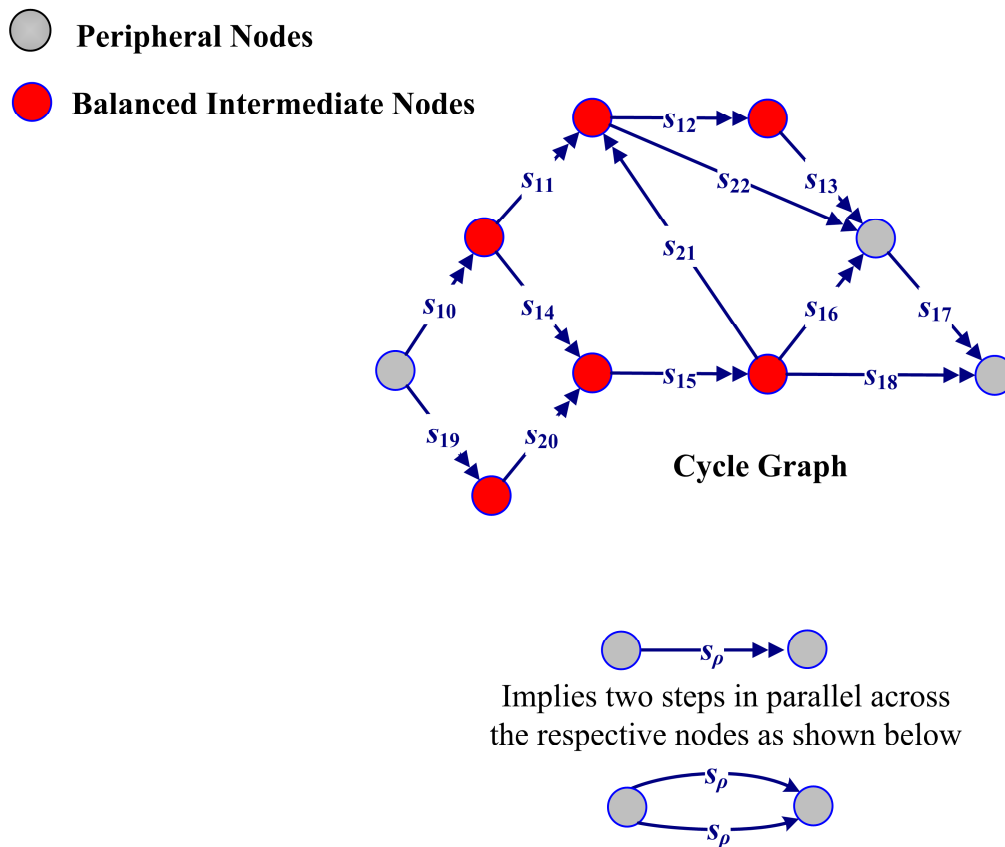
Figure 6-4a: Systematic construction of the RR Graph for the MSR reaction mechanism.
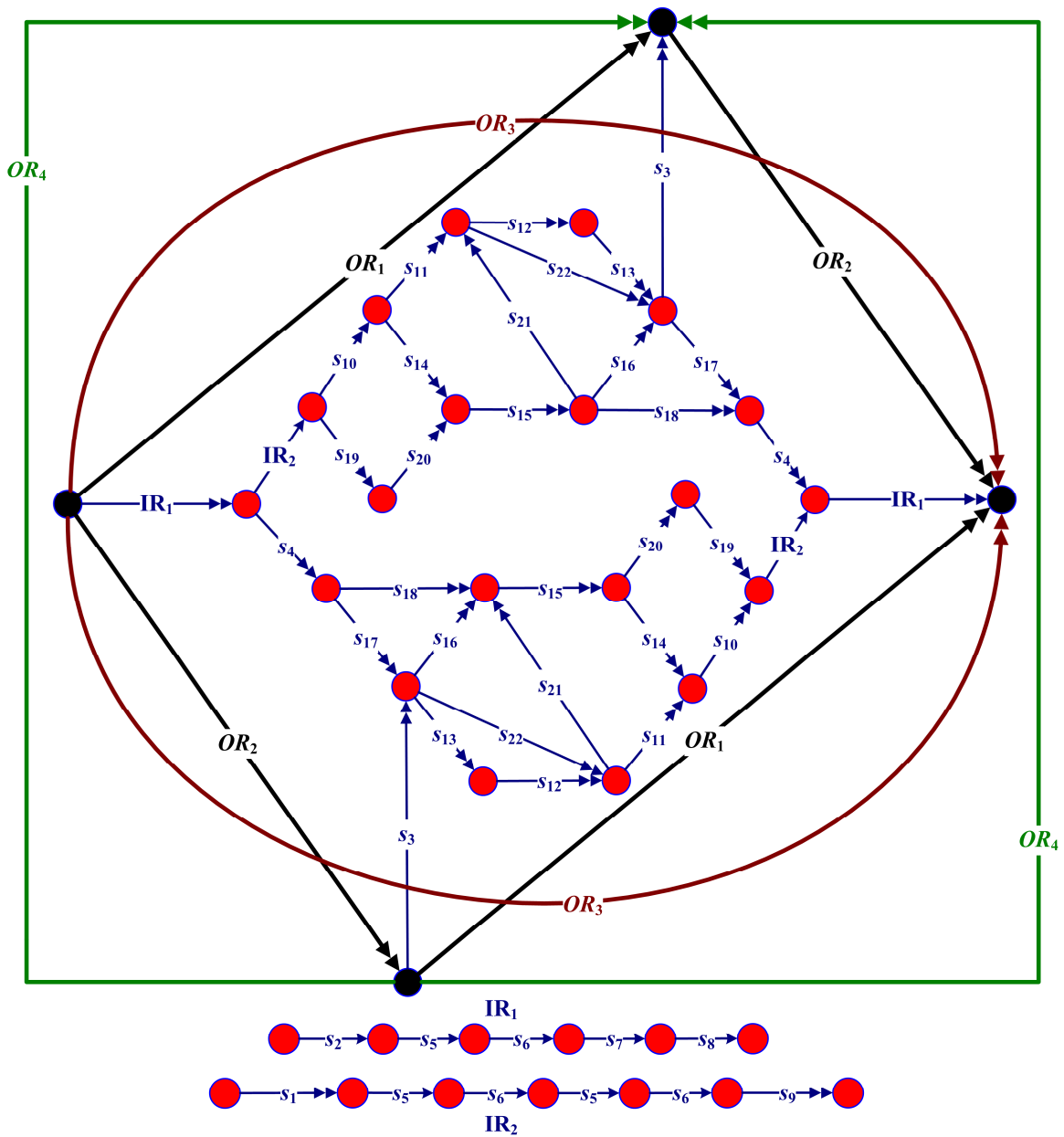
Figure 6-4b: Systematic construction of the RR Graph for the MSR reaction mechanism.

Table 6-4: QSS Conditions for Intermediates and Terminal Species in the lumped MSR reaction mechanism.

<ins>Intermediate Species:</ins>

$Q_{CH_4 \cdot S}:$ $\qquad$ $r_1 - r_9 = 0$

$Q_{CH_3 \cdot S}:$ $\qquad$ $r_9 - r_{10} - r_{19} = 0$

$Q_{CH_2 \cdot S}:$ $\qquad$ $r_{10} - r_{11} - r_{14} = 0$

$Q_{CH \cdot S}:$ $\qquad$ $r_{11} - r_{12} + r_{21} - r_{22} = 0$

$Q_{C \cdot S}:$ $\qquad$ $r_{12} - r_{13} = 0$

$Q_{CH_3O \cdot S}:$ $\qquad$ $r_{19} - r_{20} = 0$

$Q_{CH_2O \cdot S}:$ $\qquad$ $r_{14} - r_{15} + r_{20} = 0$

$Q_{CHO \cdot S}:$ $\qquad$ $r_{15} - r_{16} - r_{18} - r_{21} = 0$

$Q_{CO \cdot S}:$ $\qquad$ $-r_3 + r_{13} + r_{16} - r_{17} + r_{22} = 0$

$Q_{O \cdot S}:$ $\qquad$ $r_{IR_1} - r_{13} - r_{14} - r_{17} - r_{18} - r_{19} + r_{21} - r_{22} = 0$

$Q_{H \cdot S}:$ $\qquad$ $-2r_5 + r_9 + r_{10} + r_{11} + r_{12} + r_{15} + r_{16} + r_{18} + r_{20} + r_{22} = 0$

$Q_{H_2 \cdot S}:$ $\qquad$ $r_5 - r_6 = 0$

$Q_{CO_2 \cdot S}:$ $\qquad$ $-r_4 + r_{17} + r_{18} = 0$

<ins>Terminal Species:</ins>

$Q_{CH_4}:$ $\qquad$ $-r_{OR_1} - r_1 = 0$

$Q_{H_2O}:$ $\qquad$ $-r_{OR_1} - r_{OR_2} - r_{IR_1} = 0$

$Q_{CO}:$ $\qquad$ $r_{OR_1} - r_{OR_2} + r_3 = 0$

$Q_{H_2}:$ $\qquad$ $3r_{OR_1} + r_{OR_2} + r_{IR_1} + r_6 = 0$

$Q_{CO_2}:$ $\qquad$ $r_{OR_2} + r_4 = 0$

Next, note that FR_1 consists of non-unit stoichiometric number, suggesting that the RR graph will contain each step s_ρ as well as the OR more than once, which must furthermore be symmetrical. This is achieved by duplicating the cycle graph as shown in Figure 6-4b. The only steps missing are s_1, s_5, s_6, s_9 and s_3. We note here, that steps s_1, s_5, s_6, s_9 will be present in all stoichiometrically distinct RRs for OR_1, while s_3 corresponds only to OR_2.

In order to present the RR graph in less complex looking form, we combine s_1, s_5, s_6, s_9 into IR_2.

$$\underline{\sigma_\rho}$$

$$
\begin{array}{llll}
s_1\colon & CH_4 + S \leftrightarrows CH_4{\cdot}S & +1 & \\
s_5\colon & H{\cdot}S + H{\cdot}S \leftrightarrows H_2{\cdot}S + S & +2 & \\
s_6\colon & H_2{\cdot}S \leftrightarrows H_2 + S & +2 & (6.17) \\
s_9\colon & CH_4{\cdot}S + S \leftrightarrows CH_3{\cdot}S + H{\cdot}S & +1 & \\
\hline
IR_2\colon & CH_4 + 3H{\cdot}S \leftrightarrows CH_3{\cdot}S + 2H_2 + 2S & &
\end{array}
$$
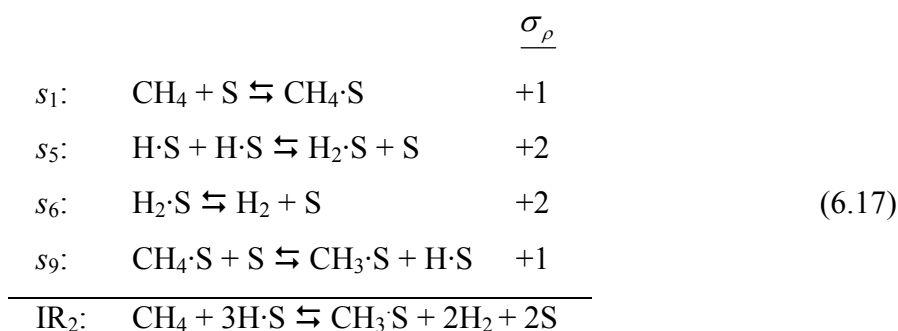
Finally, we add IR_2 and step s_3 to the cycle graph as shown in Figure 6-4b. The final step in the construction of the RR graph is the addition of the ORs, completing the connectivity of TNs. Finally, many of the steps are represented as doubled across two given nodes, in order to satisfy the KFL condition at that particular node. Thus, the final RR Graph for the MSR on Ni(111) is shown in Figure 6-4b.

6.5 Network Consistence with Kirchhoff's Laws

As shown in chapter II, RR graphs concur with KFL and KPL. Thus, each ER in the RR graph is subject to thermodynamic constraints imposed by KPL. Thus, for the 5 linearly independent ERs, for MSR we have

$$ER_1: \quad \frac{\vec{k}_{10}}{\overleftarrow{k}_{10}} \frac{\vec{k}_{14}}{\overleftarrow{k}_{14}} \frac{\vec{k}_{19}}{\overleftarrow{k}_{19}} \frac{\vec{k}_{20}}{\overleftarrow{k}_{20}} = 1$$

$$ER_2: \quad \frac{\vec{k}_{11}}{\overleftarrow{k}_{11}} \frac{\overleftarrow{k}_{14}}{\vec{k}_{14}} \frac{\overleftarrow{k}_{15}}{\vec{k}_{15}} \frac{\overleftarrow{k}_{21}}{\vec{k}_{21}} = 1$$

$$ER_3: \quad \frac{\vec{k}_{12}}{\overleftarrow{k}_{12}} \frac{\vec{k}_{13}}{\overleftarrow{k}_{13}} \frac{\overleftarrow{k}_{22}}{\vec{k}_{22}} = 1 \tag{6.18}$$

$$ER_4: \quad \frac{\vec{k}_{16}}{\overleftarrow{k}_{16}} \frac{\vec{k}_{21}}{\overleftarrow{k}_{21}} \frac{\vec{k}_{22}}{\overleftarrow{k}_{22}} = 1$$

$$ER_5: \quad \frac{\vec{k}_{16}}{\overleftarrow{k}_{16}} \frac{\vec{k}_{17}}{\overleftarrow{k}_{17}} \frac{\overleftarrow{k}_{18}}{\vec{k}_{18}} = 1$$

Furthermore, the affinities, A_ρ of the elementary reactions ($A_\rho = -\Delta G_\rho$), in a FR are interrelated with the affinity of the OR, A_{OR}, via similar KPL relation. For instance, for FR_1: $s_1 + IR_1 + s_3 + 2s_5 + 2s_6 + s_9 + s_{10} + s_{11} + s_{12} + s_{13}$, we have

$$A_1 + A_{IR_1} + A_3 + 2A_5 + 2A_6 + A_9 + A_{10} + A_{11} + A_{12} + A_{13} = A_{OR} \quad \text{i.e.,}$$
$$K_1 K_{IR_1} K_3 K_5^2 K_6^2 K_9 K_{10} K_{11} K_{12} K_{13} = K_{OR} \tag{6.19}$$

where, K_ρ and K_{OR} is the equilibrium constant of the elementary reaction step s_ρ and OR respectively. The kinetic data provided in Table 6-2, is indeed consistent with these KPL relations.

6.6 Network Analysis and Pruning

For the 22-step MSR on Ni(111), the equivalent electrical circuit can be obtained simply by replacing the branches in the final RR Graph in Figure 6-4b by the step resistances. Figure 6-5, thus, provides the electrical analog or the reaction circuit of the MSR reaction mechanism. First of all, note that only the independent ORs (2 in this case) are required on the network. As long as the driving force (power source) for any two overall reactions is known, the network can be simulated in order to calculate the flux through individual steps. This provides further justification that only the independent set of ORs is essential to describe the reaction mechanism.

Figure 6-5: Electrical Analog for the MSR reaction mechanism on Ni. The values on the circuit represent flux through each step at 900 K.
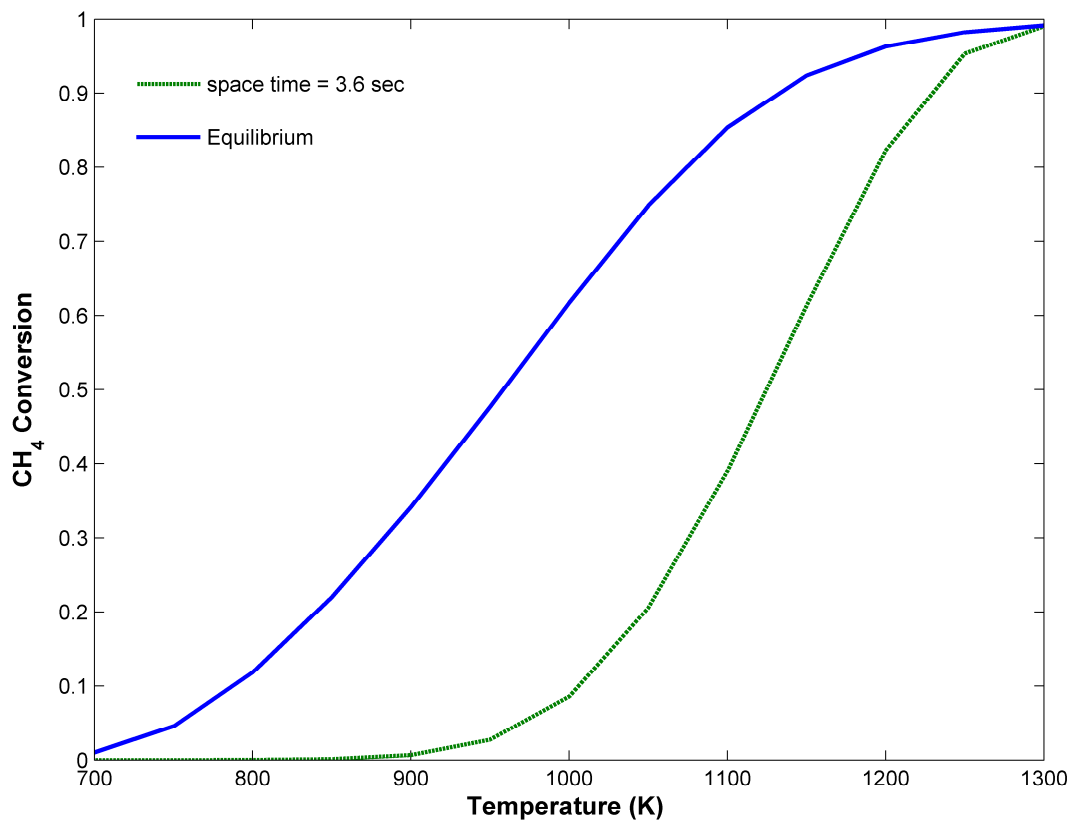
Figure 6-6: Equilibrium conversion vs. actual conversion in a PBR at a space time of 3.6 sec for MSR on Ni.

Accurate and robust simplification and reduction may now be accomplished based on a comparison of the flux (current) along different pathways in the reaction circuit. The fractional surface coverage of the intermediate species and the vacant sites are obtained by solving QSS equations and mass-balance equation for a packed-bed reactor (PBR). All numerical simulations were performed for the following conditions: surface area of 9.3 m²/g [1], surface site density of 1.86×10^{15} atoms/cm² [64], molar feed ratio $H_2O/CH_4 = 3.0$, molar feed ratio $H_2/CH_4 = 1.25$ and pressure = 10 bar, similar to that in the experimental study by Xu and Froment [1]. In order to maintain the overall reaction far away from equilibrium, we utilized a small space time of 3.6 sec (Figure 6-6). The calculated rate (flux) at $T = 900$ K for the elementary reaction steps is mentioned in Figure 6-5.

Firstly, we see from Figure 6-5 that KFL is valid at all nodes on the electrical circuit. Secondly, it is rather evident that steps s_{14}, s_{18}, s_{21} and s_{22} have negligible flux and hence can be eliminated without materially affecting the overall reaction flux. However, these conclusions may or may not be valid at a temperature other than 900 K or at other feed compositions.

Validation of this reduction and simplification of the RR network over a broad range of temperatures can be accomplished by comparing the resistances along parallel paths between two nodes, which have the same affinity drop by virtue of KPL, i.e., by considering each ER as two parallel paths and comparing the total resistance of each path. If the resistance along one path is much larger than the other, it would be safe to assume that the path contributes little to the flux and may be neglected. Finally, the effect of eliminating a resistance is validated by calculating the overall kinetics without the elementary reaction step in question.

Let us consider ER_5: $(+1)s_{16} + (+1)s_{17} + (-1)s_{18}$, which implies that there are two parallel pathways for formation of adsorbed hydrogen and CO_2 species. In the first pathway, CHO·S reacts with O·S in a single step (step s_{18}), while in the other CHO·S dissociates into CO·S (step s_{16}), which subsequently reacts with O·S (step s_{17}) to form CO_2·S and H·S. The resistance of the first pathway is simply R_{18}, while that for the second pathway comprising of two steps in series is $R_{16} + R_{17}$. Figure 6-7, compares the

resistance of these two pathways as a function of temperature for the reaction conditions mentioned above. It is evident from Figure 6-7, that R_{18} is several orders of magnitude higher than $R_{16} + R_{17}$. Since a reaction will always proceed via a minimum resistance pathway, it is reasonable to conclude that it may be possible to eliminate step s_{18} from the mechanism. Thus, the sequential formation of $CO_2 \cdot S$ and $H \cdot S$ from $CHO \cdot S$ mediated via $CO \cdot S$ is preferred over a single step reaction.

Next, we consider ER_1: $(+1)s_{10} + (+1)s_{14} + (-1)s_{19} + (-1)s_{20}$. This empty route provides two pathways for the formation of $CH_2O \cdot S$ and $H \cdot S$. The first pathway comprises of steps s_{10} and s_{14} as shown below

$$\underline{\sigma_\rho}$$

s_{10}:	$CH_3 \cdot S + S \leftrightarrows CH_2 \cdot S + H \cdot S$	$+1$
s_{14}:	$CH_2 \cdot S + O \cdot S \leftrightarrows CH_2O \cdot S + S$	$+1$

Net: $CH_3 \cdot S + O \cdot S \leftrightarrows CH_2O \cdot S + H \cdot S$
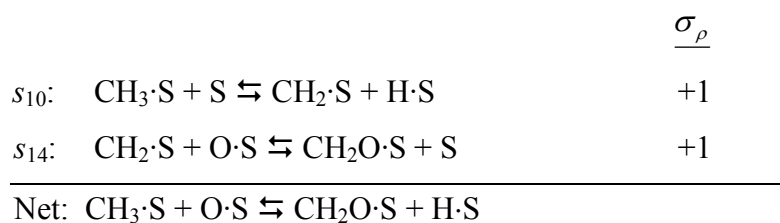
While the second pathway comprised of steps s_{19} and s_{20} is shown below

$$\underline{\sigma_\rho}$$

s_{19}:	$CH_3 \cdot S + O \cdot S \leftrightarrows CH_3O \cdot S + S$	$+1$
s_{20}:	$CH_3O \cdot S + S \leftrightarrows CH_2O \cdot S + H \cdot S$	$+1$

Net: $CH_3 \cdot S + O \cdot S \leftrightarrows CH_2O \cdot S + H \cdot S$
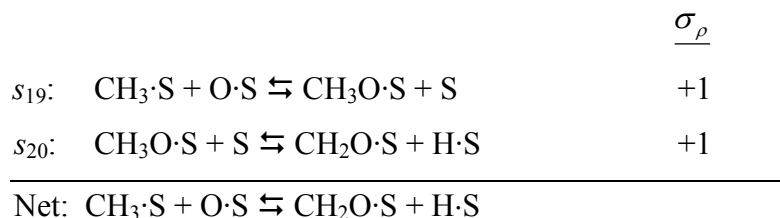
Figure 6-8, compares the resistance of these two pathways ($R_{10} + R_{14}$ vs. $R_{19} + R_{20}$) as a function of temperature for the reaction conditions mentioned above. $R_{10} + R_{14}$ is found to be several of orders of magnitude higher than $R_{19} + R_{20}$. Furthermore, it is also evident from Figure 6-8 that $R_{10} + R_{14} \sim R_{14}$, which implies all the resistance to the pathway is contributed by step s_{14}. Thus, in comparison with the parallel pathway comprising of s_{19} and s_{20}, step s_{14} can be neglected without compromising the overall reaction flux.
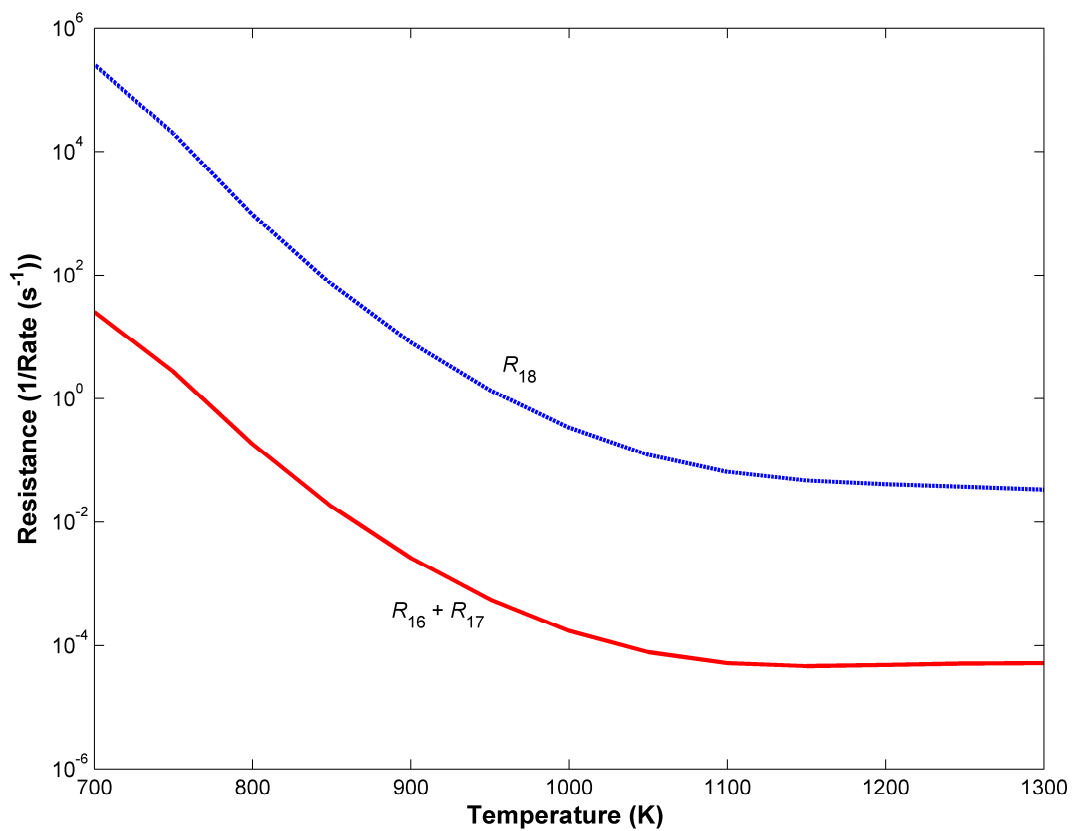
Figure 6-7: Parallel pathway resistance ($R_{16} + R_{17}$ vs. R_{18}) comparison as a function of temperature for the conditions quoted in the text.
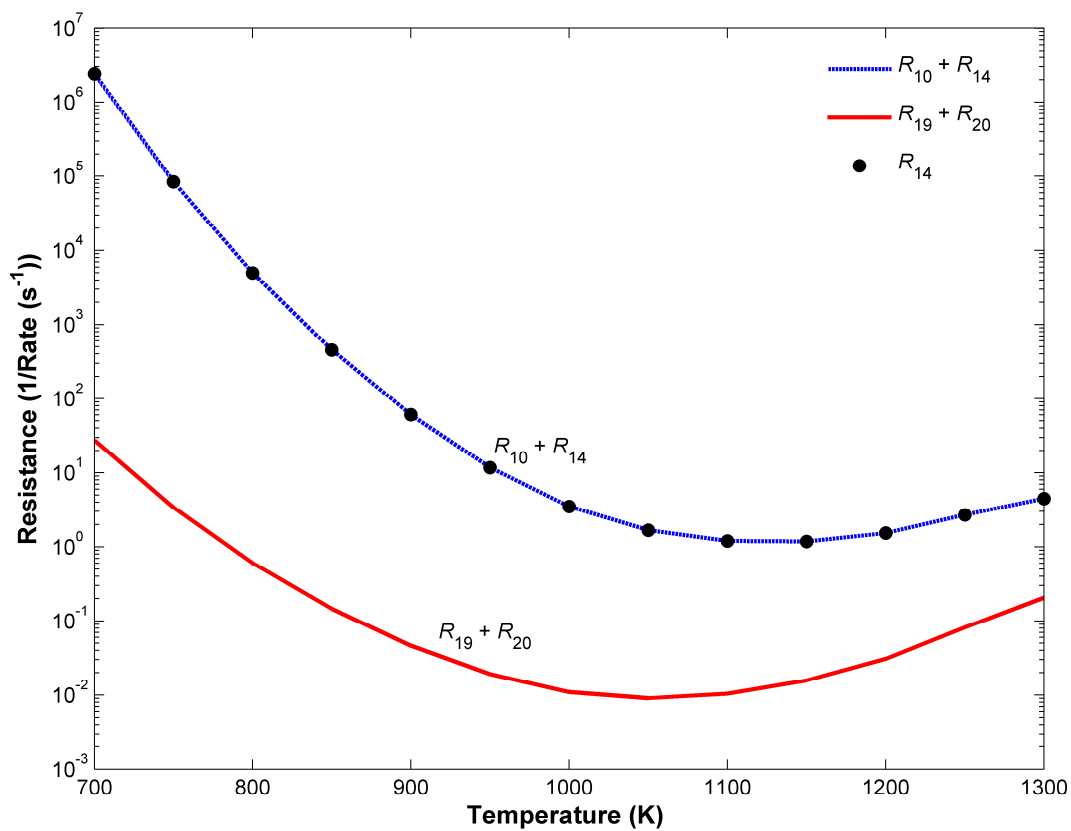
Figure 6-8: Parallel pathway resistance ($R_{10} + R_{14}$ vs. $R_{19} + R_{20}$) comparison as a function of temperature for the conditions quoted in the text.
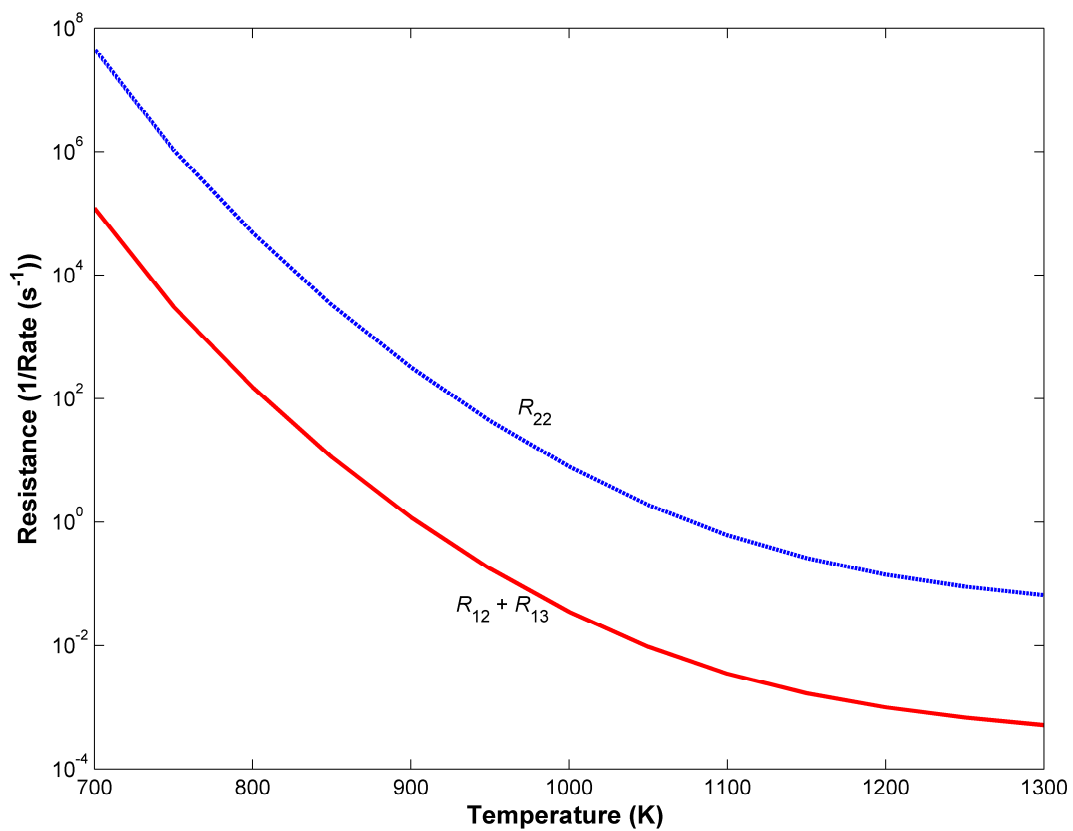
Figure 6-9: Parallel pathway resistance ($R_{12} + R_{13}$ vs. R_{22}) comparison as a function of temperature for the conditions quoted in the text.
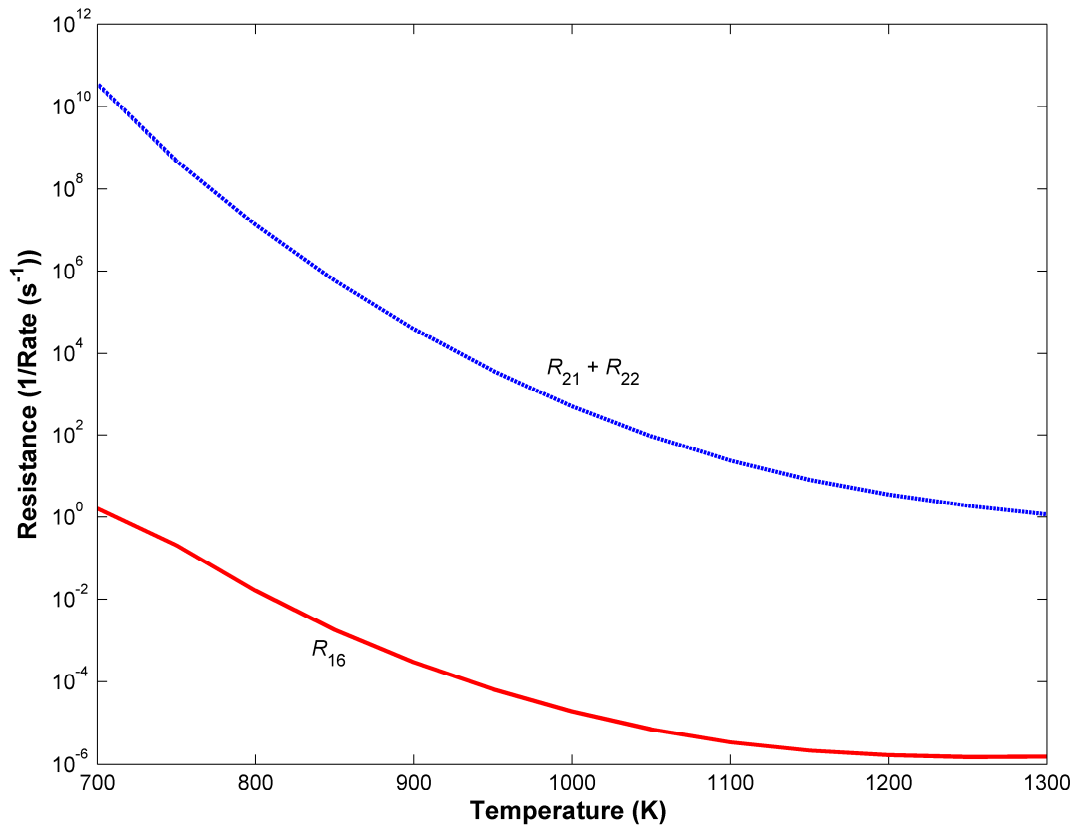
Figure 6-10: Parallel pathway resistance ($R_{21} + R_{22}$ vs. R_{16}) comparison as a function of temperature for the conditions quoted in the text.

The empty route, ER_3: $(+1)s_{12} + (+1)s_{13} + (-1)s_{22}$ is considered next. This empty route represents two parallel pathways for the formation of the CO·S and H·S. The first pathway proceeds via formation of carbon, i.e. C·S followed by surface reaction with O·S to form CO·S and H·S (i.e. step $s_{12} + s_{13}$), the resistance of which is given by $R_{12} + R_{13}$. The second pathway corresponds to the direct formation of CO·S and H·S from CH·S and O·S (step s_{22}). The resistance for the second pathway is simply R_{22}. It is evident from Figure 6-9, the pathway mediated via C·S is the preferred route. Thus, step s_{22} can be easily neglected from the overall mechanism.

Lastly, we consider the parallel pathways represented by ER_4: $(+1)s_{16} + (-1)s_{21} + (-1)s_{22}$. Figure 6-10 compares the resistance for these parallel pathways. It is clear that R_{16} is several orders of magnitude lower than $R_{21} + R_{22}$, providing enough justification for steps s_{21} and s_{22} to be deemed kinetically insignificant.

The elimination of steps, s_{14}, s_{18}, s_{21}, and s_{22} from the mechanism is validated by comparing simulated results of the complete mechanism with results from the mechanism excluding s_{14}, s_{18}, s_{21}, and s_{22}, i.e., the simplified network shown in Figure 6-11. The reduced network reveals only two pathways, namely FR_1: $IR_1 + IR_2 + s_{10} + s_{11} + s_{12} + s_{13}$ + s_3, and FR_2: $IR_1 + IR_2 + s_{19} + s_{20} + s_{15} + s_{16} + s_3$ for OR_1, i.e. $CH_4 + H_2O \leftrightarrows CO + 3H_2$. On the other hand, only a single pathway, i.e. FR_1: $-s_3 + s_{17} + s_4 + IR_1$ exists for OR_2 (CO + $H_2O \leftrightarrows CO_2 + H_2$).

The pathway resistance of the two reaction routes for OR_1 as obtained from Figure 6-5 is as follows

$$R_{FR_1} = \frac{R_{IR_1}}{2} + R_{IR_2} + \frac{R_{10}}{2} + \frac{R_{11}}{2} + \frac{R_{12}}{2} + \frac{R_{13}}{2} + \frac{R_3}{2}$$

$$R_{FR_2} = \frac{R_{IR_1}}{2} + R_{IR_2} + \frac{R_{19}}{2} + \frac{R_{20}}{2} + \frac{R_{15}}{2} + \frac{R_{16}}{2} + \frac{R_3}{2}$$

(6.20)

where, $R_{IR_1} = R_2 + R_5 + R_6 + R_7 + R_8$ and $R_{IR_2} = \frac{R_1}{2} + 2R_5 + 2R_6 + \frac{R_9}{2}$

As can be seen from Figure 6-12, FR_1 has a higher resistance as compared to FR_2, at temperatures < 1000 K, while at temperatures above 1000 K, FR_1 provides a path of minimum resistance.
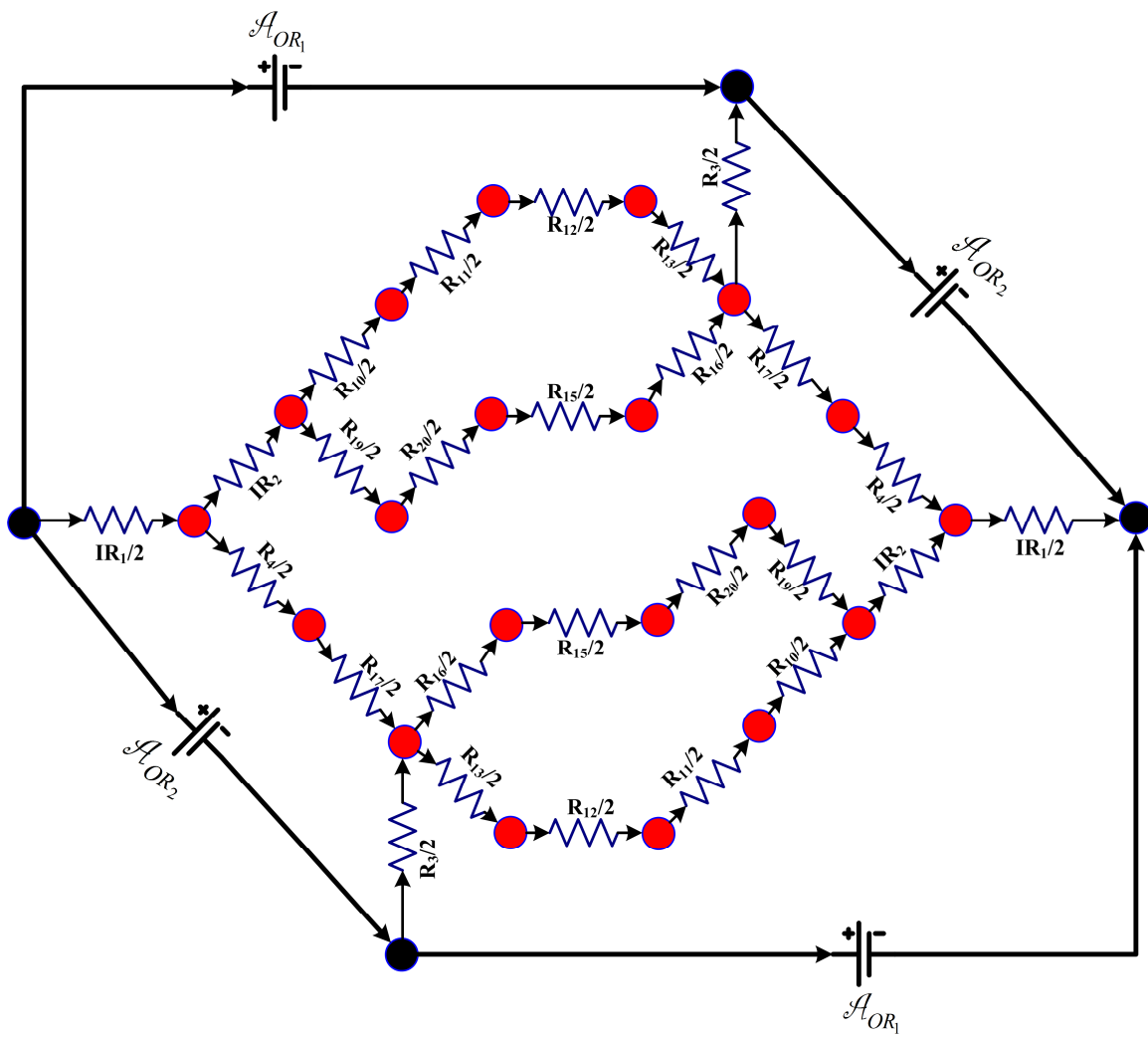
Figure 6-11: Pruned RR graph for MSR reaction mechanism on Ni.
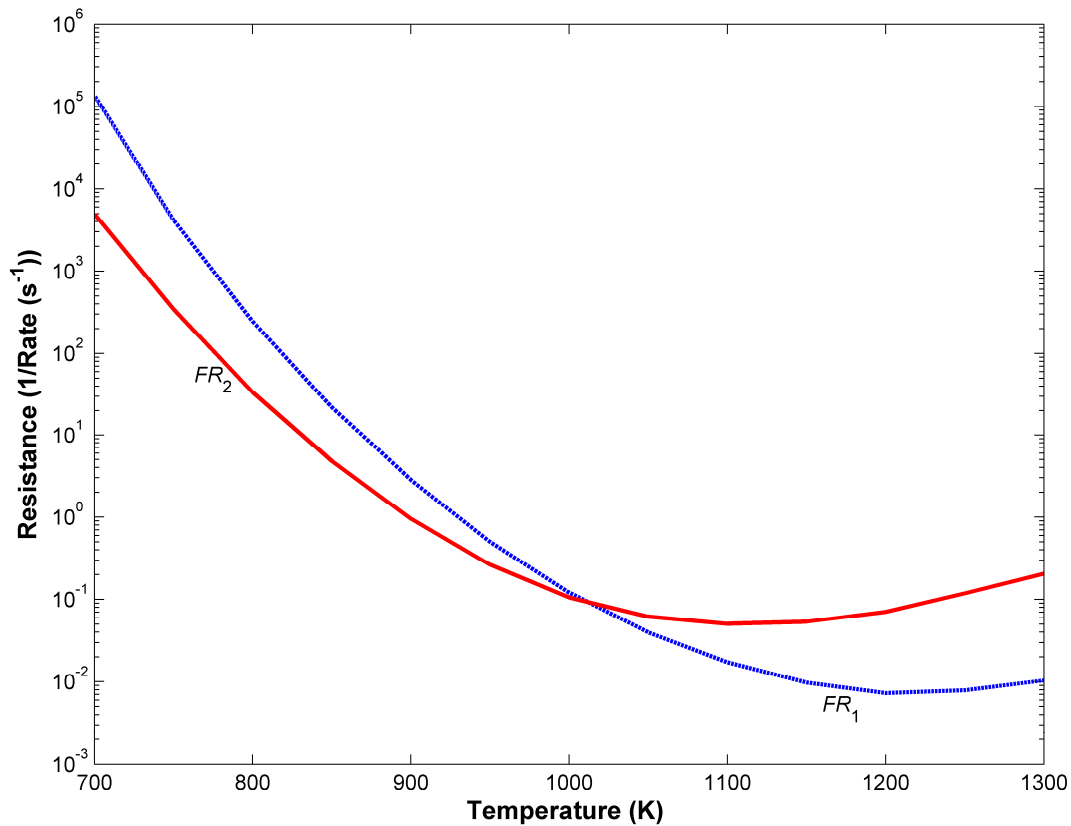
Figure 6-12: Resistance of the two dominant reaction pathways, FR_1 and FR_2 for MSR on Ni.

However, it should be noted that in the temperature of interest for MSR on Ni or direct internal reforming in a SOFC (900 < T < 1100 K), both the pathways have comparable resistances. This indicates the existence of a dual pathway mechanism depending on the temperature of operation. The two pathways in the conventional form are written as

$$\underline{\sigma_\rho}$$

s_1:	$CH_4 + S \leftrightarrows CH_4 \cdot S$	+1
s_2:	$H_2O + S \leftrightarrows H_2O \cdot S$	+1
s_3:	$CO \cdot S \leftrightarrows CO + S$	+1
s_5:	$H \cdot S + H \cdot S \leftrightarrows H_2 \cdot S + S$	+3
s_6:	$H_2 \cdot S \leftrightarrows H_2 + S$	+3
s_7:	$H_2O \cdot S + S \leftrightarrows OH \cdot S + H \cdot S$	+1
s_8:	$OH \cdot S + S \leftrightarrows O \cdot S + H \cdot S$	+1
s_9:	$CH_4 \cdot S + S \leftrightarrows CH_3 \cdot S + H \cdot S$	+1
s_{10}:	$CH_3 \cdot S + S \leftrightarrows CH_2 \cdot S + H \cdot S$	+1
s_{11}:	$CH_2 \cdot S + S \leftrightarrows CH \cdot S + H \cdot S$	+1
s_{12}:	$CH \cdot S + S \leftrightarrows C \cdot S + H \cdot S$	+1
s_{13}:	$C \cdot S + O \cdot S \leftrightarrows CO \cdot S + S$	+1

$$(6.21)$$

OR_1:	$CH_4 + H_2O \leftrightarrows CO + 3H_2$

and

$$\underline{\sigma_\rho}$$

s_1:	$CH_4 + S \leftrightarrows CH_4 \cdot S$	+1
s_2:	$H_2O + S \leftrightarrows H_2O \cdot S$	+1
s_3:	$CO \cdot S \leftrightarrows CO + S$	+1
s_5:	$H \cdot S + H \cdot S \leftrightarrows H_2 \cdot S + S$	+3
s_6:	$H_2 \cdot S \leftrightarrows H_2 + S$	+3
s_7:	$H_2O \cdot S + S \leftrightarrows OH \cdot S + H \cdot S$	+1
s_8:	$OH \cdot S + S \leftrightarrows O \cdot S + H \cdot S$	+1
s_9:	$CH_4 \cdot S + S \leftrightarrows CH_3 \cdot S + H \cdot S$	+1
s_{15}:	$CH_2O \cdot S + S \leftrightarrows CHO \cdot S + H \cdot S$ +1	

$$(6.22)$$

s_{16}:	$CHO \cdot S + S \leftrightharpoons CO \cdot S + H \cdot S$	+1
s_{19}:	$CH_3 \cdot S + O \cdot S \leftrightharpoons CH_3O \cdot S + S$	+1
s_{20}:	$CH_3O \cdot S + S \leftrightharpoons CH_2O \cdot S + H \cdot S$	+1
OR_1:	$CH_4 + H_2O \leftrightharpoons CO + 3H_2$	

Thus, both the pathways begin with adsorption of methane to form $CH_3 \cdot S$. The first pathway, FR_1, proceeds via sequential abstraction of hydrogen from $CH_3 \cdot S$ to form $C \cdot S$, which eventually reacts with adsorbed oxygen atoms, $O \cdot S$, to form $CO \cdot S$. On the other hand, the second pathway, FR_2 proceeds via surface reaction of $CH_3 \cdot S$ and $O \cdot S$ to form $CH_3O \cdot S$. Subsequent sequential removal of hydrogen from $CH_3O \cdot S$ leads to the formation of $CO \cdot S$ while avoiding any carbon formation.

Thus, according to the first mechanism, the CO is produced via elemental carbon while in the second mechanism, the CO is produced via carbon oxygenates, similar to that proposed by Temkin and coworkers [8]. In short, one pathway takes place via hydrogenated carbon species, while the other takes place via oxygenated carbon species as depicted schematically in Figure 6-13.

6.7 QSS Rate Expression for the Overall Reactions

Now that the mechanism has been appropriately pruned, we are in a position to consider the rate of the overall reactions. Let us first consider OR_1: $CH_4 + H_2O \leftrightharpoons CO + 3H_2$. We next identify the RLS for each of the two parallel pathways, namely FR_1: $IR_1 + IR_2 + s_{10} + s_{11} + s_{12} + s_{13} + s_3$, and FR_2: $IR_1 + IR_2 + s_{19} + s_{20} + s_{15} + s_{16} + s_3$. As described in the earlier chapters, RLS for a sequence is step(s) that predominantly contribute to the overall pathway resistance. In other words, in a sequence (or set of resistors connected in series), the step(s) with maximum resistance would be the slowest steps and hence kinetically dominant.

Figure 6-14 and Figure 6-15 compares the individual step resistances in the FR_1 and FR_2, respectively. For the first pathway FR_1, we observe that, step s_{11} may be considered as RLS with all the other steps at quasi-equilibrium (QE). While for the second pathway, we have step s_{15} as the RLS with all the other steps at quasi-equilibrium (QE).
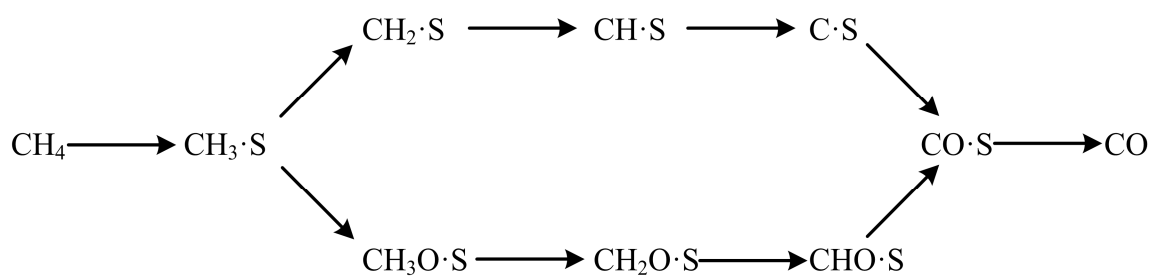
Figure 6-13: Schematic of the dominant reaction mechanism for MSR on Ni.
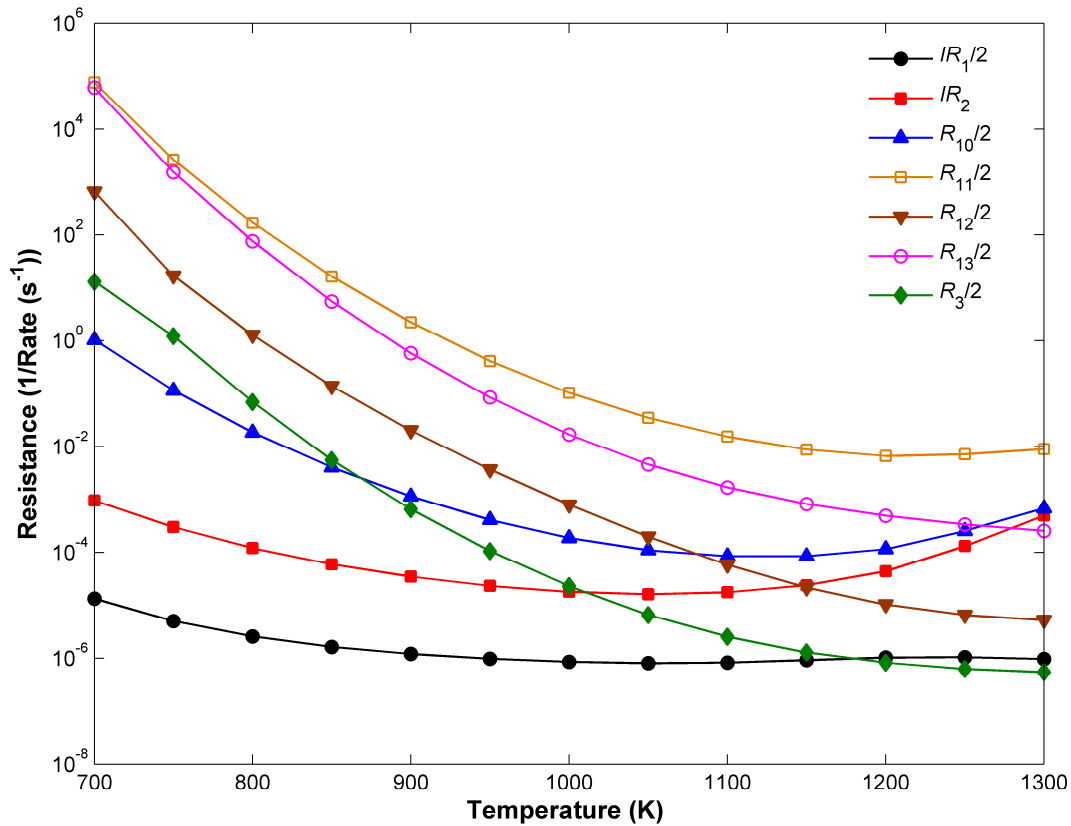
Figure 6-14: Comparison of step resistances connected in series in FR_1 in order to identify the RLS.
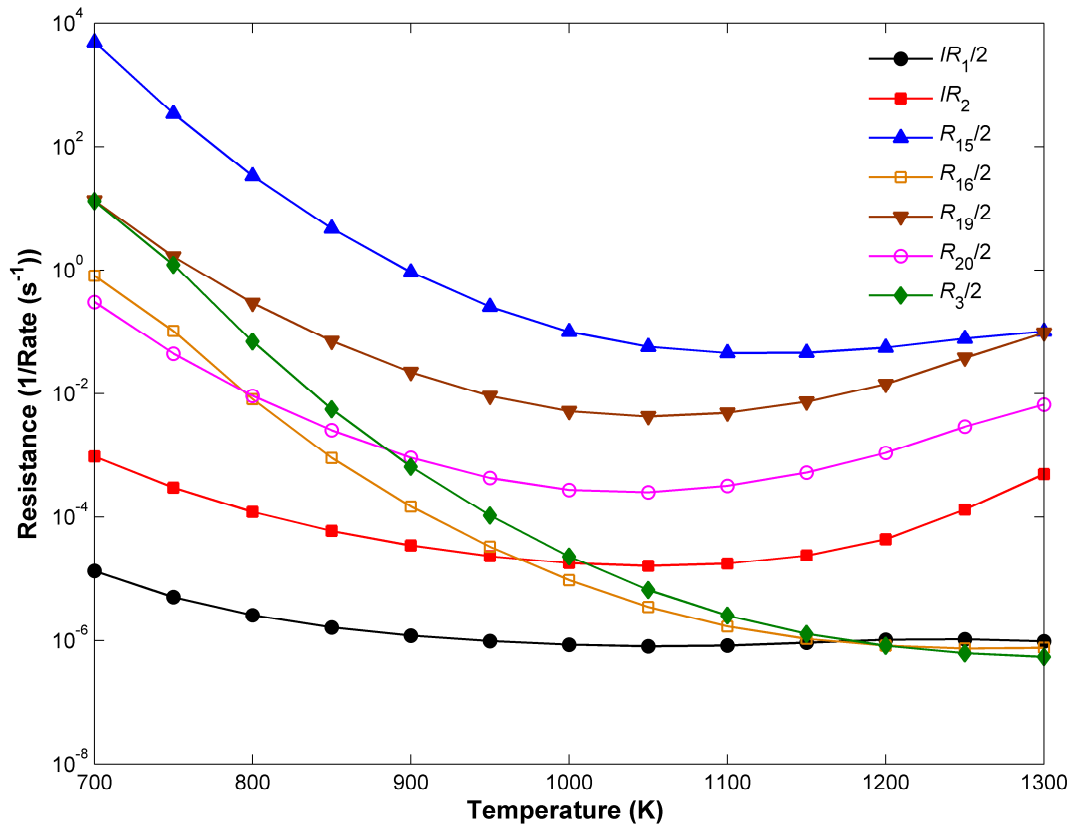
Figure 6-15: Comparison of step resistances connected in series in FR_2 in order to identify the RLS.
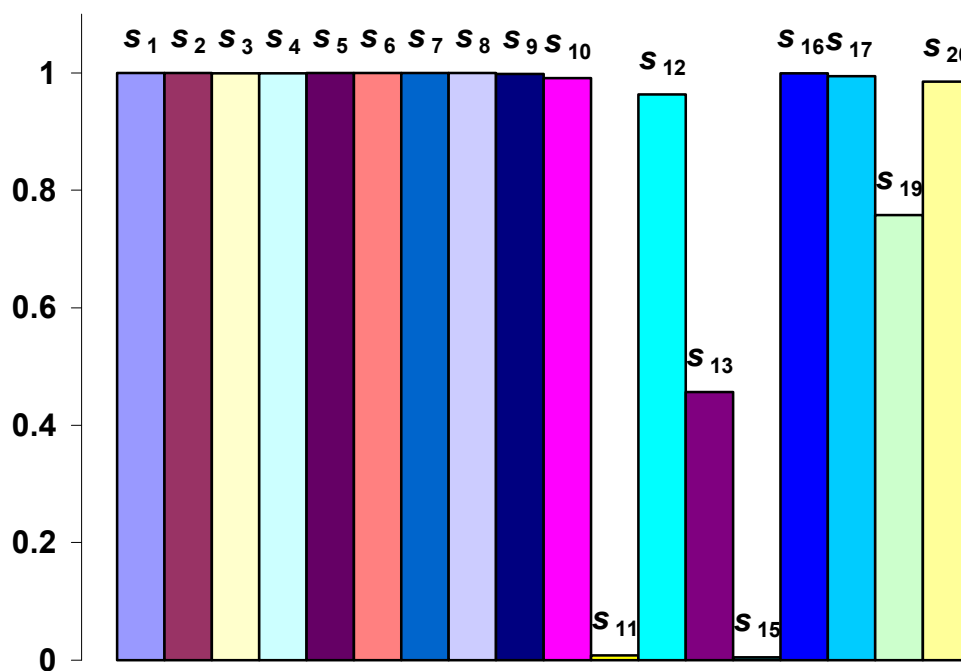
Figure 6-16: Step reversibilites of elementary reaction steps for the conditions quoted in the text.
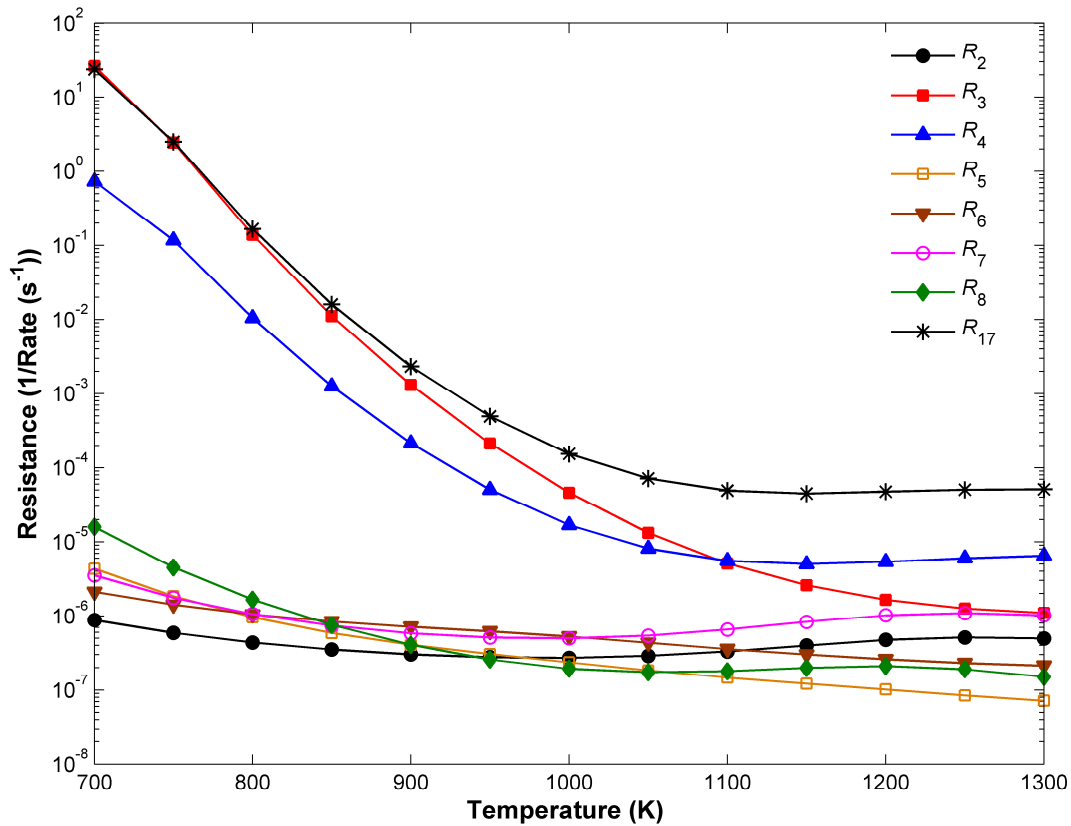
Figure 6-17: Comparison of step resistances connected in series for the dominant reaction pathway for WGS in order to identify the RLS.

The above conclusion can also be corroborated by computing the step reversibilities for a wide range of reaction conditions. One such example is shown in Figure 6-16, where the step reversibilities for steps in the reduced network are plotted for the reaction conditions quoted above and $T = 1000$ K. Thus, it can be seen that all the individual reaction steps, except s_{11}, and s_{15}, are substantially reversible. The kinetic analysis, described above can, of course, be greatly simplified based on step reversibilites. If $z_\rho \rightarrow 1$, the step may be considered as quasi-equilibrated (QE), and one of the KFL equations may be replaced by an algebraic equation expressing equilibrium of the step.

Thus, the above analysis reveals the third C–H bond activation (s_{11}: CH$_2$·S + S $\leftrightarrows$ CH·S + H·S) to be rate-limiting for the first pathway, as opposed to Iglesia and coworkers [27, 28] where the first C–H bond activation was reported to be the RDS. Xu and Froment [1] assumed CHO·S + S $\leftrightarrows$ CO·S + H·S to be the RDS in their work, however, based on our reaction circuitry analysis we find the formation of CHO·S, (i.e., s_{15}: CH$_2$O·S + S $\leftrightarrows$ CHO·S + H·S) to be rate-limiting for the second pathway.

Following a similar procedure, we can identify the RLS(s) for the only pathway, i.e., FR$_1$: $-s_3 + s_{17} + s_4 + $ IR$_1$, or $-s_3 + s_{17} + s_4 + s_2 + s_5 + s_6 + s_7 + s_8$ for OR$_2$: CO + H$_2$O $\leftrightarrows$ CO$_2$ + H$_2$. Figure 6-17, compares these step resistances and we observe step s_{17}: CO·S + O·S $\leftrightarrows$ CO$_2$·S + S to be the RLS for WGS. This is the same step assumed by Xu and Froment [1] as the RDS for WGS in their LHHW analysis.

Based on the RLSs, we can now derive QSS rate expression for both, OR$_1$ and OR$_2$. For OR$_1$, i.e. SR of methane that proceeds via two dominant RRs, the overall rate can be obtained by calculating the flux through each of the two parallel RRs. The rates along these dominant RRs may be determined using the quasi-steady state approximation (for details, see Appendix B & C) and are equal to

$$r_{11} = \frac{\vec{k}_{10}\vec{k}_{11}K_i P_{CH_4} P_{H_2}^{-1/2} \theta_0^2}{\vec{k}_{11} + \overleftarrow{k}_{10} K_v P_{H_2}^{1/2}} \left(1 - \frac{1}{K_{SR}} \frac{P_{CO} P_{H_2}^3}{P_{CH_4} P_{H_2O}} \right) \tag{6.23}$$

$$r_{21} = \frac{\vec{k}_{19}\vec{k}_{20}\vec{k}_{15}K_i K_{vi} P_{CH_4} P_{H_2O} P_{H_2}^{-3/2} \theta_0^2}{\vec{k}_{19}\overleftarrow{k}_{15} + \overleftarrow{k}_{20}\vec{k}_{15} + \vec{k}_{19}\vec{k}_{20} K_v P_{H_2}^{1/2}} \left(1 - \frac{1}{K_{SR}} \frac{P_{CO} P_{H_2}^3}{P_{CH_4} P_{H_2O}} \right) \tag{6.24}$$

where K_{SR} is the equilibrium constant of the SR reaction (OR_1: $CH_4 + H_2O \leftrightarrows CO + 3H_2$). The overall rate of this overall reaction is thus a sum of the above rates, i.e.,

$$r_{SR} = r_{11} + r_{21}$$
$$= \left(\frac{\vec{k}_{19}\vec{k}_{20}\vec{k}_{15}K_i K_{vi}P_{CH_4}P_{H_2O}P_{H_2}^{-3/2}\theta_0^2}{\vec{k}_{19}\vec{k}_{15} + \vec{k}_{20}\vec{k}_{15} + \vec{k}_{19}\vec{k}_{20}K_v P_{H_2}^{1/2}} + \frac{\vec{k}_{10}\vec{k}_{11}K_i P_{CH_4}P_{H_2}^{-1/2}\theta_0^2}{\vec{k}_{11} + \vec{k}_{10}K_v P_{H_2}^{1/2}} \right)\left(1 - \frac{1}{K_{SR}}\frac{P_{CO}P_{H_2}^3}{P_{CH_4}P_{H_2O}} \right) \qquad (6.25)$$

Next, for OR_2, i.e. WGS with only one dominant reaction pathway, we have (for details, see Appendix B & C),

$$r_{WGS} = r_{17} = \vec{k}_{17}K_{iii}K_{vi}P_{CO}P_{H_2O}P_{H_2}^{-1}\theta_0^2\left(1 - \frac{1}{K_{WGS}}\frac{P_{CO_2}P_{H_2}}{P_{H_2O}P_{CO}} \right) \qquad (6.26)$$

Here θ_0 is the fraction of the free catalyst surface and is determined from the site balance. From numerical simulations (Figure 6-18), it is evident that the major and minor MARI are $H_2O{\cdot}S$, $CO{\cdot}S$, $O{\cdot}S$, $H{\cdot}S$, $OH{\cdot}S$ and $C{\cdot}S$, i.e.,

$$S + H_2O{\cdot}S + CO{\cdot}S + H{\cdot}S + O{\cdot}S + OH{\cdot}S + C{\cdot}S \approx 1 \qquad (6.27)$$

Thus (for details, see Appendix B & C),

$$\theta_0 = \frac{1}{1 + K_{ii}P_{H_2O} + K_{iii}P_{CO} + K_v P_{H_2}^{1/2} + K_{vi}P_{H_2O}P_{H_2}^{-1} + K_{vii}P_{H_2O}P_{H_2}^{-1/2} + K_{ix}P_{CO}P_{H_2}P_{H_2O}^{-1}} \qquad (6.28)$$

The rate expressions for the two overall reactions can now be combined with mass-balance equations for a PBR. Numerical simulations (Figure 6-19) show that the model predictions are in complete agreement with the experimental data of Xu and Froment [1], without any fitting. These results further support the claim here, that only a set of independent ORs are necessary in order to describe a reaction system, and are also indicative of the robustness of the RR graph approach.

6.8 Model Significance and Concluding Remarks

Following our RR graph approach, the 22-step mechanism for MSR is whittled down to a dual path mechanism, depending upon the reaction temperature. The dominant pathways have been identified in a logical and intuitive manner. Thus, for OR_1: $CH_4 + H_2O \leftrightarrows CO + 3H_2$, we have two parallel pathways in the temperature region on interest.
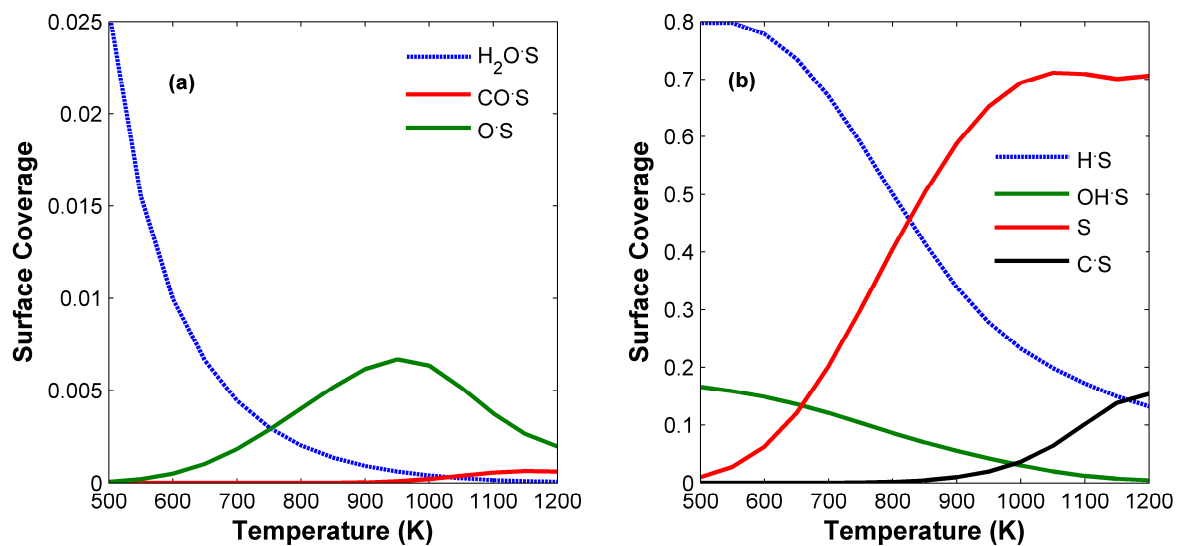
Figure 6-18: (a) Major and (b) minor surface species as a function of temperature for MSR on Ni.
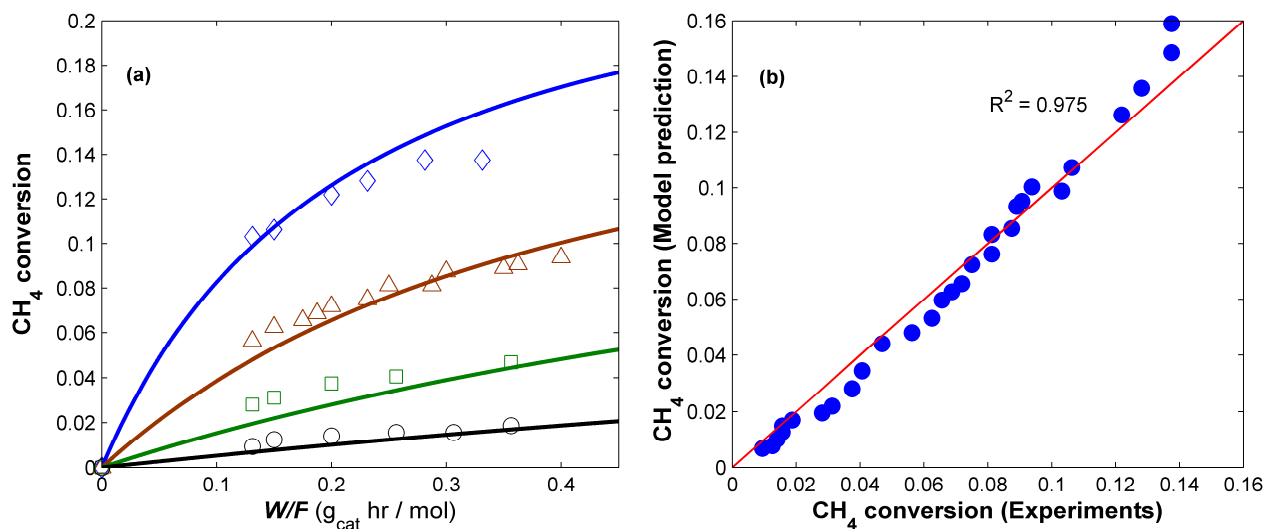
Figure 6-19: (a) Comparison of model prediction for a PBR and the experimental data by Xu and Froment [1]. (b) Parity plot of calculated methane conversion vs. the experimental conversion.
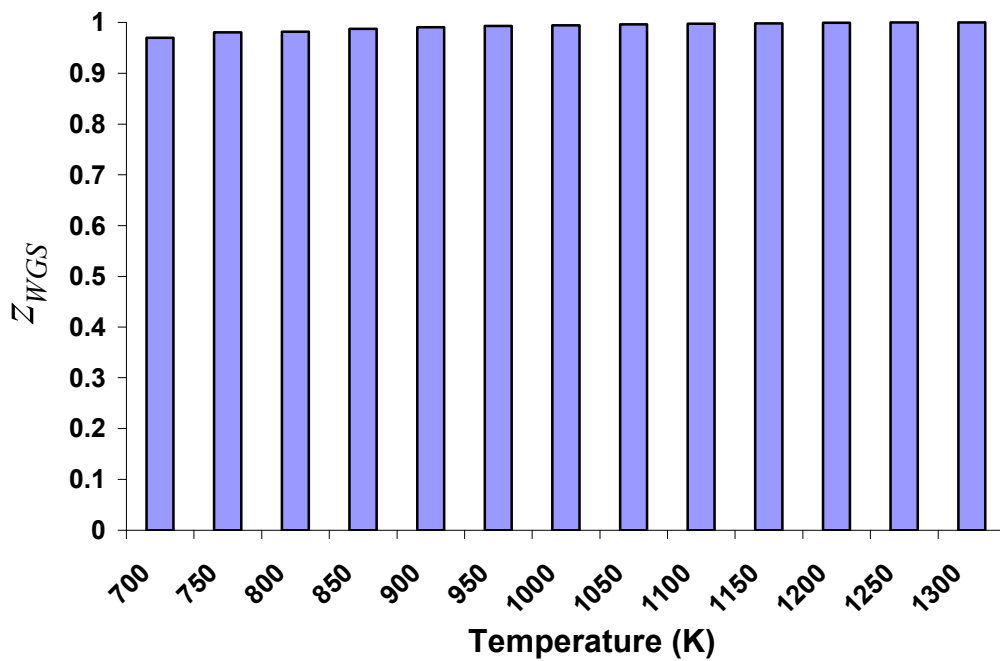
Figure 6-20: Reversibility of WGS reaction in the temperature region of interest for MSR on Ni.

One of these takes place via hydrogenated carbon species, while the other takes place via oxygenated carbon species.

Rate limiting steps (s_{11}: $CH_2 \cdot S + S \leftrightarrows CH \cdot S + H \cdot S$ and s_{15}: $CH_2O \cdot S + S \leftrightarrows CHO \cdot S + H \cdot S$ for SR of methane and s_{17}: $CO \cdot S + O \cdot S \leftrightarrows CO_2 \cdot S + S$ for WGS) along with the quasi-equilibrated steps are next identified based on the concept of step resistance and reversibility, respectively, following which explicit rate expressions are developed for each of the two overall reactions.

Finally, a comparison between the reduced model predictions for an isothermal PBR and the experimental results of Xu and Froment [1] is presented, showing good agreement. Thus, a predictive model with *a priori* kinetics has been developed that captures the experimental observations, as opposed to a LHHW-type of model fitted to the experimental data, commonly reported in the literature. We also show that for this multiple overall reaction system, comprising of five ORs, only two are independent. In fact, only the so-called independent set of ORs is required to describe the system accurately.

Lastly, we notice that the WGS reaction is essentially at equilibrium (Figure 6-20), at temperatures ($700 < T < 1200$ K), at which significant reactions involving methane occur which imply the rate expression for the WGS reaction can be replaced by its equilibrium relation. Thus, a single rate expression (Eq. (6.25)) for OR_1: $CH_4 + H_2O \leftrightarrows CO + 3H_2$, coupled with equilibrium relation for WGS, i.e. OR_2: $CO + H_2O \leftrightarrows CO_2 + H_2$ is all that is needed to adequately describe this multiple overall reaction system in the temperature region of interest ($T > 700$ K).

Semi-empirical method UBI-QEP and the transition-state theory, were utilized in this work to estimate the individual step kinetics, concluding that despite their evidently approximate character, are quite reliable in constructing physically meaningful microkinetic models for heterogeneous catalytic reactions. Although a detailed microkinetic model may in principle, be used to simulate the kinetics of the process for any reactor configuration, for numerical convenience and human interpretation of the reaction network, it is desirable to distill and simplify the mechanism further. Toward this goal, the theory of Reaction Route Graphs, applied so far only to single overall reaction

systems, has been suitably extended and applied here to the case of multiple overall reaction system.

In conclusion, we show how the 22-step MSR mechanism may be assembled into a RR Graph, which may next be converted into an equivalent reaction circuit for further analysis, simplification, and pruning, using the standard tools of circuit analysis. The result is the emergence of an unambiguous picture of MSR on Ni(111), with a clear portrayal of all possible pathways, and irrefutable identification of the dominant pathways and rate-limiting steps.

6.9 References

[1]   J. Xu, G.F. Froment, AIChE Journal. 35 (1989) 88-96.

[2]   K. Ahmed, K. Foger, Catal. Today. 63 (2000) 479–487.

[3]   E. S. Hecht, G. K. Gupta, H. Zhu, A. M. Dean, R. J. Kee, L. Maier, O. Deutschmann, Appl. Catal. A: General. 295 (2005) 40-51.

[4]   N. Laosiripojana, S. Assabumrungrat, J. Power Sources. 163 (2007) 943-951.

[5]   T. Takeguchi, Y. Kani, T. Yano, R. Kikuchi, K. Eguchi, T. K, Y. Uchida, A. Ueno, K. Omoshiki, M. Aizawa, J. Power Sources. 112 (2002) 588–595.

[6]   R. O'Hayre, S.-W. Cha, W. Colella, F.B. Prinz, Fuel Cell Fundamentals, John Wiley, Hoboken, NJ 2006.

[7]   J.R. Rostrup-Nielsen, J. Sehested, J.K. Nørskov, Adv. Catal. 47 (2002) 65.

[8]   M.I. Temkin, Adv. Catal. 28 (1979) 171.

[9]   J. Wei, E. Iglesia, J. Catal. 224 (2004) 370-383.

[10] L.M. Aparicio, J. Catal. 165 (1997) 262-274.

[11] K. Hou, R. Hughes, Chem. Eng. J. 82 (2001) 311-328.

[12] I. M. Bodrov, L. O. Apel'baum, M. I. Temkin, Kinetika i Kataliz. 9 (1968) 1065.

[13] A. A. Khomenko, L. O. Apel'baum, F. S. Shub, Y. S. Snagovskii, M. I. Temkin, Kinetika i Kataliz. 12 (1971) 423.

[14] R.J. Kee, Colorado School of Mines, SECA Annual Workshop, Asilomar, CA, 2005.

[15] J.A. Dumesic, D.F. Rudd, L.M. Aparicio, J.E. Rekoske, A.A. Trevino, The Microkinetics of Heterogeneous Catalysis, ACS, 1993.

[16] E. Shustorovich, H. Sellers, Surf. Sci. 31 (1998) 1.

[17] F. Jensen, Introduction to Computational Chemistry, Wiley, New York, 1999.

[18] L.J. Broadbelt, R.Q. Snurr, Applied Catal. A: General. 200 (2000) 23-46.

[19] I. Fishtik, R. Datta, Surf. Sci. 512 (2002) 229.

[20] N. M. Galea, D. Knapp, T. Ziegler, J. Catal. 247 (2007) 20-33.

[21] H. S. Bengaard, J. K. Nørskov, J. Sehested, B. S. Clausen, L. P. Nielsen, A. M. Molenbroek, J.R. Rostrup-Nielsen, J. Catal. 209 (2002) 365–384.

[22] M. L. Toebes, J. H. Bitter, A. J. van Dillen, K. P. de Jong, Catal. Today. 76 (2002) 33-42.

[23] D. Chen, R. Lodeng, A. Anundskas, O. Olsvik, A. Holmen, Chem. Eng. Sci. 56 (2001) 1371.

[24] A.K. Avetisov, J.R. Rostrup-Nielsen, V.L. Kuchaev, J.-H. Bak Hansen, A.G. Zyskin, E.N. Shapatina, J. Mol. Catal. A. Chemical. 315 (2010) 155-162.

[25] R.N. Bhat, W.M.H. Sachtler, Appl. Catal. A: General. 150 (1997) 279.

[26] J.R. Rostrup-Nielsen, J.H.B. Hansen, J. Catal. 144 (1993) 38.

[27] J. Wei, E. Iglesia, J. Phys. Chem. B. 108 (2004) 4094-4103.

[28] J. Wei, E. Iglesia, J. Catal. 225 (2004) 116-127.

[29] D. Chen, R. Lødeng, K. Omdahl, A. Anundskås, O. Olsvik, A. Holmen, Studies in Surf. Sci. Catal. 139 (2001) 93.

[30] D. Chen, R. Lødeng, A. Anundskås, O. Olsvik, A. Holmen, Chem. Eng. Sci. 56 (2001) 1371.

[31] K. Jarosch, T. El Solh, H. I. de Lasa, Chem. Eng. Sci. 57 (2002) 3439-3451.

[32] M.C.J. Bradford, M.A. Vannice, Appl. Catal. A: General. 142 (1996) 97-122.

[33] Y.-A. Zhu, D. Chen, X.-G. Zhou, W.-K. Yuan, Catal. Today. 148 (2009) 260–267.

[34] Y.H. Hu, E. Ruckenstein, J. Phys. Chem. B. 101 (1997) 7563-7565.

[35] E. Ruckenstein, Y.H. Hu, Catal. Lett. 51 (1998) 183-185.

[36] D.W. Blaylock, T. Ogura, W.H. Green, G.J.O. Beran, J. Phys. Chem. C. 113 (2009) 4898.

[37] S. Wang, D. Cao, Y. Li, J. Wang, H. Jiao, J. Phys. Chem. B. 109 (2005) 18956.

[38] S. Wang, X. Liao, J. Hu, D. Cao, Y. Li, J. Wang, H. Jiao, Surf. Sci. 601 (2007) 1271.

[39] G. Jones, J.G. Jakobsen, S.S. Shim, K. Kleis, M.P. Andersson, R. Rossmeisl, F. Abild-Pedersen, T. Bligaard, S. Helveg, B. Hinnemann, J.R. Rostrup-Nielsen, I. Chorkendorff, J. Sehested, J.K. Nørskov, J. Catal. 259 (2008) 147–160.

[40] E. Shustorovich, A.T. Bell, Surf. Sci. 253 (1991) 386-394.

[41] E. Shustorovich, A.T. Bell, Surface Science Letters. 259 (1991) L791-L796.

[42] E. Shustorovich, A.T. Bell, Surface Science. 248 (1991) 359-368.

[43] E. Shustorovich, A.T. Bell, Surface Science. 289 (1993) 127-138.

[44] M.J. Hei, H.B. Chen, J. Yi, Y.J. Lin, Y.Z. Lin, G.Wei, D.W. Liao, Surf. Sci. 417 (1998) 82–96.

[45] Y.-Z. Lin, J. Sun, J. Yi, J.-D. Lin, H.-B. Chen, D.-W. Liao, J. Mol. Struc. (Theochem). 587 (2002) 63-71.

[46] K. Hou, R. Hughes, Chem. Eng. J. 82 (2001) 311-328.

[47] A. Erdohelyi, J. Cserenyi, F. Solymosi, J. Catal. 141 (1993) 287-299.

[48] A. M. Efstathiou, A. Kladi, V. A. Tsipouriari, X. E. Verykios, J. Catal. 158 (1996) 64-75.

[49] O. Deutschmann, L.D. Schmidt, AIChE J. 44 (1998) 2465-2477.

[50] M. Bizzi, G. Saracco, R. Schwiedernoch, O. Deutschmann, AIChE J. 50 (2004) 1289-1299.

[51] A. K. Avetisov, V. L. Kuchaev, D. Y. Murzin, AIChE J. 52 (2006) 4273-4275.

[52] W.-S. Yang, H.-W. Xiang, Y.-W. Li, Y.-H. Sun, Catal. Today. 61 (2000) 237-242.

[53] S. Wang, G. Q. (Max) Lu, Ind. Eng. Chem. Res. 38 (1999) 2615-2625.

[54] P. Aghalayam, Y.K. Park, N. Fernandes, V. Papavassiliou, A.B. Mhadeshwar, D.G. Vlachos, J. Catal. 213 (2003) 23–38.

[55] I. Alstrup, J. Catal. 151 (1995) 216-225.

[56] C. Pistonesi, A. Juan, B. Irigoyen, N. Amadeo, Appl. Surf. Sci. 253 (2007) 4427–4437.

[57] E.M. Patrito, P.P. Olivera, H. Sellers, Surf. Sci. 306 (1994) 447.

[58] C.R.F. Lund, Ind. Eng. Chem. Res. 35 (1996) 2531-2538.

[59] NIST Chemistry WebBook (http://webbook.nist.gov/chemistry).

[60] M.F. Mark, F. Mark, W.F. Maier, Chem. Eng. Technol. 20 (1997) 361-370.

[61] G. Froment, F.,, J. Mol. Catal. A: Chemical. 163 (2000) 147–156.

[62] I. Fishtik, R. Datta, Chem. Eng. Comm. 191 (2004) 373-397.

[63] W.R. Smith, R.W. Missen, Chemical Reaction Equilibrium Analysis: Theory and Algorithms, John Wiley, New York, 1982.

[64] H.S. Bengaard, I. Alstrup, I. Chorkendorff, S. Ullmann, J.R. Rostrup-Nielsen, J.K. Nørskov, J. Catal. 187 (1999) 238.

Chapter VII

H$_2$ – O$_2$ Polymer Electrolyte Membrane (PEM) Fuel Cells

Before discussing the fuel cell performance model, we first elucidate the cause and the extent of the effect of the fuel and/or oxidant crossover on the observed fuel cell open circuit voltage (OCV). The OCV in PEM fuel cells is only ~0.95 – 1.05 V, despite the thermodynamic potential being around 1.23 V (~ room temperature). Based on *a priori* parameters, we show that hydrogen cross-over to the cathode explains all of the observed loss under open circuit conditions.

We next discuss within a lumped framework the performance of a single fuel cell, for the case when conditions on either electrode may be relatively uniform, typically characterized in terms of the polarization plot, i.e., a plot of the output voltage *V* available from a fuel cell versus the current density *i* drawn from it. The emphasis is to develop a simple model for PEM fuel cells that incorporates the cross-over effects. The framework discussed here is applicable to all types of fuel cells, albeit with different parameters.

7.1 The Effect of Hydrogen Crossover on Open-Circuit Voltage (OCV) in PEM Fuel Cells

7.1.1 Background

It is an irksome fact of life that the open-circuit voltage (OCV) of the low temperature polymer electrolyte membrane (PEM) fuel cell is typically only around 0.95 - 1.05 V, as shown in Figure 7-1 [1] versus temperature, rather than the reversible voltage V_0 (1.229 V at 25 °C) promised by thermodynamics. What is worse is that, despite extensive study over the course of three-quarters of a century, there is no clear explanation in the literature for this loss of around 20% in OCV, which causes a corresponding loss in the fuel cell efficiency, since efficiency of a fuel cell, $\varepsilon = (V/V_0)\varepsilon_0$, where V is the fuel cell voltage, V_0 is the thermodynamic voltage, and ε_0 is the thermodynamic efficiency. Clearly, an unambiguous understanding of the main reason for this in PEM fuel cells is important, which is the objective of this work.

The various hypotheses advanced to rationalize this observation center around the extremely low exchange current density for the 4-electron oxygen reduction reaction (ORR) on Pt ($i_0^* \sim 10^{-10}$ mA/cm^2) coupled with one or more side reactions occurring at the cathode in addition to the ORR [2, 3]. The presence of side reactions results in either a "rest potential," i.e., an *equilibrium* potential for a closed system, or a "mixed potential," i.e., a *steady-state* potential for an open system, e.g., a fuel cell, that is significantly lower than the thermodynamic potential (Figure 7-1).

Some of the possible side reactions ρ proposed are summarized in Table 7-1 [3], which can, of course, proceed in either direction depending upon the overpotential of electrode reaction ρ, $\eta_\rho = \Phi - \Phi_{\rho,0}$, where Φ is the electrode (rest, or mixed) potential, and $\Phi_{\rho,0}$ is the equilibrium potential for an individual reaction ρ. However, there is little consensus on which, if any, is the dominant parasitic reaction in this list.
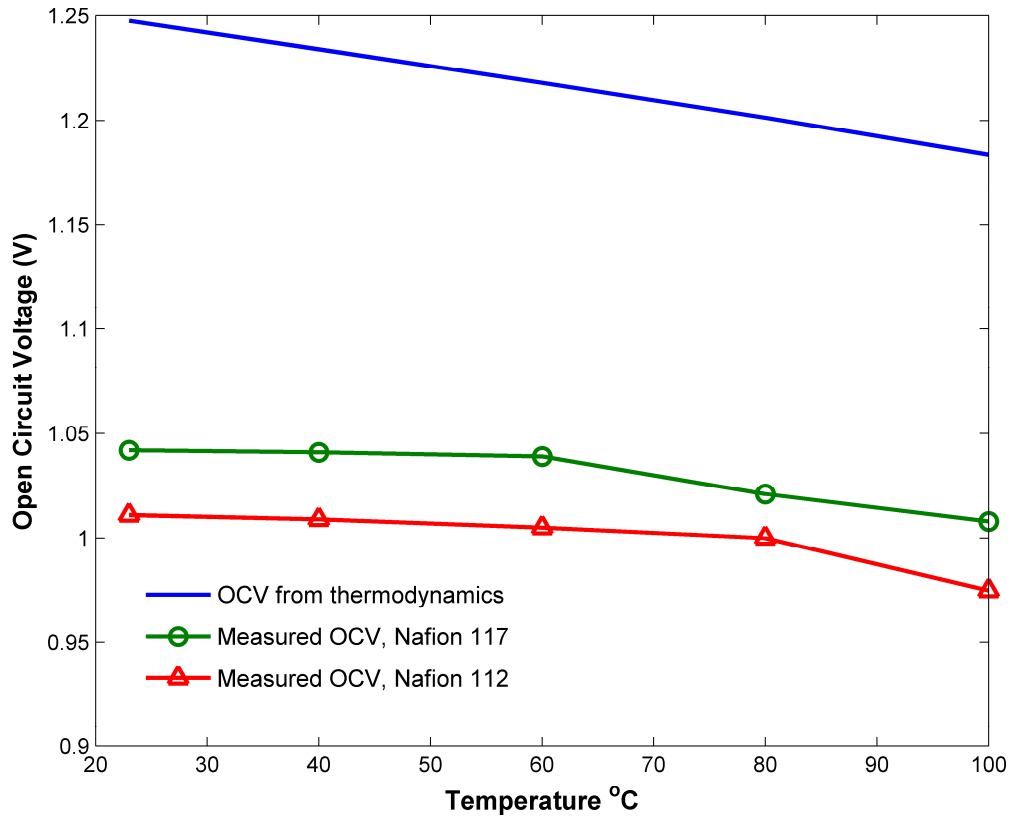
Figure 7-1: Open Circuit Voltage (OCV) for a PEM fuel cell as a function of temperature and membrane thickness. Experimental values are taken from Ref. [1]. (Anode: H_2, Cathode: Air, 3 atm, 100% RH)

Table 7-1: Possible reactions involving O_2, H_2, carbon support C, impurity CH_x, and Pt at the PEM fuel cell cathode [3].

Reaction No., ρ	Overall Reaction	Standard Electrode Potential, $\Phi^o_{\rho,0}$, V
1	$H_2O_2 + 2H^+ + 2e^- \leftrightarrows 2H_2O$	1.77
2	$PtO_3 + 2H^+ + 2e^- \leftrightarrows PtO_2 + H_2O$	1.48
3	$O_2 + 4H^+ + 4e^- \leftrightarrows 2H_2O$	1.229
4	$PtO_2 + 2H^+ + 2e^- \leftrightarrows Pt(OH)_2$	1.11
5	$Pt(OH)_2 + 2H^+ + 2e^- \leftrightarrows Pt + 2H_2O$	0.98
6	$PtO + 2H^+ + 2e^- \leftrightarrows Pt + H_2O$	0.88
7	$O_2 + 2H^+ + 2e^- \leftrightarrows H_2O_2$	0.68
8	$C + 2H_2O \leftrightarrows CO_2 + 4H^+ + 4e^-$	0.207
9	$CH_x + 2H_2O \leftrightarrows CO_2 + (x+4)H^+ + (x+4)e^-$	?
10	$2H^+ + 2e^- \leftrightarrows H_2$	0.00

If the fuel cell OCV were determined by the thermodynamic equilibrium potential in the presence of side reactions, the overpotential η_ρ as well as the net current of each electrode reaction ρ must individually be zero, i.e., $i_\rho = \vec{i}_\rho - \overleftarrow{i}_\rho = 0$, so that the rest potential $\Phi = \Phi_{\rho,0}$ is determined via simultaneous solution of the corresponding Nernst equations for the independent reaction set

$$\Phi_{\rho,0} = \Phi^o_{\rho,0} + \frac{RT}{\nu_{\rho e^-} F} \ln \prod_{\substack{i=1 \\ i \neq e^-}}^{n} a_i^{\nu_{\rho i}} \tag{7.1}$$

where $\Phi^o_{\rho,0}$ is the standard electrode potential, i.e., for unit activities a_i of species i, and $\nu_{\rho i}$ is its stoichiometric coefficient in reaction ρ, while $\nu_{\rho e^-}$ is that for electrons in it. For instance, if H_2O_2 were considered a side product, even though minor, at the cathode, there are two independent overall reactions (ORs) at the cathode, namely, the ORR (reaction 3 in Table 7-1), along with one more OR involving H_2O_2, e.g., reaction 7 in Table 7-1.

On the other hand, in a steady-state system, the overpotentials $\eta_\rho \neq 0$, and are such that the currents from anodic (electron generating) and cathodic (electron consuming) reactions occurring simultaneously on the electrode add up to zero, i.e., there is no net current, $\sum_\rho i_\rho = 0$, which determines the resulting mixed potential Φ as well as the parasitic current, as shown schematically in Figure 7-2. In other words, there is at least one anodic reaction occurring at the cathode that provides the electrons and protons consumed by the cathodic ORR and resulting in an overpotential. This, of course, is akin to corrosion.

Thus, a common explanation for the OCV is the formation of H_2O_2 via one of the reactions mentioned in Table 7-1, which could, in principle, alter the cathode thermodynamic potential. Alternately, the presence of H_2O_2 could sustain an anodic current density necessary for a mixed potential. However, it has been argued that the concentration of any H_2O_2 is far too small for this [3].
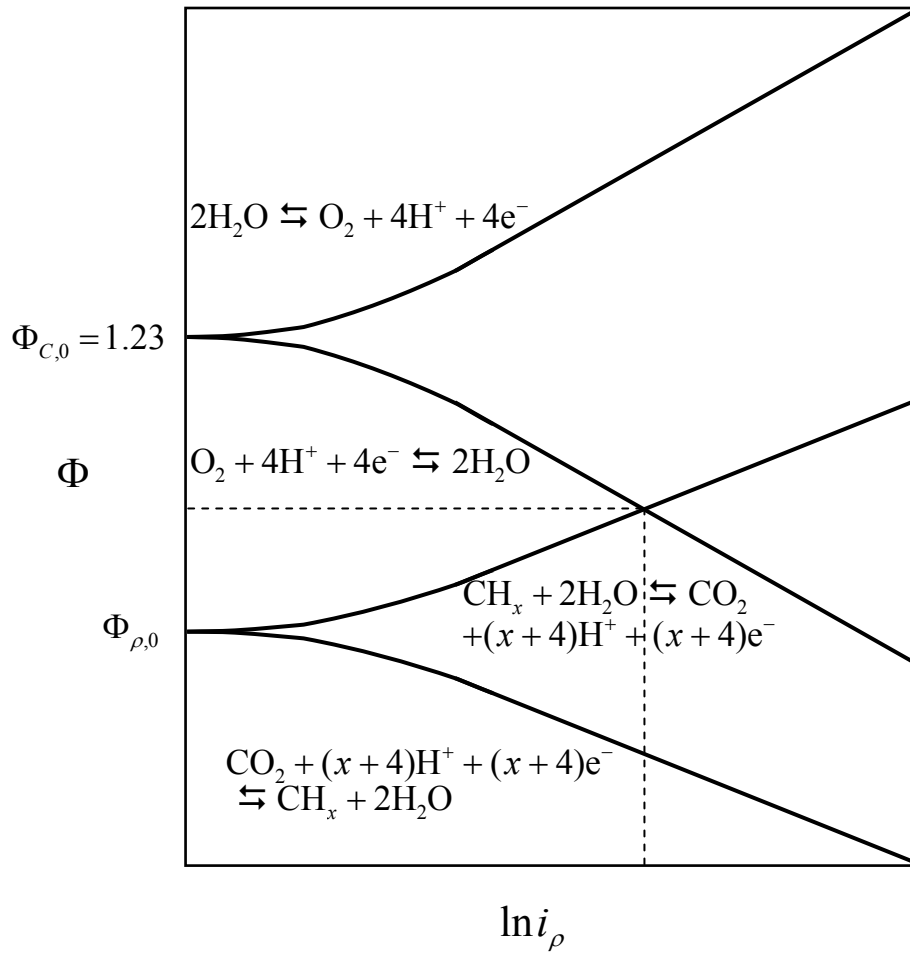
Figure 7-2: Current-potential curves for ORR and a hypothetical impurity oxidation reaction intersecting at mixed potential and a corresponding parasitic current.

An alternate explanation involves the presence of surface oxides via Pt corrosion via one or more reactions mentioned in Table 7-1. However, in an open system such as a fuel cell, reactions involving Pt or C support (reaction 8 in Table 7-1) cannot go on indefinitely and, hence, must also be rejected as the explanation for the observed OCV.

The explanation favored by Bockris and Srinivasan [3] in the study of the half-cell open-circuit potential of ORR in a liquid electrolyte, is an anodic oxidation reaction (reaction 9 in Table 7-1) due to the presence of "an organic impurity present at low concentrations in solution and having a reversible potential of 0.2 to 0.3 V," that compromises the cathodic current of the ORR, i.e., reaction 3 in Table 7-1. In careful experiments they found that the OCV tended toward the 1.23 V value for the ORR when care was taken to rigorously free the electrolyte solution of any traces of impurities. A schematic representation of the resulting mixed potential is given in Figure 7-2, showing anodic and cathodic potential versus current relations for ORR and the oxidation of an organic impurity, the intersection of the two curves representing the graphical solution for OCV as the mixed potential. However, again this explanation involving an organic impurity seems unlikely for the OCV of a H_2-O_2 PEM fuel cell operating for hundreds or thousands of hours.

A more plausible explanation attributes the observed OCV in an operating fuel cell to H_2 crossover and/or internal electrical short-circuiting [4]. Thus, Laraminie and Dicks [4] suggest that the electrolyte supports a very small amount of electronic conductivity, so that small short-circuiting currents are possible. More importantly, however, they propose that hydrogen crossover supports a small "internal current" of around, $i_X \approx 2$ mA, which can cause an activation overpotential of around 0.3 V at the cathode, estimated based on a Tafel equation, $\eta = b\ln(i_X / i_0)$, for ORR with empirical parameters, i.e., a Tafel slope $b = 60$ mV, and an ORR exchange current density $i_0 = 4.0 \times 10^{-5}$ mA/cm². Thorough and careful theoretical analysis presented in this chapter below based on *a priori* parameters supports the latter explanation as the exclusive reason for the observed phenomenon.

A recent experimental investigation of Zhang et al. [1] on the effect of temperature on OCV considered a variety of possible explanations: 1) reduced partial pressures of O_2 and H_2 at higher temperatures due to humidification, as explained by the Nernst equation, 2)

mixed potential of the Pt/PtO catalyst surface, and 3) hydrogen crossover. They concluded that the loss of OCV is due mainly (135 mV at 80 ºC) to the Pt/PtO catalyst surface, and secondarily (56 mV at 80 ºC with Nafion 112) to hydrogen crossover.

In another recent study on membrane degradation and OCV, Sompalli et al. [5] also assume that the OCV is determined by the parasitic current caused by a combination of the permeation of H_2 and Ohmic shorting through the membrane, the latter being a minor contributor. Like Laraminie and Dicks [4], these authors calculate the resulting cathode overpotential via an empirical Tafel equation. Further, they propose OCV as a key diagnostic indicator of membrane health [5]. Thus, membrane thinning and pinhole formation leads to an increase in hydrogen crossover and consequently a decline in OCV. They further reason that the OCV is higher at lower relative humidity (RH), due to the lower H_2 crossover rate [5]. Based on the hypothesis that higher OCVs lead to enhanced chemical degradation of the membrane, the degradation rate would thus be higher at lower RH. They further conclude that any parasitic currents caused by carbon corrosion at the cathode are also negligible, being an order of magnitude smaller as compared with those from hydrogen crossover $(0.1 - 1 \text{ mA/cm}^2)$.

In a more recent publication by Wu et al. [6], the authors conducted a 1200 hrs durability testing close to open-circuit conditions. The drop in the OCV was primarily attributed to mixed potential of Pt/PtO catalyst surface and hydrogen crossover. The authors further argue that at fixed operating conditions, the loss in OCV due to partial oxidation of Pt catalyst if any, should reach a steady state and cannot possibly explain the drop in OCV over time. The authors also observed a dramatic reduction in the electrochemical surface area and increase in the hydrogen crossover current over the 1200 hr test, which could be correlated with the observed drop in the OCV.

In short, despite its ubiquitous nature and practical significance, there is an absence of a clear, quantitative, and unambiguous explanation for the observed OCV in a low temperature PEM fuel cell. We theoretically analyze below the role of hydrogen crossover in PEM fuel cells, in shortchanging the OCV from its promised value of around 1.23 V, and show that hydrogen crossover can, in fact, explain the entire potential loss under open-circuit conditions. Further, it is able to rationalize the commonly observed

effect of temperature and the presence of any pinholes or membrane thinning on the drop in OCV of a PEM fuel cell.

7.1.2 Theory

In addition to serving as the medium for ion transport, the electrolyte layer, e.g., the polymer electrolyte membrane in a PEM fuel cell, serves the important function of keeping the fuel and the oxidant apart, which, of course, is crucial to the proper functioning of a fuel cell. However, since it is not a perfect separator, some of the fuel, e.g., H$_2$, and the oxidant, e.g., O$_2$, crossover to the opposite electrode where they encounter the other reactant in the presence of an electrocatalyst and an electrolyte. These are ideal conditions for the ready occurrence of an electrocatalytic reaction between them, with a consequent electrode overpotential. A schematic of the various processes that occur as a result of the permeation is provided in Figure 7-3. Thus, as shown in Figure 7-3, even though there is no external current i under open-circuit conditions, there are internal short-circuiting currents i_{int} because of: 1) the minor electronic conductivity of the electrolyte membrane, namely the electrical-short circuit current, $i_{S,M}$; and 2) due to the permeating H$_2$ and O$_2$ across the membrane that cause small local crossover currents at the cathode and the anode, respectively (i.e., $i_{X,C}$ and $i_{X,A}$), thus polarizing the two electrodes even under open-circuit conditions. The H$_2$ that permeates over to the cathode from the anode can, in principle, undergo oxidation on the Pt catalyst with O$_2$ either chemically, or electrochemically, or via both of these pathways. However, keeping in mind that the cathode potential Φ_C is very high (~1.0 V) as compared to the thermodynamic potential of hydrogen oxidation reaction (HOR), i.e., $\Phi_{A,0} = 0.0$ V, there is a huge overpotential of around $\eta \sim 1.0$ V for the HOR at the cathode, thus dramatically enhancing the electrochemical route, and making it the likely pathway [7]. Therefore, the chemical route to the hydrogen oxidation at the cathode is ignored. Thus, the electrochemical HOR provides electrons, or a crossover current at cathode, $i_{X,C}$, for the ORR at the cathode even under open-circuit conditions (Figure 7-3).

Similarly, in principle, there is some ORR occurring at the anode because of the small amount of O$_2$ permeating through the PEM from the cathode to the anode.
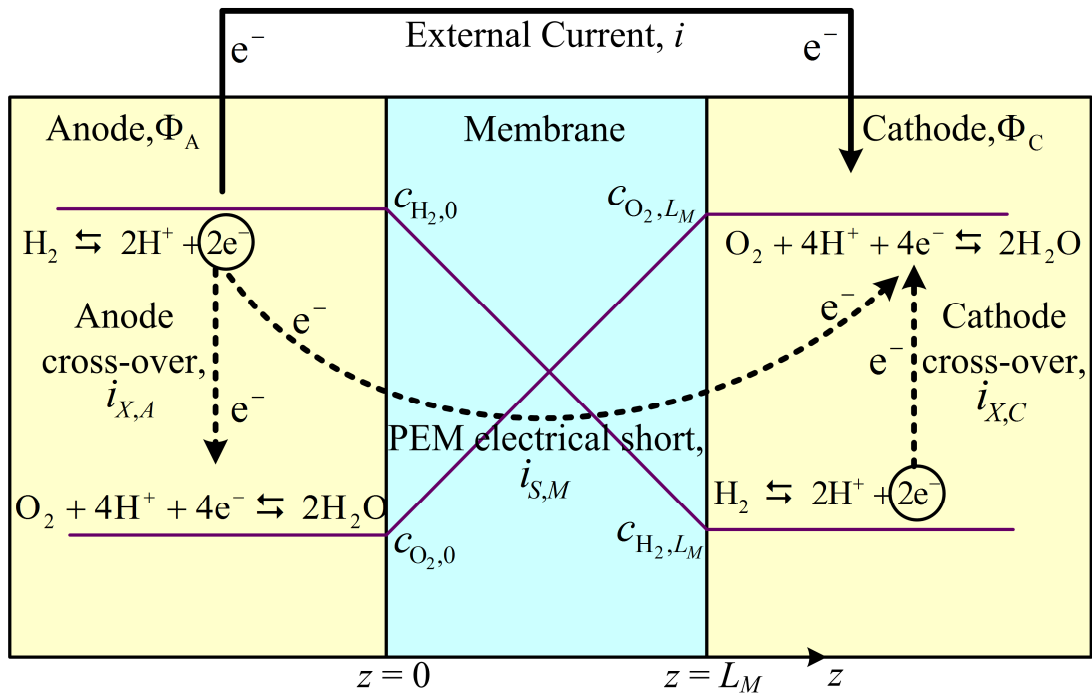
Figure 7-3: Schematic representation of various electrode reactions and the resulting external and internal crossover and electrical short-circuit currents.

This robs electrons from the HOR occurring at the anode, thus resulting in a crossover current at anode, $i_{X,A}$ (Figure 7-3). In addition, there is an electrical-short circuit current across the PEM, $i_{S,M}$ even under open-circuit conditions due to the tiny electronic conductivity of the electrolyte, as shown schematically in Figure 7-3.

Thus, the total internal current, i_{int} at a given electrode consists of the electrical-short circuit current and the crossover current due to fuel permeation, e.g., at the cathode, $i_{int,C} = i_{X,C} + i_{S,M}$.

In other words, the open-circuit condition is not strictly an equilibrium condition, but is rather a steady-state condition with small internal currents. As mentioned above, the steady-state condition is defined at each electrode by the sum over all electrode reactions (HOR and ORR) at a given electrode, $\sum_{\rho} i_{\rho} = 0$, rather than by individual $i_{\rho} = 0$, as required by the equilibrium condition. Thus, at either electrode, the current for the HOR and that for the ORR are equal and opposite at steady state, akin to corrosion currents.

These parasitic currents cause overpotentials at the anode and the cathode, so that the observed OCV is given as

$$OCV = V_0 - \eta_{X,A} + \eta_{X,C} \tag{7.2}$$

where $\eta_{\rho} = \Phi - \Phi_{\rho,0}$ is the overpotential for the electrode reaction ρ. Thus, it is positive for anode and negative for the cathode.

The thermodynamic cell voltage, $V_0 = (\Phi_{0,C} - \Phi_{0,A})$. For the case of liquid water being produced in the low temperature PEM fuel cell, i.e., for $2H_2 + O_2 \leftrightarrows 2H_2O(l)$, the thermodynamic voltage is

$$V_0 = 1.229 - 8.46 \times 10^{-4}(T - 298) + \frac{RT}{4F} \ln p_{H_2}^2 p_{O_2} \tag{7.3}$$

In order to compute the crossover electrode overpotentials $\eta_{X,A}$ and $\eta_{X,C}$ under open-circuit conditions, let us first consider the crossover flux of gaseous species i (H₂ or O₂) across the PEM. Under steady state, isothermal conditions, and no reaction ($\Delta r_i = 0$)

within the Nafion layer, the one-dimensional species diffusion equation in Cartesian coordinates reduces to

$$0 = D_i \frac{\partial^2 c_i}{\partial z^2} \tag{7.4}$$

where c_i is the concentration of the gaseous species i within the Nafion phase, and D_i is the diffusion coefficient of i within Nafion. Note that here we have neglected the convective term since the concentration of H_2 or O_2 is very small, however this may not be the case for direct methanol fuel cells. Integration provides

$$c_i = C_1 z + C_2 \tag{7.5}$$

which may be further differentiated to provide the flux through PEM

$$N_{iz} = -D_i \frac{dc_i}{dz} = -D_i C_1 \tag{7.6}$$

The applicable boundary conditions are (Figure 7-3):

$$
\left.
\begin{array}{lll}
\text{B.C. 1:} & \text{at } z = 0, & c_i\big|_{z=0} = c_{i,0} \\
\text{B.C. 2:} & \text{at } z = L_M, & c_i\big|_{z=L_M} = c_{i,L_M}
\end{array}
\right\} \tag{7.7}
$$

Evaluating the two constants of integration with these two boundary conditions, the concentration profile of species i within the electrolyte layer

$$\frac{c_{i,0} - c_i}{c_{i,0} - c_{i,L_M}} = \frac{z}{L_M} \tag{7.8}$$

i.e., the concentration profile within the membrane is linear for both H_2 and O_2 (Figure 7-3).

The species flux in the membrane then from Fick's law is

$$N_{i,z} = \frac{D_i}{L_M}(c_{i,0} - c_{i,L_M}) = \frac{k_i}{L_M}(p_{i,0} - p_{i,L_M}) \tag{7.9}$$

where c_i is the concentration of the gaseous species i within the Nafion phase, D_i is the diffusion coefficient of i within Nafion, and the membrane permeability, $k_i = D_i \kappa_i / RT$

($mol\,atm^{-1}\,cm^{-1}\,s^{-1}$). Here, the partition-coefficient, $\kappa_i = (c_i/c_{iG})_{eq}$ represents the solubility of the gaseous species i in the membrane.

The permeating species (H₂ or O₂) undergoes electrochemical reaction ρ (HOR or ORR) at the electrode, as shown schematically in Figure 7-3. Thus, the corresponding current density

$$i_X = F\nu_{\rho e^-}N_{i,z} = \frac{F\nu_{\rho e^-}k_i}{L_M}(p_{i,0} - p_{i,L_M})$$ (7.10)

where F is the Faraday's constant. At steady-state, this diffusion flux is equal to the rate of the electrode reaction, which may be described via Butler-Volmer equation of the form, with $\eta_\rho = \Phi - \Phi_{\rho,0}$ [8]

$$i_X = i_{\rho,0}\left|2\sinh\left\{\frac{\alpha_\rho^\bullet\nu_{\rho e^-}^\bullet F(\Phi - \Phi_{\rho,0})}{RT}\right\}\right|\qquad (\rho = A,\,C)$$ (7.11)

where $\alpha_\rho^\bullet$ is the effective transfer coefficient of the electrode reaction ρ, taken as symmetry factor of the rate-limiting step (RLS) (typically ½) in the sequence of molecular steps involved in the electrode reaction ρ, and $\nu_{\rho e^-}^\bullet$ is the stoichiometric coefficient of electrons in the RLS. Alternatively, $\alpha_\rho^\bullet$ and $\nu_{\rho e^-}^\bullet$ may be clubbed together into an effective transfer coefficient α_ρ, as done by Thampan et al. [8].

In the above, the exchange current density on the basis of the geometric electrode area [8]

$$i_X = \gamma_M i_X^* \qquad ; \qquad i_0 = \gamma_M i_0^*$$ (7.12)

where, the current density with the asterisk, i_0^*, is defined in terms of per unit active metal catalyst surface area and γ_M is the catalyst roughness factor defined as

$$\gamma_M = \frac{\text{Actual electrocatalyst active interfacial area}}{\text{Geometric electrode area}}$$ (7.13)

When the interfacial area at the atomic level is considered, it can be substantially more than the geometric area. In typical fuel cells, e.g., depending upon the catalyst particle

size and loading γ_M is of the order of 100. The roughness factor may be estimated from [8]

$$\gamma_M = \varphi_I m_M \left(\frac{6\varphi_M}{\rho_M d_M} \right) \tag{7.14}$$

where φ_M accounts for the part of the metal crystallite of diameter d_M which is not accessible for reaction, e.g., the side which is in contact with the support, and φ_I is the fraction of the available metal surface participating in electrocatalysis. This would be less than unity, e.g., if not all of the available metal area is in contact with the ionomer, and hence depends upon ionomer loading.

Further, the exchange-current density under actual conditions in a PEM fuel cell is related to that under reference conditions via

$$i_0 = \gamma_M \left(\frac{p_i}{p_{i,ref}} \right) \exp\left\{ -\frac{E_{\Phi_0}}{R} \left(\frac{1}{T} - \frac{1}{T_{ref}} \right) \right\} i_{0,ref}^* \tag{7.15}$$

where p_i is the partial pressure of the permeating species at the electrode.

The final equation needed for the steady-state at an electrode under OCV conditions (i.e., when the external current $i = 0$) is

$$\sum_\rho i_\rho = 0 \tag{7.16}$$

i.e., the sum of current densities of HOR and ORR occurring at an electrode (anode or cathode) is zero. Finally, for completeness, we must account for the electrical-short circuit current $i_{S,M}$ across the PEM as well, which from Ohm's law

$$i_{S,M} \approx V \left(\frac{\sigma_{M,e^-}}{L_M} \right) \tag{7.17}$$

where σ_{M,e^-} is the electronic conductivity of the membrane. This current must be added to the crossover currents at the two electrodes to compute the overpotential.

7.1.3 PEM Fuel Cell Analysis

Let us apply the above analysis to the crossover of H$_2$ and the ensuing HOR at the cathode (Figure 7-3). The crossover current density corresponding to the hydrogen flux in the membrane is

$$i_{X,C} = \frac{(F\nu_{HOR,e^-})k_{H_2}}{L_M}(p_{H_2,0} - p_{H_2,L_M})$$

(7.18)

which is also equal to that from the HOR kinetics at the cathode at the overpotential $\eta_{X,C}$

$$i_{X,C} = \gamma_{M,C}i^*_{HOR,0,ref}\left(\frac{p_{H_2,L_M}}{p_{H_2,ref}}\right)\exp\left\{-\frac{E_{HOR,\Phi_0}}{R}\left(\frac{1}{T}-\frac{1}{T_{ref}}\right)\right\}2\sinh\left\{\frac{\alpha^\bullet_{HOR}\nu^\bullet_{HOR,e^-}F(\eta_{X,C}+V_0)}{RT}\right\}$$

(7.19)

where we have combined the Butler-Volmer equation with the correlation for exchange-current density. Of course, since this is equal and opposite of the ORR current at the cathode

$$i_{X,C} = \gamma_{M,C}i^*_{ORR,0,ref}\left(\frac{p_{O_2,L_M}}{p_{O_2,ref}}\right)\exp\left\{-\frac{E_{ORR,\Phi_0}}{R}\left(\frac{1}{T}-\frac{1}{T_{ref}}\right)\right\}2\sinh\left\{\frac{\alpha^\bullet_{ORR}\nu^\bullet_{ORR,e^-}F(\eta_{X,C})}{RT}\right\}$$

(7.20)

The above 3 equations, Eq. (7.18) - (7.20) contain 3 unknowns, namely, the partial pressure of H$_2$ at the cathode p_{H_2,L_M}, the crossover current at the cathode $i_{X,C}$, and the cathode overpotential $\eta_{X,C}$ under open-circuit conditions, which can all hence be found via simultaneous solution.

Limiting Case

Let us consider the limiting case when $p_{H_2,L_M} \to 0$. This is entirely plausible because of the very high overpotential at the cathode for HOR. Then the solution is greatly simplified. Thus, from Eq. (7.18), we have

$$i_{X,C} \approx \frac{(F\nu_{HOR,e^-})k_{H_2}}{L_M}p_{H_2,0}$$

(7.21)

which can, hence, be directly evaluated from the permeability data for H_2. Thereupon, the cathode overpotential $\eta_{X,C}$ can be found from either of the two kinetics equations for HOR or ORR above (Eq. (7.19) or (7.20)). Finally, including the electrical-short circuit current $i_{S,M}$, Eq. (7.17), as well, we have

$$\eta_{X,C} = \left(\frac{RT}{\alpha^{\bullet}_{ORR} v^{\bullet}_{ORR,e^-} F} \right) \sinh^{-1} \left\{ \frac{(F v_{HOR,e^-}) k_{H_2} p_{H_2,0} + V \sigma_{M,e^-}}{2 L_M i_{ORR,0}} \right\} \tag{7.22}$$

An identical analysis can be done for the permeation of O_2, and the resulting open-circuit anode overpotential. For the limiting case, as above,

$$\eta_{X,A} = \left(\frac{RT}{\alpha^{\bullet}_{HOR} v^{\bullet}_{HOR,e^-} F} \right) \sinh^{-1} \left\{ \frac{(F v_{ORR,e^-}) k_{O_2} p_{O_2,L_M} + V \sigma_{M,e^-}}{2 L_M i_{HOR,0}} \right\} \tag{7.23}$$

Equations (7.22) and (7.23) may finally be substituted into Eq. (7.2) to evaluate V, i.e., OCV. In the event that the electronic conductivity of the membrane is small, the second term in the curly brackets can further be neglected. Clearly, however, the validity of the model depends upon the veracity of the model parameters, discussed next.

7.1.4 Model Parameters

Sakai et al. [9, 10] hypothesized that H_2 or O_2 permeates mainly through the hydrated ion-cluster regions of the Nafion membrane, while Broka and Ekdurge [11] suggest that the permeation process involves both, the hydrated ionic clusters and the amorphous region of Nafion. It is known, thus, that hydrated Nafion has higher gas permeability as compared to dry Nafion but lower than that in water [7]. Thus, dry Nafion has permeability coefficient for H_2 or O_2 similar to or lower than that for Teflon, while hydrated Nafion membrane has permeability coefficient approaching that in water [7, 9, 10]. The correlation provided by Kocha et al. [7] for the permeability of hydrogen in Nafion is used in this study,

$$k_{H_2} = 6.6 \times 10^{-8} \exp\left(-\frac{21030 \, \text{J mol}^{-1}}{RT} \right) \text{mol bar}^{-1} \, \text{cm}^{-1} \, \text{s}^{-1} \tag{7.24}$$

The permeability of oxygen in Nafion is approximately half that of hydrogen in Nafion [7, 9, 11]. Thus, we assume

$$k_{O_2} = \frac{k_{H_2}}{2} \quad \text{mol bar}^{-1} \text{ cm}^{-1} \text{ s}^{-1} \tag{7.25}$$

The electrical conductivity of Nafion, however, is not as well documented in the literature. Using a similar rationale as above, the electrical resistivity of Nafion in the dry state may be expected to be close to that of Teflon, while in the hydrated state it would be approaching the electrical resistivity of deionized water. The resistivity of Nafion at 50% RH is about $6 \times 10^5 \, \Omega \, \text{cm}$ [12], which provides an estimate for the electrical conductivity of Nafion, $\sigma_{M,e^-} \approx 1 \times 10^{-6} \, \text{S cm}^{-1}$, a value similar to the electrical conductivity of water in equilibrium with CO_2 in air [13]. On the other hand, Sompalli et al. [5] give a membrane electronic resistance of $1 - 20 \, \text{k}\Omega \, \text{cm}^2$, which results in $0.1 - 0.02 \, \text{mA cm}^{-2}$.

For the HOR, $\alpha_{HOR}^{\bullet}$ is assumed to be $1/2$, and the exchange current density is taken as $i_{HOR,0,ref}^{*} = 1 \times 10^{-3} \, \text{A cm}^{-2}$ of metal catalyst surface, commonly reported in the literature [8]. The effective activation energy for HOR on PtRu/C is taken as $E_{HOR,\Phi_0} = 34.6 \, \text{kJ mol}^{-1}$, higher than that on Pt [14]. For the ORR the exchange current density is of the order $10^{-10} \, \text{A cm}^{-2}$, i.e., $i_{ORR,0,ref}^{*} = 1 \times 10^{-10} \, \text{A cm}^{-2}$ of metal catalyst surface [15]. $\alpha_{ORR}^{\bullet}$ similar to $\alpha_{HOR}^{\bullet}$ is considered to be $1/2$, and the effective activation energy on Pt/C as given by Neyerlin et al. [16], is taken as $E_{ORR,\Phi_0} = 67 \, \text{kJ mol}^{-1}$.

The roughness factor may be estimated using catalyst loading and nanoparticles size as described above [8]. However, here, values reported by Song et al. [14], obtained experimentally utilizing the surface cyclic voltammetry measurements and shown in Table 7-2 are adopted for analysis. Thus, all the model parameters are adopted from the literature as discussed above, and are summarized in Table 7-3.

Table 7-2: Roughness factor (cm^2 metal cm^{-2} geometric electrode area) for anode and cathode as determined by Song et al. [14] in low current density region, measured at 3.0 atm pressure and 100% RH.

Temperature ^oC	$\gamma_{M,Anode}$	$\gamma_{M,Cathode}$
23	44.5	305.0
40	28.3	168.0
60	28.3	152.0
80	30.7	106.0
100	13.0	78.0

Table 7-3: Parameters employed in the OCV model

Parameter	Value	Units
k_{H_2}	$6.6 \times 10^{-8} \exp\left(-\dfrac{21030\,\text{J mol}^{-1}}{RT}\right)$	mol bar^{-1} cm^{-1} s^{-1}
k_{O_2}	$\dfrac{k_{\text{H}_2}}{2}$	mol bar^{-1} cm^{-1} s^{-1}
σ_{M,e^-}	1×10^{-6}	S cm^{-1}
$\alpha^{\bullet}_{HOR}$	$1/2$	–
$i^{*}_{HOR,0,ref}$	1×10^{-3}	A cm^{-2}
E_{HOR,Φ_0} #	34.6	kJ mol^{-1}
$\alpha^{\bullet}_{ORR}$	$1/2$	–
$i^{*}_{ORR,0,ref}$	1×10^{-10}	A cm^{-2}
E_{ORR,Φ_0} *	67.0	kJ mol^{-1}
T_{ref}	293	K
$c_{\text{H}_2,ref}$	3.96×10^{-5}	mol cm^{-3}
$c_{\text{O}_2,ref}$	8.32×10^{-6}	mol cm^{-3}

\# Activation energy for PtRu/C

* Activation energy for Pt/C
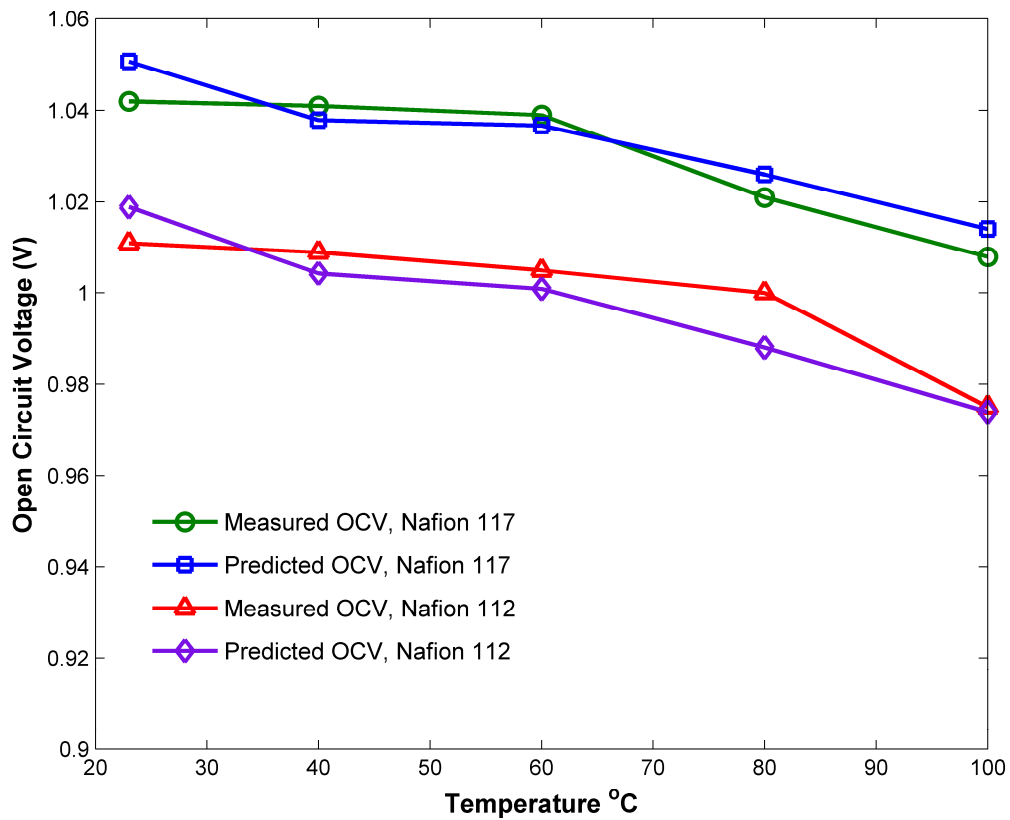
Figure 7-4: Comparison of model prediction with experimentally observed OCV for PEM fuel cell. Experimental values are taken from Ref. [1]. (Anode: H$_2$, Cathode: Air, 3 atm, 100% RH)
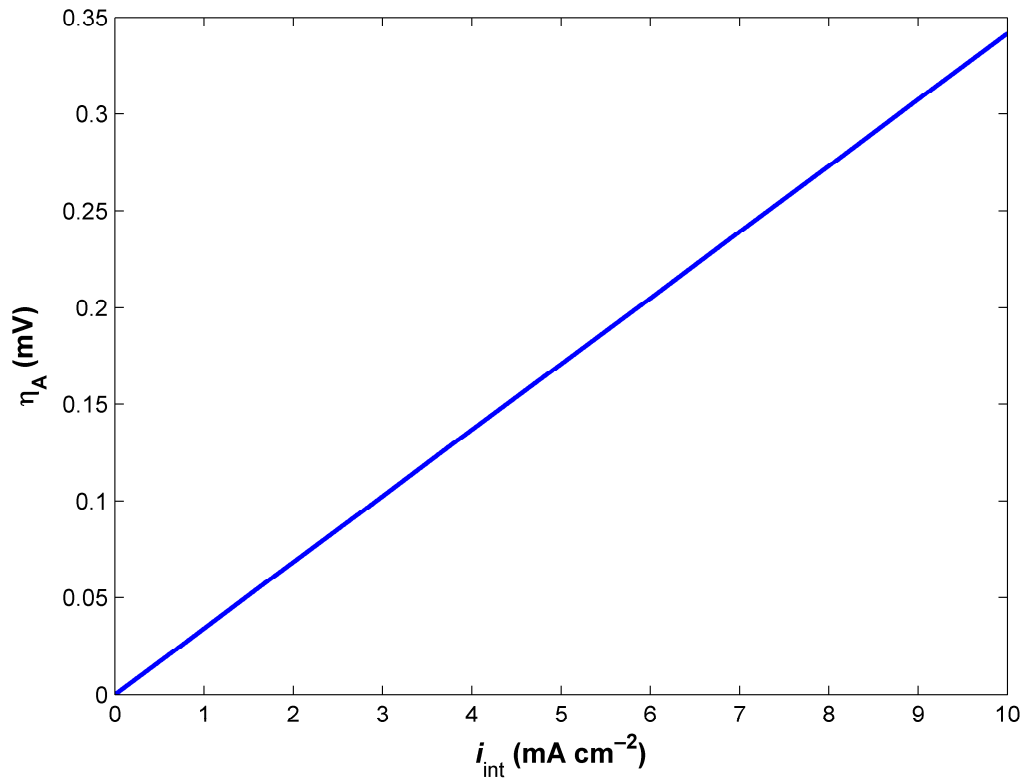
Figure 7-5: Anode overpotential as a function of total internal current.
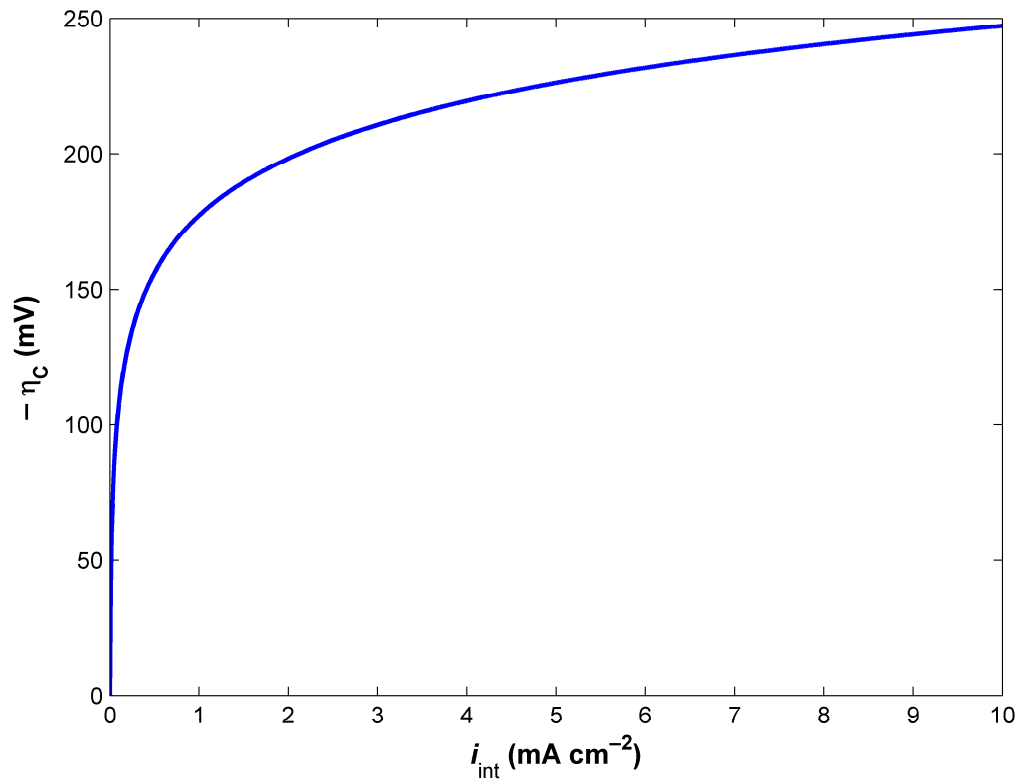
Figure 7-6: Cathode overpotential as a function of total internal current.

7.1.5 Results and Discussion

Zhang et al. [1] have experimentally monitored the OCV for PEM fuel cell with H_2 as the anode feed and air as the cathode. In their experiments, the anode and cathode consisted of PtRu/C and Pt/C, respectively with a total loading of 1.0 mg cm^{-2}, and the roughness factors for the anode and the cathode provided in Table 7-2. Thus, Eq. (7.2), (7.22) and (7.23) are solved simultaneously to calculate the OCV using the parameters from Table 7-2 and Table 7-3. Figure 7-4 compares the model predictions with experimental observations of Zhang et al. [1] for PEM fuel cell at 100% RH and 3.0 atm pressure, as a function of temperature and membrane thickness. The comparison between theory and experiments is hence quantitative with no fitted parameters. Further, as expected, the thicker membrane (Nafion 117) would have lower crossover currents and hence, higher observed OCV. Finally, the variation in the observed OCV as a function of temperature depends on a number of parameters, e.g. ORR activation energy, roughness factor. In this particular case, the change in slope of observed OCV may be attributable to the change in slope of the roughness factor as a function of temperature (Table 7-2).

In order to further investigate the relative significance of the hydrogen and oxygen crossover, Figure 7-5 and Figure 7-6 provide the effect of the total internal current, i_{int} on the anode and cathode overpotential, respectively.

It is evident from Figure 7-5, that the anode overpotential is insignificant even for an internal current as high as 10 mA cm^{-2}. However, Figure 7-6 indicates that the cathode overpotential is substantial and, in fact accounts for practically all of the observed incongruity between experimental OCV and the reversible potential. Further, we find that the electrical short-circuit current is approximately one order of magnitude lower than the crossover current for a pin-hole free MEA, an observation similar to that by Cleghorn et al. [17]. Thus, the Ohmic shorting does not noticeably affect the observed OCV. In view of this, thus, Eq. (7.22), can be further simplified into

$$\eta_{X,C} = \left(\frac{RT}{\alpha^{\bullet}_{ORR} \nu^{\bullet}_{ORR,e^-} F} \right) \sinh^{-1} \left\{ \frac{(F \nu_{HOR,e^-}) k_{H_2} p_{H_2,0}}{2 L_M i_{ORR,0}} \right\} \qquad (7.26)$$

Further, since the anode overpotential is negligible as compared to the cathode overpotential, we have, $V \approx V_0 + \eta_{X,C}$. Substituting Eq. (7.3) and (7.26) in this, thus

$$OCV = 1.229 - 8.46 \times 10^{-4}(T - 298) + \frac{RT}{4F}\ln p_{H_2}^2 p_{O_2} + \left(\frac{RT}{\alpha_{ORR}^\bullet v_{ORR,e^-}^\bullet F}\right)\sinh^{-1}\left\{\frac{(Fv_{HOR,e^-})k_{H_2}p_{H_2,0}}{2L_M i_{ORR,0}}\right\}$$

$$(7.27)$$

In short, thus, the observed OCV at a given temperature and gas partial pressures and its deviation from the thermodynamic potential of 1.23 V is entirely explained by the cathode overpotential due to hydrogen permeation, which is adequately described by the above relation.

Pronounced effect of oxygen and hydrogen crossover on membrane degradation under open-circuit conditions have been reported by Inaba et al. [18] and Endoh et al. [19], respectively. Ionomer loss and membrane thinning has been observed under open circuit conditions by Liu and Crum [20], which may result in pinhole formation and increased gas crossover. Of course, with the onset of membrane thinning and pinhole formation due to chemical degradation and fatigue, the crossover current increases, eventually leading to the failure of the MEA. It must be noted that gas crossover in the absence of catalyst does not cause membrane degradation. Consequently, the permeation of reactants and their subsequent catalyzed electrochemical reaction is critical for the degradation of membrane.

While the mechanism is not entirely clear, the high rate of membrane degradation at OCV may be attributed to H_2O_2 [21]. Thus, it may be argued that at the low cathode overpotential under OCV conditions, more H_2O_2 is produced, which is an intermediate species in the ORR. At higher overpotentials at the cathode, H_2O_2 can be further reduced into water. These qualitative observations insinuate a strong dependence between fuel permeation and OCV. Understanding the correlation between gas crossover and OCV, is thus of fundamental significance. The model presented in this study quantitatively shows that OCV is an indication of the fuel crossover and its electrochemical consumption, implicated by the enhanced membrane degradation under OCV conditions.

Furthermore, crossover of the reactant gases can also cause carbon corrosion [22]. Catalyst dissolution and precipitation within the membrane has been observed under open circuit conditions and it was found that the location of catalyst precipitation is affected by the fuel permeation through the membrane [23]. Finally, the negative effect of fuel crossover on OCV is particularly significant for direct alcohol fuel cells [24-27]. The current modeling framework can also be extended to explicate these findings.

7.2 Fuel Cell Performance Model

7.2.1 Kinetic and Diffusional Processes at an Electrode

Let us consider the case where the rate of the interfacial electrode *OR* is limited by the diffusion of one of the terminal species participating in it, as shown schematically by Figure 7-7a. As shown in this figure, one might encounter a situation where availability at the electrode interface of a gaseous component, e.g., O_2, is diffusion limited through the electrolyte layer (e.g., Nafion®, or molten carbonate) coating the catalyst surface. Alternatively, O_2 diffusion might be limited across the GDL or H^+ diffusion to the electrode interface might be limited across the polymer electrolyte membrane, e.g., under hot and dry conditions. Let us, for specificity, consider here the case of diffusion limitation of species *i* across the electrolyte layer (Figure 7-7a), although the analysis is readily adapted to the other situations.

Within the framework of the RR Graph approach, the overall process (*OP*) of diffusion and surface reaction might be construed as a two-step process, as shown schematically in Figure 7-7b. Here s_D refers to the film diffusion step, while s_K is the electrode kinetic step in the *OP*. It is then clear that at the intermediate node, n_2, the flux of step s_D is equal to that of step s_K, as suggested by KFL.

Applying Fick's law for describing the diffusive flux of species *i* in the *z*-direction across the film,

$$N_{iz} = -D_i^e \frac{dc_i}{dz} \qquad (7.28)$$
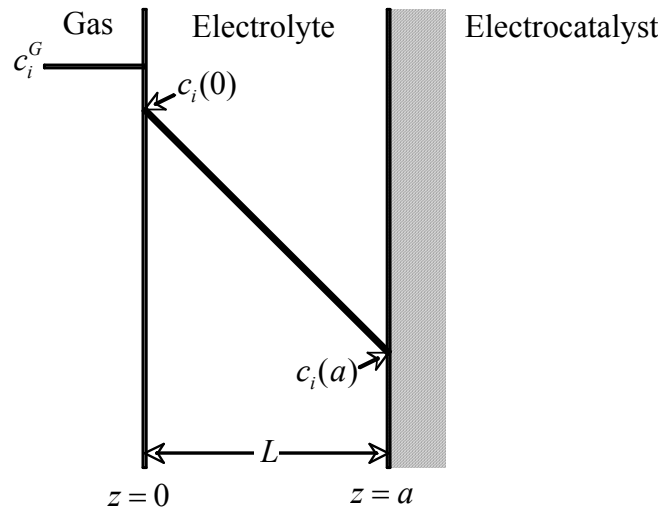
(a)
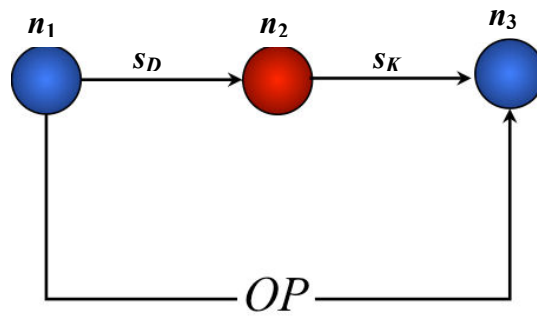
(b)

Figure 7-7: Diffusion-limited electrode reaction at three-phase interface.

where D_i^e is the effective diffusion coefficient of i in the film. The solution for flux in the film is obtained by integrating the Fickian equation by assuming that the flux $N_{iz} =$ constant, as is the effective diffusivity, along with quasi-equilibrium of gas dissolution process at the gas-electrolyte interface (Figure 7-7a). Thus

$$N_{iz} = P_i \left\{ c_i^G - \frac{c_i(a)}{\kappa_i} \right\} \qquad \frac{\text{mol}}{\text{cm}^2 \text{ MEA.s}} \qquad (7.29)$$

where the partition coefficient κ_i and the permeability P_i of species i in the film are

$$\kappa_i \equiv \left(\frac{c_i}{c_i^G} \right)_0 \quad ; \quad P_i \equiv \frac{\kappa_i D_i^e}{L} \qquad (7.30)$$

Further, adopting the pseudo-irreversible form for the interfacial electrode kinetics and assuming first-order kinetics in species i

$$r_\rho^* = k_\rho^* c_i(a) \qquad \frac{\text{mol}}{\text{cm}^2 \text{ cat.s}} \qquad (7.31)$$

where k_ρ^* is obtained by a similar relationship as Eq. (7.11)

$$\frac{k_\rho^*}{\vec{k}_{\rho,\Phi_0}^*} = \frac{r_\rho^*}{r_{\rho,0}^*} = \frac{i_\rho^*}{i_{\rho,0}^*} = \left\{ 2\sinh\left(\frac{\alpha_\rho^\bullet v_{\rho e^-}^\bullet F \eta_\rho}{RT} \right) \right\} \qquad (7.32)$$

To equate the steady-state diffusion and reaction fluxes at the interface $z = a$ (Figure 7-7a) or at node, n_2 (Figure 7-7b), the reaction rate must be written in terms of unit area of MEA, as is the case in Eq. (7.29) Thus,

$$N_{iz}(a) = (-v_{\rho i})r_\rho = (-v_{\rho i})\gamma_M k_\rho^* c_i(a) \qquad \frac{\text{mol}}{\text{cm}^2 \text{ MEA.s}} \qquad (7.33)$$

Equating Eqs. (7.29) and (7.33), and solving for the unknown interfacial concentration $c_i(a)$ we have

$$c_i(a) = \frac{\kappa_i c_i^G}{1 + \dfrac{(-v_{\rho i})\gamma_M k_\rho^* \kappa_i}{P_i}} \qquad (7.34)$$

where the term besides 1 in the denominator represents the ratio of the maximum rate of reaction (i.e., when $c_i(a) = \kappa_i c_i^G$) to the maximum rate of diffusion (i.e., when $c_i(a) = 0$).

Using $c_i(a)$ from Eq. (7.34) in Eq. (7.31) along with

$$i_\rho = \gamma_M i_\rho^* = \gamma_M (F v_{\rho e^-} r_\rho^*) \tag{7.35}$$

provides the current density as

$$i_\rho = \frac{\gamma_M F v_{\rho e^-} k_\rho^* \kappa_i c_i^G}{1 + \dfrac{(-v_{\rho i})\gamma_M k_\rho^* \kappa_i}{P_i}} \tag{7.36}$$

When the rate of diffusion $\ll$ the rate of the overall electrode reaction, the 1 in the denominator in this expression can be neglected as compared with the companion term, resulting in the current density under diffusion limited conditions, i.e.,

$$i_{\rho,L} \equiv \left(\frac{v_{\rho e^-}}{-v_{\rho i}}\right) F P_i c_i^G \tag{7.37}$$

which is called the limiting current density, corresponding to the maximum possible diffusion flux across the film, i.e., corresponding to $c_i(a) \to 0$. Combining the last two equations

$$\frac{i_\rho}{i_{\rho,L}} = \frac{\dfrac{(-v_{\rho i})\gamma_M k_\rho^* \kappa_i}{P_i}}{1 + \dfrac{(-v_{\rho i})\gamma_M k_\rho^* \kappa_i}{P_i}} \tag{7.38}$$

which may be rearranged into

$$\frac{(-v_{\rho i})\gamma_M k_\rho^* \kappa_i}{P_i} = \frac{i_\rho / i_{\rho,L}}{1 - i_\rho / i_{\rho,L}} \tag{7.39}$$

Now, from Eq. (7.35) at equilibrium

$$i_{\rho,0} = \gamma_M F v_{\rho e^-} r_{\rho,0}^* = \gamma_M F v_{\rho e^-} \vec{k}_{\rho,\Phi_0}^* c_{i,0}(a) \tag{7.40}$$

Further, since there are no diffusional limitations at equilibrium, $c_{i,0}(a) = \kappa_i c_i^G$, so that

$$i_{\rho,0} = \gamma_M F v_{\rho e^-} \vec{k}^*_{\rho,\Phi_0} \kappa_i c_i^G \tag{7.41}$$

From this equation and that for the limiting current density, the ratio

$$\frac{i_{\rho,0}}{i_{\rho,L}} = \frac{(-v_{\rho i})\gamma_M \vec{k}^*_{\rho,\Phi_0} \kappa_i}{P_i} \tag{7.42}$$

which may be used in Eq. (7.38) to provide

$$\frac{k^*_\rho}{\vec{k}^*_{\rho,\Phi_0}} = \frac{i_\rho / i_{\rho,0}}{1 - i_\rho / i_{\rho,L}} \tag{7.43}$$

Comparing this to Eq. (7.32)

$$2\sinh\left(\frac{\alpha^\bullet_\rho v^\bullet_{\rho e^-} F \eta_\rho}{RT}\right) = \frac{i_\rho / i_{\rho,0}}{1 - i_\rho / i_{\rho,L}} \tag{7.44}$$

rearranging which yields [8]

$$\eta_\rho = \left(\frac{RT}{\alpha^\bullet_\rho v^\bullet_{\rho e^-} F}\right)\sinh^{-1}\left[\frac{1}{2}\left\{\frac{i_\rho / i_{\rho,0}}{1 - i_\rho / i_{\rho,L}}\right\}\right]$$
$$= \eta_{\rho,K} + \eta_{\rho,D} \tag{7.45}$$

which is the combined overpotential associated with kinetic and diffusional processes at the electrode, as evident from Figure 7-7a, i.e., $\eta_{OP} = \eta_K + \eta_D$, which is the equivalent of Kirchhoff's potential law (KPL) of electrical circuits.

7.2.2 Lumped Fuel Cell Model

A schematic of a typical membrane-electrode-assembly (MEA) consisting of a five layer assembly is provided in Figure 7-8. We can treat this MEA in terms of RR Graph approach as shown in Figure 7-9a. The different branches in Figure 7-9a represent the interconnected steps of diffusion of reactant gases through the GDL at the anode, electrode reaction at the anode, electrolyte diffusion, reaction at the cathode, and gas diffusion in the cathode GDL.
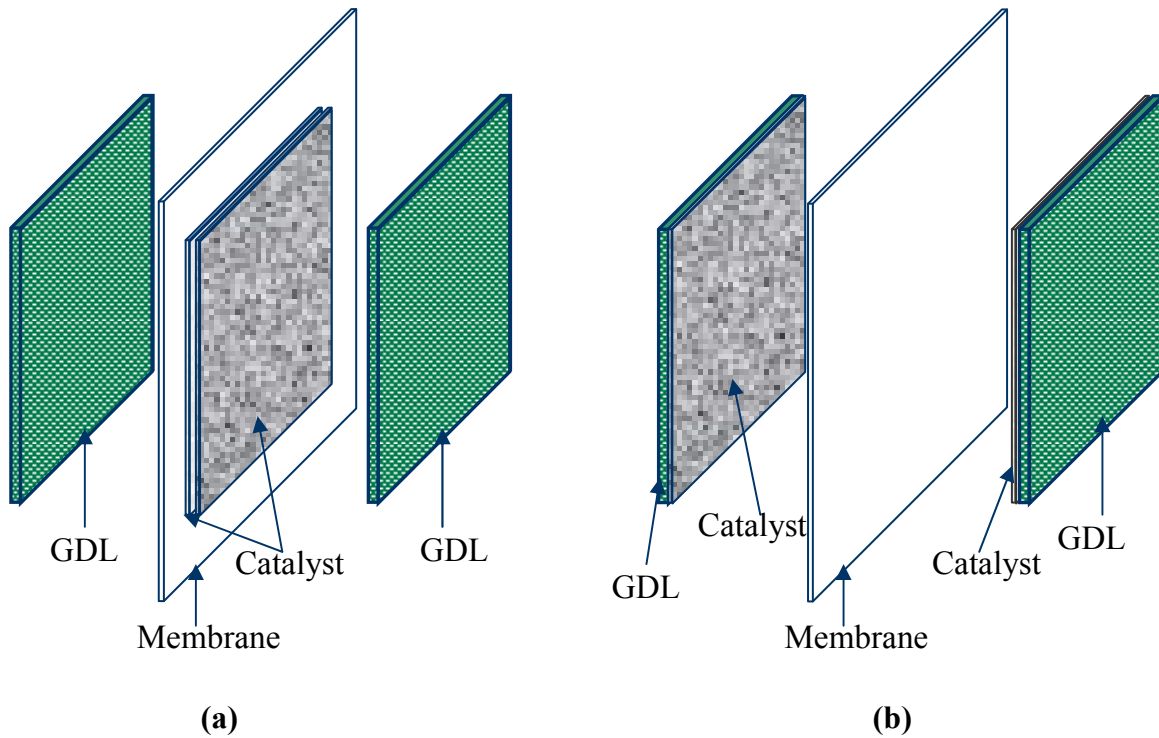
Figure 7-8: Five layer membrane-electrode assembly for fuel cells a) catalyzed membrane, b) catalyzed GDL

While different species participate in these different steps, it is remarkable that continuity of flux at the different intermediate nodes can be assumed, in addition to the sum of affinity (potential) drop in the branches adding up to that for the overall process (*OP*). These are, actually, the equivalent of Kirchhoff's flux and potential laws (KFL and KPL). In fact, the electrical equivalent of the fuel cell shown in Figure 7-9b is another form of the RR graph in Figure 7-9a, where the branches have been replaced by resistors representing the different elements.

In the absence of current, $V = V_0$, i.e., potential drop η across each branch is zero, where we imagine the OP to be replaced by a power source, as shown in Figure 7-9b. As a current i is drawn, the drop in potential registered by the power source is equal to the sum of the potential drops across all the branches in series. Thus, the KPL implies that

$$V_0 - V = \underbrace{(\eta_{A,D} + \eta_{A,K})}_{\eta_A} + \eta_{EL} - \underbrace{(\eta_{C,D} + \eta_{C,K})}_{\eta_C} + \eta_I \tag{7.46}$$

where we have included η_I as another possible potential drop across an interface with the MEA, if it is not well-assembled, or may become delaminated during use. Further, it may be recalled that the sum of diffusion and electrode reaction overpotential is given by Eq. (7.45). Thus,

$$V = V_0 - \eta_A + \eta_C - \eta_{EL} - \eta_I \tag{7.47}$$

which accounts for the fact that the sign of η_C is negative as $v_{Ce^-} < 0$. Next, the losses for the anode may be written from Eq. (7.45), with $\rho = A$, as

$$\eta_A = \left(\frac{RT}{\alpha_A^\bullet v_{Ae^-}^\bullet F} \right) \sinh^{-1} \left[\frac{1}{2} \left\{ \frac{i_A / i_{A,0}}{1 - i_A / i_{A,L}} \right\} \right] \tag{7.48}$$

When using this expression, we will assume that $v_{Ae^-}^\bullet = +1$ for the RLS in the anode mechanism for PEM (or acid electrolyte) fuel cell, while $\alpha_A^\bullet = 1/2$.

On the other hand, for cathode, with $\rho = C$, the evidence is that $v_{Ce^-}^\bullet = -2$ (based on Tafel slope) for the RLS in the mechanism for the ORR in PEM (or acid electrolyte) fuel cell, and we will further assume that $\alpha_C^\bullet = 1/2$.
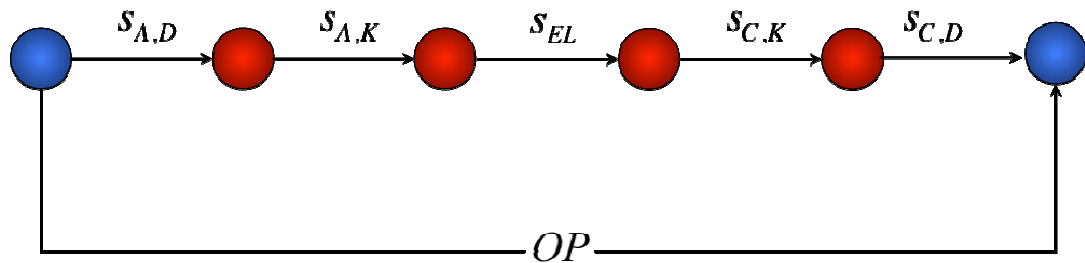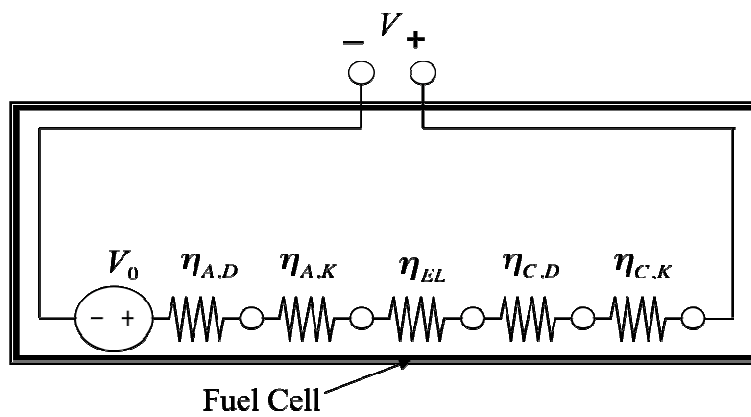
Figure 7-9: a) RR Graph for transport and reaction in a fuel cell MEA. b) An electrical analog of fuel cell internals including an ideal voltage source and internal resistances.

Furthermore, we need to account for the parasitic current at the cathode due to hydrogen crossover, as discussed in the last section

$$\eta_C = \left(\frac{RT}{\alpha_C^\bullet v_{Ce^-}^\bullet F} \right) \sinh^{-1}\left[\frac{1}{2}\left\{ \frac{(i_C + i_{C,X})/i_{C,0}}{1 - (i_C + i_{C,X})/i_{C,L}} \right\} \right] \tag{7.49}$$

where the crossover current is given by Eq. (7.21).

For the electrolyte layer, we assume that ohm's law is applicable, namely

$$i_{EL} = -\sigma_{EL} \frac{d\phi_{EL}}{dz} \tag{7.50}$$

which may be integrated for constant current density in the electrolyte layer to yield

$$\eta_{EL} = \Delta\phi_{EL} = i_{EL}\left(\frac{L_{EL}}{\sigma_{EL}} \right) \tag{7.51}$$

Thus, combining the above equations, along with KFL evident from the equality of fluxes or currents at each of the nodes in Figure 7-9, i.e., $i = i_A = i_C = i_{EL}$, there results [8]

$$V = V_0 - \frac{RT}{\alpha_A^\bullet v_{Ae^-}^\bullet F} \sinh^{-1}\left\{ \frac{1}{2}\left(\frac{i/i_{A,0}}{1 - i/i_{A,L}} \right) \right\} + \frac{RT}{\alpha_C^\bullet v_{Ce^-}^\bullet F} \sinh^{-1}\left\{ \frac{1}{2}\left(\frac{(i + i_{C,X})/i_{C,0}}{1 - (i + i_{C,X})/i_{C,L}} \right) \right\} - i\left(\frac{L_{EL}}{\sigma_{EL}} \right) - i(R_I) \tag{7.52}$$

which is the final expression for V versus the current density i in terms V_0 and the characteristic parameters, namely, the exchange current densities for the anode and the cathode reactions, and the limiting current densities for the two electrodes, and the electrolyte conductivity, etc. An example of a resulting plot is provided in Figure 7-10. $\gamma_M = 116.62$ is predicted for the ETEK electrodes using correlations provided in Ref. [8]. It is evident that the predictions are reasonable with the *a priori* parameters, and that the crossover current makes a material difference only at very low current densities.
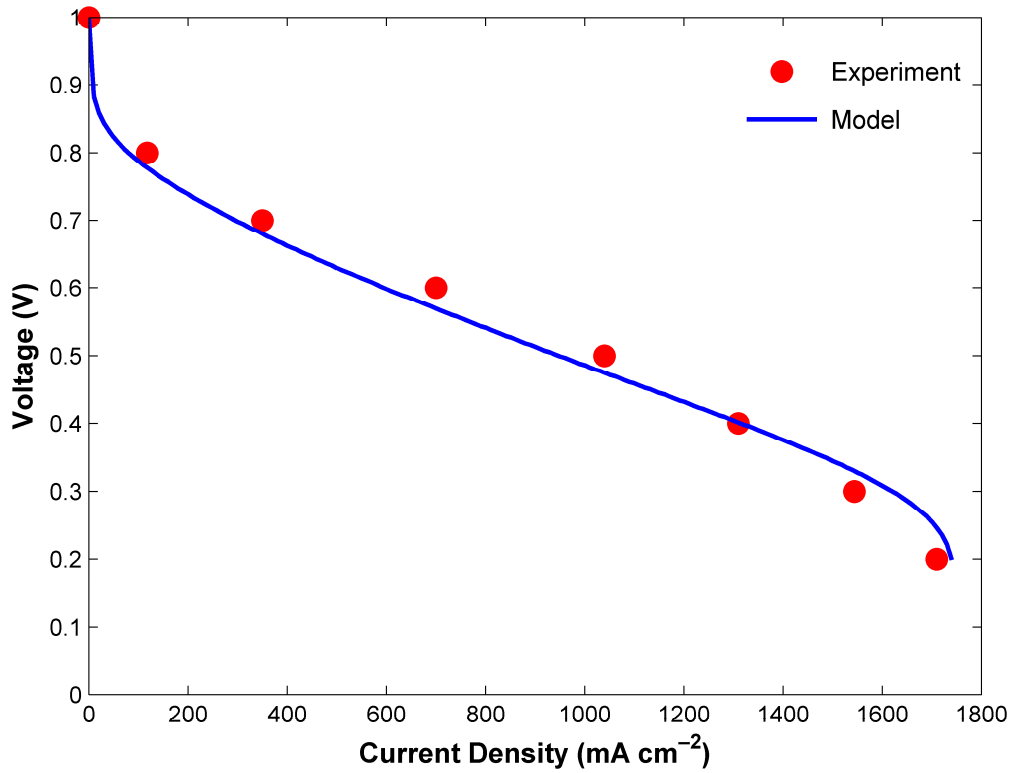
Figure 7-10: Polarization curve for H$_2$-O$_2$ fuel cell with Pt/C electrodes (0.5 mg/cm^2) from ETEK, Nafion 115, $T = 70$ ^{o}C, $P = 1$ atm, 100% RH, $\sigma_{EL} = 0.1$ S/cm, $E_{A,\Phi_0} = 18$ kJ/mol for Pt/C, $i_{C,L} = 1.75$ A/cm^2, $i_{A,L} = 4$ A/cm^2, $R_I = 0$, $\gamma_M = 116.62$. Rest of the values are provided in Table 7-3.

The majority of the initial precipitous drop in cell voltage at low current densities is due to the huge cathode-side activation overpotential due to its very low exchange-current density or activity. This loss levels off at higher current densities. The rather straight-line region at intermediate current densities is largely due to the Ohmic potential drop in the electrolyte layer, while the final sharp drop is by virtue of the mass transport resistance of oxygen in the GDL, as reflected in the limiting current density, when the cell potential drops to zero.

7.3 Conclusions

In summary, a simple model is presented here that predicts the effect of fuel permeation on open circuit voltage in PEM fuel cells. Model predictions are entirely consistent with the experimental observation. To segregate the effect of oxygen vs. hydrogen crossover, we find that the crossover current due to oxygen permeation does not significantly affect the anode overpotential and hence has no noticeable effect on the observed OCV. For a pin-hole free membrane, electrical short-circuit current is an order of magnitude smaller than the H_2 permeation current. Thus, it is shown that hydrogen crossover entirely accounts for the observed loss of about 0.2V under open circuit conditions. The OCV, furthermore, is an important diagnostic tool to determine the physical well-being of the membrane during prolonged operation, and to identify any membrane degradation in the form of membrane thinning or pin-hole formation. The cross-over effect can be easily incorporated in the lumped fuel cell performance model, which adequately describes the experimental data.

7.4 References

[1]   J. Zhang, Y. Tang, C. Song, J. Zhang, H. Wang, J. Power Sources. 163 (2006) 532-537.

[2]   J.P. Hoare, The Electrochemistry of Oxygen, Interscience Publishers, New York, 1968.

[3]   J.O.M. Bockris, S. Srinivasan, Fuel Cells: Their Electrochemistry, McGraw-Hill, New York, 1969.

[4]   J. Laraminie, A. Dicks, Fuel Cell Systems Explained, John Wiley, Chichester, England, 2000.

[5]   B. Sompalli, B.A. Litteer, W. Gu, H.A. Gasteiger, J. Electrochem. Soc. 154 (2007) B1349-B1357.

[6]   J. Wu, X.-Z. Yuan, J.J. Martin, H. Wang, D. Yang, J. Qiao, J. Ma, J. Power Sources. 195 (2010) 1171-1176.

[7]   S.S. Kocha, J.D. Yang, J.S. Yi, AIChE. J. 52 (2006) 1916-1925.

[8]   T. Thampan, S. Malhotra, J. Zhang, R. Datta, Catal. Today. 67 (2001) 15-32.

[9]   T. Sakai, H. Takenaka, N. Wakabayashi, Y. Kawami, E. Torikai, J. Electrochem. Soc. 132 (1985) 1328-1332.

[10] T. Sakai, H. Takenaka, E. Torikai, J. Electrochem. Soc. 133 (1986) 88-92.

[11] K. Broka, P. Ekdunge, J. Appl. Electrochem. 27 (1997) 117-132.

[12] F. Damay, L.C. Klein, Solid State Ionics. 162-163 (2003) 261-267.

[13] R.M. Pashley, M. Rzechowicz, L.R. Pashley, M.J. Francis, J. Phys. Chem. B. 109 (2005) 1231-1238.

[14] C. Song, Y. Tang, J.L. Zhang, J. Zhang, H. Wang, J. Shen, S. McDermid, J. Li, P. Kozak, Electrochim. Acta. 52 (2007) 2552-2561.

[15] C. Song, J. Zhang, in: J. Zhang (Ed.), PEM fuel cell electrocatalysts and catalyst layers, Springer, New York, NY, 2008.

[16] K.C. Neyerlin, W. Gu, J. Jorne, H.A. Gasteiger, J. Electrochem. Soc. 153 (2006) A1955-A1963.

[17] S. Cleghorn, J. Kolde, W. Liu, in: W. Vielstich, A. Lamm, H.A. Gasteiger (Eds.), Handbook of Fuel Cells - Fundamentals, Technology and Applications, John Wiley & Sons, New York, 2003, p. 566.

[18] M. Inaba, T. Kinumoto, M. Kiriake, R. Umebayashi, A. Tasaka, Z. Ogumi, Electrochim. Acta. 51 (2006) 5746-5753.

[19] E. Endoh, S. Terazono, H. Widjaja, Y. Takimoto, Electrochem Solid-State Lett. 7 (2004) A209-A211.

[20] W. Liu, M. Crum, ECS Trans. 3 (2006) 531-540.

[21] H. Tang, S. Peikang, S.P. Jiang, F. Wang, M. Pana, J. Power Sources. 170 (2007) 85-92.

[22] C.A. Reiser, L. Bregoli, T.W. Patterson, J.S. Yi, J.D. Yang, M.L. Perry, J.D. Jarvi, Electrochem Solid-State Lett. 8 (2005) A273-A276.

[23] J.-X. Zhang, B.A. Litteer, W. Gu, H. Liu, H.A. Gasteiger, J. Electrochem. Soc. 154 (2007) B1006-B1011.

[24] V.M. Barragan, A. Heinzel, J. Power Sources. 104 (2002) 66-72.

[25] K.-M. Yin, J. Power Sources. 167 (2007) 420-429.

[26] B.K. Kho, B. Bae, M.A. Scibioh, J. Lee, H.Y. Ha, J. Power Sources. 142 (2005) 50-55.

[27] S. Song, W. Zhou, J. Tian, R. Cai, G. Sun, Q. Xin, S. Kontou, P. Tsiakaras, J. Power Sources. 145 (2005) 266-271.

Chapter VIII

Topology, Mechanism and Kinetics of Electro-catalytic Reaction Systems in Fuel Cells

An improved understanding of the hydrogen electrode and oxygen reduction reactions is essential for deeper fundamental understanding of fuel cells, which would assist in improved catalyst design and detailed fuel cell modeling. In this chapter, we utilize the RR graph framework for analysis of these archetypical electrochemical reaction systems. The approach highlighted in this chapter can be easily adopted for a detailed and robust analysis for a host of different electrochemical systems, e.g. methanol electro-oxidation at the anode of DMFCs.

8.1 Introduction

Due to their practical significance, the hydrogen oxidation reaction (HOR), its reverse, i.e., the hydrogen evolution reaction (HER), and oxygen reduction reaction (ORR) are by far the most extensively investigated of electrocatalytic reactions [1-15]. However, even for the simplest of the electrochemical reaction systems, namely hydrogen electrode reaction, the mechanistic and kinetic understanding is still incomplete.

It is well-recognized that the standard Butler-Volmer equation is lacking in an adequate description of the kinetics of the hydrogen electrode reaction over the complete range of potentials for the alkaline as well as the acid electrolytes. Further, it is unable to explain the asymmetry in current-versus-potential observed in the hydrogen evolution reaction (HER) versus the hydrogen oxidation reaction (HOR). In fact, even kinetic descriptions via two-step mechanisms (Volmer-Heyrovsky, Volmer-Tafel, or Heyrovsky-Tafel)) are individually applicable only in limited potential ranges.

The significance of dual-pathway kinetics has recently been shown for the case of HOR on Pt electrode [1]. However, no general rate expression exists that can simultaneously account for these alternate pathways in terms of the accepted three-step mechanism, namely, the Tafel, Volmer, and the Heyrovsky steps. Further, no realistic first principles prediction of step kinetics yet exists for the hydrogen electrode reaction, although there is now a great interest in *ab initio* predictions [2-9] as well as in their experimental validation [5, 10-17]. Were an accurate rate expression for HOR/HER in terms of its three step kinetics available, it would not only be revealing, allowing fundamental questions to be answered, such as those posed recently by Gasteiger et al. [16], but, when available, it could utilize the first principles predictions of step kinetics to construct a comprehensive picture of this important and intriguing reaction system, including elucidation of the parallel pathways and the dominant steps. A thorough understanding of HOR and HER would also serve as a yardstick for understanding other electrocatalytic reactions.

One of the major pitfalls of PEM fuel cells is related to the sluggish kinetics of the irreversible ORR at the cathode, establishing a significant overpotential. Thus, ORR has

been the focus of investigation for decades. An elegant review of ORR on Pt and bimetallic surface is provided by Markovic et al. [18]. Several research groups have attempted prediction of the potential dependent activation energies for the ORR [19-24]. While, previous theoretical predictions of catalyst activity were based on the assumption of single RDS [19], which of course might not hold true over a broad range of potentials [25], there exists no general rate expression that can explain the observed kinetics. In this chapter, we provide such an explicit rate expression for the ORR on Pt(111) based on our RR graph approach. The deeper theoretical understanding of the ORR kinetics can enable us to improve the ORR activity of Pt based cathode electrocatalysis, by e.g. alloying Pt with other transition metals like Co, Ni.

8.2 Step Kinetics for Electrocatalytic Reactions

The net rate of a generic elementary step, $r_\rho = \vec{r}_\rho - \bar{r}_\rho$, is written as follows

$$\vec{r}_\rho = \underbrace{\vec{k}_\rho \prod_{i=1}^{n} a_i^{-\vec{v}_{\rho i}}}_{\vec{\omega}_\rho} \prod_{k=0}^{q} \theta_k^{-\vec{\alpha}_{\rho k}} = \vec{\omega}_\rho \prod_{k=0}^{q} \theta_k^{-\vec{\alpha}_{\rho k}};$$

$$\bar{r}_\rho = \underbrace{\bar{k}_\rho \prod_{i=1}^{n} a_i^{\bar{v}_{\rho i}}}_{\bar{\omega}_\rho} \prod_{k=0}^{q} \theta_k^{\bar{\alpha}_{\rho k}} = \bar{\omega}_\rho \prod_{k=0}^{q} \theta_k^{\bar{\alpha}_{\rho k}}$$

(8.1)

where θ_k is the (unknown) activity of intermediate species I_k ($k = 0, 1, 2, \ldots, q$), a_i is the (known, or specified) activity of terminal species T_i ($i = 1, 2, \ldots, n$), $\vec{\alpha}_{\rho k}$ is the stoichiometric coefficient of I_k in reaction step s_ρ as a *reactant* and that as a *product* is $\bar{\alpha}_{\rho k}$, while that for T_i is $\vec{v}_{\rho i}$ and $\bar{v}_{\rho i}$, respectively. We, club together, as done in earlier chapters, in the above mass-action kinetics, the product of the known rate parameters and activities of terminal species into *reaction weights*, ω_ρ, leaving behind the rates explicitly in terms of the *unknown* intermediates concentrations and *known* ω_ρ.

The thermodynamic transition-state theory gives the rate constants of the forward and reverse steps as [26]

$$\vec{k}_\rho \equiv \kappa \frac{k_B T}{h} \exp\left(-\frac{\Delta \vec{G}_\rho^{\ddagger,o}}{RT}\right) \ ; \ \overleftarrow{k}_\rho \equiv \kappa \frac{k_B T}{h} \exp\left(-\frac{\Delta \overleftarrow{G}_\rho^{\ddagger,o}}{RT}\right) \tag{8.2}$$

where the Gibbs-free energy of activation involves electrostatic potential as well, $\Delta \vec{G}_\rho^{\ddagger,o} = \Delta \vec{G}_{\rho,\Phi=0}^{\ddagger,o} - \beta_\rho(\nu_{\rho e^-}F\Phi)$, as per the linear free energy relation (LFER). Further, use of the relation: $\Delta \vec{G}_\rho^{\ddagger,o} = \Delta \vec{H}_\rho^{\ddagger,o} - T\Delta \vec{S}_\rho^{\ddagger,o}$, provides, e.g., the forward rate constant as

$$\vec{k}_\rho = \kappa \underbrace{\frac{k_B T}{h} \exp\left(\frac{\Delta \vec{S}_{\rho,\Phi=0}^{\ddagger,o}}{R}\right)}_{\vec{\Lambda}_\rho} \exp\left(-\frac{\Delta \vec{H}_{\rho,\Phi=0}^{\ddagger,o}}{RT}\right) \exp\left\{\frac{(\beta_\rho)\nu_{\rho e^-}F\Phi}{RT}\right\}$$

$$= \vec{\Lambda}_\rho \exp\left(-\frac{\vec{E}_{\rho,\Phi=0}}{RT}\right) \exp\left\{\frac{(\beta_\rho)\nu_{\rho e^-}F\Phi}{RT}\right\} = \vec{k}_{\rho,\Phi_0} \exp\left\{\frac{(\beta_\rho)\nu_{\rho e^-}F\eta_\rho}{RT}\right\} \tag{8.3}$$

where the symmetry factor is assumed to be $\beta_\rho = 1/2$ for an elementary reaction, $\vec{k}_{\rho,\Phi_0}$ is the rate constant corresponding to equilibrium electrode potential Φ_0, and $\eta_\rho \equiv \Phi - \Phi_0$, is the overpotential. The "standard" (for unit activities) electrode potentials (denoted by superscript o) for the hydrogen electrode reaction are, of course, $\Phi_0^o = 0.000$ V for acidic electrolytes, and $\Phi_0^o = -0.828$ V for alkaline electrolytes. Further, $\vec{k}_{\rho,\Phi_0}$ and $\overleftarrow{k}_{\rho,\Phi_0}$ in the above are rate constants corresponding to equilibrium electrode potential Φ_0, i.e.,

$$\vec{k}_{\rho,\Phi_0} = \vec{\Lambda}_\rho \exp\left(-\frac{\vec{E}_{\rho,\Phi=0}}{RT}\right) \exp\left\{\frac{(\beta_\rho)\nu_{\rho e^-}F\Phi_0}{RT}\right\} \tag{8.4}$$

and,

$$\overleftarrow{k}_{\rho,\Phi_0} = \overleftarrow{\Lambda}_\rho \exp\left(-\frac{\overleftarrow{E}_{\rho,\Phi=0}}{RT}\right) \exp\left\{\frac{(\beta_\rho - 1)\nu_{\rho e^-}F\Phi_0}{RT}\right\} \tag{8.5}$$

This clearly shows the nature of the pre-exponential factor, $\vec{\Lambda}_\rho = \kappa \frac{k_B T}{h} \exp\left(\frac{\Delta \vec{S}_{\rho,\Phi=0}^{\ddagger,o}}{R}\right)$, the activation energy that explains the temperature dependence in the usual Arrhenius form with the activation energy being related to the enthalpy of activation in the absence of potential, $\vec{E}_{\rho,\Phi=0} = \Delta \vec{H}_{\rho,\Phi=0}^{\ddagger,o}$, and the potential dependence via the usual Butler-Volmer

form. Clearly, both temperature and potential have a substantial effect on the rate constant of an electrochemical step. However, for the non-electrochemical steps, e.g., the Tafel step, clearly the potential dependence is zero, and the rate constant simplifies to the Arrhenius expression, $\vec{k}_\rho = \vec{\Lambda}_\rho \exp\left(-\dfrac{\vec{E}_{\rho,\Phi=0}}{RT}\right)$. It should be further apparent that the pre-exponential factor is the same for both chemical and non-electrochemical steps. Further, any conclusions about the RDS, and the importance of the different pathways, etc., is temperature as well as potential dependent.

8.3 Hydrogen Electrode Reaction Mechanism, Network and Step Kinetics

The hydrogen electrode reaction has been investigated over a long period of time due to its technological and fundamental significance. The most common and well accepted mechanism involves the Tafel, Volmer, Heyrovsky steps [27-29] which have been found to adequately explain the overall reaction kinetics [1, 5, 9, 30, 31]. This 3-step mechanism involves only a single reaction intermediate, $H \cdot S$, where S represents an unoccupied catalyst surface site. It should, however, be noted that more recently other intermediates have been proposed. For instance, intermediates such as adsorbed water ($H_2O \cdot S$), and adsorbed hydroxyl ($OH \cdot S$) have been shown to exist on Pt surfaces by Ertl and co-workers [32, 33] and others [34]. Thus, Nørskov et al. [31] consider $OH \cdot S$ and $O \cdot S$ species to calculate the effect of molecular water on adsorption. Additional intermediates, of course, imply additional elementary steps in the mechanism and would alter the site balance. Nonetheless, we simply adopt the standard Tafel-Volmer-Heyrovsky mechanism shown below to avoid being distracted by the additional complexities of a more detailed mechanism, which are left for future work.

$$
\begin{array}{llccc}
\underline{s_\rho} & & \underline{\sigma_{VT,\rho}} & \underline{\sigma_{VH,\rho}} & \underline{\sigma_{HT,\rho}} \\
s_V : & H \cdot S + OH^- \leftrightarrows H_2O + S + e^- & +2 & +1 & \\
s_T : & H_2 + 2S \leftrightarrows 2H \cdot S & +1 & & -1 \\
s_H : & H_2 + S + OH^- \leftrightarrows H_2O + H \cdot S + e^- & & +1 & +2 \\
\hline
OR = & \sum_\rho \sigma_{g\rho} s_\rho : H_2 + 2OH^- \leftrightarrows 2H_2O + 2e^- & & &
\end{array}
\tag{8.6}
$$
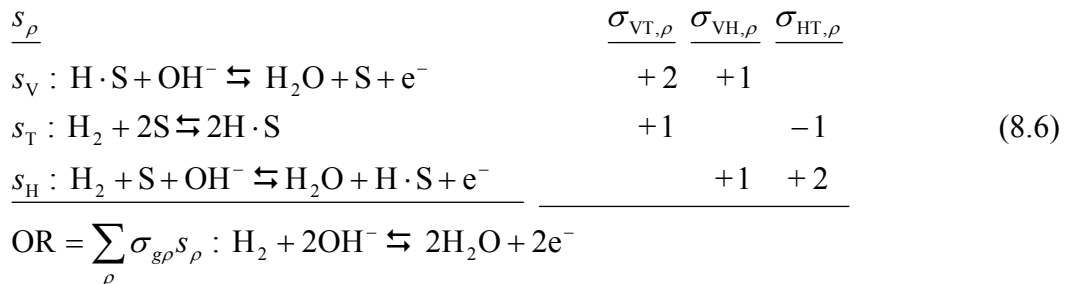
Eq. (8.6) above describes the hydrogen oxidation reaction (HOR) in an alkaline electrolyte. In an acidic electrolyte, on the other hand, the corresponding mechanism is

$$
\begin{array}{lccc}
\underline{s_\rho} & \underline{\sigma_{VT,\rho}} & \underline{\sigma_{VH,\rho}} & \underline{\sigma_{HT,\rho}} \\
s_V : H \cdot S + H_2O \leftrightarrows H_3O^+ + S + e^- & +2 & +1 & \\
s_T : H_2 + 2S \leftrightarrows 2H \cdot S & +1 & & -1 \\
s_H : H_2 + S + H_2O \leftrightarrows H_3O^+ + H \cdot S + e^- & & +1 & +2 \\
\hline
OR = \sum_\rho \sigma_{g\rho} s_\rho : H_2 + 2H_2O \leftrightarrows 2H_3O^+ + 2e^-
\end{array} \tag{8.7}
$$
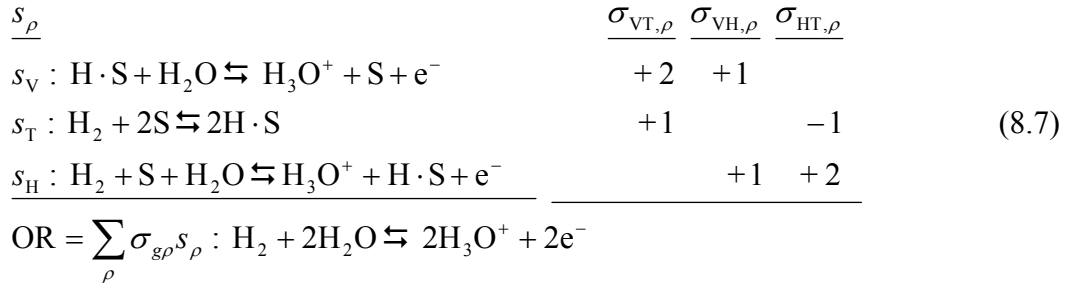
The Volmer step, s_V, above describes the electrochemical consumption of the key intermediate, namely, the surface atomic hydrogen, $H \cdot S$, while the non-electrochemical Tafel step, s_T, and the electrochemical Heyrovsky step, s_H, describe the generation of $H \cdot S$ from molecular H_2. As indicated by the stoichiometric numbers $\sigma_{g\rho}$ above, when these steps are combined in a manner that eliminates the only intermediate $H \cdot S$ ($q = 1$), the overall reaction (OR) results. Clearly, this can be accomplished in more than one way, which represent the alternate reaction routes (RRs), or pathways. The overall reaction and the elementary steps for the case of the hydrogen evolution reaction (HER) are simply the reverse of those written above for the case of HOR.

For the hydrogen electrode reaction, a direct FR must not contain more than any two ($q + 1$) of the three steps, while a direct ER must be restricted to less than three steps. As shown in Eqs. (8.6) and (8.7), the three FRs for the HOR are

$$
\left.
\begin{array}{ll}
FR_{VH} : & (+1)s_V + (+1)s_H = OR \\
FR_{VT} : & (+2)s_V + (+1)s_T = OR \\
FR_{HT} : & (+2)s_H + (-1)s_T = OR
\end{array}
\right\} \tag{8.8}
$$

The full-route FR_{VH} represents the Volmer-Heyrovsky pathway, while FR_{VT} and FR_{HT} are the Volmer-Tafel and the Heyrovsky-Tafel pathways, respectively. Further, subtracting one FR from the other, e.g., $FR_{VT} - FR_{VH}$, eliminates all species (both intermediate and terminal), and thus provides an ER, namely, $(+1)s_V + (-1)s_H + (+1)s_T = 0$, is an empty route, ER_1:

$$
\begin{array}{lll}
\underline{s_\rho} & & \underline{\sigma_{1\rho}} \\
s_V: & H\cdot S + OH^- \leftrightharpoons H_2O + S + e^- & +1 \\
s_H: & H_2 + S + OH^- \leftrightharpoons H_2O + H\cdot S + e^- & -1 \quad\quad (8.9)\\
s_T: & H_2 + 2S \leftrightharpoons 2H\cdot S & +1 \\
\hline
ER_1: & 0 \leftrightharpoons 0 &
\end{array}
$$
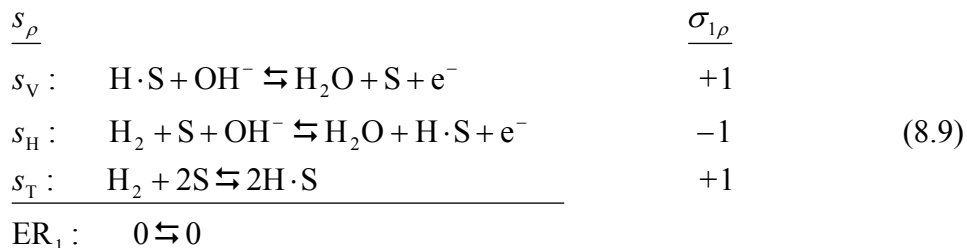
This finite and unique set of FRs and ERs are listed in Table 8-1 for the above HOR/HER mechanism. As per the Horiuti-Temkin theorem, an independent RR set for the 3-step HOR/HER mechanism is $\mu = p - q = 3 - 1 = 2$ RRs, which may include both FRs and ERs, so long as they include among them all of the steps in the mechanism. Moreover, the number of linearly independent ERs is given $p - (q + 1) = 3 - 2 - 1 = 1$ for the reaction mechanism considered [35]. Thus, a set of 2 linearly independent RRs may be readily determined by identifying one independent ER and one FR by simple inspection of the HER/HOR mechanism, as done above, thus avoiding the stoichiometric enumeration of RRs used for complex mechanisms [35-37]. Let us consider the FR_{VH} and ER_1, mentioned above as the independent set of RRs for the considered HOR/HER mechanism, from which the remaining set of unique RRs can be obtained. Thus, a linear combination of FR_{VH} and ER_1 results in FR_{VT} and FR_{HT} (Table 8-1).

These RRs, or pathways, may, in fact, be simply traced as walks on the Reaction Route Graph of a mechanism for an overall reaction. The construction of such a graph is is described below with regard to the hydrogen electrode reaction.

8.3.1 Reaction Route Graph

With the independent set of RRs (i.e., FRVH and ER1) in hand, the construction of the RR graph is straightforward and is illustrated in Figure 8-1 [38]. We start by assembling the empty routes, only ER1 in this case, into a cycle graph.

Table 8-1: Stoichiometrically distinct direct FRs and ERs for the 3-step hydrogen electrode reaction mechanism.

Reaction Route	Expression
Full RRs	
FR_{VH} (Volmer-Heyrovsky):	$s_V + s_H = OR$
FR_{VT} (Volmer-Tafel):	$2s_V + s_T = OR$
FR_{HT} (Heyrovsky-Tafel):	$2s_H - s_T = OR$
Empty RRs	
ER_1:	$s_V - s_H + s_T = 0$

a) Cycle Graph
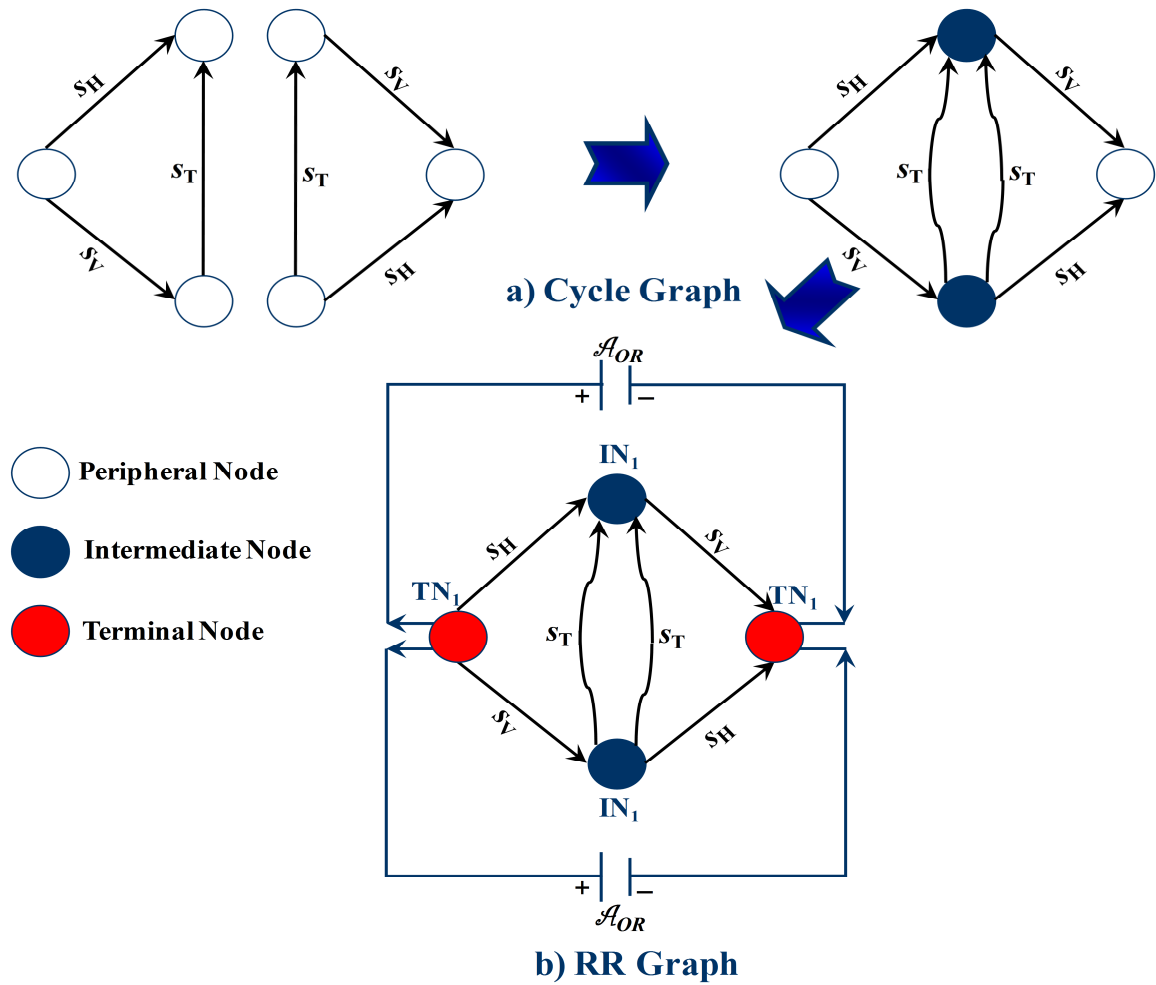
b) RR Graph

Figure 8-1: RR Graph construction for the 3-step hydrogen electrode reaction mechanism.

It is further noted that there exists non-unit stoichiometric ($\sigma_{g\rho} = +2$) numbers in some of the RRs in the unique set (Table 8-1), i.e., in FR_{VT} and in FR_{HT}. This implies that every elementary reaction step s_ρ as well as the OR must occur twice in the RR graph, which must furthermore be symmetrical [37, 39].

This can be accomplished by fusing two ER_1's as shown in Figure 8-1a. Next, we note that the remaining RR of the independent set, namely, FR_{VH}, can be included in the graph by simply connecting the OR (also twice) across terminal nodes (TNs), yielding the final RR Graph (Figure 8-1b). It is next noted that all of the 4 unique RRs (Table 8-1) for HOR can be traced on the resulting RR Graph as walks between the TNs. In fact, it may be noticed that every RR in the graph is involved twice. This is a consequence of the fact that the mechanism is non-minimal [37], i.e., the elementary steps are involved more than once in a FR. Nonetheless, the affinity (or any other thermodynamic potential change across it) and the rate of a step (e.g., s_H, s_V or s_T) remain unchanged regardless of their placement because of the network symmetry. For HER, the FR walks are simply in the opposite direction.

Let us next check, if the RR graph, so obtained, concurs with the condition that the intermediate nodes (INs) and the TNs must be consistent with the quasi-steady state (QSS) condition for the intermediate and terminal species. Since there is only one linearly independent intermediate, $H \cdot S$, here, its QSS condition is

$$Q_{H \cdot S}: \quad (-2)r_T + (+1)r_V + (-1)r_H = 0 \tag{8.10}$$

which is consistent with the connectivity, $\sum_{\rho} m_{\rho j} s_\rho = 0$, where the incidence coefficient $m_{\rho j} = +1$, if a branch leaves the node j, and $m_{\rho j} = -1$, if a branch is coming into the node j, of the only one IN (although present twice) in the RR Graph, i.e.,

$$IN_1: \quad (-2)s_T + (+1)s_V + (-1)s_H = 0 \tag{8.11}$$

Similarly, the QSS condition for the terminal species (H_2, OH^-, H_2O, e^-) for the HOR in alkaline electrolyte (Eq. (8.6)) are

$$
\left.\begin{array}{ll}
Q_{H_2} & : \ (-1)r_{OR} + (-1)r_T + (-1)r_H = 0 \\[4pt]
Q_{H_2O} & : \ (+2)r_{OR} + (+1)r_V + (+1)r_H = 0 \\[4pt]
Q_{e^-} & : \ (+2)r_{OR} + (+1)r_V + (+1)r_H = 0 \\[4pt]
Q_{OH^-} & : \ (-2)r_{OR} + (-1)r_V + (-1)r_H = 0
\end{array}\right\} \tag{8.12}
$$

It is seen that the QSS condition for OH^-, e^-, and H_2O is the same, and is represented by the TN_1 (represented twice in the graph) in the RR Graph, namely

$$
TN_1: \ 2OR - s_V - s_H = 0 \tag{8.13}
$$

Thus, the resulting RR graph satisfies all of the conditions imposed on the RR graph, i.e., all nodes are balanced in that they satisfy the QSS conditions of one or more surface intermediate (in case of INs) and of one or more terminal species (in case of TNs). Further, all the RRs can be traced as walks or paths on the RR graph. The network includes the commonly considered Volmer-Heyrovsky and Volmer-Tafel pathways, along with the not so common Heyrovsky-Tafel pathway [38]. Thus, this is an appropriate RR Graph for the hydrogen electrode reaction.

Finally, a curious observation by Chialvo et al. [5, 30], that two distinct sets of alternate parameters provide identical HOR/HER kinetics, can be explained simply from the topology of the RR Graph. Thus, it is clear from the symmetry of the RR Graph in Figure 8-1b that the Volmer and the Heyrovsky steps can be interchanged without affecting the properties of the circuit. As a result, interchanging the kinetic parameters of the Volmer and the Heyrovsky steps does not alter the current density versus overpotential predictions, as found by Chialvo et al. [5, 30], even though it changes the dependence of surface coverage on η from $\theta_{H \cdot S}(\eta)$ to $1 - \theta_{H \cdot S}(\eta)$.

We will use the RR Graph in Figure 8-1b below for deriving a QSS rate law based on its electrical analog, which would include the flux along all the three pathways (FRs), so that one need not select a pathway individually for kinetic analysis, as is the usual practice.

8.3.2 Step Kinetics

Following the discussion above in section 8.2, the net rates, $r_\rho = \vec{r}_\rho - \bar{r}_\rho$, of the three elementary steps in the HOR/HER mechanism may be written as

$$\left. \begin{aligned} r_T &= \vec{\omega}_T (1 - \theta_{H \cdot S})^2 - \bar{\omega}_T \theta_{H \cdot S}^2 \\ r_V &= \vec{\omega}_V \theta_{H \cdot S} - \bar{\omega}_V (1 - \theta_{H \cdot S}) \\ r_H &= \vec{\omega}_H (1 - \theta_{H \cdot S}) - \bar{\omega}_H \theta_{H \cdot S} \end{aligned} \right\} \tag{8.14}$$

where the site balance, namely, $\theta_0 + \theta_{H \cdot S} = 1$, has been incorporated.

The step weights in the above may be written as

$$\begin{aligned} \vec{\omega}_T &= \vec{k}_T a_{H_2} & ; \quad \bar{\omega}_T &= \bar{k}_T \\ \vec{\omega}_V &= \vec{\omega}_{V,0} e^{\psi} & ; \quad \bar{\omega}_V &= \bar{\omega}_{V,0} e^{-\psi} \\ \vec{\omega}_H &= \vec{\omega}_{H,0} e^{\psi} & ; \quad \bar{\omega}_H &= \bar{\omega}_{H,0} e^{-\psi} \end{aligned} \tag{8.15}$$

where the dimensionless electrode overpotential, $\psi \equiv \dfrac{1}{2} \dfrac{F\eta}{RT}$. Further, for the case of alkaline electrolytes, the parameters above, in terms of the rate constants at equilibrium electrode potential and the activities of the terminal species, are

$$\begin{aligned} \vec{\omega}_{V,0} &= \vec{k}_{V,\Phi_0} a_{OH^-} & ; \quad \bar{\omega}_{V,0} &= \bar{k}_{V,\Phi_0} a_{H_2O} \\ \vec{\omega}_{H,0} &= \vec{k}_{H,\Phi_0} a_{OH^-} a_{H_2} & ; \quad \bar{\omega}_{H,0} &= \bar{k}_{H,\Phi_0} a_{H_2O} \end{aligned} \tag{8.16}$$

Furthermore, in these expressions, the activity of water is usually assumed to be unity, i.e., $a_{H_2O} = 1$, for saturated conditions, while the activity of hydrogen is written as its partial pressure, i.e., $a_{H_2} = p_{H_2}$, in atm.

8.3.3 Consistence with Network Laws

Figure 8-2 below represents the electrical analog for the HER/HOR mechanism, obtained directly from the RR Graph in Figure 8-1. In doing this, the elementary steps are viewed as resistances, while the OR is viewed as a power source [38].

8.3.3.1 Kirchhoff's Potential Law (KPL)

The RR graphs, as explained in chapter II follows Kirchhoff's potential law (KPL) [35-37], that provides an important thermodynamic consistency check on the given kinetic parameters. For example, KPL relation for ER_1, i.e., $A_V - A_H + A_T = 0$, implies, with the help of the relation $A_\rho / RT = \ln(\vec{r}_\rho / \overleftarrow{r}_\rho)$

$$\left(\frac{\vec{r}_V}{\overleftarrow{r}_V}\right)\left(\frac{\overleftarrow{r}_H}{\vec{r}_H}\right)\left(\frac{\vec{r}_T}{\overleftarrow{r}_T}\right) = 1; \quad \text{or} \quad \left(\frac{\vec{\omega}_V}{\overleftarrow{\omega}_V}\right)\left(\frac{\overleftarrow{\omega}_H}{\vec{\omega}_H}\right)\left(\frac{\vec{\omega}_T}{\overleftarrow{\omega}_T}\right) = 1 \tag{8.17}$$

The calculated or experimentally determined rate constants must be consistent with these constraints.

Alternatively, not all rate constants need to be predicted, some may be found from KPL relations. The affinities of the elementary reaction steps s_ρ in a full route are related to the overall reaction affinity via a similar reaction.

$$\mathscr{A}_{OR} = \mathscr{A}_V + \mathscr{A}_H = 2\mathscr{A}_V + \mathscr{A}_T = 2\mathscr{A}_H - \mathscr{A}_T \tag{8.18}$$

8.3.3.2 Kirchhoff's Flux Law (KFL)

The Kirchhoff's Flux Law (KFL), analogous to the QSS analysis [5, 30], applies at each node [35-37], i.e., $\sum_{\rho=1}^{p} m_{j\rho} r_\rho = 0$. Thus, at the intermediate node

$$IN_1 : \quad (-2)r_T + (+1)r_V + (-1)r_H = 0 \tag{8.19}$$

The use of the step kinetics (Eq. (8.14)) in this, thus, allows one to determine the unknown site fraction $\theta_{H \cdot S}$ from

$$\underbrace{2(\overleftarrow{\omega}_T - \vec{\omega}_T)\theta_{H \cdot S}^2}_{a} + \underbrace{\left\{4\vec{\omega}_T + (\overleftarrow{\omega}_V + \vec{\omega}_V) + (\overleftarrow{\omega}_H + \vec{\omega}_H)\right\}\theta_{H \cdot S}}_{b} \underbrace{- (2\vec{\omega}_T + \vec{\omega}_V + \overleftarrow{\omega}_H)}_{c} = 0 \tag{8.20}$$

The solution to which is
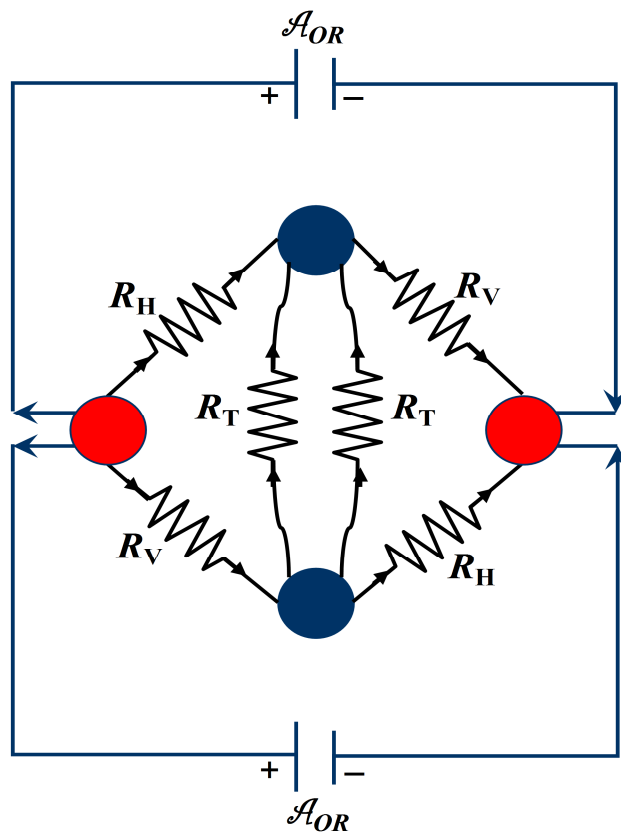
Figure 8-2: The equivalent electrical circuit for the 3-step HER mechanism.

$$\theta_{\text{H·S}} = \frac{1}{4(\bar{\omega}_{\text{T}} - \vec{\omega}_{\text{T}})} \Big[-\{4\vec{\omega}_{\text{T}} + (\bar{\omega}_{\text{V}} + \vec{\omega}_{\text{V}}) + (\bar{\omega}_{\text{H}} + \vec{\omega}_{\text{H}})\}$$
$$+ \sqrt{\{4\vec{\omega}_{\text{T}} + (\bar{\omega}_{\text{V}} + \vec{\omega}_{\text{V}}) + (\bar{\omega}_{\text{H}} + \vec{\omega}_{\text{H}})\}^2 + 8(\bar{\omega}_{\text{T}} - \vec{\omega}_{\text{T}})(2\vec{\omega}_{\text{T}} + \bar{\omega}_{\text{V}} + \vec{\omega}_{\text{H}})} \Big]$$

$$(8.21)$$

The other root of the quadratic equation does not provide a value between 0 and 1 [30]. This may be used to obtain the surface coverage of adsorbed hydrogen for a given set of kinetic parameters, using which the step rates as well as step affinities and step resistances may be calculated.

The OR rate can next be calculated from the application of KFL at the terminal node, namely

$$\text{TN}_1: \quad (-2)r_{OR} + (+1)r_{\text{V}} + (+1)r_{\text{H}} = 0 \qquad (8.22)$$

Thus, although an explicit OR rate expression that contains all the three mechanistic steps cannot be obtained, numerical calculations of the OR rate can be readily performed for a variety of conditions, as shown later. Such QSS analysis is performed for the HOR/HER by many authors, for instance, by Chialvo et al. [5, 30], although we interpret this as KFL applicable to the RR Graph. Consequently, the results are similar [5, 30].

One can similarly compute QSS (KFL) rate for each of the individual limiting cases of the 2-step mechanisms, namely, the VH, VT and HT mechanisms. Of course, the QSS (KFL) condition will change for each such limiting case, as will the dependence of $\theta_{\text{H·S}}$ on overpotential.

A specific advantage of the RR Graph approach, however, is that once the step rates, affinities, and resistances are hence obtained via KFL, a robust identification of the dominant reaction pathways may be accomplished based on a comparison of the flux (current) along different branches in the RR Graph or via a comparison of pathway resistance. Moreover, comparison of resistance enables us to identify the rate-limiting steps (RLS), without making any *ad hoc* assumptions. We followed such a numerical analysis for many of the examples in earlier chapters. Here, we follow the alternate circuitry approach for an explicit treatment of rate law for the general case involving all three steps, as well as explicit rate expressions for limiting 2-step mechanisms.

8.3.4 Ohm's Law Kinetics

The overall resistance of a reaction network may be calculated in terms of branch resistances using standard electrical circuit methods [40]. For the case of the HOR/HER, the overall rate may be written as

$$2r_{OR} = \frac{\mathcal{A}_{OR}}{R_{OR}} \tag{8.23}$$

where for the circuit shown in Figure 8-2, the overall resistance R_{OR}, can be obtained by employing, e.g., a $\Delta - Y$ conversion utilized in electrical circuits [38], [40]. The rate, r_{OR} on the left-hand side of Eq. (8.23) has been doubled since the network involves the OR twice (Figure 8-2). The overall network resistance for HOR/HER may be shown to be equal to

$$R_{OR} = \frac{R_T R_V + R_H (R_T + 4R_V)}{2(R_T + R_V + R_H)} \tag{8.24}$$

While such a representation of reaction rate is entirely consistent with the numerical results obtained from the conventional KFL/QSS analysis discussed in the last section [38], unfortunately, the step resistances in Eq. (8.24) as defined in chapter II, involve step kinetics including activity of the intermediate species $\theta_{H \cdot S}$, which is, of course, not known *a priori*, the determination of which is, in fact, the key goal of kinetic analysis. We thus, follow an alternate Ohm's law representation of Eq. (8.23) of the form [41]

$$2r_{OR} = \frac{E_{OR}}{R_{OR}^{\bullet}} \tag{8.25}$$

in which the network resistance $R_{OR}^{\bullet}$, of a form similar to Eq. (29) as described below, can, in fact, be determined *a priori*. Here, the thermodynamic driving force is defined as

$$E_{OR} \equiv 1 - z_{OR} \tag{8.26}$$

while the reversibility of the OR

$$z_{OR} = \vec{r}_{OR} / \vec{r}_{OR} = \exp(-\mathcal{A}_{OR}) = \frac{1}{K_{OR}} \prod_{i=1}^{n} a_i^{v_i} \tag{8.27}$$

Furthermore, based on KPL, the above OR reversibility can be written in terms of the step weights, thus making it a known quantity for a given set of reaction conditions

$$z_{OR} = \prod_{\rho=1}^{q+1} \left(\frac{\bar{\omega}_\rho}{\vec{\omega}_\rho} \right)^{\sigma_{g\rho}} \tag{8.28}$$

For the HOR, thus, for the different FRs (Eq. 3)

$$z_{OR} = \frac{\bar{\omega}_V}{\vec{\omega}_V} \frac{\bar{\omega}_H}{\vec{\omega}_H} = \frac{\bar{\omega}_V^2}{\vec{\omega}_V^2} \frac{\bar{\omega}_T}{\vec{\omega}_T} = \frac{\bar{\omega}_H^2}{\vec{\omega}_H^2} \frac{\bar{\omega}_T}{\vec{\omega}_T} \tag{8.29}$$

The OR reversibility in the above relations may be written as follows by combining Eq. (8.15) with, e.g., the first of the relations in Eq. (8.29). Thus

$$z_{OR} = \left(\frac{\bar{\omega}_{V,0}}{\vec{\omega}_{V,0}} \frac{\bar{\omega}_{H,0}}{\vec{\omega}_{H,0}} \right) e^{-4\psi} \tag{8.30}$$

When equilibrium is brought about by changing the hydrogen electrode overpotential to zero, i.e., as $\psi \to 0$, $z_{OR} \to 1$, and $R_\rho \to R_{\rho,0}$. Thus, the term in the parenthesis in the above expression must be unity, i.e., $\bar{\omega}_{V,0}\bar{\omega}_{H,0} = \vec{\omega}_{V,0}\vec{\omega}_{H,0}$, where these parameters in terms of rate constants at equilibrium potential and species concentrations are given in Eqs. (8.4) and (8.16).

The equation also explains the reciprocity in rate constants of the Volmer and Heyrovsky steps observed and commented on by Chialvo et al. [5, 30]. As a result, furthermore, the reversibility simply becomes

$$z_{OR} = e^{-4\psi} \tag{8.31}$$

It is, thus, clear from above that when $\psi > 0$, i.e., when the overpotential is positive, the OR proceeds as depicted in Eqs. (8.6), i.e., as HOR. On the other hand, when $\psi < 0$, the OR is the HER. Further, at high overpotential in either direction, i.e., when $|\psi| \gg 0$, the reaction is essentially irreversible.

The above relation may alternately be obtained if either of the other two forms in Eq. (8.29) were used for this analysis, which further require $\bar{\omega}_{V,0}^2 \bar{\omega}_T = \vec{\omega}_{V,0}^2 \vec{\omega}_T$ and $\bar{\omega}_{H,0}^2 \bar{\omega}_T = \vec{\omega}_{H,0}^2 \vec{\omega}_T$ as additional KPL relations.

Further, using Eqs. (8.25), (8.26) and (8.31) in $i = v_{OR,e^-} F r_{OR}$, where r_{OR} is in units of mol cm^{-2} s^{-1} and v_{OR,e^-} is the stoichiometric coefficient of electrons in the overall electrode reaction (i.e., $v_{OR,e^-} = +2$ for HOR and $v_{OR,e^-} = -2$ for HER), and rearranging, the current density

$$i = \frac{v_{OR,e^-} F(e^{2\psi} - e^{-2\psi})}{e^{2\psi}(2R_{OR}^\bullet)} \tag{8.32}$$

This relation may alternately be expressed in terms of the exchange current density as follows. Thus, when equilibrium is brought about by changing the hydrogen electrode overpotential to zero, i.e., as $\psi \to 0$, then the net electrode current density $i \to 0$, but the current density in each direction $\vec{i}$, and $\bar{i} \to i_0$. Of course, then the step resistance changes as well, $R_\rho^\bullet \to R_{\rho,0}^\bullet$, and the OR resistance changes concomitantly, $R_{OR}^\bullet \to R_{OR,0}^\bullet$. Thus,

$$i_0 = \frac{\left|v_{OR,e^-}\right| F}{2R_{OR,0}^\bullet} \tag{8.33}$$

and the current density then may be written in the alternate form

$$\frac{i}{i_0} = \frac{R_{OR,0}^\bullet (e^{2\psi} - e^{-2\psi})}{e^{2\psi}(R_{OR}^\bullet)} \tag{8.34}$$

As mentioned above, $R_{OR}^\bullet$ in the above relations is the total network resistance, which may be written in terms of step resistance in the same form as Eq. (8.24), i.e.,

$$R_{OR}^\bullet = \frac{R_T^\bullet R_V^\bullet + R_H^\bullet (R_T^\bullet + 4R_V^\bullet)}{2(R_T^\bullet + R_V^\bullet + R_H^\bullet)} \tag{8.35}$$

where $R_\rho^\bullet$ is defined explicitly in chapter II, as the resistance of the step s_ρ when it is considered as the rate-determining step (RDS), with all other steps are at quasi-

equilibrium (QE). $R_\rho^\bullet$ can next be ascertained *a priori* following the LHHW approach along with notion of IRRs, elucidated in chapter II. Thus, with step s_T as the RDS

$$R_T^\bullet = \frac{1}{\vec{r}_T^\bullet} = \frac{1}{\vec{\omega}_T (\theta_{0,T}^\bullet)^2} \tag{8.36}$$

The corresponding intermediate reaction for $H \cdot S$ is $IR_{HS} = (-1)s_V$. Using Eq. 2.25 , we thus have $\theta_{H\cdot S,T}^\bullet / \theta_{0,T}^\bullet = \bar{\omega}_V / \vec{\omega}_V$. Next from Eq. 2.26 , $1/\theta_{0,T}^\bullet = 1 + \bar{\omega}_V / \vec{\omega}_V$. Finally, using this in Eq. (8.36) along with Eq. (8.15)

$$R_T^\bullet = \frac{1}{\vec{\omega}_T}\left(1 + \frac{\bar{\omega}_V}{\vec{\omega}_V}\right)^2 = \frac{1}{\vec{\omega}_T}\left(1 + \frac{\bar{\omega}_{V,0}}{\vec{\omega}_{V,0}}e^{-2\psi}\right)^2 \tag{8.37}$$

Next, with step s_V as the RDS

$$R_V^\bullet = \frac{1}{\vec{r}_V^\bullet} = \frac{1}{\vec{\omega}_V \theta_{H\cdot S,V}^\bullet} = \frac{1}{\vec{\omega}_V \left(\dfrac{\theta_{H\cdot S,V}^\bullet}{\theta_{0,V}^\bullet}\right)\theta_{0,V}^\bullet} \tag{8.38}$$

The corresponding intermediate reaction for $H \cdot S$ is $IR_{HS} = (+1)s_H$. Thus, $\theta_{H\cdot S,V}^\bullet / \theta_{0,V}^\bullet = \bar{\omega}_H / \vec{\omega}_H$ along with $1/\theta_{0,V}^\bullet = 1 + \bar{\omega}_H / \vec{\omega}_H$. Using the above in Eq. (8.38),

$$R_V^\bullet = \frac{1}{\vec{\omega}_{V,0}e^{\psi}}\left(1 + \frac{\bar{\omega}_{H,0}}{\vec{\omega}_{H,0}}e^{-2\psi}\right) \tag{8.39}$$

Similarly

$$R_H^\bullet = \frac{1}{\vec{r}_H^\bullet} = \frac{1}{\vec{\omega}_H \theta_{0,H}^\bullet} = \frac{1}{\vec{\omega}_{H,0}e^{\psi}}\left(1 + \frac{\bar{\omega}_{V,0}}{\vec{\omega}_{V,0}}e^{-2\psi}\right) \tag{8.40}$$

8.3.5 General Tafel-Volmer-Heyrovsky Kinetics

Assuming all three steps are significant, and combining Eqs. (8.32) and (8.35)

$$i = \frac{v_{OR,e^-}F}{e^{2\psi}}\left\{\frac{R_T^\bullet + R_V^\bullet + R_H^\bullet}{R_T^\bullet R_V^\bullet + R_H^\bullet(R_T^\bullet + 4R_V^\bullet)}\right\}(e^{2\psi} - e^{-2\psi}) \tag{8.41}$$

Using the step resistances obtained above in this and rearranging provides

$$
i = \frac{(v_{OR,e^-}F)\vec{\omega}_T\vec{\omega}_{V,0}^2\left\{1+\dfrac{\vec{\omega}_{H,0}}{\vec{\omega}_T\vec{\omega}_{V,0}}\left(\vec{\omega}_{V,0}e^{\psi}+\tilde{\omega}_{V,0}e^{-\psi}\right)+\dfrac{\left(\vec{\omega}_{H,0}e^{\psi}+\tilde{\omega}_{H,0}e^{-\psi}\right)}{\left(\vec{\omega}_{V,0}e^{\psi}+\tilde{\omega}_{V,0}e^{-\psi}\right)}\right\}(e^{2\psi}-e^{-2\psi})}{\left(\vec{\omega}_{V,0}e^{\psi}+\tilde{\omega}_{V,0}e^{-\psi}\right)^2+\left(\vec{\omega}_{H,0}e^{\psi}+\tilde{\omega}_{H,0}e^{-\psi}\right)\left\{\dfrac{4\vec{\omega}_T\vec{\omega}_{V,0}}{\vec{\omega}_{H,0}}+\left(\vec{\omega}_{V,0}e^{\psi}+\tilde{\omega}_{V,0}e^{-\psi}\right)\right\}}
$$

$$(8.42)$$

Although complex-looking, it is noteworthy that this is the first explicit expression available in the literature that provides the kinetics of the hydrogen electrode reaction in terms of the kinetics of *all* of the three accepted steps (Tafel-Volmer-Heyrovsky) considered together.

Further, when equilibrium is brought about by changing the hydrogen electrode overpotential to zero, i.e., as $\psi \to 0$, then the net electrode current density $i \to 0$, but the current density in each direction $\vec{i}$, and $\tilde{i} \to i_0$. The above equation then provides the exchange current density

$$
i_0 = \frac{\left|v_{OR,e^-}\right|F\vec{\omega}_T\vec{\omega}_{V,0}^2\left\{1+\dfrac{\vec{\omega}_{H,0}}{\vec{\omega}_T\vec{\omega}_{V,0}}\left(\vec{\omega}_{V,0}+\tilde{\omega}_{V,0}\right)+\dfrac{\left(\vec{\omega}_{H,0}+\tilde{\omega}_{H,0}\right)}{\left(\vec{\omega}_{V,0}+\tilde{\omega}_{V,0}\right)}\right\}}{\left(\vec{\omega}_{V,0}+\tilde{\omega}_{V,0}\right)^2+\left(\vec{\omega}_{H,0}+\tilde{\omega}_{H,0}\right)\left\{\dfrac{4\vec{\omega}_T\vec{\omega}_{V,0}}{\vec{\omega}_{H,0}}+\left(\vec{\omega}_{V,0}+\tilde{\omega}_{V,0}\right)\right\}}
$$

$$(8.43)$$

The last two expressions can be further combined to alternately express the current density in terms of exchange current density

$$
i = i_0\frac{\left[\left(\vec{\omega}_{V,0}+\tilde{\omega}_{V,0}\right)^2+\left(\vec{\omega}_{H,0}+\tilde{\omega}_{H,0}\right)\left\{\dfrac{4\vec{\omega}_T\vec{\omega}_{V,0}}{\vec{\omega}_{H,0}}+\left(\vec{\omega}_{V,0}+\tilde{\omega}_{V,0}\right)\right\}\right]\left\{1+\dfrac{\vec{\omega}_{H,0}}{\vec{\omega}_T\vec{\omega}_{V,0}}\left(\vec{\omega}_{V,0}e^{\psi}+\tilde{\omega}_{V,0}e^{-\psi}\right)+\dfrac{\left(\vec{\omega}_{H,0}e^{\psi}+\tilde{\omega}_{H,0}e^{-\psi}\right)}{\left(\vec{\omega}_{V,0}e^{\psi}+\tilde{\omega}_{V,0}e^{-\psi}\right)}\right\}(e^{2\psi}-e^{-2\psi})}{\left\{1+\dfrac{\vec{\omega}_{H,0}}{\vec{\omega}_T\vec{\omega}_{V,0}}\left(\vec{\omega}_{V,0}+\tilde{\omega}_{V,0}\right)+\dfrac{\left(\vec{\omega}_{H,0}+\tilde{\omega}_{H,0}\right)}{\left(\vec{\omega}_{V,0}+\tilde{\omega}_{V,0}\right)}\right\}\left[\left(\vec{\omega}_{V,0}e^{\psi}+\tilde{\omega}_{V,0}e^{-\psi}\right)^2+\left(\vec{\omega}_{H,0}e^{\psi}+\tilde{\omega}_{H,0}e^{-\psi}\right)\left\{\dfrac{4\vec{\omega}_T\vec{\omega}_{V,0}}{\vec{\omega}_{H,0}}+\left(\vec{\omega}_{V,0}e^{\psi}+\tilde{\omega}_{V,0}e^{-\psi}\right)\right\}\right]}
$$

$$(8.44)$$

Although the above expressions are approximate, they are highly accurate as shown later in comparison with the QSS numerical results over the entire range of potentials of interest for both HOR and HER.

8.3.6 Limiting Cases of Dual-Step Kinetics

When one of the 2-step mechanisms (Volmer-Heyrovsky or Volmer-Tafel) is dominant, the third step may be removed from the RR Graph, and the corresponding simplified $R_{OR}^{\bullet}$ computed for the hence reduced circuit (Figure 8-3). The Heyrovsky-Tafel mechanism is not considered here further based on the QSS results presented later in the chapter. Thus, the overall resistances of the two-step pathways involved in HER/HOR are

$$\left.\begin{array}{l} R_{VH}^{\bullet} = (R_V^{\bullet} + R_H^{\bullet})/2 \\ R_{VT}^{\bullet} = 2R_V^{\bullet} + R_T^{\bullet}/2 \end{array}\right\} \tag{8.45}$$

which may be used for $R_{OR}^{\bullet}$ in Eqs. (8.32) to (8.34), i.e., in $r_{OR} = E_{OR}/(2R_{OR}^{\bullet}) \approx E_{OR}/(2R_{FR}^{\bullet})$.

8.3.6.1 Volmer-Heyrovsky Mechanism

For the Volmer-Heyrovsky mechanism, using the expressions for the Volmer and Heyrovsky resistances in Eq. (8.45) and rearranging

$$i_{VH} = \frac{\nu_{OR,e^-} F \vec{\omega}_{V,0} \vec{\omega}_{H,0} (e^{2\psi} - e^{-2\psi})}{\left(\vec{\omega}_{H,0} + \vec{\omega}_{V,0}\right)e^{\psi} + \left(\overleftarrow{\omega}_{H,0} + \overleftarrow{\omega}_{V,0}\right)e^{-\psi}} \tag{8.46}$$

This rate expression can, in fact, be derived via the KFL/QSS analysis as well, which provides an explicit solution in this case because the kinetics for both the Volmer and Heyrovsky steps are linear in the unknown surface intermediate concentration.

The rate expression may further be written in an alternate form by using the identities, $e^{\psi} = \cosh\psi + \sinh\psi$, $e^{-\psi} = \cosh\psi - \sinh\psi$, and $\sinh(2\psi) = 2\sinh\psi\cosh\psi$, and rearranging, to provide
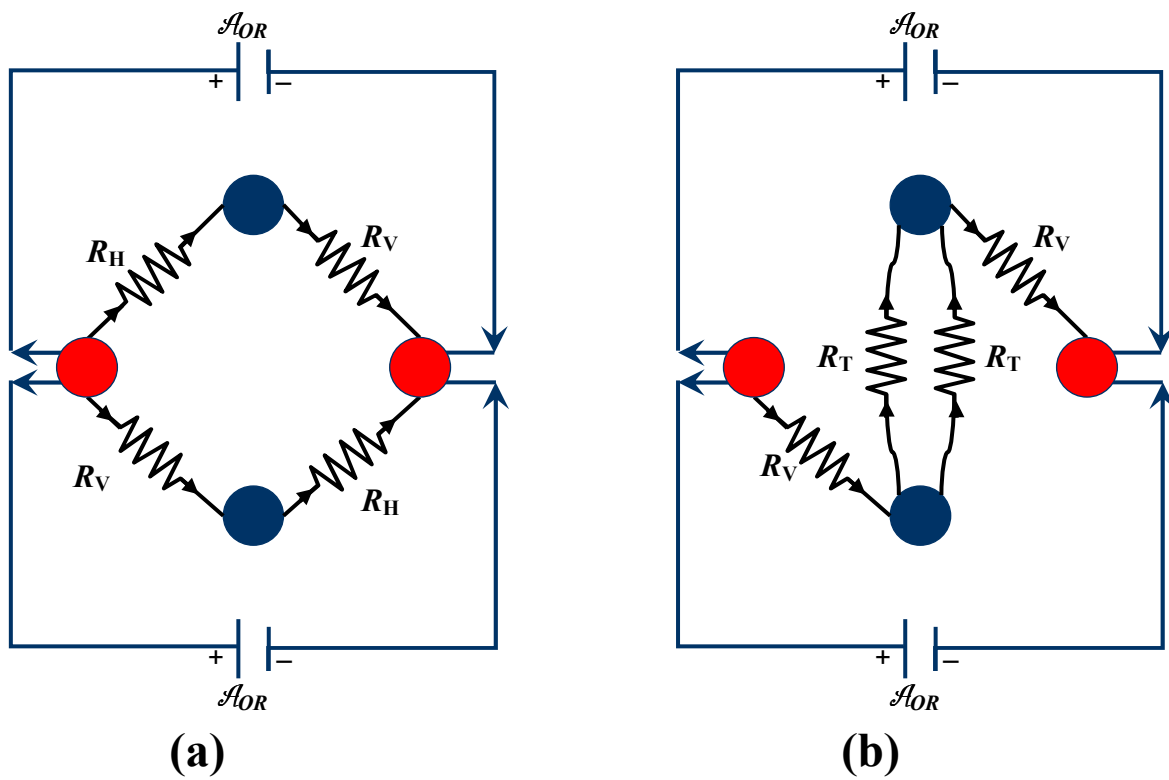
Figure 8-3: Reduced RR circuit for (a) Volmer-Heyrovsky mechanism and (b) Volmer-Tafel mechanism.

$$i_{VH} = \frac{4\nu_{OR,e^-} F\left(\dfrac{\vec{\omega}_{H,0}\vec{\omega}_{V,0}}{\bar{\omega}_{V,0} + \bar{\omega}_{H,0}}\right)\sinh\psi}{2 - \left\{1 - \dfrac{(\bar{\omega}_{V,0} + \bar{\omega}_{H,0})}{(\vec{\omega}_{V,0} + \vec{\omega}_{H,0})}\right\}(1 - \tanh\psi)} \tag{8.47}$$

Further, the exchange current density from Eq. (8.33)

$$i_{VH,0} = \frac{\left|\nu_{OR,e^-}\right| F\left(\dfrac{\vec{\omega}_{V,0}\vec{\omega}_{H,0}}{\vec{\omega}_{V,0} + \vec{\omega}_{H,0}}\right)}{1 + \dfrac{(\bar{\omega}_{V,0} + \bar{\omega}_{H,0})}{(\vec{\omega}_{V,0} + \vec{\omega}_{H,0})}} \tag{8.48}$$

Thus, an alternate form of the rate expression is obtained by combining the last two expressions

$$i_{VH} = \frac{4i_{VH,0}\left\{1 + \dfrac{(\bar{\omega}_{V,0} + \bar{\omega}_{H,0})}{(\vec{\omega}_{V,0} + \vec{\omega}_{H,0})}\right\}\sinh\psi}{2 - \left\{1 - \dfrac{(\bar{\omega}_{V,0} + \bar{\omega}_{H,0})}{(\vec{\omega}_{V,0} + \vec{\omega}_{H,0})}\right\}(1 - \tanh\psi)} \tag{8.49}$$

8.3.6.2 Volmer-Tafel Mechanism

For the Volmer-Tafel mechanism, using the expressions for the Volmer and Tafel resistances, along with $\bar{\omega}_{V,0}\bar{\omega}_{H,0} = \vec{\omega}_{V,0}\vec{\omega}_{H,0}$, and Eq. (8.45) in Eq. (8.33) and rearranging provides the exchange current density

$$i_{VT,0} = \frac{\left|\nu_{OR,e^-}\right| F(\vec{\omega}_T \vec{\omega}_{V,0}^2)}{(\vec{\omega}_{V,0} + \bar{\omega}_{V,0})^2 \left\{1 + \dfrac{4\vec{\omega}_T\vec{\omega}_{V,0}}{\bar{\omega}_{V,0}(\bar{\omega}_{V,0} + \vec{\omega}_{V,0})}\right\}} \tag{8.50}$$

which may be combined with Eq. (8.34) to provide

$$i_{VT} = \frac{i_{VT,0}\left\{1 + \dfrac{4\vec{\omega}_T\vec{\omega}_{V,0}}{\bar{\omega}_{V,0}(\bar{\omega}_{V,0} + \vec{\omega}_{V,0})}\right\}(e^{2\psi} - e^{-2\psi})}{\dfrac{1}{(\vec{\omega}_{V,0} + \bar{\omega}_{V,0})^2}\left\{(\vec{\omega}_{V,0}e^\psi + \bar{\omega}_{V,0}e^{-\psi})^2 + \dfrac{4\vec{\omega}_T\vec{\omega}_{V,0}}{\bar{\omega}_{V,0}}(\vec{\omega}_{V,0}e^\psi + \bar{\omega}_{V,0}e^{-\psi})\right\}} \tag{8.51}$$

which can alternately be written in terms of hyperbolic functions as above

$$
i_{\mathrm{VT}} = \frac{4i_{\mathrm{VT},0}\left\{1 + \dfrac{4\vec{\omega}_{\mathrm{T}}\bar{\omega}_{\mathrm{V},0}}{\bar{\omega}_{\mathrm{V},0}(\bar{\omega}_{\mathrm{V},0} + \vec{\omega}_{\mathrm{V},0})}\right\}\sinh\psi}{\cosh\psi\left\{1 + \dfrac{(\bar{\omega}_{\mathrm{V},0} - \vec{\omega}_{\mathrm{V},0})}{(\bar{\omega}_{\mathrm{V},0} + \vec{\omega}_{\mathrm{V},0})}\tanh\psi\right\}^2 + \dfrac{4\vec{\omega}_{\mathrm{T}}\bar{\omega}_{\mathrm{V},0}}{\bar{\omega}_{\mathrm{V},0}(\bar{\omega}_{\mathrm{V},0} + \vec{\omega}_{\mathrm{V},0})}\left\{1 - \dfrac{(\bar{\omega}_{\mathrm{V},0} - \vec{\omega}_{\mathrm{V},0})}{(\bar{\omega}_{\mathrm{V},0} + \vec{\omega}_{\mathrm{V},0})}\tanh\psi\right\}}
$$

$$(8.52)$$

It is noteworthy that this is the first such explicit expression for the Volmer-Tafel mechanism, as the corresponding QSS analysis cannot be written explicitly in such a form due to the nonlinearity of the kinetics. Thus, the QSS site coverage for the Volmer-Tafel kinetics is

$$
\theta_{\mathrm{H\cdot S}} = \frac{1}{4(\vec{\omega}_{\mathrm{T}} - \bar{\omega}_{\mathrm{T}})}\left[\left\{4\vec{\omega}_{\mathrm{T}} + (\bar{\omega}_{\mathrm{V}} + \vec{\omega}_{\mathrm{V}})\right\} - \sqrt{\left\{4\vec{\omega}_{\mathrm{T}} + (\bar{\omega}_{\mathrm{V}} + \vec{\omega}_{\mathrm{V}})\right\}^2 - 8(\vec{\omega}_{\mathrm{T}} - \bar{\omega}_{\mathrm{T}})(2\vec{\omega}_{\mathrm{T}} + \bar{\omega}_{\mathrm{V}})}\right]
$$

$$(8.53)$$

which may be used in Eq. (8.14) for calculating the OR rate via the KFL/QSS approach.

8.3.7 Case of Hydrogen Electrode Reaction in Alkaline Medium

Unfortunately, the rate constants for electrocatalytic elementary reactions are not yet available from first principles predictions, although important progress is being made in this direction [2-4, 8, 9, 31]. Therefore, for our analysis, we adopt rate constants obtained in the literature by fitting experimental rate data. Thus, the set of rate constants used here for the case of Pt catalyst in 0.5M NaOH solution at 296 K is provided in Table 8-2 [30, 42]. Moreover, this kinetic data is found to be consistent with KPL relations described in the earlier sections.

Figure 8-4 provides a plot of $1/R_\rho^\bullet$ (maximum possible forward step rate) versus overpotential η. Based on Figure 8-4, Volmer step seems to be the fastest over the entire range of overpotential, while the resistances of the Heyrovsky and Tafel steps are of similar magnitude and may be rate-limiting over limited potential ranges, as discussed in more detail below. However, all three resistances are not of dramatically different magnitude. Finally, the potential dependence of $R_{\mathrm{T}}^\bullet$ is curious, and explained by Eq. (49).

Table 8-2: Reaction rate constants for HER on Pt in 0.5M NaOH at 296 K [30].

Reaction Step, s_ρ	$\vec{k}_{\rho,\Phi_0} \, (\mathrm{mol\,cm^{-2}\,s^{-1}})$	$\overleftarrow{k}_{\rho,\Phi_0} \, (\mathrm{mol\,cm^{-2}\,s^{-1}})$
$s_T : H_2 + 2S \leftrightarrows 2H \cdot S$	$\vec{k}_T = 8.8 \times 10^{-10}$	$\overleftarrow{k}_T = 8.8 \times 10^{-8}$
$s_V : H \cdot S + OH^- \leftrightarrows H_2O + S + e^-$	$\vec{k}_{V,\Phi_0} = 4.4 \times 10^{-7}$	$\overleftarrow{k}_{V,\Phi_0} = 4.4 \times 10^{-8}$
$s_H : H_2 + S + OH^- \leftrightarrows H_2O + H \cdot S + e^-$	$\vec{k}_{H,\Phi_0} = 2.4 \times 10^{-10}$	$\overleftarrow{k}_{H,\Phi_0} = 2.4 \times 10^{-9}$
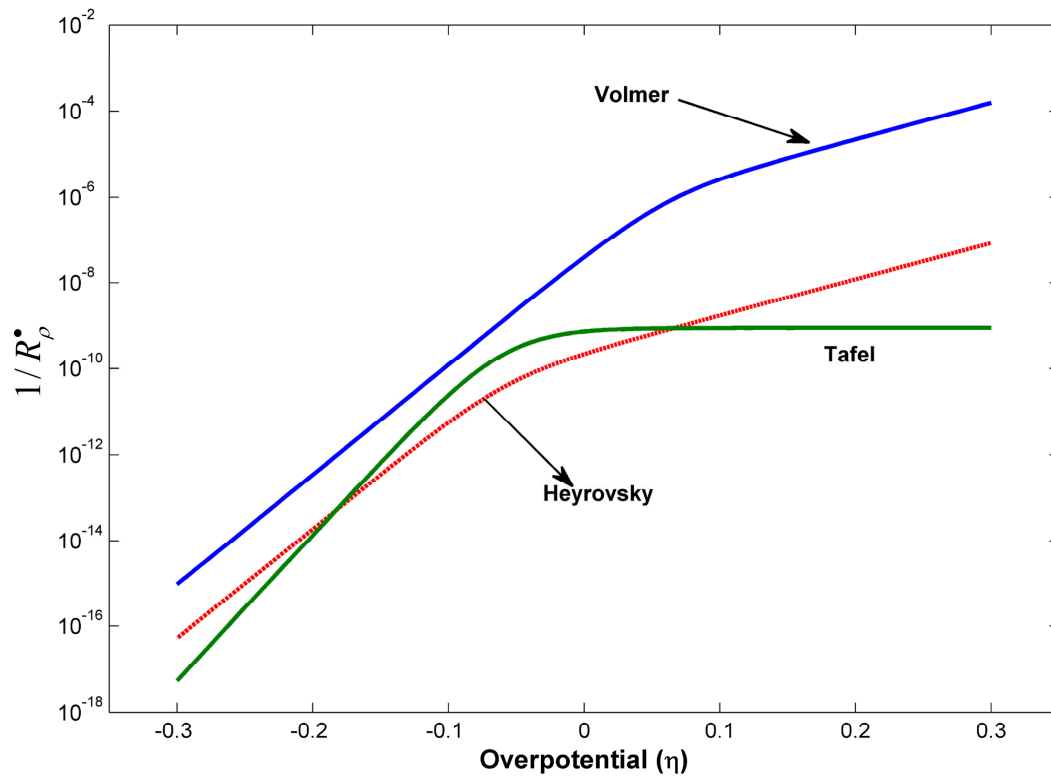
Figure 8-4: Semilog plot of $1/R_\rho^\bullet$ vs. overpotential, η (V) for hydrogen electrode reaction on Pt in alkaline medium.
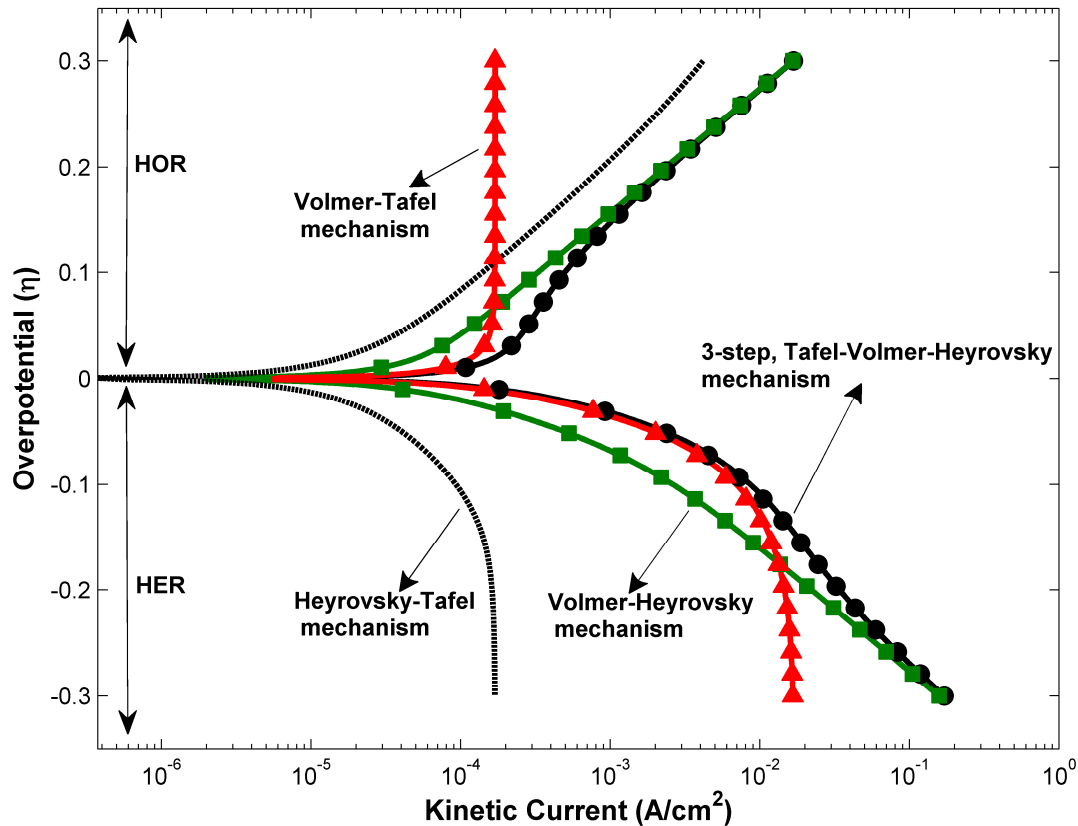
Figure 8-5: Semilog plot of overpotential (V), η vs. absolute value of kinetic current, i for hydrogen electrode reaction on Pt in alkaline midium. Solid lines represent data obtained from solving QSS equation for the 3-step Tafel-Volmer-Heyrovsky (black) mechanism and each of the 2-step mechanism, namely, Volmer-Heyrovsky (green), Volmer-Tafel (red) and Heyrovsky-Tafel (dotted, black) mechanism, while symbols represent calculations from Ohm's law. ● 3-step mechanism Eq. (8.42), ■ 2-step Volmer-Heyrovsky mechanism Eq. (8.49), ▲ 2-step Volmer-Tafel mechanism Eq. (8.52).

Finally, Figure 8-5, provides QSS rates for HOR/HER mechanism in alkaline medium obtained numerically by solving the KFL relations for each of the three two-step mechanisms as well for the case of the 3-step mechanism. It is evident from Figure 8-5 that the HT mechanism is not a significant contributor over any part of the range of overpotentials considered here for the alkaline system. In fact, even the VH and VT mechanisms are individually applicable only in limited potential ranges.

Figure 8-5, also plots the QSS rate obtained from the explicit rate expression for the complete 3-step mechanism, as well as those for the limiting cases. Although these expressions (i.e., Eqs. (8.44), (8.49) and (8.52)) are approximate, they are highly accurate as shown in comparison with the QSS numerical results over the entire range of potentials of interest for both HOR and HER, as shown in Figure 8-5. Moreover, they quite nicely explain the asymmetry between the kinetics in the HER region versus that in the HOR region (Figure 8-5).

It is clear that the expression is adequate in the overpotential range of $-0.3\,\text{V} < \eta < -0.24\,\text{V}$ for HER and $0.13\,\text{V} < \eta < 0.3\,\text{V}$ for HOR in the alkaline system. The asymmetry between the kinetics in the HER region versus that in the HOR region for the Vomer-Heyrovsky mechanism is a result of the coefficient of the tanh term in the denominator (Eq. (8.49)). For small ψ, this would be small, and the result would be a simple symmetric behavior as described by a Butler-Volmer kinetic expression [26].

Further, there is a great asymmetry in the Volmer-Tafel mechanism, described by the form of the denominator in the expression (i.e. Eq. (8.52))! This mechanism is important for HER in an alkaline system in the overpotential range of $-0.1\,\text{V} < \eta < 0\,\text{V}$. $-0.1\,\text{V} < \eta < 0\,\text{V}$. For HOR in an alkaline system, the VT mechanism is only applicable in a narrow overpotential range of $0 < \eta < 20\,\text{mV}$.

Finally, for the kinetic data provided in Table 8-2, this relation provides an exchange current density of $i_0 = 1.7 \times 10^{-4}\,\text{A cm}^{-2}$ for HER on Pt in 0.5M NaOH at $T = 296$ K. This value compares well with that predicted using the correlation provided by Chiavlo et al. [30] based on an extension of the Temkin development for a single reaction route. Many

others have also suggested i_0 to be $\sim 10^{-4}$ A cm^{-2} on Pt for alkaline electrolytes [15, 43, 44].

8.3.8 Case of Hydrogen Electrode Reaction in Acidic Medium

Let us now consider the case of hydrogen electrode reaction in acidic medium, of fundamental importance with the connection to PEM fuel cells. The HOR and HER reactions are represented by Eq. (8.7) and the kinetic rate constants are written as

$$\vec{k}_\rho \equiv \Lambda \exp\left(-\frac{\Delta \vec{G}_\rho^{\ddagger,o}}{RT}\right) \; ; \; \overleftarrow{k}_\rho \equiv \Lambda \exp\left(-\frac{\Delta \overleftarrow{G}_\rho^{\ddagger,o}}{RT}\right) \qquad \frac{\text{molecules}}{\text{site.s}} \qquad (8.54)$$

where $\Delta \vec{G}_\rho^{\ddagger,o} = \Delta \vec{G}_{\rho,\Phi=0}^{\ddagger,o} - \beta_\rho(\nu_{\rho e^-}F\Phi)$, as per the linear free energy relation (LFER). In terms of free energy, $\Delta \vec{G}_\rho^{\ddagger,o} = \Delta \vec{H}_\rho^{\ddagger,o} - T\Delta \vec{S}_\rho^{\ddagger,o}$. Thus,

$$\vec{\Lambda}_\rho = \Lambda \exp\left(\frac{\Delta \vec{S}_\rho^{\ddagger,o}}{R}\right) \qquad \frac{\text{molecules}}{\text{site.s}} \qquad (8.55)$$

In short, Λ acts like a scaling factor in order to express the differences in the intrinsic exchange currents by the corresponding activation free energies [9]. $\Delta G_\rho^{\ddagger,o}$, on the other hand, is a function of the electrostatic potential given by LFER as explained earlier.

The activation free energies for the three reactions involved in the hydrogen electrode reaction are shown schematically in Figure 8-6. ΔG_{ad}^{o} in Figure 8-6 represents the standard adsorption free energy for $1/2\mathrm{H}_2 + \mathrm{S} \rightarrow \mathrm{H}\cdot\mathrm{S}$ at zero overpotential. We can see from Figure 8-6,

$$\begin{aligned}
\Delta \vec{G}_{V,\Phi=0}^{\ddagger,o} &= \Delta G_{V,\Phi=0}^{\ddagger,o} \\
\Delta \overleftarrow{G}_{V,\Phi=0}^{\ddagger,o} &= \Delta G_{V,\Phi=0}^{\ddagger,o} + \Delta G_{ad}^{o} \\
\Delta \vec{G}_{T,\Phi=0}^{\ddagger,o} &= \Delta G_{T,\Phi=0}^{\ddagger,o} \\
\Delta \overleftarrow{G}_{T,\Phi=0}^{\ddagger,o} &= \Delta G_{T,\Phi=0}^{\ddagger,o} - 2\Delta G_{ad}^{o} \\
\Delta \vec{G}_{H,\Phi=0}^{\ddagger,o} &= \Delta G_{H,\Phi=0}^{\ddagger,o} \\
\Delta \overleftarrow{G}_{H,\Phi=0}^{\ddagger,o} &= \Delta G_{H,\Phi=0}^{\ddagger,o} - \Delta G_{ad}^{o}
\end{aligned} \qquad (8.56)$$
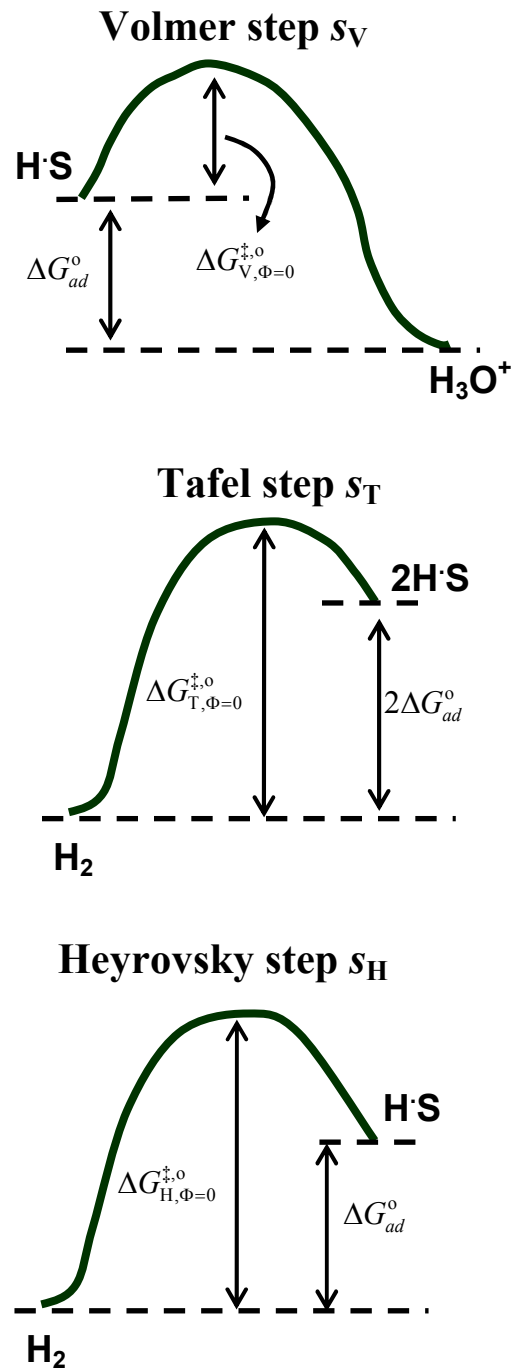
Figure 8-6: Schematic representation of free energy of activation and adsorption for the Volmer, Heyrovsky and Tafel steps.

Based on dual-pathway kinetic equation, Wang et al. [1] provided fitted step kinetics that were able to describe the kinetic behavior of the hydrogen electrode reaction over the entire relevant potential region for $T = 298$ K. In a subsequent publication [9], the authors estimated the standard adsorption free energy, $\Delta G_{ad}^0 = 75$ meV at zero overpotential, and the activation free energies for each of the three elementary steps based on the fitted kinetic data. Thus, activation free energies were calculated as $\Delta G_{T,\Phi=0}^{\ddagger,o} = 196$ meV, $\Delta G_{H,\Phi=0}^{\ddagger,o} = 294$ meV and $\Delta G_{V,\Phi=0}^{\ddagger,o} = 48$ meV for the Tafel, Heyrovsky and the Volmer steps, respectively. The DFT calculations by the authors [9] yielded $\Delta G_{ad}^0 = 58$ meV, agreeing reasonably with that obtained from fitting. It must, however, be noted that the quantum mechanical calculations by Cai and Anderson [4] obtained the activation energy for the Heyrovsky step as 76 meV which is considerably smaller than that estimated by Wang et al. [9]. The authors [9] attributed the difference to entropy contribution and the effect of lateral repulsion from the H_{UPD}, neglected by Cai and Anderson [4]. Nørskov and coworkers [45] estimated the activation energy for the Volmer step as ~150 meV, in consistence with calculated barriers for proton transfer in water. Their calculations for the Volmer reaction suggested that the energetics are given essentially by the reaction energy with a small extra contribution to the energy barrier due to the proton transfer in the water bilayer. This would indicate a very small barrier for this process close to the equilibrium potential. The energy barrier for the Tafel step was found to be significantly higher ~550 meV, than that for the Volmer step. Finally, energy barrier for the Heyrovsky step (~350 mev) was estimated to be lower than that for the Tafel step. However, the authors acknowledge the approximate nature of the method used to estimate the effect of the electrode potential which calls for more self-consistent approaches with utilization of more water molecules in the simulation to be able to distinguish between protons in the solution and protons in the double layer. Thus, there is a great deal of discrepancy in the literature reported values, largely due to the difficulties in accurately simulating the electrochemical environment from first principles calculations and is an area of active research.

Table 8-3: Reaction rate constants for hydrogen electrode reaction on Pt in acidic medium.

Reaction Step, s_ρ	Wang et al. [9]	This work
$\Delta G^{\ddagger,\mathrm{o}}_{\mathrm{T},\Phi=0}$	196 meV	185 meV
$\Delta G^{\ddagger,\mathrm{o}}_{\mathrm{H},\Phi=0}$	294 meV	120 meV
$\Delta G^{\ddagger,\mathrm{o}}_{\mathrm{V},\Phi=0}$	48 meV	48 meV
$\Delta G^{0}_{\mathrm{ad}}$	75 meV	58 meV
Λ	$3.1211\times10^{6}\ \dfrac{\text{molecules}}{\text{site.s}}$	$2.1848\times10^{5}\ \dfrac{\text{molecules}}{\text{site.s}}$

In the absence of consistent and realistic rate constants for all the electrocatalytic elementary reactions from first principles, we utilize the semi-empirical kinetic data (Table 8-3) provided by Wang et al. [9] for the case of Pt catalyst in acidic electrolyte. The kinetic analysis presented here, however, is independent of how the rate constants might have been estimated.

Finally, the specific rate r_ρ, written in terms of mol per unit supported metal catalyst surface area, is given as

$$r_\rho = \vec{r}_\rho - \bar{r}_\rho = \left\{ \vec{k}_\rho \prod_{i=1}^{n} a_i^{-\vec{\nu}_{\rho i}} - \bar{k}_\rho \prod_{i=1}^{n} a_i^{\bar{\nu}_{\rho i}} \right\} \left(\frac{C_t}{N_{Av}} \right) \qquad \frac{\text{mol}}{\text{cm}^2\text{cat.s}} \qquad (8.57)$$

where C_t is the number of reaction sites/cm^2 of catalyst surface (typically $\sim 10^{15}$ atoms/cm^2 on a metal surface), and N_{Av} (6.0221415 × 10^{23}) is the Avogadro's number. The current density can next be obtained in the units of A/cm^2, i.e., $i = \nu_{OR,e^-} F r_{OR}$ as shown in earlier analysis for alkaline medium.

It should be noted that the kinetic data in Table 8-3 is also consistent with KPL relations detailed in the earlier sections. We next utilize the data provided by Wang et al. [9] (Table 8-3), to simulate the kinetic current for hydrogen electrode reaction on Pt in acidic system at T = 298 K as presented in Figure 8-7. A close agreement of the kinetic current obtained by employing Eq. (8.44) with the QSS rate, elucidates the brute-force of the reaction route graph approach. Finally, for the kinetic data by Wang et al. [9] provided Table 8-3, an exchange current density (Eq. (8.43)) of ~370 mA/cm^2 is obtained for HOR on Pt in acidic media at 298 K, which is two orders of magnitude higher than the conventionally accepted value of 1 mA/cm^2 [46]. This is, however, in accord with the data reported by Wang et al. [1, 9] based on their dual kinetic equation. Moreover, recently, Neyerlin et al. [16] experimentally obtained the exchange current density within the range of 235 – 600 mA/cm^2 using a hydrogen pump configuration, which agrees reasonable well with our predictions.

Lastly, even though the asymmetry between the kinetics in the HER region versus that in the HOR region is captured by the rate expression derived using the circuitry approach, the degree of the asymmetry between the two regions is striking (Figure 8-7).
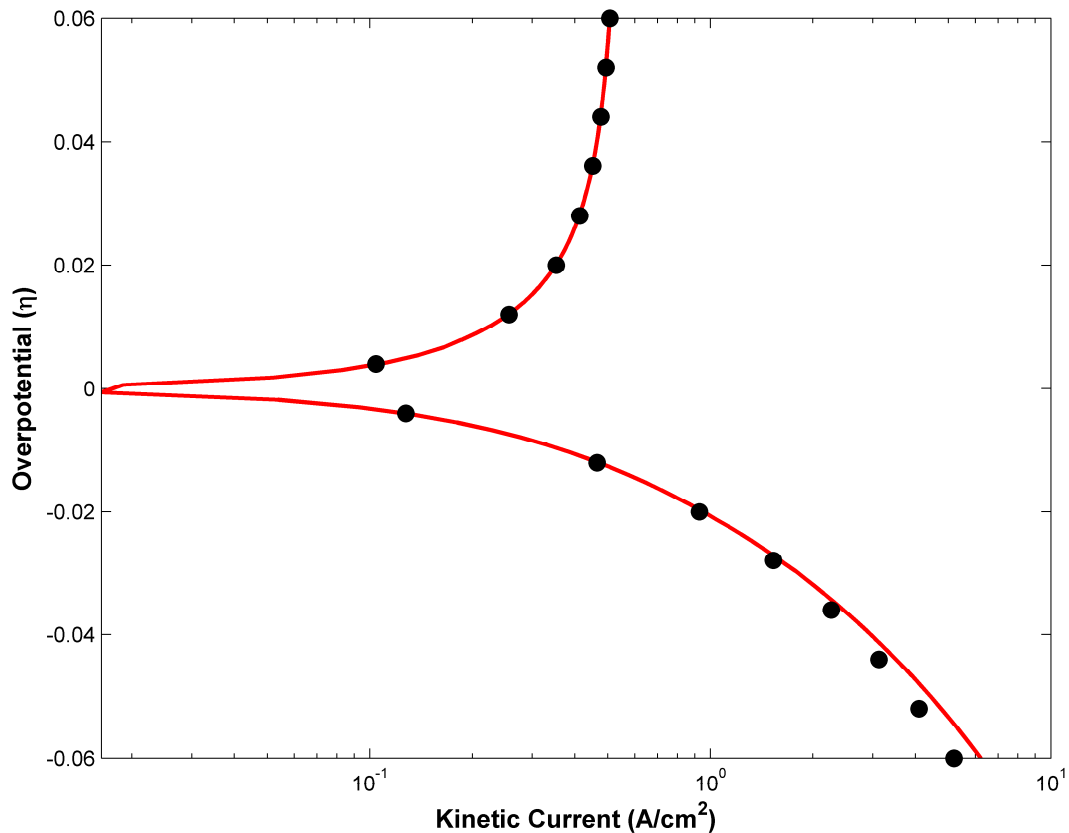
Figure 8-7: Semilog plot of overpotential, η (V) vs. absolute value of kinetic current, i for hydrogen electrode reaction on Pt in acidic medium at 298 K, Solid line represents data obtained from solving QSS equation for the 3-step Tafel-Volmer-Heyrovsky mechanism while symbols (●) represent calculations from Ohm's law for the 3-step mechanism (Eq. (8.44)).

The experimental data presented by Neyerlin et al. [16] for a fuel cell at $T = 80$ $^{\circ}$C, on the other hand is relative symmetric.

The kinetic data was next modified by us in order to fit the experimental data by Neyerlin et al. [16] at $T = 80$ $^{\circ}$C, with reasonable agreement as shown in Figure 8-8. We use $\Delta G_{T,\Phi=0}^{\ddagger,o} = 185\,\text{meV}$, a value similar to that obtained from UBI-QEP method for the Tafel step, $\Delta G_{H,\Phi=0}^{\ddagger,o} = 120\,\text{meV}$ as reported on Pt(100) by Markovic et al. [47] and $\Delta G_{V,\Phi=0}^{\ddagger,o} = 48\,\text{meV}$ provided by Wang et al [9]. Lastly, we use the value for the adsorption free energy for $1/2 H_2 + S \rightarrow H \cdot S$ at zero overpotential, $\Delta G_{ad}^0 = 58\,\text{meV}$, as determined from the DFT calculations by Wang et al. [9]. Λ, on the other hand, is the fitted parameter. It can be seen from Figure 8-8, that the kinetic current predicted by Eq. (8.44) well captures the experimental observations by Neyerlin et al. [16]. For this set of rate constants, the exchange current density was determined to be ~700 mA/cm^2, higher than that estimated by Neyerlin et al. [16].

Figure 8-8, also plots the kinetic current predicted by the more limiting rate expression for the two-step Volmer-Heyrovsky mechanism, i.e. Eq. (8.49). Thus, based on our analysis, in the entire overpotential region of interest for PEM fuel cells ($-60\,\text{mV} < \eta < 60\,\text{mV}$) in the acidic system, the Volmer-Heyrovsky is found to be the dominant reaction mechanism. The RDS, if any, can next be identified by comparing the step resistances connected in series in this pathway, as shown in Figure 8-9. Even though Heyrovsky appears to be slower of the two steps, both the steps have resistances of similar order and further pruning is unwarranted.

A number of experimental studies of HER on various Pt single crystal surfaces or polycrystalline Pt films have suggested either the Vomer-Tafel [48-50] or the Vomer-Heyrovsky dual-step reaction mechanism [51]. Thus, Volmer-Heyrovsky mechanism was suggested by Tavares et al. [51] based on fitting kinetic equations for H$_2$ evolution over polycrystalline Pt electrodes in acid to Tafel plots. Based on Tafel plots, Markovic et al. [47], suggested that the Volmer-Heyrovsky mechanism was being followed over Pt(100), and the Volmer-Tafel mechanism over the (110) surface.
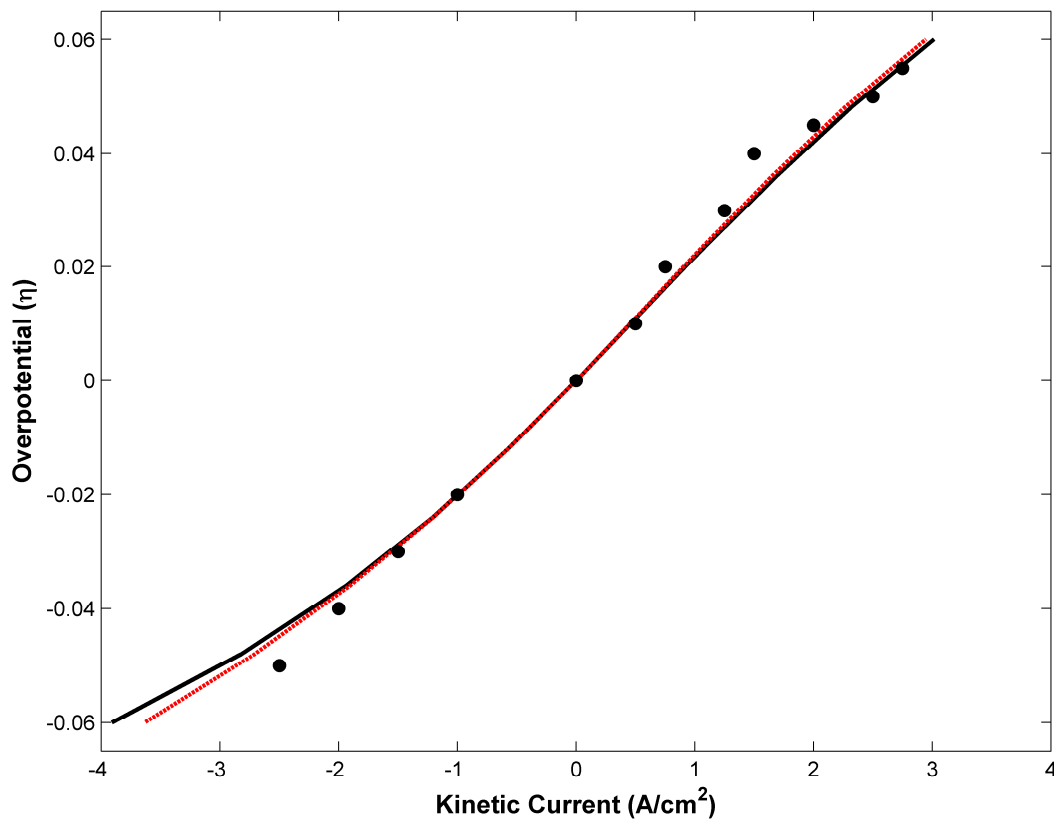
Figure 8-8: Overpotential, η (V) vs. kinetic current, i for hydrogen electrode reaction on Pt in acidic medium at 353 K, Symbols (●) represent the experimental data [16]. Solid line represents kinetic current for the 3-step Tafel-Volmer-Heyrovsky mechanism from Ohm's law for the complete 3-step mechanism (Eqs. (8.44)). Dotted line represents the kinetic current for the limiting case via Volmer-Heyrovsky mechanism (Eqs. (8.49)).
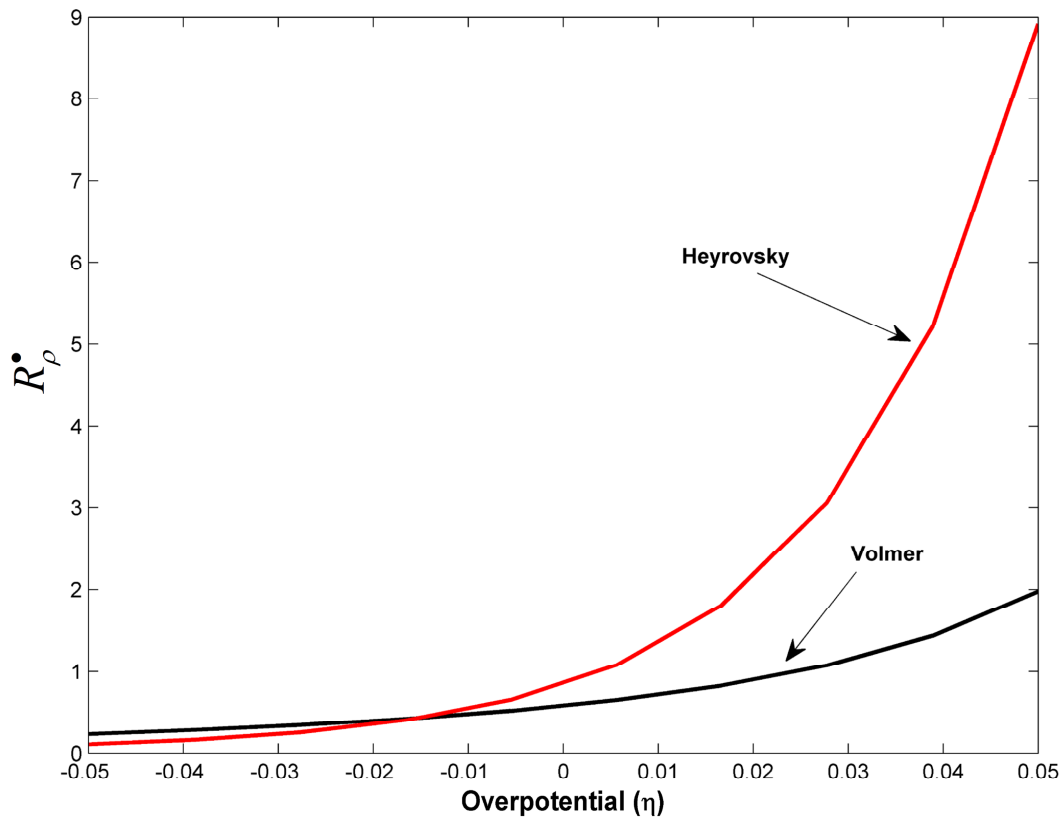
Figure 8-9: Comparison of $R_{\mathrm{V}}^{\bullet}$ and $R_{\mathrm{H}}^{\bullet}$ connected in series for the Volmer-Heyrovsky

pathway.

Results regarding the dominant reaction mechanism, however, were rather unclear over Pt(111) [47]. Others have also suggested a dual-pathway mechanism [1, 9]. Nevertheless, a general rate expression like the one developed here, for the 3-step complete mechanism has not been obtained so far, which would still be valid for all the Pt surfaces. Thus, more reliable kinetic data supplemented by consistent experimentation is necessary for a clear portrayal of the dominant reaction mechanism. The approach developed in this chapter, when combined with such kinetic data, should allow an unambiguous determination of the mechanism and kinetics.

8.4 Oxygen Reduction Reaction: Mechanism and Kinetics

Oxygen reduction reaction (ORR) accounts for a significant overpotential, even for the best known ORR catalyst, i.e., Pt, in a PEM fuel cell. A fundamental understanding of the said reaction is pivotal in designing better ORR catalysts and also for sound fuel cell modeling. Unfortunately, the mechanism and kinetics of ORR on different electrode surfaces is far from being clear. The complexity of the mechanism is due to the associated multielectron transfer and its dependence on the electrode material and electrolyte. Rotating-ring-disk electrode has been widely employed to probe the oxygen reduction mechanism. However, the method suffers from the drawback that the intermediates which do not desorb from the disk electrode surface cannot be detected.

Here we consider the simple 4-step reaction mechanism for ORR proposed by Wang et al. [25] as shown in Table 8-4, along with the activation free energies on Pt(111) in 0.1 M $HClO_4$ solution, deduced by analyzing the measured polarization curves. The physisorbed $O_2 \cdot S$ [18] and associated $O_2H \cdot S$ [19, 52-54] are neglected in the mechanism, since these species are much less stable than $O \cdot S$ or $OH \cdot S$ [25]. $O_2H \cdot S$ is, in fact, not even detected in an acidic medium [55]. Other mechanisms for ORR have been shown to be mediated via H_2O_2 [18, 53, 56-61]. However, Paulus et al. [62] showed that H_2O_2 formation at typical operating conditions of 0.7 – 0.8V is close to only ~0.2%. Similarly, Markovic et al. [18] have also shown that the fraction of peroxide formed on Pt catalyst is rather minimal (Figure 8-10), can thus be neglected to simplify the reaction mechanism as done in this case.
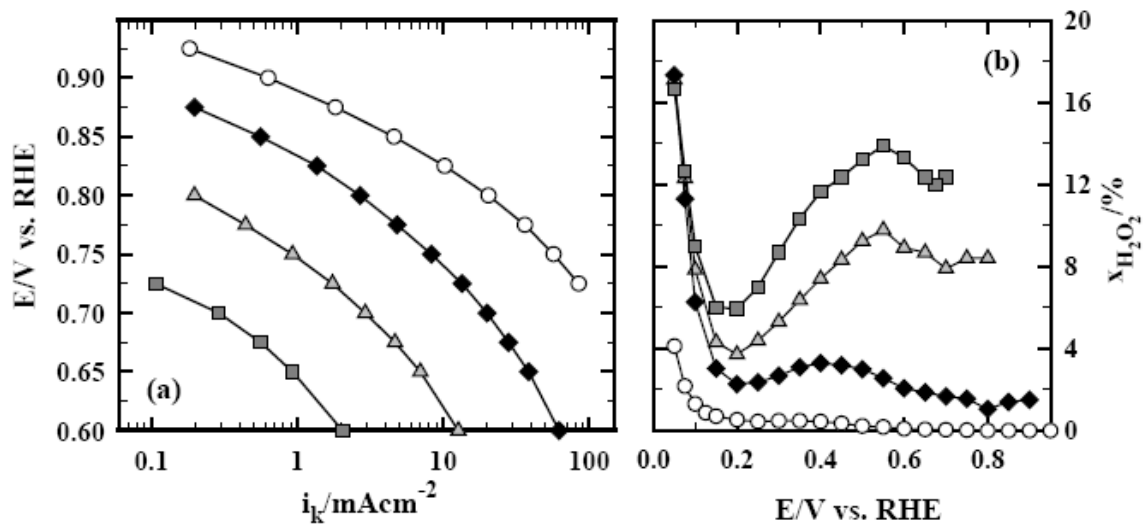
Figure 8-10: (a) Tafel plots for the ORR on Pt/Vulcan in 0.5 M HClO$_4$ (white circles) and after addition of 10^{-4} M Cl$^-$ (black diamonds), 10^{-3} M Cl$^-$ (gray triangles), and 10^{-2} M Cl$^-$ (gray squares). (b) Fraction of peroxide formed during the ORR in the presence of chloride [18].

Table 8-4: Free energy of activation for the 4-step ORR reaction mechanism on Pt(111) in acidic medium [25].

	$\Delta \vec{G}_{\rho,\Phi=0}^{\ddagger,o}$ (eV)	Elementary Reactions	$\Delta \overleftarrow{G}_{\rho,\Phi=0}^{\ddagger,o}$ (eV)
s_1:	0.258	½ O_2 + S $\leftrightarrows$ O·S	0.735
s_2:	0.459	½ O_2 + H^+ + e^- + S $\leftrightarrows$ OH·S	0.579
s_3:	0.502	O·S + H^+ + e^- $\leftrightarrows$ OH·S	0.145
s_4:	0.455	OH·S + H^+ + e^- $\leftrightarrows$ H_2O + S	0.335

Further, the kinetic data utilized in this study is also consistent with the values reported in the literature. $\Delta \vec{G}_{2,\Phi=0}^{\ddagger,o}$ was predicted to be 0.22 eV by Hyman and Medlin [23], 0.4 eV by Wang and Balbuena [22], and 0.45 eV by Anderson et al. [24]. On the other hand, DFT calculations by Nørskov and coworkers [19] yielded $\Delta \vec{G}_{3,\Phi=0}^{\ddagger,o} = 0.51\,\text{eV}$ and $\Delta \vec{G}_{4,\Phi=0}^{\ddagger,o} = 0.49\,\text{eV}$. These values are in harmony with the kinetic data employed in this work. Finally, we utilize a pre-exponential factor, $\Lambda = 3.1211 \times 10^6 \dfrac{\text{molecules}}{\text{site.s}}$, calculated from Ref. [25].

The net rates, $r_\rho = \vec{r}_\rho - \bar{r}_\rho$, of the four elementary steps in the ORR mechanism may be written as

$$
\left.
\begin{aligned}
r_1 &= \vec{\omega}_1 (1 - \theta_{\text{O·S}} - \theta_{\text{OH·S}}) - \bar{\omega}_1 \theta_{\text{O·S}} \\
r_2 &= \vec{\omega}_2 (1 - \theta_{\text{O·S}} - \theta_{\text{OH·S}}) - \bar{\omega}_2 \theta_{\text{OH·S}} \\
r_3 &= \vec{\omega}_3 \theta_{\text{O·S}} - \bar{\omega}_3 \theta_{\text{OH·S}} \\
r_4 &= \vec{\omega}_4 \theta_{\text{OH·S}} - \bar{\omega}_4 (1 - \theta_{\text{O·S}} - \theta_{\text{OH·S}})
\end{aligned}
\right\}
\tag{8.58}
$$

where, the site balance, namely, $\theta_0 + \theta_{\text{O·S}} + \theta_{\text{OH·S}} = 1$, has been incorporated to exclude θ_0.

The step weights in the above are given as

$$
\begin{aligned}
\vec{\omega}_1 &= \vec{k}_1 & ; \quad \bar{\omega}_1 &= \bar{k}_1 \\
\vec{\omega}_2 &= \vec{\omega}_{2,0} e^{-\psi} & ; \quad \bar{\omega}_2 &= \bar{\omega}_{2,0} e^{\psi} \\
\vec{\omega}_3 &= \vec{\omega}_{3,0} e^{-\psi} & ; \quad \bar{\omega}_3 &= \bar{\omega}_{3,0} e^{\psi} \\
\vec{\omega}_4 &= \vec{\omega}_{4,0} e^{-\psi} & ; \quad \bar{\omega}_4 &= \bar{\omega}_{4,0} e^{\psi}
\end{aligned}
\tag{8.59}
$$

Further,

$$
\begin{aligned}
\vec{\omega}_{2,0} &= \vec{k}_{2,\Phi_0} \sqrt{a_{\text{O}_2}} & ; \quad \bar{\omega}_{2,0} &= \bar{k}_{2,\Phi_0} \\
\vec{\omega}_{3,0} &= \vec{k}_{3,\Phi_0} \sqrt{a_{\text{O}_2}} & ; \quad \bar{\omega}_{3,0} &= \bar{k}_{3,\Phi_0} \\
\vec{\omega}_{4,0} &= \vec{k}_{4,\Phi_0} & ; \quad \bar{\omega}_{4,0} &= \bar{k}_{4,\Phi_0} a_{\text{H}_2\text{O}}
\end{aligned}
\tag{8.60}
$$

In these expressions, the activity of water is usually assumed to be unity, i.e., $a_{\text{H}_2\text{O}} = 1$, for saturated conditions, while the activity of oxygen is written as its partial pressure, i.e.,

$a_{O_2} = p_{O_2}$, in atm. Finally, $\vec{k}_{\rho,\Phi_0}$ and $\overleftarrow{k}_{\rho,\Phi_0}$ is obtained similar to that in the case of hydrogen electrode reaction in the acidic system, i.e., Eq. (8.54) and Eq. (8.3).

8.4.1 Reaction Route Graph

For the 4-step ORR reaction mechanism considered here, with two linearly independent intermediates species, O·S and OH·S, a direct full route must not contain more than any three (q +1) of the four steps, while a direct ER must be restricted to less than four (q + 2) steps.

The system, in fact consists of two FRs and 1 ER as shown below

$$
\left.\begin{array}{ll}
\text{FR}_1: & (+1)s_1 + (+1)s_3 + (+1)s_4 = \text{OR} \\
\text{FR}_2: & (+1)s_2 + (+1)s_4 = \text{OR} \\
\text{ER}_1: & (+1)s_1 + (-1)s_2 + (+1)s_3 = 0
\end{array}\right\} \tag{8.61}
$$

It is relatively easy to assemble these RRs into a RR graph which is provided in Figure 8-11. We first assemble the only empty route, ER$_1$ into a cycle graph. The only step missing, i.e., s_4 in next added to complete the full route. The overall reaction is then added across the terminal nodes to complete the RR Graph.

Finally, the kinetic data provided in Table 8-4, is consistent with the KPL relation, i.e.

$$
\mathscr{A}_{OR} = \mathscr{A}_1 + \mathscr{A}_3 + \mathscr{A}_4 = \mathscr{A}_2 + \mathscr{A}_4 \tag{8.62}
$$

and

$$
\mathscr{A}_1 - \mathscr{A}_2 + \mathscr{A}_3 = 0, \text{i.e,} \quad \left(\frac{\vec{\omega}_1}{\overleftarrow{\omega}_1}\right)\left(\frac{\vec{\omega}_2}{\overleftarrow{\omega}_2}\right)\left(\frac{\vec{\omega}_3}{\overleftarrow{\omega}_3}\right) = 1 \tag{8.63}
$$

8.4.2 QSS Rate Expression

Numerical QSS rate can be obtained by solving the KFL equation at the nodes of the RR graph, i.e.

$$
\begin{array}{ll}
n_1: & (-1)r_4 + (+1)r_1 + (+1)r_2 = 0 \\
n_2: & (-1)r_1 + (+1)r_3 = 0
\end{array} \tag{8.64}
$$
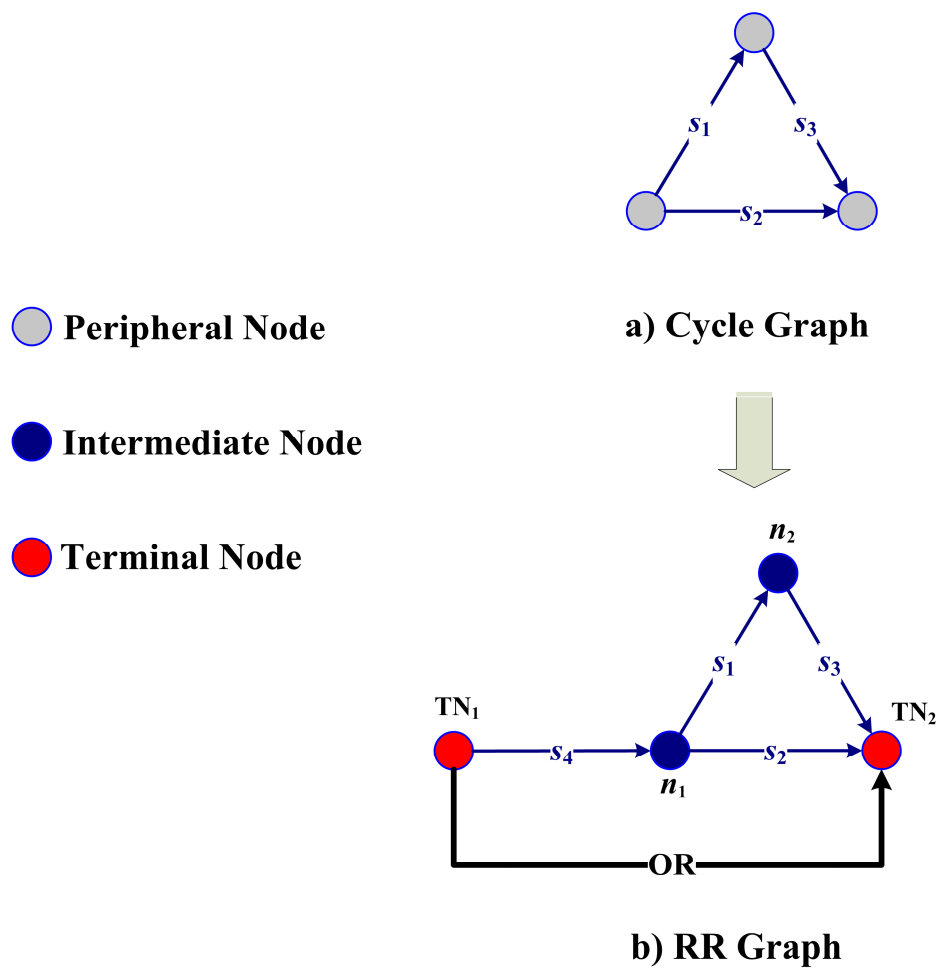
Figure 8-11: RR Graph construction for the 4-step ORR mechanism.

Solving the above equations simultaneously, provides $\theta_{O\cdot S}$ and $\theta_{OH\cdot S}$, and hence the step rates. Using the same in the KFL at the terminal nodes (Figure 8-11) gives the overall reaction rate, i.e.

$$r_{OR} = r_4 = r_2 + r_3 \tag{8.65}$$

We will, however, use the electrical analog of the RR Graph, shown in Figure 8-12 below for deriving a QSS rate law based on its electrical analog, which would include the flux along both pathways (FRs).

The rate of the overall reaction can be cast into a Ohm's law form as shown below

$$r_{OR} = \frac{\mathscr{A}_{OR}}{R_{OR}} \tag{8.66}$$

Where, the resistance of the network can be easily obtained from its electrical network (Figure 8-12).

$$R_{OR} = R_4 + \cfrac{1}{\cfrac{1}{R_2} + \cfrac{1}{R_1 + R_3}} \tag{8.67}$$

Such a representation, even though consistent with the numerical results obtained from the conventional KFL/QSS analysis, cannot provide explicit rate expressions. Thus, following the alternate circuitry approach, we may write the overall rate as

$$r_{OR} \approx \frac{E_{OR}}{R_{OR}^\bullet} = \cfrac{E_{OR}}{R_4^\bullet + \cfrac{1}{\cfrac{1}{R_2^\bullet} + \cfrac{1}{R_1^\bullet + R_3^\bullet}}} \tag{8.68}$$

where, the driving force E_{OR} is known quantity

$$E_{OR} = 1 - z_{OR} = 1 - \frac{\bar{\omega}_2 \bar{\omega}_4}{\vec{\omega}_2 \vec{\omega}_4} = 1 - \frac{\bar{\omega}_1 \bar{\omega}_3 \bar{\omega}_4}{\vec{\omega}_1 \vec{\omega}_3 \vec{\omega}_4} \tag{8.69}$$
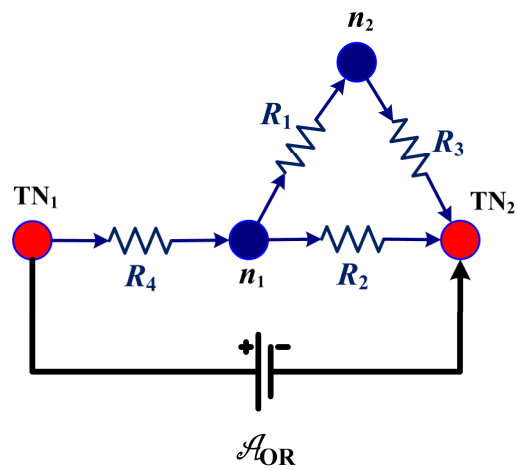
Figure 8-12: The equivalent electrical circuit for the 4-step ORR mechanism.

$R_\rho^\bullet$ can next be ascertained *a priori* following the LHHW approach along with notion of IRRs, described in chapter II. Thus, with step s_1 as the RDS, the intermediate reactions for the two intermediates are

$IR_{O\cdot S} : (-1)s_3 + (-1)s_4 \qquad : H_2O + S \rightleftharpoons O\cdot S + 2H^+ + 2e^-$

$IR_{OH\cdot S} : (-1)s_4 \qquad\qquad : H_2O + S \rightleftharpoons OH\cdot S + H^+ + e^-$
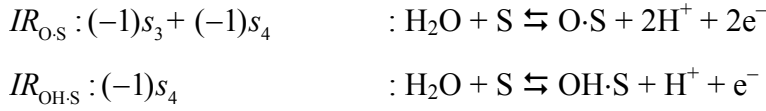
Using Eq. 2.25, for the QE steps, the site fraction ratios are

$$\left.\begin{aligned}
\frac{\theta_{O\cdot S,1}^\bullet}{\theta_{0,1}^\bullet} &= \left(\frac{\vec{\omega}_3}{\bar{\omega}_3}\right)^{-1}\left(\frac{\vec{\omega}_4}{\bar{\omega}_4}\right)^{-1} \\
\frac{\theta_{OH\cdot S,1}^\bullet}{\theta_{0,1}^\bullet} &= \left(\frac{\vec{\omega}_4}{\bar{\omega}_4}\right)^{-1}
\end{aligned}\right\}
\tag{8.70}$$

Once the site fractions are known, the step resistance $R_1^\bullet$ can be ascertained using the site balance equation

$$R_1^\bullet = \frac{1}{\vec{r}_1^\bullet} = \frac{1}{\vec{\omega}_1 \theta_{0,1}^\bullet} = \frac{1}{\vec{\omega}_1}\left(1 + \frac{\bar{\omega}_3\bar{\omega}_4}{\vec{\omega}_3\vec{\omega}_4} + \frac{\bar{\omega}_4}{\vec{\omega}_4}\right)
\tag{8.71}$$

Similarly with step s_2 as the RDS, the intermediate reactions for the two intermediates are

$IR_{O\cdot S} : (-1)s_3 + (-1)s_4 \qquad : H_2O + S \rightleftharpoons O\cdot S + 2H^+ + 2e^-$
$IR_{OH\cdot S} : (-1)s_4 \qquad\qquad : H_2O + S \rightleftharpoons OH\cdot S + H^+ + e^-$
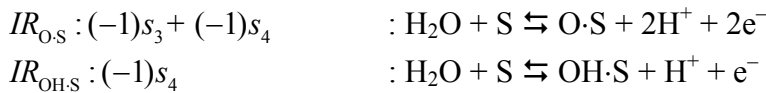
Using Eq. 2.25, for the QE steps, the site fraction ratios are

$$\left.\begin{aligned}
\frac{\theta_{O\cdot S,2}^\bullet}{\theta_{0,2}^\bullet} &= \left(\frac{\vec{\omega}_3}{\bar{\omega}_3}\right)^{-1}\left(\frac{\vec{\omega}_4}{\bar{\omega}_4}\right)^{-1} \\
\frac{\theta_{OH\cdot S,2}^\bullet}{\theta_{0,2}^\bullet} &= \left(\frac{\vec{\omega}_4}{\bar{\omega}_4}\right)^{-1}
\end{aligned}\right\}
\tag{8.72}$$

Thus, using the above and the site balance equation Eq. 2.26, we have,

$$R_2^\bullet = \frac{1}{\vec{r}_2^\bullet} = \frac{1}{\vec{\omega}_2 \theta_{0,2}^\bullet} = \frac{1}{\vec{\omega}_2}\left(1 + \frac{\bar{\omega}_3\bar{\omega}_4}{\vec{\omega}_3\vec{\omega}_4} + \frac{\bar{\omega}_4}{\vec{\omega}_4}\right)
\tag{8.73}$$

Following a similar procedure for step s_3 and s_4, we get

$$R_3^\bullet = \frac{1}{\vec{r}_3^\bullet} = \frac{1}{\vec{\omega}_3 \theta_{O\cdot S,3}^\bullet} = \frac{1}{\vec{\omega}_3 \left(\dfrac{\theta_{O\cdot S,3}^\bullet}{\theta_{0,3}^\bullet} \right) \theta_{0,3}^\bullet} = \frac{\bar{\omega}_1}{\vec{\omega}_3 \vec{\omega}_1} \left(1 + \frac{\bar{\omega}_1}{\bar{\omega}_1} + \frac{\bar{\omega}_4}{\bar{\omega}_4} \right) \tag{8.74}$$

$$R_4^\bullet = \frac{1}{\vec{r}_4^\bullet} = \frac{1}{\vec{\omega}_4 \theta_{OH\cdot S,4}^\bullet} = \frac{1}{\vec{\omega}_3 \left(\dfrac{\theta_{O\cdot S,4}^\bullet}{\theta_{0,4}^\bullet} \right) \theta_{0,4}^\bullet} = \frac{\bar{\omega}_2}{\vec{\omega}_4 \vec{\omega}_2} \left(1 + \frac{\bar{\omega}_1}{\bar{\omega}_1} + \frac{\bar{\omega}_2}{\bar{\omega}_2} \right) \tag{8.75}$$

Substituting Eqs. (8.71), (8.73), (8.74), and (8.75) in Eq. (8.68) along with Eq. (8.69), and using $i = v_{OR,e^-} Fr_{OR}$, provides a complex, albeit explicit rate expression for ORR on Pt in acidic medium, we have

$$i = \frac{v_{OR,e^-} F(1 - z_{OR})}{\dfrac{\bar{\omega}_2}{\vec{\omega}_4 \vec{\omega}_2} \left(1 + \frac{\bar{\omega}_1}{\bar{\omega}_1} + \frac{\bar{\omega}_2}{\bar{\omega}_2} \right) + \dfrac{1}{\dfrac{1}{\dfrac{1}{\bar{\omega}_2} \left(1 + \frac{\bar{\omega}_3 \bar{\omega}_4}{\vec{\omega}_3 \vec{\omega}_4} + \frac{\bar{\omega}_4}{\bar{\omega}_4} \right)} + \dfrac{1}{\dfrac{1}{\bar{\omega}_1} \left(1 + \frac{\bar{\omega}_3 \bar{\omega}_4}{\vec{\omega}_3 \vec{\omega}_4} + \frac{\bar{\omega}_4}{\bar{\omega}_4} \right) + \dfrac{\bar{\omega}_1}{\vec{\omega}_3 \vec{\omega}_1} \left(1 + \frac{\bar{\omega}_1}{\bar{\omega}_1} + \frac{\bar{\omega}_4}{\bar{\omega}_4} \right)}}} \tag{8.76}$$

Moreover, under conditions of interest, ORR is essentially an irreversible reaction, thus $z_{OR} \to 0$, or $E_{OR} \to 1$. Thus,

$$i = \frac{v_{OR,e^-} F}{\dfrac{\bar{\omega}_2}{\vec{\omega}_4 \vec{\omega}_2} \left(1 + \frac{\bar{\omega}_1}{\bar{\omega}_1} + \frac{\bar{\omega}_2}{\bar{\omega}_2} \right) + \dfrac{1}{\dfrac{1}{\dfrac{1}{\bar{\omega}_2} \left(1 + \frac{\bar{\omega}_3 \bar{\omega}_4}{\vec{\omega}_3 \vec{\omega}_4} + \frac{\bar{\omega}_4}{\bar{\omega}_4} \right)} + \dfrac{1}{\dfrac{1}{\bar{\omega}_1} \left(1 + \frac{\bar{\omega}_3 \bar{\omega}_4}{\vec{\omega}_3 \vec{\omega}_4} + \frac{\bar{\omega}_4}{\bar{\omega}_4} \right) + \dfrac{\bar{\omega}_1}{\vec{\omega}_3 \vec{\omega}_1} \left(1 + \frac{\bar{\omega}_1}{\bar{\omega}_1} + \frac{\bar{\omega}_4}{\bar{\omega}_4} \right)}}} \tag{8.77}$$

Moreover, when equilibrium is brought about by changing the electrode overpotential to zero, i.e., as $\psi \to 0$, then the net electrode current density $i \to 0$, and the current density in each direction $\vec{i}$, and $\bar{i} \to i_0$. Thus, Eq. (8.77) at $\psi = 0$ provides the exchange current density for ORR on Pt as $i_0 = 1.43 \times 10^{-11}$ A/cm^2. This is within the normal reported range of exchange current density for ORR, i.e. $10^{-9} - 10^{-11}$ A/cm^2 [63]. Antoine et al. [52] predicted exchange current density in the range of $10^{-10} - 10^{-7}$ A/cm^2.

Parthasarathy et al. have reported exchange current density for ORR as 2.2×10^{-10} A/cm^2 [64], 8.3×10^{-10} A/cm^2 [65] and 3.25×10^{-11} A/cm^2 [66] in their work.

QSS rate expressions can also be derived for the limiting cases for each of the two pathways. Thus,

$$\left. \begin{aligned} R^\bullet_{FR_1} &= R^\bullet_1 + R^\bullet_3 + R^\bullet_4 \\ R^\bullet_{FR_2} &= R^\bullet_2 + R^\bullet_4 \end{aligned} \right\} \tag{8.78}$$

Thus, for each of the two pathways with $E_{OR} \to 1$ we have

$$i_{FR_1} \approx \frac{v_{OR,e^-} F E_{OR}}{R^\bullet_{FR_1}} \approx \frac{v_{OR,e^-} F}{R^\bullet_1 + R^\bullet_3 + R^\bullet_4} \tag{8.79}$$

$$i_{FR_2} \approx \frac{v_{OR,e^-} F E_{OR}}{R^\bullet_{FR_2}} \approx \frac{v_{OR,e^-} F}{R^\bullet_2 + R^\bullet_4} \tag{8.80}$$

Figure 8-13 plots the kinetic current for the 4-step mechanism and for each of two pathways for the ORR on Pt rotating disc electrode in an oxygen saturated ($a_{O_2} = p_{O_2} = 1$ atm) 0.1 M HClO$_4$ solution. The rate expression for the complete 4-step reaction mechanism is in good agreement with the experimental data. It should be noted that the current density obtained from Ohm's law representation of kinetics, Eq. (8.77) is in complete agreement with the numerical QSS rate obtained from solving the KFL equations, i.e. Eqs. (8.64) and (8.65). In order to avoid clutter, the numerical QSS rate is not provided on Figure 8-13. Moreover, Figure 8-13 reveals that majority of the flux is through FR$_2$, i.e. $s_2 + s_4 = OR$. Thus, the reductive adsorption and reductive desorption is the favorable path via OH·S species.

Thus, one may derive the reduced rate expression for ORR on Pt in acidic system,

$$i = \frac{v_{OR,e^-} F}{R^\bullet_2 + R^\bullet_4} \tag{8.81}$$

or
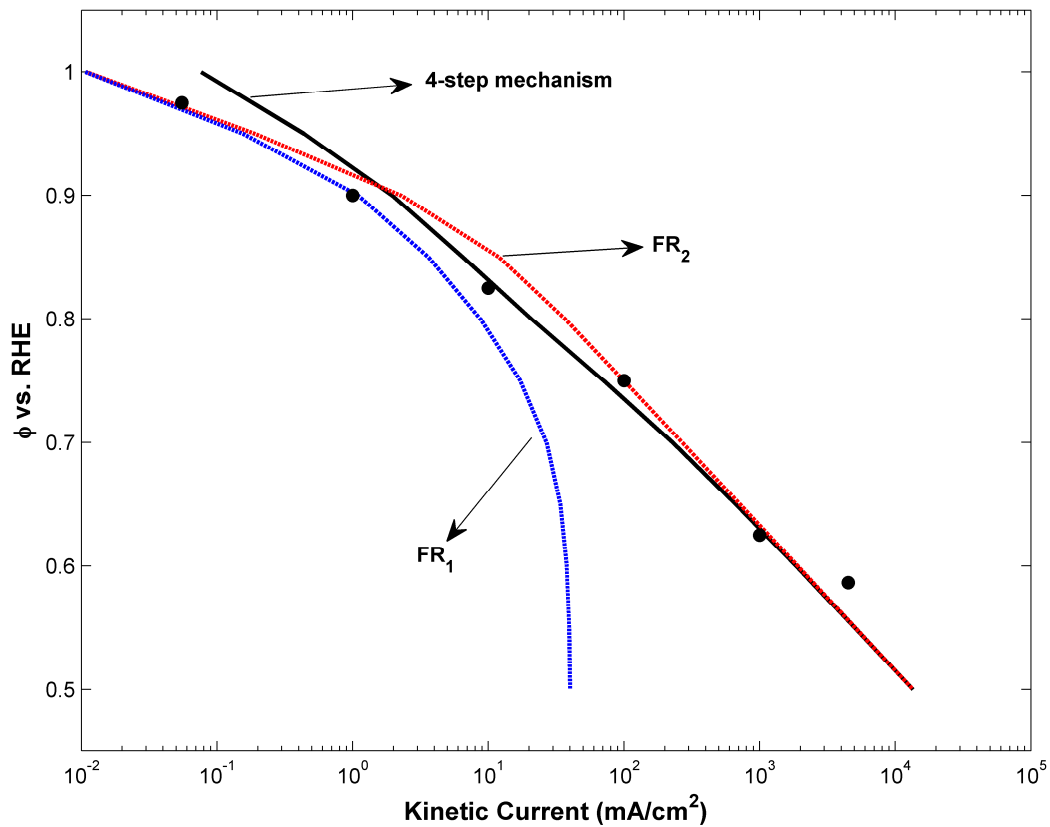
Figure 8-13: Potential (V) vs. kinetic current for ORR on Pt electrode in 0.1 M HClO$_4$ solution. Symbols (●) represent the experimental data [25]. Solid line represents kinetic current for the 4-step mechanism from Ohm's law (Eq. (8.77)). Dotted lines represent the kinetic current for the limiting case via FR$_1$ (blue) and FR$_2$ (red) (i.e., Eqs. (8.79) and (8.80)).
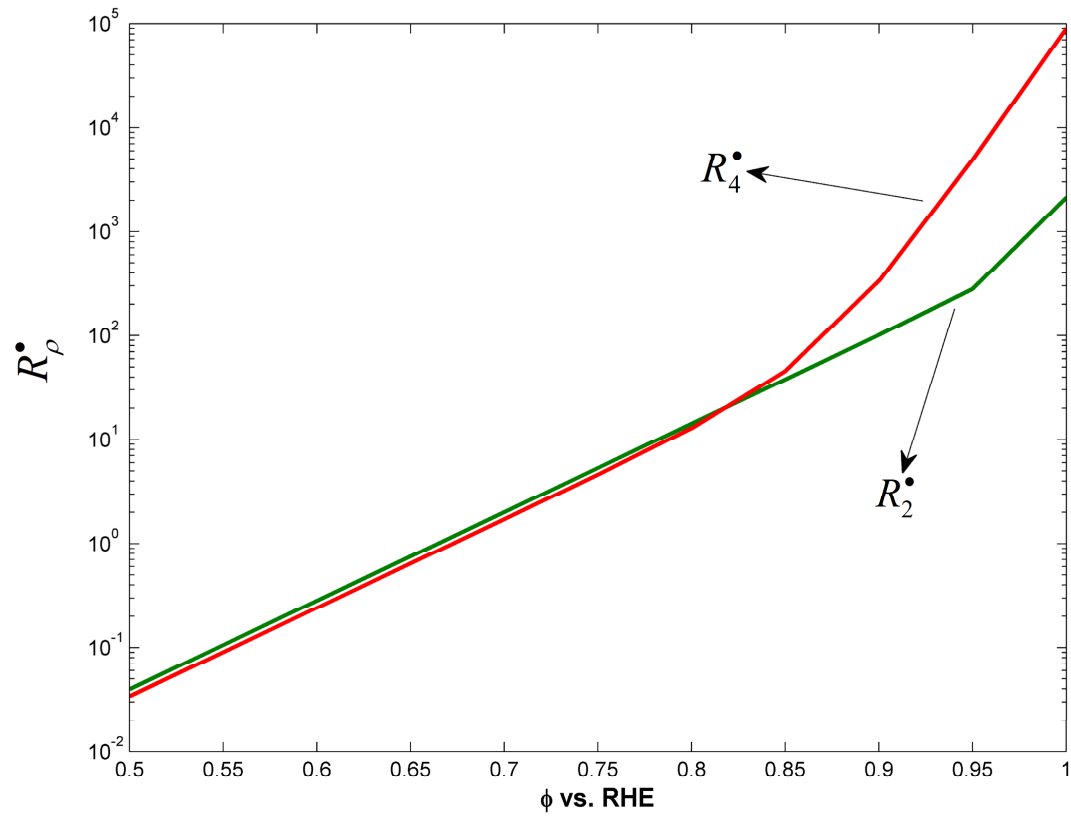
Figure 8-14: Comparison of $R_2^\bullet$ and $R_4^\bullet$ connected in series for the FR$_2$.

$$i = \frac{v_{OR,e^-} F}{\frac{1}{\vec{\omega}_2}\left(1 + \frac{\bar{\omega}_3\bar{\omega}_4}{\vec{\omega}_3\vec{\omega}_4} + \frac{\bar{\omega}_4}{\vec{\omega}_4}\right) + \frac{\bar{\omega}_2}{\vec{\omega}_4\vec{\omega}_2}\left(1 + \frac{\bar{\omega}_1}{\vec{\omega}_1} + \frac{\bar{\omega}_2}{\vec{\omega}_2}\right)} \tag{8.82}$$

Figure 8-14, next compares the relative resistances in FR_2. We see that only for $\Phi > 0.8\,V$, can step s_4, i.e., reductive desorption be labeled as the RDS. Thus, the rate-limiting step is not constant over the entire potential range. We conclude that the step s_2, i.e., the reductive adsorption cannot be considered as the RDS for the process as proposed by Wang et al. [25].

8.5 Conclusions

The Reaction Route (RR) Graph approach has been applied here to the hydrogen electrode reaction and the oxygen reduction reaction of immense importance in fuel cells. Explicit new rate expressions involving all 3 steps ((Volmer-Heyrovsky-Tafel) as well as for more limiting 2-step ((Volmer-Heyrovsky, Volmer-Tafel) mechanisms for the hydrogen electrode reaction have been derived. These expressions not only agree very well with the QSS analysis, and nicely explain the asymmetry in current-versus-potential observed in the hydrogen evolution reaction (HER) versus the hydrogen oxidation reaction (HOR), but also agree with the literature reported experimental data.

Thus, for the 3-step hydrogen electrode reaction mechanism on Pt in 0.5M NaOH at T = 296 K, we find that the Volmer-Heyrovsky pathway is dominant in the potential region $-0.3\,V < \eta < -0.24\,V$ for HER and in the range $0.13\,V < \eta < 0.3\,V$ for HOR, while the Volmer-Tafel mechanism dominates in the potential region $-0.1\,V < \eta < 0\,V$ for HER and in $0 < \eta < 20\,mV$ for HOR. All three steps, however, need to be retained over the complete range of potentials of interest.

For the case of HOR on Pt in acidic system in connection to fuel cells, we find that the Volmer-Heyrovsky mechanism adequately describes the experimental findings in the potential region of interest to PEM fuel cells. Moreover, the exchange current density for HOR in the acidic system was found to be two orders of magnitude higher than what has been assumed for more than four decades.

A 4-step simple mechanism for ORR was also analyzed using the reaction circuitry approach to deduce explicit rate expression which is in good agreement with the experimental data from the literature. Reduced rate expression based on the dominant reaction pathway is next obtained in a logical manner by comparing the resistance across different possible pathways.

Our topological approach is, thus, revealing and intuitive in depicting all possible reaction pathways as walks or paths on the RR Graph, and by visualizing the steps as resistances in an electrical circuit analog involving series and parallel pathways. It furthermore provides for an explicit analysis in an easy and tractable manner. Based on this approach, we were able to report explicit rate expressions for the first time ever, for both the electrochemical reaction systems occurring at the anode and cathode of a $H_2 - O_2$ PEM fuel. A deeper fundamental understanding of fuel cells, thus developed can aid improved catalyst design and detailed fuel cell modeling. The approach highlighted in this chapter can be easily adopted for a detailed and robust analysis for a host of different electrochemical systems, e.g., methanol electro-oxidation at the anode of DMFCs.

8.6 References

[1]   J.X. Wang, T.E. Springer, R.R. Adzic, J. Electrochem. Soc. 153 (2006) A1732-A1740.

[2]   Y. Ishikawa, J.J. Mateo, D.A. Tryk, C.R. Cabrera, J. Electroanal. Chem. 607 (2007) 37-46.

[3]   A.B. Anderson, N.M. Neshev, R.A. Sidik, P. Shiller, Electrochim. Acta. 47 (2002) 2999-3008.

[4]   Y. Cai , A.B. Anderson, J. Phys. Chem. B. 108 (2004) 9829 -9833.

[5]   M.R. Gennero de Chialvo, A.C. Chialvo, Phys. Chem. Chem. Phys. 3 (2001) 3180-3184.

[6]   J.K. Norskov, T. Bligaard, A. Logadottir, J.R. Kitchin, J.G. Chen, S. Pandelov, U. Stimming, J. Electrochem. Soc. 152 (2005) J23-J26.

[7]   S. Wolfgang, T. Sergio, J. Electrochem. Soc. 153 (2006) L31-L32.

[8]   J. Meier, J. Schiøtz, P. Liu, J.K. Nørskov, U. Stimming, Chem. Phys. Lett. 390 (2004) 440-444.

[9]   J.X. Wang, T.E. Springer, P. Liu, M. Shao, R.R. Adzic, J. Phys. Chem. C. 111 (2007) 12425-12433.

[10] P.M. Quaino, J.L. Fernandez, M.R. Gennero de Chialvo, A.C. Chialvo, J. Mol. Catal. A: Chemical. 252 (2006) 156-162.

[11] B.E. Conway, L. Bai, J. Electroanal. Chem. 198 (1986) 149-175.

[12] N. Krstajic, M. Popovic, B. Grgur, M. Vojnovic, D. Sepa, J. Electroanal. Chem. 512 (2001) 16-26.

[13] N. Krstajic, M. Popovic, B. Grgur, M. Vojnovic, D. Sepa, J. Electroanal. Chem. 512 (2001) 27-35.

[14] R.-B. Lin, S.-M. Shih, J. Chin. Inst. Chem. Eng. 39 (2008) 475-481.

[15] N.M. Markovic, S.T. Sarraf, H.A. Gasteiger, P.N.J. Ross, J. Chem. SOC., Faraday Trans. 92 (1996) 3719-3725.

[16] K.C. Neyerlin, W. Gu, J. Jorne, H.A. Gasteiger, J. Electrochem. Soc. 154 (2007) B631-B635.

[17] C.A. Marozzi, M.R. Canto, V. Costanza, A.C. Chialvo, Electrochim. Acta. 51 (2005) 731-738.

[18] N. M. Markovic, T.J. Schmidt, V.Stamenkovic, P.N. Ross, Fuel Cells-From Fundamentals to Systems. 1 (2001) 105-116.

[19] J.K. Nørskov, J. Rossmeisl, A. Logadottir, L. Lindqvist, J.R. Kitchin, T. Bligaard, H. Jonsson, J. Phys. Chem. B. 108 (2004) 17886.

[20] Y. Xu, A.V. Ruban, M. Marvrikakis, J. Am. Chem. Soc. 126 (2004) 4717.

[21] A.B. Anderson, T.V. Albu, J. Electrochem. Soc. 147 (2000) 4229.

[22] Y.X. Wang, P.B. Balbuena, J. Phys. Chem. B. 108 (2004) 4376.

[23] M.P. Hyman, J.W. Medlin, J. Phys. Chem. 110 (2006) 15338.

[24] A.B. Anderson, Y. Cai, A.S. Reyimjan, D.B. Kang, J. Electroanal. Chem. 580 (2005) 17.

[25] J.X. Wang, J. Zhang, R.R. Adzic, J. Phys. Chem. A. 111 (2007) 12702-12710.

[26] T. Thampan, S. Malhotra, J. Zhang, R. Datta, Catal. Today. 67 (2001) 15-32.

[27] J. Tafel, Z. Phys. Chem. 50 (1905) 641.

[28] J. Heyrovsky, Recl. Trav. Chim. Pays-Bas. 46 (1927) 582.

[29] T. Volmer, M. Erdey-Gruz, Z. Phys. Chem. Abt. A. 150 (1930) 203.

[30] M.R. Gennero de Chialvo, A.C. Chialvo, J. Electrochem. Soc. 147 (2000) 1619-1622.

[31] J.K. Nørskov, T. Bligaard, A. Logadottir, J.R. Kitchin, J.G. Chen, S. Pandelov, U. Stimming, J. Electrochem. Soc. 152 (2005) J23-J26.

[32] S. Völkening, K. Bedürftig, K. Jacobi, J. Wintterlin, G. Ertl, Phys. Rev. Lett. 83 (1999) 2672-2675.

[33] K. Bedurftig, S. Volkening, Y. Wang, J. Wintterlin, K. Jacobi, G. Ertl, J. Chem. Phys. 111 (1999) 11147-11154.

[34] J. Rossmeisl, J.K. Nørskov, C.D. Taylor, M.J. Janik, M. Neurock, J. Phys. Chem. B. 110 (2006) 21833-21839.

[35] I. Fishtik, C.A. Callaghan, R. Datta, J. Phys. Chem. B. 108 (2004) 5671-5682.

[36] I. Fishtik, C.A. Callaghan, R. Datta, J. Phys. Chem. B. 108 (2004) 5683-5697.

[37] I. Fishtik, C.A. Callaghan, R. Datta, J. Phys. Chem. B. 109 (2005) 2710-2722.

[38] I. Fishtik, C.A. Callaghan, J.D. Fehribach, R. Datta, J. Electroanal. Chem. 576 (2005) 57-63.

[39] S.A. Vilekar, I. Fishtik, R. Datta, J. Catal. 252 (2007) 258-270.

[40] N. Balabanian, T. Bickart, Electrical Network Theory, John Wiley, New York, 1969.

[41] S.A. Vilekar, I. Fishtik, R. Datta, Chem. Eng. Sci. 64 (2009) 1968-1979.

[42] L. Bai, J. Electroanal. Chem. 355 (1993) 37.

[43] V.S. Bagotzky, V. Osterova, J. Electroanal. Chem. 43 (1973) 233.

[44] K. Machida, M. Enyo, Bull. Chem. Soc. Jpn. 59 (1986) 725-731.

[45] E. Skulason, G.S. Karlberg, J. Rossmeisl, T. Bligaard, Greeley J., H. Jonsson, J.K. Nørskov, Phys. Chem. Chem. Phys. 9 (2007) 3241–3250.

[46] J.O.M. Bockris, S. Srinivasan, Fuel Cells: Their Electrochemistry, McGraw-Hill, New York, 1969.

[47] N.M. Markovic, B.N. Grgur, P.N. Ross, J. Phys. Chem. B. 101 (1997) 5405-5413.

[48] K. Kunimatsu, T. Senzaki, M. Tsushima, M. Osawa, Chem. Phys. Lett. 401 (2005) 451.

[49] B. E. Conway, G. Jerkiewicz, Electrochim. Acta. 45 (2000) 4075.

[50] J. Barber, S. Morin, B. E. Conway, J. Electroanal. Chem. 446 (1998) 125.

[51] M.C. Tavares, S.A.S. Machado, L.H. Mazo, Electrochim. Acta. 46 (2001) 4359-4369.

[52] O. Antoine, Y. Bultel, D. Durand, J. Electroanal. Chem. 499 (2001) 85–94.

[53] A. Damjanovic, V. Brusic, Electrochim. Acta. 12 (1967) 615-628.

[54] Y. Suga, Chem. Lett. 35 (2006) 1406-1407.

[55] M.H. Shao, P. Liu, R.R. Adzic, J. Am. Chem. Soc. 128 (2006) 7408.

[56] A.B. Anderson, T.V. Albu, Electrochem. Comm. 1 (1999) 203-206.

[57] T.V. Albu, A.B. Anderson, Electrochim. Acta. 46 (2001) 3001–3013.

[58] A.B. Anderson, T.V. Albu, J. Am. Chem. Soc. 121 (1999) 11855-11863.

[59] R.A. Sidik, A.B. Anderson, J. Electroanal. Chem. 528 (2002) 69-78.

[60] V. Stamenkovic, T. J. Schmidt, P. N. Ross, N. M. Markovic, J. Phys. Chem. B. 106 (2002) 11970-11979.

[61] V. Stamenkovic, B. N. Grgur, P. N. Ross, N. M. Markovic, J. Electrochem. Soc. 152 (2005) A277-A282

[62] U.A. Paulus, T.J. Schmidt, H.A. Gasteiger, R.J. Behm, J. Electroanal. Chem. 495 (2001) 134–145.

[63] K. Kinoshita, Electrochemical Oxygen Technology, Wiley, New York, 1992.

[64] A. Parthasarathy, C.R. Martin, S. Srinivasan, J. Electrochem. Soc. 138 (1991) 916.

[65] A. Parthasarathy, B. Dave, S. Srinivasan, A.J. Appleby, C.R. Martin, J. Electrochem. Soc. 139 (1992) 1634.

[66] A. Parthasarathy, S. Srinivasan, A.J. Appleby, C.R. Martin, J. Electrochem. Soc. 139 (1992) 2530.

Chapter IX

Conclusions and Recommendations for Future Work

9.1 Theory of Reaction Route Graphs

The objective of this research was to develop fundamental understanding of the kinetics and mechanism of the journey of a fuel (e.g. methane or methanol) to electricity involving a number of catalytic steps in fuel reformation into hydrogen as well as electro-catalytic steps in the converting hydrogen to electricity in a fuel cell. Kinetic data via first principles calculations is becoming a commonplace providing the foundation for such an understanding. The accuracy of such approaches can only be expected to improve in near future. Moreover, there are semi-empirical approaches like the UBI-QEP that can also provide accurate activation energies for many catalytic systems, and are associated with radically less computational expense. The next logical question is how to utilize this information for logical and rational catalyst design.

Toward this goal, we have developed a graph-theoretic approach based on the rigors of flow network laws. Such a graph-theoretic description of a reaction mechanism is in principle different than the conventional depiction afforded via reaction graphs. In conventional reaction graphs, species are depicted as nodes interconnected via arrows representing elementary reaction steps. While appropriate for linear-kinetics mechanisms, for most catalytic and electro-catalytic reaction schemes of interest (which are non-linear in nature), such a representation is merely a pretty picture, providing no more information than the qualitative depiction of its molecular reaction mechanism. Our graph-theoretic approach developed here avoids this pitfall, overcoming the limitations of current methodologies and providing a self-consistent topological, mechanistic, and kinetic analysis tool, based on the reaction route (RR) theory. The basic difference from the conventional approach is that the nodes, or hubs, do not necessarily represent an individual species, but rather simply represent the connectivity among elementary reaction steps in the network at a juncture. As a result, the RR Graphs become quantitative that follow network laws. Exploiting their analogy with electrical circuits, equivalent circuitry for a given reaction mechanism can be developed, simply by

replacing each branch by its equivalent resistance, defined as $R_\rho \equiv \ln(\vec{r}_\rho / \bar{r}_\rho) / (\vec{r}_\rho - \bar{r}_\rho)$.

With the dimensionless De Donder affinity, $\mathscr{A}_\rho$, as the driving force, the step kinetics can be written in an Ohm's law form, $r_\rho = \mathscr{A}_\rho / R_\rho$. The corresponding overall rate then takes the form $r_{OR} = \mathscr{A}_{OR} / R_{OR}$, where R_{OR} may be obtained in terms of R_ρ from the RR Graph in a manner completely equivalent to that in electrical circuits. Dominant reaction pathways can be identified simply from flux analysis. Further the slow or the rate-limiting steps are identified rationally with ease based on comparison of step resistances, rather than the cursory approach of assuming a RLS (as is the case with the common LHHW approach), or the limited notion of step reversibilities (i.e. labeling the step with $z_\rho \approx z_{OR}$ as the RLS) or even the robust but numerically exhaustive sensitivity analysis. However, only numerical analysis is possible in this manner, since the step rates, $\vec{r}_\rho$ and $\bar{r}_\rho$, and, hence, the step resistances are not known *a priori*, involving the unknown intermediates concentrations.

Thus, the theory of RR graph was extended so as to allow for an explicit topological analysis of reaction mechanisms, in which the final result was of a form that could be cast into an alternate Ohm's law form, i.e., $r_{OR} = E_{OR} / R_{OR}^\bullet$, where the OR driving force is in the conventional form, $E_{OR} = 1 - z_{OR} = \{1 - \exp(-\mathscr{A}_{OR})\}$, and the OR resistance $R_{OR}^\bullet$ relates to step resistances $R_\rho^\bullet$ in the usual manner of electrical circuits, and can be further ascertained *a priori*. Thus, this approach not only provides an explicit QSS rate expression for a given mechanism in terms of step kinetics, but also affords perceptive insights into the dominant pathways and rate-limiting steps, allowing rigorous network pruning. This new form of the electrical analogy provides results that are exactly the same as that obtained via linear algebra from the conventional QSS analysis, for mechanisms that are linear in step kinetics. However, for non-linear kinetic reaction mechanism the results are rather accurate, albeit approximate. It should be, however, noted that in general, of course, for the non-linear case, an explicit solution via the QSS approach is not possible. Rather, only numerical solution is generally obtained. Therefore, even though approximate, an explicit solution is very useful, for instance, in reactor design and analysis.

Thus, our new graph-theoretic approach is an easy to use addendum to the quantum chemical software. It allows thermodynamic consistence check of the predicted kinetics, while providing a road-map for all possible pathways from the reactants to the products. Microkinetic analysis is similar to circuit analysis, based on the analogous equivalent electrical circuit. Thus, in conjunction with DFT calculations, RR graphs form a powerful combination for visualizing the myriad pathways, developing detailed network kinetics, performing flux analysis along with network pruning, and developing steady-state rate expressions.

We have employed our rigorous RR graph approach to a host of catalytic and electro-catalytic systems in connection with fuel cells. The catalytic reaction systems of significance with the fuel processing train, namely, the methanol decomposition, water gas shift, ammonia decomposition, and methane steam reforming, have been studied mechanistically and kinetically. Application of the RR graph theory to the case of methane steam reforming is also a significant advancement, which implies that the theory is applicable to reaction mechanisms consisting of multiple overall reactions. All the other examples involve only a single overall reaction. Finally, the topological analysis of the electro-catalytic reactions in connection to the anode and cathode of fuel cells, i.e. hydrogen electrode reaction and the oxygen reduction reaction has been accomplished.

9.1.1 Methanol Decomposition

In chapter III, a 13-step reaction mechanism was assembled into a RR graph, and combined with DFT predicted step kinetics on Pt(111), we showed how a detailed flux analysis could be accomplished that lays bare the dominant reaction pathways and steps in a reaction network allowing insightful pruning of the mechanism. It was, thus, found that methanol decomposition proceeds exclusively via the initial C–H dehydrogenation step rather than through O–H bond activation on Pt.

This 13-step mechanism was chosen since this was the most complete reaction mechanism reported in the literature with *a priori* kinetics predicted from first principles. Of course, other elementary steps have been reported and should be considered for a detailed analysis of the reaction mechanism. Experimental results clearly suggest that methanol decomposition reaction is a more complex process.
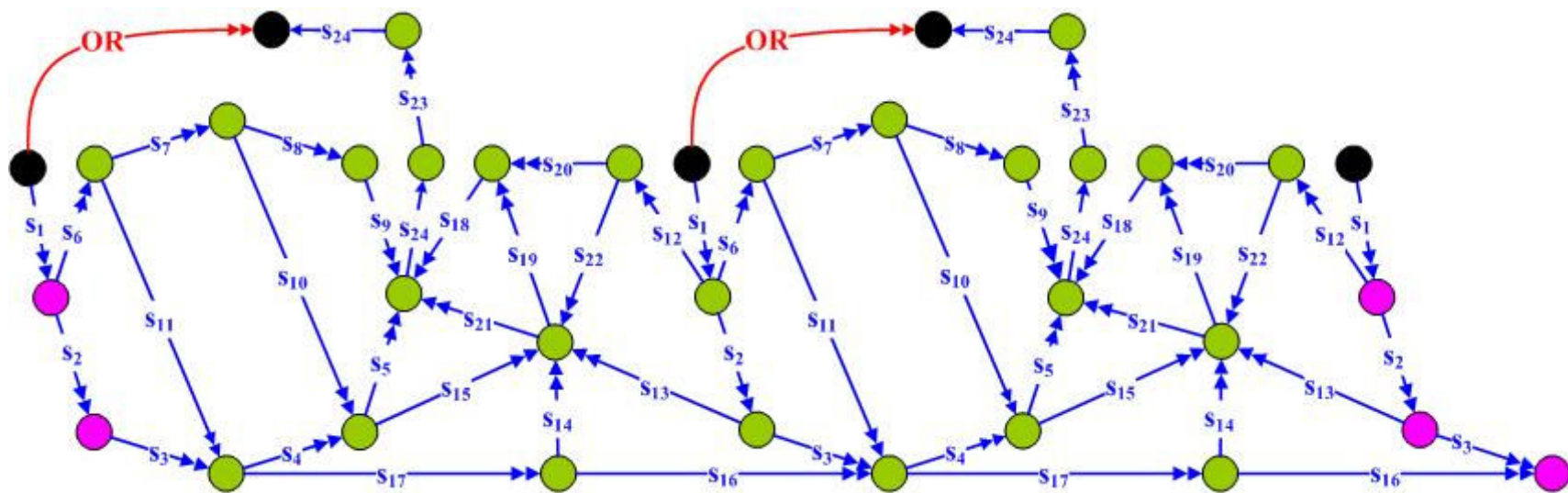
Figure 9-1: RR graph for the 24-step methanol decomposition reaction mechanism (Eq. (9.1)).

On many metals, even on Cu, the carbon deposition has been observed. In view of the above, it is important to develop more complete mechanisms that can be used to quantitatively describe the kinetics of the processes on various catalysts. One such example is shown below, where 24 elementary reactions comprising the mechanism of heterogeneous catalytic decomposition of methanol on various transition metals have been assembled into a RR Graph. The mechanism involves a sequence of elementary reactions representing the hydrogen abstraction from both CH_3 and OH groups as well as C–O bond activation.

$$
\begin{aligned}
&s_1: & CH_3OH + S &\rightleftarrows CH_3OH{\cdot}S \\
&s_2: & CH_3OH{\cdot}S + S &\rightleftarrows CH_3O{\cdot}S + H{\cdot}S \\
&s_3: & CH_3O{\cdot}S + S &\rightleftarrows CH_2O{\cdot}S + H{\cdot}S \\
&s_4: & CH_2O{\cdot}S + S &\rightleftarrows CHO{\cdot}S + H{\cdot}S \\
&s_5: & CHO{\cdot}S + S &\rightleftarrows CO{\cdot}S + H{\cdot}S \\
&s_6: & CH_3OH{\cdot}S + S &\rightleftarrows CH_2OH{\cdot}S + H{\cdot}S \\
&s_7: & CH_2OH{\cdot}S + S &\rightleftarrows CHOH{\cdot}S + H{\cdot}S \\
&s_8: & CHOH{\cdot}S + S &=\rightleftarrows COH{\cdot}S + H{\cdot}S \\
&s_9: & COH{\cdot}S + S &\rightleftarrows CO{\cdot}S + H{\cdot}S \\
&s_{10}: & CHOH{\cdot}S + S &\rightleftarrows CHO{\cdot}S + H{\cdot}S \\
&s_{11}: & CH_2OH{\cdot}S + S &\rightleftarrows CH_2O{\cdot}S + H{\cdot}S \\
&s_{12}: & CH_3OH{\cdot}S + S &\rightleftarrows CH_3{\cdot}S + OH{\cdot}S \\
&s_{13}: & CH_3O{\cdot}S + S &\rightleftarrows CH_3{\cdot}S + O{\cdot}S \\
&s_{14}: & CH_2O{\cdot}S + S &\rightleftarrows CH_2{\cdot}S + O{\cdot}S \\
&s_{15}: & CHO{\cdot}S + S &\rightleftarrows CH{\cdot}S + O{\cdot}S \\
&s_{16}: & CH_3{\cdot}S + S &\rightleftarrows CH_2{\cdot}S + H{\cdot}S \\
&s_{17}: & CH_2{\cdot}S + S &\rightleftarrows CH{\cdot}S + H{\cdot}S \\
&s_{18}: & CH{\cdot}S + S &\rightleftarrows C{\cdot}S + H{\cdot}S \\
&s_{19}: & C{\cdot}S + OS &\rightleftarrows CO{\cdot}S + S \\
&s_{20}: & C{\cdot}S + OH{\cdot}S &\rightleftarrows CO{\cdot}S + H{\cdot}S \\
&s_{21}: & CH{\cdot}S + O{\cdot}S &\rightleftarrows CO{\cdot}S + H{\cdot}S
\end{aligned}
$$

(9.1)

$$s_{22}: OH{\cdot}S + S \leftrightarrows O{\cdot}S + H{\cdot}S$$

$$s_{23}: CO{\cdot}S \leftrightarrows CO + S$$

$$s_{24}: H{\cdot}S + H{\cdot}S \leftrightarrows H_2 + 2S$$

$$OR: CH_3OH = CO + 2H_2$$

The corresponding RR graph (which happens to be an infinite network) for this mechanism is provided in Figure 9-1. The RR graph comprises of the entire set of RRs, namely the 122 direct FRs and 192 direct ERs. For all the elementary steps with no first principles energetic data, semi-empirical method of UBI-QEP could be employed. Once the kinetic data for all the steps is available, detailed flux analysis can be performed, that can enable us to bottleneck the dominant reaction pathways.

Furthermore, the case of methanol decomposition should be extended to consider methanol steam reforming, an important pathway for hydrogen production [1-4]. Of course, oxidative methanol decomposition or auto-thermal methanol reforming is more lucrative, since it offers thermo neutrality [5, 6]. We consider here a simple case where the 13-step methanol decomposition reaction mechanism (considered in chapter III) [7, 8], has been combined with the relatively simple WGS reaction mechanism [9]. The simple 23-step methanol steam reforming reaction mechanism is shown below, along with the corresponding RR graph in Figure 9-2, where OR_1: $CH_3OH \leftrightarrows CO + 2H_2$, OR_2: $CO_2 + H_2 \leftrightarrows CO + H_2O$, and OR_3: $CH_3OH + H_2O \leftrightarrows CO_2 + 3H_2$. Of course, only two ORs ($OR_3 = OR_1 - OR_2$) are independent and required for a detailed kinetic and mechanistic analysis. The WGS mechanism, however, should be suitably updated in the light of conclusions reached in chapter IV to include the carboxyl mechanism. Nevertheless, this is a good starting point for developing detailed kinetic model for methanol steam reforming.

$$s_1: CH_3OH + S \leftrightarrows CH_3OH{\cdot}S$$

$$s_2: CH_3OH{\cdot}S + S \leftrightarrows CH_3O{\cdot}S + H{\cdot}S$$

$$s_3: CH_3O{\cdot}S + 2S \leftrightarrows CH_2O{\cdot}S_2 + H{\cdot}S$$

$$s_4: CH_2O{\cdot}S_2 \leftrightarrows CHO{\cdot}S + H{\cdot}S$$

$$s_5: CHO{\cdot}S + S \leftrightarrows CO{\cdot}S + H{\cdot}S$$

$$s_6: CH_3OH{\cdot}S + S \leftrightarrows CH_2OH{\cdot}S + H{\cdot}S$$

s_7: $CH_2OH \cdot S + S \leftrightarrows CHOH \cdot S + H \cdot S$

s_8: $CHOH \cdot S + S \leftrightarrows COH \cdot S + H \cdot S$

s_9: $COH \cdot S + S \leftrightarrows CO \cdot S + H \cdot S$

s_{10}: $CHOH \cdot S + 2S \leftrightarrows CO \cdot S + 2H \cdot S$

s_{11}: $CH_2OH \cdot S + 2S \leftrightarrows CH_2O \cdot S_2 + H \cdot S$

s_{12}: $CO \cdot S \leftrightarrows CO + S$　　　　　　　　　　　　　　　　(9.2)

s_{13}: $H \cdot S + H \cdot S \leftrightarrows H_2 + 2S$

s_{14}: $H \cdot S + H \cdot S \leftrightarrows H_2 \cdot S + S$

s_{15}: $H_2 \cdot S \leftrightarrows H_2 + S$

s_{16}: $H_2O + S \leftrightarrows O \cdot S + H_2$

s_{17}: $H \cdot S + O \cdot S \leftrightarrows OH \cdot S + S$

s_{18}: $CO \cdot S + OH \cdot S \leftrightarrows H \cdot S + CO_2 \cdot S$

s_{19}: $CO \cdot S + OH \cdot S \leftrightarrows HCOO \cdot S + S$

s_{20}: $HCOO \cdot S + S \leftrightarrows H \cdot S + CO_2 \cdot S$

s_{21}: $HCOO \cdot S + O \cdot S \leftrightarrows OH \cdot S + CO_2 \cdot S$

s_{22}: $CO \cdot S + O \cdot S \leftrightarrows CO_2 \cdot S + S$

s_{23}: $CO_2 \cdot S \leftrightarrows CO_2 + S$
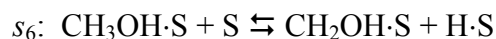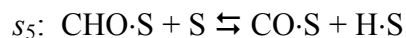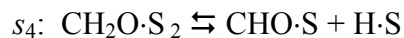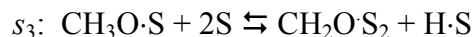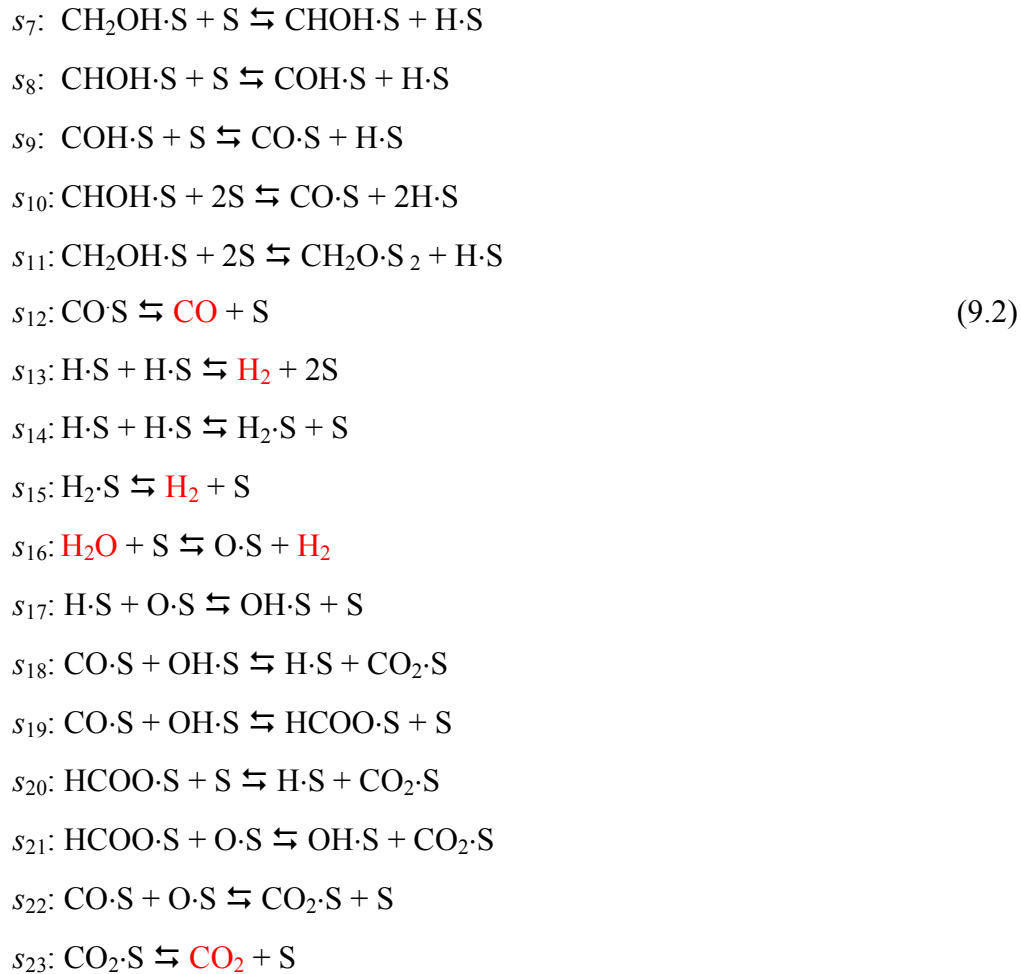
Methanol decomposition is also an important reaction taking place at the anode of DMFC. The analysis can be easily extended to methanol electro-oxidation by assuming that the mechanism largely remains same, as shown by Janik et al. [10] that a similar dual-path mechanism exists for methanol decomposition in an electrochemical environment using *ab initio* quantum chemical methods. The authors [10] provide an approach to theoretically calculate potential dependent activation energies. However, one could well assume, the activation energies and pre-exponential factors to be similar for both catalytic and electrocatalytic systems. The only difference being for electrochemical counterparts of the catalytic reactions, the reaction rate would be affected by the electrode potential described by the Butler-Volmer equation. The said approach coupled with RR graph analysis can possibly provide a detailed portrayal of the electrochemical reaction system at the DMFC anode.
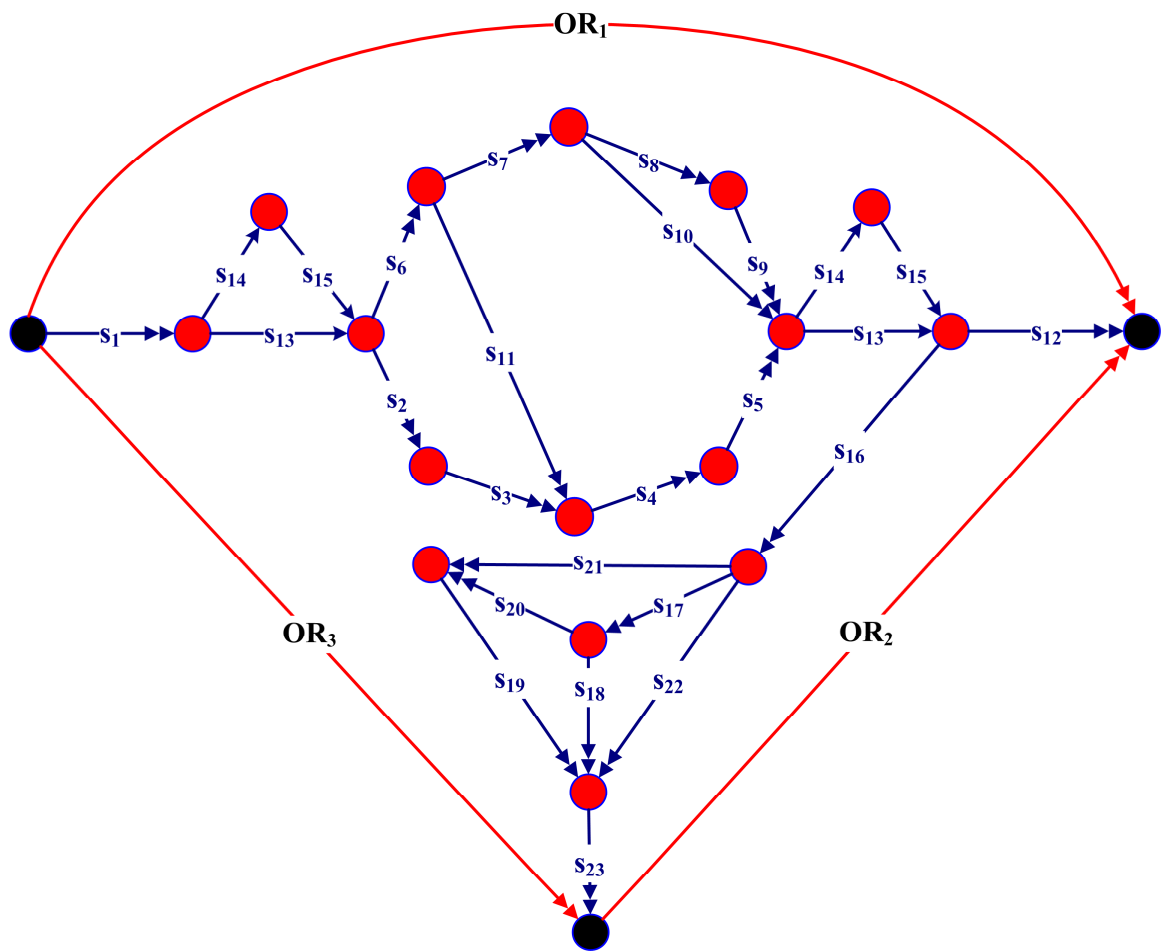
Figure 9-2: RR graph for the 23-step methanol steam reforming reaction mechanism (Eq. (9.2)).

Finally, if methanol is to play an important role in the hydrogen economy, either for direct internal reforming in a fuel cell or for catalytic production of hydrogen, it is imperative to analyze in detail the dominant reaction pathways for methanol synthesis. Methanol, also known as wood alcohol as it was originally produced by the dry distillation of wood, is mainly produced from a mixture of CO, CO_2 and H_2. Several researchers have attempted to answer the question whether the carbon in methanol originates from CO or CO_2. Chinchen et al. [11, 12] experimentally concluded that the methanol is produced from hydrogenation of CO_2 rather than CO. Millar et al. [13] reported that the formation of methanol from CO, historically considered to be the preferred path was almost 2 orders of magnitude slower than methanol synthesis from CO_2 and H_2. The model of Waugh [14] similarly proposed methanol to be synthesized almost entirely by the hydrogenation of CO_2 via a bidentate surface formate, where the RDS was the hydrogenation of the surface formate species. Calculations based on dipped adcluster model (DAM) combined with *ab initio* Hartree–Fock (HF) and second-order Møller–Plesset (MP2) by Hu et al. [15], identified formate, dioxomethylene, formaldehyde, and methoxy as the key reactive intermediates. The authors [16] further suggested the RDS to be the hydrogenation of adsorbed formate leading to formaldehyde with dioxomethylene intermediate. Of course, in a mixture of CO, CO_2 and H_2, CO could potentially be oxidized to CO_2 via WGS, which then later gets converted into methanol. The importance of incorporating WGS in the methanol synthesis modeling was duly noted by Villa et al. [17]. Graaf et al. [18, 19] also considered both the hydrogenation of CO and CO_2 as well as the water gas shift reaction, assumed to proceed via the formate route. Bussche and Froment [20] followed a similar approach, where WGS was considered essentially to oxidize CO to CO_2, the precursor to methanol with the generally accepted hydrogenation of formate assumed as the RDS. Taylor et al. [21], on the other hand suggested that hydrogenation of formate cannot be labeled as the RDS. On the contrary, hydrogenation of the dioxomethylene intermediate to form adsorbed methoxy, eventually leading to methanol was proposed to be rate-determining. Askgaard et al. [22] similarly concluded that the RDS was the hydrogenation of dioxomethylene to methoxide. Thus, the identification of the true rate-determining step in methanol synthesis is still a topic of research. Our RR graph approach serves as the perfect tool to

answer these questions. A compilation of the literature reported mechanism for methanol synthesis from CO_2 is provided below. Of course, one can also add the WGS reaction to the following set of elementary reactions, to include the role of CO in the system.

s_1: $CO_2 + S \leftrightarrows CO_2 \cdot S$

s_2: $H_2 + 2S \leftrightarrows 2H \cdot S$

s_3: $CO_2 \cdot S + H \cdot S \leftrightarrows HCOO \cdot S + S$

s_4: $CO_2 \cdot S + OH \cdot S \leftrightarrows HCOO \cdot S + O \cdot S$

s_5: $HCOO \cdot S + S \leftrightarrows CHO \cdot S + O \cdot S$

s_6: $HCOO \cdot S + H \cdot S \leftrightarrows CH_2O \cdot S + O \cdot S$

s_7: $H \cdot S + O \cdot S \leftrightarrows OH \cdot S + S$

s_8: $OH \cdot S + H \cdot S \leftrightarrows H_2O \cdot S + S$

s_9: $CHO \cdot S + H \cdot S \leftrightarrows CH_2O \cdot S + S$

s_{10}: $CH_2O \cdot S + H \cdot S \leftrightarrows CH_3O \cdot S + S$

s_{11}: $CH_3O \cdot S + H \cdot S \leftrightarrows CH_3OH \cdot S + S$

s_{12}: $H_2O \cdot S \leftrightarrows H_2O + S$ (9.3)

s_{13}: $CH_3OH \cdot S \leftrightarrows CH_3OH + S$

s_{14}: $CH_2O \cdot S + H \cdot S \leftrightarrows CH_2OH \cdot S + S$

s_{15}: $CH_2OH \cdot S + H \cdot S \leftrightarrows CH_3OH \cdot S + S$

s_{17}: $HCOO \cdot S + H \cdot S \leftrightarrows H_2COO \cdot S + S$

s_{18}: $H_2COO \cdot S + H \cdot S \leftrightarrows CH_3O \cdot S + O \cdot S$

s_{19}: $H_2COO \cdot S + H \cdot S \leftrightarrows CH_2O \cdot S + OH \cdot S$

s_{20}: $H_2 + S \leftrightarrows H_2 \cdot S$

s_{21}: $H_2 \cdot S + S \leftrightarrows 2H \cdot S$

OR: $CO_2 + 3H_2 \leftrightarrows CH_3OH + H_2O$
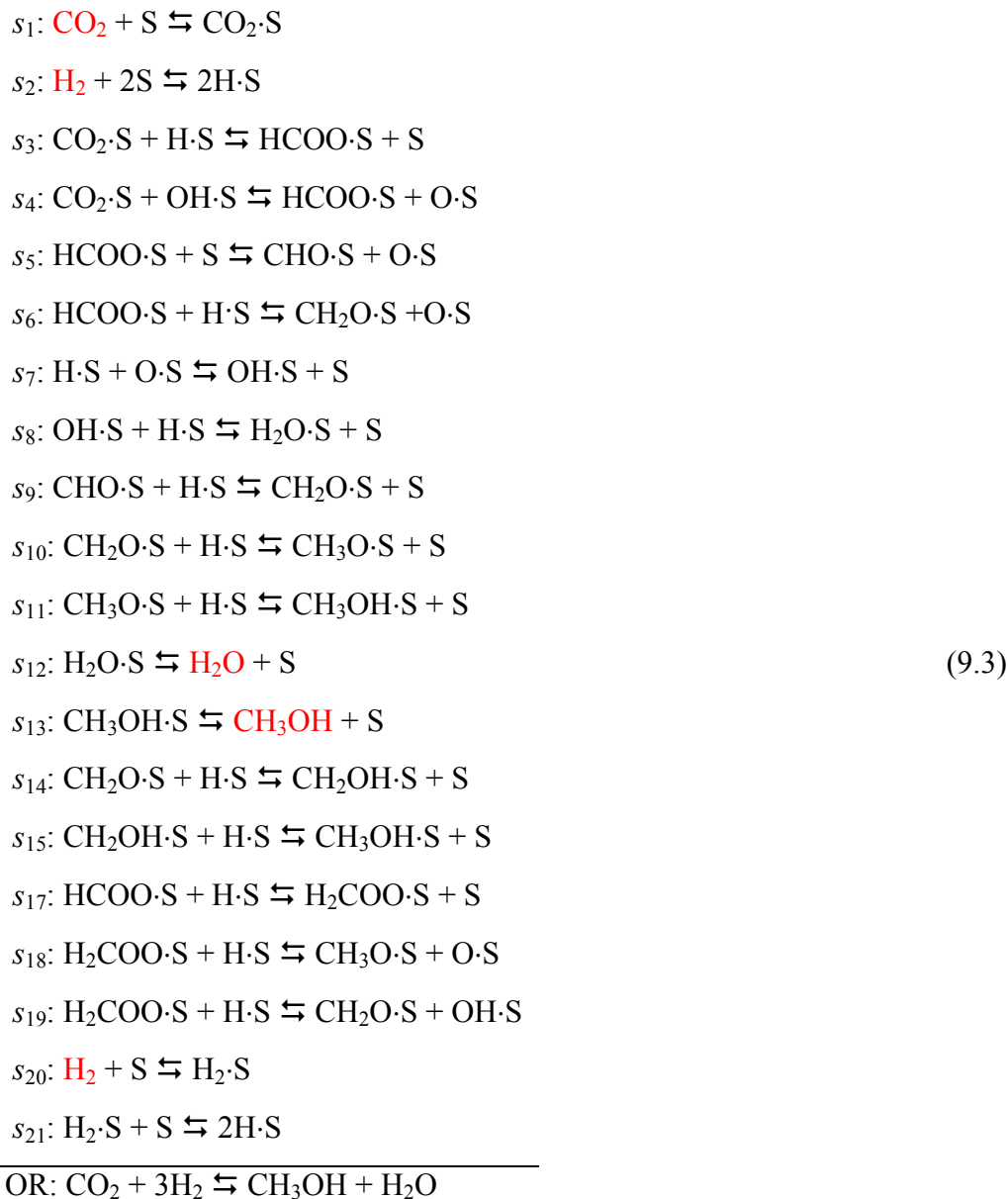
A detailed topological analysis of the above reaction mechanism can unequivocally reveal the dominant reaction pathways and the key rate-limiting steps.

9.1.2 Water Gas Shift

In chapter IV, we considered the 17-step associative mechanism through a carboxyl intermediate, proposed by Grabow et al. [23] on Pt(111) with DFT-predicted kinetic data.

A RR Graph was constructed that incorporates all the 17 steps, on which all of the 71 direct FRs and 49 ERs may be traced as walks! The RR network was subsequently simplified and reduced to a network involving only a single dominant RR, i.e. associative mechanism mediated via carboxyl species. Dissociation of water and direct decomposition of carboxyl species were identified to the rate-limiting steps. A QSS rate expression was next derived based on the slow steps, agreeing reasonably well with the 17-step microkinetic model.

However, others [24] have suggested that the redox and the associative route via carboxyl intermediate could co-exist and the dominant reaction pathway depends on the system under consideration, typically the nature of the catalytic surface. Our previous RR graph analysis on Cu(111) [9] surface also revealed that associative route (without the carboxyl species) and formate route were dominant at temperatures < 550 K, while the modified redox mechanism dominated at higher temperatures. A more complete picture of the WGS mechanism can be developed by combining all of these proposed pathways into a single RR graph, so that flux analysis can be performed over the entire system. This should readily reveal the dominant pathways as a function of operation conditions.

9.1.3 Preferential Oxidation (PrOx)

Preferrential oxidation (PrOx) of CO is an integral part of the fuel processing train, following the shift reactors, especially for low temperature PEM fuel cells, in order to reduce the CO in the reformate down to 20 – 25 ppm range. Due to the limited selectivity, however, O_2 in excess of stoichiometry is required to reduce CO to low levels, which burns the hydrogen present in the reformate, thus reducing the overall efficiency. Choi and Stenger [25] studied preferential oxidation of CO on a Pt–Fe/γ-Al_2O_3 catalyst between 100 and 300 °C, proposed rate expressions for a 3-step mechanism, and suggested performance improvement with addition of water. Bissett et al. [26] have developed a rate equation for PrOx on a supported Pt catalyst based on a 6-step mechanism, which explicitly accounts for the presence of H_2O, H_2 and CO_2 in addition to CO and O_2 in the PrOx reactor and involves both CO oxidation and H_2 oxidation. Further, the authors [26] reported minimal methanation on Pt catalyst. Ouyang et al. [27] simulated a PROX microreactor applying plug-flow model with 28 surface

reactions for the Pt–Fe/γ-Al$_2$O$_3$ catalyst using CHEMKIN package. A 20-step PrOx reaction mechanism is provided below along with the corresponding RR graph (Figure 9-3).

$$s_1: CO + S \leftrightarrows CO{\cdot}S$$

$$s_2: H_2 + 2S \leftrightarrows 2H{\cdot}S$$

$$s_3: O_2 + 2S \leftrightarrows 2O{\cdot}S$$

$$s_4: O{\cdot}S + H{\cdot}S \leftrightarrows OH{\cdot}S + S$$

$$s_5: OH{\cdot}S + H{\cdot}S \leftrightarrows H_2O + 2S$$

$$s_6: CO{\cdot}S + O{\cdot}S \leftrightarrows CO_2 + 2S$$

$$s_7: CO{\cdot}S + O{\cdot}S \leftrightarrows CO_2{\cdot}S + S$$

$$s_8: CO_2{\cdot}S \leftrightarrows CO_2 + S$$

$$s_9: O_2 + S \leftrightarrows O_2{\cdot}S$$

$$s_{10}: O_2{\cdot}S + S \leftrightarrows 2O{\cdot}S$$

$$s_{11}: H_2 + S \leftrightarrows H_2{\cdot}S$$

$$s_{12}: H_2{\cdot}S + S \leftrightarrows 2H{\cdot}S \tag{9.4}$$

$$s_{13}: OH{\cdot}S + H{\cdot}S \leftrightarrows H_2O{\cdot}S + S$$

$$s_{14}: H_2O{\cdot}S \leftrightarrows H_2O + S$$

$$s_{15}: CO{\cdot}S + OH{\cdot}S \leftrightarrows HCOO{\cdot}S + S$$

$$s_{16}: CO{\cdot}S + OH{\cdot}S \leftrightarrows CO_2{\cdot}S + H{\cdot}S$$

$$s_{17}: HCOO{\cdot}S + S \leftrightarrows CO_2{\cdot}S + H{\cdot}S$$

$$s_{18}: HCOO{\cdot}S + O{\cdot}S \leftrightarrows CO_2{\cdot}S + OH{\cdot}S$$

$$s_{19}: OH{\cdot}S + H{\cdot}S \leftrightarrows O{\cdot}S + H_2{\cdot}S$$

$$s_{20}: HCOO{\cdot}S + H{\cdot}S \leftrightarrows CO_2{\cdot}S + H_2{\cdot}S$$
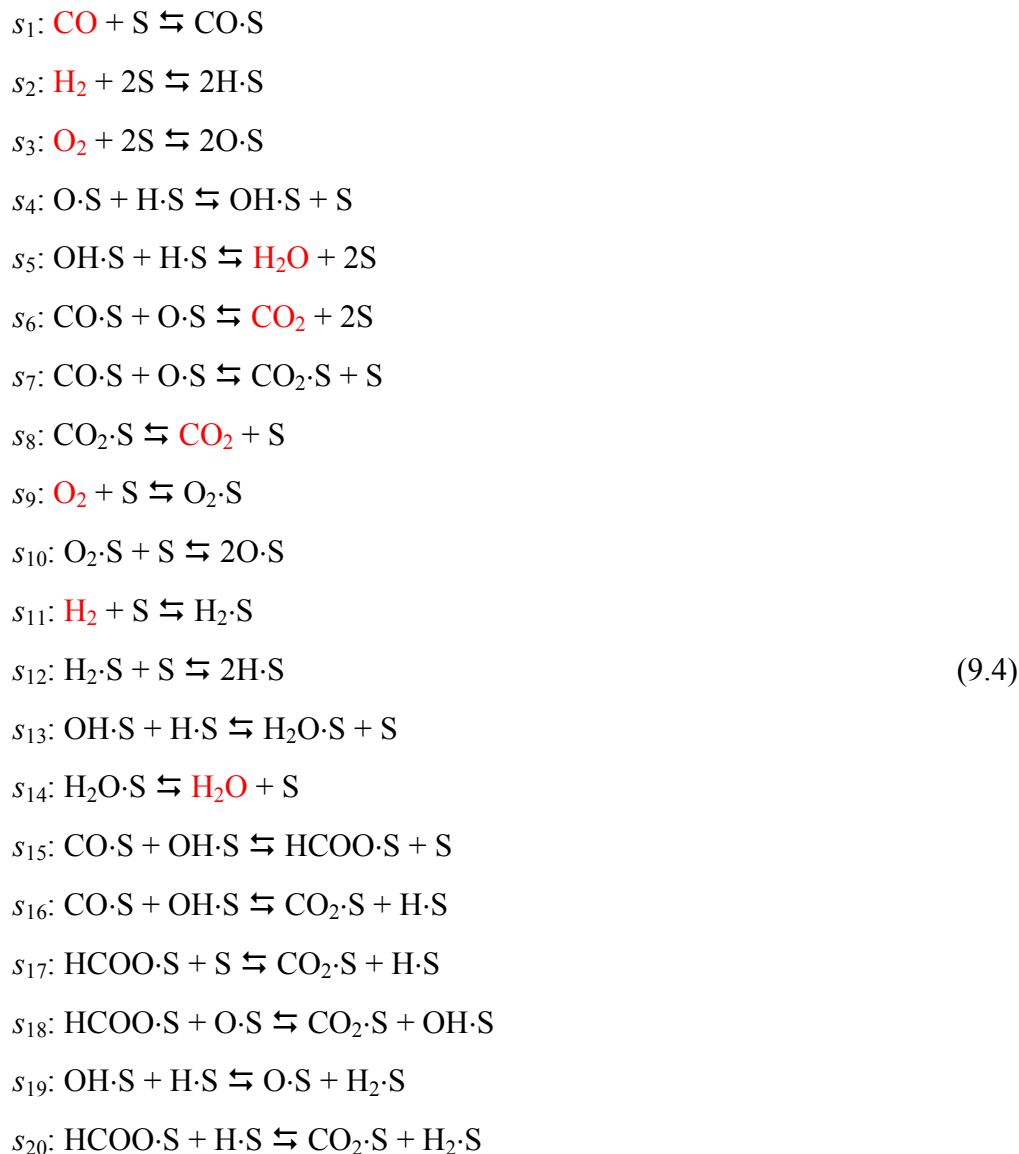
A detailed analysis of catalytic PrOx can be accomplished based on the above mentioned mechanism, along with either DFT-predicted kinetics or those from UBI-QEP. Moreover, the analysis can also be extended to simulate anode kinetics of a PEM fuel cell operating with CO containing reformate feed, where competitive electro-oxidation of CO and H$_2$ takes place.
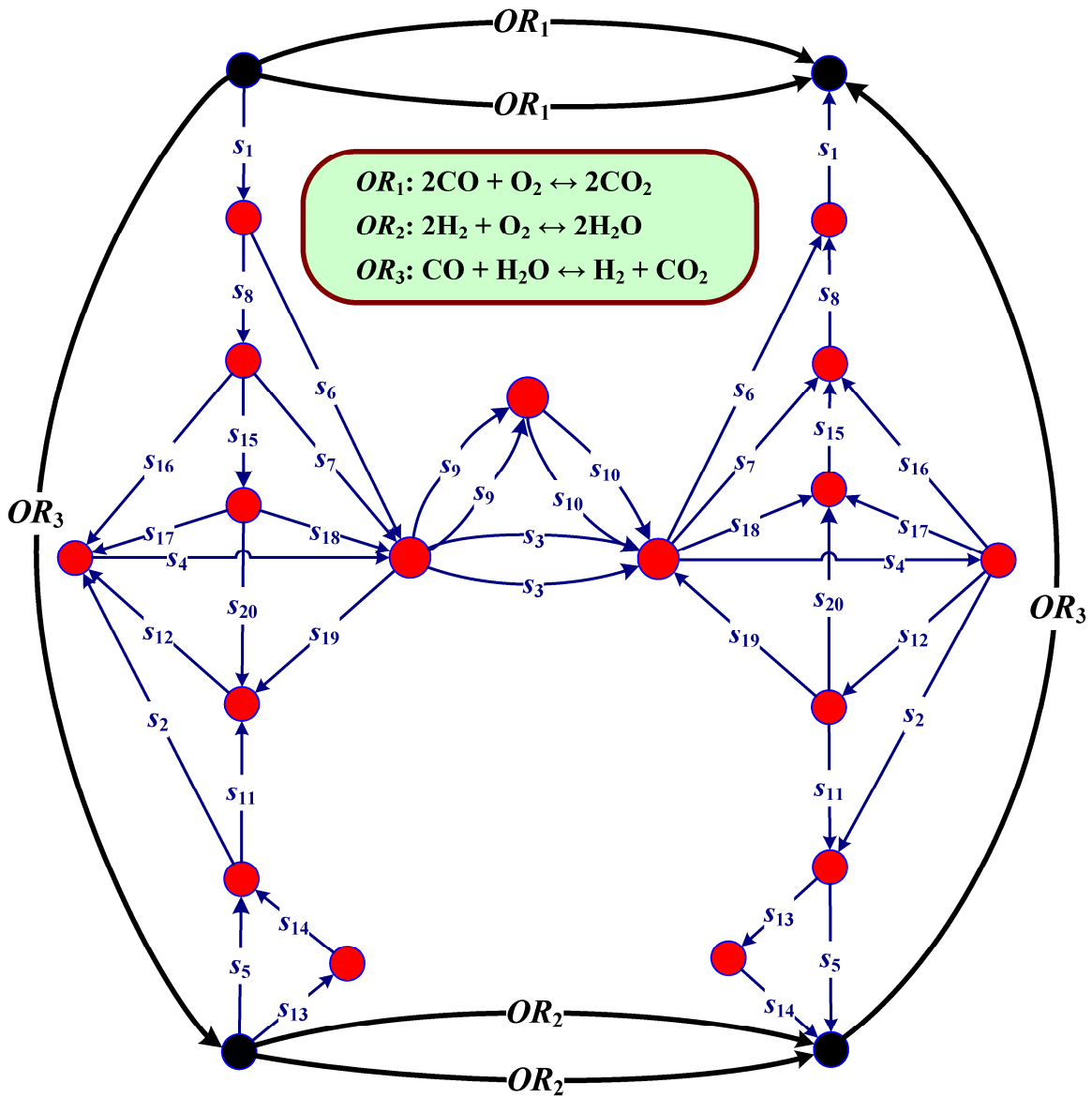
Figure 9-3: RR graph for the 20-step preferential oxidation (PrOx) reaction mechanism (Eq. (9.4)).

9.1.4 Multiple OR system

In chapter VI, the theory of RR graphs was developed further and its applicability and utility for systems with multiple overall reactions was elucidated for the case of methane steam reforming on Ni. We, further, showed that one only needs the independent set of ORs to describe a multiple OR reaction system, as opposed to the general notion [28]. Following our RR graph approach, the 22-step mechanism was whittled down to a dual path mechanism for MSR, depending upon the reaction temperature and the reaction conditions considered in this study. Based on the comparison the step resistances, R_ρ, the rate-limiting steps for each of the two dominant reaction pathways were identified. Based on the knowledge of the rate-limiting steps and QE steps, the steady-state rate expression for MSR was derived using the QSS analysis.

On the other hand, the new form of electrical analogy $r_{OR} = E_{OR} / R_{OR}^\bullet$ can also allow us to derive explicit rate expressions for the independent ORs. However, the theory, i.e., the alternate form of Ohms's law, is still in the developing stages and needs to be rigorously evaluated in order to apply the same for multiple OR systems. We have shown that this form of representation, $r_{OR} = E_{OR} / R_{OR}^\bullet$ provides exact results for the case of *single* OR mechanisms with linear kinetics. Thus, an ideal system for the further development of this theory would consist of a multiple OR mechanism with linear kinetics. One such example is the N_2O decomposition on Fe-ZSM-5 in the presence of NO. A simple 16-step reaction mechanism with DFT-predicted kinetics is provided in Table 9-1. The corresponding RR graph along with the qualitative representation is provided in Figure 9-4. This example should serve as the perfect model to develop the theory of RR graphs further, in order to develop QSS rate expressions for multiple OR system, directly from the electrical analog with no *a priori* assumptions about the RLSs.

Table 9-1: Elementary reaction steps and their rates in the N_2O decomposition on Fe-ZSM-5 [29-31].

s_ρ	Reaction Step	$r_\rho = \vec{r}_\rho - \bar{r}_\rho$	$\vec{\omega}_\rho$	$\bar{\omega}_\rho$	$\vec{\Lambda}_\rho$	$\bar{\Lambda}_\rho$	$\vec{E}_\rho$	$\bar{E}_\rho$
s_1:	$N_2O + I_0 \leftrightarrows I_1$	$r_1 = \vec{\omega}_1\theta_0 - \bar{\omega}_1\theta_1$	$\vec{k}_1 p_{N_2O}$	$\bar{k}_1$	$1.06\ 10^7$	$1.67\ 10^{13}$	0.0	6.4
s_2:	$I_1 \leftrightarrows I_2 + N_2$	$r_2 = \vec{\omega}_2\theta_1 - \bar{\omega}_2\theta_2$	$\vec{k}_2$	$\bar{k}_2 p_{N_2}$	$2.09\ 10^{14}$	$4.43\ 10^8$	30.7	41.9
s_3:	$I_1 \leftrightarrows I_3 + N_2$	$r_3 = \vec{\omega}_3\theta_1 - \bar{\omega}_3\theta_3$	$\vec{k}_3$	$\bar{k}_3 p_{N_2}$	$6.98\ 10^{13}$	$5.82\ 10^7$	30.4	50.0
s_4:	$I_2 \leftrightarrows I_3$	$r_4 = \vec{\omega}_4\theta_2 - \bar{\omega}_4\theta_3$	$\vec{k}_4$	$\bar{k}_4$	$2.15\ 10^{13}$	$8.46\ 10^{12}$	14.1	22.5
s_5:	$N_2O + I_3 \leftrightarrows I_6$	$r_5 = \vec{\omega}_5\theta_3 - \bar{\omega}_5\theta_6$	$\vec{k}_5 p_{N_2O}$	$\bar{k}_5$	$3.99\ 10^6$ $(4.39\ 10^8)^\#$	$1.67\ 10^{13}$	0.0	2.7
s_6:	$I_6 \leftrightarrows I_5 + N_2$	$r_6 = \vec{\omega}_6\theta_6 - \bar{\omega}_6\theta_5$	$\vec{k}_6$	$\bar{k}_6 p_{N_2}$	$3.12\ 10^{10}$ $(3.12\ 10^{12})^\#$	$3.19\ 10^8$	20.1 $(20.2)^\#$	31.5
s_7:	$I_5 \leftrightarrows I_0 + O_2$	$r_7 = \vec{\omega}_7\theta_5 - \bar{\omega}_7\theta_0$	$\vec{k}_7$	$\bar{k}_7 p_{O_2}$	$1.67\ 10^{13}$	$1.51\ 10^5$	8.0	8.1
s_8:	$N_2O + I_2 \leftrightarrows I_4$	$r_8 = \vec{\omega}_8\theta_2 - \bar{\omega}_8\theta_4$	$\vec{k}_8 p_{N_2O}$	$\bar{k}_8$	$2.74\ 10^6$	$1.67\ 10^{13}$	0.0	4.5
s_9:	$I_4 \leftrightarrows I_5 + N_2$	$r_9 = \vec{\omega}_9\theta_4 - \bar{\omega}_9\theta_5$	$\vec{k}_9$	$\bar{k}_9 p_{N_2}$	$3.25\ 10^{14}$	$8.16\ 10^7$	16.5	34.4
s_{10}:	$I_3 \leftrightarrows I_7 + O_2$	$r_{10} = \vec{\omega}_{10}\theta_3 - \bar{\omega}_{10}\theta_7$	$\vec{k}_{10}$	$\bar{k}_{10} p_{O_2}$	$1.67\ 10^{13}$	$1.4\ 10^6$	54.2 $(54.17)^\#$	1.1
s_{11}:	$N_2O + I_7 \leftrightarrows I_8$	$r_{11} = \vec{\omega}_{11}\theta_7 - \bar{\omega}_{11}\theta_8$	$\vec{k}_{11} p_{N_2O}$	$\bar{k}_{11}$	$5.3\ 10^9$	$1.67\ 10^{13}$	0.03	0.0
s_{12}:	$I_8 \leftrightarrows I_0 + N_2$	$r_{12} = \vec{\omega}_{12}\theta_8 - \bar{\omega}_{12}\theta_0$	$\vec{k}_{12}$	$\bar{k}_{12} p_{N_2}$	$6.43\ 10^9$	$8.54\ 10^5$	2.8	70.0
s_{13}:	$I_2 + NO \leftrightarrows I_9$	$r_{13} = \vec{\omega}_{13}\theta_2 - \bar{\omega}_{13}\theta_9$	$\vec{k}_{13} p_{NO}$	$\bar{k}_{13}$	$5.75\ 10^5$	$1.67\ 10^{13}$	3.7	34.6 $(34.7)^\#$
s_{14}:	$I_9 \leftrightarrows I_0 + NO_2$	$r_{14} = \vec{\omega}_{14}\theta_9 - \bar{\omega}_{14}\theta_0$	$\vec{k}_{14}$	$\bar{k}_{14} p_{NO_2}$	$1.67\ 10^{13}$	$1.81\ 10^5$	16.0	0.0
s_{15}:	$I_2 + NO \leftrightarrows I_{10}$	$r_{15} = \vec{\omega}_{15}\theta_2 - \bar{\omega}_{15}\theta_{10}$	$\vec{k}_{15} p_{NO}$	$\bar{k}_{15}$	$3.10\ 10^4$	$1.67\ 10^{13}$	4.6	38.2
s_{16}:	$I_{10} \leftrightarrows I_0 + NO_2$	$r_{16} = \vec{\omega}_{16}\theta_{10} - \bar{\omega}_{16}\theta_0$	$\vec{k}_{16}$	$\bar{k}_{16} p_{NO_2}$	$1.67\ 10^{13}$	$9.77\ 10^3$	19.2	0.6

$I_0 = Z^-[FeO]^+$; $I_1 = Z^-[FeO]^+(ON_2)$; $I_2 = Z^-[OFeO]^+$; $I_3 = Z^-[FeO_2]^+$; $I_4 = Z^-[OFeO]^+(ON_2)$; $I_5 = Z^-[O_2FeO]^+$; $I_6 = Z^-[FeO_2]^+(ON_2)$; $I_7 = Z^-[Fe]^+$; $I_8 = Z^-[Fe]^+(ON_2)$; $I_9 = Z^-[OFeONO]^+$; $I_{10} = Z^-[OFeO_2N]^+$.

Activation energies in $k_\rho = \Lambda_\rho \exp(-E_\rho/RT)$ are in kcal/mol; the units of the pre–exponential factors are $bar^{-1}\ s^{-1}$ for adsorption/desorption reactions and s^{-1} for surface reactions. ω_ρ represents the reaction step weights where rate parameters and activities of terminal species are clubbed together. θ_k is the surface coverage of species I_k. $^\#$Values in parenthesis are modified to ensure thermodynamic consistency in the light of Kirchhoff's potential law [31].
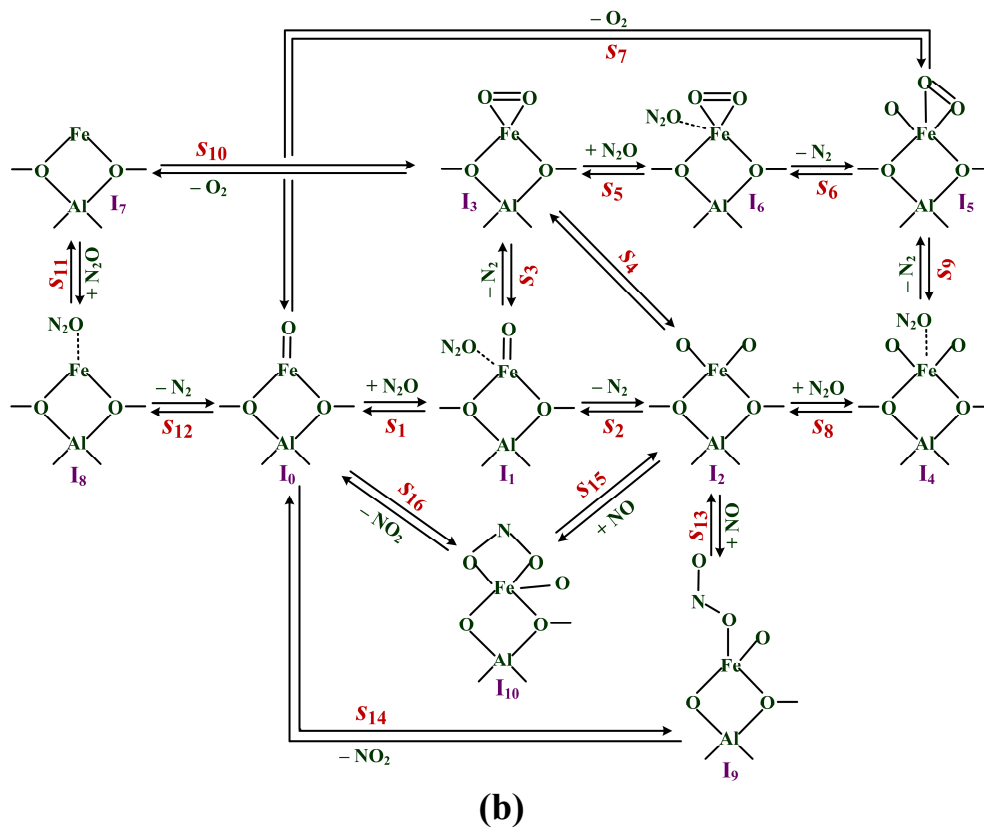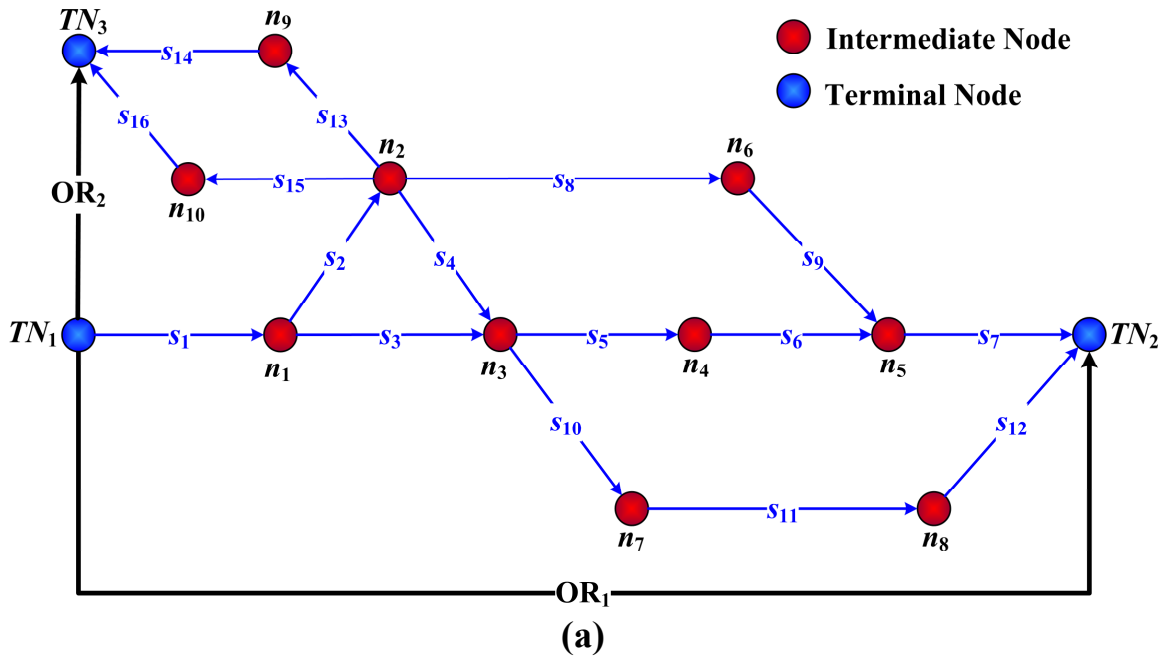
Figure 9-4: (a) Reaction Route (RR) Graph and (b) reaction mechanism for the 16-step N_2O decomposition on Fe-ZSM-5 in the presence of NO

9.2 Fuel Cell Model

In Chapter VII we discussed within a lumped framework the performance of a single PEM fuel cell that incorporates the fuel cross-over effects. A simple model was developed that showed the effect of fuel permeation on open circuit voltage in PEM fuel cells. The observed loss of about 0.2V under open circuit conditions was attributed to the hydrogen cross-over and the ensuing HOR at the cathode side, causing a significant overpotential. The cross-over effect was later incorporated in the lumped fuel cell performance model, which adequately described the experimental data.

The negative effect of fuel crossover on OCV is particularly significant for direct alcohol fuel cells [32-35]. Crossover of methanol is a huge challenge that impacts both the performance of the fuel cell, as well its Voltage and Faradaic efficiencies. Moreover, the flux of methanol across the PEM is not simply by diffusion, but is also proportional to the current. This methanol that crosses over to the cathode significantly reduces the cathode potential by virtue of the simultaneous methanol oxidation and oxygen reduction reactions taking place on the same electrode.

The current modeling framework developed in chapter VII should be extended to explicate these findings.

9.3 References

[1] Y. Choi, H.G. Stenger, J. Power Sources. 142 (2005) 81-91.

[2] Y. Choi, H.G. Stenger, Appl. Catal. B: Environmental. 38 (2002) 259–269.

[3] R. He, R.R. Davda, J.A. Dumesic, J. Phys. Chem. B. 109 (2005) 2810-2820.

[4] B.A. Peppley, J.C. Amphlett, L.M. Kearns, R.F. Mann, Appl. Catal. A: General. 179 (1999) 31-49.

[5] J.R. Lattner, M.P. Harold, Catal. Today. 120 (2007) 78–89.

[6] M. Lyubovsky, D. Walsh, J. Power Sources. 162 (2006) 597–605.

[7] A.A. Gokhale, S. Kandoi, J.P. Greeley, M. Mavrikakis, J.A. Dumesic, Chem. Eng. Sci. 59 (2004) 4679-4691.

[8] S. Kandoi, J. Greeley, M.A. Sanchez-Castillo, S.T. Evans, A.A. Gokhale, J.A. Dumesic, M. Mavrikakis, Topics in Catal. 37 (2006) 17-28.

[9] C.A. Callaghan, S.A. Vilekar, I. Fishtik, R. Datta, Appl. Catal. A: General. 345 (2008) 213-232.

[10] M.J. Janik, C.D. Taylor, M. Neurock, Top. Catal. 46 (2007) 306–319.

[11] G. C. Chinchen, P. J. Denny, D. G. Parker, M. S. Spencer, D. A. Whan, Appl. Catal. 30 (1987) 333.

[12] G. C. Chinchen, P. J. Denny, J. R. Jennings, M. S. Spencer, K. C. Waugh, Appl. Catal. 36 (1988) 1.

[13] G.J. Millar, C.H. Rochester, K.C. Waugh, J. Chem. Soc., Faraday Trans. 87 (1991) 2795.

[14] K.C. Waugh, Catal. Today. 15 (1992) 51-75.

[15] Z.-M. Hu, K. Takahashi, Nakatsuji. H., Surf. Sci. 442 (1999) 90-106.

[16] Nakatsuji. H., Z.-M. Hu, Int. J. Quant. Chem. 77 (2000) 341–349.

[17] P. Villa, P. Forzatti, Buzzi-Ferraris, G. G., G.,, I. Pasquon, Ind. Eng. Chem. Process Des. Dev. 24 (1985) 12.

[18] G.H. Graaf, E.J. Stamhuis, A.A.C.M. Beenackers, Chem. Eng. Sci. 43 (1988) 3185.

[19] G.H. Graaf, H. Scholtens, E.J. Stamhuis, A.A.C.M. Beenackers, Chem. Eng. Sci. 45 (1990) 773.

[20] K.M. Vanden Bussche, G.F. Froment, J. Catal. 161 (1996) 1-10.

[21] P.A. Taylor, P.B. Rasmussen, I. Chorkendorff, J. Chem. Soc., Faraday Trans. 91 (1995).

[22] T. S. Askgaard, J. K. Nørskov, C. V. Ovsen, P. Stoltze, J. Catal. 156 (1995) 229.

[23] L. C. Grabow, A. A. Gokhale, S. T. Evans, J. A. Dumesic, M. Mavrikakis, J. Phys. Chem. C (2008) A-J.

[24] P. Liu, J.A. Rodriguez, J. Chem. Phys. 126 (2007) 164705.

[25] Y. Choi, H.G. Stenger, J. Power Sources. 129 (2004) 246–254.

[26] E.J. Bissett, S.H. Oh, R.M. Sinkevitch, Chem. Eng. Sci. 60 (2005) 4709–4721.

[27] X. Ouyang, L. Bednarova, R.S. Besser, AIChE J. 51 (2005) 1758–1771.

[28] J. Xu, G.F. Froment, AIChE Journal. 35 (1989) 88-96.

[29] A. Heyden, B. Peters, A.T. Bell, F.J. Keil, J. Phys. Chem. B. 109 (2005) 1857-1873.

[30] A. Heyden, N. Hansen, A.T. Bell, F.J. Keil, J. Phys Chem. B. 110 (2006) 17096-17114.

[31] S.A. Vilekar, I. Fishtik, R. Datta, in: I. Halasz (Ed.), Silica and Silicates in Modern Catalysis, Transworld Research Network, Kerala, India, 2010, pp. 49-79.

[32] V.M. Barragan, A. Heinzel, J. Power Sources. 104 (2002) 66-72.

[33] K.-M. Yin, J. Power Sources. 167 (2007) 420-429.

[34] B.K. Kho, B. Bae, M.A. Scibioh, J. Lee, H.Y. Ha, J. Power Sources. 142 (2005) 50-55.

[35] S. Song, W. Zhou, J. Tian, R. Cai, G. Sun, Q. Xin, S. Kontou, P. Tsiakaras, J. Power Sources. 145 (2005) 266-271.

Appendix A: Stoichiometric algorithm for enumeration of direct RRs and nodes for a given reaction mechanism

In order to construct the RR graph for complex reaction mechanisms, the enumeration of some direct RRs and direct nodes is essential. Although only knowledge of the independent set is essential, we describe below the mathematical underpinnings of our stoichiometric enumeration of all possible direct RRs and direct nodes (both intermediate and terminal). The details can be found in our earlier publications (Fishtik et al., J. Phys. Chem. B. 108 (2004) 5671-5682; J. Phys. Chem. B. 108 (2004) 5683-5697; J. Phys. Chem. B. 109 (2005) 2710-2722). The MAPLE code developed based on this framework is also provided at the end.

Notation and Definitions

Let us consider the general case of a chemical reaction system comprising of p elementary reaction steps s_ρ (ρ = 1, 2, …, p). The species involved in the elementary reaction steps are divided into l intermediates I_1, I_2, ..., I_l of which q are independent, and n terminal species (reactants and products) T_1, T_2, …,T_n. Thus, the elementary reaction steps may be presented as

$$s_\rho: \qquad \sum_{k=1}^{l} \alpha_{\rho k} I_k + \sum_{i=1}^{n} \beta_{\rho i} T_i = 0 \qquad (\rho = 1, 2, …, p) \qquad (A.1)$$

By convention, the stoichiometric coefficients of the intermediates $\alpha_{\rho k}$ (ρ = 1, 2, ..., p; k = 1, 2, ..., l) and terminal species $\beta_{\rho i}$ (ρ = 1, 2, ..., p; i = 1, 2, ..., n), are assumed to be positive for products and negative for reactants. For simplicity, we assume that the overall chemical process is described by only one overall reaction (*OR*)

$$OR: \qquad v_1 T_1 + v_2 T_2 + ... + v_n T_n = 0 \qquad (A.2)$$

The columns in the stoichiometric matrix of the mechanism, defined without the *OR*,

$$\mathbf{v} = \begin{bmatrix} \alpha_{11} & \alpha_{12} & ... & \alpha_{1l} & \beta_{11} & \beta_{12} & ... & \beta_{1n} \\ \alpha_{21} & \alpha_{22} & ... & \alpha_{2l} & \beta_{21} & \beta_{22} & ... & \beta_{2n} \\ ... & ... & ... & ... & ... & ... & ... & ... \\ \alpha_{p1} & \alpha_{p2} & ... & \alpha_{pl} & \beta_{p1} & \beta_{22} & ... & \beta_{2n} \end{bmatrix} \qquad (A.3)$$

are, in general, linearly dependent. We next define as follows two sub-matrices of $\mathbf{v}$ in which the columns are linearly independent. First, we observe that the columns in the two sub-matrices comprising the intermediates and terminal species may be linearly dependent, that is

$$
rank\ \boldsymbol{\alpha}' = rank
\begin{bmatrix}
\alpha_{11} & \alpha_{12} & \ldots & \alpha_{1l} \\
\alpha_{21} & \alpha_{22} & \ldots & \alpha_{2l} \\
\ldots & \ldots & \ldots & \ldots \\
\alpha_{p1} & \alpha_{p2} & \ldots & \alpha_{pl}
\end{bmatrix}
= q \leq l
\tag{A.4}
$$

$$
rank\ \boldsymbol{\beta}' = rank
\begin{bmatrix}
\beta_{11} & \beta_{12} & \ldots & \beta_{1n} \\
\beta_{21} & \beta_{22} & \ldots & \beta_{2n} \\
\ldots & \ldots & \ldots & \ldots \\
\beta_{p1} & \beta_{p2} & \ldots & \beta_{pn}
\end{bmatrix}
= t \leq n
\tag{A.5}
$$

In such cases, the linearly dependent columns in $\boldsymbol{\alpha}'$ may be omitted. Without lost of generality, we assume that the first q columns in $\boldsymbol{\alpha}'$ are linearly independent and define the sub-matrix

$$
\boldsymbol{\alpha} =
\begin{bmatrix}
\alpha_{11} & \alpha_{12} & \ldots & \alpha_{1q} \\
\alpha_{21} & \alpha_{22} & \ldots & \alpha_{2q} \\
\ldots & \ldots & \ldots & \ldots \\
\alpha_{p1} & \alpha_{p2} & \ldots & \alpha_{pq}
\end{bmatrix}
\tag{A.6}
$$

so that $rank\ \boldsymbol{\alpha} = q$. The sub-matrix $\boldsymbol{\alpha}$ is referred to as the *intermediate* sub-matrix. Next, we notice that the rank of the stoichiometric matrix $\mathbf{v}$ is equal to $q + 1$. Without loss of generality, we eliminate the last $n - 1$ columns from $\boldsymbol{\beta}'$ and define a *reduced* stoichiometric sub-matrix

$$
\boldsymbol{\gamma} =
\begin{bmatrix}
\alpha_{11} & \alpha_{12} & \ldots & \alpha_{1q} & \beta_{11} \\
\alpha_{21} & \alpha_{22} & \ldots & \alpha_{2q} & \beta_{21} \\
\ldots & \ldots & \ldots & \ldots & \ldots \\
\alpha_{p1} & \alpha_{p2} & \ldots & \alpha_{pq} & \beta_{p1}
\end{bmatrix}
\tag{A.7}
$$

such that $rank\ \mathbf{v} = rank\ \boldsymbol{\gamma} = q + 1$.

We define, further, the rate vector

$$\mathbf{r} = (r_1, r_2, ..., r_p)^{\mathrm{T}} \tag{A.8}$$

where r_ρ (ρ = 1, 2, ..., p) is the rate of the elementary reaction steps. Finally, we assume that the rates of formation and consumption of the intermediates are approximately equal and, hence, the quasi-steady state (QSS) approximation holds. Thus, we introduce the vector $\mathbf{Q}$,

$$\mathbf{Q} = (Q_1, Q_2, ..., Q_q)^{\mathrm{T}} \tag{A.9}$$

where the Q_k's (k = 1, 2, ..., q) denote the QSS conditions of the linearly independent intermediates I_k (k = 1, 2, ..., q) and may be written in vector form as

$$\mathbf{Q:} \qquad \boldsymbol{\alpha}^{\mathrm{T}} \mathbf{r} = 0 \tag{A.10}$$

or

$$Q_1: \qquad \alpha_{11} r_1 + \alpha_{21} r_2 + ... + \alpha_{p1} r_p = 0$$

$$Q_2: \qquad \alpha_{12} r_1 + \alpha_{22} r_2 + ... + \alpha_{p2} r_p = 0$$

$$... \tag{A.11}$$

$$Q_q: \qquad \alpha_{1q} r_1 + \alpha_{2q} r_2 + ... + \alpha_{pq} r_p = 0$$

Eq. (A.11) is referred to as the *intermediate QSS* condition. On the other hand, the rate r_{OR} of the *OR* under QSS conditions is related to the rates of the elementary reaction steps via

$$r_{OR} = \frac{1}{v_1} \sum_{\rho=1}^{p} \beta_{\rho 1} r_\rho = \frac{1}{v_2} \sum_{\rho=1}^{p} \beta_{\rho 2} r_\rho = ... = \frac{1}{v_n} \sum_{\rho=1}^{p} \beta_{\rho n} r_\rho \tag{A.12}$$

where r_ρ (ρ = 1, 2, ..., p) are subject to the QSS conditions, Eq. (A.11). Furthermore, Eq. (A.12) is referred to as the *OR* QSS conditions.

*i) **Full RRs:*** A *RR* that eliminates *all* intermediates while retaining *only* the terminal species, thus producing an *OR,* is referred to as a *full RR* or, simply, *FR*. Mathematically, the *g*-th *FR* is defined as

$$FR_g: \quad \sum_{\rho=1}^{p} \sigma_{g\rho} s_\rho = OR \tag{A.13}$$

The FR_g, i.e., a set of stoichiometric numbers $\sigma_{g1}, \sigma_{g2}, ..., \sigma_{gp}$, may be generated based on the following considerations. Substituting Eq. (A.1) into Eq. (A.13), we have

$$\sum_{\rho=1}^{p} \sigma_{g\rho} \left(\sum_{k=1}^{l} \alpha_{\rho k} I_k + \sum_{i=1}^{n} \beta_{\rho i} T_i \right) = \sum_{k=1}^{l} \left(\sum_{\rho=1}^{p} \alpha_{\rho k} \sigma_{g\rho} \right) I_k + \sum_{i=1}^{n} \left(\sum_{\rho=1}^{p} \beta_{\rho i} \sigma_{g\rho} \right) T_i = OR \tag{A.14}$$

By definition, the intermediates in a *FR* should cancel. That is,

$$\sum_{\rho=1}^{p} \alpha_{\rho k} \sigma_{g\rho} = 0 \qquad (k = 1, 2, ..., l)$$

or

$$\boldsymbol{\alpha'}^{\mathrm{T}} \boldsymbol{\sigma}_g = 0$$

where $\boldsymbol{\sigma}_g$ is the vector of stoichiometric numbers

$$\boldsymbol{\sigma}_g = (\sigma_{g1}, \sigma_{g2}, ..., \sigma_{gp})^{\mathrm{T}} \tag{A.15}$$

After eliminating the linearly dependent columns in $\boldsymbol{\alpha'}$, we have

$$\boldsymbol{\alpha}^{\mathrm{T}} \boldsymbol{\sigma}_g = 0 \tag{A.16}$$

Thus, $\boldsymbol{\sigma}_g$ may be determined by solving a system of homogeneous linear equations, i.e., Eq. (A.16). The number of linearly independent *FR*s is equal to p - *rank* $\boldsymbol{\alpha} = p - q$.

Direct FRs: According to Milner, a direct *FR* involves no more than *rank* $\boldsymbol{\alpha} + 1 = q + 1$ *linearly independent* elementary reaction steps. Let the $q + 1$ linearly independent elementary reaction steps that are involved in a direct *FR* be $s_{i_1}, s_{i_2}, ..., s_{i_q}, s_{i_{q+1}}$, where the subscripts $i_1, i_2, ..., i_q, i_{q+1}$ represent an ordered set of $q + 1$ integers from among the p elementary steps, i.e., $1 \le i_1 < i_2 < ... < i_q < i_{q+1} \le p$. A direct *FR* may be denoted by $FR(s_{i_1}, s_{i_2}, ..., s_{i_q}, s_{i_{q+1}})$, thus specifying the elementary reaction steps $s_{i_1}, s_{i_2}, ..., s_{i_q}, s_{i_{q+1}}$ that are involved in the *FR*. Thus, in general,

$$FR(s_{i_1}, s_{i_2}, ..., s_{i_q}, s_{i_{q+1}}): \quad \sigma_{i_1} s_{i_1} + \sigma_{i_2} s_{i_2} + ... + \sigma_{i_q} s_{i_q} + \sigma_{i_{q+1}} s_{i_{q+1}} = OR \tag{A.17}$$

where the stoichiometric numbers $\sigma_{gi_1}, \sigma_{gi_2}, ..., \sigma_{gi_q}, \sigma_{gi_{q+1}}$ are obtained by solving Eq. (A.16), where the solution is

$$\sigma_{i_k} = \begin{vmatrix} \alpha_{i_1,1} & \alpha_{i_1,2} & \cdots & \alpha_{i_1,q} & 0 \\ \alpha_{i_2,1} & \alpha_{i_2,2} & \cdots & \alpha_{i_2,q} & 0 \\ \cdots & \cdots & \cdots & \cdots & \cdots \\ \alpha_{i_{k-1},1} & \alpha_{i_{k-1},2} & \cdots & \alpha_{i_{k-1},q} & 0 \\ \alpha_{i_k,1} & \alpha_{i_k,2} & \cdots & \alpha_{i_k,q} & 1 \\ \alpha_{i_{k+1},1} & \alpha_{i_{k+1},2} & \cdots & \alpha_{i_{k+1},q} & 0 \\ \cdots & \cdots & \cdots & \cdots & \cdots \\ \alpha_{i_q,1} & \alpha_{i_q,2} & \cdots & \alpha_{i_q,q} & 0 \\ \alpha_{i_{q+1},1} & \alpha_{i_{q+1},2} & \cdots & \alpha_{i_{q+1},q} & 0 \end{vmatrix} \tag{A.18}$$

More succinctly, the general equation of a *FR* may, thus, be written as

$$FR(s_{i_1}, s_{i_2}, ..., s_{i_q}, s_{i_{q+1}}): \quad \begin{vmatrix} \alpha_{i_1,1} & \alpha_{i_1,2} & \cdots & \alpha_{i_1,q} & s_{i_1} \\ \alpha_{i_2,1} & \alpha_{i_2,2} & \cdots & \alpha_{i_2,q} & s_{i_2} \\ \cdots & \cdots & \cdots & \cdots & \cdots \\ \alpha_{i_q,1} & \alpha_{i_1,2} & \cdots & \alpha_{i_1,q} & s_{i_q} \\ \alpha_{i_{q+1},1} & \alpha_{i_{q+1},2} & \cdots & \alpha_{i_{q+1},q} & s_{i_{q+1}} \end{vmatrix} = OR \tag{A.19}$$

Clearly, not every subset of $q + 1$ elementary reaction steps from the total of p is linearly independent. Also, not every subset of $q + 1$ linearly independent elementary reaction steps will necessarily result in a distinct *RR*. The direct *FR*s may be enumerated by considering all of the possible choices of $q + 1$ elementary reaction steps from among the total of p. The number of stoichiometrically distinct direct *FR*s enumerated, however, usually far exceeds $p - q$, the number of linearly independent *FR*s.

*ii) **Empty RRs**:* A *RR* that eliminates *all species*, both intermediate and terminal species, thus producing a reaction in which the stoichiometric coefficients of all of the species are equal to zero is referred to as an *empty RR* or, simply, an *empty route (ER)*. Mathematically, the *g*-th *ER* is defined as

$$ER_g: \quad \sum_{\rho=1}^{p} \sigma_{g\rho} s_{\rho} = 0 \tag{A.20}$$

Substituting Eq. (A.1) into Eq. (A.20) and requiring all of the species to cancel, we have

$$\sum_{\rho=1}^{p} \alpha_{\rho k} \sigma_{g\rho} = 0 \qquad\qquad (k = 1, 2, \ldots, l)$$

$$\sum_{\rho=1}^{p} \beta_{\rho i} \sigma_{g\rho} = 0 \qquad\qquad (i = 1, 2, \ldots, n)$$

or

$$\mathbf{v}^{\mathrm{T}} \boldsymbol{\sigma}_g = \mathbf{0}$$

Eliminating the linearly dependent columns from the stoichiometric matrix $\mathbf{v}$ gives

$$\boldsymbol{\gamma}^{\mathrm{T}} \boldsymbol{\sigma}_g = \mathbf{0} \tag{A.21}$$

Thus, the *ER*s are also generated by solving a set of homogeneous linear equations, i.e., Eq. (A.21). The number of linearly independent *ER*s is equal to $p - rank\ \mathbf{v} = p - (q + 1)$.

Direct ERs: By analogy with a direct *FR*, we define a *direct ER* as a *RR* that involves no more than $rank\ \boldsymbol{\gamma} + 1 = q + 2$ elementary reaction steps, where $\boldsymbol{\gamma}$ is the reduced stoichiometric matrix, Eq. (A.7). Let the $q + 2$ elementary reaction steps that are involved in an *ER* be $s_{j_1}, s_{j_2}, \ldots, s_{j_q}, s_{j_{q+1}}, s_{j_{q+2}}$, where the subscripts $j_1, j_2, \ldots, j_q, j_{q+1}, j_{q+2}$ represent an ordered set of $q + 2$ integers from among p satisfying the condition $1 \le j_1 < j_2 < \ldots < j_q < j_{q+1} < j_{q+2} \le p$. A direct *ER* is denoted by $ER(s_{j_1}, s_{j_2}, \ldots, s_{j_q}, s_{j_{q+1}}, s_{j_{q+2}})$, thus specifying the elementary reaction steps $s_{j_1}, s_{j_2}, \ldots, s_{j_q}, s_{j_{q+1}}, s_{j_{q+2}}$ that are involved in the *ER*. Thus, in general,

$$ER(s_{j_1}, s_{j_2}, \ldots, s_{j_q}, s_{j_{q+1}}, s_{j_{q+2}}): \sigma_{j_1} s_{j_1} + \sigma_{j_2} s_{j_2} + \ldots + \sigma_{j_q} s_{j_q} + \sigma_{j_{q+1}} s_{j_{q+1}} + \sigma_{j_{q+2}} s_{j_{q+2}} = 0 \tag{A.22}$$

where the stoichiometric numbers are obtained by solving Eq. (A.21). The solution is given as

$$
\sigma_{j_k} = \begin{vmatrix} \alpha_{j_1,1} & \alpha_{j_1,2} & \cdots & \alpha_{j_1,q} & \beta_{j_1,1} & 0 \\ \alpha_{j_2,1} & \alpha_{j_2,2} & \cdots & \alpha_{j_2,q} & \beta_{j_2,1} & 0 \\ \cdots & \cdots & \cdots & \cdots & \cdots & \cdots \\ \alpha_{j_{k-1},1} & \alpha_{j_{k-1},2} & \cdots & \alpha_{j_{k-1},q} & \beta_{j_{k-1},1} & 0 \\ \alpha_{j_k,1} & \alpha_{j_k,2} & \cdots & \alpha_{j_k,q} & \beta_{j_k,1} & 1 \\ \alpha_{j_{k+1},1} & \alpha_{j_{k+1},2} & \cdots & \alpha_{j_{k+1},q} & \beta_{j_{k+1},1} & 0 \\ \cdots & \cdots & \cdots & \cdots & \cdots & \cdots \\ \alpha_{j_q,1} & \alpha_{j_q,2} & \cdots & \alpha_{j_q,q} & \beta_{j_q,1} & 0 \\ \alpha_{j_{q+1},1} & \alpha_{j_{q+1},2} & \cdots & \alpha_{i_{q+1},q} & \beta_{j_{q+1},1} & 0 \\ \alpha_{j_{q+2},1} & \alpha_{j_{q+2},2} & \cdots & \alpha_{i_{q+1},q} & \beta_{j_{q+2},1} & 0 \end{vmatrix}
\tag{A.23}
$$

Alternatively, this result may be represented as

$$
ER(s_{j_1}, s_{j_2}, \ldots, s_{j_q}, s_{j_{q+1}}, s_{j_{q+2}}) : \begin{vmatrix} \alpha_{j_1,1} & \alpha_{j_1,2} & \cdots & \alpha_{j_1,q} & \beta_{j_1,1} & s_{j_1} \\ \alpha_{j_2,1} & \alpha_{j_2,2} & \cdots & \alpha_{j_2,q} & \beta_{j_2,1} & s_{j_2} \\ \cdots & \cdots & \cdots & \cdots & \cdots & \cdots \\ \alpha_{j_q,1} & \alpha_{j_q,2} & \cdots & \alpha_{j_q,q} & \beta_{j_q,1} & s_{j_q} \\ \alpha_{j_{q+1},1} & \alpha_{j_{q+1},2} & \cdots & \alpha_{j_{q+1},q} & \beta_{j_{q+1},1} & s_{j_{q+1}} \\ \alpha_{j_{q+2},1} & \alpha_{j_{q+2},2} & \cdots & \alpha_{j_{q+2},q} & \beta_{j_{q+2},1} & s_{j_{q+2}} \end{vmatrix} = 0
\tag{A.24}
$$

Again, not necessarily every subset of $q + 2$ elementary reaction steps will result in a distinct *ER*. A complete set of distinct *ER*s may be generated either by considering all of the possible combinations of $q + 2$ elementary reaction steps from among the total of *p*.

*iii) **Direct QSS Conditions and Direct Nodes**:* In order to generate meaningful RR graphs, it is necessary to specify the rules that govern the connectivity of the elementary reaction steps at the nodes of a RR graph. Thus, the nodes of the RR graph are subject to Kirchhoff's Flux Law (KFL), i.e., the rates of the elementary reaction steps leaving and entering the nodes satisfy the intermediate and *OR* QSS conditions, Eqs. (A.11) and (A.12). Further there are two types of nodes. Thus, the nodes that satisfy the QSS conditions for intermediate species are referred to as the *intermediate nodes* (*IN*s), while those that satisfy the QSS conditions for terminal species are referred to as *terminal nodes* (*TN*s). Furthermore, the QSS is a limiting form of KFL, which actually applies to non-steady state conditions as well. Further, INs or TNs do not necessarily represent QSS conditions (*Q*) of an individual species, but in general represents a group of species, i.e.,

Catalytic and Electrocatalytic Pathways in Fuel Cells

they represent a certain linear combination of Q_1, Q_2, ..., Q_q. Thus, nodes only denote the reaction connectivity.

Finally, the concept of directness is extended to the nodes as well. More specifically, we assume that the number of elementary reaction steps connected at a direct node, either *IN* or *TN*, should be *minimal* in the sense that if a reaction is dropped from the node, it is not possible to satisfy the QSS conditions for the given set of species at that node by employing only the remaining reaction steps. In other words, it is postulated that *only the nodes that connect a minimum number of reaction steps satisfying the QSS conditions for a given set of species are allowed*. By analogy with *RR*s, the QSS conditions involving a minimal number of rates of the elementary reaction steps are called *direct QSS conditions*, while the corresponding nodes are called *direct IN*s and *direct TN*s.

Direct INs: Consider first the enumeration of the direct intermediate QSS conditions. Let an arbitrary linear combination of the intermediate QSS conditions Q_1, Q_2, ..., Q_q be

$$
\begin{aligned}
Q = \lambda_1 Q_1 + \lambda_2 Q_2 + ... \lambda_q Q_q = \\
(\alpha_{11} r_1 + \alpha_{21} r_2 + ... + \alpha_{p1} r_p)\lambda_1 + (\alpha_{12} r_1 + \alpha_{22} r_2 + ... + \alpha_{p2} r_p)\lambda_2 + ... \\
+ (\alpha_{1q} r_1 + \alpha_{2q} r_2 + ... + \alpha_{pq} r_p)\lambda_q = 0
\end{aligned}
\tag{A.25}
$$

where $\lambda_1, \lambda_2, ..., \lambda_q$ are constants corresponding to the intermediate species. Now, to obtain the direct QSS conditions, i.e., those that involve a minimum number of rates, the constants $\lambda_1, \lambda_2, ..., \lambda_q$ should be chosen so as to eliminate a maximum number of rates. This results in a system of homogeneous equations in the unknowns $\lambda_1, \lambda_2, ..., \lambda_q$. As well known from linear algebra, in order to obtain a non-trivial solution for $\lambda_1, \lambda_2, ..., \lambda_q$ it is necessary to have no more than $q - 1$ linear homogeneous equations. That is, the intermediate QSS conditions Q_1, Q_2, ..., Q_q should be linearly combined so as to eliminate at least $q - 1$ rates. In turn, this means that a direct intermediate QSS condition should involve no more than $p - (q - 1) = p - q + 1$ rates. This, of course, specifies the maximum degree of an intermediate nodes.

Let us partition the set of rates $\{r_1, r_2, ..., r_p\}$ of the elementary reaction steps into two subsets: a subset of $q - 1$ rates $\{r_{l_1}, r_{l_2}, ..., r_{l_{q-1}}\}$ $(1 \le l_1 < l_2 < ... < l_{q-1} \le p)$ that *are not*

involved in a direct intermediate QSS condition, and a subset of $p - q + 1$ rates $\{r_{h_1}, r_{h_2}, ..., r_{h_{p-q+1}}\}$ $(1 \le h_1 < h_2 < ... < h_{p-q+1} \le p)$ that *are involved* in a direct QSS condition. Here $\{l_1, l_2, ..., l_{q-1}\}$ and $\{h_1, h_2, ..., h_{p-q+1}\}$ are two ordered subsets of integers chosen such that

$$\{l_1, l_2, ..., l_{q-1}\} \cup \{h_1, h_2, ..., h_{p-q+1}\} = \{1, 2, ..., p\} \tag{A.26}$$

A direct intermediate QSS may, thus, be characterized by either the selection of $q - 1$ rates $r_{l_1}, r_{l_2}, ..., r_{l_{q-1}}$ that *are not involved*, or by the $p - q + 1$ rates $\{r_{h_1}, r_{h_2}, ..., r_{h_{p-q+1}}\}$ that *are involved* in a direct intermediate QSS condition. We denote a direct intermediate QSS condition by $Q(r_{h_1}, r_{h_2}, ..., r_{h_{p-q+1}})$, thus specifying the rates of the elementary reaction steps that are involved in a direct intermediate QSS condition. The latter may be obtained by choosing $\lambda_1, \lambda_2, ..., \lambda_q$ in Eq. (A.25) so as to eliminate the rates $r_{l_1}, r_{l_2}, ..., r_{l_{q-1}}$. This gives

$$
\begin{aligned}
\alpha_{l_1,1}\lambda_1 + \alpha_{l_1,2}\lambda_2 + ... + \alpha_{l_1,q}\lambda_q &= 0 \\
\alpha_{l_2,1}\lambda_1 + \alpha_{l_2,2}\lambda_2 + ... + \alpha_{l_2,q}\lambda_q &= 0 \\
... \\
\alpha_{l_{q-1},1}\lambda_1 + \alpha_{l_{q-1},2}\lambda_2 + ... + \alpha_{l_{q-1},q}\lambda_q &= 0
\end{aligned}
\tag{A.27}
$$

The solution to this system of homogeneous linear equations is

$$
\lambda_k = \begin{vmatrix}
\alpha_{l_1,1} & \alpha_{l_2,1} & ... & \alpha_{l_{q-1},1} & 0 \\
\alpha_{l_1,2} & \alpha_{l_2,2} & ... & \alpha_{l_{q-1},2} & 0 \\
... & ... & ... & ... & ... \\
\alpha_{l_1,k-1} & \alpha_{l_2,k-1} & ... & \alpha_{l_{q-1},k-1} & 0 \\
\alpha_{l_1,k} & \alpha_{l_2,k} & ... & \alpha_{l_{q-1},k} & 1 \\
\alpha_{l_1,k+1} & \alpha_{l_2,k+1} & ... & \alpha_{l_{q-1},k+1} & 0 \\
... & ... & ... & ... & ... \\
\alpha_{l_1,q} & \alpha_{l_2,q} & ... & \alpha_{l_{q-1},h_q} & 0
\end{vmatrix}
\quad (k = 1, 2, ..., q)
\tag{A.28}
$$

Substituting Eq. (A.28) into Eq. (A.25) gives the following general formula for a direct intermediate QSS condition

$$Q(r_{h_1}, r_{h_2}, ..., r_{h_{p-q+1}}): \quad \begin{vmatrix} \alpha_{l_1,1} & \alpha_{l_2,1} & ... & \alpha_{l_{q-1},1} & Q_1 \\ \alpha_{l_1,2} & \alpha_{l_2,2} & ... & \alpha_{l_{q-1},2} & Q_2 \\ ... & ... & ... & ... & ... \\ \alpha_{l_1,q} & \alpha_{l_2,q} & ... & \alpha_{l_{q-1},q} & Q_q \end{vmatrix} = 0 \qquad (A.29)$$

or, taking into account Eq. (A.11), the direct QSS condition (KFL) for a node is

$$Q(r_{h_1}, r_{h_2}, ..., r_{h_{p-q+1}}): \quad \sum_{k=1}^{p-q+1} \begin{vmatrix} \alpha_{l_1,1} & \alpha_{l_2,1} & ... & \alpha_{l_{q-1},1} & \alpha_{h_k,1} \\ \alpha_{l_1,2} & \alpha_{l_2,2} & ... & \alpha_{l_{q-1},2} & \alpha_{h_k,2} \\ ... & ... & ... & ... & ... \\ \alpha_{l_1,q} & \alpha_{l_2,q} & ... & \alpha_{l_{q-1},q} & \alpha_{h_k,q} \end{vmatrix} r_{h_k} = 0 \qquad (A.30)$$

As a result, the general connectivity of an *IN* denoted by $n(s_{h_1}, s_{h_2}, ..., s_{h_{p-q+1}})$ is

$$n(s_{h_1}, s_{h_2}, ..., s_{h_{p-q+1}}): \quad \sum_{k=1}^{p-q+1} \begin{vmatrix} \alpha_{l_1,1} & \alpha_{l_2,1} & ... & \alpha_{l_{q-1},1} & \alpha_{h_k,1} \\ \alpha_{l_1,2} & \alpha_{l_2,2} & ... & \alpha_{l_{q-1},2} & \alpha_{h_k,2} \\ ... & ... & ... & ... & ... \\ \alpha_{l_1,q} & \alpha_{l_2,q} & ... & \alpha_{l_{q-1},q} & \alpha_{h_k,q} \end{vmatrix} s_{h_k} \qquad (A.31)$$

The complete enumeration of direct intermediate QSS conditions and *IN*s may be, in principle, performed by considering all of the possible combinations of $p - q + 1$ species from the total of p. Normally, the number of direct *IN*s exceeds the number of linearly independent *IN*s, i.e., the number of linearly independent intermediates q. It may be noted again, that, although the node connectivity (Eq. (A.31)) results from the QSS condition, it is more generally valid including the unsteady state.

***Direct TNs*:** Now, consider the enumeration of the direct *OR* QSS conditions, i.e., the enumeration of direct *TN*s. Since, again, a direct *OR* QSS condition should involve a minimum number of rates, it is necessary to eliminate from Eq. (A12) the maximum number of rates by employing the interrelationships provided by the intermediate QSS, Eq. (A.11). Because *rank* $\alpha = q$, we can solve Eq. (A.11) for no more than q rates. Upon substitution of these q rates into Eq. (A.12) we arrive at a direct *OR* QSS condition involving no more than $p - q$ rates of the elementary reaction steps. Let $\{r_{l_1}, r_{l_2}, ..., r_{l_q}\}$ $(1 \leq l_1 < l_2 < ... < l_q \leq p)$ be the q rates of the elementary reaction steps that *are not*

involved in a direct *OR* QSS condition, while $\{r_{h_1}, r_{h_2},...,r_{h_{p-q}}\}$ $(1 \le h_1 < h_2 < ... < h_{p-q} \le p)$ be the $p - q$ rates that *are involved* in a direct *OR* QSS condition. Here $\{l_1, l_2,...,l_q\}$ and $\{h_1, h_2,...,h_{p-q}\}$ are two ordered subsets of integers chosen so as to satisfy Eq. (A.26). A direct *OR* QSS condition is denoted by $P(r_{h_1}, r_{h_2},...,r_{h_{p-q}})$ thus specifying the rates that are involved in a direct *OR* QSS condition. Its general equation may be obtained by solving Eq. (A.11) with respect to $\{r_{l_1}, r_{l_2},...,r_{l_q}\}$

$$
\begin{aligned}
&\alpha_{l_1,1}r_{l_1} + \alpha_{l_2,1}r_{l_2} + ... + \alpha_{l_q,1}r_{l_q} = -\alpha_{h_1,1}r_{h_1} - \alpha_{h_2,1}r_{h_2} - ... - \alpha_{h_{p-q},1}r_{h_{p-q}} \\
&\alpha_{l_1,2}r_{l_1} + \alpha_{l_2,2}r_{l_2} + ... + \alpha_{l_q,2}r_{l_q} = -\alpha_{h_1,2}r_{h_1} - \alpha_{h_2,2}r_{h_2} - ... - \alpha_{h_{p-q},2}r_{p-q} \\
&... \\
&\alpha_{l_1,q}r_{l_1} + \alpha_{l_2,q}r_{l_2} + ... + \alpha_{l_q,q}r_{l_q} = -\alpha_{h_1,q}r_{h_1} - \alpha_{h_2,q}r_{h_2} - ... - \alpha_{h_{p-q},q}r_{j_{p-q}}
\end{aligned}
\tag{A.32}
$$

Substituting the solution of Eq. (A.32) into Eq. (A.12), after a few transformations based on the properties of the determinants, we obtain

$$
P(r_{h_1}, r_{h_2},...,r_{h_{p-q}}): \quad \frac{1}{v_1\Delta}\sum_{k=1}^{p-q}
\begin{vmatrix}
\alpha_{l_1,1} & \alpha_{l_1,2} & ... & \alpha_{l_1,q} & \beta_{l_1,1} \\
\alpha_{l_2,1} & \alpha_{l_2,2} & ... & \alpha_{l_2,q} & \beta_{l_2,1} \\
... & ... & ... & ... & ... \\
\alpha_{l_q,1} & \alpha_{l_q,2} & ... & \alpha_{l_q,q} & \beta_{l_q,1} \\
\alpha_{h_k,1} & \alpha_{h_k,2} & ... & \alpha_{h_k,q} & \beta_{h_k,1}
\end{vmatrix}
r_{h_k} = r_{OR}
\tag{A.33}
$$

where the determinant

$$
\Delta = \Delta(l_1, l_2,...,l_q) =
\begin{vmatrix}
\alpha_{l_1,1} & \alpha_{l_1,2} & ... & \alpha_{l_1,q} \\
\alpha_{l_2,1} & \alpha_{l_2,2} & ... & \alpha_{l_2,q} \\
... & ... & ... & ... \\
\alpha_{l_q,1} & \alpha_{l_q,2} & ... & \alpha_{l_q,q}
\end{vmatrix}
\tag{A.34}
$$

Obviously, only those selections of the set of integers $(l_1, l_2,...,l_q)$ are valid for which the determinant $\Delta = \Delta(l_1, l_2,...,l_q)$, Eq. (A.34), is different from zero. The *TN*s that correspond to these direct *OR* QSS conditions are denoted by $m(s_{h_1}, s_{h_2},...,s_{h_{p-q}})$ and their general connectivity is given by

Catalytic and Electrocatalytic Pathways in Fuel Cells

$$
n_{\mathrm{T}}\left(s_{h_1}, s_{h_2}, \ldots, s_{h_{p-q}}\right): \quad \frac{1}{v_1 \Delta} \sum_{k=1}^{p-q} \begin{vmatrix} \alpha_{l_1,1} & \alpha_{l_1,2} & \ldots & \alpha_{l_1,q} & \beta_{l_1,1} \\ \alpha_{l_2,1} & \alpha_{l_2,2} & \ldots & \alpha_{l_2,q} & \beta_{l_2,1} \\ \ldots & \ldots & \ldots & \ldots & \ldots \\ \alpha_{l_q,1} & \alpha_{l_q,2} & \ldots & \alpha_{l_q,q} & \beta_{l_q,1} \\ \alpha_{h_k,1} & \alpha_{h_k,2} & \ldots & \alpha_{h_k,q} & \beta_{h_k,1} \end{vmatrix} s_{h_k} + OR \qquad (A.35)
$$

Notice that in Eq. (A.35) the *OR* is added to the first term rather than subtracted as it would follow from Eq. (A.32). As shown below, this change in sign is dictated by the necessity to ensure that the *RR* graphs are cyclic graphs. It should also be noted that, in deriving Eqs. (A.33) and (A.34), we have arbitrarily utilized the first identity in Eq. (A.12). It may be shown, however, that, up to a constant, the final result is independent of the choice of the identities in Eq. (A.12).

The complete enumeration of the *TN*s may be, in general, performed by applying Eq. (A.33) to all possible combinations of $\{r_{l_1}, r_{l_2}, \ldots, r_{l_q}\}$ $(1 \le l_1 < l_2 < \ldots < l_q \le p)$ or $\{r_{h_1}, r_{h_2}, \ldots, r_{h_{p-q}}\}$ $(1 \le h_1 < h_2 < \ldots < h_{p-q} \le p)$ for which the determinant Δ, Eq. (A.34), is different from zero.

The connectivity of *IN*s and *TN*s, in principle, provides the necessary information for constructing the *RR* graph. Of course, not all *IN*s and *TN*s are independent; only q *IN*s (the number of independent intermediate species) and one *TN* (for the single *OR*) are independent.

Code written in MAPLE for stoichiometric enumeration of direct RRs and INs:

```
> restart;
> with(Student[LinearAlgebra]):
> with(combinat):
> ########Input stoichiometric matrix: Double click on the matrix to edit
```

Replace with the filename of your stoichimetric matrix. You need a "csv" file, accessible in Excel.

```
>
> stoich := ImportMatrix("WGS17Cu.csv", source = csv);
```

$$stoich := \begin{bmatrix} \text{18 x 15 Matrix} \\ \text{Data Type: anything} \\ \text{Storage: rectangular} \\ \text{Order: Fortran\_order} \end{bmatrix}$$

nINTS: Number of intermediates. Needs to be changed by user.
> **nINTS:=9;**

$$nINTS := 9$$

Input filename. Warning: The files will be overwritten without notice
> **filename:="WGS17Cu":**
> **AllFR_file:=cat("AllFR_",filename,".csv"):**
> **AllER_file:=cat("AllER_",filename,".csv"):**
>
> **UniqueFR_file:=cat("UniqueFR_",filename,".csv"):**
> **UniqueER_file:=cat("UniqueER_",filename,".csv"):**
> **AllIN_file:=cat("AllIN_",filename,".csv"):**
> **UniqueIN_file:=cat("UniqueIN_",filename,".csv"):**
> **nES := RowDimension(stoich)-1:**
> **nSPECIES := ColumnDimension(stoich)-1:**
> **for i from 2 to nES+1**
do
  rxnR[i] := 0;
  rxnP[i] := 0;
  for j from 2 to nSPECIES+1
  do
   if stoich[i, j] < 0
    then rxnR[i] := evalf(rxnR[i])-stoich[i, j]*convert(stoich[1, j], symbol);
    else rxnP[i] := evalf(rxnP[i])+stoich[i, j]*convert(stoich[1, j], symbol);
   end if:
  od:
od:
>
> **for i to nES**
do
  ESlist[i] := cat(stoich[i+1, 1], ":   ", convert(rxnR[i+1], string), " <-> ",
convert(rxnP[i+1], string)); print(ESlist[i]);
od:

$$\text{"s1:\quad S+H2O <-> H2OS'}$$
$$\text{"s2:\quad S+CO <-> COS"}$$
$$\text{"s3:\quad 2*HS <-> 2.*S+H2'}$$
$$\text{"s4:\quad CO2S <-> S+CO2"}$$
$$\text{"s5:\quad H2OS+S <-> HS+OHS'}$$
$$\text{"s6:\quad OHS+S <-> HS+OS'}$$
$$\text{"s7:\quad 2*OHS <-> OS+H2OS'}$$
$$\text{"s8:\quad OS+COS <-> CO2S+S'}$$
$$\text{"s9:\quad COS+OHS <-> COOHS+S}$$
$$\text{"s10:\quad COOHS+S <-> HS+CO2S}$$

```
                  "s11:   OS+COOHS  <->  OHS+CO2S
                  "s12:   OHS+COOHS  <->  CO2S+H2OS
                  "s13:   COS+COOHS  <->  CO2S+HCOS
                   "s14:   HCOOS+S  <->  HS+CO2S
                  "s15:   OS+HCOOS  <->  OHS+CO2S
                  "s16:   OHS+HCOOS  <->  CO2S+H2OS
                    "s17:   HCOS+S  <->  HS+COS'
```

```
> for i from 1 to nINTS
do
  Q[i]:=0:
  for k from 1 to nES
    do
      Q[i]:=Q[i]+stoich[k+1,i+1]*convert(stoich[k+1,1],symbol);
    od:
  print(cat("Q",i,"=",convert(Q[i],string))):
od:
>
```

```
                  "Q1=-2*s3+s5+s6+s10+s14+s17"
                       "Q2=s6+s7-s8-s11-s15"
                       "Q3=s2-s8-s9-s13+s17"
                  "Q4=s5-s6-2*s7-s9+s11-s12+s15-s16"
                       "Q5=s9-s10-s11-s12-s13"
                          "Q6=-s14-s15-s16"
                  "Q7=-s4+s8+s10+s11+s12+s13+s14+s15+s16"
                        "Q8=s1-s5+s7+s12+s16"
                             "Q9=s13-s17"
```

```
> intM := Matrix(nES, nINTS): #Intermediate submatrix
> for i to nINTS
do
  for j to nES
  do intM[j, i] := stoich[j+1, i+1]
  od:
od:
> print("intM:=",intM);
```

$$
\text{"intM:=",} \begin{bmatrix}
\text{17 x 9 Matrix} \\
\text{Data Type: anything} \\
\text{Storage: rectangular} \\
\text{Order: Fortran\_order}
\end{bmatrix}
$$

```
> ES:=Rank(intM)+1;
```

$$ES := 10$$

Full Routes enumeration:

```
> FRmax := factorial(nES)/(factorial(nES-ES)*factorial(ES));
```

$$FRmax := 19448$$

```
> RRsubmatrix := Matrix(ES-1, nINTS): #Submatrix used to determine the Si
coefficient in the reaction route
> Enumerated:=choose(nES,ES):
> ORcounter:=0:
unique:=1:
AllFR := fopen(AllFR_file, WRITE):
UniqueFR:= fopen(UniqueFR_file,WRITE):
fprintf(UniqueFR,cat(", , Number of steps, Associated OR \n")):
for k  from 1 to FRmax
do
 counter:=0:
 Steps[k]:="";
 for i from 1 to ES
 do
   for l from 1 to ES-1
   do
     for m from 1 to nINTS
     do
       if (l=i)
         then jump:=1;
       end if;
       RRsubmatrix[l,m]:=intM[Enumerated[k,l+jump],m];
       #print(jump,k,l,m,RRsubmatrix[l,m],Enumerated[k,l+jump]);
     od:
   od:
  Scoeff[i]:= (-1)^((i+1))*Determinant(RRsubmatrix);
  jump:= 0;
  #print(Enumerated[k],RRsubmatrix,jump,k,l,m, Scoeff[i]);
 od:
 #Determine gcd of Scoeff
 g:=0;
 for i from 1 to ES
 do
   g:= gcd(g,Scoeff[i]);
   if (g=1) then break end if:
 od:
 #Check sign of the first non-zero Si coefficient
 neg:=1:
 for i from 1 to ES
 do
   if (Scoeff[i]<>0)
   then
     if (Scoeff[i]<0)
     then
       neg:=-1;
       break;
```

```
    else
      neg:=1;
      break;
    end if;
   else
     neg:=0;
   end if;
 od:
 #Puts possible FR into "canonical" form
 for i from 1 to ES
 do
  if (neg<>0) and (g<>0)
  then
    Scoeff[i]:=(Scoeff[i])/(neg*g);
  end if;
 od:
 FR[k]:=0;
 for i from 1 to ES
 do
  FR[k]:=FR[k]+convert(stoich[Enumerated[k,i]+1,1],symbol)*Scoeff[i];
  if (i<>ES)
  then
    Steps[k]:=cat(Steps[k],stoich[Enumerated[k,i]+1,1],";")
  else Steps[k]:=cat(Steps[k],stoich[Enumerated[k,i]+1,1])
  end if:
 od:
 ###Check if the reaction obtained is "zero"
 OR[k]:=0;
 for i from 1 to ES
 do
  for j from 2 to nSPECIES+1
  do

OR[k]:=OR[k]+Scoeff[i]*stoich[Enumerated[k,i]+1,j]*convert(stoich[1,j],symbol);
  od:
 od:
 OR[k]:=simplify(OR[k]);
 ER[k]:=0:
 if (OR[k]=0)
 then
   ER[k]:=1
 end if:
 fprintf(AllFR,cat("FR(",Steps[k],")=", convert(FR[k], string),"\n")):
 #print(cat("FR(",Steps[k],")=", convert(FR[k], string)));
 if (ER[k]=1)
 then
```

```
  Buffer[k]:=0;
 else
  unique:=1:
  for i from 1 to k-1
   do
    if (Buffer[i]=FR[k])
    then
     #print(Buffer[i],FR[k]);
     unique:=0:
     break:
    end if:
   od:
  if (unique=1)
  then
   #uniqueOR:=1:
   for i from 1 to ES
   do
    if (Scoeff[i]<>0) then counter:=counter+1 end if:
   od:
   uniqueORtrue:=1:
   #print(ORcounter):
   for i from 1 to ORcounter
   do
    if (OR[k]<>0)
    then
     #print(OR[k],uniqueOR[i]);
     if (abs(uniqueOR[i])=abs(OR[k]))
     then
      uniqueORtrue:=0:
      ORnumber:=i:
      #print("break",OR[k],OR[i],k,i);
      break:
     else
      uniqueORtrue:=1:
     end if:
    else
     #print("zero",k,i);
    end if:
   od:
   if (uniqueORtrue=1)
   then
    ORcounter:=ORcounter+1:
    ORnumber:=ORcounter:
    #print("no zero",OR[k],OR[i],ORcounter,i);
    uniqueOR[ORcounter]:=OR[k]:
   end if:
```

Catalytic and Electrocatalytic Pathways in Fuel Cells

```
    fprintf(UniqueFR,cat("FR(",Steps[k],")=,", convert(FR[k],
string),",",convert(counter,string),",OR",convert(ORnumber,string),"\n"));
   end if:
   Buffer[k]:=FR[k]
  end if:
od:
fprintf(UniqueFR,"\n \n \n"):
for i from 1 to ORcounter
do

fprintf(UniqueFR,cat("OR",convert(i,string),"=",convert(uniqueOR[i],string),"\n")
);
od:
fclose(AllFR):
fclose(UniqueFR):
> #uniqueOR;
> for i from 1 to ORcounter
do
 print(uniqueOR[i]);
 #fprintf(UniqueFR,cat("FR(",Steps[k],")=,", convert(FR[k],
string),",",convert(counter,string),"\n"));
od:
```

$$-H2O - CO + H2 + CO2$$

Empty Routes Enumeration

```
> gammaM := Matrix(nES, nINTS+1): #reduced stoichiometric submatrix
>
> for i to nINTS
do
  for j to nES
  do gammaM[j, i] := stoich[j+1, i+1]
  od:
od:
> for j from 1 to nES
do
  gammaM[j, nINTS+1] := stoich[j+1, nINTS+3]:
od:

> print("gammaM:=",gammaM);
```

$$\text{"gammaM:=",} \begin{bmatrix} \text{17 x 10 Matrix} \\ \text{Data Type: anything} \\ \text{Storage: rectangular} \\ \text{Order: Fortran\_order} \end{bmatrix}$$

```
> qp2:=Rank(gammaM)+1;
```

$$qp2 := 11$$

```
> ERmax := factorial(nES)/(factorial(nES-qp2)*factorial(qp2));
                              ERmax := 12376
> ERsubmatrix := Matrix(qp2-1, nINTS+1): #Submatrix used to determine the Si
coefficient in the reaction route
> Enumerated:=choose(nES,qp2):
>

AllER := fopen(AllER_file, WRITE):
UniqueER:= fopen(UniqueER_file,WRITE):
for k  from 1 to ERmax
do
 counter:=0:
 Steps[k]:="";
 for i from 1 to qp2
 do
  for l from 1 to qp2-1
  do
    for m from 1 to nINTS+1
    do
     if (l=i)
       then jump:=1;
     end if;
     ERsubmatrix[l,m]:=gammaM[Enumerated[k,l+jump],m];
    od:
  od:
  Scoeff[i]:= (-1)^((i+1))*Determinant(ERsubmatrix);
  #print(Scoeff[i],i,k);
  jump:= 0;
 od:
 #Determine gcd of Scoeff
 g:=0;
 for i from 1 to qp2
 do
  g:= gcd(g,Scoeff[i]);
  if (g=1) then break end if:
 od:
 #Check sign of the first non-zero Si coefficient
 neg:=1:
 for i from 1 to qp2
 do
  if (Scoeff[i]<>0)
  then
    #print(Scoeff[i],i,k);
    if (Scoeff[i]<0)
    then
      neg:=-1;
```

```
      break;
    else
      neg:=1;
      break;
    end if;
  else
    neg:=0;
  end if;
od:
#Puts possible ER into "canonical" form
for i from 1 to qp2
do
  if (neg<>0) and (g<>0)
  then
    Scoeff[i]:=(Scoeff[i])/(neg*g);
  end if;
od:
ER[k]:=0;
for i from 1 to qp2
do
  ER[k]:=ER[k]+convert(stoich[Enumerated[k,i]+1,1],symbol)*Scoeff[i];
  if (i<>qp2)
  then
    Steps[k]:=cat(Steps[k],stoich[Enumerated[k,i]+1,1],";")
  else Steps[k]:=cat(Steps[k],stoich[Enumerated[k,i]+1,1])
  end if:
od:
###Check if the reaction obtained is "zero"
OR[k]:=0;
for i from 1 to qp2
do
  for j from 2 to nSPECIES+1
  do

OR[k]:=OR[k]+Scoeff[i]*stoich[Enumerated[k,i]+1,j]*convert(stoich[1,j],symbol);

    #print("OR,Scoeff,stoich,stoich coeff,
i,j,k",OR[k],Scoeff[i],stoich[Enumerated[k,i]+1,j],stoich[1,j],i,j,k);
  od:
  #print(" j loop end");
od:
#print("i loop end");
#OR[k]:=simplify(OR[k]);
#print("Final",OR[k],k);
ERcheck[k]:=0:
if (OR[k]=0)
```

```
    then
      ERcheck[k]:=1
    end if:
    fprintf(AllER,cat("ER(",Steps[k],")=", convert(ER[k], string),"\n"));
    #print(cat("ER(",Steps[k],")=", convert(OR[k], string)));
    if (ERcheck[k]<>1)
    then
      Buffer[k]:=0;
    else
      unique:=1:
      for i from 1 to k-1
        do
          if (Buffer[i]=ER[k])
          then
            unique:=0:
            break:
          end if:
        od:
      if (unique=1)
      then
        for i from 1 to qp2
        do
          if (Scoeff[i]<>0) then counter:=counter+1 end if:
        od:
        fprintf(UniqueER,cat("ER(",Steps[k],")=", convert(ER[k],
string),",",convert(counter,string),"\n"));
      end if:
    Buffer[k]:=ER[k]
    end if:
od:
fclose(AllER);
fclose(UniqueER);
```

Intermediate Nodes Enumeration
>
> **intMT:=Transpose(intM);**

$$intMT := \begin{bmatrix} 9 \text{ x } 17 \text{ Matrix} \\ \text{Data Type: anything} \\ \text{Storage: rectangular} \\ \text{Order: Fortran\_order} \end{bmatrix}$$

> **nES;**
> **ES;**
>

$$17$$
$$10$$

> **q:=Rank(intMT);**

$$q := 9$$

Catalytic and Electrocatalytic Pathways in Fuel Cells

```
> INmax := factorial(nES)/(factorial(nES-(q-1))*factorial(q-1));
                                   INmax := 24310
> INsubmatrix := Matrix((q-1), (q-1) ): #Submatrix used to determine the Si
coefficient in the reaction route
> Enumerated:=choose(nES,q-1):
>
> AllIN := fopen(AllIN_file, WRITE):
UniqueIN:= fopen(UniqueIN_file,WRITE):
for k  from 1 to INmax
do
  counter:=0:
  jump:=0:
  Steps[k]:="";
  for l from 1 to nINTS
  do
    for i from 1 to q-1
    do
      for j from 1 to q-1
      do
        if (j=l) then jump:=1 end if:
        INsubmatrix[j,i]:=intMT[j+jump,Enumerated[k,i]];
        #print("something",i,j,k,l,jump);
      od:
      jump:=0:
    od:
    #jump:=0:
    #print(INsubmatrix);
    Qcoeff[l]:=(-1)^(l+1)*Determinant(INsubmatrix):
    #print("plus");
  od:
  #print("out");
  Steps:=cat("IN("):
  for i from 1 to nES
  do
    fait:=0:
    for j from 1 to q-1
    do
      if (i<>Enumerated[k,j]) and (fait=0)
      then
        Steps:=cat(Steps,stoich[i+1,1],";"):
        fait:=1:
      end if:
    od:
  od:
  Steps:=cat(Steps,")"):
  IN[k]:=0:
```

```
for i from 1 to nINTS
do
  IN[k]:=IN[k]+Qcoeff[i]*Q[i]:
  #print("do"):
od:
simplify(IN[k]):
#fprintf(AllIN,cat(Steps,"=, ",convert(IN[k],string),"\n"));
#Calculate individual Si coefficients
for j from 1 to nES
do
  Scoeff[j]:=0:
od:
#print("done");
for i from 1 to nINTS
do
  for j from 1 to nES
  do
    Scoeff[j]:=Scoeff[j]+Qcoeff[i]*stoich[j+1,i+1]:
    #print("OK");
  od:
od:
Scoeffprint:=0:
for i from 1 to nES
do
  Scoeffprint:=Scoeffprint+ Scoeff[i]*convert(stoich[i+1,1],symbol);
od:
#print(Scoeffprint);
#Check sign of the first nonzero coeff
neg:=1:
for i from 1 to nES
do
  if (Scoeff[i]<>0)
  then
    if (Scoeff[i]<0)
    then
      neg:=-1:
      break:
    else
      neg:=1:
      break:
    end if:
  else
    neg:=0:
  end:
od:
#Determine GCD of Scoeff
```

```
  g:=0:
  for i from 1 to nES
  do
    g:=gcd(g,Scoeff[i]):
    if (g=1) then break end if:
  od:
  #Puts IN into canonical form
  for i from 1 to nES
  do
    if (neg<>0) and (g<>0)
    then
      Scoeff[i]:=Scoeff[i]/(neg*g);
    end if:
  od:
    Scoeffprint:=0:
  for i from 1 to nES
  do
    Scoeffprint:=Scoeffprint+ Scoeff[i]*convert(stoich[i+1,1],symbol);
  od:
  fprintf(AllIN,cat(Steps,"=, ",convert(Scoeffprint,string),"\n"));
  #Determine Unique INs
  unique:=1:
  for i from 1 to k-1
  do
    if (Buffer[i]=Scoeffprint)
    then
      unique:=0:
      break:
    end if:
  od:
  if (unique=1)
  then
    Buffer[k]:=Scoeffprint:
    fprintf(UniqueIN,cat(Steps,"=, ",convert(Scoeffprint,string),"\n"));
  end if:
od:

> fclose(AllIN);
fclose(UniqueIN);
```

Catalytic and Electrocatalytic Pathways in Fuel Cells

Appendix B: Derivation of QSS rate expressions Eqs. (6.23) – (6.28).

The rate of the elementary reaction s_{11} is

$$r_{11} = \vec{k}_{11}\theta_{CH_2 \cdot S}\theta_0 - \bar{k}_{11}\theta_{CH \cdot S}\theta_{H \cdot S} \tag{B.1}$$

From Appendix C we have

$$\theta_{H \cdot S} = K_v P_{H_2}^{1/2}\theta_0 \tag{B.2}$$

$$\theta_{CH \cdot S} = K_x P_{CO} P_{H_2}^{3/2} P_{H_2O}^{-1}\theta_0 \tag{B.3}$$

The coverage of the surface intermediate $CH_2 \cdot S$ may be obtained from the quasi-steady state condition

$r_{10} = r_{11} + r_{14}$. However, the flux through step s_{14} is negligible, thus,

$r_{10} = r_{11}$

or

$$\vec{k}_{10}\theta_{CH_3 \cdot S}\theta_0 - \bar{k}_{10}\theta_{CH_2 \cdot S}\theta_{H \cdot S} = \vec{k}_{11}\theta_{CH_2 \cdot S}\theta_0 - \bar{k}_{11}\theta_{CH \cdot S}\theta_{H \cdot S} \tag{B.4}$$

From Appendix C we have

$$\theta_{CH_3 \cdot S} = K_i P_{CH_4} P_{H_2}^{-1/2}\theta_0 \tag{B.5}$$

Solving (B.4) gives

$$\theta_{CH_2 \cdot S} = \frac{\vec{k}_{10}K_i P_{CH_4} P_{H_2}^{-1/2} + \bar{k}_{11}K_v K_x P_{CO} P_{H_2}^2 P_{H_2O}^{-1}}{\vec{k}_{11} + \bar{k}_{10}K_v P_{H_2}^{1/2}}\theta_0 \tag{B.6}$$

Substituting Eqs. (B.2), (B.3) and (B.6) into Eq. (B.1)

$$r_{11} = \frac{\vec{k}_{10}\vec{k}_{11}K_i P_{CH_4} P_{H_2}^{-1/2}\theta_0^2}{\vec{k}_{11} + \bar{k}_{10}K_v P_{H_2}^{1/2}}\left(1 - \frac{K_v^2 K_x}{K_{10}K_{11}K_i}\frac{P_{CO}P_{H_2}^3}{P_{CH_4}P_{H_2O}}\right) \tag{B.7}$$

Eq. (6.23) is obtained by recognizing that

$$\frac{K_v^2 K_x}{K_{10}K_{11}K_i} = \frac{1}{K_{SR}}$$

The rate of the elementary reaction s_{15} is

$$r_{15} = \vec{k}_{15}\theta_{CH_2O \cdot S}\theta_0 - \bar{k}_{15}\theta_{CHO \cdot S}\theta_{H \cdot S} \tag{B.8}$$

From Appendix C we have

$$\theta_{CHO \cdot S} = K_{viii} P_{CO} P_{H_2}^{1/2} \theta_S \tag{B.9}$$

$\theta_{H \cdot S}$ is given in Eq. (B.2)

Surface coverage of $CH_2O \cdot S$ is determined from the quasi-steady state condition $r_{20} + r_{14} = r_{15}$. However, the flux through step s_{14} is negligible, thus

$$r_{20} = r_{15}$$

or

$$\vec{k}_{20} \theta_{CH_3O \cdot S} \theta_0 - \overleftarrow{k}_{20} \theta_{CH_2O \cdot S} \theta_{H \cdot S} = \vec{k}_{15} \theta_{CH_2O \cdot S} \theta_0 - \overleftarrow{k}_{15} \theta_{CHO \cdot S} \theta_{H \cdot S} \tag{B.10}$$

Solving Eq. (B.10) gives

$$\theta_{CH_2O \cdot S} = \frac{\vec{k}_{20}}{\overleftarrow{k}_{15} + \overleftarrow{k}_{20} K_v P_{H_2}^{1/2}} \theta_{CH_3O \cdot S} + \frac{\overleftarrow{k}_{15} K_v K_{viii} P_{CO} P_{H_2}}{\overleftarrow{k}_{15} + \overleftarrow{k}_{20} K_v P_{H_2}^{1/2}} \theta_0 \tag{B.11}$$

In turn, from the steady-state condition of $CH_3O \cdot S$ we have

$$r_{19} = r_{20}$$

or

$$\vec{k}_{19} \theta_{CH_3 \cdot S} \theta_{O \cdot S} - \overleftarrow{k}_{19} \theta_{CH_3O \cdot S} \theta_0 = \vec{k}_{20} \theta_{CH_3O \cdot S} \theta_0 - \overleftarrow{k}_{20} \theta_{CH_2O \cdot S} \theta_{H \cdot S} \tag{B.12}$$

where $\theta_{CH_3 \cdot S}$ is given by Eq. (B.5) and $\theta_{O \cdot S}$ according to Appendix C, is given by

$$\theta_{O \cdot S} = K_{vi} P_{H_2O} P_{H_2}^{-1} \theta_0 \tag{B.13}$$

From Eq. (B.12) we have

$$\theta_{CH_3O \cdot S} = \frac{\vec{k}_{19} K_i K_{vi} P_{CH_4} P_{H_2O} P_{H_2}^{-3/2}}{\overleftarrow{k}_{19} + \vec{k}_{20}} \theta_0 + \frac{\overleftarrow{k}_{20} K_v P_{H_2}^{1/2}}{\overleftarrow{k}_{19} + \vec{k}_{20}} \theta_{CH_2O \cdot S} \tag{B.14}$$

Solving simultaneously Eqs. (B.11) and (B.14) we have

$$\theta_{CH_2O \cdot S} = \left(\frac{\overleftarrow{k}_{19} \overleftarrow{k}_{15} K_v K_{viii} P_{CO} P_{H_2} + \vec{k}_{20} \overleftarrow{k}_{15} K_v K_{viii} P_{CO} P_{H_2} + \vec{k}_{19} \vec{k}_{20} K_i K_{vi} P_{CH_4} P_{H_2O} P_{H_2}^{-3/2}}{\overleftarrow{k}_{19} \overleftarrow{k}_{15} + \vec{k}_{20} \overleftarrow{k}_{15} + \overleftarrow{k}_{19} \overleftarrow{k}_{20} K_v P_{H_2}^{1/2}} \right) \theta_0 \tag{B.15}$$

Substituting Eqs. (B.2), (B.9) and (B.15) into Eq. (B.8) results in

$$r_{15} = \frac{\vec{k}_{19} \vec{k}_{20} \overleftarrow{k}_{15} K_i K_{vi} P_{CH_4} P_{H_2O} P_{H_2}^{-3/2} \theta_0^2}{\overleftarrow{k}_{19} \overleftarrow{k}_{15} + \vec{k}_{20} \overleftarrow{k}_{15} + \overleftarrow{k}_{19} \overleftarrow{k}_{20} K_v P_{H_2}^{1/2}} \left(1 - \frac{\overleftarrow{k}_{19} \overleftarrow{k}_{20} \overleftarrow{k}_{15} K_v^2 K_{viii}}{\vec{k}_{19} \vec{k}_{20} \overleftarrow{k}_{15} K_i K_{vi}} \frac{P_{CO} P_{H_2}^3}{P_{CH_4} P_{H_2O}} \right) \tag{B.16}$$

or

$$r_{15} = \frac{\vec{k}_{19} \vec{k}_{20} \overleftarrow{k}_{15} K_i K_{vi} P_{CH_4} P_{H_2O} P_{H_2}^{-3/2} \theta_0^2}{\overleftarrow{k}_{19} \overleftarrow{k}_{15} + \vec{k}_{20} \overleftarrow{k}_{15} + \overleftarrow{k}_{19} \overleftarrow{k}_{20} K_v P_{H_2}^{1/2}} \left(1 - \frac{K_v^2 K_{viii}}{K_{19} K_{20} K_{15} K_i K_{vi}} \frac{P_{CO} P_{H_2}^3}{P_{CH_4} P_{H_2O}} \right) \tag{B.17}$$

Eq. (6.24) is obtained by recognizing that

$$\frac{K_v^2 K_{viii}}{K_{19}K_{20}K_{15}K_i K_{vi}} = \frac{1}{K_{SR}}$$

The rate of the elementary reaction s_{17} is

$$r_{17} = \vec{k}_{17}\theta_{CO\cdot S}\theta_{O\cdot S} - \overleftarrow{k}_{17}\theta_{CO_2\cdot S}\theta_0 \qquad \text{(B.18)}$$

Based on Appendix C,

$$\theta_{CO\cdot S} = K_{iii}P_{CO}\theta_0$$

$$\theta_{O\cdot S} = K_{vi}P_{H_2O}P_{H_2}^{-1}\theta_0$$

$$\theta_{CO_2\cdot S} = K_{iv}P_{CO_2}\theta_0$$

Substituting above in Eq. (B.18), we have

$$r_{17} = \vec{k}_{17}K_{iii}K_{vi}P_{CO}P_{H_2O}P_{H_2}^{-1}\theta_0^2\left(1 - \frac{\overleftarrow{k}_{17}K_{iv}}{\vec{k}_{17}K_{iii}K_{vi}}\frac{P_{CO_2}P_{H_2}}{P_{H_2O}P_{CO}}\right) \qquad \text{(B.19)}$$

or

$$r_{17} = \vec{k}_{17}K_{iii}K_{vi}P_{CO}P_{H_2O}P_{H_2}^{-1}\theta_0^2\left(1 - \frac{K_{iv}}{K_{17}K_{iii}K_{vi}}\frac{P_{CO_2}P_{H_2}}{P_{H_2O}P_{CO}}\right) \qquad \text{(B.20)}$$

Eq. (6.26) is obtained by recognizing that

$$\frac{K_{iv}}{K_{17}K_{iii}K_{vi}} = \frac{1}{K_{WGS}}$$

Finally θ_0 in the above expressions is obtained based on the concept of MARI. Thus,

$$\theta_0 = 1 - \theta_{H_2O\cdot S} - \theta_{CO\cdot S} - \theta_{H\cdot S} - \theta_{O\cdot S} - \theta_{OH\cdot S} - \theta_{C\cdot S} \qquad \text{(B.21)}$$

Based on Appendix C, we have

$$\theta_{H_2O\cdot S} = K_{ii}P_{H_2O}\theta_0$$

$$\theta_{CO\cdot S} = K_{iii}P_{CO}\theta_0$$

$$\theta_{H\cdot S} = K_v P_{H_2}^{1/2}\theta_0$$

$$\theta_{O\cdot S} = K_{vi}P_{H_2O}P_{H_2}^{-1}\theta_0$$

$$\theta_{\text{OH·S}} = K_{vii} P_{\text{H}_2\text{O}} P_{\text{H}_2}^{-1/2} \theta_0$$

$$\theta_{\text{C·S}} = K_{ix} P_{\text{CO}} P_{\text{H}_2} P_{\text{H}_2\text{O}}^{-1} \theta_0$$
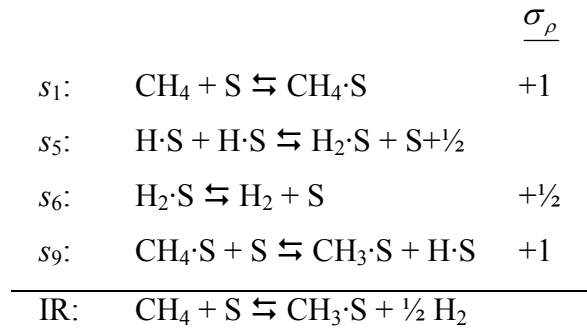
Eq. (6.28) can be obtained by substituting the above in Eq. (B.21)

Appendix C: Intermediate Reactions for the formation of key intermediates utilized in Appendix B

We show here the derivation of surface coverage of intermediate species based on QE approximation and the notion of intermediate reactions. The methodology is illustrated for one species, $CH_3 \cdot S$. The surface coverage of the other intermediate species can be derived following a similar procedure, unless otherwise stated in the text.

In order to obtain the QE surface coverage of $CH_3 \cdot S$, we first identify the Intermediate Reaction for the formation of $CH_3 \cdot S$ from amongst steps that can be considered to be quasi-equilibrated. Thus, for $CH_3 \cdot S$, the appropriate intermediate reaction is

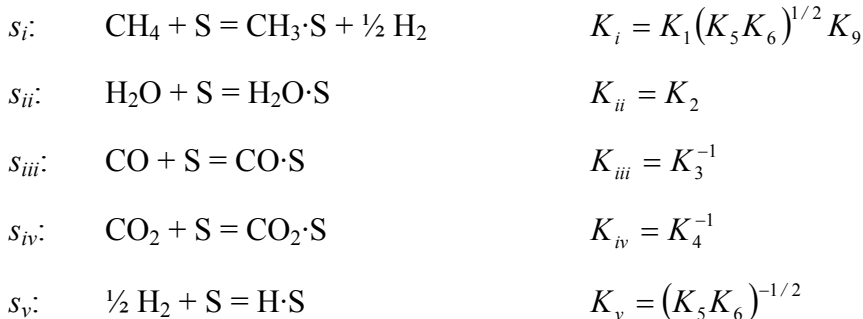s_i: $CH_4 + S = CH_3 \cdot S + \frac{1}{2} H_2$ as shown below

$$\sigma_\rho$$

s_1:	$CH_4 + S \leftrightarrows CH_4 \cdot S$	$+1$
s_5:	$H \cdot S + H \cdot S \leftrightarrows H_2 \cdot S + S + \frac{1}{2}$	
s_6:	$H_2 \cdot S \leftrightarrows H_2 + S$	$+\frac{1}{2}$
s_9:	$CH_4 \cdot S + S \leftrightarrows CH_3 \cdot S + H \cdot S$	$+1$
IR:	$CH_4 + S \leftrightarrows CH_3 \cdot S + \frac{1}{2} H_2$	

Thus, the equilibrium constant for this intermediate reaction is $K_i = K_1 \left(K_5 K_6 \right)^{1/2} K_9$ and
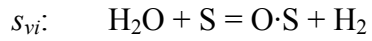
$$\theta_{CH_3 \cdot S} = K_i P_{CH_4} P_{H_2}^{-1/2} \theta_0$$

A list of the intermediate reactions for relevant intermediate species utilized in Appendix B is as follows:

s_i:	$CH_4 + S = CH_3 \cdot S + \frac{1}{2} H_2$	$K_i = K_1 \left(K_5 K_6 \right)^{1/2} K_9$
s_{ii}:	$H_2O + S = H_2O \cdot S$	$K_{ii} = K_2$
s_{iii}:	$CO + S = CO \cdot S$	$K_{iii} = K_3^{-1}$
s_{iv}:	$CO_2 + S = CO_2 \cdot S$	$K_{iv} = K_4^{-1}$
s_v:	$\frac{1}{2} H_2 + S = H \cdot S$	$K_v = \left(K_5 K_6 \right)^{-1/2}$

s_{vi}: $H_2O + S = O \cdot S + H_2$ $K_{vi} = K_2 K_5 K_6 K_7 K_8$

s_{vii}: $H_2O + S = OH \cdot S + \frac{1}{2} H_2$ $K_{vii} = K_2 \left(K_5 K_6 \right)^{1/2} K_7$
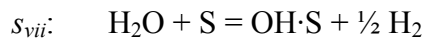
s_{viii}: $\frac{1}{2} H_2 + CO + S = CHO \cdot S$ $K_{viii} = \left(K_3 K_5^{1/2} K_6^{1/2} K_{16} \right)^{-1}$
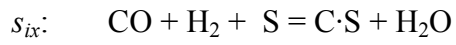
s_{ix}: $CO + H_2 + S = C \cdot S + H_2O$ $K_{ix} = \left(K_2 K_3 K_5 K_6 K_7 K_8 K_{13} \right)^{-1}$
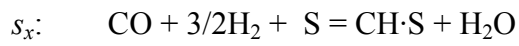
s_{x}: $CO + 3/2 H_2 + S = CH \cdot S + H_2O$ $K_{x} = \left(K_2 K_3 K_5^{3/2} K_6^{3/2} K_7 K_8 K_{12} K_{13} \right)^{-1}$

Appendix D: Overview of energetic predictions via first-principles and UBI-QEP

A brief overview of the first-principles calculations that are fast becoming a commonplace for energetic predictions for catalysis and electrocatalysis is provided here. The electronic structure theories are based on the Time-Independent Schrödinger Equation (TISE),

$$H\Psi = \left(-\frac{\hbar^2}{2m_{mol}}\nabla^2 + V \right)\Psi = E\Psi \tag{D.1}$$

where, H is the Hamiltonian (total energy operator) comprising of potential (V), and kinetic energy, i.e., $-(\hbar^2/2m_{mol})\nabla^2$, E is the total energy of the system, and ψ is the wavefunction, i.e., a function of space containing all possible information about the system. $\hbar = h/2\pi$ and m_{mol}, the mass of the molecule are constants. Solution of this equation yields fundamental information about the system, including probability distributions for all particles within it and energetic information about particular particle configurations. The above TISE is simplified by the Born-Oppenheimer Approximation, which relies on the fact that atomic nuclei move at a pace which is several orders of magnitude slower than that of the electrons, thus allowing us to perform separate calculations for nuclear and electronic structure by splitting the TISE into two parts. Chemical engineers are concerned with the electronic structure solution, which may be visualized as fixed configurations of nuclei surrounded by an "electron gas." The electronic structure of this gas is determined by solution of the electronic TISE, and the resulting total energy is interpreted as a potential energy for the nuclei. Solution of the TISE for many different nuclear arrangements permits the construction of potential energy surfaces (PES's) for the nuclei, which can be utilized to analyze the nuclear dynamics. However, analytical solution is not possible and only approximate numerical schemes can be employed. The simplest technique for the calculation of the electronic orbitals is the Hartree Fock Self-Consistent Field (HFSCF) approach, where the full, many-electron wavefunction for the system, ψ, is written as a product of one-electron wavefunctions containing adjustable parameters. The number of one-electron orbitals is equal to the number of electrons in the system. Corresponding to each electron, Eqs.

similar to Eq. (D.1) are written such that V represents the effective one-electron potential energy function, and E the one-electron eigenvalue. Being the simplest of the techniques, the HFSCF approach generally gives very inaccurate molecular energies due to the lack of explicit electron correlation effects. Configuration Interaction (CI) methods account for these correlation effects, albeit at additional computation time by making use of the unoccupied (virtual) states. Other approaches include the use of Density Functional Theory (DFT), which nicely approximates the correlation effects while not being too computationally demanding. The methodology is largely similar to the HFSCF approach with an additional term, known as the exchange-correlation (XC) energy, added to the effective one-electron potential energy function, V while solving the set of one electron equations. A host of different XC energy expressions have developed built on a similar platform of being explicit functionals of the electron density. The LDA (Local Density Approximation) uses an XC functional that depends only on the electron density itself and takes the XC energy to be the exact XC energy for a homogeneous electron gas. LDA calculations, however, often produce poor estimates of binding energies and molecular structures. The GGA (Generalized Gradient Approximation) incorporates density gradient terms into the XC functional. State-of-the-art GGA, like PW91, PBE, and RPBE are known to give accurate results for trends in binding energies and in lattice constants of transition metals.

Accurate representation of the core electrons is also vital to obtain accurate results. However, the computational effort can be greatly reduced by approximating the behavior of these core electrons, based on the assumption that they do not generally play an active role in chemical bonding as they are located in the innermost shell of an atom. Frozen Core Approximation (FCA) is one such approximation.

Apart from the above mentioned approximations, the biggest stumbling block for accurate energetic prediction is the catalyst surface representation in heterogeneous catalysis. Of course, for electrocatalysis, simulating the effect of electrode potential on the energetics presents additional difficulties. Some research groups employ cluster calculations that use finite ensembles of metal atoms to model surfaces. These are computationally less expensive since they employ atomic or molecular orbital basis sets to satisfy the boundary condition of zero electron density at infinite distance from the

cluster. The other approach is to utilize slab calculations, with the use periodic boundary conditions (and hence require the use of a periodic basis set to match the boundary conditions) to model extended surfaces. These models avoid the electronic structure artifacts that sometimes trouble cluster calculations.

DFT calculations provide an efficient way to calculate the total electronic energy (TE) of a system, which may be used for calculation of ΔH. For the case of adsorption of a species on a surface, ΔH is approximated by the binding energy (BE) of the species. Knowledge of the total energies of the adsorbed configuration, the clean slab representing the catalytic surface and the isolated gas phase species can be used to calculate this BE as:

$$BE_{I_k \cdot S} = TE(\text{adsorbed configuration}) - TE(\text{clean slab}) - TE(\text{isolated gas phase species})$$

$$(D.2)$$

The binding energies are also corrected using zero point energies, and temperature corrections, which may be obtained from the vibrational frequencies of the species. Thus,

$$H^{\circ}_{I_k \cdot S} = H^{\circ}_{I_k(g)} + BE_{I_k \cdot S} + \Delta(ZPE_{I_k})$$

$$(D.3)$$

where $H^{\circ}_{I_k(g)}$ is the standard enthalpy of formation in the gas phase, $BE_{I_k \cdot S}$ is the binding energy, and $\Delta(ZPE_{I_k})$ is the zero point energy correction to binding energy of the intermediate species I_k. The enthalpy change and the entropy change are

$$\Delta H^{\circ}_{\rho} = \sum_{k=1}^{l} \alpha_{\rho k}(H^{\circ}_{I_k \cdot S}) + \sum_{i=1}^{n} \beta_{\rho i}(H^{\circ}_{T_i(g)})$$
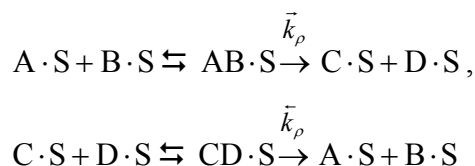
$$(D.4)$$

The recent advances in first principles calculations, has made possible the direct calculation of the activation barriers using DFT. The state of the art CI-NEB method determines the minimum energy path between the initial and final state of a given elementary step by optimizing several discrete intermediate images and is shown to give excellent convergence to saddle points, verified by the existence of a single imaginary frequency at the transition state.

Entropy of the adsorbed species can be approximated as shown in chapter III, i.e. by assuming total loss of translational entropy from gas phase to the adsorbed phase. On the

other, it may be rigorously calculated from DFT based on the knowledge of the vibrational, translational and rotational modes of the adsorbed species. Thus,

$$\Delta S_\rho^o = \sum_{k=1}^{l} \alpha_{\rho k} (S_{I_k \cdot S}^o) + \sum_{i=1}^{n} \beta_{\rho i} (S_{T_i(g)}^o) \tag{D.5}$$

Finally, the surface reactions, the rate constants are calculated using transition state theory (TST), while for adsorption/desorption reactions collision theory can be used. TST assumes equilibrium between the reactants and the activated complex. Thus, for a surface reaction $A \cdot S + B \cdot S \leftrightarrows C \cdot S + D \cdot S$, we have

$$A \cdot S + B \cdot S \leftrightarrows AB \cdot S \xrightarrow{\vec{k}_\rho} C \cdot S + D \cdot S,$$

$$C \cdot S + D \cdot S \leftrightarrows CD \cdot S \xrightarrow{\vec{k}_\rho} A \cdot S + B \cdot S$$

The forward rate constant rate constant $\vec{k}_\rho$ is given as

$$\vec{k}_\rho = \vec{\Lambda}_\rho \exp\left(\frac{-\vec{E}_\rho}{k_B T}\right); \ K_\rho = \frac{\vec{k}_\rho}{\overleftarrow{k}_\rho} \tag{D.6}$$

$\vec{E}_\rho$ is the activation energy for the forward reaction and $\vec{\Lambda}_\rho$ is the pre-exponential factor given as

$$\vec{\Lambda}_\rho = \frac{k_B T}{h} \exp\left(\frac{\Delta \vec{S}_\rho^{\ddagger,o}}{k_B}\right) \tag{D.7}$$

where, $\Delta \vec{S}_\rho^{\ddagger,o} = \Delta S_{AB \cdot S}^o - \Delta S_{A \cdot S}^o - \Delta S_{B \cdot S}^o$ is the standard state entropy change accompanying the formation of the transition state. $\Delta S_{AB \cdot S}^o$ for the activated complex is calculated following a similar procedure as that for the adsorbed species.

Collision theory can be used to obtain rate constants for adsorption processes, which give the pre-exponential factor as

$$\vec{\Lambda}_\rho = \frac{\sigma^0(T,\theta)}{\sqrt{2\pi m_A k_B T}} \tag{D.8}$$

where, m_A is the molecular weight of the species and $\sigma^0(T,\theta)$ denotes the sticking probability.

UBI-QEP approach for predicting the activation energies of elementary reaction steps:

The method of UBI-QEP is the improved version of the BOC-MP. Here we provide only the relevant equations useful in predicting the activation energies for elementary reactions. The details can be found in the publications by Shustorovich and co-workers (Shustorovich, E. M., and Sellers, H., Surf. Sci., 31, (1998), 1; Zeigarnik, A. V. et al., Surf. Sci., 541, (2003), 76; Shustorovich, E. M., and Zeigarnik, A. V., Russian J. Phys. Chem., 80, (2006), 4)

1) The heats of chemisorption for diatomic molecules are based on the type of binding. Atomic heat of adsorption of species A, in an n-fold site (a site making n-bonds with the adsorbed atom) is

$$Q_A = Q_{0A}\left(2 - \frac{1}{n}\right) \tag{D.9}$$

where Q_{0A} is the heat of adsorption in the on-top position or, alternatively, the two-center bond energy.

2) For the weak bonding ad-molecule typical of adsorption of closed-shell molecules, the heat of adsorption of an AB molecule, $Q_{AB,n}$, on n-fold site, which adsorbed via A atom is given by

$$Q_{AB,n} = \frac{Q_{0A}^2}{\left(\dfrac{Q_{0A}}{n} + D_{AB}\right)} \tag{D.10}$$

where D_{AB} is the gas-phase dissociation energy of the A-B bond.

Weakly bound molecules such as closed shell molecules (i.e., CO, N_2) or molecular radicals with strongly delocalized unpaired electrons (i.e., O_2, NO) tend to have heats of chemisorption in the range 10-35 kcal/mol.

3) For the strong bonding ad-molecules, which typically occurs upon the adsorption of molecular radicals, heat of adsorption is given by

$$Q_{AB,n} = \frac{Q_A^2}{Q_A + D_{AB}} \tag{D.11}$$

Strongly bound molecules have heats of chemisorption in the range 35-120 kcal/mol. Medium binding gives an average of the two extremes.

4) The enthalpy changes in the course of adsorption and reaction are accordingly given by

$$\Delta H = \sum_r Q_r - \sum_p Q_p + \sum_b D_b - \sum_f D_f \tag{D.12}$$

where Q_r and Q_p are the heats of chemisorption for the reactants (r) and products (p), respectively; D_b and D_f are the binding energies for the bonds that are broken (b) and formed (f), respectively.

Heats of chemisorption (Q) and total bond energies in a gas phase (D) for various species on different catalyst surfaces are well documented in the literature (Shustorovich, E. M., and Sellers, H., Surf. Sci., 31, (1998), 1; Hei, M. J. et al., Surf. Sci., 417, (1998), 82; Lin, Y.-Z. et al., J. Mol. Struc. (Theochem), 587, (2002), 63; Olivera, P. P. et al., Surf. Sci, 327, (1995), 330; Sellers, H., and Shustorovich, E. M., Surf. Sci., 504, (2002), 167).

In the case of the disproportionation reaction, A·S + BC·S ⇆ AB·S + C·S, the direction of the reaction is defined such that the condition that $D_{BC} > D_{AB}$ is satisfied. If it is not, the direction of the reaction should be reversed for the analysis. The activation energy of the reaction in the forward direction, corresponding to the appropriate form of the reaction, may be determined using

$$\vec{E} = \frac{1}{2}\left[\Delta H + \frac{Q_{AB}Q_C}{Q_{AB} + Q_C}\right] \tag{D.13}$$

Similarly, for an AB·S ⇆ A·S + B·S, we have

$$\vec{E} = \frac{1}{2}\left[\Delta H + \frac{Q_A Q_B}{Q_A + Q_B}\right] \tag{D.14}$$

The activation energy of the reverse direction may then be determined from the relationship between the reaction enthalpy and the reaction's forward activation barrier

$$\Delta H = \vec{E} - \bar{E} \tag{D.15}$$

Let us calculate the activation energy on Ni(111) for the following elementary reaction, CHO·S + S $\leftrightarrows$ CH·S + O·S, as an example.

$$Q_{\text{CHO·S}} = 49.9\,\text{kcal/mol}, \quad D_{\text{CHO·S}} = 274\,\text{kcal/mol}$$

$$Q_{\text{CH·S}} = 116\,\text{kcal/mol}, \quad D_{\text{CH·S}} = 81\,\text{kcal/mol}$$

$$Q_{\text{O·S}} = 115\,\text{kcal/mol}, \quad D_{\text{O·S}} = 0\,\text{kcal/mol}$$

Using above in Eq. (D.12), we have $\Delta H = \sum_r Q_r - \sum_p Q_p + \sum_b D_b - \sum_f D_f = 11.9$ kcal/mol.

Using these in Eq. (D.13), we have,

$$\vec{E} = \frac{1}{2}\left[\Delta H + \frac{Q_{AB}Q_C}{Q_{AB}+Q_C}\right] = \frac{1}{2}\left[11.9 + \frac{(116)(115)}{116+115}\right] = 34.82 \text{ kcal/mol}$$

Using the above in Eq. (D.15), we have

$$\bar{E} = \vec{E} - \Delta H = 22.92 \text{ kcal/mol}$$